2009

AN ENHANCED -1800-YEAR RECORD OF RECENT VOLCANIC ASH-FALL EVENTS FOR NORTHERN NEW ZEALAND FROM THE ANAlYSIS OF CRYPTOTEPHRA

GEHRELS, MARIA J.

AN ENHANCED ~1800-YEAR RECORD OF RECENT VOLCANIC ASH-FALL EVENTS FOR NORTHERN NEW ZEALAND FROM THE ANALYSIS OF CRYPTOTEPHRA

by

MARIA J. GEHRELS

A thesis submitted to the University of Plymouth

in partial fulfilment for the degree of

DOCTOR OF PHILOSOPHY

School of Geography

Faculty of Science

August 2009

An enhanced ~1800-year record of recent volcanic ash-fall events for northern New Zealand from the analysis of cryptotephra

Maria J. Gehrels

The history of volcanic eruptions in North Island, New Zealand, based on the visible stratigraphic record of tephras is not fully representative of the type, frequency and magnitude of eruptions that have occurred in the past or that are likely to occur in the future. Relatively small-scale eruptions from the region's andesitic volcanoes can produce widespread fine tephra falls with considerable impact, such as during recent eruptions of Mt Ruapehu (1995-1996) and Mt Ngauruhoe (1974-1975), and their threat is therefore likely to be underestimated. The aim of this study was to develop an enhanced stratigraphic record of recent ash-fall events in the Auckland and Waikato regions through the application of cryptotephrostratigraphic techniques. Cryptotephras in sediment cores from two peat bogs and two lakes were quantified and characterised for the period since deposition of the AD 233 ± 13 Taupo Tephra. A complex record of primary and reworked rhyolitic and andesitic tephra-fall is revealed. A stratigraphic and geochemical protocol for distinguishing primary from likely reworked tephras was developed and enabled the identification of ten post-Taupo cryptotephra-fall events. The rhyolitic Okataina Volcanic Centre-derived Kaharoa Tephra (AD 1314 ± 12), a key chronostratigraphic marker for human settlement in New Zealand, was found in all sites together with four pre-historic Mt Ruapehu-derived tephras of the Tufa Trig Formation (Tf4, Tf5, Tf6, and Tf14). In the Waikato Region, an additional Tufa Trig tephra (Tf8) was detected, as well as ash fallout from historical eruptions of Mt Ruapehu (1861, 1945 and 1996) and Mt Ngauruhoe (1975). These findings represent a considerable extension to the known geographical ranges of tephra-fall events and demonstrate that cryptotephrostratigraphic techniques can enhance the historical and geological record of ash-fall events as a guide to future volcanic hazard assessment for countries such as New Zealand.

TABLE OF CONTENTS

APPENDICES*

i. Shard counts data

ii. Major element geochemistry, raw data

iii. Radiocarbon age results

iv. PDFs of publications

v. PDF of this thesis

***Included on a CDRom on the back cover of this thesis.**

LIST OF FIGURES

LIST OF TABLES

LIST OF PLATES

Acknowledgements

This project was made possible by a School of Geography PhD scholarship at the University of Plymouth. The following grants were also obtained to support fieldwork, analyses and conference attendance:

- Natural Environmental Research Council, two weeks analytical time at the Tephra Analytical Unit, Edinburgh, 2007.
- Quaternary Research Association, travel award to attend INQUA Congress, Cairns, Australia, July 2007, £600, 2007.
- Natural Environmental Research Council, Radiocarbon dating allocation no. 1204.1006, £9880, 2007.
- Geological Society of America, student travel award, Geological Society of America Annual Meeting, Philadelphia, 22-25 October, $200, 2006.
- University of Waikato, New Zealand, Radiocarbon dating award, equivalent to £1000, 2005.
- The Royal Society, Dudley Stamp Memorial Fund, fieldwork support, £200, 2005.

I wish to thank many people and organisations who have provided help and support in one way or another during the time frame of this project. Firstly, my very special thanks go to my academic advisors and mentors Professors Rewi Newnham (Plymouth) and David Lowe (Waikato) for their unrelenting support and encouragement throughout this project. I have learnt a great deal from them both. I am also very grateful to Professor Valerie Hall who helped with the formulation and early stages of this project and to Professor Dan Charman for his expertise and for reading through drafts of this thesis. For the material used in this project I am grateful to the New Zealand Department of Conservation (Waikato) for allowing access and sampling at Moanatuatua and Opuatia bog sites. My thanks go to Paul Augustinus from the University of Auckland who very generously supplied valuable core material from Lake Pupuke site used in this study. Thanks also to

Michael Turner (Massey University, NZ) for providing some trial core material from Lake Rotomanuaka. Discussions with Dr Phil Shane (University of Auckland, NZ), Dr Beverly Clarkson (Landcare Research, NZ), Prof. Stefan Wastegård (Stockholm University) and Prof. John Pilcher (Queen's University, Belfast) provided many helpful insights.

For help and support with laboratory analysis I wish to thank the technical staff from the School of Geography, University of Plymouth (UoP), and from the Department of Earth and Ocean Sciences, University of Waikato. At UoP labs I am particularly grateful to Ms Ann Kelly for her technical expertise and assistance. Thanks also to the cartographers, especially Jamie Quinn and Tim Absalom (UoP) for help with figures, maps and technical problems. At the NERC radiocarbon facility I am grateful to Drs Mark Garnett and Charlotte Bryant for a very informative training visit to the laboratory. Thank you to Drs Alan Hogg and Fiona Petchey at the Waikato Radiocarbon Dating Laboratory for radiocarbon dates and calibrations. At the NERC Tephrochronology Analytical Unit, University of Edinburgh, I am particularly grateful to Dr David Steele, now at JTek in Queensland, Australia, for his expertise and guidance in using the electron microprobe.

My thanks also go the following persons who have supported me or the project in some way in the last four years: Dr Brent Alloway (GNS, New Zealand), Dr Christina Magill (Risk Frontiers, Macquarie University, NSW, Australia), Dr Bruce Hayward (University of Auckland) and Dr Francois De Vleeschouwer (University of Leige, Belgium). My thanks also go to my friends for support of another kind - especially to Veronica Hohl, Afraa Sallowm and Jessie Woodbridge. Last but not least, I wish to thank my dear husband Roland, for being so supportive and patient these last four years. Thank you!

Author's declaration, research contributions and word count

At no time during the registration for the degree of Doctor of Philosophy has the author been registered for any other University award.

Publications

The following publications, relevant to this research, were produced during the timeframe of this project:

Gehrels, M.J., Newnham, R.M., Lowe, D.J., Wynne, S., Hazell, Z.J., Caseldine, C., 2008. Towards rapid assay of cryptotephra in peat cores: review and evaluation of various methods. *Quaternary International* 178, 68-84.

Gehrels, M.J., Lowe, D.J., Hazell, Z.J., Newnham, R.M., 2006. A continuous 5300-yr Holocene cryptotephrostratigraphic record from northern New Zealand and implications for tephrochronology and volcanic-hazard assessment. *The Holocene* 16, 173-187.

On the basis of these two publications the author was awarded the 2008 New Zealand Geological Society's Vucetich and Pullar prize, an award for most merititious contribution to tephra studies in New Zealand in the past three years.

Conference contributions

Gehrels, M.J., Newnham, R.M., Lowe, D.J., Charman, D., Hall, V.A., Augustinus, P., 2008. An enhanced record of recent ash-fall events from northern New Zealand based on cryptotephra analysis. IAVCEI General Assembly, Iceland. 17 - 22 August 2008. Oral presentation.

Gehrels, M.J., Newnham, R.M., Lowe, D.J., Hall, V.A., Augustinus, P., 2007. Cryptotephrostratigraphic records from northern New Zealand for the last two millennia. XVII INQUA Congress, Cairns, Australia, 28 July – 3 August. Oral Presentation.

Gehrels, M.J., Newnham, R.M., Lowe, D.J, Hall, V.A., Augustinus, P., 2007. Enhancing the record of volcanic ash-fall events in northern New Zealand for palaeoenvironmental and archaeological applications. Quaternary Environments and Human Past. Quaternary Environments and Geoarchaeological Research Group at the University of Manchester. 20 June. Poster presentation.

Gehrels, M.J., Newnham, R.M., Lowe, D.J., and Hall, V.A., 2006. Enhancing the record of volcanic ash-fall events in New Zealand for palaeoenvironmental and archaeological applications. Geological Society of America Abstracts with Programs, Vol. 38, No. 7, p. 177. Geological Society of America, Philadelphia, 22-25 October 2006. Oral presentation.

Gehrels, M.J., 2006. The use of cryptotephrostratigraphy to enhance and extend the late Holocene tephra record for northern New Zealand. Quaternary Research Association, 5th

International Postgraduate Symposium, University of Edinburgh, 29 August – 1 September. Oral presentation.

Gehrels, M.J., 2005. Developing a Holocene crypto-tephrostratigraphic record for the North Island, New Zealand. SCOTAV Field Conference and Workshop, Whitehorse and Dawson City, Yukon Territory, Canada, 31 July – 8 August. Oral presentation.

Gehrels, M.J., 2005. A crypto-tephrostratigraphic study of lakes and peat bogs in the Waikato Region, North Island, New Zealand. Quaternary Research Association, 4th International Postgraduate Symposium, University of Plymouth, 31 August – 2 September. Oral presentation.

Word count of this thesis.....**79415**.....

Signed.....M.J. Gehrels.....Date.....2/2/07.....

CHAPTER 1: INTRODUCTION

1.1 Introduction and rationale

A considerable part of the North Island of New Zealand is volcanically active. Subduction-related and intraplate volcanism are manifest across the North Island as a number of active and potentially active rhyolitic or andesitic volcanic centres or basaltic volcanic fields. The centres include large magnitude rhyolitic caldera-forming volcanoes that include two of the most active and highly explosive rhyolitic volcanoes in the world, and numerous very frequently active andesitic stratovolcano complexes. Explosive ash-producing (pyroclastic) eruption phases from these volcanoes (and from vents of the volcanic fields) have provided an extensive legacy of tephra which have mantled contemporaneous surfaces and which can be identified as distinct visible layers in many terrestrial sedimentary archives on land and in adjacent marine environments (Froggatt & Lowe, 1990; Carter *et al.*, 1995; Shane, 2000; Carter *et al.*, 2003; Lowe *et al.*, 2008b).

The tephra record has revealed a very detailed history of volcanic activity in North Island during the late Cenozoic (Lowe, 1988b; Froggatt & Lowe, 1990; Wilson, 1993; Lowe *et al.*, 1999; Shane, 2000; 2005). The tephras have provided numerous, important

stratigraphic markers for dating and correlating sequences representing key periods of climatic, environmental and archaeological change in the region (Lowe *et al.*, 2000; 2002; Newnham *et al.*, 2003; Lowe & Newnham, 2004; 2008b). These records also form the basis for assessing future ash-fall hazards from active and potentially active volcanoes in the region.

However, it is widely acknowledged that the history of volcanic eruptions based on these records is not necessarily fully representative of the actual types, frequency and magnitude of eruptions that have occurred in the past or that are likely to occur in the future (Lowe & Newnham, 1999; Newnham *et al.*, 1999a; 1999b; Wilson *et al.*, 2004). In comparison with the well-represented deposits from the large magnitude, millennial frequency eruptions of the rhyolitic volcanoes (Froggatt & Lowe, 1990; Shane, 2000; Lowe *et al.*, 2008b), tephra fall events from the smaller, yet more frequently active, andesitic volcanoes are poorly represented. Nevertheless, andesitic eruptions are capable of wide tephra dispersal and impact, as revealed by recent eruption events (e.g. Ruapehu 1995-1996 and Ngauruhoe 1974-1975) (Nairn & Self, 1978; Weinstein & Patel, 1997; Johnston *et al.*, 2000; Becker *et al.*, 2001). On the other hand, the less frequent but thick deposits of silicic tephra from large magnitude rhyolitic eruptions are generally well studied (Lowe, 1988b; Froggatt & Lowe, 1990; Shane, 2000) but provide only a limited guide to future volcanic activity on timescales of immediate social and economic relevance.

As a consequence, recent work has placed more emphasis on the study of thin, medial to distally deposited tephra layers in New Zealand to extend the known dispersal of tephra layers for stratigraphic applications and to model ash-fall hazards with higher reliability

(e.g. Lowe, 1988a; 1988b; Sandiford *et al.*, 2001; Shane & Hoverd, 2002; Shane *et al.*, 2002; Shane, 2005; Molloy & Shane, 2007). In these studies, peat deposits and lake sediments from northern New Zealand in particular have proved to be effective archives for preservation of fine tephra deposits including products from andesitic eruptions. Significantly, these investigations have revealed a greater range of deposits in distal settings than previously recognised and more eruptions than determined from proximal deposits alone.

A small number of studies have attempted to extend studies of fine tephra further through the detection and identification of tephra which may be present in such low concentrations in the matrix of sediments so as to be not visible to the naked eye (Hogg, 1979; Lowe *et al.*, 1981; Gardner *et al.*, 1985; Eden & Froggatt, 1996; Gehrels *et al.*, 2006). The analysis and application of this cryptic tephra (cryptotephra; Lowe & Hunt, 2001) is well established throughout Europe (e.g., Hall & Pilcher, 2002; Davies *et al.*, 2002; 2003; Davies & Lowe, 2004) and increasingly in other regions of the world (e.g. Russia, Wastegård *et al.*, 2000b; New Zealand, Gehrels *et al.*, 2006; Iceland, Kristjansdottir *et al.*, 2007; Africa, Feakins *et al.*, 2007; Australia, S.E. Davies *et al.*, 2007; Alaska, Payne *et al.*, 2008; Canada, Lakeman *et al.*, 2008; Japan, Lim *et al.*, 2008). Cryptotephra can be preserved in distal sedimentary archives, including peat bogs, lake, marine and aeolian sediments, and in ice cores (Lowe, 2008). Cryptotephra study is an emerging discipline with the potential to revolutionise understanding of sediment chronologies and volcanic hazards. This is largely the result of new methods developed to detect and isolate the very fine-grained and sparse components of distal tephra and techniques that allow characterisation of very small tephra grains (down to ~20-40 μm in diameter). These

advances have made it possible to extend the geographical limits of tephra applications well beyond the immediate area around volcanoes by hundreds and sometimes thousands of kilometres. For example, the Iceland-derived Vedde Ash has been detected as a cryptotephra >3000 km away in the Alps (Blockley *et al.*, 2007). Cryptotephrostratigraphy has allowed for wide scale correlations between sites (e.g. Davies *et al.*, 2002; Turney *et al.*, 2004; Davies *et al.*, 2008). In some cases, these distally deposited tephras have revealed eruption events that were previously overlooked in sites proximal to volcanic source (e.g. Wastegård, 2002; Davies *et al.*, 2003; Chambers *et al.*, 2004; Ranner *et al.*, 2005; Lim *et al.*, 2008). The detection of very fine grained, distally deposited, tephras has also helped to reveal the wider impacts of distal tephra fallout on the environment (Grattan *et al.*, 1999; Giles *et al.*, 1999; e.g. Payne & Blackford, 2005) and on human health and community infrastructure (Newnham *et al.*, 1999a; Horwell & Baxter, 2006; Molloy & Shane, 2007; Payne *et al.*, 2008).

Although these studies illustrate the considerable capacity of cryptotephra analyses to enhance tephrostratigraphic records, they also point to a number of potential problems. It has been suggested that cryptotephra are subject to considerable reworking, mixing and weathering processes, which could render them of little value for stratigraphic studies (Shane, 2000). Preservation problems of cryptotephra, their physical and chemical weathering and their taphonomy are now topics of high interest (Dugmore *et al.*, 1992; Turney & Lowe, 2001; Payne & Blackford, 2004; S.M. Davies *et al.*, 2007; Pyne-O'Donnell *et al.*, 2008; Matthews, 2008).

This investigation concerns the application of cryptotephra analysis at selected sites in the Waikato and Auckland regions of northern New Zealand, with records spanning the interval since deposition of the AD 233 ± 13 Taupo Tephra (1717 ± 13 cal yr BP, Sparks *et al.*, 1995; 2008). Because well-developed tephrostratigraphies, based on visible tephra layers, already exist for these regions, this investigation will be able to explore both the potential and the problems for using cryptotephra to enhance the existing visible tephrostratigraphic framework. The study area includes large centres of population and so provides the opportunity to consider implications for contemporary volcanic hazards assessment that arise from a tephrostratigraphic record enhanced by cryptotephra analyses. The Taupo Tephra provides a baseline readily identifiable at all four sites investigated (described below) whilst the overlying sedimentary records span the last *ca.* 1800, a critical period in recent environmental change and archaeology in New Zealand (e.g., Lowe *et al.*, 1998; 2008b). The sedimentary record of the past ~1800 years spans an interval of most direct relevance for contemporary hazards assessment, incorporating both large and small scale eruption events, and enables detailed high-resolution analyses to be undertaken with good potential for inter-site replication within the timeframe of this study.

1.2 Aims, objectives and significance

The main aim of this study is to develop an enhanced stratigraphic record of recent ash fall events in peat bogs and lakes in northern North Island, New Zealand, through the application of cryptotephrostratigraphic techniques. To achieve this aim, the following objectives are defined:

(1) To use cryptotephrostratigraphic techniques to detect, quantify and characterise primary tephra-fall events preserved as cryptotephra in sediment cores from peat bogs and lakes in the region for the period following deposition of the AD 233 ± 13 Taupo Tephra.

(2) To link identified cryptotephras to a volcanic source and if possible to an individual eruptive event and tephra.

(3) To appraise the depositional sites in terms of cryptotephra preservation and to advance methodologies for distinguishing primary fall tephras from 'background' or reworked concentrations of tephra-derived shards.

(4) To consider the implications of enhanced records of ash fall derived through cryptotephra analysis for the assessment of ash-fall hazards to the wider regions of Waikato and Auckland.

Cryptotephrostratigraphy is traditionally applied at sites that are positioned *distally* from volcanic source. This study is distinctive in that it is concerned with developing, adapting and applying cryptotephrostratigraphic techniques at sites which are *medially* positioned in relation to volcanic source and hence are likely to detect smaller-scale eruptions and higher concentrations of tephra. In addition to enhancing the local tephrostratigraphic records at these sites, it is anticipated that the likely greater abundance (concentration) of glass

associated with cryptotephras will enable stronger insights into the potential advances as well as limitations of this developing method than might be gleaned from more distal sites.

There are various potentially significant outcomes from this study including: (1) increasing the number of isochronous markers in the tephrostratigraphic records; (2) extending the application of key chronostratigraphic marker tephras; (3) providing a more realistic appraisal of ash-fall hazards to include medial/distal hazards posed by small concentrations of ash; (4) developing the methodological approaches for detecting and analysing cryptotephra in volcanic regions.

1.3 A note on terminology used in this thesis

The terminology related to tephra studies varies in the literature in part due to the wide range of different research disciplines where tephra are applied, but also between different regions and researchers. The terminology used in this thesis follows that recommended by Lowe and Hunt (2001) and Alloway *et al.* (2007).

Tephra: the unconsolidated, fragmental material (pyroclasts) erupted explosively from a volcano and deposited as airborne fallout or as co-ignimbrite material. The deposits studied typically were fine to medium ash (<1 mm in size), and mainly glassy or pumiceous compositionally. Coarse ash (1-2 mm) and fine lapilli (2-4 mm) were present as Taupo Tephra.

Glass shards or shards: individual fragments of glassy, vitric particles which comprise the main component of a medial or distal tephra deposit. This term is used primarily in the context of microscopic examination during shard counts and microprobe analysis.

Cryptotephra or cryptic tephra: tephra-derived glass-shard concentrations which are not immediately recognisable in the sediments as a distinct layer and which require separation from the sediment matrix to identify definitively, normally through microscopy. Cryptotephra are also referred to as microtephra and non-visible tephra in the literature.

1.4 Thesis structure

This thesis contains seven chapters in addition to this introductory section. Chapter 2 provides a short background to the study and reviews key developments and themes of relevance. Chapter 3 outlines the methodology used in this study, the rationale for site selection and details of laboratory techniques and analyses. Chapters 4 and 5 present results from the four sites investigated separated into the two main geographical regions, Waikato and Auckland. Chapter 6 includes a detailed synthesis and interpretation of the main results and findings from this study. Chapter 7 concludes the thesis with a summary of the main research findings.

CHAPTER 2: BACKGROUND

2.1 Introduction

This chapter provides a short introduction to the main research field and study region discussed in this thesis. It includes: (1) the terminology and main sub disciplines in tephra studies; (2) the general environment of New Zealand and the timing and impact of human settlement; (3) the regional plate tectonic setting, late Quaternary volcanism and tephra layers; and (4) North Island's volcanic activity for the past ~2000 years, the time span covered in this thesis. More detailed information about relevant tephras is given in the chapters of results.

2.2 Tephra studies: terminology, principles and methods

For more than half a century tephra layers have been recognised as both highly valuable stratigraphic markers for dating and correlating sedimentary sequences in addition to providing an important dossier of past volcanic activity (Grange, 1931; Vucetich & Puller, 1964; Kittleman, 1979; Thorarinsson, 1981).

Tephra

The word tephra derives from the Greek word τεφρα, meaning 'ashes'. The first recorded use of 'tephra' in the western literature was by Aristotle more than 2000 years ago when describing an eruption of Hiera (Vulcano) in the Aeolian or Lipari islands near Sicily (Thorarinsson, 1981; Lowe, 2008). The term was resurrected by Sigurdur Thorarinsson in the 1940s and is now used as a collective term for all explosively erupted, unconsolidated products of a volcanic eruption (including tephra fall deposits, unconsolidated deposits of pyroclastic flows and surges, and co-ignimbrite ash/lapilli deposits) (Lowe & Hunt, 2001). Thorarinsson chose the word 'tephra' specifically to tie in linguistically with terms 'lava' and 'magma' and with classical Mediterranean volcanology, and to avoid grain size connotations. Thus tephra encompasses particles of any size including (1) large blocks (angular) and bombs (rounded) >64 mm in diameter; (2) lapilli (singular: lapillus), which means "little stones" in Latin, including scoria, pumice, rock fragments and large crystals 2-64 mm in diameter; and (3) ash <2 mm (coarse ash is 2-0.5 mm, medium ash 0.5-0.0625 mm, very fine ash <0.004 mm). Ash is typically composed of vitreous glass fragments, and in some cases ash-sized micropumice particles, together with crystals and rock fragments depending on proximity to the source volcano (Heiken & Wohletz, 1985). The widespread, thinly deposited tephra fall deposits of primary interest in this thesis study typically comprise fine to very fine ash which is likely to travel the furthest and be less easily observed in the sedimentary record.

The different sub-disciplines and terms related to tephra studies are summarised in Figure 2.1. Tephrochronology in its original sense (*sensu stricto*) is the use of tephra layers as isochrons to connect or correlate sequences and to transfer ages to such sequences where

the tephras have been dated (Alloway *et al.*, 2007). In this sense, tephrochronology is a linking, dating, and synchronising tool (Lowe, 2008). In contrast, tephrochronometry is the dating of a tephra layer either directly or indirectly. In recent times, the term tephrochronology (*sensu lato*) has been used more broadly to describe all aspects of tephra studies (Shane, 2000; Lowe, 2008).

Tephostratigraphy and tephrochronology (tephra studies)

Tephra layers, provide valuable stratigraphic markers for dating and correlating sedimentary sequences in addition to providing an important dossier of past volcanic activity. As a dating and correlating tool, tephras encompass three special features (Alloway *et al.*, 2006): (1) they are deposited over a very short period of time (days, weeks or months at most); (2) they can be widely dispersed; and (3) they can be characterised, or 'fingerprinted' to link them to a volcanic source or to a specific eruption or deposit. These features form the basis of the interlinking disciplines of tephrostratigraphy and tephrochronology.

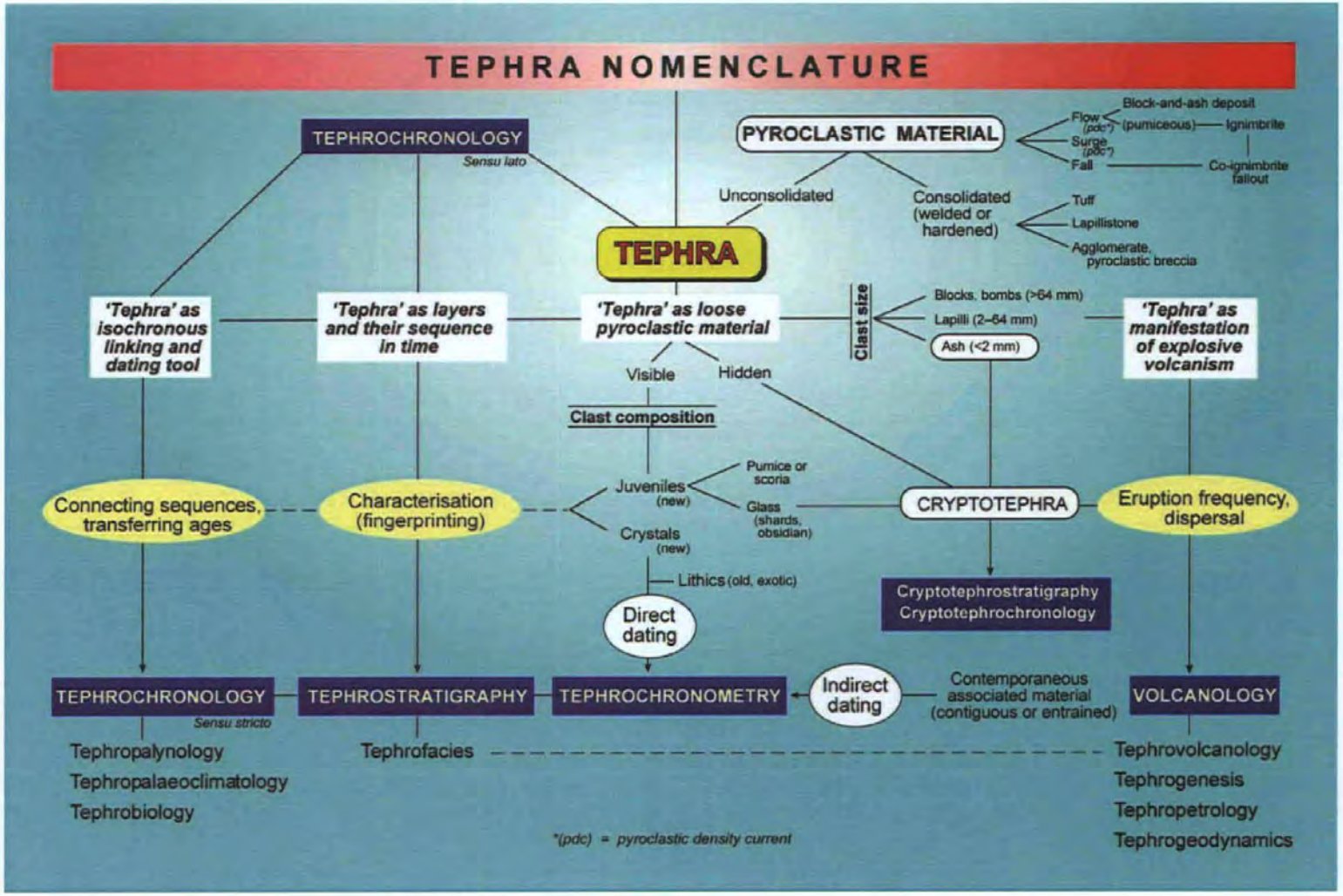

Figure 2.1. Tephra nomenclature and relationships. Figure from Lowe (2008).

Tephrostratigraphy is the study of sequences of tephras and associated deposits and their stratigraphic relationships and relative ages. It involves defining, describing and characterizing tephra layers using their physical, mineralogical or geochemical properties from field and laboratory-based observations (Fig. 2.1, Lowe, 2008). Several criteria are used to characterise tephras and include: (1) stratigraphic position in relation to other tephra layers or associated deposits, or relative age; (2) diagnostic physical and compositional properties; and (3) numerical age determined from radiometric (e.g. radiocarbon dating), incremental (e.g. layer counting), or age-equivalent (e.g. paleomagnetism) methods.

As noted above, tephrochronology (*sensu stricto*) is the use of individual 'characterised' tephra layers as age-equivalent markers or isochrons in the stratigraphic record. Because of widespread dispersal, many tephra layers can be used to correlate, link or synchronize sequences from a wide range of different sedimentary archives. They can also be used as a dating tool when tephras have been independently dated (Alloway *et al.*, 2007). As a chronological tool, some tephra layers have provided almost unrivalled precision amongst many other dating methods across a wide range of geological, palaeoenvironmental and geoarchaeological applications (Buckland *et al.*, 1981; Einarsson, 1986; Sarna-Wojcicki, 2000; Turney & Lowe, 2001; Alloway *et al.*, 2006).

Cryptotephrostratigraphy and cryptotephrochronology (cryptotephra studies)

Cryptotephra, from the Greek word *kryptein*, meaning 'to hide', are the sparse, very fine grained components of tephra, typically comprising ash-grade glass-shard concentrations, which are 'hidden', i.e. not visible to the naked eye, in distal sedimentary archives such as peat bogs, lake, marine and aeolian sediments, and in ice cores (Lowe, 2008). 'Cryptotephra' is now a well established and recommended term (e.g. Turney *et al.*, 2004) in tephra studies and supersedes the term 'microtephra'. Microtephra was one of the original terms used to describe 'hidden' tephras (Turney *et al.*, 1997), possibly to convey the need for microscopy for detection and analysis. This term is still used by some researchers (e.g. Pollard *et al.*, 2006; Feakins *et al.*, 2007). Although it can be argued that microscopy is necessary to confirm the occurrence of these deposits in a sediment sample, once extracted or separated from the enclosing sediments, tephra-derived glass shards may be quite visible. Microscopy is used anyway in the study of visible or 'macro' tephras as well as cryptotephras. The term 'non-visible' tephra has also been used to describe cryptotephra (e.g. Blockley *et al.*, 2007; Matthews, 2008).

Cryptotephra studies are an emerging and, according to Lowe (2008), revolutionary discipline because the development of methods to detect and characterise very small concentrations of tephra-derived glass have made it possible to extend tephrochronological applications to geographical regions well beyond the volcanic sources, >3000 km in some cases. Cryptotephra studies have now been undertaken in more than 24 countries and in sediment cores from oceans and from ice cores (Lowe, 2008). Methods to detect, isolate, and analyse very fine grained components of tephra (mainly glass shards) from a wide range of sediment compositions have been undertaken (e.g., Pilcher & Hall, 1992; Turney,

1998; Blockley *et al.*, 2005; Gehrels *et al.*, 2008). Both destructive and non-destructive techniques have been developed (e.g., see Gehrels *et al.*, 2006; 2008) and these are explored further in this thesis.

Once isolated, the analysis of glass from cryptotephras to characterise and correlate them has been mainly undertaken using the electron microprobe (EMP) for major and some minor elements. Originally developed by Smith & Westgate (1969), advances in EMP were made by Froggatt (1983; 1992) and then by Hunt & Hill (1993; 1996; 2001), with the most recent discussion on EMP protocol for tephra analysis being that of Turney *et al.* (2004). Analysis by EMP is critical to cryptotephra studies because medial and distal cryptotephras have no (or very limited) field characteristics, and typically have sparse or only limited amounts of crystals (mineral assemblages) that are used to aid identification and correlation at more proximal sites (e.g., Froggatt & Lowe, 1990; Lowe, 2008). The analysis of glass to obtain trace element or rare-earth element (REE) data on a grain-by-grain basis has only recently become more readily available after more than a decade in development. Techniques include laser ablation, inductively-coupled plasma mass spectrometry (LA-ICPMS) (e.g. Westgate *et al.*, 1994; Pearce *et al.*, 1999; Pearce *et al.*, 2004), and the ion microprobe (secondary ionisation mass spectrometry, SIMS) (e.g., Shane *et al.*, 2007; Denton & Pearce, 2008). These methods potentially allow tephras which are compositionally similar based on major elements to be distinguished using trace elements or REEs (Lowe, 2008).

Some of the first systematic cryptotephra studies were centred in Scotland and Northern Ireland where very fine and sparse deposits of Icelandic-derived volcanic ash were found preserved in peat bogs and lakes (Pilcher & Hall, 1992; Dugmore & Newton, 1992; Hall *et*

al., 1993; Dugmore *et al.*, 1995). Since those early studies, there has been a rapid expansion in the application of cryptotephra across many other regions (summarised by Lowe, 2008). In Europe, cryptotephrostratigraphy has developed rapidly and a comprehensive stratigraphic framework of tephra layers from Icelandic, Faroese, Italian and German volcanoes across large parts of Europe now enables wide scale correlations between sites (Davies *et al.*, 2002; Turney *et al.*, 2004). Cryptotephra have also been identified in North America (Payne & Blackford, 2004; Lakeman *et al.*, 2008); Africa (Feakins *et al.*, 2007), Russia (Wastegård *et al.*, 2000b) and Australia (S.E. Davies *et al.* 2007). More recently, cryptotephras have been utilized to enhance and extend regional tephrostratigraphic records in volcanic provinces such as Iceland (Kristjansdottir *et al.*, 2007) Japan (Lim *et al.*, 2007), Alaska (Payne *et al.*, 2008) and New Zealand (Gehrels *et al.*, 2006). Recent identification of cryptotephra in polar ice cores (e.g., Davies *et al.*, 2008) represent an exciting new development in the field.

This work illustrates the potential of cryptotephra for extending the role and applications of tephra studies generally as well as drawing attention to key methodological issues and fundamental assumptions. It is widely assumed for example that a concentrated zone of cryptotephra represents the original depositional point in the record and that glass-shard geochemistry has not been altered significantly after deposition. Parallel assumptions underpin conventional tephra work (on visible layers) as well. However, it is recognised that very thin tephras may be more vulnerable to post-depositional movement and/or chemical weathering and hence these assumptions may be more challenging for cryptotephra (S.E. Davies *et al.*, 2007).

In the case of peat bogs and lakes, glass shard concentrations representing individual cryptotephra have been identified as diffuse or attenuated zones of shards with attendant difficulties for defining the original stratigraphic position or isochron represented by the tephra (e.g., Gehrels *et al.*, 2006; S.M. Davies *et al.*, 2007; Pyne-O'Donnell *et al.*, 2008). In peat sites, the vertical spread of tephra shards is thought to represent vertical movement of tephra in the profile as a result of bioturbation or hydrological effects (Pilcher & Hall, 1992; Charman *et al.*, 1995; Matthews, 2008). Contributions of wind-blown tephras from reworked deposits adjacent to the site may also result in persistence of tephra shards in the sediments and may have the additional impact of obscuring additional primary fall tephras in the sediments (Gehrels *et al.*, 2006). The impact of shard attenuation may be particularly pronounced in archaeological sites as a result of human-induced disturbance (Matthews, 2008). At lake sites, this pattern of shards has been attributed to a range of taphonomic and sedimentary processes including bioturbation, and the remobilisation, reworking and redeposition of tephra into or within the site (S.M. Davies *et al.*, 2007).

In some acid peat bogs, the increased surface area of thin tephras may result in the leaching of chemical elements over time but it may require several thousand years before the correlative potential of thin tephras is affected (Dugmore *et al.*, 1992; De Vleeschouwer *et al.*, 2008). Tephra shards with lower silica content (i.e. intermediate and basic composition) are thought to be most vulnerable to these effects (Hodder *et al.*, 1991).

2.3 Environment of New Zealand

New Zealand comprises an isolated group of islands in the mid-latitudinal South Pacific Ocean spanning 34 to 47 degrees of latitude. The archipelago consists of two main islands, the North Island and the South Island, a third island, Stewart Island, and a number of smaller islands. The total land area is 268,680 sq km, an area slightly larger than that of the United Kingdom. The New Zealand environment has been shaped and modified largely by tectonism, climate (including climatic change through the Quaternary), volcanism, and very recently by human activities and impacts (Newnham et al., 1999b). The resulting landscape is characterised by strong relief marked by diversity, complexity, and youthfulness (Soons & Selby, 1992; Molloy & Christie, 1998; Newnham et al., 1999b; Fitzsimons, 2001; Leathwick et al., 2003). Volcanic landforms were described by Neall (2001). The remainder of this section briefly outlines the topography, climate, and earliest human arrival and impacts in New Zealand, all of which are directly relevant to interpretation of the results of this investigation.

Topography and climate

The New Zealand islands form a long (~1900 km), narrow, northeast–southwest trending archipelago with an often mountainous to hilly terrain. More than 66% of the land is above 200 m elevation: about 25% is steep to very steep (slopes > 26°), about 20% is hilly (slopes 16-25°), and about 55% is flat, undulating, and rolling (slopes 0-15°) (Palmer *et al.*, 2009). The South Island and southern North Island have high axial mountain ranges which generate strongly differentiated regional climates. Latitudinal variations and topographic

controls result in major contrasting and complex climate regimes across the islands ranging from subtropical in the north to temperate conditions in the south (NIWA, 2007b). The climate of New Zealand is oceanic with no part of the country more than 130 km from the sea. Most areas of New Zealand receive between 600 and 1600 mm of rain throughout the year, but extremes range from ~16,000 mm pa in Westland, South Island, to ~160 mm pa in eastern rain shadow areas of South Island. Mean annual temperature ranges from ~10°C in the south to ~16°C in the north.

The climate of New Zealand is strongly influenced by the circum-polar westerly winds (NIWA, 2007b) (Fig. 2.2). Contemporary prevailing winds have a strong westerly component although easterly or north-easterly winds may predominate in some months. These strong winds have been an important factor in the variable dispersal of tephras in the Quaternary. For example it has been suggested that tephra dispersal patterns indicate much stronger westerly winds during glacial phases (Carter *et al.*, 1995; Shane, 2000).

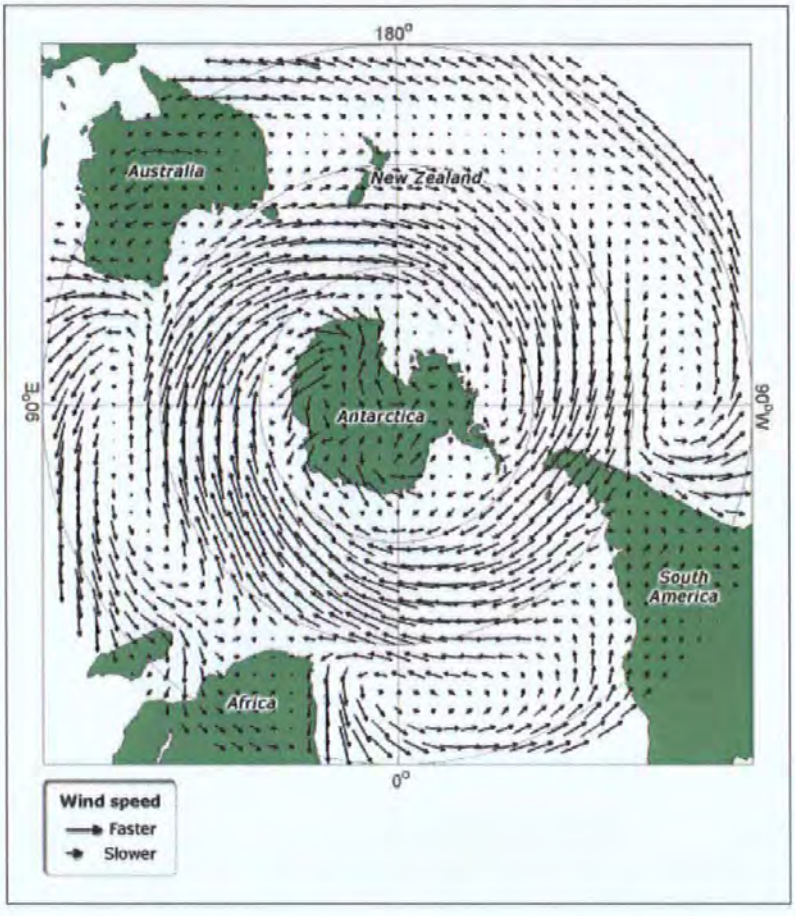

Figure 2.2. Generalised wind patterns in the Southern Hemisphere today. New Zealand straddles the mid-latitude transition from predominantly circum polar westerly winds in the south to predominantly easterly trade winds to the north. Image from: Mullan *et al.* (2007).

Human arrival and impact

Because of New Zealand's isolated position, it was the last major land mass (outside Antarctica) to have been settled by people, first by Polynesians and then later by Europeans. Tephra records have provided important marker horizons for dating settlement history and impacts (Newnham *et al.*, 1998; Lowe *et al.*, 2000; 2002) (Fig. 2.3). The earliest settlement by Polynesian sailors (from eastern Polynesia) took place probably *c.* AD 1250-1300 (Newnham *et al.*, 1998; Hogg *et al.*, 2003). This timing is now supported

by a wide range of palaeoenvironmental data and archaeological evidence (e.g. see Wilmshurst *et al.*, 2008).

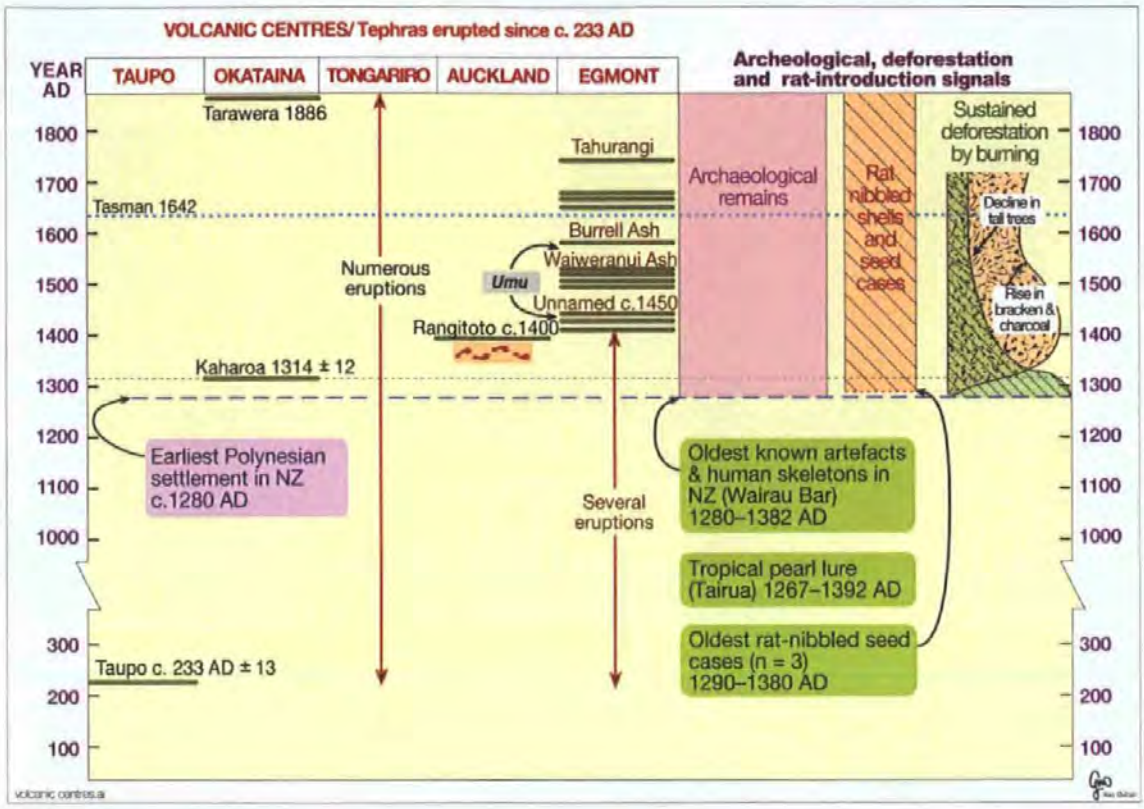

Figure 2.3. Summary of post-AD 200 tephras from the main active volcanic centres, showing relationships with archaeological and palynological data for Polynesian settlement. From: Lowe (2008a) after Higham *et al.* (1999) and Lowe & Newnham (2004). Archaeological and rat introduction signals show presence versus absence. Deforeststion signals show a model of relative changes in tree cover in relation to bracken and charcoal through time as revealed from a pollen records in the region.

Prior to human settlement, most of the forests in New Zealand comprised an evergreen mixed conifer-broadleaved rainforest, with two main forest types; conifers (podocarps, kauri, cedar) and southern beeches (see Wilmshurst *et al.*, 2007). Sedimentary records reveal widespread burning of these forests by early Polynesians settlers (e.g., Wilmshurst, 1997; McGlone & Wilmshurst, 1999; Newnham *et al.*, 1999b). Pollen records in particular show a distinctive signal of sustained rise in bracken (*Pteridium*) spores and grasses

together with a decline in forest taxa coupled with an increase in charcoal (Newnham *et al.*, 1998). It is evident that the largely forested landscape (~85% cover) was reduced to ~55% forest cover prior to European settlement. About one-third of North Island forests and about one-half of South Island forests were destroyed (Wilmshurst *et al.*, 2007). Primarily as a consequence of deforestation, rates of erosion increased dramatically in some areas at least (e.g., Gomez *et al.*, 2007). The Polynesian rat (*Rattus exulans*) was also introduced and recent dates on rat bones, and on rat-nibbled seed cases and gnawed snail shells, have aligned with the earliest dates for deforestation and for the earliest archaeological sites at around AD 1280 (Wilmshurst & Higham, 2004; Wilmshurst *et al.*, 2008).

The arrival of European missionaries, sealers and others in the early 1800s, and settlers substantially from around 1840 onwards, marked another dramatic change in the New Zealand environment. Forest cover was further reduced to ~25% of original pre-human cover in the next ~100 years, an extremely fast rate of deforestation. Wetlands were drained leaving tiny remnants. Rates of erosion generally increased tenfold or more (e.g., Newnham *et al.*, 1999b). Much of the New Zealand landscape is now covered in exotic grassland which underpins a predominantly agricultural economy.

2.4 Plate tectonic setting, volcanism and late Quaternary tephras

Plate tectonic setting

The North Island of New Zealand owes its volcanic heritage to a complex and dynamic plate tectonic setting (Kamp, 1992; Briggs *et al.*, 2005; Wilson & Leonard, 2008). The North and South islands are bisected obliquely by the boundary of the Australian and Pacific tectonic plates on the south-western edge of the Pacific 'ring of fire'. On the western edge of the South Island, plate margin collision results in the uplift of the Southern Alps and a zone of corresponding transcurrent faults, the largest of which is the Alpine Fault (Fig. 2.4). To the south, the Australian plate is being subducted beneath the Pacific Plate marked by the Puysegur Trough. To the east of the North Island, the Pacific Plate is being subducted under the Indian Plate and is marked by a large submarine trench – the Hikurangi Trough which is the southern extension of the Tonga-Kermadec trench and arc system (Fig. 2.4).

One of the on-land expressions of this current subduction activity and the locus of volcanism for the last ~2 Ma (Cole, 1990; Wilson *et al.*, 1995) is a 300-km long and 60-km wide volcano-tectonic complex across the North Island referred to as the Taupo Volcanic Zone (TVZ) (Houghton *et al.*, 1995; Price *et al.*, 2005) (Fig. 2.5). This comprises a central area containing a number of overlapping rhyolitic calderas lying between areas of largely andesitic stratovolcanoes at southwestern and northeastern ends (Fig. 2.5). The

rhyolite calderas include the highly active Taupo and Okataina volcanoes, and at least six older calderas including Mangakino, Kapenga, Whakamaru, Reporoa, Rotorua, and Maroa.

Figure 2.4. Plate tectonic setting of New Zealand showing the boundary between the Australian and Pacific plates bisecting New Zealand and the submerged continental crust of 'Zealandia'. Image from: McSaveney & Nathan (2007).

The TVZ also extends offshore and includes the currently active White Island and numerous submarine volcanoes stretching northeastward towards Tonga (Smith *et al.*, 2007). Mayor Island or Tuhua Volcanic Centre is a peralkaline rhyolite caldera volcano in western Bay of Plenty. Back-arc extension related basaltic volcanism is also evident across

the north western edge of the North Island (Cassidy *et al.*, 1999), forming basaltic volcanic fields including the most recently active Auckland Volcanic Field (Fig. 2.5).

Figure 2.5. The North Island, New Zealand, showing the plate boundary defined by the Hikurangi Trough, with relative movement (cm per year), and main tephra-producing volcanic centres that have been active in the late Quaternary. TVZ, Taupo Volcanic Zone. W, White Island (Whakaari). Image kindly provided by Prof. David Lowe (Lowe *et al.*, 2008a).

Late Quaternary tephrostratigraphic records

Tephrostratigraphic records from the North Island show prolific volcanic activity over the last ~50;000–60,000 years (Froggatt & Lowe, 1990; Shane, 2000; Lowe *et al.*, 2008b). In this time period there have been >60 rhyolitic tephra eruptions from the caldera volcanoes in central TVZ (Fig. 2.6) and numerous eruptions (probably hundreds) from the andesitic volcanoes of Tongariro Volcanic Centre and from Egmont Volcano (also known as Mt Taranaki) (Froggatt & Lowe, 1990). Basaltic volcanism has produced a localised record of basaltic lavas, scoria cones, tuff rings and tephra layers in the Auckland region (Shane & Smith, 2000b). Brief notes on these volcanoes follow.

Rhyolitic caldera volcanoes

By far the best recorded eruption events have been those from the large silicic, caldera forming volcanoes of the Taupo and Okataina volcanic centres since about 55,000 calendar years BP (Fig. 2.6). The widespread tephra fall events from these volcanoes have resulted in an exceptional stratigraphic record providing a number of precise age markers for late Quaternary studies (Newnham *et al.*, 2003; Lowe *et al.*, 2008b). The offshore peralkaline volcano of Mayor Island (Tuhua; Fig. 2.5) has also resulted in at least one large eruption in the Mid-Holocene resulting in the widespread Tuhua Tephra (ca. 7000 cal. years BP) (Hogg & McCraw, 1983; Manighetti *et al.*, 2003).

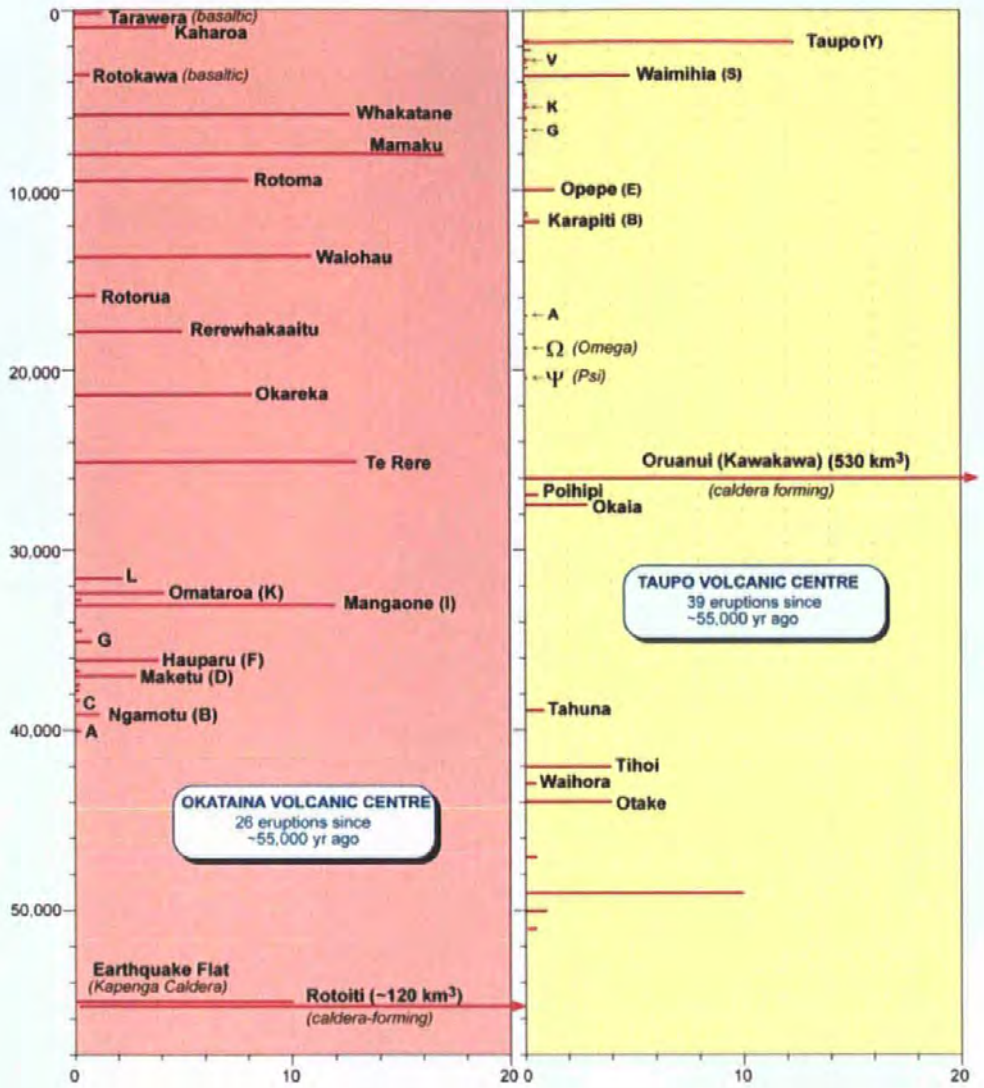

Figure 2.6. Late Quaternary tephrostratigraphic record from the Okataina and Taupo volcanic centres. Image from: Lowe *et al.* (2008a) after Smith *et al.* (2005). Vertical scale, age in cal. yr BP; horizontal scale, magma volume as dense rock equivalent (km^3).

Andesitic stratovolcanoes

Although tephra layers from andesitic and basaltic volcanoes have provided comparatively limited value as stratigraphic tools (Shane, 2000) they are becoming increasingly important for time periods and sites poorly represented by rhyolitic tephras (Shane & Smith, 2000;

Shane, 2005). Detailed tephostratigraphic studies have been undertaken on volcanic ring plains (Alloway *et al.*, 1995; Donoghue *et al.*, 1995b; Cronin *et al.*, 1997; Cronin & Neall, 1997). Some eruptive events from Egmont and Tongariro volcanic centres have been recorded as visible tephra layers 200-300 km from vent in the Waikato, Hawke's Bay and Auckland regions (Sandiford *et al.*, 2001; Shane & Hoverd, 2002; Shane, 2005; Molloy & Shane, 2007).

Tongariro Volcanic Centre is a relatively young, active centre consisting of three main volcanic edifaces of Mt Ruapehu (2797 m asl), Mt Tongariro (1968 m) and Mt Ngauruhoe (2287 m) (Fig. 2.5). Strictly, Ngauruhoe is part of the Tongariro massif but it is usually given separate volcano status. Activity commenced at these volcanoes ~275 ka with intervals of more rapid activity (cone growth), which includes the period ~25 ka to the present day (Hobden *et al.*, 1996). The erupted tephras have been the focus of detailed tephrostratigraphic studies of proximal deposits (Donoghue *et al.*, 1995b; Cronin & Neall, 1997; Hobden *et al.*, 2002). Many of the andesitic tephra formations comprise composite units made up of multiple deposits from numerous very small scale eruptions.

Egmont volcano (2518 m) is the most westerly volcano on the North Island and is the latest of a succession of stratovolcanoes in the area comprising the Sugar Loaf, Kaitake, Pouakai, and Egmont centres. The current edifice has been active since *ca.* 150-200 ka (Alloway *et al.*, 1995). The general history of Egmont is one of frequent small eruptions interspersed with occasional major collapses that generated large volcanic landslides (Neall & Alloway, 1996).

It has been argued that the limited dispersal range of these typically thin andesitic ash-fall events (as visible tephra) is partly a result of poor preservation (Donoghue *et al.*, 1997; Shane, 2005; Magill *et al.*, 2006a). A general lack of compositional data for proximal andesitic tephras and limited age constraints also provide limitations for their application tephrochronologically (Shane *et al.*, 2002). It is also the case that andesitic glasses are inherently heterogeneous in composition and can be inclusion-rich which presents difficulties in establishing a geochemical fingerprint (Platz *et al.*, 2007). Recent and ongoing work has been important in redressing some of these limitations (Cronin *et al.*, 1996a; 1996b; Shane, 2005; Molloy & Shane, 2007; Donoghue *et al.*, 2007; Platz *et al.*, 2007; Turner *et al.*, 2008), and is discussed further in subsequent chapters.

Basaltic volcanoes of the Auckland Volcanic Field

The Auckland Volcanic Field (AVF) has been active for *c.* 200 ka or longer (Marra *et al.*, 2006), generating small volume phreatomagmatic and magmatic activity. Around 50 separate basaltic cones or craters have been identified in the field, the result of (mainly) monogenetic activity (Cassidy *et al.*, 1999). Tephras from these eruptions are localised. Most eruptions are poorly dated (Shane & Smith, 2000a), but magnitude and frequency are thought to be sporadic. A number of deep maar lakes occur in the AVF and these have preserved very long sediment records including tephra layers from AVF eruptions and distal volcanoes of TVZ, Egmont, and Mayor Island (Shane *et al.*, 2002; Pepper *et al.*, 2004; Molloy & Shane, 2007; Augustinus *et al.*, 2008).

2.5 Post ~AD 200 volcanic activity and tephras

The history of known volcanic activity and some related events in North Island since *c.* 200 AD are summarised in Fig. 2.7 (from Lowe *et al.*, 2002). The time-scale is divided into three main periods: a pre-human (pre-settlement) period from *ca.* 200 to *ca.* 1300 AD; a Polynesian (prehistoric) period from *ca.* AD 1300 to 1800; and a European (historic) period since *ca.* AD 1800. The benchmarks at *ca.* AD 200 and *ca.* AD 1300 are defined by two widespread rhyolitic tephra marker beds, the Taupo and Kaharoa tephras, respectively. Single-line isopach distributions of these two tephras are shown in Fig. 2.8.

The Taupo Tephra provides a pre-Polynesian benchmark and it has been dated precisely at AD 233 ± 13 (1717 ± 13 cal. yr BP; Sparks *et al.*, 1995; 2008). Kaharoa Tephra represents a critical 'settlement layer' datum in eastern and northern North Island associated with the arrival of Polynesians as noted earlier (Newnham *et al.*, 1998; Lowe *et al.*, 1998), and it has been dated precisely at AD 1314 ± 12 (636 ± 12 cal yr BP) by dendrochronological 'wiggle-matching' of a carbonized *Phyllocladus* tree killed in the eruption (Hogg *et al.*, 2003).

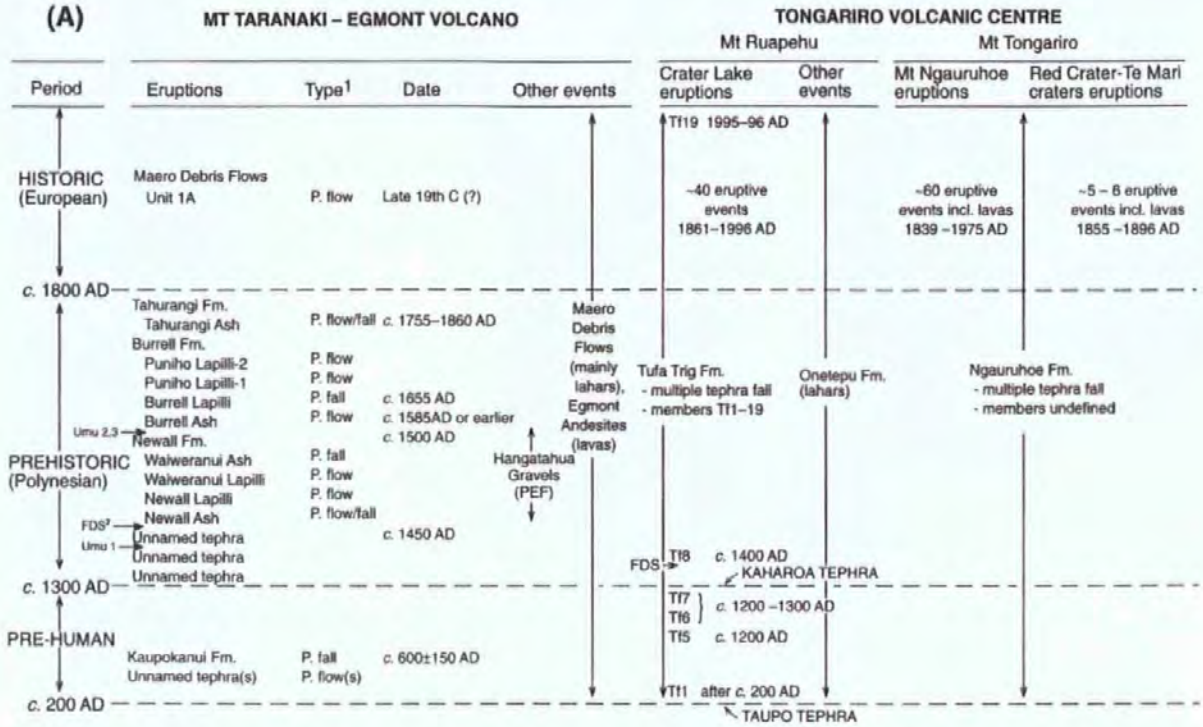
(A)
MT TARANAKI – EGMONT VOLCANO
TONGARIRO VOLCANIC CENTRE
Mt Ruapehu
Mt Tongariro
Period
Eruptions
Type1
Date
Other events
Crater Lake eruptions
Other events
Mt Ngauruhoe eruptions
Red Crater-Te Mari craters eruptions
HISTORIC (European)
Maero Debris Flows Unit 1A
P. flow
Late 19th C (?)
Tf19 1995–96 AD
~40 eruptive events 1861–1996 AD
~60 eruptive events incl. lavas 1839 –1975 AD
~5 – 6 eruptive events incl. lavas 1855 –1896 AD
c. 1800 AD
Tahurangi Fm.
Tahurangi Ash
P. flow/fall
c. 1755–1860 AD
Maero Debris Flows (mainly lahars), Egmont Andesites (lavas)
Burrell Fm.
Puniho Lapilli-2
P. flow
Puniho Lapilli-1
P. flow
Burrell Lapilli
P. fall
c. 1655 AD
Burrell Ash
P. flow
c. 1585AD or earlier
Umu 2,3
Newall Fm.
c. 1500 AD
Tufa Trig Fm.
- multiple tephra fall
- members Tf1–19
Onetepu Fm. (lahars)
Ngauruhoe Fm.
- multiple tephra fall
- members undefined
PREHISTORIC (Polynesian)
Waiweranui Ash
P. fall
Hangatahua Gravels (PEF)
Waiweranui Lapilli
P. flow
Newall Lapilli
P. flow
FDS?
Newall Ash
P. flow/fall
Umu 1
Unnamed tephra
c. 1450 AD
FDS
Tf8
c. 1400 AD
KAHAROA TEPHRA
Unnamed tephra
Unnamed tephra
c. 1300 AD
Tf7
Tf6
c. 1200 –1300 AD
Tf5
c. 1200 AD
PRE-HUMAN
Kaupokanui Fm.
Unnamed tephra(s)
P. fall
P. flow(s)
c. 600±150 AD
Tf1 after c. 200 AD
c. 200 AD
TAUPO TEPHRA

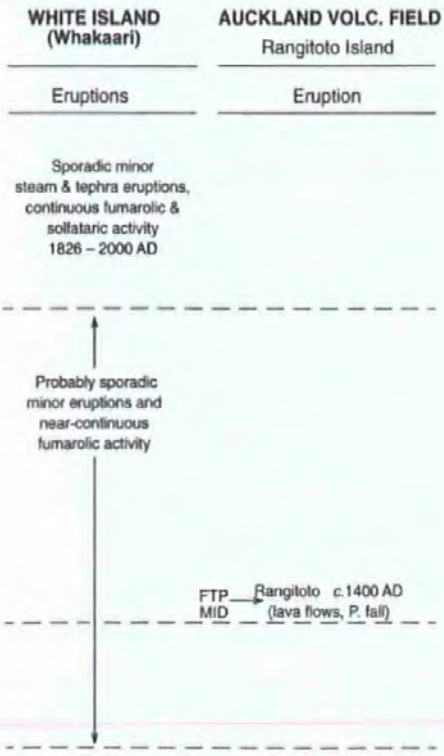
WHITE ISLAND (Whakaari)
AUCKLAND VOLC. FIELD
Rangitoto Island
Eruptions
Eruption
Sporadic minor steam & tephra eruptions, continuous fumarolic & solfataric activity 1826 – 2000 AD
Probably sporadic minor eruptions and near-continuous fumarolic activity
FTP
MID
Rangitoto c.1400 AD
(lava flows, P. fall)

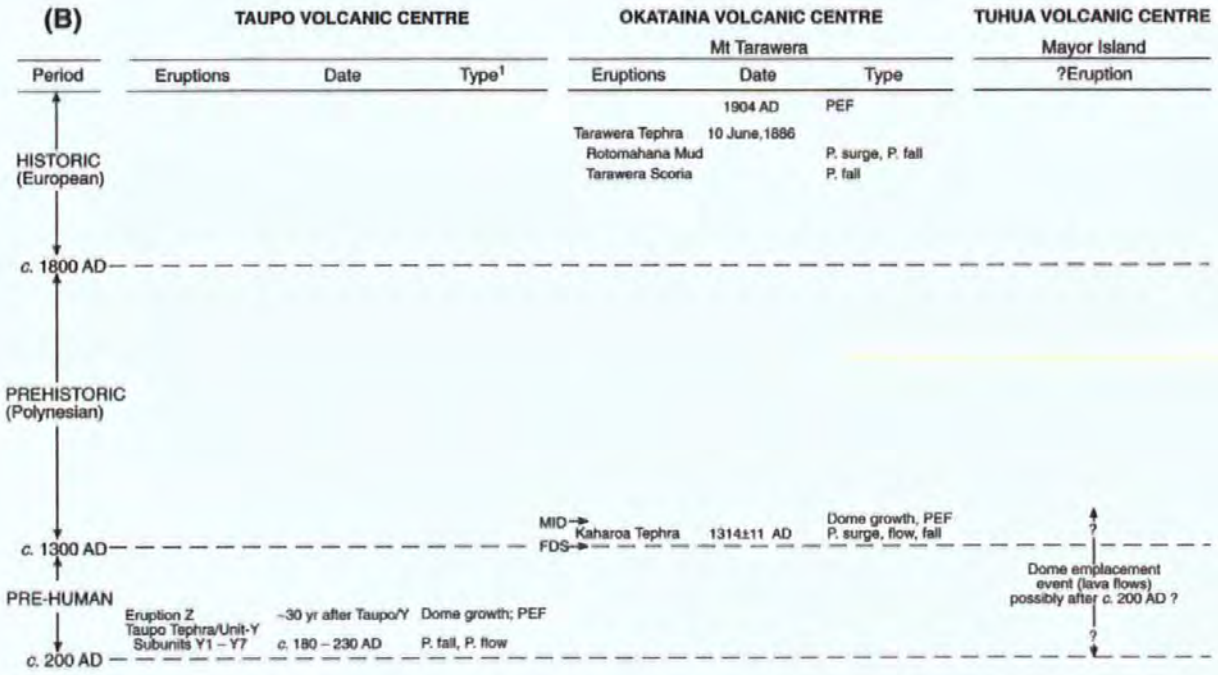

Figure 2.7. Summary of eruptions of North Island volcanic centres, and some other events, since *ca.* AD 200 A, andesitic and basaltic volcanoes; B, rhyolitic volcanoes. (From: Lowe *et al.*, 2002, p.130-131). Note that the dates for Taupo and Kaharoa are AD 233 ± 13 and AD 1314 ± 12 respectively.

[1]Dominant style of eruption: P. flow, pyroclastic flows; P. fall, pyroclastic falls; PEF, post-eruptive flooding. Pyroclastic flows at Mt Taranaki were block-and-ash flows.

[2]FDS, first (sustained) deforestation signal (inferred to be human-induced).

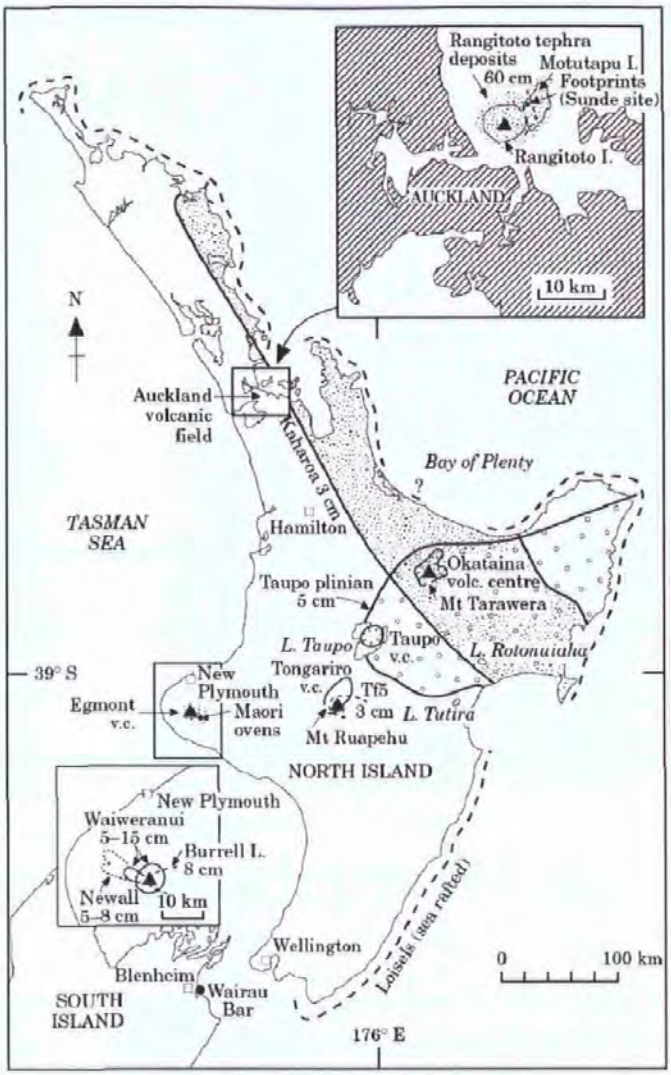

Figure 2.8 Locations of volcanic centres and distribution of selected post-AD ~200 tephras relevant to dating the region's pre-history. The 5-cm isopach of Taupo deposits is after Wilson & Walker (1985) (see also Wilson & Leonard, 2008), and the 3-cm isopach of Kaharoa deposits is after Pullar *et al.* (1977). From: Lowe *et al.* (2000).

Thus six or seven spatially separate volcanic centres or fields have been active in the North Island since *ca.* AD 200 (Fig. 2.7). The andesitic centres (Taranaki, Tongariro, White Island) have all erupted very frequently; the basaltic Auckland Volcanic Field is characterised by a single eruptive episode (Rangitoto Island, *ca.* AD 1400); and the rhyolitic centres (Taupo, Okataina, Tuhua) have each erupted just once or twice. The latest eruption from the Okataina Volcanic Centre (the so-called Tarawera eruption of 10 June,

1886) was a basaltic rather than rhyolitic event as usually occurs at this centre. The uncertain timing of the latest dome-building eruption on Mayor Island/Tuhua precludes it from further discussion because it may not have been active during the past ~2000 years (Fig.2.7).

In the Tongariro Volcanic Centre, the most recent phase of activity of Mt Ruapehu is represented by the Tufa Trig Formation, which consists of 19 defined tephra members (Tf1-19) overlying the Taupo Tephra (Donoghue *et al.*, 1995b; 1997; Donoghue & Neall, 1996). The latest eruptions of Mt Ruapehu (defined as Tf19) were in 1995 and 1996 (Donoghue *et al.*, 1997). The post-Taupo eruptions of Ngauruhoe are referred to as the Ngauruhoe Formation which comprises multiple, undefined members (Fig. 2.7). The latest eruption was in February, 1975 (Nairn & Self, 1978).

Egmont's most recent definitive eruption was that of Tahurangi Ash dated at about AD 1755, but there may have been another small eruptive event since then (Lowe *et al.*, 2000; 2002). Earlier eruptions (each comprising several members recognised within each formation) include the Kaupokanui (*ca.* AD 600), Newall (*ca.* AD 1500), and Burrell (*ca.* AD 1655) episodes as well as a number of unnamed events (Fig. 2.7).

White Island is New Zealand's most active volcano, more-or-less constantly venting steam and gases, and intermittently forming new vents and producing clouds of ash. Europeans first observed the volcano in 1826, and it has probably been active since Polynesian arrival. The volcano is 48 km off the Bay of Plenty coast, however, so its effect on the mainland has been minor, largely resulting to infrequent dustings of volcanic ash (McSaveney *et al.*, 2007).

The main types or styles of eruption for each volcanic centre and associated events including lahar emplacement and post-eruptive flooding are given in Fig. 2.7. Based on these data, the types of volcanic hazards likely to have been experienced or witnessed by prehistoric Polynesians (the ancestors of Maori) and early European settlers were summarised by Lowe *et al.* (2002).

CHAPTER 3: METHODOLOGY

As outlined in Chapter 1, the main aim of this study was to develop an enhanced stratigraphic record of volcanic ash-fall events in northern New Zealand for the last ~1800 years. The approach is to detect and identify fine volcanic ash deposits preserved as cryptotephra in sediment cores taken at sites from the Auckland and Waikato regions which lie beyond the proximal volcanic zone, thus extending the current known depositional range of post-Taupo tephra events beyond their visible occurrence. Of particular interest are recent ash-fall events from andesitic volcanoes that are poorly represented as visible layers beyond the proximal volcanic zone and ash-fall events with a restricted depositional range including the Kaharoa Tephra, an important stratigraphic marker tephra for palaeoenvironmental and archaeological research (Newnham *et al.*, 1998; Lowe *et al.*, 1998).

The protocol developed in this study for detecting and identifying cryptotephra in selected sites and linking them to known eruption events comprises a sequence of steps (Fig. 3.1): (1) sub-sampling of sediment sequence; (2) extraction of tephra-derived glass shards from sediment matrix; (3) microscopic identification and quantification of shard content; (4) determination of individual ash-fall events from background glass using the shard concentrations, (5) geochemical fingerprinting, and (5) construction of core chronology.

Investigations of cryptotephra in distal environments must also consider the possibility that cryptotephra layers may have resulted from secondary deposition rather than primary airfall (Gehrels *et al.*, 2006; S.M. Davies *et al.*, 2007). Therefore an objective of this study was to develop a methodological approach aimed at making this distinction with a greater degree of confidence. This approach was based on the following steps: (1) establish a high resolution and continuous record of glass shard content to evaluate the spread and sedimentological properties of cryptotephra horizons; (2) detailed geochemical fingerprinting throughout selected cryptotephra horizons; (3) where possible, replicate cores from each site are used to evaluate within-site variability of concentrations and temporal spread of tephra. In addition, both peat and lake sites are used to compare these two different sedimentary archives in terms of cryptotephra deposition and preservation.

An additional objective of this study was to consider the implications of an enhanced record of volcanic ash-fall events for future assessments of volcanic hazards to the region. For this purpose, sites were selected near or within the cities of Auckland and Hamilton respectively, the largest and fourth largest population centres in New Zealand. Cryptotephras detected in these localities could represent ash-fall events of comparable or greater magnitude than the 1995-1996 Ruapehu eruption and therefore would have a significant impact today should a further eruption of similar magnitude occur.

3.1 Site selection and coring strategy

The two principal criteria for site selection are: (1) suitable archival sediments to preserve fine ash-fall, and (2) preserve continuous sediment accumulation since the Taupo Tephra depositional event. In February 2005, after consultation and coring reconnaissance eight sediment cores were collected from two raised bog sites (Moanatuatua and Opouatia bogs) and one lake site (Lake Rotoroa, Hamilton) in northern New Zealand (Fig. 3.2). Two cores were also provided from a lake site (Lake Pupuke) in Auckland. A summary of the core stratigraphies are shown in Figure 3.3. Details of each site and cores collected are provided in the results chapters (Chapters 4 and 5).

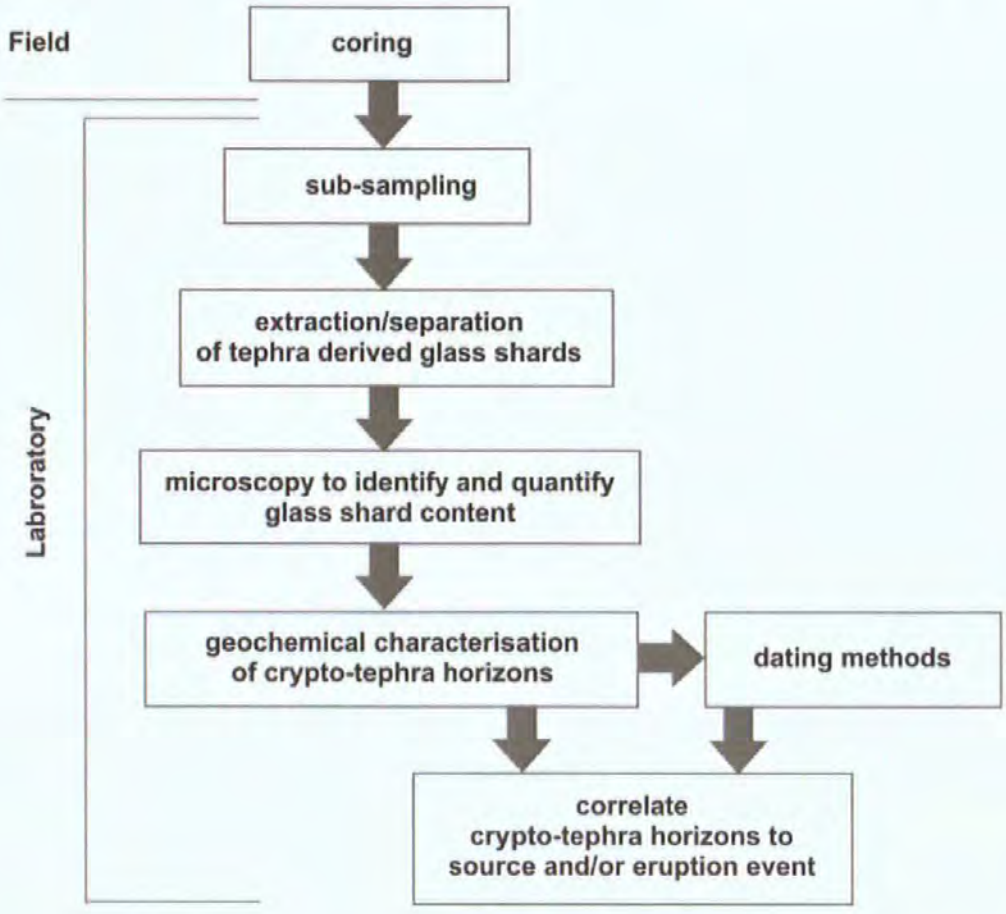

Figure 3.1. Sequence of methods used to detect and identify cryptotephra in sediment cores

The peat bog and lake sites selected are located beyond the proximal zone of recent ash-fall from andesitic cone volcanoes and beyond the recorded visible limits of the Kaharoa Tephra (Hogg *et al.* 2003; Fig. 3.2). Both peat and lake sites are well established as effective archives for the preservation and detection of fine ash-fall. All sites were known to contain well-preserved sediments representing at least the last few thousand years of sediment accumulation and are therefore suitable as recorders of ash-fall events over this time period.

Multiple cores were collected from each site (Fig. 3.3), each marked at the base by the visible Taupo Tephra (1717 ± 13 cal. yr BP[1], Lowe *et al.*, 2008; Sparks *et al.*, 2008; Fig. 3.3) and in most cases extend up to the modern surface and incorporate modern sediments. In the peat sequence from Opuatia Bog the Taupo Tephra is represented by pumice alluvium derived from the Taupo eruption and subsequently presumed deposited by the ancestral Waikato River very shortly after the eruption. With the exception of Lake Pupuke, which also contained an additional locally-derived basaltic tephra (Rangitoto Tephra, *ca.* AD 1400; Lowe *et al.* 2000; Horrocks *et al.* 2005; Fig. 3.3), none of the cores contained any additional visible (macroscopic) post-Taupo tephras.

The collection of multiple cores from each site provides the means to assess intra-site variability and reproducibility of the cryptotephra record at each site. In particular, intra-site variability is used as a means to differentiate between depositional and site-dependent processes affecting the preservation of cryptotephra, thus addressing the second aim of this study. Two sites, Moanatuatua and Lake Rotoroa, are in close proximity (~15 km apart) and provide a basis for comparing the cryptotephra records in a bog compared to a lake.

Collectively, the samples sites form a rough transect between Auckland and the volcanoes in the central North Island and Mt Taranaki which have been active in the Late Holocene (Shane, 2000) (Fig. 3.2). This spatial distribution is used to construct isopach maps of ash-fall events from various sources for considering distribution and potential impact of future

[1] All ages cal yr BP referred to in this thesis refer to calibrated years before AD1950

ash-fall events. In addition, the two lake sites occur today within the urban environment of the two largest cities in northern New Zealand, Auckland (pop. 1.3 million) and Hamilton (130,000; 2006 census: http://www.stats.govt.nz/census/default.htm). As stated previously, a more complete record of ash fall from these sites is important for reassessing volcanic hazards to these regions.

Figure 3.2. Location of core sites in the North Island New Zealand, in relation to Hamilton and Auckland and volcanic centres which have been active in the Late Holocene. Dashed red line shows the limit of the Kaharoa Tephra recorded as a distinct visible tephra horizon. H, Haroharo volcano; TR, Tarawera volcano; Tg, Mt. Tongariro; N, Ngauruhoe; R, Mt. Ruapehu; Tn, Mt. Taranaki.

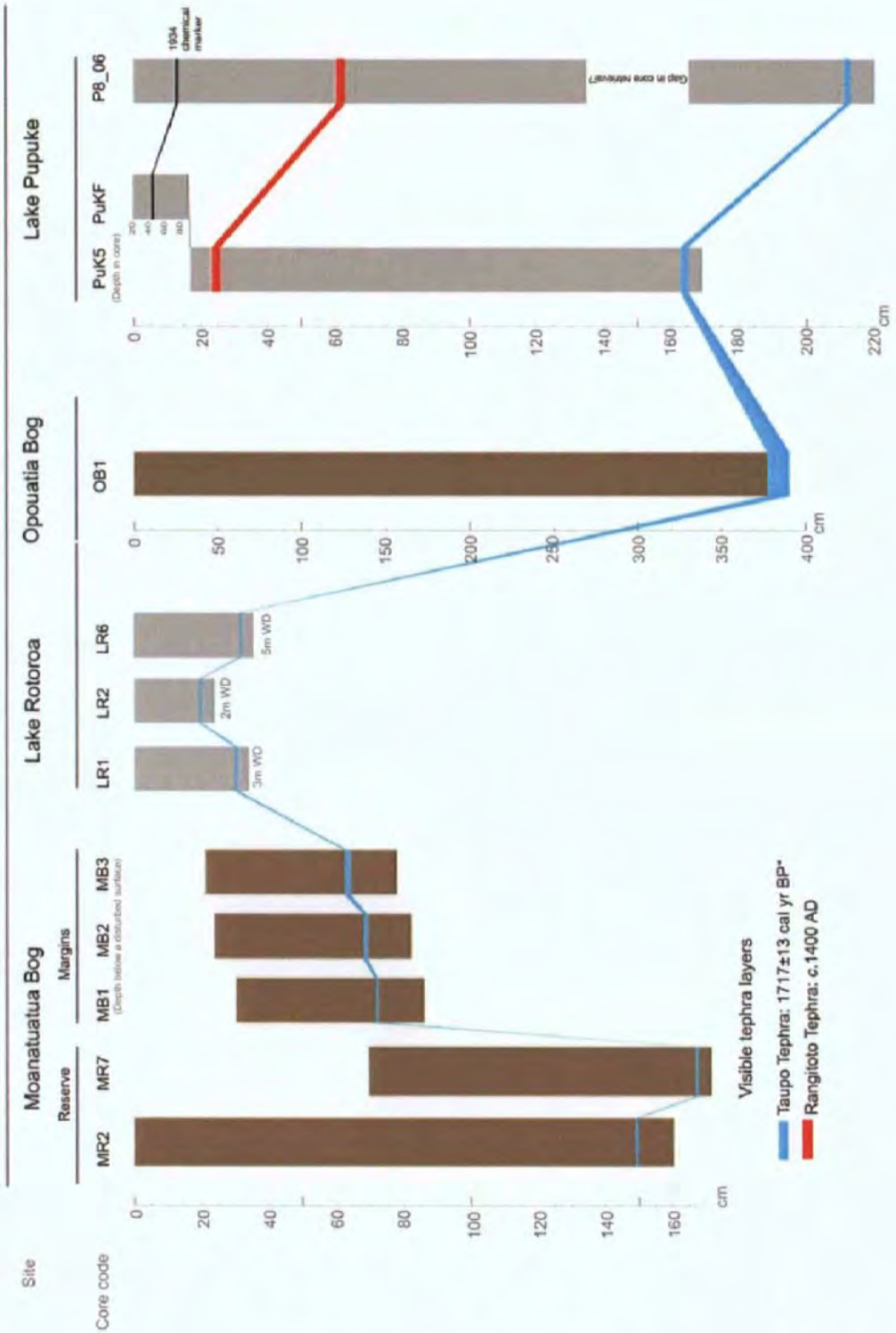

Figure 3.3 Summary of core reference information, including visible tephrostratigraphy used in this study. All depths are from the surface unless otherwise stated. * Cal yr BP, calibrated or calendar years before present (AD 1950).

3.2 Sediment description: lithology and sedimentology

Following collection, the peat and lake sediment cores were described in detail. The keys to the sediment logs described in this study are shown for the individual sites in the results sections (Chapters 4 and 5) and reflect the unique nature of each site. These descriptions provided crucial information for interpreting the resulting tephra content, specifically in terms of changes in sedimentation processes and rates and inter and intra site disturbance which could have resulted in the addition of reworked tephra-derived shards. In addition, detailed sediment logs helped in relocating levels in the cores for re-sampling for additional cryptotephra analyses, particularly in the case of core shrinkage due to de-watering following core retrieval. A measurement of organic content, using loss-on-ignition (LOI), also provided an important guide to changing lithology and, in peat samples, to possible cryptotephra horizons (Gehrels *et al.* 2008).

Unlike *Sphagnum* peats, restiad peats are conventionally described based on the visual examination of identifiable components, e.g. plant remains, charcoal layers and wood, and peat texture following Clarkson (2004), Campbell (1975) and Lowe (1988b). The texture of the peat was defined primarily by the degree of humification; a measure of plant decomposition (Blackford & Chambers, 1993). Humification was assessed using simple field techniques (von Post scale) to observe the colour of interstitial water from the peat and texture of wet peat between fingertips (dark fluid and smooth texture = well humified; light or clear fluid and rough texture = poorly humified). Two broad categories of peat were recognized for the sections collected in this study: (1) well to moderately well humified peat, comprising a dense and compact peat with no discernable plant remains and

generally dark in colour; and (2) poorly to very poorly humified peat with a porous texture and comprising distinguishable, poorly decomposed plant material and roots. Additional levels included the upper, aerated acrotelm layer of the peat.

The lithostratigraphy of the lake cores was described using the conventional Troels-Smith (1955) classification scheme for unconsolidated sediments. The Munsell colour chart was used to characterize the colour of the sediments. As with peat sections, additional identificable components, e.g. charcoal layers and plant remains, were also noted.

3.3 Determining cryptotephra content

The conventional method of extraction for microscopy was used to determine a continuous and high resolution account of the tephra-derived glass shards in sediment profiles collected (Pilcher & Hall, 1992; TEPHRATRACE, 2002). As discussed in the following sections, this involves a three stage process: (1) sampling, (2) extraction of glass shards from sediment matrix, and (3) microscopy to identify and quantify glass shard content. This approach provides a reliable quantitative measure of glass concentrations to assist with the differentiation of primary fall tephras from secondary sources ('background') and to assess the nature and extent to which taphonomic processes have affected the stratigraphic integrity of the deposits (Gehrels *et al.*, 2008). A summary of procedures used to extract glass shards from peat and lake samples for microscopy as well as for geochemical analysis is provided in Figure 3.4.

3.3.1 Sampling considerations

The conventional method of extraction for microscopy, where applied in very distal settings, traditionally follows an iterative sampling strategy process to narrow down areas of the core likely to contain tephra (Hall & Pilcher, 2002). In this study, however, it was anticipated that given the proximity of the sites to primary and secondary sources of tephra, a high-resolution sampling strategy would be necessary from the outset (Gehrels *et al.*, 2006). As with the majority of cryptotephra studies the sampling strategy was designed to establish a continuous record of tephra-derived glass in the sediment sequences.

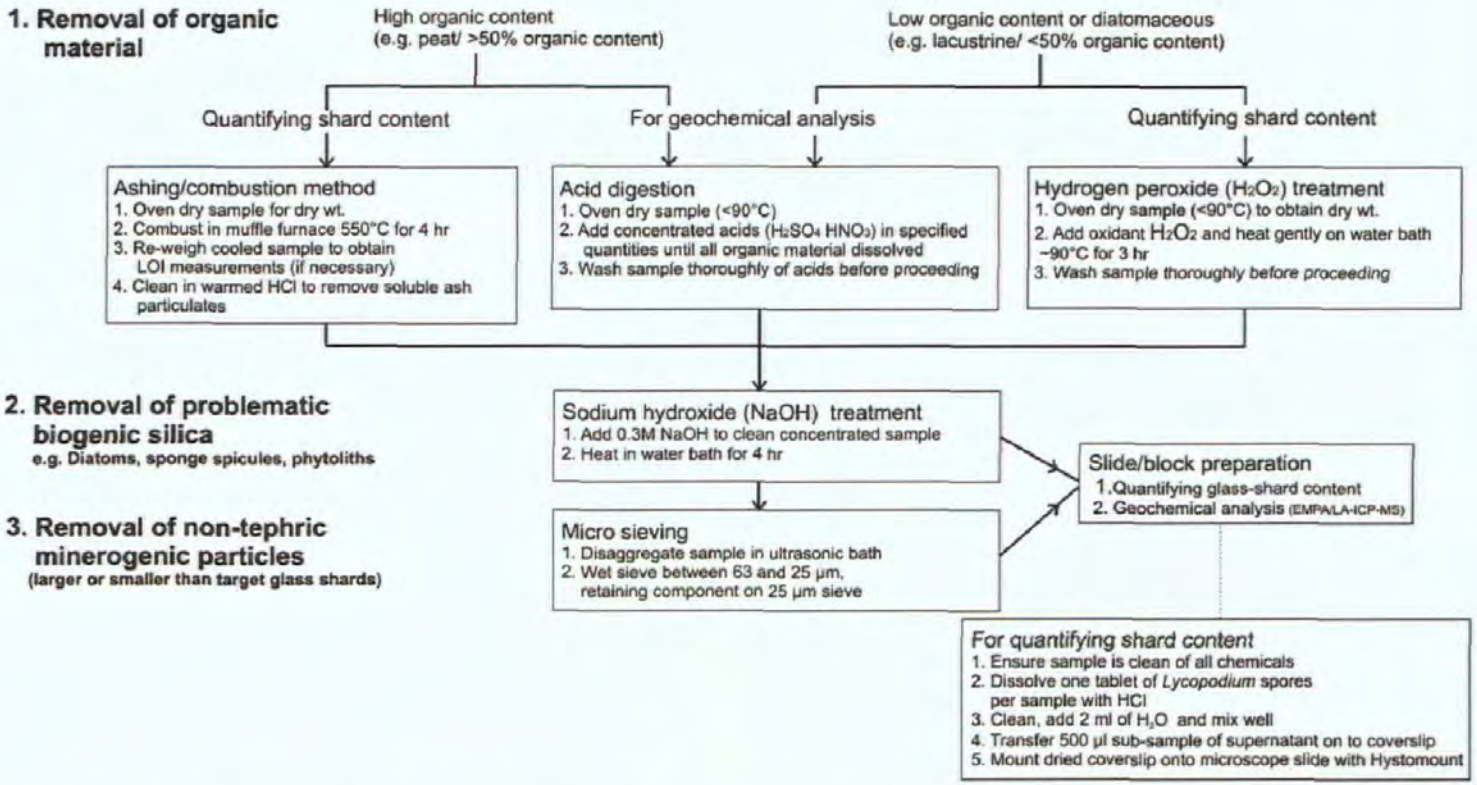

Figure 3.4. Summary of laboratory procedures for glass extraction from peat and lake samples in preparation for microscopic examination, quantifying shard content and geochemical analysis. Adapted from Davies *et al.* (2005).

3.3.2 *Peat sites: sampling and extraction*

The procedure used for extracting tephra-derived glass shard content from peat samples used in this study follows the ashing method described by Pilcher and Hall (1992) (demonstrated in the online workshop TEPHRABASE (2002). In this study modifications are made to this method for fibrous restiad peats (Gehrels *et al.*, 2008; enclosed in this thesis). This method involves the combustion of organic material in a high temperature furnace to liberate any inorganic material for microscopic examination to identify and quantify glass shard content. This is considered to be the quickest, simplest and most economical method to remove organic material from a variety of organic rich samples, but has the disadvantage of potentially altering the geochemical composition of the glass shards (Dugmore *et al.*, 1992). Ashing is therefore unsuitable for samples destined to be used for geochemical characterization (see section 3.3). Whilst this method is suitable for a range of organic-rich sediments, it was not used for the lake samples used in this study for reasons discussed later.

Although the majority of peat sequences are composed almost entirely of organic material, in some cases additional inorganic components are also present, e.g. plant phytoliths and minerogenic particles. In high concentrations these may prove problematic for the microscopic examination of glass grains by obscuring the microscope slide or glass. Minerogenic particles can be particularly abundant in peat sections representing the last few centuries as a result of intensifying agricultural activities (Pilcher and Hall, 1992). Plant phytoliths are recognised as being particularly problematic in restiad peats because they form in the stems of the restiad species (Dugmore *et al.*, 1992; Meney & Pate, 1999; Ballinger, 2003). In some cases they can look very similar to glass shards which can be

problematic if the latter are small and lack distinct morphology (Hall & Pilcher, 2002). In such cases the samples were treated as with lake sediment samples using additional chemical methods and sieving (Fig. 3.4.; section 3.2.3.) to further concentrate glass content.

A 1cm to 2 cm-thick contiguous sampling strategy was employed for all peat sequences from just above the visible Taupo Tephra up to the top of the core (modern land surface in most cases). A 1 cm-resolution sampling strategy was used on targeted areas of cores where a more detailed measure of shard content was required, i.e. around identified cryptotephra horizons. For each sample, approximately 1g of wet peat was extracted from a cleaned surface using a sharp blade. This was particularly important for very fibrous, poorly-humified sections of the peat sequences. Samples were collected by weight rather than by volume as part of the method employed in this study to quantify tephra-shard content (section 3.2.4).

The samples were placed into pre-weighed, numbered, furnace proof, nickel crucibles and oven dried at ~90°C overnight. This was to obtain oven-dry weight, required to calculate the concentration of glass shards per unit weight of the sample. In preparation for combustion, the oven-dry samples were crushed gently in crucibles using a plastic pestle to ensure a thorough burn. Crucibles were covered (to avoid any cross-contamination or to prevent debris from entering sample) and burnt in a high temperature furnace at 550°C for 4-6 hours. This is slightly longer than used conventionally on *Sphagnum* peats in European cryptotephra studies (Hall & Pilcher, 2002) because of the very fibrous nature of the New Zealand peat, which can also contain thick roots and stems (Gehrels *et al.*, 2006, 2008).

Upon cooling, samples were reweighed so that loss-on-ignition (LOI) may be calculated. LOI is an effective measure of organic content which is useful for assessing sedimentological changes in a sequence (Aaby & Berglund, 1986; Barber, 1993; Blackford & Chambers, 1993). In particular, LOI measurements have proved a useful guide to locating concentrations of glass in some highly organic sequences such as those from raised bogs (Gehrels *et al.*, 2008) . These measurements are also easy to obtain as part of ashing/combustion procedure.

The remaining inorganic component was washed into correspondingly numbered glass beakers with 10% hydrochloric acid (HCl). This ensured that the entire sample was removed from the crucible. The HCl also helped to dissolve remaining ash particulates and soluble inorganics in the sample when gently heated on a hotplate for approximately 1 hour or until particulates had noticeably dissolved (Pilcher & Hall, 1992; Gehrels *et al.*, 2008). The remaining clean solution was then diluted with distilled water and left to settle.

Once remaining particulates had settled it was easy to see the sample though the glass beaker and to decide if further cleaning procedures were necessary. Where problematic samples were encountered, subsamples were mounted onto glass slides with water and viewed under the microscope to identify the nature of the substance and to select the appropriate cleaning method (Fig. 3.4).

3.3.3 Lake sites: sampling and extraction

Unlike peats, which have a sediment matrix that is almost exclusively organic, lake sediments are inherently heterogeneous in composition and require a more complex approach to liberate glass shards (Turney, 1998; Blockley *et al.*, 2005; Davies *et al.*, 2005). The approach found to be most effective for glass recovery from lake sequences used in this study involved the sequential removal of the main non-tephric components of sediments including (1) organic material, (2) biogenic silica and (3) minerogenic particles above and below the size range of the majority of glass shards. Density separation technique (e.g. Turney, 1998) did not prove suitable for the recovery of glass shards with intermediate and basic chemistries (Mackie *et al.*, 2002) present in the sequences, and as a result was used only in a limited way on a few samples following procedures described by Blockley *et al.* (2005). The sequence of methods used for preparing lake sediment samples for microscopy is summarized in Figure 3.4.

Sampling

Wet samples were extracted from a cleaned surface of lake sediment from contiguous levels at 0.5-1 cm resolution using clean blades. This higher resolution sampling strategy compared to that used for the peat sequences helped compensate for the slower accumulation rates of lake sediments in this study so that samples representing comparable time slices were obtained. Samples were oven dried as with peat samples to obtain dry weight needed for determining glass shard concentrations through the profiles.

Removal of organic material

The removal of organic material from the samples followed the method described by Bennett *et al.* (1992) (cited in Rose *et al.*, 1996) of chemical digestion with hydrogen peroxide (H_2O_2). This method is commonly used for samples with a low to moderate organic composition for microfossil analysis because it does not affect the biogenic or siliceous components. It was found to be an effective replacement of the ashing method for samples containing large concentrations of biogenic silica which hardened on combustion and made remaining samples difficult to disaggregate for further processing. The use of H_2O_2 is also unlikely to compromise geochemical composition of shards and means that when necessary samples can be reused for geochemical analysis.

Laboratory grade H_2O_2 (30%) was added to glass beakers containing the dried samples and left overnight at room temperature. More H_2O_2 was added to the samples which were heated in water bath 80-90° C for 3 hours. Regular checks were made to ensure samples did not dry out. Samples were then washed thoroughly with distilled water and concentrated into centrifuge tubes before proceeding to the next stage, that of removing biogenic silica.

Some samples provided for this study (Lake Pupuke, core P8_06; Fig. 3.3) had been previously combusted for loss-on-ignition measurements as part of another study. This made effective use of the limited material in the core. The combustion process did, however, result in very dry compacted sediment samples. To disaggregate samples, they

were soaked in Calgon (sodium hexametaphosphate) for several hours and placed in an ultrasonic bath for 20 minutes before the next stage.

Removal of problematic biogenic silica

Both lake sequences of lake sediments used in this study (Pupuke and Rotoroa) contained large components of biogenic silica in the form of diatom frustules and sponge spicules. The high concentrations of these particles in the sediment samples obscured glass content at times, making microscopy problematic. Biogenic silica is, however, easily removed using the chemical procedure described by Rose *et al.* (1996), involving strong alkaline solution which dissolves biogenic silica without affecting minerogenic or siliceous particles (Fig. 3.4).

A 5 ml solution of 0.3M (molar) laboratory grade sodium hydroxide (NaOH) was added to the cleaned-and-concentrated samples in centrifuge tubes. The sample tubes were heated in a water bath at 80-90° C for three to four hours. This period of heating is considered sufficient in order to dissolve most silica in the sample without damaging or dissolving glass shards (Dugmore *et al.*, 1995; Rose *et al.*, 1996). This method also proved quite effective for dissolving plant phytoliths in peat samples (Dugmore *et al.*, 1995; Gehrels *et al.*, 2008).

Removal of minerogenic particles

Wet sieving was the most effective method for separating glass shards from most of the mineral particles remaining in the lake sediment samples (and any remaining fine particulates). Sieving thus replaced the use of heavy liquids (Dugmore *et al.*, 1995; Turney, 1998; Blockley *et al.*, 2005) which, as discussed above, was unsuitable for the range of glass compositions in the samples and was time consuming given the relatively small component of minerogenic material in the samples. Wet sieving concentrated glass shard content by removing particles greater or lesser in size than the majority of glass shards observed in the lake sediments.

In preparation for sieving, samples were placed in glass beakers, diluted in distilled water and placed in an ultrasonic bath for ~20 minutes to fully disaggregate making sieving quicker and more efficient. In some cases (in conjunction with the ultrasonic treatment) Calgon was used to disaggregate stubborn samples. While still in suspension, samples were passed through 63 μm and 25 μm mesh micro-sieves with water, the retained sample containing the majority of glass shards on the 25 μm sieve. In general this sieving resulted in very clean samples that needed no further cleaning.

3.3.4 Microscopy and quantifying glass shard content

Remaining samples were examined by microscopy to identify and quantify glass shard content following the method described in Gehrels *et al.* (2006). This method, adapted from palynology (Maher, 1981), uses a spike containing a known concentration of the exotic marker spore *Lycopodium* to each sample to derive a semi-quantitative measure of

glass shard content without having to count all glass particles on the slide (see Maher, 1981, for a discussion on the statistics involved in the use of exotic markers). The spike contains a known number of spores which are counted alongside glass shards per field of view under the microscope and a 'concentration' of shards (in relation to number of spores counted) is derived. This is particularly useful for the analysis of sequences containing relatively large concentrations of glass shards or where long sequences are being analysed which contained abundant tephra layers or glass concentrations (Gehrels *et al.*, 2006; Payne *et al.*, 2008). The resulting shard concentrations provide a starting point for distinguishing primary fall deposits from the background levels derived from post-depositional or secondary processes based on the pattern and concentration of shards in the sediment sequence.

The *Lycopodium* spike was added to cleaned samples prior to undertaking the microscopy (Stockmarr, 1971). One tablet (18,583 spores ± 2.1 %, batch # 483216) was added to each cleaned sample concentrate and dissolved in 10% HCl to release spores from their coating (samples were washed twice using distilled water to remove remaining HCl before mounting on to slides). It was important that the tablet was fully dissolved and the sample well mixed in a vortex mixer to distribute the spores evenly and to ensure that the subsample being counted is representative of the whole sample.

Slide preparation

Using a micropipette, 0.5 ml of the well-mixed spiked supernatant was transferred on to glass cover slips, air dried and mounted onto glass micro slides using Hystomount.

Hystomount (from Hughs and Hughs, Somerset, UK) is an improved synthetic (polymer) mounting medium for biological slides. It is solvent based with a neutral pH and provides a fast drying, permanent setting. In preference to other mounting media (Ballinger, 2003), Hystomount was found to give better visual clarity for examining glass shards under the microscope. Only a few drops of the mountant were added to the centre of the glass microscope slide. The cover slips were placed, dried material downwards, over the Hystomount, and pushed down gently to produce an even spread across the sample. However, once mounted, slides are suitable for counting only for a few months before the *Lycopodium* spores start to deteriorate and become difficult to identify.

Microscopy

Slides were examined at 400× magnification under polarised light using a Zeiss Standard 25 binocular microscope viewed under crossed polarisers. Tephra-derived glass shards were identified by shard form, vesicularity, colour and isotropy under crossed polars (Fisher, 1961; Kittleman, 1979; Ballinger, 2003). It was also possible to tentatively distinguish between andesitic and rhyolitic shards primarily on the basis of colour. Rhyolitic shards were colourless (Fig. 3.5a) with few if any microlites (small crystals) and with a distinct bubble wall or pumiceous form. Andesitic shards (Fig. 3.5b) on the other hand were orange-brown to dark brown in colour, blocky in form and contained abundant microlites (Cronin *et al.*, 1996a; 1996b; Shane, 2005). At the Auckland site, basaltic shards (Fig. 3.5c) were also present in the cores; these were dark brown and blocky with abundant microlites. The basaltic shards were similar in appearance to andesitic shards

where populations where mixed and it was difficult to differentiate between them conclusively under microscopic examination.

Clear (rhyolitic) and brown (andesitic or basaltic) shards > ~25 µm in diameter were identified and counted separately alongside *Lycopodium* spores along transects across the slide. At least four transects or up to 400 spores were counted alongside the glass shards to determine shard concentrations from original dry weight of sample (shards per mg dry weight) (Gehrels *et al.*, 2006). Although some ferromagnesian minerals (crystals) were seen in some samples, which *may* have been associated with the tephra fall events these were not identified as part of this study.

Glass shard concentrations (c) are expressed as shards per mg dry weight using the formula:

$$c = l \times \frac{a}{bd}$$

where a = glass shard count; b = *Lycopodium* spore count; d = sample oven dry weight in milligrams; and l = number of *Lycopodium* spores in a tablet.

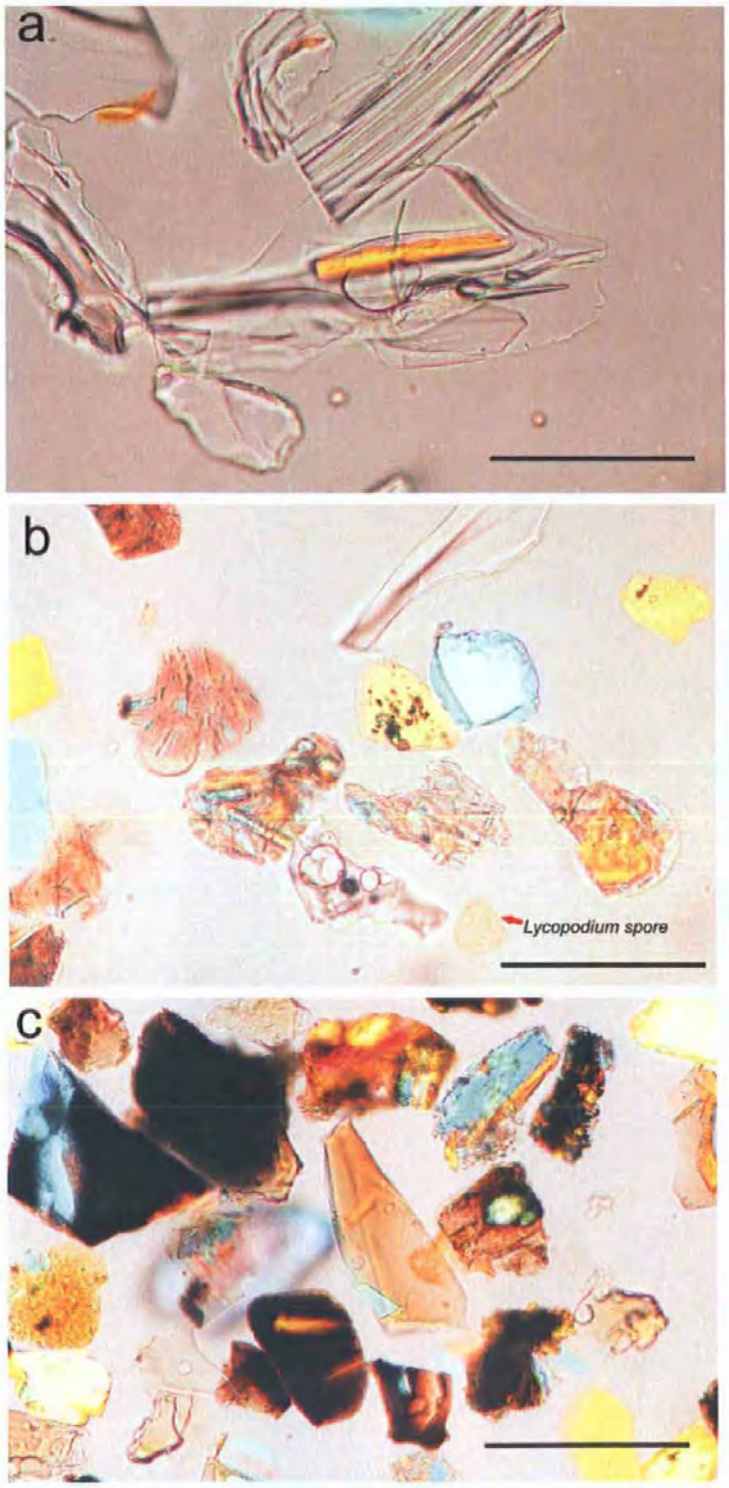

Figure 3.5. Photomicrographs of characteristic glass shards encountered in the peat and lake sediment sequences: (a) large, clear rhyolitic shards (core MR2, 142 cm, Taupo Tephra); (b) microlite-rich andesitic shards (Pup5, 52 cm). (c) Dark brown basaltic shards (Rangitoto Tephra) with large crystal inclusions, amongst associated ferromagnesian minerals (Pup5 24 cm). Scale bar bottom right of images represents 50 µm.

3.4 Geochemical characterisation

The major element compositions of glass shards were used to identify and correlate cryptotephras identified within the peat and lake sediment sequences. The compositions were determined using single grain analysis by wavelength-dispersive electron microprobe analysis (W-D EMPA) carried out at the NERC funded Tephrochronology Analytical Unit based at the University of Edinburgh during two separate, week-long visits. The main aim of this analysis was to determine if glass shard populations were sufficiently homogenous geochemically to confirm their origin from a single eruptive event and, if so, if analyses could be matched geochemically to those of the established tephrostratigraphic record in the region (e.g. Shane & Smith, 2000a; Shane & Hoverd, 2002; Shane, 2005; Smith *et al.*, 2005; Gehrels *et al.*, 2006; Alloway *et al.*, 2007). Analyses were conducted and presented in accordance with recommendations by Froggatt (1992) and Pearce *et al.* (2008). Detailed below are the procedures for selecting stratigraphic positions of cryptotephra analysis, sample and slide preparation and analytical conditions and measures.

3.4.1 Identifying cryptotephra levels for analysis

Geochemical characterisation of tephra is an expensive and time-consuming process. It would have been preferable to analyse glass shards continuously through the sedimentary record in order to maximise information about provenance and taphonomy. In practice, this level of detail is rarely justified therefore investigations such as this focus on key criteria and selected horizons within the stratigraphic sequences.

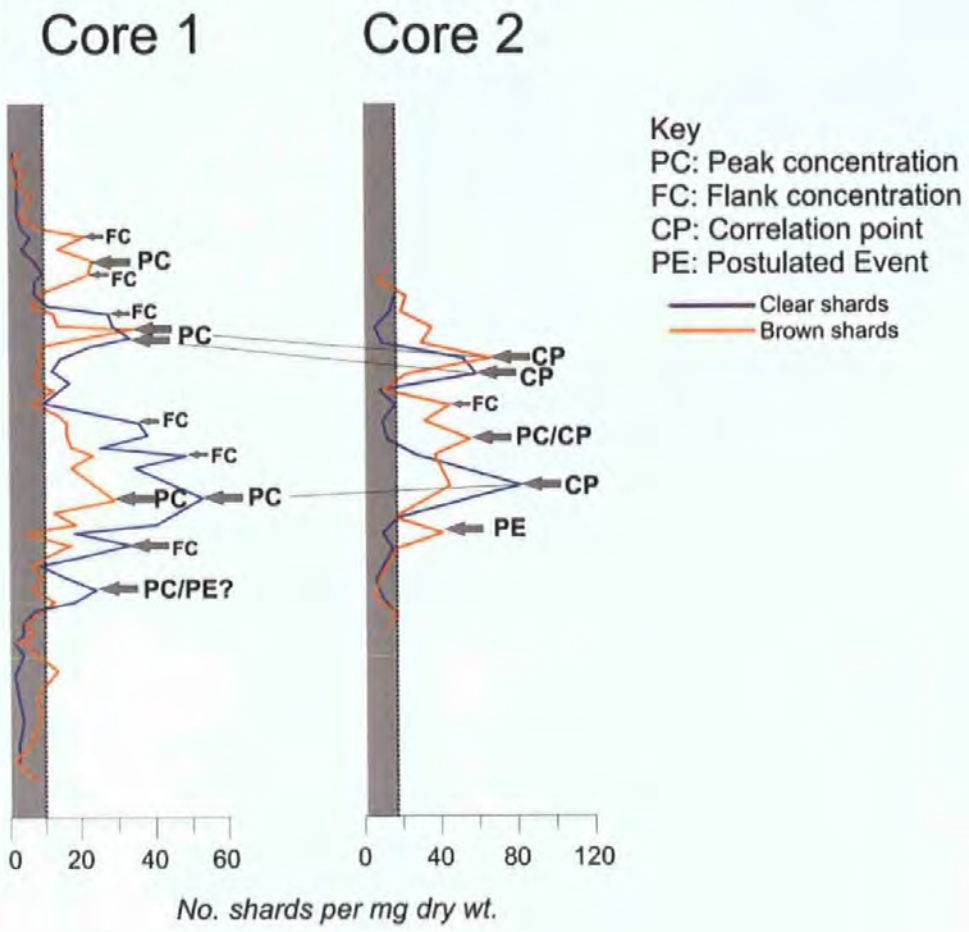

Figure 3.6. A conceptual model of the criteria used to select samples for EMPA from two cores based on glass shard concentrations. Grey line delineates arbitrary threshold for background shard concentrations where content constitutes less than 10% of total shards in a sequence (minus components from visible tephras). See text for definition of defining criteria.

The cryptotephra sampling levels for EMPA were selected using the shard concentrations determined for each sequence based on four defining criteria (Fig. 3.6). These were particularly important in sequences where individual cryptotephra 'horizons' were difficult to define. In such cases, levels for sampling were identified throughout sections marked by

continuous cryptotephra glass concentrations or zones. This strategy was used to (a) identify likely primary fall events and background concentrations of shards derived from secondary deposition, (b) identify the overlaps between mixed populations, (c) to confirm, geochemically, putative andesitic and rhyolitic groups identified on the basis of colour through microscopy and stratigraphic position, and (d) establish the degree of homogeneity to provide insights into the taphonomic processes involved. Defining criteria were as follows:

1. The level containing a marked Peak Concentration **(PC)** of shards. These were initially assumed to represent major depositional events most likely from primary tephra-fall events and were the foci of the analysis for most sequences.

2. The concentrations of shards above and below a PC or the Flank Concentrations **(FC)**, selected on the basis that EMPA will help to define the vertical extent of a given cryptotephra above and below the PC. The levels selected to represent FC, where possible, represent the first and third quartile as derived from the sum of shards from a distinct cryptotephra zone. The selection of the FC sampling positions was particularly important where cryptotephra concentrations were highly dispersed through the sediment profile (e.g. Gehrels *et al.*, 2006). In this case an individual cryptotephra zone is defined as a discrete zone of shards where shard concentrations increase above the background counts for the core. Background counts are arbitrarily defined by samples containing less than 10% overall shard concentrations for a given sequence, although defining the cut-off for background concentrations was not always possible in practice. Also considered was the

spread of shards as well as changes in sedimentology, particularly where this may have affected resulting shard concentrations.

3. Levels where there is a Postulated Event **(PE),** a peak concentrations thought to be linked to a known eruption, i.e. historical or well-dated ash falls which are likely to be present as cryptotephra in the profile.

4. Levels selected based on the tephra profile and stratigraphic relationships as the most likely to provide Correlation Points **(CP)** between all the cores.

In addition to these considerations for sampling strategy, further consideration was given to the numbers and types of shards analysed within samples (see section 3.3.5). Further details of sampling strategy for geochemical analysis, including exact stratigraphic positions of samples, are provided in the relevant results chapters.

3.4.2 Sampling and sample preparation

Fresh samples were extracted from the identified stratigraphic levels with a clean blade with due care to ensure that the samples were taken at the original levels identified through shards counts, i.e. same stratigraphic interval. Such care is particularly important in peat sections that are subject to considerable shrinkage through water loss over time. Samples needed to be sufficiently large to ensure enough shards were retrieved and to allow for any loss during processing. Publishable datasets generally require at least 10-12 shards per population to show reproducibility (Froggatt, 1992). It was thus also necessary that

samples were sufficiently clean of non-tephric components to concentrate the glass particles for analysis.

Sample preparation to concentrate shard content for EMPA followed standard procedures to remove non-tephric components which do not compromise geochemical composition of shards as described above (TEPHRATRACE, 2002). As with the preparation of samples for microscopy, this step involves the removal of organic material followed by additional chemical processes and sieving (Fig. 3.4). The acid digestion method (Dugmore *et al.*, 1992) was used to remove organic material from both peat and lake sediments as an alternative to the ashing method, which is known to alter levels of certain elements, specifically the alkalis, in the shards (Dugmore *et al.*, 1992; 1995). Although it has been suggested (Blockley *et al.*, 2005) that this method may result in the deterioration of shard surface after sustained treatment, there is no evidence that the geochemical composition of the shards is compromised.

For the acid digestion, wet samples were added to large (> 150 ml) conical flasks followed by the sequential addition of chemicals to digest organic material. Firstly, 50 ml of 98% concentrated sulphuric acid (1.84 SG, analytical reagent grade) was added to each sample and flasks shaken carefully. This was followed by several additions of 2-3 ml of 70% concentrated nitric acid (1.42 SG, laboratory reagent grade) until the reaction (foaming) had subsided. The flasks were carefully shaken in between each addition of acids to reduce the impact of any strong reactions (foaming). The liquid was then set to boil on a hotplate until it turned a clear yellow - when all organic material had been digested. Samples were left to settle so that most of the chemicals could be removed and the

remaining sediment recovered. Samples were cleaned thoroughly of chemical residue in distilled water until the solution returned to a neutral pH.

Samples were wet sieved to <25 >63 μm to remove any remaining fines as well and to remove the majority of any minerogenic particles present. The narrow size range provided an even layer of shards on the slide and ensured maximum exposure for smaller andesitic shards.

Where necessary, the NaOH treatment was used, prior to sieving, to dissolve biogenic silica content in samples with high concentrations. The use of NaOH is generally considered safe for using in preparation of samples for EMPA although there has been some concern regarding leaching (Blockley *et al.*, 2005) which is unsubstantiated. A query to tephra workers through the SCOTAV (now INTAV, International focus group on Tephrochronology and Volcanism) list server (SCOTAV list server accessed 18/9/2007) revealed a general consensus that the use of this chemical is unlikely to have any impact on the major element composition of glass shards. Only after sustained use would NaOH possibly etch the very outer layer of the shard surface only. This surface would nevertheless be removed during the polishing stage (section 3.3.3) to expose interior shard surfaces for analysis. Details of the procedure to remove organic content using NaOH was given in section 3.2.3.

3.4.3 Slide preparation

The preparation of samples for EMPA followed the grain mounting procedure recommended by the Tephra Analytical Unit (under the guidance of Dr David Steele). This involved mounting glass samples onto glass microslides with Epoxy resin and polishing sequentially with finer wet and dry carborundum papers to expose glass interiors. Slides were prepared carefully to ensure effective coverage and exposure of glass shard surfaces.

Samples were mounted onto glass, thin section slides of an appropriate size for the sample holder in the microprobe (28x48 mm, 1.2-1.5 mm thick, 50 OTG 90° (Menzel Glaser). In preparation, the surface of the slide was frosted using coarse grained (190 grit) carborundum (wet and dry) grinding paper to allow the resin to stick to the glass. Using a pencil, each slide was labelled and boxes, approximately 1cm^2, were drawn to outline the area on the slide for each sample. Space was allocated for four to six samples per slide. The most effective way to transfer small amounts of sample on to the slide was to pipette diluted sample on to slide which was then dried on a warm hotplate.

Small quantities of Epoxy resin (EPO-Thin resin, a two part Epoxy resin supplied by Buehler) were prepared and added using a cocktail stick on to each dried sample to ensure even coverage and to avoid contamination between samples. Resin was left to dry at room temperature for 1-2 hours and then placed onto a hotplate for ~1 hour to allow the resin to fully set/cure. Once cooled, the slides were polished to expose shard surfaces through the resin mount for EMP analysis as described below.

Sequentially finer grades of wet and dry carborundum papers (400, 800, 1200, 2500 and 4000 grits) were used to carefully expose the interior surfaces of shards on each slide. Slides were placed surface down firstly on the coarsest grain paper (400), which was kept moistened with distilled water. The polishing was done on a flat glass plate using steady pressure to ensure a uniform thickness across the slide. A micrometer was used at each stage to measure thickness of resin and to reduce the risk of over-grinding. Regular checks were also made using a light microscope on the exposure of shards. Before the final polish, slides were cleaned of any loose material in an ultrasonic bath for ~10 minutes.

A final fine polish was produced using a 6 μm diamond polishing lap and then a 1 μm polishing lap each for about 15 minutes each. Slides were again cleaned in an ultrasonic bath and examined using reflected light microscope to check for grain exposure. Slides were carbon coated to produce a conductive surface for analysis immediately prior to EMPA.

3.4.4 Electron microprobe (EMP) specifications and operating conditions

The glass samples were analysed for major elements using a CAMECA SX100 electron microprobe equipped with five WD spectrometers. The software used for analysis and data reduction was CAMECA's PC-based PeakSight software. All analyses were undertaken using beam conditions of 10 kV accelerating voltage, 10 nA (Faraday cup) beam current, and a 4 μm spot size. The small spot size made it possible to avoid microlites which are typically abundant in andesitic shards (Donoghue *et al.*, 2007; Platz *et al.*, 2007). (Although it has been suggested that beam size smaller than 10 μm could distort

compositional output (Hunt & Hill, 2001), careful use of standards throughout the analysis suggest that was not the case using the conditions described here.) The instrument crystal configuration and analysed elements were TAP(Si, P) - LPET(K,Ca) - LLiF(Mn, Fe) - TAP(Al, P) - LTAP(Na, Mg). Analysis times for 'first cycle' elements (Si, K, Mn, Al, Na) were 30 s peak, 30 s background. For Na and Si the 30 s peak time was split into 6.5 sec intervals and a decay curve procedure employed to correct for count rate decrease or increase in Na and Si, respectively. Second cycle elements counting times were 20 s peak and 20 s background. Independently characterised basaltic glasses including Lipari and BCR2G were analysed at regular intervals throughout the analysis session (results in appendices). The standard nine major elements (as oxides) were measured for glass composition: silicon (Si), aluminium (Al), potassium (K), sodium (Na), calcium (Ca), magnesium (Mg), manganese (Mn), iron (Fe) and titanium (Ti).

3.4.5 Shard selection and analytical strategy

During the analysis of each sample, considerations were given to the numbers and types of shards analyzed. As recommended by Froggatt (1992), at least 10 analyses were conducted on different shards per sample but 15-20 shards were attempted, particularly for key tephras (e.g. Kaharoa Tephra) and andesitic tephras. It is considered that at least 10 consistent analyses are required to be acceptable for publication (Froggatt, 1992; Turney *et al.*, 2004). In practice, however, it was not always possible to achieve this number. Each set of analyses from a sample were checked for outliers and multiple populations. For each sample a range of shards was analysed to produce a representative overview of each sample. The range included the dominant shard population or populations identified from

shard counts and a small number of shards from background concentrations to assess possible sources of reworked material.

Individual glass shards were identified in each sample using a range of imaging facilities on the EMP before analysing. The light microscope facility on the EMP was particularly useful for identifying shards of a particular chemistry, i.e. andesitic or rhyolitic in samples with mixed populations and for distinguishing between glass shards and crystals (minerals). For the analysis of andesitic shards, setting the EMP to obtain backscattered electron images of shards (Fig 3.7a) was useful for identifying and avoiding microlite inclusions which would potentially contaminate the resulting analysis (Platz *et al.*, 2007). Backscattered electron (BSE) images also provided a way of checking surface exposure of shards above resin; the resin appears as a black background (Fig. 3.7 a, b) around shard surface. Using BSE it was also possible to discriminate between andesitic and rhyolitic shards, the latter appearing slightly darker due to higher silica composition (compare Fig. 3.7 a and b).

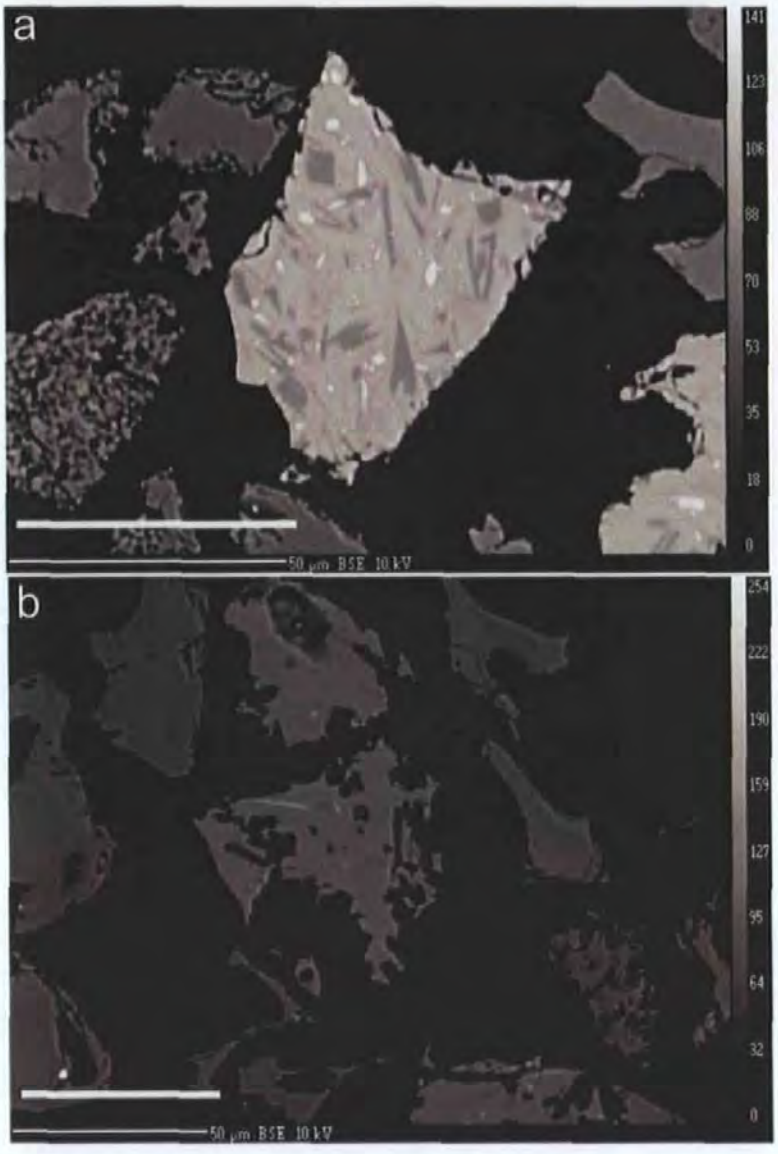

Figure 3.7. Backscattered electron (BSE) images of exposed surfaces of glass shards in resin mount: (a) andesitic shards (core MR2, 8 cm) showing distinct microlite inclusions (small crystals); (b) rhyolitic shards (LR1, 17 cm) appear slightly darker than andesitic shards due to compositional differences. Bar is 50 µm long.

3.5 *Chronology construction*

It was necessary to develop chronologies for each sequence, both (a) to develop a robust age-model for key profiles, and (b) to date targeted areas of the cores which record potentially significant tephra falls. Four dating methods were used for this objective:

radiocarbon dating, tephrochronology, palynology and historical markers. The age models provided the means to date individual cryptotephras and link them with known eruption events or correlate with other cores and or sites where individual tephras could not be differentiated by geochemistry. In addition to dating significant ash fall, dating was used also used to constrain the time-stratigraphic interval over which some significant cryptotephras occupy as a result of taphonomic processes affecting shards.

3.5.1 Tephrochronology

Tephrochronology, via tephrostratigraphy provided a useful dating method for the cores used in this study. This included using visible tephra layers present in the cores as well as any cryptotephras identified that could be linked to well-dated tephra depositing events, e.g. the Kaharoa Tephra. The visible Taupo Tephra (1717 ± 13 cal yr BP; (Fig 3.3) provided a well defined age horizon for marking the base of all sequences. Lake Pupuke cores also included a localised basaltic tephra, the Rangitoto Tephra, *ca.* AD 1400 (Fig. 3.3).

3.5.2 Radiocarbon dating

Radiocarbon dating was selected as the primary method to date selected sediment sequences from the two peat bogs (Moanatuatua and Opouatia) and from Lake Rotoroa, also contained enough organic material for dating. As previous studies of Lake Pupuke suggested a problem with a radiocarbon hard-water effect, radiocarbon dating was not used at this site (Horrocks *et al.*, 2005). Measurements of ^{14}C for dating the sequences used in

this study were carried out at the University of Waikato radiocarbon facility in New Zealand and the NERC radiocarbon facility in East Kilbride, UK.

Four samples were processed at the University of Waikato Radiocarbon Laboratory in July 2005. The samples were submitted shortly after cores were collected, with the aim of constructing an outline chronology using conventional liquid scintillation spectrometry. These samples were taken from *in situ* sections and included bulk samples of peat and large pieces of wood. Samples were not treated to any physical or chemical pre-treatments prior to submission. In the laboratory, samples were acid washed using 10% HCl, and 1% NaOH to remove contaminants and the base-insoluble fraction was selected for dating.

Samples collected for dating by accelerator mass spectrometry (AMS) at the NERC facility comprised plant macrofossils, pollen concentrates and bulk sediment samples. For peat bog sites, plant macrofossils comprised stems, seeds and leaves which were handpicked from the coarse fraction of peat samples that were suspended in water using a low power microscope. Samples were prepared by wet sieving peat through a >180 μm sieve to retain the fraction then suspended in distilled water for hand picking, with care taken to avoid roots that may have penetrated the peat from younger levels. Plant macrofossils were particularly sparse in lower levels of the peat sequences. To obtain the required minimum sample size of at least 1-2 mg of carbon for AMS dating, most of the peat samples were composed of a mixture of various macrofossil types.

Pre-treatment of plant macrofossil samples to remove contaminants was completed at the radiocarbon facility. Samples were digested in 2M HCl (80°C, 8 hours), washed free from

mineral acid with deionised water then dried and homogenised. Carbon content was recovered as CO_2 gas which was converted to graphite for analysis using 5MV AMS.

There were not enough plant macrofossils in the lake cores from Lake Rotoroa for dating and an attempt was made to extract pollen concentrates (using method detailed in Newnham *et al.*, 2007b). However, these samples resulted in a very low amount of CO_2, close to the limit for routine samples (c. 1 ml CO_2). As a result of low precision only preliminary results were obtained from these samples. In these cases bulk sediment samples containing ~40% organic content were dated in addition to the pollen concentrates.

3.5.3 Palynology

Each profile spans the interval from Taupo Tephra to present (the last ~1800 years), during which two major anthropogenic events are clearly discernible in New Zealand pollen records: the initial forest clearance that accompanied earliest Polynesian settlement and the introduction of adventive plants with European settlement. The former occurred at around the time of the eruption of the Kaharoa Tephra (AD 1314 ± 12) (Newnham *et al.*, 1998; McGlone & Wilmshurst, 1999; Lowe *et al.*, 2000), whilst the latter occurred during the first few decades of the nineteenth century, with historical records supporting existing age models. Palynological analysis may therefore potentially provide two additional time lines for each profile.

3.5.4 *Additional age markers*

These include charcoal layers from recorded fire events and chemical markers from pollution events (e.g. a copper layer in Lake Pupuke cores from the addition of copper sulphate in the 1920s; Fig. 3.3). These markers are especially important for providing dates in the last 300 years when radiocarbon dating is compromised by industrial effects such as atomic bomb testing, industrial pollution and agricultural affects. Details of the particular historical markers applied are given in the relevant results chapters.

CHAPTER 4: WAIKATO REGION

4.1 Waikato Region sites

In this chapter the results of analyses outlined in the previous chapter are described for the three research sites within the Waikato Region of the North Island, New Zealand. These sites include Moanatuatua and Opuatia peat bogs, and Lake Rotoroa (Fig. 4.1.). The results from the Auckland Region site are described in the following chapter. Under the heading for each site each section includes: (1) a description and background to the site; (2) details of the sample collection and retrieval; (3) lithostratigraphy of the sediment sequences, (4) construction of age-models for sediment sequences; (5) the tephra-derived glass content; and (6) geochemical composition and identification of cryptotephras. A final section includes a summary of the main findings from each site including any resultant issues.

The Waikato Region of the North Island covers an area ~25,000 km^2 and consists of large areas of pastoral farmland, several small towns and one city. Though defined as a political district, the Waikato Region is in general terms defined by the course of the Waikato River. This is the longest river in New Zealand, extending ~425 km northwest from its source at Lake Taupo, through the Waikato lowlands up to where it empties into the

Tasman Sea at Port Waikato (Fig. 4.1.1). The city of Hamilton is the region's only city and largest population centre with ~130,000 permanent residents, and is the seventh largest population centre in New Zealand (Statistics New Zealand, 2008).

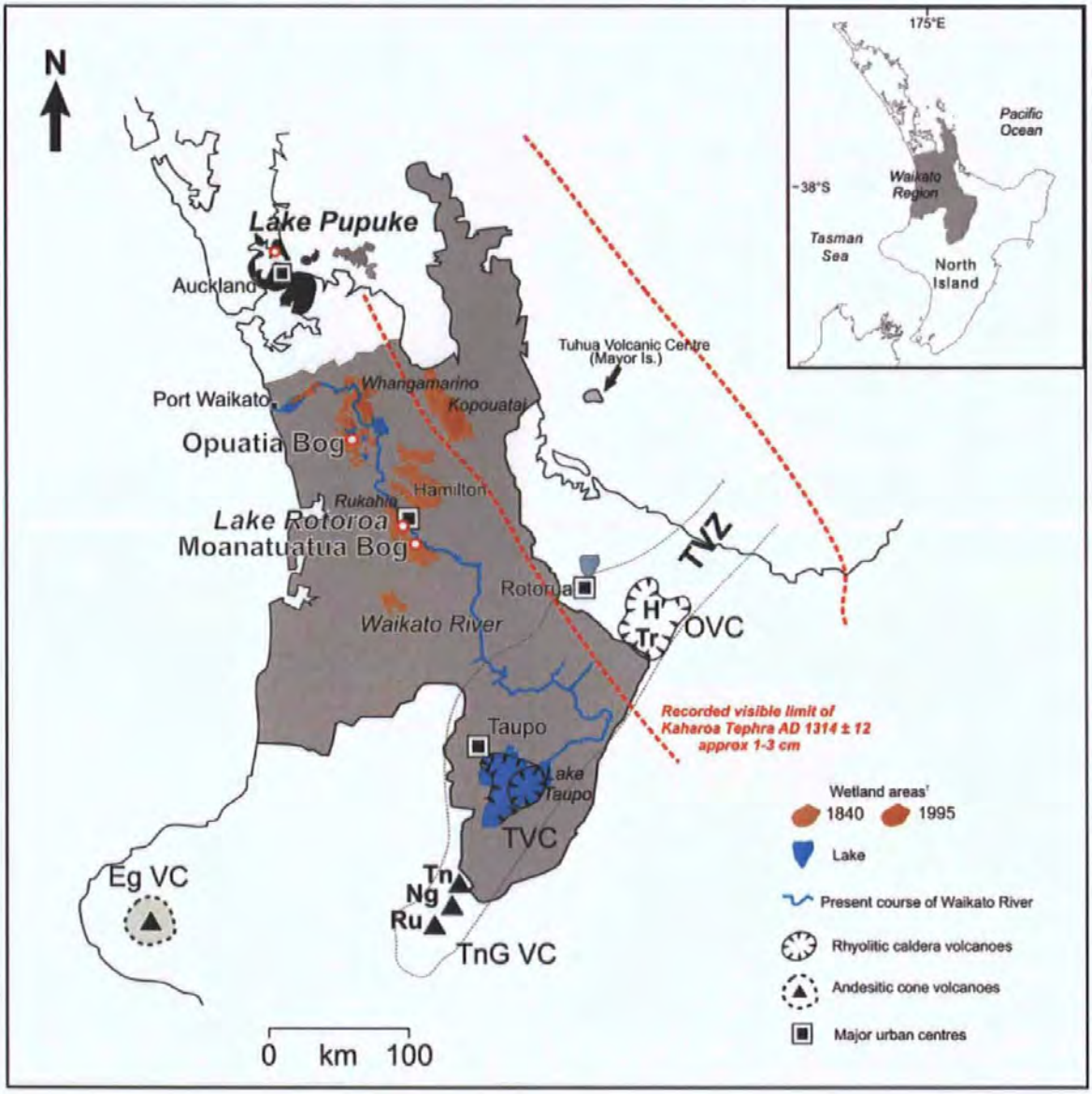

Figure 4.1. The Waikato Region with locations of core sites and the present and past extent of significant wetland areas, †from Environment Waikato (1999b). The names of significant peatlands are in italics.

The landscape of the central Waikato Region (Hamilton Basin) is dominated by broad alluvial plains formed by the ancestral Waikato River, and numerable swamps, peatlands and small lakes (Fig. 4.1.). Many of these wetland sites and bogs developed as a result of increased rainfall that accompanied the climate amelioration at the end of the last glacial stage (Green & Lowe, 1985; Newnham *et al.*, 1989). Wetlands typically formed in poorly drained depressions of the volcaniclastic alluvium (known as the Hinuera Formation) deposited by ancestral Waikato River (Selby & Lowe, 1992). The raised peatlands in the region represent the final stage in the succession of these wetland areas through a process of hydroseral succession (Aaby & Berglund, 1986). Peat growth is thought to start on the margins of swamp lakes which gradually encroach on the lake. This is coupled with the replacement of plant species with less nutrient-demanding plant species. The key plant species in this succession includes the Southern Hemisphere species of jointed rushes (*Restionaceae* or restiad species) which have unique hydrological and peat forming properties and form a distinct type of raised ombrotrophic bog which are found only in New Zealand (Selby & Lowe, 1992; de Lange *et al.*, 1999). High water table conditions suitable for this peat development have been maintained by the region's high annual rainfall, mild temperatures and high humidity (Shearer, 1997). The current mean annual rainfall for the Hamilton area is ~1252 mm year^{-1}.

The ombrotrophic bogs are characterized by a raised, dome-like surface which rises above the surrounding land surface that is hydrologically separate, receiving all water and nutrients from precipitation resulting in an acidic and nutrient poor environment dominated by only a few specialised plant species. Allogenic inputs to these raised bogs are therefore likely to solely reflect atmospheric inputs which are of key importance to this investigation. The resulting peat is highly organic in nature providing effective repositories

for preserving and detecting a wide range of palaeoenvironmental proxies as well as airfall tephras. Raised restiad bogs are a distinctive type of bog that is unique to New Zealand. These are dominated by a Southern Hemisphere family of jointed rushes, *Restionacea* which includes species *Sporadanthus ferrugineus* (henceforth *Sporadanthus*) and *Empodisma minus* which produce a fibrous and highly acidic type of peat (pH ~3-4) (Campbell, 1975; de Lange *et al.*, 1999; Clarkson *et al.*, 2004).

Large areas of wetlands once covered ~5% of the Waikato landscape but this has reduced to <1% since the arrival of Europeans (~AD 1840) who instigated extensive drainage programmes to convert the land for agriculture (de Lange *et al.*, 1999). Drainage activities took place over a ~150 year period reducing wetland area from 111,000 ha (estimated AD 1840 cover from Environment Waikato, 1999) to ~30,000 ha (AD 1995 measurements) (Fig. 4.1.). Many of the remaining wetlands were reduced to isolated remnants which are now protected as reserves in recognition of the many unique and endangered species of plant and animals found in them. Moanatuatua and Opuatia bogs are representative of the few remaining raised restiad peat domes in New Zealand.

Both peat bog and lake sites in the region have provided important archives for palaeoenvironmental proxies and for distal tephras from TVZ volcanoes (Lowe *et al.*, 1980; Lowe, 1981; 1986; 1988b; Green & Lowe, 1985; Newnham *et al.*, 1995; Gehrels *et al.*, 2006). More than 40 individual Late Quaternary tephras have been detected in peat and lake sites in the region from both rhyolitic and andesitic sources (Hogg *et al.*, 1987; Lowe, 1988a; de Lange & Lowe, 1990).

4.2 Moanatuatua Bog

Moanatuatua Bog (37° 58'S, 175° 72'E) is one of only a few remaining raised, ombrotrophic (rain fed), restiad peat bog in New Zealand, and with Lake Rotoroa, represents the sites positioned closest to potential volcanic sources of ash from TVZ and Egmont/Taranaki volcanoes.

4.2.1 Site description

Moanatuatua Bog is located ~17 km southeast of Hamilton city (Fig. 4.2.1a) and is situated within the Hamilton Basin (as is Lake Rotoroa), an oval shaped, tectonically controlled depression >80 km N-S and > 40 km wide surrounded by hills to the east and west (Selby & Lowe, 1992; McCraw, 2002). Quaternary deposits that fill the basin include sediments from the Waikato River and older thick deposits of tephras from volcanoes of the TVZ and from Egmont/Taranaki volcano (Selby & Lowe, 1992). Moanatuatua Bog developed on Waikato River derived volcanogenic alluvium approximately 13, 300 ^{14}C yrs BP (*ca.* 15, 500 cal. yrs BP) based on radiocarbon ages (from the deepest peat (Wk-529; Hogg *et al.*, 1987, p. 287).

The bog itself was once a large raised peatland in excess of 7500 ha in size with a maximum peat thickness of ~15 m (Shearer, 1997; Clarkson *et al.*, 2004). It has

significantly reduced in size in recent centuries. An extensive drainage programme that started in the early 1900s to convert land to pasture and farmland has reduced the peat bog to two small isolated remnants ~120 ha in total size (Fig. 4.2.1b). The largest of these, marked by a line of planted pines (*Pinus radiata*) on its eastern margin, is now protected as a scientific reserve in recognition of the unique and threatened species (including *Sporadanthus*) in these types of bog. However, due to its small size it is considered very vulnerable to change (Shearer, 1997) and the sampling strategy adapted for this site was constrained in recognition of this fragile habitat.

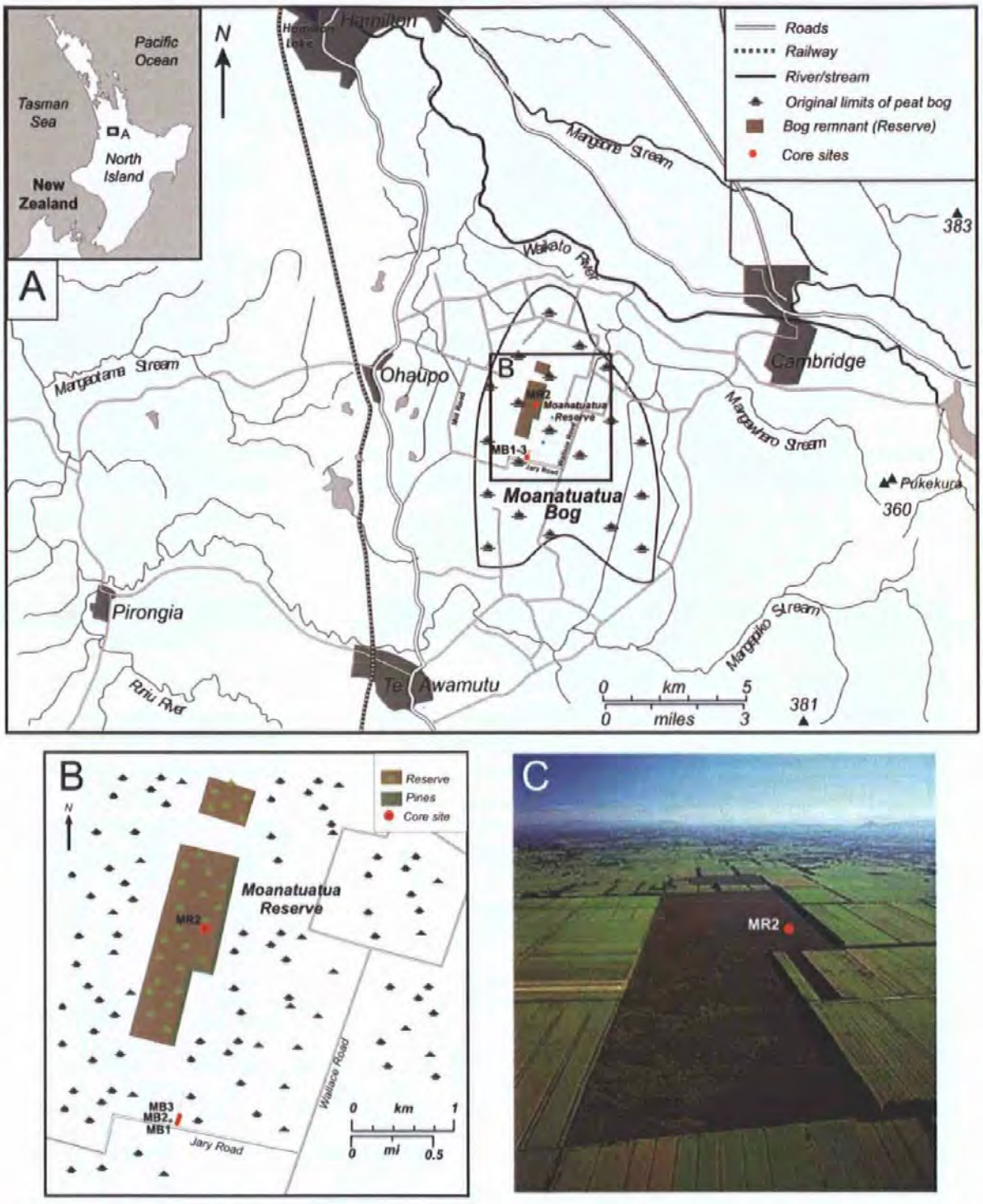

Figure 4.2.1 Location map of Moanatuatua Bog: (A) in relation to Hamilton and other significant population centres in Hamilton Basin, (B) close up of the remnant bog and core sites. The larger of the remnants is the scientific reserve. (C) Oblique aerial photograph of the peat bog remnant and surrounding drains, red dot indicates the approximate location of core site (source of photograph:

http://erth.waikato.ac.nz/research.campbell/carbon.flux/index.shtml, University of Waikato).

The modified (drained) peatland is crossed with a dense network of maintained drainage ditches. This drainage has resulted in significant subsidence of the underlying peat caused by losses of organic matter and consolidation (Mc Lay *et al.*, 1992; Schipper & McLeod, 2002). An average of ~2.5 m of subsidence has been measured for the drained peat from this site over a 77 year period (Schipper & McLeod, 2002). This has had an inevitable effect on the water table conditions of the remaining remnant which is now too small to maintain its own water table conditions. Since 1974 (to 1999) mean water table levels on the bog were found to have declined by ~25 cm (Clarkson, 1997). A manifestation of this change is the development of an unusually thick acrotelm layer (aerated root zone) in the peat. This is typically 50-60 cm thick in the bog as opposed to 20-30 cm for unmodified bogs (Shearer, 1997). Subsequent changes to the plant composition in parts of the bog, particularly on the margins are thought to have stemmed peat accumulation altogether (Dr David Campbell, Waikato University pers. comm. February, 2005). Frequent fires associated with early drainage and other land activities have also had a significant impact on the remaining remnant affecting the restiad species which are particularly sensitive to disturbance (Thompson *et al.*, 1999; Campbell *et al.*, 2002; Schipper & McLeod, 2002).

The plant species in the Scientific Reserve (~74 ha) are dominated by the jointed rush species including *Sporadanthus* which is a late successional species endemic to the North Island and restricted to highly acidic (pH <5) ombrotrophic peat bogs (de Lange *et al.*, 1999). *Sporadanthus* are long lived perennial plants which spread vegetatively by rhizomes that produce dense clusters of upright culms (10-15 mm in diameter) (de Lange *et al.*, 1999). In Moanatuatua the pH of the peat has been measured to between 4.1 and 4.6 (Clarkson *et al.*, 2004). The root system produces 25-30 cm long, horizontal roots but have

been known to penetrate >2 m in the peat (Dr Beverley Clarkson, pers. comm. October, 2007). The culms (stems) extend up to ~2 m in height to form a dense lofty canopy sheltering the underlying peat from the Sun and reducing evapotranspiration and providing an important habitat for a number of plant and animal species (Bell, 1986; de Lange *et al.*, 1999) (Plate 4.2.1a).

In the reserve, *Empodisma* forms a dense understory to *Sporadanthus*. This restiad species also spreads vegetatively producing denser but finer culms which extend up to ~1.2 m in height (Plate 4.2.1c; Clarkson 1997). The fine, dense cluster roots from this species are the main peat formers in restiad bogs, producing a mat like structure which has unique water-retaining properties. The living roots from this species can penetrate >1 m down in the peat (Dr Beverley Clarkson, pers. comm. October, 2007). The dense culms from both restiad species form a raft-like construction on the underlying peat upon which a number of other plant species thrive. Intermittent species identified in the understory of the bog include shrubs such as *Leptospermum* (manuka) and *Gleichenia dicarpa* (umbrella fern), Liverworts *Goebelobryum unguiculatum* and mosses *Campylopus acuminatus* and *Lycopodium laterale* (Clarkson, 1997). Shrubs are particularly prominent in the drier areas of the bog which have been most affected by the surrounding drainage.


a


b


c


d


e

Plate 4.2.1 Moanatuatua Reserve, showing site vegetation and sampling methods: (a) surface vegetation dominated by dense restiad species (Prof. David Lowe (standing upright) is holding a full length *Sporadanthus* culm). The understory vegetation includes predominantly *Empodisma*. (b) View of the raised surface of the bog from bog margins. The pine trees *(Pinus radiata)* mark the eastern margins of the Reserve (Fig. 4.1b); (c) Close up of the *Empodisma* understory with other intermittent plant species (the *Empodisma* is ~40 cm in height in this picture). (d) The surface pit dug to collect monolith samples. (e) Narrow reconnaissance core used to determine the depth of the Taupo Tephra (marked by trowel tip but barely visible in this picture). All photographs by author.

Moanatuatua Bog has been the focus of a range of scientific studies. In particular, it has become an important site for monitoring the impact of drainage and modification of the region's peat bogs to bog hydrology and xeromorphic vegetation characteristics (Clarkson, 1997; Thompson *et al.*, 1999; Campbell *et al.*, 2002; Norton & de Lange, 2003). Studies have also focussed on the impact of fire on restiad species using recent fires at the site to monitor plant recovery (e.g. Clarkson, 1997; 2002). Peat sequences from the remaining bog and margins also proved to be useful archives of palaeoenvironmental proxies in a recent study by Hazell (2004). These records were dated successfully using a number of distal rhyolitic tephras preserved as visible deposits at the site. In addition to the Taupo Tephra, additional tephras detected at the site include the peralkaline Tuhua Tephra (~7000 cal yr BP) and Okataina-derived Mamaku Tephra (~8000 cal yr BP), which were found in peat sequences collected from the drained margins of the bog (Hazell, 2004). Within the same sequences a number of cryptotephra concentrations were also detected using measurements of organic content and magnetic susceptibility as a guide to tephra concentrations (Ballinger, 2003). No geochemical analyses were undertaken to characterise these visible or cryptic tephras definitively, they were tentatively correlated with known rhyolitic and andesitic ash-fall events based on stratigraphic position, physical characteristics and ages. No brown glass shards were recorded from the cryptotephra study, but microlite-rich glass shards were observed which were tentatively linked to known

Egmont-sourced tephras. It is likely that the presence of brown shards, which are typically smaller in size and in lower concentrations than rhyolitic glass shards, were overlooked in that particular study.

4.2.2 Peat collection

Five peat sequences were retrieved in total from Moanatuatua Bog during field visits in 2005 and 2007 (Fig. 4.2.2.). These include two sections from the Scientific Reserve (MR2 and MR7) and three short sections (MB1-3) from a peat exposure in a partly drained region of the bog where blueberries are cultivated. A summary of material collected is shown in Table 4.2.1 and coring locations are shown in Figure 4.2.1b.

Section MR2 was collected from the unmodified peat in the Scientific Reserve (GR: E2718772, N6361319; Fig. 4.2.1) and represents the most complete sequence obtained from Moanatuatua Bog. The sequence was collected from a depth just below the visible Taupo Tephra at 1.5 m up to the modern surface of the bog which was composed of living plants (Table 4.2.1; Fig. 4.2.1b). The Taupo Tephra has been identified throughout the site from previous studies by its distinct physical properties and depth (Lowe, 1988b). It represents the most recently deposited tephra detected at the site. After probing various sites, the actual core site was located ~10 m in from the margins of the reserve, where there was no visible impact of marginal drainage ditches on bog vegetation and surface. Also, at this point the thickness of the peat section was also considered sufficient to obtain a high resolution record of tephra derived glass-shard content throughout the sequence.

The peat was sampled in sections as cores and monoliths to a depth just below the visible Taupo Tephra. Monolith 'tins' were used to collect the top 90 cm of the peat up to the surface which was difficult to extract effectively using coring equipment. This was due to the loose nature of the un-compacted acrotelm layer which is also unusually thick at this site. The use of monolith tins also allowed for large sections of peat to be collected and which were also undisturbed by the action of any coring processes.

To collect the monolith samples, a pit was dug from the surface of the bog to form vertical face in the peat. Plastic boxes (length = 30 cm, width = 20 cm, depth = 20 cm) were adapted to provide lightweight monolith containers which were cut into the peat exposure and dug out to obtain contiguous sections of undisturbed peat. A narrow Russian type corer with a 50-cm long and 5-cm diameter barrel was used to extract the replicate sections from the remaining sequence down to the Taupo Tephra from the base of the pit (at 90 cm depth).

Section MR7 was an additional core taken from the reserve in February 2007 (by Professors Rewi Newnham and David Lowe) to provide replicate analysis for section MR2 (Table 4.2.1). It was anticipated that this section would provide replicate analysis for section MR2 for the section containing the Kaharoa Tephra to examine some of the taphonomic processes affecting this particular tephra. The core site was located *ca.* 10 m from the previous core site (MR2) where peat accumulation rates would be similar. Three 0.5-m-long sections were retrieved using a narrow Russian type corer down to just below the visible Taupo Tephra. Problems were encountered, however, in obtaining the top section of the peat with the corer due to the thick actotelm layer, and so peat was only retrieved immediately below the root zone. The core retrieved extends from 57 cm (bottom

of root zone) down to the Taupo Tephra at 173 cm - a total of 116cm of peat core (Fig. 4.2.2.).

Monoliths MB1, MB2 and MB3 were collected from a 90-m-long section of exposed peat in a partially water filled, 1.5-m deep, drainage ditch located on the north side of Jary Road (Fig. 4.2.1b; Plate 4.2.2a), approximately 500 m south of the present day bog margins (GR: E2718472, N6359349). These ditches from part of a blueberry farm and are used to control water tables seasonally. These ditch-based sections were collected to examine the spatial variability of cryptotephras in the site as well as provide more detailed, replicate analysis for the lower 50 cm of the peat sequence above the Taupo Tephra which was only obtained in narrow cores from the reserve. The peat exposure consisted of a well preserved peat below a disturbed agricultural soil ~20-30 cm thick on the surface. The Taupo Tephra formed a distinct and laterally continuous layer visible along the exposure at a depth ~67 to 75 cm below the surface, a difference of at least 80 cm of peat height compared with the unmodified peat sequence in the reserve. Samples of the peat were collected in overlapping monoliths tins from the cleaned, exposed sides of the drain using plastic boxes as monoliths, as for MR2, taken just below the disturbed peat surface (Plate 4.2.2 b-e).

4.2.3 Lithostratigraphy and peat characteristics

All monoliths and cores retrieved from Moanatuatua Bog contained restiad peat characterized by restiad plant and root matter of varying levels of decomposition, and interspersed with woody fragments and charcoal layers (Figs. 4.2.3. and 4.2.4). Generic

descriptions were used in this study to describe the restiad peat sequences based on the visual examination of identifiable components, e.g. plant remains, charcoal layers and wood, and peat texture (after Campbell, 1975; Lowe, 1988b; Clarkson, 2004).

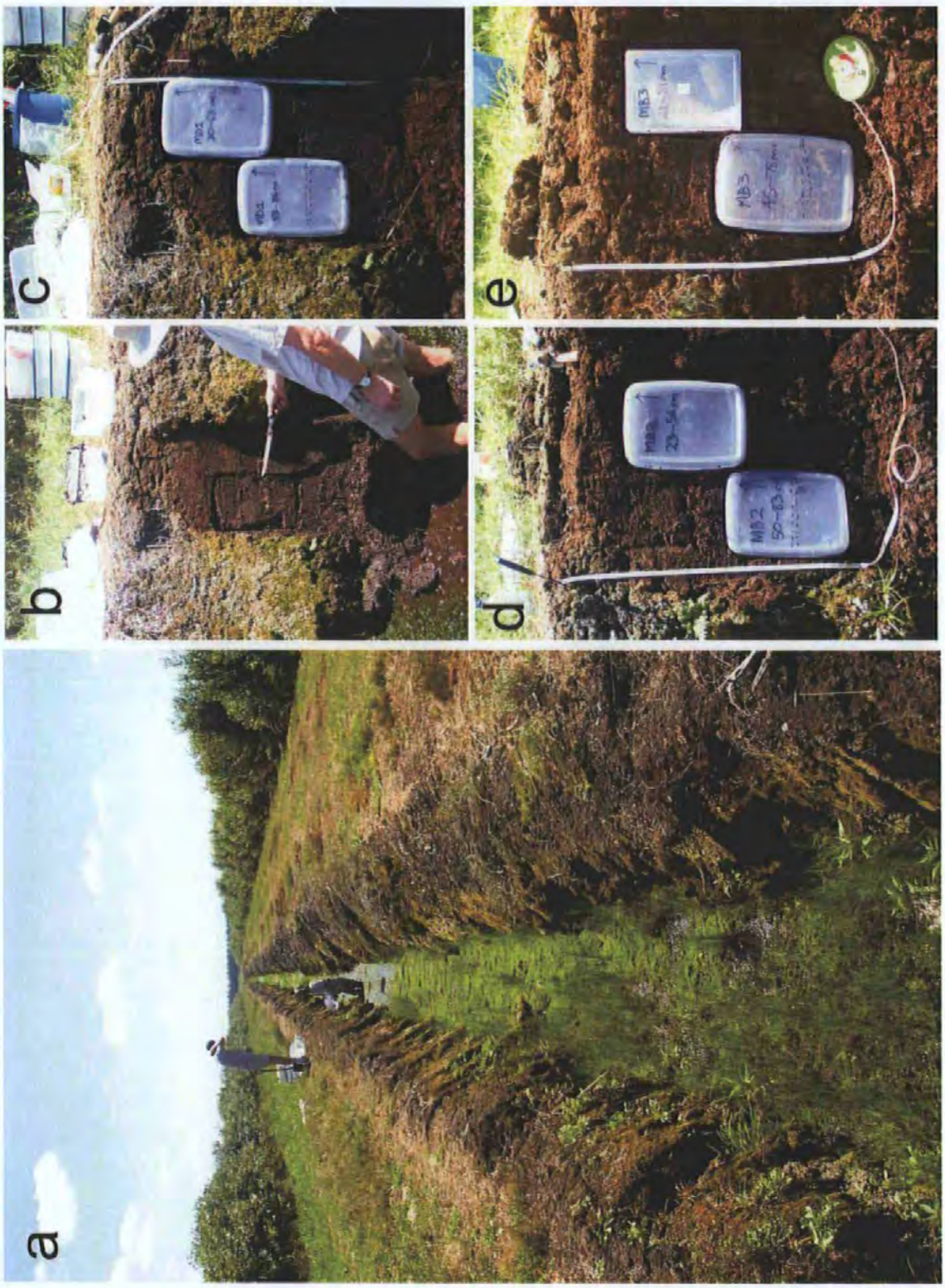

Plate 4.2.2 Moanatuatua margins (blueberry farm) and detail of peat exposure and sample collection: (a) site of drainage ditch and peat exposure (Fig. 4.1); (b) preparation of exposure for sample collection; (c-e) plastic containers (~ 30 cm in length) used to collect overlapping monolith samples from peat exposure: (c) MB1, (d) MB2, (e) MB3. All photographs by author.

Table 4.2.1 Summary of material collected from Moanatuatua site

Core site (date collected)	Core site details [grid ref of core site]	Sample code	Depth retrieved from surface (cm)	Sample retrieval	Notes on stratigraphy
Reserve (8-2-05)	Taken from the Reserve, 10 m from margin and drainage ditch, amongst *in situ* vegetation (Plate 4.2.1a) [E271877, N636131]	**MR2**	**0-190**	x3 contiguous 30 cm long monolith tins (0-65 cm); cores (90-190 cm; taken in triplicate A-C) from surface	Taupo Tephra at 149-150 cm (fine lapilli) identified by field characteristics and stratigraphic position
(17-2-07)		**MR7**	**74-170**	3 x 0.5 m long contiguous sections from below acrotelm	Taupo Tephra at 170 cm
Partly drained margins (9-2-05)	Peat exposure in drainage ditch on the margins of reserve (Fig. 4.2.1b; Plate 4.2.2a) [E271847,N635934]	**MB1**	**30-86**	x2 parallel monolith tins with 10 cm overlap (30-63 cm and 53-86 cm; Plate 4.2.2c)	Taupo Tephra at 75 cm Several distinct charcoal layers
	17 m north of MB1	**MB2**	**23-83**	x2 parallel monolith tins with 6 cm overlap (23-56 cm and 50-83 cm) (Plate 4.2.2d)	Taupo Tephra at 69-71 cm (~ 2 cm fine lapilli) Several distinct charcoal layers
	53 m north of MB2	**MB3**	**21-78**	x2 parallel monolith tins with 6 cm overlap (21-51 and 45-78 cm) (Plate 4.2.2e)	Taupo Tephra at 67-69 cm Charcoal layers

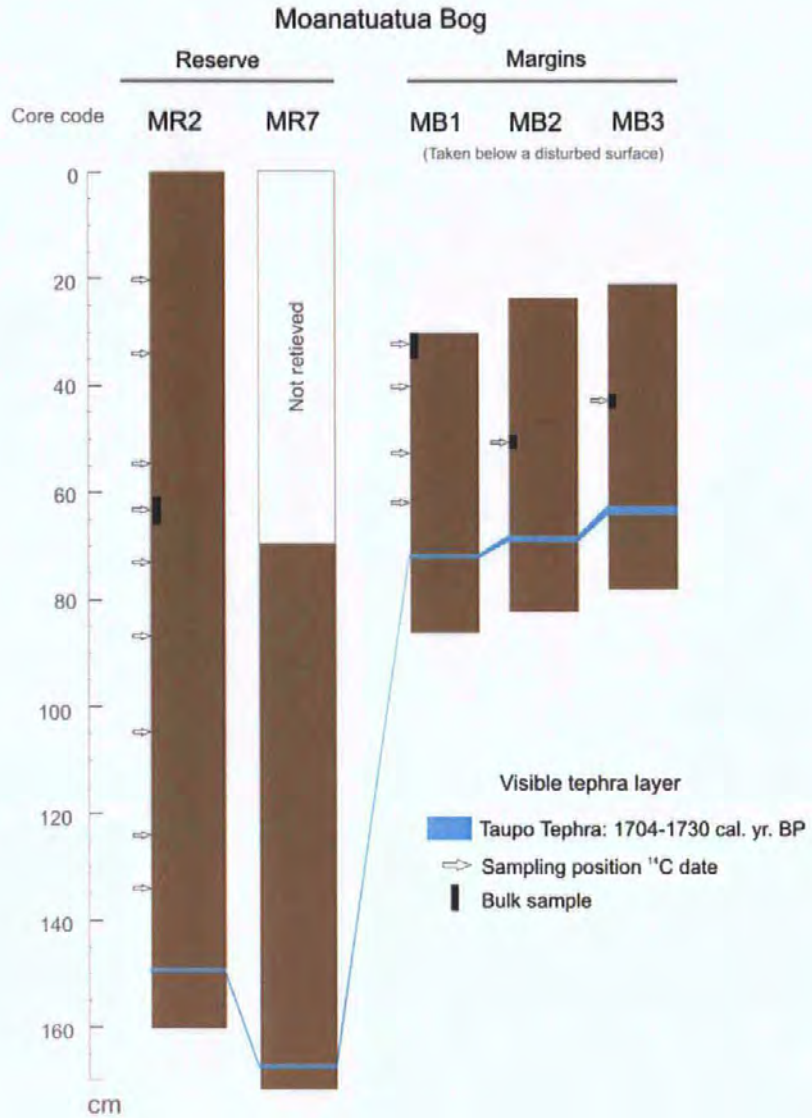

Figure 4.2.2 Summary of all cores from Moanatuatua Bog – reserve and margins used in this study, showing visible tephrostratigraphy and positions of samples for radiocarbon dating.

The texture of the peat is defined primarily by the degree of humification; a measure of plant decomposition (Blackford & Chambers, 1993). For the purposes of this study humification was assessed using simple field techniques (von Post scale) to observe the colour of interstitial water from the peat and texture of wet peat between fingertips (dark fluid and smooth texture = well humified; light or clear fluid and rough texture = poorly humified). Two broad categories of peat were recognized for the sections collected: (1)

well to moderately well humified peat, comprising a dense and compact peat with no discernable plant remains and generally dark in colour; and (2) poorly to very poorly humified peat with a porous texture and comprising distinguishable, poorly decomposed plant material and roots. The fibrous, aerated zone which forms the acrotelm forms a separate category for section MR2 which extends up to the surface. Measurements of loss on ignition (LOI) were also used to provide a measure of changing organic content through the peat sequence.

Section MR2 (Fig. 4.2.3)

MR2 was the longest and most complete sequence retrieved from this site, comprising a continuous section of restiad peat taken from just below the Taupo Tephra at 150 cm depth in the peat up to the modern surface where peat is still actively accumulating. Based on the depth of the tephras an approximate peat accumulation rate at this site is 0.8 mm yr^{-1}.

Measurements of LOI revealed a highly organic peat typical of restiad peatlands consisting of 93-99% organic material, with a mean of 96.6% for the peat above 140 cm depth up to the surface. LOI values decrease markedly immediately above the Taupo Tephra and then increase steadily to the mean value at ~115 cm, 35 cm above that layer. Distinct fluctuations in LOI values at 70, 60, 55 and 8 cm amount to ~5% decrease in organic content and were suggestive of several possible cryptotephra concentrations prior to microscopic examination. Changes in organic content at 18-34 cm coincide with changes in peat composition.

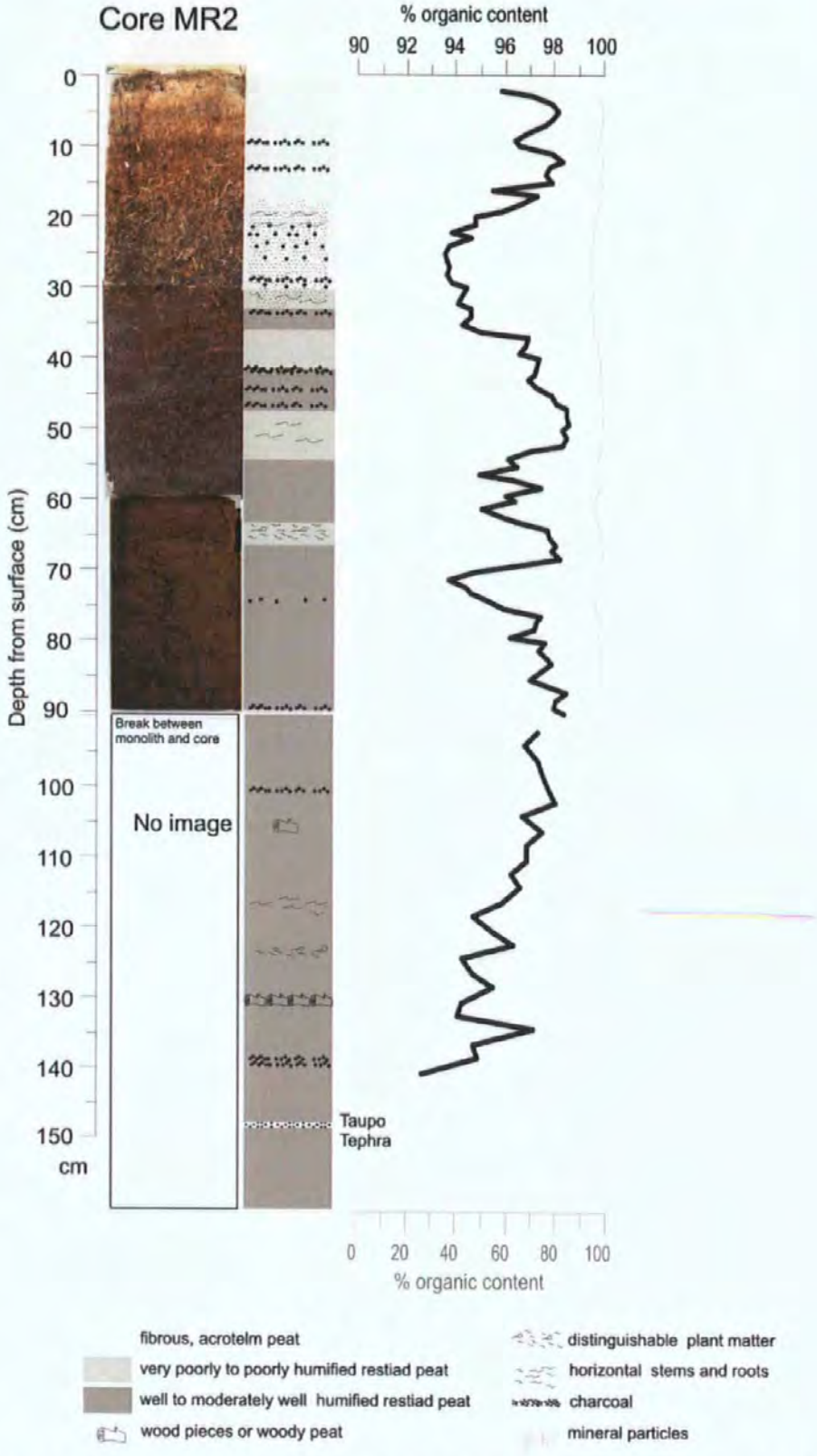

Figure 4.2.3 Section MR2 showing position of charcoal layers and other observable lithostratigraphic changes, shown alongside measurements of loss on ignition showing down-core changes in organic content.

At the base of the sequence the Taupo Tephra comprises a unit of coarse ash and lapilli visibly disseminated over ~1.5 cm. The peat immediately above and up to ~55 cm depth is a relatively homogenous unit consisting of well to moderately well humified peat. This peat is interspersed with a few narrow horizons of woody peat and wood pieces, visible horizontal stems, a few poorly humified layers and four distinct charcoal layers. The lowest of these at ~140 cm is disseminated over ~3 cm and comprises charred wood and peat suggestive of *in situ* burning. At 75 cm, the charcoal layer is indistinct, comprising very fine charred particles.

Above 55 cm the peat becomes significantly less humified, comprising distinguishable plant material including roots and stems. The peat was relatively dry on collection and uncompacted and is likely to represent the extent of the aerated, acrotelm peat zone. Between 35 and 20 cm, the peat becomes distinctly more fibrous and dry and contains abundant charcoal particles and some sparse quartz and other mineral grains. A distinct inflection in LOI in this section of the core is also suggestive of disturbance. This inflection is most likely to reflect shrinkage of the bog size due to large scale drainage activities which commenced in the early 1900s. This would have resulted in more windblown material hence the presence of increase in minerogenic material. The charcoal is likely to have derived from the frequent fires associated with machinery used to drain the bog (Clarkson, 1997). The top 20 cm consists of the living cluster roots of *Empodisma*. In the top ~50 cm section there are at least seven distinct charcoal layers including two in the top 20 cm.

Section MR7 (Fig. 4.2.7)

MR7 was retrieved below the aerated zone at ~75 cm depth in the peat down to the visible Taupo Tephra, at 170 cm depth. The peat was well humified throughout. Measurements of organic content are comparable to those of section MR2, showing a steady increase in organic content up to ~30 cm above the visible tephra. Above 130 cm and up to 74 cm (top of retrieved sequence), LOI fluctuates between 97.4 - 98.8 %. No distinguishable charcoal layers were identified, possibly due to the narrowness of the core. A possible charcoal layer was identified during sample preparation at ~107 cm depth.

Monoliths MB1-3 (Fig. 4.2.4)

The three sequences obtained from the drain exposure comprised relatively dry compact restiad peat above the Taupo Tephra and below a disturbed surface. Structures and stratification of the undisturbed peat section appeared all the more distinct because of its dryness but made it difficult to evaluate degree of decomposition. Components of the peat included abundant charcoal layers, wood and wood fragments, and distinguishable plant material. Many features could be traced across the section. In all sequences charcoal layers formed some distinct layers but there were also less distinct sections containing charcoal fragments disseminated through several centimeters of peat, particularly in combination with plant and wood fragments and in poorly humified horizons.

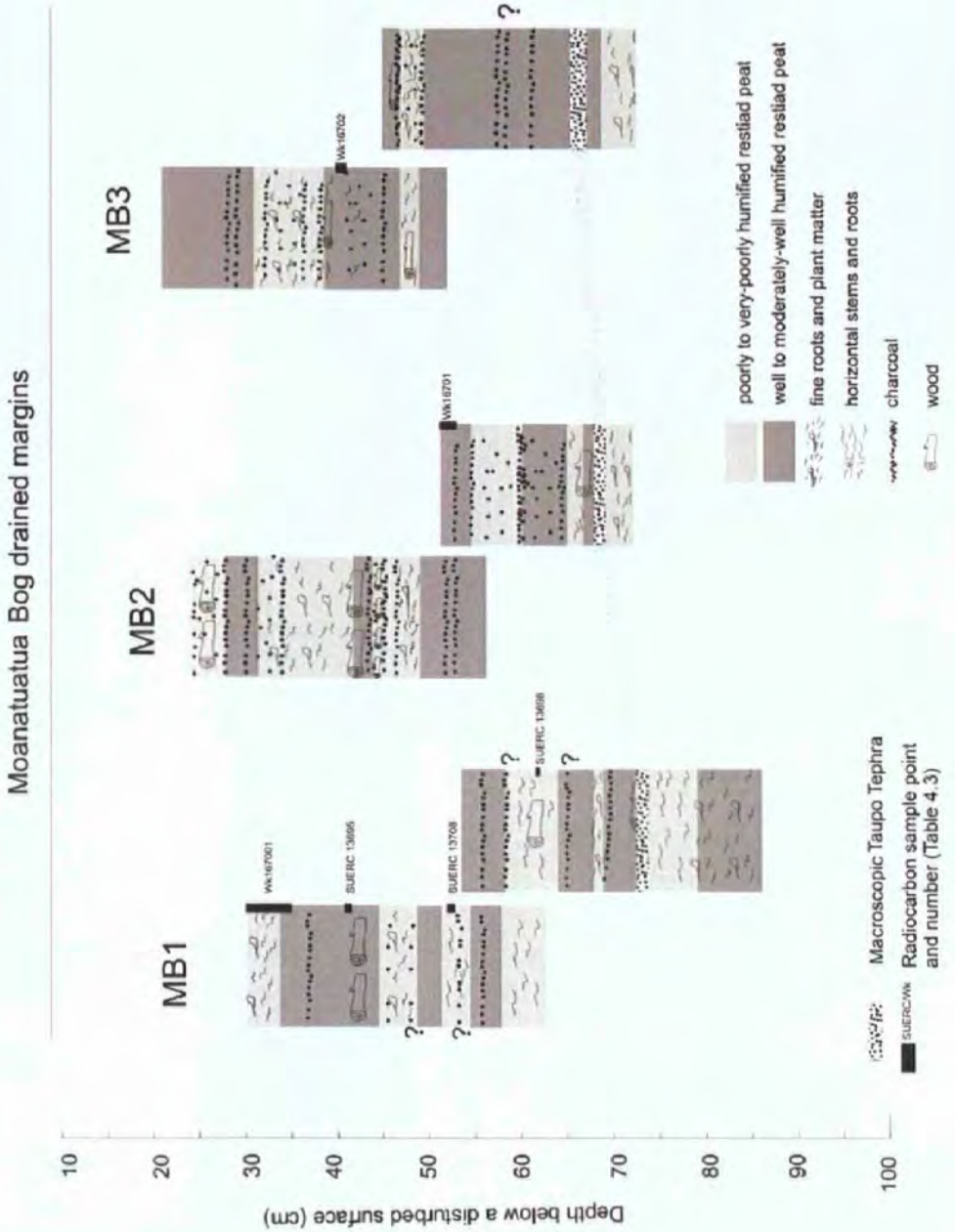

Figure 4.2.4 Stratigraphy of sections MB1-3 collected from bog margins (Fig. 4.2.1, Plate 4.2.2 a-e) showing levels and results of radiocarbon dating (Table 4.2.4). Question marks by charcoal layers indicate where these are not well defined.

4.2.4 Age depth models

Age depth models are developed for cores MR2, MR7 and MB1-3 using AMS and radiocarbon ages, tephrochronological ages for the visible Taupo Tephra (1717 ±13 cal yr. BP), and where present the cryptic Kaharoa Tephra (identification described later) as well as charcoal and pollen markers. In total 15 radiocarbon ages were obtained for the site (Table 4.2.2). These include four radiocarbon dates provided by University of Waikato Radiocarbon Dating Laboratory (New Zealand) and 11 AMS ages from plant macrofossils performed at the NERC radiocarbon facility in East Kilbride, Scotland. Table 4.2.4 provides a summary of radiocarbon and AMS dates from all sections.

Table 4.2.2 Radiocarbon ages and calibrated ages on samples from cores MR2 and MB1-MB3. Sample positions are shown in Figures 4.2.2, 4.2.5 and 4.2.8. Samples: WPMF, woody plant macrofossils; PMF, plant macrofossils; BP, bulk peat; WP, woody peat; PC, peat with charcoal.

Lab code	Sample ID	Core	Stratigraphic position (cm)	Sample material	Conv. RC age years BP	±1 sd	$\delta^{13}C_{VPDB}$ ‰*	Estimated BP**	Calibrated age range*** (2σ) cal yr BP	Median age
SUERC-13691	MR2_20	MR2	20-22	WPMF	84	37	-26.0	250	0-101	70
SUERC-13702	MR2_34		34-35	PMF	123	37	-23.9	300	0-265	95
SUERC-13703	MR2_54		54-54.5	PMF	126	37	-24.4	400	0-267	96
Wk:MR2	MR2-65		60-65	BP	344	35	-27.8		319-464	395
SUERC-13704	MR2_74		74-75	PMF	354	37	-27.6	500	305-472	392
SUERC-13686	MR2_86		85.5-86	WPMF	885	35	-25.8	750	678-897	749
SUERC-13693	MR2_104		104-106	WPMF	1132	35	-25.0	1000	931-1056	988
SUERC-13705	MR2_122		121.5-122.5	PMF	1248	37	-26.3	1350	988-1256	1118
SUERC-13694	MR2_133		131-133	WPMF	1560	35	-24.4	1450	1309-1423	1387
Wk:MB1	MB1_35	MB1	30-35	BP	879	35	-28.2		727-911	789
SUERC-13695	MB1_41		41-41.5	WPMF	1135	37	-26.4	1000	930-1059	992
SUERC-13708	MB1_53		52.9-53.5	PMF	1469	35	-27.0	1300	1282-1380	1322
SUERC-13698	MB1_62		62.2-62.7	WPMF	1582	37	-25.0	1500	1339-1522	1413
Wk:MB2	MB2-51	MB2	50-51	WP	1296	42	-27.0		1093-1300	1232
Wk:MB3	MB3-43	MB3	42-43	PC	1196	36	-27.8		1003-1256	1122

***isotopic fractionation $\delta^{13}C$ is expressed as ‰ wrt PDP, ± 0.2 for Waikato dates (Wk prefix to lab code) and ± 0.1 for NERC dates (SUERC prefix). **based on a linear interpolation using tephrochronological age of Taupo Tephra and existing ages. *** Calibration curve shcal 04.14c (Southern Hemisphere calibration curve).**

MR2

A detailed age-depth model is constructed for this section using six of the nine AMS ages obtained for the sequence together with the tephrochronological age from the visible Taupo Tephra (Fig. 4.2.5; Table 4.2.2). In addition, two charcoal layers close to the top of the core are linked to two historically documented fire events on the bog in 1962 (at 12 cm depth) and 1972 (at 10 cm depth). The lowest occurrence of the glass concentrations representing the Kaharoa Tephra also provides an additional marker at 85 cm (*ca.* 1314 AD) and this fits within the age model based on 2σ age ranges from the bracketing ^{14}C dates. Three of the AMS ages (22, 35, 54 cm) not used in age model on the basis that they resulted in overlapping near-modern ages but all 2σ distributions fit with the age-depth model. Only the lowest age (at 54 cm) is used to constrain a maximum age. The age determined from bulk peat sample from 60-65 cm (wk-16702) in the section was also rejected and the underlying AMS age is used because it is considered more precise based on its close relationship with the Kaharoa Tephra (Fig. 4.2.5). The stratigraphy and resulting tephra content also suggest that contamination of older material may have been an issue as a result of disturbance. The calibrated AMS ages are plotted using the median value against the midpoint of the depth, as recommended by Telford *et al.* (2004) (Hazell, 2004; Gehrels *et al.*, 2006). This has proved effective for previous age models constructed for peat sections in the region.

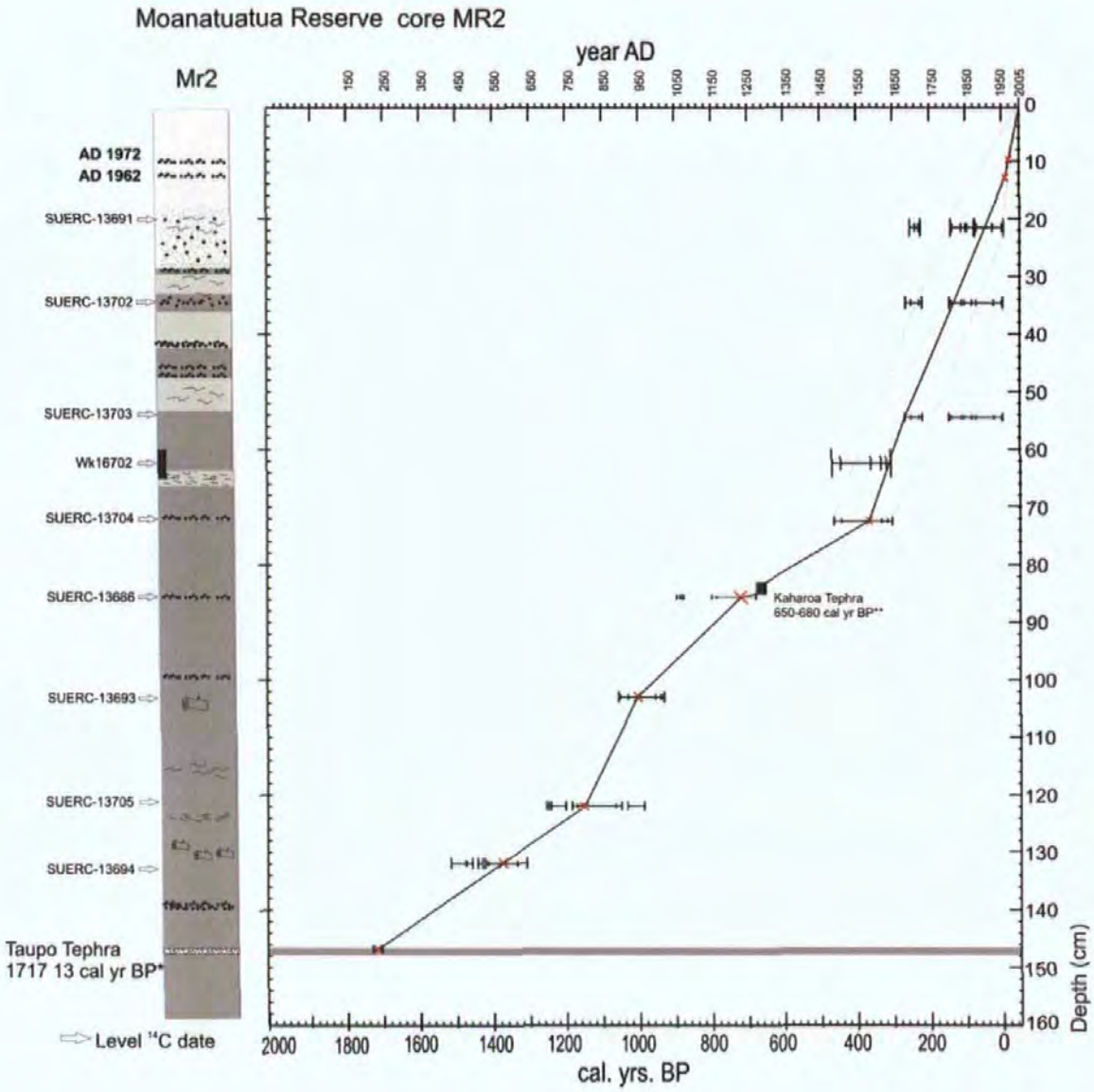

Figure 4.2.5 Age-depth model for core MR2 based on a linear interpolation through the median ages of six AMS dates (Table 4.2.2.), tephrochronological dates on the Taupo (*from Sparks *et al.* 2008) and Kaharoa (wiggle match date from Hogg *et al.* 2003) tephras and two historical charcoal layers (refer to text). Levels sampled for ^{14}C dating indicated by white arrows in relation to stratigraphy.**

MR7

An age-depth model is constructed for the replicate sequence to MR2 using tephrochronological ages of the Taupo Tephra and the first occurrence of the Kaharoa Tephra in the sequence. These tie points at *ca.* AD 233 and *ca.* AD 1314 were used to calculate an approximate age for intervening shard concentrations (Fig. 4.2.7).

MB1

The age-depth model for this partial peat sequence taken from the margins of the reserve is constructed from one radiocarbon age from a bulk peat sample (Wk prefix), two AMS ages (dates with SUERC prefix) from plant macrofossils, and the tephrochronological age for the visible Taupo Tephra (Fig. 4.2.8; Table 4.2.2). The Kaharoa Tephra was not detected in the sections from the bog margins and as a result could not be used as an additional age marker. One of the AMS dates was rejected on the basis that it was discordant with age models derived for MB2 and MB3 based on the pattern of glass content. It is possible that the charcoal in the sample was a source of contamination affecting age determination. Charcoal is known to retain contaminants very strongly (e.g. mobile carbon sources in the sediments) (Walker, 2005). As for MR2, the age model is plotted using the median value against the midpoint of the depth.

MB2 and MB3

The age depth model for replicate sections to MB1 were constructed from one radiocarbon age and the tephrochronological age for the visible Taupo Tephra as above.

4.2.5 Tephra derived glass-shard content

The results of down-core tephra-derived glass shard counts from each section obtained from Moanatuatua Bog are presented as concentrations of glass shards calculated as particles per mg dry weight (mg d-wt.) for sections MR2 (Fig. 4.2.6), MR7 (Fig. 4.2.7) and MB1-3 (Fig. 4.2.8). Two distinct glass shard types were recognised at the site, primarily on the basis of colour: clear and brown shards which were tentatively identified prior to geochemical fingerprinting as originating from rhyolitic and andesitic sources, respectively (Shane, 2000). The possible occurrence of any basaltic tephra in the peat sequences from this site was very unlikely for the time period investigated. Shard counts are differentiated on the basis of colour rather than source in the following descriptions.

Clear shards are typically the larger of the two types of shards (~50 - 200 μm) consisting of vesicular and bubble wall glass fragments, which were isotropic under crossed polars and show a moderate to high degree of stretching. Brown shards were highly variable in nature but were typically smaller (~30-60 μm) and orange-brown in colour with a blocky morphology and poorly vesicular. Many of the shards encountered from this site contained abundant small crystals. These were present in two distinct forms: rod shaped microlites 10-20 μm in length and ~1-5 μm in diameter, and larger euhedral and subhedral crystals of feldspar and pyroxene, 15-20 μm in length and ~5-10 μm wide (Sharp *et al.*, 1996). Both types of crystals appear randomly oriented in the majority of shards. Variability in the typical character of brown shards was observed at different levels in the sections. Brown shards also appeared to show a greater degree of chemical weathering than clear shards. Weathering features of brown shards included surfacial "gaps" arising from the loss of microlites and feldspar crystals, and the structural break down of the shards shown by

fractures and pitting which could be the result of the acidic conditions of the peat (Hodder *et al.*, 1991). Photographic examples of the shard types found in samples from this site are shown in Plate 4.2.3.

Shard contents derived for each sequence are shown for clear and brown shard concentrations alongside measurements of organic content derived from loss on ignition. A measure of total shard concentrations (brown and clear shards combined) provides an indicator of total-derived tephra shard influx and a reference to visually compare shard content from the two different sources. Because of the high concentrations of glass shards within and immediately above the visible Taupo Tephra, the results of these shard counts are omitted from the diagrams for clarity.

The glass shard content for each section is described from the base to the top of the sequence for clear and then brown shards. These include reference to any observations of shard character and morphology using descriptions based on a combination of generic and technical terms for ash-sized glass shards (Heiken, 1972; Fisher & Schmincke, 1984; Heiken & Wohletz, 1985).

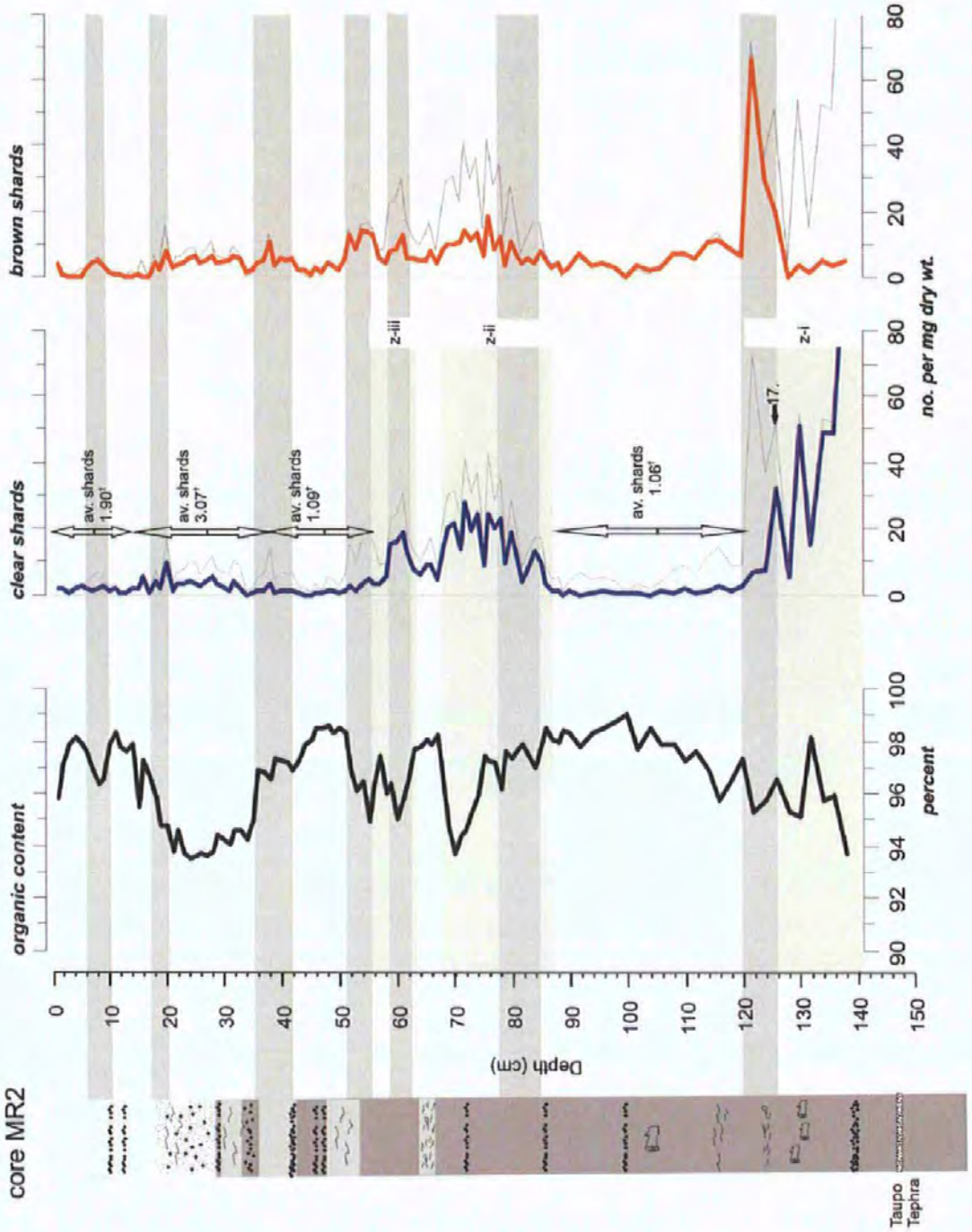

Figure 4.2.6 Results of glass shard concentrations derived for core MR2 shown alongside stratigraphy and organic content. Shard counts are shown in colour, blue for clear shards and orange for brown shards. The background grey line represents total shards, brown and clear combined. Organic content is derived from loss-on-ignition (LOI) measurements. Light grey bands mark zones (z-i to z-iii) of elevated concentrations of clear shard. Darker grey bands represent elevated shard content for brown and clear shards. †average concentrations of clear shards derived to number per mg dry wt. in sections of the core marked by vertical arrows. Key for core stratigraphy shown in Fig. 4.2.3.

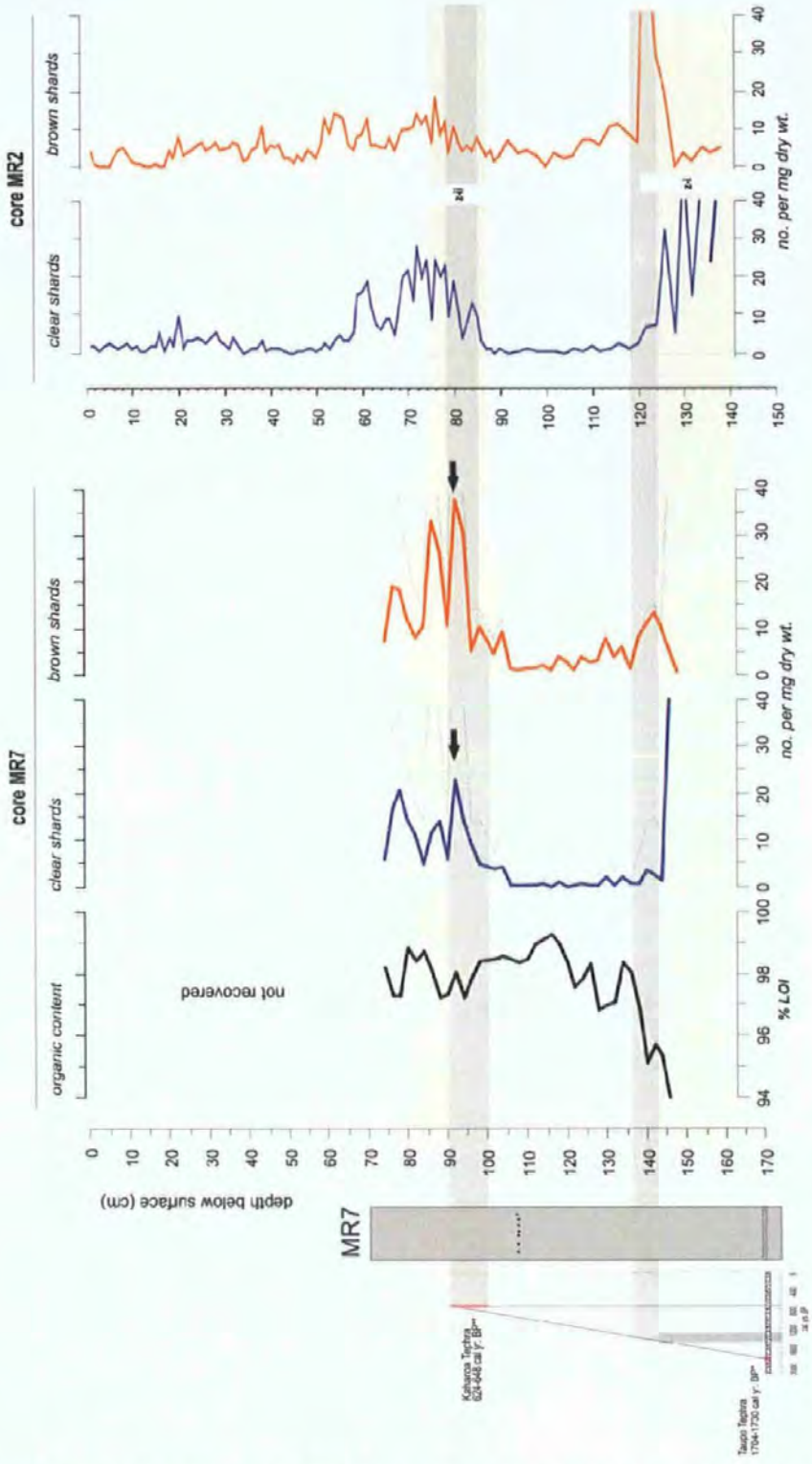

Figure 4.2.7 Results of clear and brown shard counts for core section MR7 shown with organic content derived from loss on ignition (LOI) and age model (Table 4.2.2). Shown alongside shard content derived for section MR2 to illustrate replicability. Grey bands mark possible tie points between the cores based on the pattern of shard concentrations. Refer to Figure 4.2.3 for the key to stratigraphy. Black arrow marks the level sampled for EMPA.

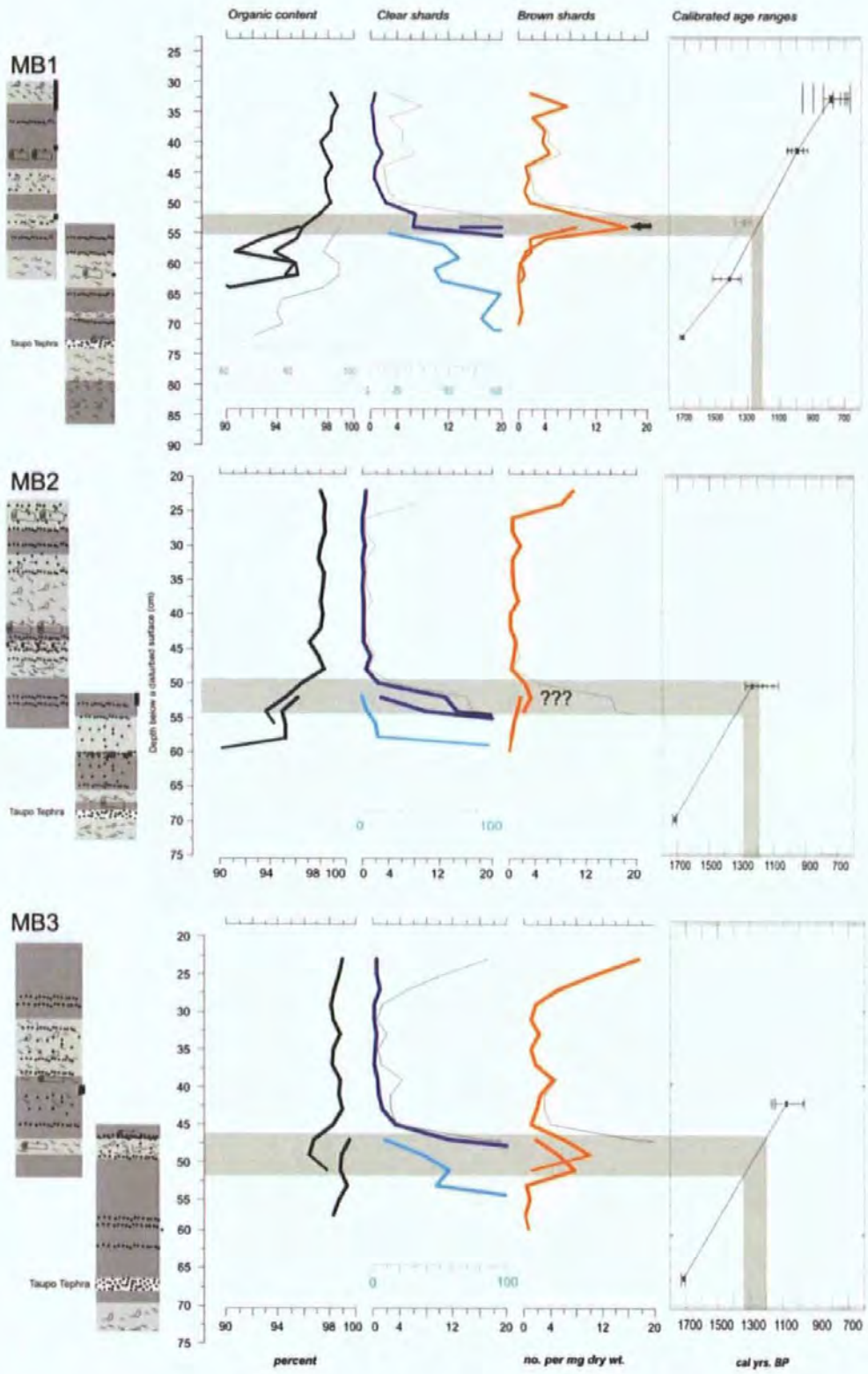

Figure 4.2.8 The result of glass shard counts from monolith sections MB1-3 showing overlap between the two monoliths. Shown alongside stratigraphy (Fig. 4.2.4), organic content and age models based on a limited set of radiocarbon dates (Table 4.5). Black arrow marks the level sampled for EMPA.

Glass-shard content MR2

The results of down-core glass-shard counts for sequence MR2 are shown in Figure 4.2.5. The shard content derived from this section is based on analysis of 114 contiguous samples 1-cm thick from the top of the sequence to 90 cm depth and then 2-cm thick to the Taupo Tephra at 150 cm. Individual glass shards were detected and counted in almost every sample viewed from this section containing a mix of both clear and brown shards in varying proportions. Concentrations of these two shard types are represented by distinctly different patterns down through the core. Measurements of organic content provide an effective gauge for tephra content for large parts of this sequence (Fig. 4.2.6).

Clear glass shards are present throughout this section of peat with three distinct zones of elevated shard concentrations (z-i to z-iii in Fig. 4.2.6). Small but varying "background" concentrations of shards were seen – these defined as samples containing ~ <4 shards per mg d-wt. The first and lowest of the zones (z-i) of clear shards extends above the upper limit of the visible Taupo Tephra at 147 cm for at least ~ 26 cm up through the peat represented by fluctuating but generally very high concentrations of shards. These typically comprise a mix of pumiceous and striate shards of fine to medium ash size and with a moderate degree of vesicularity and stretching, typical of rhyolitic sourced glass shards.

The second zone of clear shards (z-ii) forms a wide but broad spread of fluctuating shard content between 86 and 70 cm (a total of 16 cm) in the peat, coincident with decreases in LOI values. Elevated brown shard concentrations coincide with this zone of clear shards in this section of the core which together contribute to high total shard concentrations (dashed line; Fig 4.2.6) that are reflected by LOI measurements. This zone is marked by several 'peaks' in clear shard content. The lowest of these 'peaks' at ~85 cm is separated by ~1 cm

of peat where shard concentrations fall below background levels. Between 82-70 cm, concentrations of clear shards, however, remain consistently elevated above background levels. The level of maximum shard concentrations is at 70 cm, coinciding with a distinct decrease in LOI values. Glass shards in this section of the core comprise a mixture of cuspate and pumiceous shards with a moderate to high degree of stretching and vesicularity. Shards in this zone consist of fine-ash sized particles (~50-70 μm across), typically smaller than for the lower zone of clear shards (Plate 4.2.3 h-i). Shards appear well preserved throughout the zone with no distinguishable weathering features observed during microscopy.

The peak of clear shards at 59- 62 cm forms a discrete concentration of shards separated from zii by ~4 cm of peat where shard content decrease significantly but do not return to background concentrations. This thickness of peat (4 cm) represents in excess of 50 years of peat accumulation using the age-depth model as a basis for assessing accumulation rates in this section of the core (Fig. 4.2.9). The peak in shards is therefore likely to represent a separate phase of deposition. Shard morphology is comparable to morphologies of the previous zone of clear shards and with no discernable signs of shard weathering.

The background concentrations of clear shards between these zones of elevated shard content also show an interesting change in pattern and concentrations up through the core which could be attributed to changes in the environment and land use surrounding the bog (refer to Figs. 4.2.6; 4.2.9). Between shard zones z-i and z-ii (121-86 cm depth; 35 cm of peat), clear shard content remains very low with an average of 1.06 (± 0.8) shards per mg d-wt. Shard concentrations return to low levels above z-iii, from 52-39 cm (13 cm in the core) with an average content of 1.09 (± 0.7) shards per mg d-wt. The background shard

content, however, increases and becomes more irregular 15-37 cm depth with average shard content of 3.07 (± 2.13) shards per mg d-wt. Marking the end of this zone concentrations of both clear and brown shards show a distinct increase (~20 cm) that possibly relate to the proximity of disturbance activities. In the final phases of drainage of the bog, disturbance activities were likely to have been closer to core site in the remaining remnant. Above this disturbed zone clear shard content appear to stabilize but shard content is still slightly higher than determined for lower sections of the core with an average of 1.80 (± 0.65) shards per mg d-wt. up to the surface of the sequences.

The content of brown shards determined throughout MR2 reveals a much less distinct pattern of changing shard content with typically lower maximum shard concentrations than rhyolitic (clear shard) counterparts. In this section, brown shards are present in almost continuous concentrations represented by a highly fluctuating pattern of shard content. Shard concentrations remain below ~14 shards per mg d-wt. throughout much of the core apart from one distinct peak in brown shards at 122 cm which coincides with the upper limit of the clear shard zone above the Taupo Tephra. The calculated shard content for this particular level may, however, be distorted as it is not reflected by a similar change in LOI values. The woody nature of peat at this levels meant that the sample extracted contained very little peat and this is likely to have affected the calculation of shard content determined from the dry weight of the sample. Elevated shard concentrations persist throughout the sequence with noticeable increases coincident with the upper zone of clear shards, between 85-50 cm and at levels 35-40 cm and 7-8 cm where brown shard content exceeds ~5 shards per mg d-wt.

Although the visible features of brown shards are highly variable, there are some distinguishing characteristics observed between some shard concentrations (Plate 4.2.3 a-g, j). For example, brown shards at 122 cm are quite distinct from brown shards observed at other levels. The 122-cm-depth shards are typically smaller (25-40 μm) and comprise a mix of pale yellowish-brown, moderately-vesicular shards and some very dark brown platy, bubble wall shards which are microlite poor. The pale brown shards (Plate 4.2.3j) contained very fine microlites, and some shards had rod shaped holes where microlites were once present, indicating chemical etching. The concentration of brown shards at 65-80 cm contain large (50-70 μm across), pumiceous, light orange-brown shards with large euhedral feldspar crystals (Plate 4.2.3 g). These shards are mixed with smaller blocky shards with abundant microlites. At 59 cm depth brown shards are typically blocky in shape with a very dense microlite and crystal content (Plate 4.2.3f). A predominance of shards at 51-55 cm show a moderate degree of stretching and vesicularity and contain fewer microlites. At 38 cm depth, shards are typically blocky shaped but with very fine, dense microlites. There is a very varied mix of shards observed at 20-30 cm, some of which appeared chemically or physically weathered (Plate 4.2.3 c) suggestive of reworking. At 8 cm, shards range in size but many display a moderate degree of stretching. These shards contain very distinct contents of microlite crystals which appear to be orientated in the direction of stretching (Plate 4.2.3b). Shards at the top of the sequence (0-2 cm) comprise predominantly large (40-60 μm) and blocky shaped clasts with abundant microlites (Plate 4.2.3a).

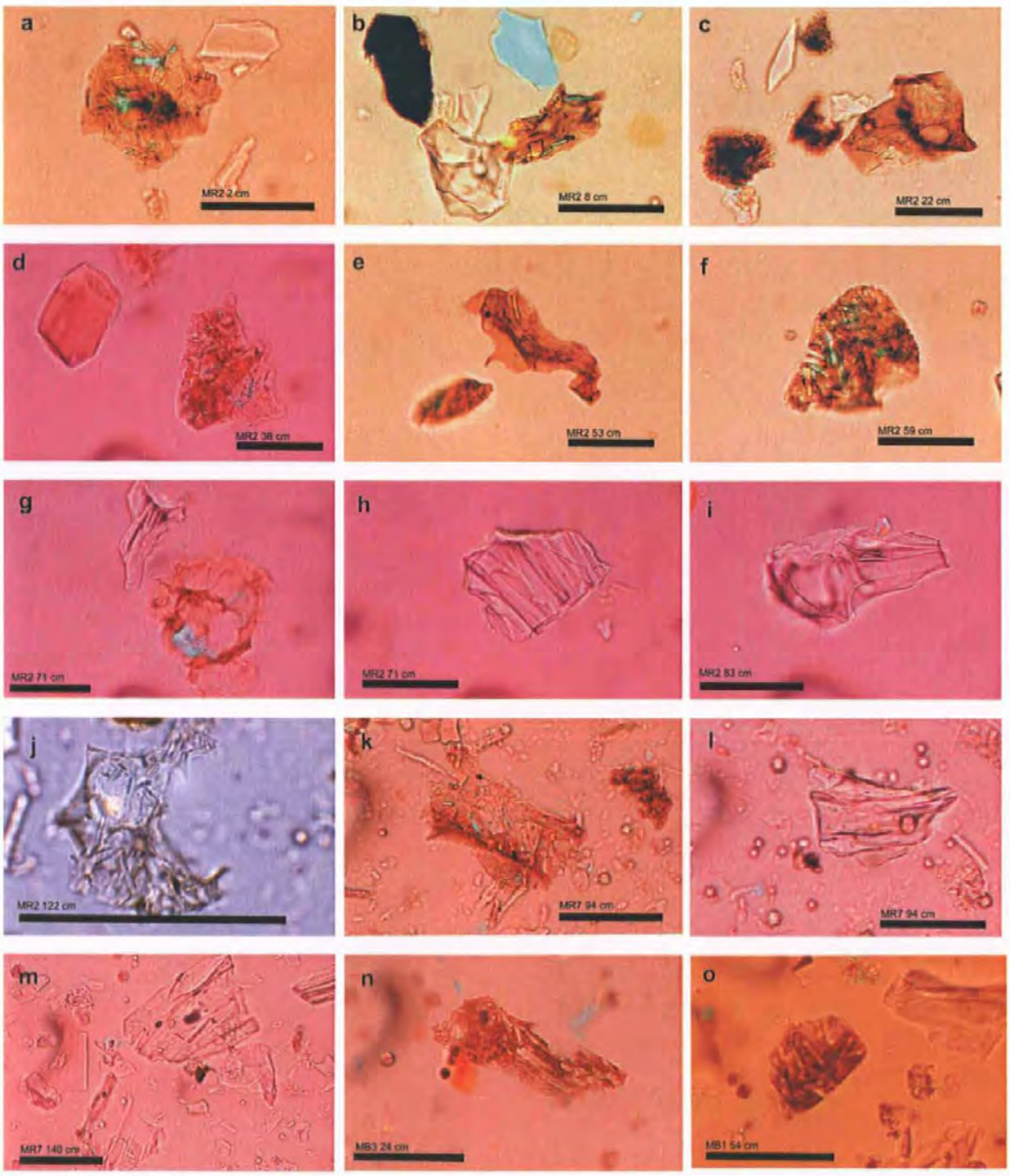

Plate 4.2.3 Photomicrographs of various glass (tephra) shards (types and morphologies) observed in samples from sections MR2 (a-j) in order of depth in section), MR7 (k-m) and MB3 (n-o) as referred to in the text.

All shards are photographed from glass slide setting using manual SLR camera attached to a petrographic microscope and viewed under plain light at x400 magnification. Black bar on each image equals 50 µm in length. Section number and depth are labelled on each image. Additional images of shards from selected levels are provided in the appendix.

Shard content MR7

Glass shard content derived from sequence MR7 was determined from 36, 2-cm-thick, contiguous samples from 74 to 144 cm depth (Fig. 4.2.7). As for MR2, both clear and brown glass shards were encountered in almost every sample examined from this sequence. The pattern of shard concentrations is very similar to that from the lower half of the MR2 sequence. Similarly, the subtle fluctuations in organic content in this section also appear to be an effective gauge to changing concentrations of glass shards.

Two zones of clear shards are revealed in this sequence represented at comparable stratigraphic level to those detected in MR2 (z-i and z-ii; Fig. 4.2.6). Clear shards persist in very high concentrations above the Taupo Tephra (at 173 cm) up to 144 cm depth, a distance of ~30 cm. These shards typically comprise a mix of pumiceous and striate fine-medium ash-size grains (Plate 4.2.3 m). The second zone of clear shards appears in the peat at 104 cm depth and is represented by differing concentrations of shards, peaking at 78 cm and extending up to the top of the retrieved sequence. These shards in this second zone are predominantly smaller (40-70 μm) in size than the shards found above the Taupo Tephra (Plate 4.2.3 i). In the intervening section of peat between these two zones (142-106 cm; 36 cm of peat) the concentrations of clear shards remain <1 shard per mg d-wt.

As for MR2, brown shards are represented in almost continuous but highly variable concentrations with an average of 9.5 shards per mg d-wt in this section (Fig. 4.2.7). In two sections of the core, brown shard concentrations exceed 10 shards per mg d-wt and are marked by distinct peaks in shard content. The lowest of these peaks is at 142 cm and, as with MR2, coincides with upper limit of clear shards above the Taupo Tephra. In this section, however, shard concentrations are significantly less prominent. Shards at this level

are comparable to those found in MR2 and consist of relatively small, pale yellow-brown coloured shards with some evidence for possible surface chemical weathering. As for MR2, the upper significant zone of brown shards coincides with increases in clear shards and forms three significant peaks up to the top of the sequence. In contrast to MR2, brown shards at this stratigraphic level are represented by a higher proportion of the total shards. A mix of shard types occurred in these levels including some relatively large (50-70 μm) platy and vesicular shards with fine microlites (Plate 4.2.3 k).

Glass shard content MB1-3

The results of down-core glass-shard counts for the three sequences MB1, MB2 and MB3 are shown in Figure 4.2.8. The shard contents derived from these sections are based on analysis of 27, 23 and 22 contiguous, 2-cm-thick, samples (respectively) from the top of the sequence (below undisturbed peat) to ~10 cm above the Taupo Tephra. For all sections this analysis includes replication from the overlap between monoliths. As for previous analyses from this site, individual glass-shard particles were detected and counted in almost every sample viewed containing a mix of both clear and brown shards.

For all three sections the records of changing shard content for clear and brown shards were similar. The clear shards in all sequences are shown to extend upwards in the peat at least 20 cm above the visible Taupo Tephra in high but steadily declining quantities. Above that point in all cores clear shard concentrations remain at <1 shard per mg d-wt. up to the top of the sections. There is no evidence in any of the sequences for the additional zone of clear shards detected in sequences from the reserve. It is therefore most likely that the section of peat containing this tephra has either become incorporated into the ploughed

soil on the surface of the peat, or oxidized and lost completely. This would represent a loss of at least one metre of peat if compared with the records from the reserve.

Brown shard content in the sections is represented by three to four zones which exceed average shard concentrations of ~4 shards per mg d-wt. (varies between sections). The lowest of these zones in all three sequences coincides with the final decline in clear shard concentrations above the Taupo Tephra. The same pattern is observed in the two sequences from the reserve (MR2 and MR7; Fig. 4.2.7). Shards found at this stratigraphic level are also typically small (25-40 μm), pumiceous and dark brown (Plate 4.2.3 o). This concentration of brown glass is also bracketed by two closely spaced charcoal layers in all three sequences. In MB2, the peak in shards is not as distinct as in the other sections and it is possible that the calculation of concentration was affected by the abundant charcoal particles in the sample. It is equally possible, however, that the deposition of the tephra was unevenly distributed on the bog surface.

Additional 'concentrations' of brown shards are represented at the very top of sections MB2 and MB3 but are not observed at MB1 which represents a shorter preserved sequence above the Taupo Tephra. There is a variety of shard types in these levels including some relatively large (50-70 μm) platy and vesicular shards with fine microlites. There are also two to three less prominent increases in brown shards amounting to 2-6 shards per mg d-wt evident in all three sections. General observations of brown shards in these sections revealed a much greater degree of chemical etching and loss of many of the microlites, particularly in shard concentrations close to the top of the weathered surface (Plate 4.2.3 n) where the peat is likely to have been most affected by disturbance.

4.2.6 Geochemical character, correlatives and interpretation

The results of major element composition of cryptotephra populations sampled from Moanatuatua Bog are based on 21 samples comprising 213 individual analyses determined by electron microprobe analysis. These include 19 samples from section MR2 (shown by numbered levels in Fig. 4.2.9 which correspond with sample numbers detailed below) with a few selected levels from the other sequences at the site. For this site the most complete sequence MR2 is used as a 'master section' for the analysis of glass-shard major element geochemistry. Table 4.2.3 provides a summary of analysis for glass populations from each level sampled. Table 4.2.4 provides a summary of the identified sources and eruption correlatives for each level together with interpolated age range and reference sources for tephra ages and geochemistry. The bivariate plots of selected oxides from this analysis are shown in Figures 4.2.10 and 4.2.11 and represent the most diagnostic oxide combinations to differentiate between individual geochemical populations for these types and sources of tephra (Shane, 2000). Other elements were, however, considered in correlating deposits and for distinguishing between individual populations. All analysis presented here have been normalized to 100 weight (wt.) % loss free basis to account for hydration which is common practice for the analysis of New Zealand tephras (Froggatt, 1992; Shane, 2000) and is now recommended for all tephra analysis by EMP by Pearce et al. (2008). The following descriptions of these analyses also refer to normalized values. Raw, non-normalized analyses can be found in appendices ii in this thesis.

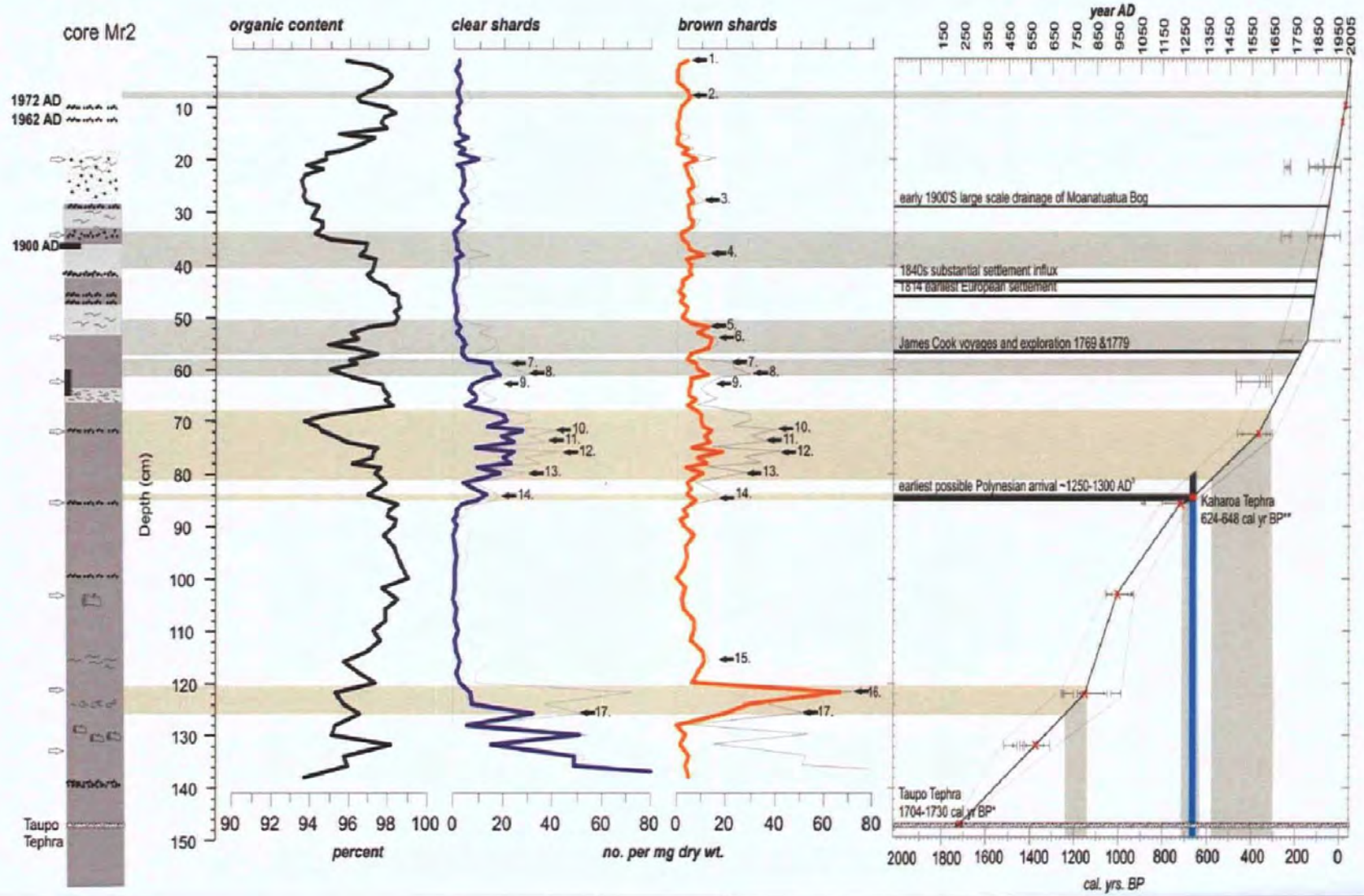
core Mr2
organic content
clear shards
brown shards
year AD
1972 AD
1962 AD
1900 AD
Taupo Tephra
Depth (cm)
percent
no. per mg dry wt.
cal. yrs. BP
early 1900's large scale drainage of Moanatuatua Bog
1840s substantial settlement influx
1814 earliest European settlement
James Cook voyages and exploration 1769 &1779
earliest possible Polynesian arrival ~1250-1300 AD*
Kaharoa Tephra
624-648 cal yr BP**
Taupo Tephra
1704-1730 cal yr BP*

Figure 4.2.9 Results of glass shard concentrations derived for core MR2 shown alongside, stratigraphy, organic content and age depth model. Shard counts and LOI are shown as for Fig. 4.2.6. Grey bands represent significant glass concentrations. The age-depth model is based on a linear interpolation through the median ages of six AMS dates (Table 4.2.2.), tephrochronological dates on the Taupo (*from Sparks *et al.*, 2008) and Kaharoa (wiggle match date from Hogg *et al.*, 2003) tephras, two historical charcoal layers (refer to text) and limited by AD 1900 date marking the impact of large scale drainage shown by drop in LOI and supported by changes in stratigraphy (see text). Positions sampled for ^{14}C dating and EMPA are indicated by arrows. Numbered arrows indicated for EMPA correspond with sample numbers in Tables 4.2.3 and 4.2.4. Age model show time lines of significant anthropogenic events, (sources of dates: [1] Shearer (1997); [2]Lowe *et al.*, (2000); [3] Taylor *et al.*, (1997) and references therein.**

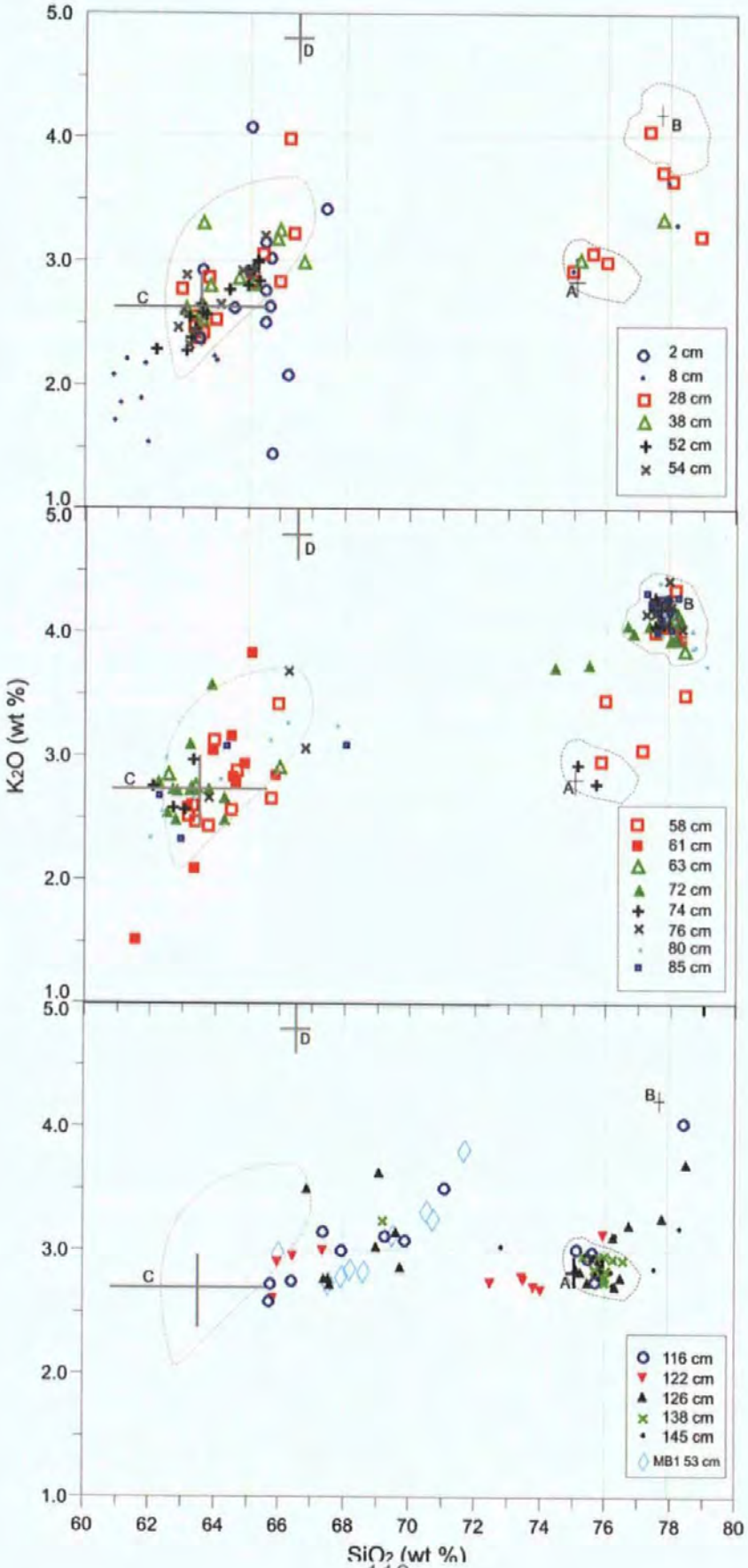
5.0
4.0
3.0
2.0
1.0
D
B
A
C
2 cm
8 cm
28 cm
38 cm
52 cm
54 cm
58 cm
61 cm
63 cm
72 cm
74 cm
76 cm
80 cm
85 cm
116 cm
122 cm
126 cm
138 cm
145 cm
MB1 53 cm
K2O (wt %)
60
62
64
66
68
70
72
74
76
78
80
SiO2 (wt %)

Figure 4.2.10 Bivariate plot of K_2O versus SiO_2 (wt%) glass composition from core MR2, Moanatuatua Bog: (a) 2-54 cm; (b) 58-85 cm; (c) 116-145 cm and section MB1 53 cm (see Figs. 4.2.7 and 4.2.8 for sampling positions) using electron microprobe analysis. Ranges A-D = compositional ranges of: A = Taupo Tephra (unit Y), B = Kaharoa Tephra (OVC) (from Lowe et al., 2008); C = Tongariro VC Tufa Trig Formation (Tf) members 5, 8, 14, 19 from Donoghue *et al.*, (1997); D = Egmont sourced glass (Burrell Lapilli) from Platz *et al.*, (2007). Envelopes are shown for visual comparison.

The major element composition of glass samples from this site reveal both acidic rhyolitic (SiO_2 = > 69 wt.%) and intermediate glasses (SiO_2 = 58-69 wt.%) and confirms the initial identification for clear and brown shards (Table 4.2.3; Fig. 4.2.10). The analyses for both types of tephra-derived glasses are comparable to previously obtained compositional ranges for TVZ eruptives (Shane, 2000; Lowe *et al.*, 2008b) (Fig. 4.2.10). For rhyolitic shard analysis total alkalis (K_2O and Na_2O) were especially in accord with previously recorded values and suggest that there has been no significant chemical alteration for these shards resulting from the acid conditions in the peat or from sample pre-treatments (Hodder *et al.*, 1991; Blockley *et al.*, 2005). With limited geochemistry available for intermediate tephras the alteration of glass composition due to chemical weathering was uncertain.

The analysis of rhyolitic glass reveals a range of compositions (SiO_2 72-78 wt.%) with low standard deviations (range 0.17-0.94 wt.%) for individual glass populations (Table 4.2.3; Fig. 4.2.8). Raw analytical totals range from 93.3 to >100 wt.%, with an average total of 97.9 wt.%. Analyses were not, however, rejected on the basis of analytical totals which are known to vary considerably for rhyolitic TVZ eruptives (Lowe *et al.*, 2008b). For these glasses major element composition was sufficient to identify two distinct populations from Taupo and Okataina volcanic centres and preclude a small number of older reworked

tephras from analysis (Fig. 4.2.10) based on diagnostic oxide combinations. These analyses confirm the identification of the visible Taupo Tephra in this site and for the first time, the presence of the Kaharoa Tephra represented by the additional zone of shards recorded in the sequence. Small quantities of glass shards from both rhyolitic tephras are found throughout the peat above the main concentrations of the tephras up to very top of the sequence (Fig. 4.2.10). These represent the main background source to concentrations of glass representing primary fall deposits.

Intermediate glass populations consist predominantly of dacitic glasses (SiO_2 = 63-69 wt.%) with at least one population with an andesitic chemistry (SiO_2 = 57-63 wt.%) and a few individual analyses fitting into trachy-dacite and trachy-andesite chemistries (Fig. 4.2.11 a). Individual populations typically comprise a heterogeneous set of glass analyses (SiO_2 = 58.7-71.0 wt.%; $Na_2O + K_2O$ (total alkalis) = 4.78-7.89 wt.%) characterized by high standard deviations for individual oxides (e.g. SD: 0.75-2.14 for SiO_2; Table 4.2.3) compared with rhyolitic counterparts. Raw analytical totals for these glasses, however, remained consistently high ranging from 97-100 wt.% with an average of 98.6 wt.%. These high totals suggest that hydration have not unduly affected these glasses which are typically more vulnerable to chemical weathering than rhyolitic glasses (Hodder *et al.*, 1991).

The majority of dacitic glasses were characteristic of tephras of the Tufa Trig Formation from Ruapehu volcanic centre (SiO_2= av. 63.0 wt.%; total alkalis = av. 6.5 wt.%) (Donoghue & Neall, 1996) (Fig. 4.2.11). These tephras represent eruption activity of Ruapehu volcano subsequent to the Taupo Tephra eruption (1717 ± 13 cal yr BP; Sparks *et*

al., 2008) which are geochemically distinct from preceding Ruapehu eruptives (Donoghue & Neall, 1996). As with previous Tongariro VC-derived members detected in distal deposits these analyses are likely to plot within the high-Si range of tephra deposits from proximal sites and from whole rock analysis (Lowe, 1988b; Froggatt & Rogers, 1990; cited within Shane *et al.*, 2002). Egmont-sourced tephra, which typically have much higher K_2O composition, were not evident from the analyses from this site. All intermediate glasses were evaluated for "contamination" from microlite phases using procedure by Platz et al. (2007) which estimates plagioclase proportions in contaminated glass (Fig. 4.2.11 b). Outliers affected by microlite contamination or analytical error were also identified using a range of plots of incompatible oxides (e.g. FeO_2 v Al_2O_3 and K_2O v Al_2O_3; Figs. 4.2.11 b, c) (Platz *et al.*, 2007).

There is a limited number of published compositional data or age determinations for recent andesitic sourced tephras and correlation is uncertain for many andesitic ash-fall events (Donoghue *et al.*, 2007). Identifications of individual populations are, as a result, tentative and attributed to individual eruptives based on a number of factors that includes any compositional disparity or distinctness, where possible, together with stratigraphic position and likely age where the age range for a deposit is well constrained. Where possible these attributes are linked with available compositional data for Tf members sampled from proximal sources (Donoghue *et al.*, 1995b; 1997; 2007). Consideration of potential Tf candidate correlatives is also given to the thickness of the deposit in proximal sequences which are thought to have resulted in more widespread dispersal (Donoghue *et al.*, 1995b).

---

[2]Total Fe = Fe_2O_3 + FeO

The dispersal range of the thin Tf members was thought to have been limited to the ring plain of the volcano (Donoghue *et al.*, 1995b). Compositional ranges from these tephra units are plotted for the mean and standard deviations in Figure 4.2.11 (d). However, direct correlation between these published datasets and analyses obtained from the sites presented here remain tentative. With only a limited set of published analyses any inaccuracies cannot be ruled out. Differences in analytical conditions may also limit correlation as well as possible discrepancies between the composition of proximal and distal deposits. Interpolated age ranges for all tephra units described below are based on 2σ ages ranges derived from the age-depth model for individual sections unless otherwise stated (Figs. 4.2.7, 4.2.8 and 4.29) (see section 4.2.6).

The following descriptions refer to numbered samples shown in Figure 4.2.9.

Sample 1 (MR2 0-2 cm): TnG VC, Ruapehu, June 17th 1996

A sample from the very top of the sequence (Fig. 4.2.9) was analysed to test for evidence that very light ash fall from the most recent eruption from Mt Ruapehu (1995-1996 activity; Tufa Trig member Tf 19) is preserved at the site. The sample obtained from the top 2 cm of peat recovered abundant, brown glass for analysis of major element geochemistry. The results of this analysis revealed the brown shards to be of dacitic chemistry with a relatively heterogeneous glass composition (SiO_2= 65.35 (SD 1.03); FeO = 6.25 (0.42); K_2O = 2.75 (0.64)) (Table 4.2.3; Figs. 4.2.10; 4.2.11). A number of outliers in the analyses were encountered, and were attributed to contamination from the abundant microlites that were very distinct in this particular glass population (Platz *et al.*, 2007). With the outliers removed the glass population showed at least one relatively homogenous

cluster of analyses (Fig. 4.2.11 d). The majority of these glass analyses do, however, fit within the compositional envelope for recent Mt. Ruapehu derived tephras of the Tufa Trig Formation (as derived from Tufa Trig members Tf 2, 4-6, 9, 10, 14 and 19; Fig. 4.2.11) (Donoghue *et al.*, 1997) and overlap with analyses from several additional levels in the section. In addition, it was not likely that the shards were derived from reworking of preexisting deposits in the peat because the glass population is geochemically distinct from that of the underlying shard population at 8 cm (sample 2).

There are three sets of published glass compositional data that exist for the most recent ash falls from Mt Ruapehu which provides possible means of correlating the analyses derived from the uppermost sample in the core (Fig. 4.2.11a). These include EMPA of samples from two episodes of ash fall in October 1995 (11-12th and 14-15th) from Donoghue (1997) and Platz *et al.* (2007) (14th October) which result in slightly different compositional ranges possibly resulting from differences in analytical conditions (Fig. 4.2.11 d). The analyses from Platz *et al.* (2007) were screened for contamination by microlite phases. However, only a few analyses from sample 1 appear to overlap with the compositional range derived for this early phase of Tf19 from these studies which result in slightly lower mean SiO_2 values: 63.25 (SD: 1.91) (Platz *et al.*, 2007) (Table 4.2.3). This variation could result from variations discussed above, i.e. including small differences in analytical conditions. Alternatively, Donoghue *et al.* (2007) noted compositional differences between the different eruption phases of the eruption episode (e.g. Donoghue *et al.*, 2007). The only analyses from the widespread 1996 ash fall event were derived by XRF on bulk samples (Gamble *et al.*, 1999), which is less useful for direct correlation (Fig. 4.2.11). The only additional data available for the recent eruptive deposits were derived as part of this recent study. I collected a 1996 tephra sample from the flanks of Ruapehu volcano in 2005 (Table

4.2.3). This sample was considered very likely to contain predominantly glass from the 1996 ash fall events from the volcano (Gamble *et al.*, 1999). Glass from the sample was analyzed using the same analytical conditions as glass from the peat samples. The resulting analyses form a distinct cluster (SiO_2 = 64.77 (SD 1.46); K_2O = 2.69 (0.68)) which encompasses the compositional ranges for the majority of TnG derived glasses analysed from the peat site including those of sample 1.

It was very likely that ash was deposited on the bog during the 1996 Ruapehu eruption. The climactic episode of the eruption from Mt. Ruapehu culminated in a large ash plume being generated on 17th June 1996. This was one of the largest recorded (historical) eruption events from Mt. Ruapehu since the 1945 eruption with a Volcanic Explosivity Index (VEI) of 3 and tephra volume ~5 x 10^6 m^3 (Siebert & Simkin, 2002-; Cronin *et al.*, 2003). On June 16th the ash plume was transported by strong southerly winds dispersed ash over a wide areas >300 km from the volcano in a predominantly east, north east direction (Cronin *et al.*, 2003). Ash falls a few millimeters thick were recorded within 150 km of the volcano, but as reported by Johnston *et al.* (2000), fine deposit of ash were reported in newspaper accounts as far as 200 km from source in a northeast direction with fine ash recorded at Hamilton airport (located near Moanatuatua Bog). In Hamilton, there were also reports of air conditioning unit malfunctions at the time of the eruption which were attributed to fine tephra (Dr Richard Smith, pers. comm., 2008). This would suggest that although the tephra were very fine it is likely to have resulted in deposition on the surface of the bog. It does, however, remain possible that some of the glass population from 2 cm in the peat represents a combination of both primary fall deposits as well as reworked deposits from older Tf members.

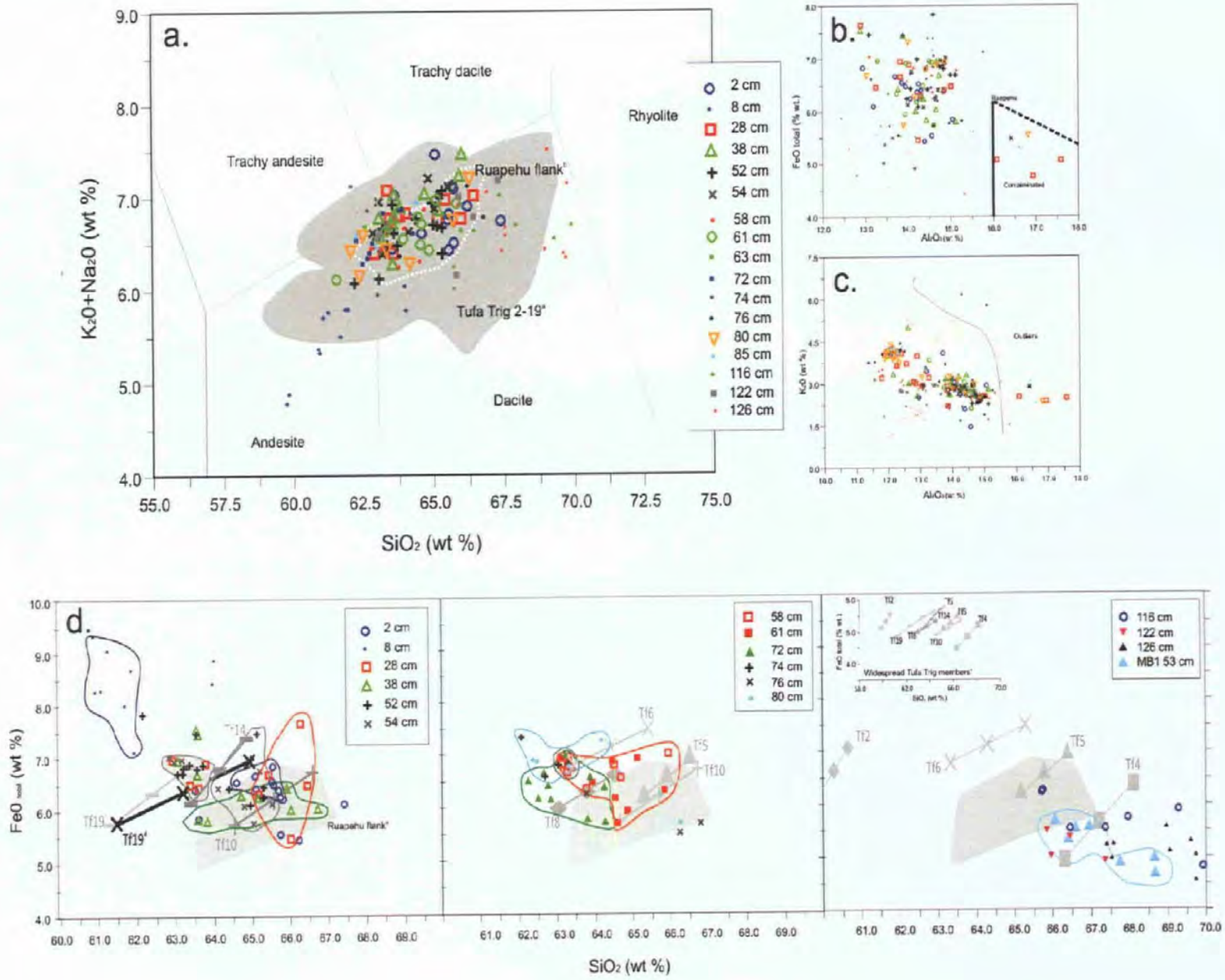
a.
Trachy dacite
Rhyolite
Trachy andesite
Ruapehu flank*
Tufa Trig 2-19*
Dacite
Andesite
K2O+Na2O (wt %)
SiO2 (wt %)
2 cm
8 cm
28 cm
38 cm
52 cm
54 cm
58 cm
61 cm
63 cm
72 cm
74 cm
76 cm
80 cm
85 cm
116 cm
122 cm
126 cm
b.
c.
d.
Tf19*
Tf10
Tf18
Tf6
Tf5
Tf4
Tf2
MB1 53 cm

Figure 4.2.11 Bivariate plots of normalized analyses from MR2 and MB1. All data are normalised to 100% loss-free. (a) Total alkali-silica diagram (TAS; after Le Bas *et al.* 1986) showing compositions of brown glass from section MR2 against compositional envelope for Tufa Trig members after Donoghue *et al.* (1997, 2007). (b) Plot of FeO versus Al_2O_3 used to identify glass analysis contaminated by plagioclase microlites. Note that dashed line represents mean compositional value for microlite plagioclase from Mt Ruapehu tephras. Solid line marks the threshold value for plagioclase contamination following Platz *et al.* (2007). (c) Plot of alkalis for all data (rhyolitic and andesitic) showing distinct outliers within main chemical populations. (d) FeO versus SiO_2 for brown glass analyses separated into three sections of the sequence with depth (2-54 cm. 58-80 cm, and 116-126 cm).

[a] Compositional ranges for Ruapehu Tufa Trig (Tf) members Tf2, 4-6, 9, 10, 14 and 19 from Donoghue *et al.* (2007; data presented are normalized to loss free basis).
[b] Tephra sample taken from the flank of Mt Ruapehu in 2005.
[c] Mean and standard deviation of compositions derived from widespread Tufa Trig Formation members from Donoghue et al. (1997; 2007; normalised to loss free basis). Data points represent mean and standard deviation. Tf19 from Donoghue et al., (2007) includes only glass from 11-15th October 1995 fall event.
[d] Compositional range of Mt . Ruapehu derived glass from 14th October 1995 eruption corrected for microlite contamination. Data points represent mean and standard deviation.

Table 4.2.3 Electron microprobe analyses of tephra-derived glass shards from 19 sample depths in core MR2 and 3 samples from MB1 and MR7, Moanatuatua Bog Sampling positions for MR2 are shown in Figure 4.2.9; MB1 shown in 4.2.8 and for MR7 in Fig. 4.2.7. Means (in bold) and standard deviations of total number (*n*) analysis (of individual shards) normalized to a 100% loss-free basis (wt%). Analysis undertaken at NERC Tephra Analytical Unit, University of Edinburgh, February and June 2007. Proximal sample collected from Mt. Ruapehu in 2005 representative of recent ash falls. †Mean values for independently characterized laboratory standards. TB1G and Lipari analysed at 3-4 hours intervals during analyses of glass samples from this site. Full details of standards including inter-laboratory statistics are provided in the appendices.

Anal.no.	1	2	3	4	5	6	7a	7b
Core/depth	**MR2/2cm**	**MR2/8cm**	**MR2/28cm**	**MR2/38cm**	**MR2/52cm**	**MR2/54cm**	**MR2/58 cm**	
Source	TnG VC	TnG VC	TnG VC	TnG VC	TnG VC	TnG VC	TnG VC	Okataina
(Tephra)	Tf19 June 1996	Ngauruhoe 1974	Tf, incl 1945?	Tf, Feb, 1861		Tf8 +	Tf8 +	Kaharoa Tephra
SiO_2	**65.34** 1.03	**61.57** 1.40	**64.18** 1.48	**64.52** 1.25	**64.08** 1.03	**64.01** 1.05	**64.27** 1.03	**77.56** 0.88
Al_2O_3	**14.12** 0.59	**14.09** 1.18	**14.71** 1.35	**14.29** 0.60	**14.42** 0.52	**14.76** 0.66	**14.27** 0.83	**12.04** 0.28
TiO_2	**1.12** 0.08	**1.27** 0.18	**1.16** 0.13	**1.14** 0.06	**1.12** 0.10	**1.10** 0.11	**1.12** 0.16	**0.10** 0.08
FeO*	**6.25** 0.42	**8.74** 0.94	**6.40** 1.12	**6.47** 0.61	**6.79** 0.49	**6.43** 0.55	**6.63** 0.96	**1.01** 0.39
MnO	**0.10** 0.07	**0.12** 0.07	**0.10** 0.06	**0.12** 0.04	**0.11** 0.07	**0.08** 0.05	**0.07** 0.06	**0.05** 0.06
MgO	**1.68** 0.44	**2.47** 1.12	**1.69** 0.76	**1.91** 0.74	**1.90** 0.28	**1.90** 0.26	**1.95** 0.50	**0.10** 0.06
CaO	**4.33** 0.44	**5.93** 0.60	**4.77** 0.77	**4.61** 0.48	**4.76** 0.42	**4.72** 0.48	**4.87** 0.54	**0.79** 0.30
Na2O	**4.08** 0.49	**3.59** 0.35	**4.02** 0.28	**3.86** 0.70	**3.94** 0.21	**4.06** 0.11	**3.84** 0.21	**4.16** 0.19
K_2O	**2.75** 0.64	**1.94** 0.25	**2.75** 0.45	**2.87** 0.28	**2.66** 0.25	**2.73** 0.28	**2.73** 0.34	**3.78** 0.47
P_2O_5	**0.23** 0.03	**0.27** 0.05	**0.22** 0.04	**0.21** 0.04	**0.21** 0.03	**0.21** 0.03	**0.26** 0.05	**0.00** 0.02
*H2O***	*1.49 0.55*	*1.22 0.44*	*1.24 0.87*	*1.00 0.55*	*1.42 1.54*	*1.18 0.43*	*1.21 0.52*	*1.51 1.43*
n	***13***	***11***	***14***	***14***	***15***	***10***	***9***	***9***

Anal.no.	8	8b	9a	9b	10a	10b	11a	11b
Core/depth	**MR2/61 cm**		**MR2/63 cm**		**MR2/72 cm**		**MR2/74cm**	
Source	TnG VC	Okataina	TnG VC	Okataina	TnG VC	Okataina	TnG VC	Okataina
(Tephra)	Tf8 +	Kaharoa T.	Tf8 +	Kaharoa T.	Tf6 +	Kaharoa T.	Tf6 +	Kaharoa T.
SiO_2	**64.43** 0.86	**77.97** 0.25	**63.81** 1.50	**77.97** 0.21	**63.25** 0.75	**77.63** 0.57	**62.78** 0.53	**77.68** 0.17
Al_2O_3	**14.15** 0.44	**12.06** 0.06	**14.34** 0.53	**12.19** 0.14	**14.39** 0.59	**12.14** 0.07	**14.54** 0.09	**12.19** 0.14
TiO_2	**1.14** 0.09	**0.08** 0.05	**1.10** 0.06	**0.08** 0.04	***1.11*** *0.10*	**0.09** 0.02	**1.10** 0.03	**0.08** 0.02
FeO*	**6.48** 0.47	**0.86** 0.08	**6.75** 0.50	**0.75** 0.12	***6.37*** *0.39*	**0.88** 0.12	**6.92** 0.32	**0.86** 0.10
MnO	**0.09** 0.06	**0.04** 0.02	**0.12** 0.11	**0.06** 0.03	***0.11*** *0.08*	**0.05** 0.06	**0.16** 0.12	**0.04** 0.07
MgO	**2.06** 0.31	**0.07** 0.01	**2.15** 0.40	**0.07** 0.01	**2.09** 0.31	**0.07** 0.01	**2.40** 0.21	**0.07** 0.01
CaO	**4.73** 0.41	**0.62** 0.03	**4.89** 0.41	**0.60** 0.04	**4.89** 0.31	**0.60** 0.02	**5.21** 0.26	**0.60** 0.04
Na2O	**3.77** 0.41	**4.24** 0.10	**3.81** 0.07	**4.16** 0.11	**3.82** 0.27	**4.09** 0.11	**3.95** 0.45	**4.28** 0.14
K_2O	**2.89** 0.46	**4.06** 0.10	**2.81** 0.08	**4.11** 0.11	**2.78** 0.33	**4.05** 0.07	**2.71** 0.19	**4.18** 0.08
P_2O_5	**0.26** 0.04	bd	**0.22** 0.04	**0.00** 0.02	**0.24** 0.03	bd	**0.23** 0.06	bd
*H2O***	*1.63 0.97*	*1.55 0.80*	*0.76 0.70*	*0.50 0.62*	**1.26** 0.63	**0.77** 0.48	*1.18 0.43*	*1.41 0.98*
n	***9***	***5***	***3***	***11***	***10***	***9***	***4***	***13***

*Total iron as FeO; ** Water by difference; bd= below detection. TnG VC, Tongariro Volcanic Center.

Table 4.2.3 Continued.

Anal.no.	12	13a	13b	14	15a	15b	16a	16b
Core/depth	**MR2/76cm**	**MR2/80 cm**		**MR2/85 cm**	**MR2/116cm**		**MR2/122 cm**	
Source (Tephra)	**Okataina Kaharoa T.**	**TnG VC Tf6 +**	**Okataina Kaharoa T.**	**Okataina Kaharoa T.**	**TnG VC Tf5 +**	**Taupo Taupo Tephra**	**TnG VC Tf5**	**Taupo Taupo T.**
SiO_2	**77.79** 5.82	**64.28** 2.11	**78.20** 0.45	**77.74** 0.29	**67.95** 2.00	**76.05** 1.21	**66.38** 2.14	**73.85** 1.15
Al_2O_3	**12.24** 3.06	**14.50** 1.10	**12.14** 0.14	**12.27** 0.15	**13.59** 0.77	**12.68** 0.41	**14.61** 1.99	**12.30** 0.36
TiO_2	**0.09** 0.36	**1.13** 0.16	**0.08** 0.03	**0.06** 0.02	**1.08** 0.16	**0.23** 0.08	**0.92** 0.12	**0.25** 0.07
FeO*	**0.81** 1.86	**6.52** 0.62	**0.85** 0.11	**0.86** 0.09	**5.47** 0.79	**1.78** 0.58	**4.58** 0.99	**1.78** 0.43
MnO	**0.06** 0.06	**0.11** 0.06	**0.11** 0.04	**0.06** 0.06	**0.09** 0.04	**0.08** 0.06	**0.07** 0.08	**0.15** 0.06
MgO	**0.07** 0.67	**1.87** 0.59	**0.07** 0.01	**0.07** 0.01	**1.27** 0.38	**0.23** 0.09	**1.06** 0.44	**0.24** 0.07
CaO	**0.59** 1.95	**4.85** 0.93	**0.62** 0.05	**0.62** 0.05	**3.65** 0.65	**1.48** 0.30	**3.70** 1.74	**1.42** 0.21
Na2O	**4.18** 0.96	**3.64** 0.35	**3.89** 0.29	**4.13** 0.13	**3.70** 0.25	**4.35** 0.37	**4.05** 0.30	**4.08** 0.34
K_2O	**4.17** 1.03	**2.86** 0.34	**4.04** 0.16	**4.18** 0.11	**2.98** 0.29	**3.08** 0.47	**3.32** 1.42	**2.80** 0.17
P_2O_5	**0.00** 0.10	**0.26** 0.04	**0.00** 0.03	**0.00** 0.03	**0.23** 0.04	**0.04** 0.03	**0.20** 0.03	**0.03** 0.03
*H_2O***	*1.23 1.20*	*1.59 0.75*	*0.86 1.14*	*1.16 1.64*	*1.76 0.38*	*2.54 1.78*	***2.04*** *0.49*	***3.09*** *0.50*
n	***12***	***8***	***14***	***10***	***8***	***6***	***6***	***6***

Anal.no.	17a	17b	18	19
Core/depth	**MR2/126 cm**		**MR2/138cm**	**MR2/145 cm**
Source (Tephra)	**TnG VC Tf1+**	**Taupo Taupo T.**	**Taupo Taupo T.**	**Taupo Taupo T.**
SiO_2	**68.50** 1.14	**76.02** 0.68	**75.96** 0.34	**75.74** 0.94
Al_2O_3	**13.36** 0.61	**12.81** 0.29	**12.82** 0.28	**12.87** 0.24
TiO_2	**1.13** 0.17	**0.24** 0.07	**0.26** 0.04	**0.26** 0.06
FeO*	**5.32** 0.67	**1.85** 0.24	**1.95** 0.20	**1.96** 0.27
MnO	**0.06** 0.05	**0.09** 0.07	**0.13** 0.08	**0.10** 0.06
MgO	**1.04** 0.23	**0.24** 0.05	**0.25** 0.02	**0.26** 0.07
CaO	**3.58** 0.46	**1.49** 0.15	**1.59** 0.05	**1.57** 0.22
Na2O	**3.70** 0.32	**4.32** 0.30	**4.12** 0.29	**4.18** 0.34
K_2O	**3.03** 0.33	**2.90** 0.17	**2.88** 0.08	**3.02** 0.60
P_2O_5	**0.27** 0.04	**0.03** 0.02	**0.04** 0.02	**0.03** 0.02
*H_2O***	*1.50 0.71*	*3.38 1.31*	*3.98 1.45*	**3.57** 1.97
n	***9***	***14***	***9***	***17***

	a	b	
	MB1/54 cm		**MR7/90 cm**
	TnG VC Tf5	**Taupo Taupo T.**	**Okataina Kaharoa T.**
SiO_2	**68.72** 1.83	**75.77** 0.45	**77.92** 0.87
Al_2O_3	**13.47** 0.53	12.84 0.27	**11.97** 0.31
TiO_2	**0.97** 0.20	**0.25** 0.04	**0.11** 0.07
FeO*	**5.10** 1.06	**1.96** 0.11	**0.92** 0.35
MnO	**0.12** 0.06	**0.07** 0.08	**0.07** 0.07
MgO	**1.08** 0.28	**0.25** 0.04	**0.09** 0.07
CaO	**3.54** 0.57	**1.48** 0.13	**0.69** 0.30
Na2O	**3.70** 0.25	**4.51** 0.21	**4.16** 0.20
K_2O	**3.07** 0.36	**2.85** 0.13	**4.05** 0.40
P_2O_5	**0.23** 0.07	**0.02** 0.02	**0.02** 0.02
*H_2O***	**0.65** 0.35	**1.15** 1.10	**1.00** 1.36
n	***9***	***9***	***12***

Anal.no.	Proximal sample
Sample	**Ruapehu flank**
SiO_2	**64.77** 1.46
Al_2O_3	**14.62** 1.64
TiO_2	**1.04** 0.17
FeO	**6.24** 1.28
MnO	**0.10** 0.09
MgO	**1.49** 0.38
CaO	**4.88** 0.95
Na_2O	**3.90** 0.61
K_2O	**2.69** 0.68
P_2O_5	**0.26** 0.06
H_2O	*0.95 0.84*
n	***8***

	Standards†				
	TB1G	**Lipari**	**BCR2G**	**A-ALK**	**S-OBS**
	53.88 0.22	**74.19** 0.23	**53.49** 0.18	**73.47** 0.16	**76.91** 0.32
	16.17 0.17	**12.84** 0.08	13.09 0.13	**12.16** 0.05	**12.44** 0.06
	0.89 0.05	**0.07** 0.03	**2.41** 0.06	**0.18** 0.03	**0.09** 0.05
	8.55 0.26	**1.60** 0.13	**13.09** 0.33	**3.10** 0.25	**0.62** 0.15
	0.19 0.07	**0.06** 0.08	**0.18** 0.07	**0.10** 0.07	**0.12** 0.05
	3.62 0.04	**0.04** 0.01	**3.69** 0.02	**0.05** 0.01	**0.05** 0.01
	6.89 0.12	**0.75** 0.04	**7.26** 0.11	**0.37** 0.03	**0.46** 0.04
	3.32 0.07	**4.17** 0.08	**3.23** 0.06	**5.67** 0.09	**4.23** 0.07
	4.44 0.08	**5.19** 0.09	**1.78** 0.05	**4.60** 0.09	**4.81** 0.09
	0.60 0.03	**0.00** 0.03	**0.37** 0.03	**0.00** 0.03	**-0.02** 0.02
Total	**98.54** 0.48	**98.92** 0.32	**98.59** 0.41	**99.72** 0.26	**99.75** 0.37
	41	***41***	***10***	***10***	***10***

Sample 2 (MR2 7-8 cm): TnG VC, Ngauruhoe, 19th February, 1975, with reworked Taupo glass shards

The sample from 8 cm depth in core MR2 marks a discrete peak in glass concentrations observed to contain well preserved, microlite rich, brown shards (Plate 4.2.3b). EMP analysis reveals a moderately homogenous glass population with an andesitic chemistry. This forms a population distinct from other brown glasses in the sequences which are predominantly dacitic in composition (Fig. 4.2.10 a, d). The composition of this glass set is characterized by lower values of K_2O (1.94, SD 1.40) and SiO_2 (61.57, SD 1.40) and higher FeO (8.74, SD 0.94 %). Tephras with andesitic chemistry and high FeO are characteristic of tephras from the Tongariro volcano and adjacent Ngauruhoe cone (Donoghue *et al.*, 1995b; Cronin *et al.*, 1996a; Donoghue *et al.*, 1997; Hobden *et al.*, 2002). Tephras from these volcanoes erupted since the Taupo eruption of AD 233 are defined as the Ngauruhoe Formation (Hobden *et al.*, 2002). The sample also contains a relatively minor component of rhyolitic shards (four grains analyzed) that correlate with Taupo Tephra (Fig. 4.2.9). These most likely represent deposits remobilized and re-deposited from disturbed exposures of the tephra in nearby drainage ditches.

Identifying potential correlatives for this andesitic population is facilitated by both the age constraints, historical records of ash fall distribution as well as the distinctive geochemical composition. This tephra unit stratigraphically overlies a charcoal layer at 10 cm depth which can be linked to the last fire event on the reserve in 1972 (Clarkson, 1997) which limits deposition to within the last 35 years. A linear interpolation on the age-depth model between 1971 and the surface of the peat section (collected in 2005) would suggest that the concentration of glass was actually deposited before 1980 (Fig. 4.2.9). During this time

period (1972-1980) there was only one significant eruptive event from the TnG VC which could have resulted in widespread ash deposit. Between 1974 and 1975 the Ngauruhoe volcano (part of the TnGVC) erupted with series of intermittent block-and-ash flows which culminated in a large ash eruption on 19th February 1975 (Nelson, 1975; Nairn & Self, 1978; Hobden *et al.*, 2002). This was one of the largest events recorded from the volcano in historical times with a VEI 3 and with an estimated tephra volume of ~3.7 x 10^6 m^3 (Nelson, 1975). Observations of the eruption event by Nelson (1975) record an ash plume ~8 km above the crater rim, which, facilitated by strong southerly winds on the day, was blown across the Waikato Region in a narrow course at least as far as Hamilton. In Hamilton City a fine grained brown ash was observed to form a near-continuous covering over the surface (Donoghue *et al.*, 1997; Prof. David Lowe pers. comm. 2008). It is therefore very likely that it was also deposited on the site which is within the known trajectory and a little closer to the actual source. Comparisons with chemistry derived from the ash collected on the day of the eruption from Hamilton using XRD (Nelson, 1975) also shows very good correspondence particularly for low K_2O values (1.8 % (wt., un-normalized) in the 1975 sample, compared with ~1.9% (wt., un-normalized) for the glass from the peat sample) and high FeO values. XRF analyses of the pyroclastic deposits from the eruption by Hobden *et al.* (2002) revealed a similar composition characterized by high FeO (8.49 wt.%) and low K_2O (1.33 wt.%) compared to XRF analyses from preceding Ngauruhoe tephras and Ruapehu derived Tufa Trig members (Gamble *et al.*, 1999). A very recent study of Ngauruhoe deposits demonstrated with EMP of glass separates that tephra from Ngauruhoe source could be distinguished from Ruapehu by distinctly higher values of FeO (Mobis *et al.*, 2008).

Sample 3 (MR2 27-28 cm): TnG VC derived Tf tephras with reworked grains from Taupo and Kaharoa tephras

Analysis of glass shards from this sampling position was undertaken to gauge the possible impact of disturbance activities adjacent to the site on resulting concentrations of glass preserved in the peat. The sample from 28 cm marks the midpoint of the section of peat (20-40 cm) representing the time interval ~mid 1800s to mid 1900s (Fig. 4.2.9). This time period was characterized by large scale drainage activities at the site including frequent and related fire events. For this interval of peat, abundant brown and clear shards were recorded during microscopy but are not represented by distinct fluctuations in changing shard content characteristic of discrete depositional events (Fig. 4.2.9). The analyses of shards from this level reveal dacitic glass population equally mixed with a significant background component of rhyolitic shards (7 out of 21 shards analyzed) (Fig. 4.2.11). The dacitic glass population consists of a heterogeneous set of glass analyses that fall within the compositional range for the Tufa Trig tephras from Ruapehu (Donoghue *et al.*, 1997; Donoghue *et al.*, 2007). Within this population it is possible to identify a bi- (or possibly multi-) modal composition comprising at least one distinct clusters of analyses (Fig. 4.2.11 d). These represent a combination of glass compositions that can be compared to a number of populations identified in older stratigraphic levels in the core (e.g. samples 4 and 5). It is therefore likely that this sample is dominated by contributions from one or more reworked deposits. It is also possible that this multimodal composition represents heterogeneity arising from magma mingling during one eruption event as seen for dacitic glass populations in additional levels in the sequence. Possible sources of primary fall deposits for this level could include one or more significant (VEI > 2), tephra-generating, eruptions from Mt. Ruapehu that occurred in the late 1800s and early 1900s (Gregg, 1960

and references therein). Such eruptions include the large ash eruption from Mt Ruapehu in 1945 which was of a similar magnitude to the 1996 event (Johnston *et al.*, 2000). The ejecta within the 1945 eruption column was observed to reach >1000 feet (~300 m) above the crater wall and is likely to have been transported in the stratospheric winds across the island (Gregg, 1960; McSaveney *et al.*, 2007). Published compositional data from the 1945 and other historical eruptives from Mt Ruapehu have been determined by XRF (Gamble *et al.*, 1999). These data (on bulk samples) show the 1945 eruptive to be quite distinct from subsequent eruptives but very similar to preceding (pre-historic) eruptives. Disturbance and remobilization of one or more of these tephras deposited on or preserved close to the surface could account for the pattern of tephra shards detected in the peat at Moanatuatua.

The shards of rhyolitic glass in the sample correlate both with Taupo and Kaharoa tephras in similar proportions (Fig. 4.2.10). These tephras are both present at deeper levels in the peat and are likely to have been remobilized and re-deposited as a result of modern disturbance adjacent to the site.

Sample 4 (MR2 38-40 cm): TnG VC derived Tf tephra, Ruapehu, February, 1861

The sample from this position represents a peak in shard concentrations within a distinct zone of elevated shard content between 36 and 42 cm in the peat sequence (Fig. 4.2.8). The shard content consists of a mix of predominantly brown shards with a minor component of clear shards. Compositional analysis reveals a mix of (brown) dacitic glasses with a minor component of (clear) ryholitic shards (Fig. 4.2.10). The dacitic glasses all correlate with Tufa Trig Formation members as for previous levels and form a relatively distinct population from other dacitic glasses. These are also characterized by a distinct bi-modal

composition (Fig. 4.2.11 d). Compositionally, this glass population compares most closely with Donoghue's (1997) Tf10 member (Fig. 4.2.11 d). Although this tephra member is not dated directly it is thought to represent an eruptive event which precedes European arrival (earliest arrival AD 1814; Lowe *et al.*, 2000) and could therefore represent a subsequent eruptive event.

The approximate age of this glass population in the peat is ~ AD 1770-1890 (Fig. 4.2.9). A potential candidate for the deposition of ash for this time period is therefore likely to be a large historical ash-fall event. A possible candidate tephra includes that of the 1861 eruption of Mt Ruapehu. This central vent eruption was the first significant eruption activity witnessed by European settlers (Siebert & Simkin, 2002). With an estimated Volcanic Explosivity Index (VEI) of 2 (Donoghue *et al.*, 1995b) there is a possibility that the ash plume would have been sufficient to deposit ash over a relatively long distance from source. Although there were no witness statements of ash fall in localities close to the site at the time (that this author is aware of) it is likely that because the region was so sparsely populated the occurrence of any sparse, fine ash deposits may have gone unnoticed or unrecorded.

Samples 5 and 6 (MR2 52 and 54 cm): TnG VC, Tf14

Analysis of glass shards from 52 cm and 54 cm in the peat are representative of a distinct and prominent zone of brown shards between 51 and 57 cm depth in section MR2 (Fig. 4.2.9). Both samples comprised a relatively distinct set of dacitic glass analyses with a bimodal composition (Figs. 4.2.10 and 4.2.11 d; mean values (wt.%) of diagnostic oxides: **pop.1.** SiO_2 = 63.17 (SD: 0.39), K_2O = 2.49 (0.17), CaO = 5.10 (0.19); **pop. 2**: SiO_2 =

65.01 (0.40), K_2O = 2.90 (0.14), CaO = 4.36 (0.26). Both populations are represented by an equal number of analyses, all of which fall within the compositional ranges for Tufa Trig tephras (Donoghue *et al.*, 1995b). This bimodal population could represent different phases of the same eruptive event or the result of magma mixing which has been identified within older tephras from TnG VC (Donoghue *et al.*, 1995a; Shane *et al.*, 2008a). Alternatively, the glass population could represent the mixing of two discrete ash fall populations deposited during closely spaced eruption events but because they are so well mixed in both samples this is possibly less likely.

The age range of this shard concentration is 160-300 calendar yr BP (based on 2σ range) equivalent to calendar date AD 1650-1790 (Fig. 4.2.9) which is prior to European settlement and the commencement of records of eruptions. A possible correlative for this glass population is likely to include Tf14 or a later or an unknown Tufa Trig member. Member Tf14 is recorded as one of the thickest of Tf members preserved in sequences proximal to Mt. Ruapehu (Donoghue *et al.*, 1995b) represents one of the largest of Tf eruptives in volume (this of course only partially supports the potential for widespread dispersal (Bursik, 1998)). EMPA derived for this tephra member from proximal sequences by Donoghue (1997) (SiO_2 = 63.74 (0.74), K_2O = 2.66 (0.38), CaO = 5.08 (0.42)) show a very good correlation with analyses from samples 5 and 6 and plots between the two populations (Fig. 4.2.11 d). There were no background rhyolitic shards analyzed from this level as these were very sparse in the sample suggesting, perhaps, that remobilised glasses are not an issue in this section of the sequence.

Samples 7-9 (MR2 58, 61, 63 cm): TnG VC Tf10 or later Tf member with reworked grains from Kaharoa Tephra and Tf8

Three samples represent a discrete peak in clear shards with a minor component of brown shards 58-63 cm in the peat sequence which also marks the upper limit of the zone of clear shards in this middle part of the sequence (Fig. 4.2.9). Compositional analysis reveals a mix of shards from three sources (Fig. 4.2.10). The majority of clear shards fit within the compositional range for Okataina VC derived tephras and they correlate with Kaharoa Tephra (see samples 10-14). This glass represents the upper limit of this cryptotephra, almost 30 cm above its first occurrence in the peat. A few shards (9 % of total shards analyzed) from 58 cm also correlate with the Taupo Tephra (see sample 19). These rhyolitic shards are likely to have been reworked from exposed deposits during a single discrete erosion event. The brown shard component comprises dacitic glasses within the compositional range for TnG VC-derived Tufa Trig members. The brown shards comprise an apparently bimodal composition, similar to samples 5 and 6 but are compositionally distinct from the preceding concentration of brown shards at 72 cm (Fig. 4.2.11 d). The compositional range for the glass population at these levels does however appear to overlap with the compositional range of at least three post Kaharoa Tf members including Tf 6, 8 and 10 (Fig. 4.2.11 d).

The age range of this concentration of glass shards in the core is 260-280 cal yr BP (equivalent to AD 1670-1710) (2 σ age range: 200-370 cal yr BP) (Fig. 4.2.9). For this time period Tf 8 and Tf6 are likely to be too old as potential candidate correlatives that are more likely to be detected closer to the Kaharoa Tephra isochron. The compositional range of Tf10 shows very good correlation with at least 50% of analyses from these levels. This

tephra is another of the more widely dispersed of the Tf members, and occurs as a thick deposit in proximal sequences (Donoghue *et al.*, 1995b). There are no age estimates for this tephra but in proximal sequences it occurs approximately equidistance between Tf members 9 and 14. Given the number of reworked rhyolitic shards in this level it is very likely that this glass population also contains shards from earlier members that have also been reworked into younger stratigraphic levels.

Samples 10-14 (MR2 72, 74, 76, 80, 85 cm): Kaharoa Tephra with Tufa Trig Member 6-8

Samples 10-14 are representative of a broad zone of shards between 72 and 85 cm in sequence MR2 (Fig. 4.2.9). This zone is manifest by elevated but variable shard content containing both rhyolitic and intermediate glasses. The samples analyzed are taken from distinct peaks in shard concentration within this zone of variable shard content. Analyses of shards from all these levels (72-85 cm) reveal a distinct and homogenous composition of rhyolitic glass. High values of SiO_2 (~77.7%) are characteristic of Okataina VC derived tephras (compared to ~75% for Taupo VC) and high K_2O (~4.1%) of the compositionally distinct Kaharoa Tephra (wiggle match date AD 1314 ± 12; Hogg *et al.*, 2003). The age range of this particular tephra is very well constrained and where preserved marks the onset of distinguishable human presence on the eastern North Island (Newnham *et al.*, 1998; Lowe *et al.*, 2000). In this peat section, however, the tephra is represented by a time interval spanning ~360 years (age range 320-680 cal yr BP).

Using the age-depth model for the sequence (Fig. 4.2.9), it was possible to predict the level of the glass zone which should be representative of the primary fall layer. When plotted on the age model, the Kaharoa age marker coincides with the first occurrence of the rhyolitic

glass population in the peat at 85 cm (Fig. 4.2.9). Interestingly, this does not represent the highest concentration of shards in which is often the assumed level assigned to cryptotephra concentrations which show vertical spread in a profile (e.g. Pyne-O'Donnell *et al.*, 2008; Lowe *et al.*, 2008b). The persistence of shards above the primary fall layer up through the peat therefore may represent sustained remobilization of the deposits from disturbed exposures in or on the margins of the bog, most likely due to activities from early Polynesian settlers.

Four analyses associated with this rhyolitic glass population correlate with older Okataina VC derived eruptives as well as the Taupo Tephra. The low numbers of these analyses preclude the possibility that they represent additional phases or eruptions and most likely they are remobilized deposits which have either been incorporated into the eruption column from overlying deposits or reworked from nearby exposures. Alternately, they could be analytical outliers.

Glass shards of intermediate composition were also analyzed in all levels coincident with the Kaharoa Tephra but in most cases are represented by low numbers of analyses due to very low quantities of shards recovered. The analyses that were obtained revealed glass of dacitic chemistry in all levels which were compositionally consistent with analysis of Tufa Trig members (Donoghue & Neall, 1996). Only at 72 cm were sufficient glass analyses obtained (10 shards). These showed a moderately homogenous composition that was distinct from both underlying and overlying glass concentrations (Fig. 4.2.11 d). This population shows good correlation with the compositional ranges for Tf6 and Tf8 members (Donoghue *et al.*, 1997). The majority of glass analyses from 72 cm appear consistent with the composition range of Tf8 whereas analyses from preceding levels (74-80 cm) are more

closely matched with Tf6, with a few analyses compositionally similar to Tf5 and Tf4 tephras.

Candidate eruptives Tf6 and Tf8, are two widespread Tf members (Donoghue *et al.*, 1995b) that have been identified as closely spaced visible deposits in sequences >100 km from source (Hawkes Bay, Napier) (Wilmshurst, 1997). Neither of these Tf members have been dated directly but are found positioned immediately above the deforestation signal in the Hawkes Bay sites established through palynology (Wilmshurst, 1997; cited in Lowe *et al.*, 2000). The deforestation event in these sites has been imprecisely dated to *ca.* AD 1450 based on associations with the Kaharoa Tephra. This provides an age limit for these tephra members that suggest that they stratigraphically overlie the Kaharoa Tephra (Lowe *et al.*, 2000). Such a relationship would be consistent with the glass populations in the core in relation to the Kaharoa Tephra. Tf8 is also given an approximate age of *ca.*600 ^{14}C years BP based on the relative stratigraphic position with radiocarbon-dated member Tf5 which also provides a maximum age for Tf6 of 650 ± 50 ^{14}C years B.P (547-675 cal yr BP) (Donoghue *et al.*, 1995b). Tf5 is thought to stratigraphically underlie the Kaharoa Tephra (Lowe *et al.*, 2000). The age range of the glass peak at 72 cm in the core is ~300-460 cal yr B.P. (AD 1490-1650; Fig. 4.2.11). This age might suggest that the approximate age of *ca.*600 ^{14}C years BP is overestimated, or that the glass population at 72 cm represents a subsequent event with a similar composition.

It is likely therefore that this 'zone' of brown shards coincident with the Kaharoa Tephra represents at least three populations representing primary fall tephras from widespread Tf members (Tf8 and Tf6) as well as reworked Tf members from lower stratigraphic levels (Tf4 and Tf5).

Samples 15-17 (MR2 116, 122, 126 cm): TnG derived Tf 4, 5 with Taupo Tephra (Unit Y) and uncorrelated tephra

Samples 15-17 are representative of a zone of predominantly brown shards which marks the upper limit of abundant clear shard concentrations in the peat above the visible Taupo Tephra (Fig. 4.2.9). This zone of shards is characterised by a very distinct peak in shard content at 122 cm with elevated shard content up to 108 cm in the peat. The samples from 116 cm and 126 cm, either side of the peak in shards at 122 cm, were analyzed to assess the vertical spread of this shard population (Fig. 4.2.8). Analyses of shards from these levels were, however, affected by a poor recovery of brown shards. During microscopy some of the brown shards in these levels appeared to have been affected by chemical weathering and it is uncertain, although possible, that this may have had an effect on elemental composition of these shard populations.

Analyses of the shards that were recovered from these levels revealed a mix of intermediate and rhyolitic glasses (Fig. 4.2.10). Dacitic glasses from these levels are compositionally distinct from subsequent intermediate glass populations in the sequence and are characterized by higher SiO_2 (65.8-71.0 wt.%) and lower FeO_{total} (4.79-6.96 wt.%) (Fig. 4.2.11 d). The majority of these glass analyses do, however, still fall within the compositional range for Tufa Trig members determined by Donoghue (1997). Analyses from each level also form relatively distinct clusters (Fig. 4.2.11 d), although there were insufficient analyses to suggest that these represent separate geochemical populations. Potential candidates for these glass populations include only a limited number of Tf members which stratigraphically intervene between the Taupo and Kaharoa tephras. These include Tf1-5. However, only Tf1, 2 and 5 are found as thick proximal deposits and are

considered to be the only eruptions capable of widespread dispersal (Donoghue *et al.*, 1995b). Tf5 is considered to be one of the most widespread of all Tufa Trig members with an estimated VEI of 3 resulting in a tephra volume in excess of 10^7 m^3 (Lowe *et al.*, 2000; Siebert & Simkin, 2002). Compositionally, however, samples 15-17 most closely match the range for Tf4 after Donoghue (1997) with only a few analyses overlapping Tf5 range (Fig. 4.2.10 d). The glass population does not correlate with the distinct composition of earlier member Tf2 which is characterized by having a much lower SiO_2 content.

The age range for peat incorporating samples 15-17 is 1080-1240 cal yr BP (Fig. 4.2.9). This is much older than the maximum age given to Tf5 of 830 ± 60 ^{14}C yr BP (uncalibrated age) (671-907 cal yr BP; Eden and Froggatt, 1996), which would support the correlation of glass at Moanatuatua with the older Tf4 member tephra instead. There are no ages associated with Tf4 deposit but it is recorded in proximal deposits as a discrete and distinct unit between The Taupo Tephra and the closely spaced units Tf5-14.

Interestingly, the assays of brown-coloured glass from 122 cm comprised predominantly rhyolitic chemistry mixed with only a small population of dacitic glass (4 shards) (Figs. 4.2.10 and 4.2.11 d). These 'brown' rhyolitic glasses are uncorrelated and do not match compositions for recent Taupo or Okataina VC eruptives but could represent a previously unrecognized rhyolitic phase to the Tf5 eruption or are more likely derived from reworked deposits from much older tephras or an unknown eruption event. Similar glass compositions were not recognized from analyses of samples from comparable stratigraphic levels in replicate sequences (MB1-54 cm). Additional rhyolitic shards in the samples correlate with the Taupo Tephra.

Sample 19 (MR2 138 and 145 cm): Taupo Tephra (Unit Y)

The samples taken from 138 and 145 cm are representative of the zone of abundant clear shards observed above the visible component of the Taupo Tephra. Analyses of shards from these samples were used to confirm the occurrence of the Taupo Tephra as the visible unit identified by field characteristics and to support the hypothesis that components of this tephra were remobilized and re-deposited for long periods after initial deposition. Both samples contain a relatively homogenous set of rhyolitic glass analysis (Table 4.2.3; Fig. 4.2.10). The composition of the glass is typical of Taupo VC rhyolitic glass which has characteristically lower SiO_2 (74.8-76.7 wt. %) and K_2O (2.44-3.62 wt. %) than OVC derived tephras. These analyses also compare very closely to the compositional range for the climactic tephra-generating phase of the AD 233 ± 13 Taupo Tephra event (Unit Y) (SiO_2 = 75.04 ± 0.19; K_2O = 2.85 ± 0.07 wt. %; (Gehrels *et al.*, 2006). The analyses from these samples, however, reveal slightly higher mean SiO_2 composition and this difference very likely relates to small differences in analytical conditions. There are also a few analytical outliers associated with these samples which are likely to represent older Okataina and Taupo VC deposits (Fig. 4.2.10). The occurrence of outliers and uncorrelated analyses associated with the Taupo Tephra has been noted from previous studies (Gehrels *et al.*, 2006). This has been attributed to a number of possible causes including the incorporation of older deposits into the eruption column, additional phases of the eruption, or magma mingling (Lowe *et al.*, 2000; Siebert & Simkin, 2002).

Section MB1 - 54 cm: TnG tephra Tf4 with Taupo Tephra

Due to time constraints for analyses, only one sample was analyzed from sections MB1-3. The sample from 53 cm in section MB1 represented a peak in brown shard concentrations coincident with the decline in clear shards above the Taupo Tephra (Fig. 4.2.8). This forms a similar pattern of shards observed at comparable stratigraphic levels in section MR2 (122 cm, analysis no. 16; Table 4.2.3) and in MR7 (144 cm; Fig. 4.2.7). Analysis of shards from this level in MB1 was therefore used to test if these could be correlated within the same site based on this association of shard concentrations. The resulting analyses confirm glass populations comprising of rhyolitic and dacitic glasses. The rhyolitic glasses correlate with the Taupo Tephra and confirm this tephra as the dominant background component of rhyolitic glasses in this section of the core. The dactic glass analyses are typically heterogeneous with a possibly bi- or multi- modal composition (Fig. 4.2.10 and 4.2.11). The glass analysis fits within the high Si range of analysis (SiO_2= 65.7-71.5 % wt. %) compared to analyses determined from section MR2 (Fig. 4.2.10). These analyses also closely correspond with dacitic glass populations from all three levels in MR2 (116, 122 and 126 cm) which correspond with the decline in Taupo shard concentrations (Fig. 4.2.10). It is therefore most likely representative of Tufa Trig member tephra Tf4 identified at 122 cm in MR2. The age range of this glass population in the core is 1210-1280 cal yr BP (based on median age; Fig. 4.2.8) which fits well within the age range determined for the correlative in MR2 at 1080-1240 cal yr BP.

Section MR7- 90 cm: Kaharoa Tephra

This sample is representative of a peak in clear shards from the upper zone of clear shard concentrations in the replicate core MR7 (Fig. 4.2.7). Analysis from this level confirms the source as Kaharoa Tephra, which has been detected at comparable stratigraphic levels in section MR2. The result of compositional analysis is a homogenous set of rhyolitic glass with high SiO_2 (77.9 ± 0.9 wt.%) and K_2O (4.05 ± 0.4 wt.%) characteristic of Kaharoa Tephra from published analysis (SiO_2 = 77.61 ± 0.19 wt.%; K_2O = 4.26 ± 0.08 wt.% (Lowe *et al.*, 2000; 2008b) and compares with analysis from identified Kaharoa Tephra in the MR2 section (SiO_2 = 77.7 wt.%; K_2O = 4.1 wt.%). There are slightly higher SiO2 values for this tephra in the peat sections than for published values. This issue remains consistent for all rhyolitic shards analyzed in this study and is likely to relate to differences in analytical conditions.

Table 4.2.4 Summary of cryptic and visible tephras identified in cores MR2, MR7 and MB1 including their relative ages. Age ranges based on 2-sigma range on age depth model and taking into consideration the vertical extent of cryptotephra zone considered to represent primary fall event or depositional event identified from shard counts (Fig. 4.2.6-8) and from analysis of geochemical populations (Fig. 4.2.9-11 and Table 4.2.3). * Unable to interpolate age; **age ranges interpolated from this core between ages for Taupo Tephra and Kaharoa Tephra at level of first occurrence; * interpolated from projected age model based on MR2. RW= reworked (secondary deposition).**

Sample no. /core	Depth in core (cm) of sample shard conc.[a]	No. of shards in population analysed	Eruptive source (VC)[b]	Interpolated age of glass conc. in cal. yr BP 2σ range[c] [Calender date AD based on age model]	Identification of tephra (T.) /interpretation	Calendar ages (AD)/ Calibrated ages of tephras in cal. yr BP 2σ range[d]	Primary reference(s): ages[1] major element chemistry[2]
1/MR2	2	13	Tng	[post 1972]	1995-1996 Ruapehu (Tufa Trig 19)	Oct 1995, June 17-18th 1996	[2]Donoghue *et al.* 1997
2	8	(a) 11	Tng	[post 1972]	1974 Ngauruhoe eruption	February 19th, 1974	[1]Nelson, 1975; Nairn and Self, 1978
		(b) 2	TVC		Reworked (RW) TaupoTephra	*	[2]Nelson, 1975; Donoghue, 1995
		(c) 2	OVC		RW Kaharoa Tephra	*	Cronin *et al.*, 1996; Hobden *et al.*, 2002
3	28 [20-32]	(a) 14	Tng	[~1820-1950]	1945 plus earlier Tufa Trig members	1945 +	[1]Gregg, 1960 and references therein [2]Donoghue *et al.*, 1997
		(b) 3	TVC		RW Taupo Tephra	*	
		(c) 4	OVC		RW Kaharoa Tephra	*	
4	38 [36-42]	(a) 11	Tng	[1760-1910]	Ruapehu 1861	February 1861	As for sample 3 above
		(b) 3	TVC		RW Taupo Tephra	*	
5	52 [52-56]	15	Tng	160-300 [1790-1650]	Ruapehu, Tf 14	post- 1314 ± 12 AD	[1]Lowe *et al.*, 2000 [2]Donoghue *et al.*, 1995
6	54	10	Tng				
7	58	(a) 9	Tng				[1]Wilmshurst *et al.*, 1997 [2]Donoghue, 1995
		(b) 2	TVC		RW Taupo Tephra	*	
		(c) 11	OVC				
8	61 [58-62]	(a) 9	Tng	200-440 [1510-1750]	Ruapehu, Tf 8 or later Tf member	post- 1314 ± 12 AD	
		(b) 5	OVC		RW Kaharoa Tephra	*	
9	63	(a) 3	Tng				
		(b) 11	OVC				

Table 4.2.4 Continued

10	72	(a) 10 (b) 9	Tng OVC		Ruapehu, Tf 8 or later Tf member	* 1314 ± 12 AD	[1]Wilmshurst *et al.*, 1997 [2]Donoghue, 1995
11	74 [69-80]	(a) 4 (b) 2 (c) 13	Tng TVC OVC	280-720	RW Taupo Tephra Kaharoa Tephra	* *	[1,2]Newnham *et al.*, 1998
12	76	(a) 3 (b) 12	Tng OVC		Kaharoa Tephra	*	
13	80	(a) 8 (b) 14	Tng OVC		Ruapehu, Tf 6 or later Tf member Kaharoa Tephra	1314 ± 12 AD	[2]Donoghue *et al.*, 1997
14	85 [84-86]	(a) 4 (b) 10	Tng OVC	620-890	Ruapehu, Tf 6 or earlier Tf Mmb. Kaharoa Tephra	* 1314 ± 12 AD	[2]Donoghue *et al.*, 1997 [1]Newnham *et al.*, 1998; [2]Hogg *et al.*, 2003
15	116 [112-117]	(a) 8 (b) 6	Tng TVC		RW Taupo Tephra	*	
16	122 [120-126]	(a) 6 (b) 6	Tng TVC	1000-1260	Ruapehu, Tf 4 RW Taupo Tephra	1210±150 *	[1]Lowe *et al.*, 2000; [2]Donoghue *et al.*, 1997
17	126	(a) 9 (b) 14	Tng TVC			*	
18	138	9	TVC	1460-1600	RW Taupo Tephra	*	[1,2]Lowe *et al.*, 2008
19	145	17	TVC				
MB1	54	(a) 9 (b) 9	Tng TVC	1285-1340	Ruapehu, Tf 4 RW Taupo Tephra	1314 ± 12	[1]Lowe *et al.*, 2000; [2]Donoghue *et al.*, 1997 [1,2]Lowe *et al.*, 2008
MR7	74 78	(a) 2 (b) 1 2	Tng OVC OVC	290-330***	Ruapehu, Tf 8 or later Tf member RW Kaharoa Tephra RW Kaharoa Tephra	post-1314 ± 12 * *	[1]Wilmshurst *et al.*, 1997 [2]Donoghue, 1995
	90	12	OVC	640-680**	Kaharoa Tephra	1314 ± 12	[1,2]Hogg *et al.*, 2003

4.2.7 Summary of findings from Moanatuatua Bog and resultant issues

Material collected from Moanatuatua Bog comprises five restiad peat sequences, two sections from the scientific reserve and three sections from an exposure on the partly drained margins. Section MR2 is the most complete sequence, representing continuous accumulation since the deposition of the Taupo Tephra up to the modern surface. All peat sequences comprise restiad peat interspersed with abundant charcoal layers possibly representing several *in situ* and adjacent fire events.

Analysis of the tephra-derived glass shard content of the sequences reveals almost continuous shard concentrations throughout the sequences comprising both clear and brown shards from rhyolitic and andesitic or dacitic sources, respectively. Measurements of organic content in the peat sequences determined by loss on ignition provide a sensitive indicator (based on an inverse relationship) of these shard concentrations.

Clear shards are represented in two distinct zones in sections MR2 and MR7. These include a zone of diminishing shard content several centimeters above the Taupo Tephra and a second broad zone of clear shards in about the middle section of the sequence. Brown shards are represented by continuous and highly variable content throughout the sequences with several distinct peaks in shard concentrations. Distinct morphological characteristics are recognized: shard type, colour, microlite type and abundance and sometimes shard chemical etching features for individual concentrations of brown shards.

The lower parts of these sequences correspond very closely to the cryptotephra patterns evident in MB1-3 indicating that these three sections are truncated at approximately the higher (second) broad zone of clear shards.

Compositional analysis of selected shard concentrations by EMP confirms the identification of the Taupo Tephra (1717 ± 13 cal yr. BP) as a visible unit in the peat which remains persistent in high concentrations as a cryptotephra "tail" for at least 300 years of peat accumulation after initial deposition. The second zone of clear shards in the sequences MR2 and MR7 from the reserve correlate closely with the Kaharoa Tephra (1314 ± 12 cal yr. BP). This correlation is the first time the Kaharoa Tephra has been definitively identified in the Hamilton Basin. Glass from the tephra is spread vertically through the peat representing at least 400 years of peat accumulation. Kaharoa Tephra is not present in the truncated peat sequences from the margins (MB1-3). The age model in section MR2 is used to constrain this well-dated tephra and indicates that the first occurrence of shards in the peat sequence is most likely to represent the level of primary fall out of this tephra (i.e. the most accurate position for the Kaharoa isochron). In MR2, as with the Taupo Tephra, glass shards from the Kaharoa Tephra are detected in low concentrations almost all through the sequence above the level in the peat representing the primary fall deposit. This dissemination suggests almost continual remobilization and deposition of these tephras from disturbance in the peat bog or adjacent exposures. This background concentration of reworked clear shards increases two-fold above the Kaharoa Tephra possibly due to the latter tephra being added to the background glasses derived from the Taupo Tephra or the results of increased disturbance.

Compositional analysis of selected brown shard concentrations confirms an andesitic to dacitic source. The majority of these correlate well with known Tufa Trig members derived from Ruapehu VC since the Taupo Tephra was deposited. Unexpectedly, there are no Egmont VC derived shards identified from these sequences. Individual populations are distinguished by major element composition and stratigraphic position and age relationships. Possibly as many as nine individual tephra depositing events are recognized including three or four historical eruption events (Table 4.2.3). The probable historical events recorded include 1861 (Ruapehu), 1945 (Ruapehu), 1974 Ngauruhoe) and 1996 (Ruapehu). Earlier eruptives most likely include Tufa Trig members Tf4 (or Tf5) (*ca.* 1400 ± 150 cal yr BP), Tf6 (620-890 cal yr BP), Tf8 (290-330 cal yr BP) and Tf14 (160-300 cal yr BP). Alternatives and additional units may be present. In all sections there is a distinct maximum peak in brown shards, coincident with the decline of the Taupo Tephra-derived shards at a point *ca.*600 cal yrs after the Taupo Tephra which correlates with Tufa Trig member Tf4 or Tf5 based on major element composition and relative age.

4.3 Lake Rotoroa

4.3.1 Site description

Lake Rotoroa (37°48'S, 175°16'30''E), also known as Hamilton Lake, is a small (~54 ha), shallow, enclosed lake formed in riverine and peat deposits in the urban area of Hamilton City (Fig. 4.3.1; Plate 4.3.1). Hamilton City (Kirikiriroa in Maori) lies ~130 km south of Auckland and is the fourth largest urban centre and seventh largest city in New Zealand with a population of about 130,000 people (Statistics New Zealand, 2008).

The lake is mesotrophic to eutrophic with high organic productivity resulting in the deposition of organic rich muds (gyttja). The lake water is moderately transparent with an absence of algal blooms but contains abundant and diverse aquatic macrophytes (Tanner *et al.*, 1990). The lake has a relatively small catchment (138 ha) which comprises residential housing and a grassed recreational area (Tanner *et al.*, 1990; Clayton & de Winton, 1994). The lake is a closed basin and is fed predominantly by precipitation and overland flow but in recent times is also fed by drainage inlet pipes around the lake margins. Discharge rates into the lake are approximately 16 ls^{-1} km^{-2} of water (Tanner *et al.*, 1990).

Radiocarbon dates and tephras from basal sediments of the lake suggest that it formed ~ 20,000 cal yrs BP in an embayment dammed by alluvial deposits (Hinuera Formation) from the ancestral Waikato River (Lowe & Green, 1992; Green & Lowe, 1994). The deposition of the alluvium allowed two shallow lakes to form which deepened and coalesced to form one lake after the encroachment of a marginal peat bog concomitant with increased net precipitation (Green & Lowe, 1985). The two basins (north and south; Fig. 4.3.1; Plate 4.3.1 b) of the original lakes are still evident from the bathymetry of the lake bed. The current depth of the lake is around 5-6 m and average depth 2.4 m (Tanner *et al.*, 1990; Clayton & de Winton, 1994).

There has been a wide range of studies of the lake sediments. These include investigations of the impact of recent human activities on the lake environment that include the application of herbicides in the last few decades to control aquatic plants (Tanner & Clayton, 1990; Tanner *et al.*, 1990). There has also been a small number of palaeoenvironmental studies and investigations of the tephra layers present in the lake sediments (Green & Lowe, 1985; Lowe, 1988b; Green & Lowe, 1994). Studies of the

pollen assemblages from nearby lakes sediments show that early Polynesian settlement occurred in the area at around 700 years ago when forests appear to have been rapidly burned off and replaced by scrub (Newnham *et al.*, 1989; Lowe & Green, 1992; Giles *et al.*, 1999). This interruption is supported by measurements of $\delta^{13}C$ in the Lake Rotoroa which show a rapid change to increased terriginous inputs and increased eutrophication around this time (Newnham *et al.*, 1989; Green & Lowe, 1994). Detailed tephrostratigraphic investigation of the lake have identified at least 14 named visible rhyolitic and andesitic tephra layers in the lake sediments from a range of TVZ sources including Egmont VC (Lowe, 1988b; Spiers, 1995). No tephras have been recorded in the post –Taupo time span.

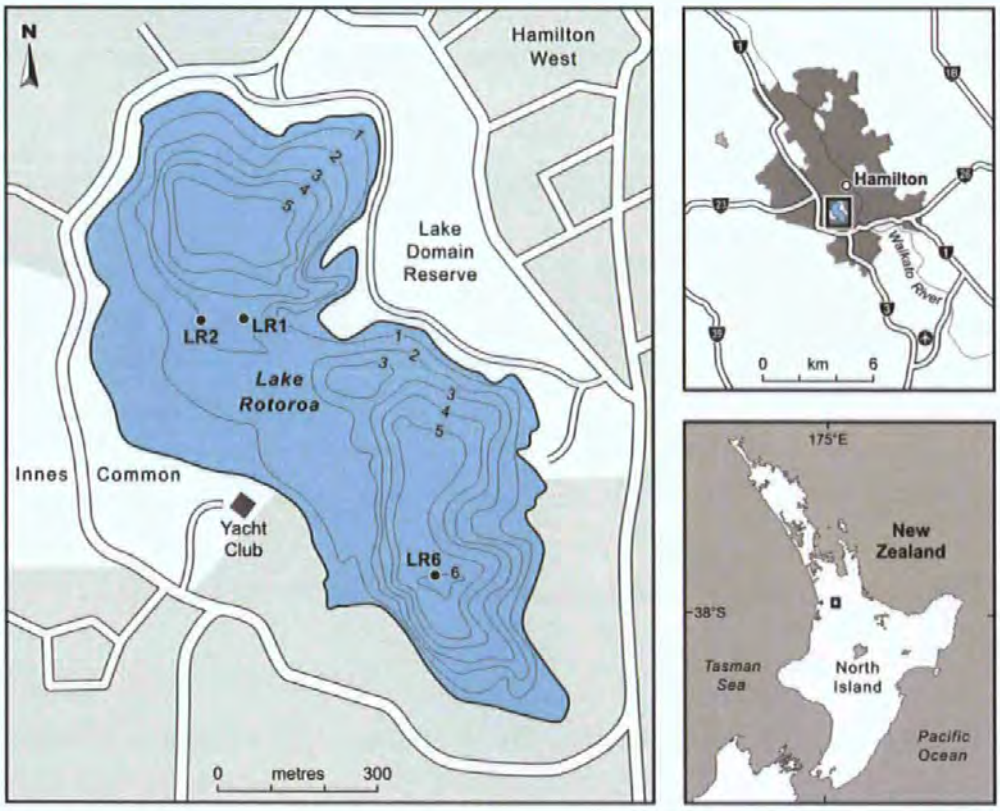

Figure 4.3.1 Location map of Lake Rotoroa with position of core sites in relation to water depth (redrawn from Tanner *et al.* 1990). Inset: the lake in relation to Hamilton City (grey shaded area), main traffic arteries and the present course of the Waikato River.

Plate 4.3.1 Satellite images of Lake Rotoroa: (a) location of lake within the greater Hamilton City area showing surrounding agricultural landscape and present course of the Waikato River. (b) Close up of the lake showing core sites and the lake bathymetry. Sourced from Orthophoto S14 Hamilton, Crown Copyright reserved: http://www.linz.govt.nz/core/topography/aerialandorthophotos/orthophotoindex/aps14/index.html).

4.3.2 Core collection

Short sediment cores were obtained from Lake Rotoroa in February 2005. Cores were collected using a modified piston corer with a 50 mm diameter collected from the side of a lightweight dinghy (Plate 4.3.2 a-c). This coring technique was possible because of the shallow nature of the lake. The original plans for core collection included several cores from different water depths from the north and south basins of the lake. However, retrieval of cores proved difficult for some of the deeper sections of the lake where sloppy sediments were encountered. In shallow parts of the lake the length of the sequence was too short to provide a high resolution account of tephra-derived glass shard content. Several cores were collected from the lake, three of which (LR1, LR2 and LR6; Table 4.3.1; Fig. 4.3.2; Plate 4.3.1 b; Plate 4.3.2 c) were used for this study.

Cores consisted of ~50 cm long sediment sequences taken from the water-sediment interface down to below the Taupo Tephra (1717 ± 13 cal yr BP; Sparks *et al.*, 1995; 2008). The Taupo Tephra was identified in the cores by field characteristics as fine lapilli ~1-2 cm in thickness in the cores at ~ 30 cm depth. This sediment interval represents a very slow sediment accumulation rate of ~ 0.17 mm yr^{-1} (based on an assumed constant sedimentation rate). Below this tephra there were at least three additional visible tephra layers down to a depth of ~90 cm in the sections retrieved (Table 4.3.1). Sections LR1 and LR2 were taken from the northern section of the lake where water depths were ~3 m and 2 m, respectively (Fig. 4.3.1). LR6 was collected from the southern basin of the lake where water depth exceeded 5 m.

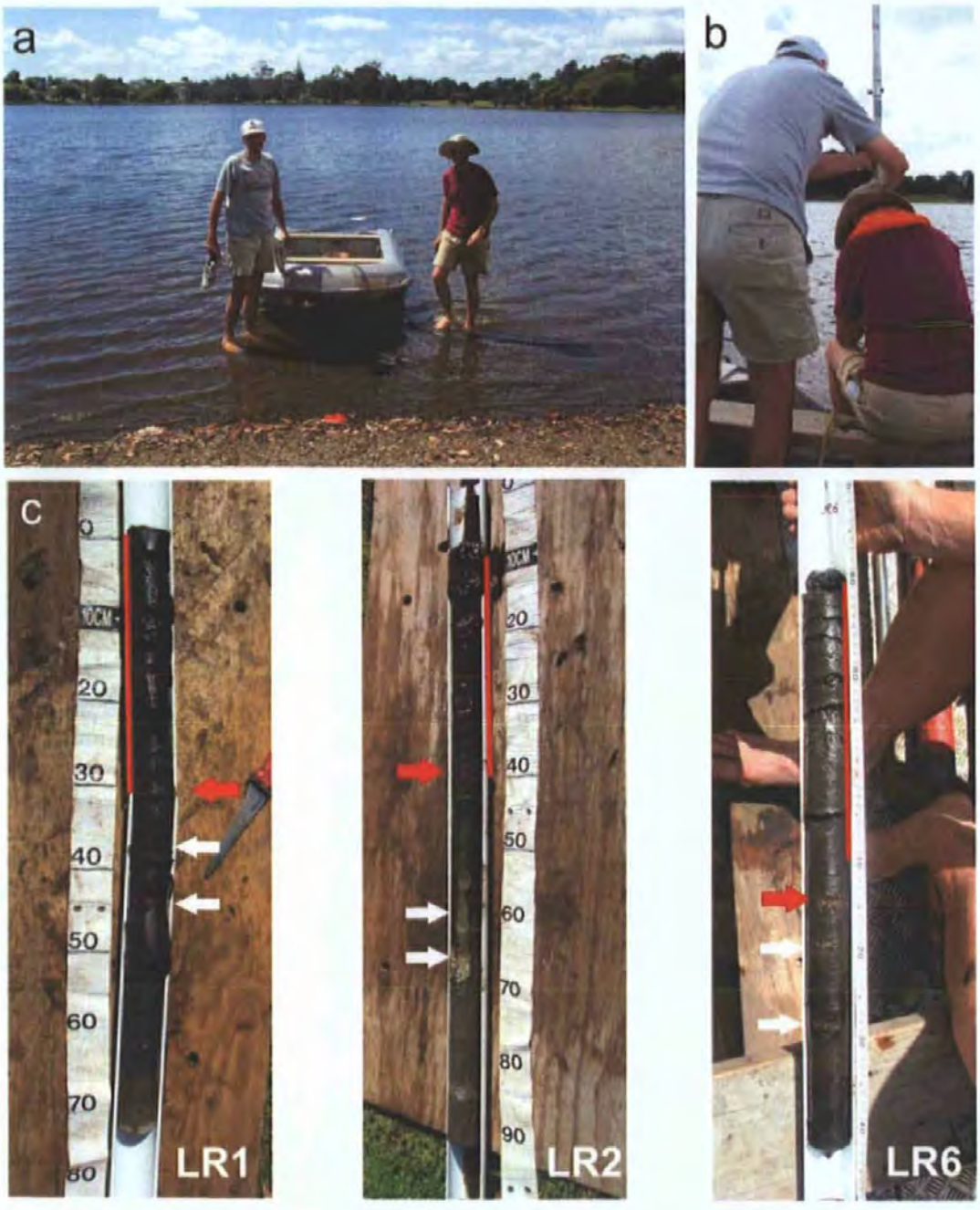

Plate 4.3.2 Photographs of Lake Rotoroa, the method of core collection and resulting sediment cores collected from the lake. (a) View of the southern basin of the lake (photo taken from the western edge by the yacht club; Fig. 4.3.1) showing the boat used to collect cores (with Profs. David Lowe and Rewi Newnham). (b) Setting the piston corer down into the water from the edge of the boat. (c) The three cores retrieved from the lake used as part of this study, LR1, LR2 and LR6 (Fig. 4.3.2; Table 4.3.1). Red lines represent 30 cm in length. Red arrows indicate position of Taupo Tephra identified from field characteristics and stratigraphic position in the cores; white arrows point to visible tephras in the cores below the Taupo Tephra. All photographs taken by author.

Table 4.3.1 Summary of cores collected from Lake Rotoroa

Sample code (date collected)	Core site details [Grid ref of core site]	Depth retrieved from surface (cm)	Sample retrieval	Notes on stratigraphy
LR1 (15-2-05)	North end of lake ~ 3 m water depth [E271035, N637600]	**0-100**	Piston corer with 50 mm diameter core barrel	Retrieved down to fine grey ash at the base of the core. At 30 m a fine lapilli identified as Taupo Tephra. Three additional macroscopic ash layers at 39, 45 and 65 cm.
LR2 (15-2-05)	North end of lake ~2 m water depth [E271027, N637592]	**0-86**		Taupo Tephra present as a very thin layer at ~22 cm depth. Three additional ash layers at 52 cm (Tuhua), 62 cm (Mamaku) and 85 cm (Opepe?)
LR6 (15-2-05)	South end of lake ~5 m water depth [E271069,N637543]	**0-61**		Fine lapilli at 35 cm possibly Taupo Tephra. Several additional tephras identified below

4.3.3 Lithostratigraphy and organic content

The lithostratigraphy of the lake cores from this site was described using the conventional Troel-Smith (1955) classification scheme for unconsolidated sediments. The Munsell colour chart was used to characterize the sediments according to colour. It was anticipated that this information could be used to identify sedimentological changes which may help to account for any variations in tephra content. Measurements of loss on ignition (LOI) were used to determine changes in organic content down through the sediment profiles and provide a guide to possible changes in lake sedimentation or catchment activities which

may have contributed or affected tephra content. Figure 4.3.2 provides an overview of the lithostratigraphy of the three cores.

The sediments in the three cores consisted of a homogenous, very fine organic rich mud (gyttja) above the Taupo Tephra with no distinguishable layering or structure. A subtle transition in colour was recognized up through all sequences changing from very dark brown (Musell: 7.5 YR/2.5/2) to dark brown (7.5 YR/3/2) approximately 10 cm above the Taupo Tephra in each sequence (Fig. 4.3.2).

LOI measurements taken from 2 cm contiguous samples in the sections revealed a relatively high component of organic material for the lake sediments ranging from 20-40% with an average of ~36 % organic matter (Fig. 4.3.4). The inorganic component revealed by microscopic examination includes a mixture of diatom frustules, sponge spicules, tephra-derived glass shards and minerogenic particles. Diatom frustules and sponge spicules form the major component of the sediments. Unlike the peat sequence from Moanatutua Bog, LOI measurements in the cores only appear to reflect the very high glass shard concentrations immediately above the Taupo Tephra.

All three cores show a similar pattern in changing organic content up from the Taupo Tephra to the surface of the core. Organic content increases steadily above the Taupo Tephra reaching peak values several centimeters above it. Values then decline very gradually up to approximately halfway in the sequences that mark an inflection to lower stable organic content. This inflection point in LOI coincides with a colour change in the sediments that possibly reflects the transition from a forested to deforested catchment resulting from human settlement in the area. This change in the catchment would have resulted in changes to hydrological and sedimentary process in the lake.

The organic content of LR1 increases to average values (36 %) ~ 2.5 cm above the Taupo Tephra and up to a maximum of 41% organic matter at 22 cm. Above 22 cm organic content in the core steadily declines up to ~14 cm where values plateau at ~33.5% organic content up to the surface. In core LR2 organic content also increases rapidly ~2.5 cm above the Taupo Tephra, with a peak organic content of 40% measured at 15 cm. Above 15 cm, values start to decline up to 10 cm where values remain consistently at ~36 % organic up to the surface. Section LR6 shows a more pronounced change in LOI values up through the sequence. Organic content increases to average values ~6 cm above the Taupo Tephra (29 cm) where values for organic content peak at 47 %, a ~6% increase compared to LR1 and LR2. Above 29 cm, values decline steadily up to 16 cm whereupon values plateau at ~24.7 %. This is a much lower value for the top section of the sequence compared with those of LR1 and LR2 (a difference of ~ 9% organic).

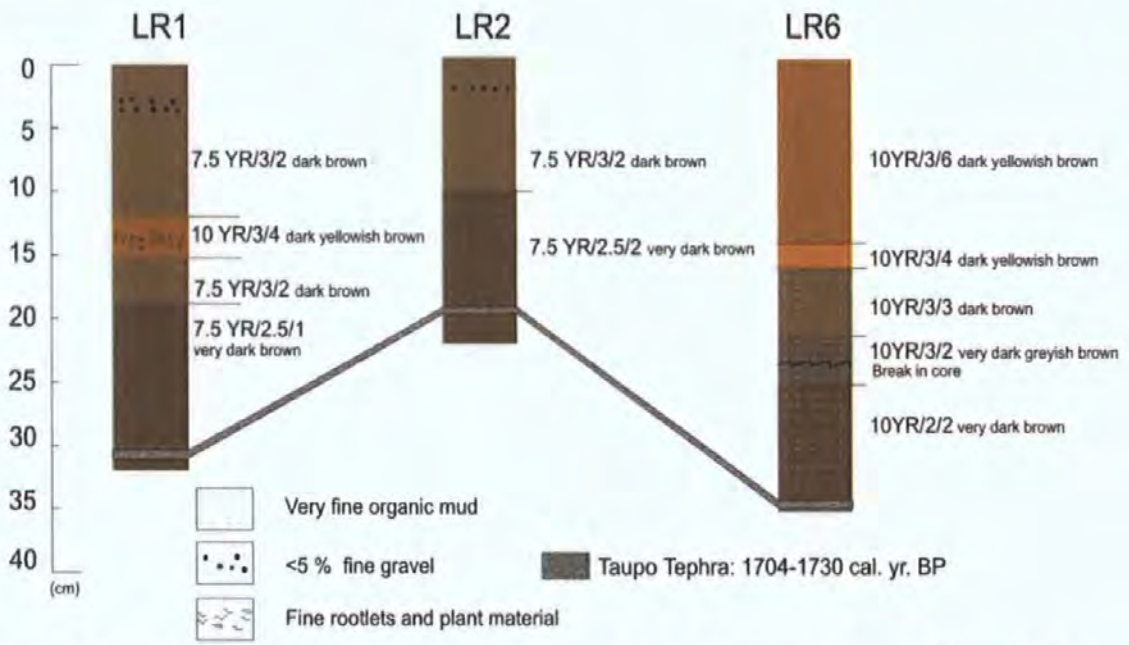

Figure 4.3.2 Stratigraphy of the three cores from Lake Rotoroa. Detailed lithostratigraphy, visible tephrostratigraphy and positions of samples for radiocarbon dating (from pollen concentrates and bulk sediment samples; see Table 4.8).

4.3.4 Age-depth models

An age-depth model was developed for core LR1 using AMS ^{14}C dating and tephra ages from the visible Taupo Tephra (1717 ± 13 cal yr BP) and from the Kaharoa Tephra (636 ± 12 cal yr BP) preserved as a cryptotephra (Fig. 4.3.3). The criteria for identifying the cryptotephra are detailed in section 4.3.6. This core was selected for dating to support the identification and interpretation of the shard concentrations confirmed by EMPA. AMS ^{14}C ages were determined at the NERC radiocarbon laboratory (RCL) in East Kilbride, Scotland (Table 4.3.2). A calibrated age was plotted with the tephrochronological ages using the median value and 2σ errors against the depth of the sample model (Fig. 4.3.3).

Dating the lake sequence with AMS ^{14}C ages proved problematic but provided an insight into the changing sedimentary process in the lake and an illustration of the difficulties of dating anthropogenically disturbed sequences. Six AMS ^{14}C ages were obtained from three replicated levels in the core firstly using pollen concentrates and then bulk sediment samples. Only one of the six AMS ages obtained is included in the age model (LR1-22; Table 4.3.2; Fig. 4.3.5) for reasons explained below.

Three pollen concentrate samples were initially extracted from the core to provide narrow time slices to circumvent the slow accumulation rates. The extraction method, however, resulted in very small samples which were near the limit for measurements of routine samples (*c.* 1 ml CO_2). Laboratory standards processed along with the samples also failed the laboratory's quality assurance programme (Dr Mark Garnett pers. comm.). The resulting ages were also considered too old and were therefore deemed unreliable. The result was that the ages were not reported formally by the RCL. The error terms for these informally reported measurements (Table 4.3.2) are higher than would be expected

for similar samples, which reflects the greater uncertainty in the results. Given problems with the sample sizes of the pollen concentrates, bulk sediment samples were used instead to date the sequence from the same or nearby horizons.

The lowest ages from samples LR1-22 and LR1-22p (p suffix from pollen concentrates), both extracted from ~22 cm in the core resulted in very similar median ages and strongly overlapping error ranges. Both ages are close to the estimated age for this level in the core (Fig. 4.3.3; Table 4.3.2) and likely represent a time period before the deforestation era, based on similarity in the two ages and the position of the Kaharoa Tephra identified in the core. A major point of inflection in the organic content curve also occurs at this level in the core. Organic content would be expected to trend to lower levels following deforestation. As a consequence, it is concluded that both these ages are reliable. The date from the bulk sample is used in the age model because it has smaller laboratory errors.

The age obtained from LR1-14p was deliberately targeted at a layer containing visible plant material but insufficient plant fragments were extracted for dating. The sample consisted of pollen concentrates but the resulting age represented a significant age reversal in the age model and has large errors. Sample LR1-16 (bulk sample) was taken just below this plant layer, yet gives a considerably younger age, albeit still too old. The upper samples LR1-6p and LR1-7 provide ages, which are closer to estimated ages but still older than expected. In particular they give ages older than the Kaharoa Tephra (which underlies this horizon). Interestingly, LR1-6p is considerably younger than LR1-7 (bulk sample) which is likely to reflect the reduced potential for contamination from pollen concentrates which derive mostly from aeolian origin in undisturbed sediments. The fine gravel layer a

few centimetres above this horizon is clear evidence that inwash is still an issue for sedimentation in the core.

Table 4.3.2 Conventional radiocarbon and calibrated ages on bulk sediment sample and pollen concentrate samples from core LR1. Sample positions are shown in Figures 4.11. *Isotopic fractionation $\delta^{13}C$ is expressed as ‰ wrt PDP, error ± 0.1 for NERC dates (SUERC prefix). Calibration curve used is shcal 04.14c (Southern Hemisphere calibration curve). *Based on a linear interpolation using tephrochronological age of Taupo Tephra and existing ages. †age estimated due to insufficient CO_2 for $\delta^{13}C$ measurements. § Laboratory standards processed commensurate with pollen concentrate samples.

Lab code	Stratigraphic position (cm)	Sample material	Conv. RC age years BP (±1sd)	plus/ minus	$\delta^{13}C_{vpdb}$ ‰	Estimated BP*	Calibrated age range (2σ) cal yr BP	Median age calibrated age cal. yr BP
SUERC-15743	6-7	Bulk sediment	**1039**	37	-29.4	400	**576-733**	**625**
SUERC-15744	14-16	Bulk sediment	**1227**	37	-29.2	800	**1176-1988**	**1555**
SUERC-15745	21.5-22	Bulk sediment	**1136**	37	-29.9	1200	**733-1243**	**968**
GR/8625	6-6.5	Pollen concentrates	**709**	83	- 28.7	400	**897-961**	**888**
GR/8626	14-14.5	Pollen concentrates	**1687**	191	- 25.0†	800	**974-1220**	**1094**
GR/8627	21.5-22	Pollen concentrates	**1101**	122	- 25.0†	1200	**930-1059**	**993**
GR/8624	Lab standard§	ST1 96H HUMIN (1)	**2729**	326	- 28.4			
GR/8628	Lab standard§	ST2 BIT. COAL (4)	**34494**	109	- 23.0			

4.3.5 Tephra derived glass-shard content

The results of glass shard counts from the three cores from Lake Rotoroa are shown in Figure 4.3.4 (and Fig. 4.3.5 for LR1) alongside measurements of organic content. Clear and brown shard types were encountered in the sediments as with Moanatuatua Bog (section 4.2) and are present in almost continuous concentrations through each core. As with the Moanatuatua sections, the high concentrations of glass shards detected immediately above the visible Taupo Tephra are omitted from the diagrams for clarity. The shard content for each section is described from the visible Taupo Tephra to the top of each

sequence for both clear and then brown shards 25-63 μm in size. Observations of size range prior to sieving were made in some instances. Observations of shard character and morphology are described with reference to images in Plate 4.3.3 based on a combination of generic and technical terms for ash sized tephra-derived glass shards (Heiken, 1972; Fisher & Schmincke, 1984; Heiken & Wohletz, 1985).

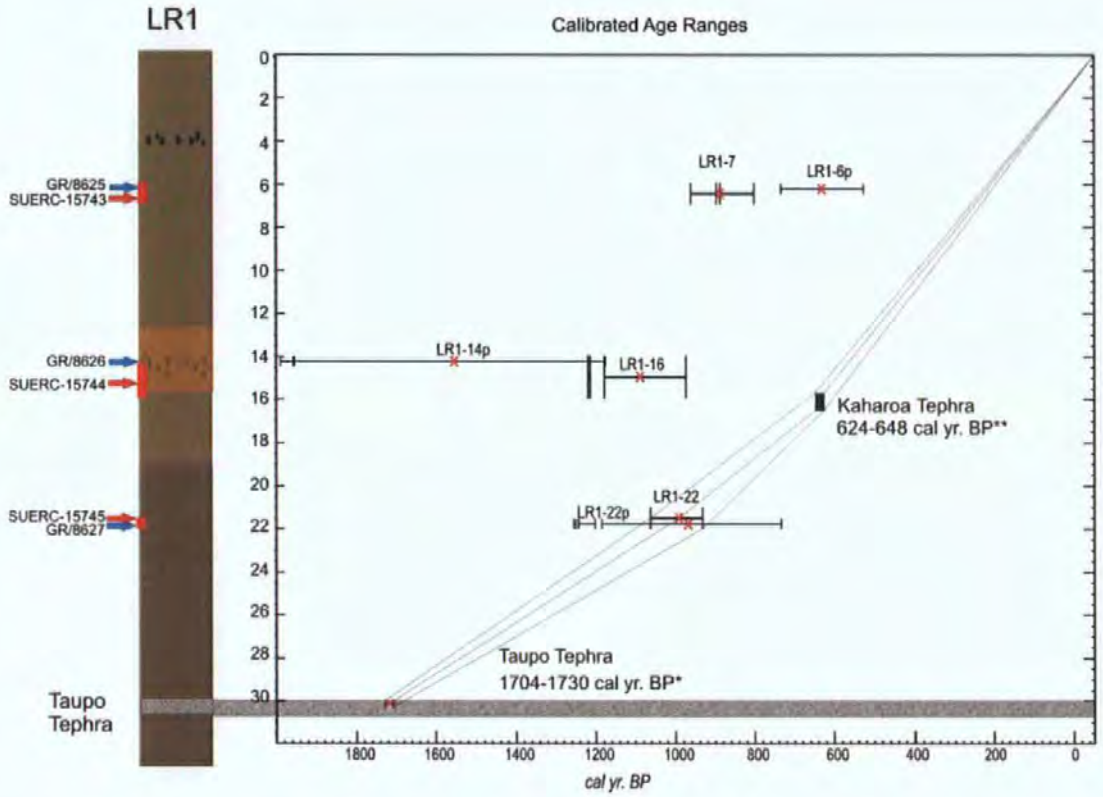

Figure 4.3.3 Age-depth model for core LR1. Based on a linear interpolation through median age of one ^{14}C AMS date (2σ error) (codes refer to sample types and depth in core detailed in Table 4.3.2), tephrochronological dates on the Taupo Tephra (*from Sparks et al. 2008) and Kaharoa Tephra (wiggle match date from Hogg et al. 2003) (refer to text). The additional five ^{14}C AMS dates not used on the model for reasons discussed in the text are shown in relation to stratigraphy which highlights possible sources of contamination.**

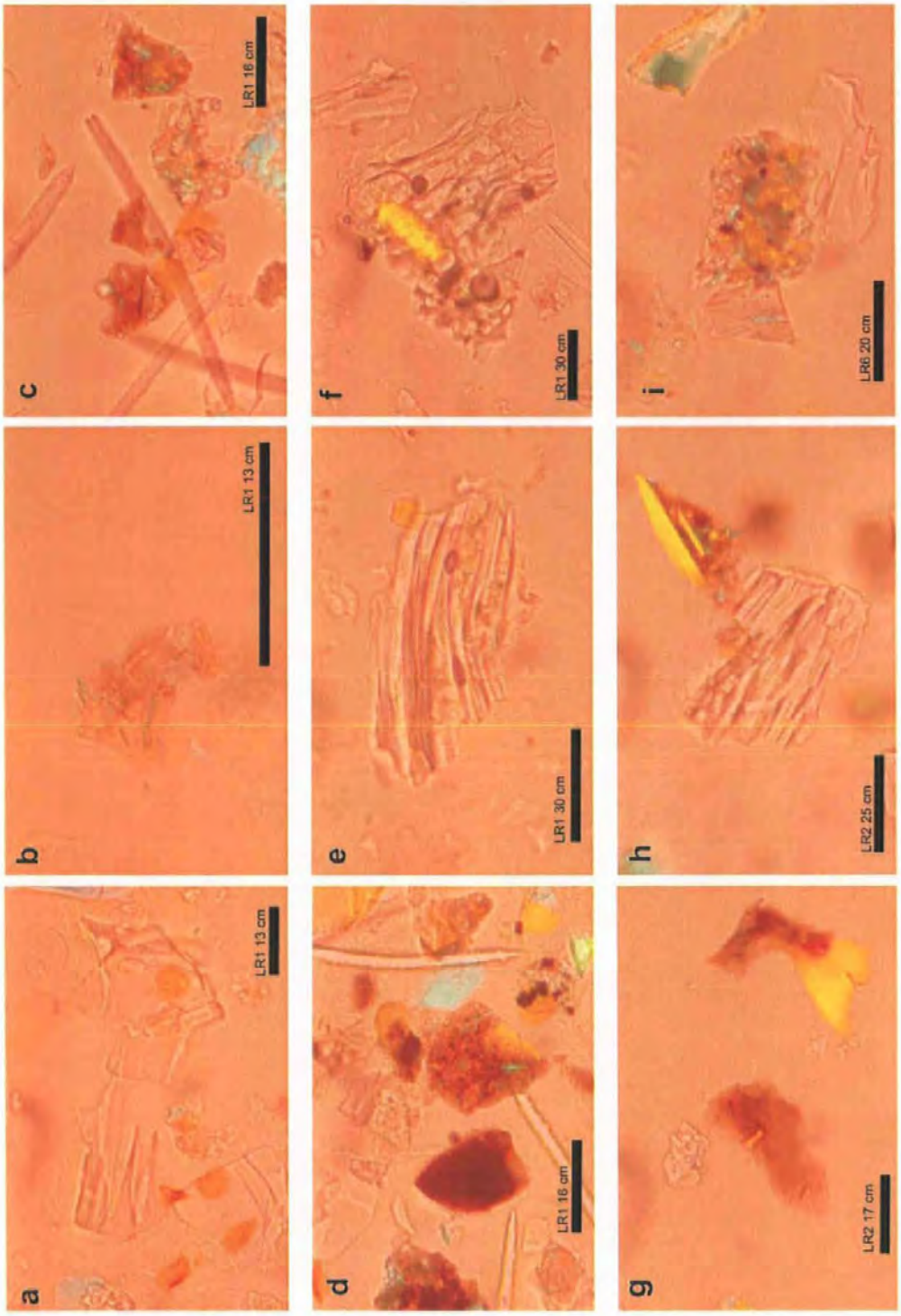

Plate 4.3.3 Photomicrographs of various glass shard types observed in samples from cores LR2 (a-f) in order of depth in section); LR2 (g, h) and LR6 (i) as referred to in the text.

All shards are photographed from glass slide setting using manual SLR camera attached to a petrographic microscope and viewed under plain polarized light at x400 magnification. Black bar on each image equals 50 µm in length. Section number and depth are labeled on each image. Additional images of shards from selected levels are provided in the appendix.

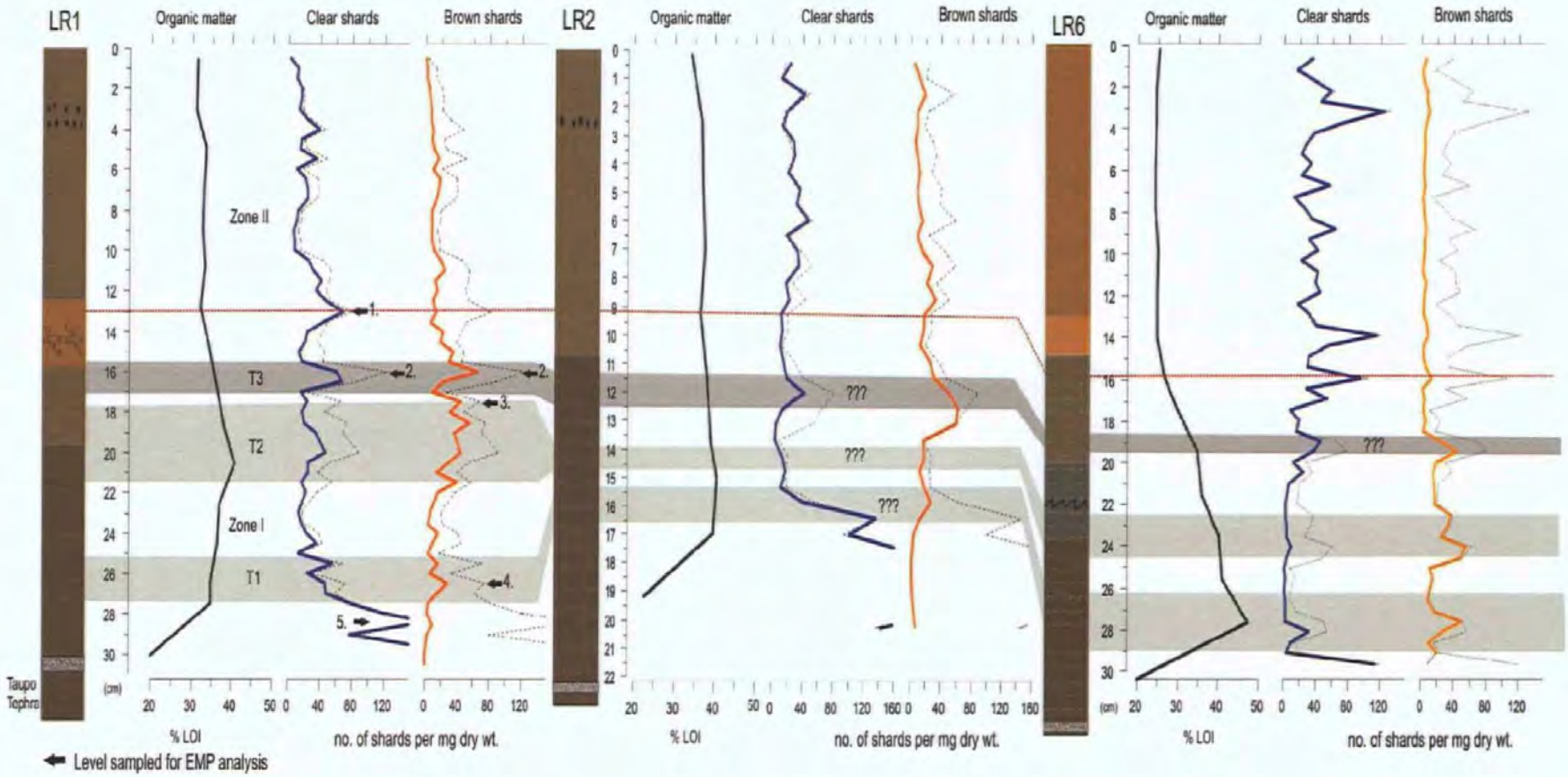

Figure 4.3.4 Results of glass shard concentrations derived for cores LR1-3 shown alongside stratigraphy (see Fig. 4.3.2 for key) and organic content. Shard counts are calculated to number of shards per mg dry weight for each core: blue for clear shards and orange for brown shards. The background dashed line represents total shards brown and clear combined. Organic content (black line) is derived from loss on ignition measurements. Thick grey bands numbered T1-3 represent possible correlative tie-points between the three sections based on a combination of shard concentrations and lithostratigraphy. The red line marks an inflection point in LOI values to lower organic content in all three cores and represents a change in the pattern of shard concentrations in the core: Zone I to Zone II.

Glass shard content core LR1

The shard counts from this sequence (Figs. 4.3.4; 4.3.5) are based on 62 contiguous samples 0.5 cm thick from the top of the sequence to just below the visible Taupo Tephra at 30-31 cm in the core. Individual glass shards were detected in almost every sample viewed through microscopy and comprised a mix of clear and brown coloured shards in varying proportions.

Clear shards form highly fluctuating concentrations up through the core with at least six distinct 'peaks' in shards which exceed mean values derived for clear shard concentrations of ~35 shards per mg d-wt. These peaks include the zone of shards immediately above the Taupo Tephra which extends up the sequence for ~4 cm in fluctuating but declining shard content before reaching mean clear-shard concentrations. This trend follows a similar pattern to that recorded in peat sites in this study, e.g. Moanatuatua Bog (Fig. 4.2.5), and is suggestive of continued remobilization and re-deposition of the deposit in the lake and from the surrounding land surface. The shards in this zone comprised predominantly fine (4-63 μm) to medium ash (63-500 μm) sized glass. The majority of shards >63 um were, however, removed during the sieving process in preparing the samples for microscopy. It is therefore likely that this zone contains much higher shard concentrations than shown here. Shards displayed low to moderate vesicularity indices and a moderate to high stretching (Plate 4.3.3 e). Interspersed within this glass were some large (>250 μm) highly vesicular shards with infrequent but distinct microlites (small crystals) (Plate 4.3.3 f).

The additional peaks in clear shards occur at ~ 4, 13, 16.5, 20 and 25.5 cm. The largest of these peak concentrations of glass is at ~13 cm and 16.5 cm which both coincide with a change in lithology. The peak in shards at 13 cm coincides with a point of LOI inflection to

lower organic content and at 16.5 cm the shard peak occurs below a change in the colour of the sediments in the sequence (Fig. 4.3.5). The character of shards for the majority of these levels was not observably different or distinct from glass attenuated above the Taupo Tephra and consists of a mix of shard sizes (Plate 4.3.3 a, b). Only the zone of clear shards at 16 cm appears to comprise a distinct population based on shard character. Shards at this level comprise predominantly small (<50 μm across longest axis) platy glass shards mixed in almost equal parts with brown shards (Plate 4.3.3 c, d).

The down-core content of brown shards shows a distinct pattern different from that of clear shard content (Fig. 4.3.5). The mean value of brown shard content for the sequence is ~16 shards per mg d-wt., less than half the mean for clear shards at ~35 shards. However, brown shard content is represented by greater fluctuations through the section with more than twice the number of 'peaks' exceeding mean shard content values than for clear shards. These peaks form discrete zones of elevated brown shard content in the core. The lowest of these zones coincides with the decline in clear shards above the Taupo Tephra, 24-25.5 cm in the core. The most prominent of these zones, however, occurs between 15 and 21 cm which coincide, in part, with peaks in clear shard content (Fig. 4.3.5). From below 14 cm up to the top of the core shard concentrations noticeably decline with only a few moderately elevated peaks in shard content.

Brown shard concentrations in all levels typically consisted of small, fine-ash sized (<63 um) blocky and poorly vesicular shards with dense microlite inclusions (Plate 4.3.3 b-d). These are comparable with andesitic and dacitic glass fragments detected in Moanatuatua Bog sequences (section 4.1.4) and exhibit Type 1 morphologies as defined by Heiken and Wohletz (1985) for andesitic type eruptives. These are typical of hydrovolcanic eruptions

which include Tufa Trig member tephras from Mt. Ruapehu (Donoghue *et al.*, 1997). At 16 cm these included some distinctly platy, microlite-poor, dark brown shards which may be characteristic of an individual tephra population or alternatively represent an influx of reworked older deposits (Plate 4.3.3 d).

Glass shard content LR2

The glass shard content from the replicate sequence LR2 is based on 43 contiguous samples 0.5 cm thick down to the Taupo Tephra at 22 cm depth in the core. Shard counts are comparable with changes in shard content for core LR1 but with slightly less well defined peaks - which are possibly an artifact of the increased time intervals represented by each sample. Some peaks in clear and brown shards in the core can be traced to comparable stratigraphic levels, based on lithological changes, in core LR1 (T1-3; Fig. 4.3.4). Comparable shard patterns include the persistence of clear shards concentrations for at least 6 cm above the Taupo Tephra (T1) in the core which is followed by a slight increase in brown shards (marked by T1). Clear and brown shards were also observed persisting below the visible Taupo Tephra for several centimetres (Plate 4.3.3 e). The brown shard concentration at 18-16 cm comprises predominantly small (<50 um), dark brown, microlite-poor shards characteristics of shard concentrations observed from comparable stratigraphic levels in LR1 (Plate 4.3.3 d). Other comparisons include a marked increase in both clear and brown shard content approximately halfway up the sequence (T2 and T3). T1 and T2 concentrations in LR1 are represented by multiple peaks, but in LR2 these are represented by a single, wide peak in shard concentration 11-15 cm depth in the core. Above 9 cm depth, coincident with an inflection in LOI to a lower,

organic content, clear shard concentrations in LR2 remain relatively high and comprise multiple peaks which do not compare with shard content at comparable levels in LR1 or LR6. Concentrations of brown shards in this level of the core remain low with no distinguishable peaks.

Glass shard content LR6

The results of glass shard content derived for core LR6 are based on 49 contiguous 0.5 cm thick samples taken from the top 30 cm of sediment in the core. Shard counts also reveal patterns comparable to those of cores LR1 and LR6 but with generally higher average shard concentrations. As for LR1 and LR2, the high concentrations of clear shards persist above the Taupo Tephra for ~5 cm in the core. Coincident with the decline in these clear shards in the lower part of the core there is a peak in brown shards that probably correlate with T1 in LR1 and LR2 (Fig. 4.3.4). Additional peaks in brown and clear shards in the lower half of the core tentatively compare with T2 and T3 concentrations identified in LR1. T3 comprises a well defined peak in both brown and clear shards where the two different shard types are observed in almost equal proportions (Plate 4.3.3 f), a characteristic observed in core LR1. Above ~17 cm there is a marked increase in the concentration and frequency of clear shards but a decline in brown shards as for LR3. The concentrations of clear shards in the upper section of this core are significantly higher than those of the cores from the northern basin of the lake. It is possible that the southern basin of the lake, which is surrounded by a steeper catchment and almost completely surrounded by residential buildings, was subject to greater degree of disturbance in recent centuries than the northern basin (Plate 4.3.1 b).

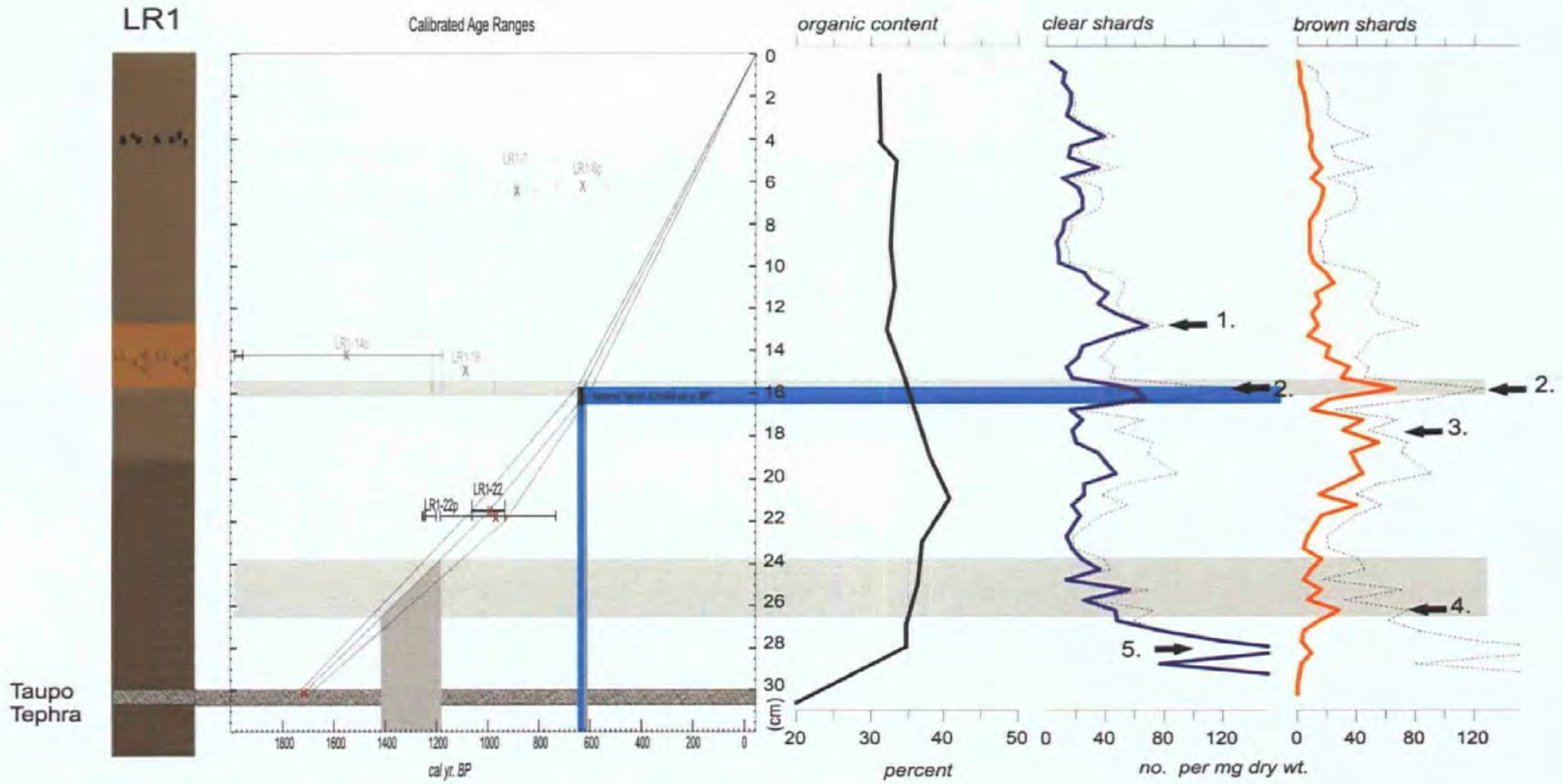

Figure 4.3.5 Results of tephra-derived glass shard counts derived from core LR1 shown alongside stratigraphy, organic content and age depth model. The age-depth model (see Fig. 4.3.3 for more detail of individual ages) is based on a linear interpolation through the median age of one AMS ^{14}C age (Table 4.3.2), and tephrochronological dates on the Taupo and Kaharoa tephras. Numbered arrows indicate positions sampled for EMPA and correspond with numbered samples in Tables 4.3.3 and 4.3.4.

4.3.6 Geochemical character, correlatives and interpretation

The results of major element analyses of cryptotephra populations sampled from Lake Rotoroa are based on five samples from core LR1 (Fig. 4.3.5). A total of 63 analyses on individual shards were determined by electron microprobe analysis (EMPA). These represent a very limited number of analyses which are for most levels insufficient for a full evaluation of the core. Interpretations of the results presented below therefore remain tentative. Sampling positions in the core were selected for EMPA on the basis of defining criteria outlined in section 3.3.1 (Chapter 3). Table 4.3.3 summarises the compositional analyses from the main populations identified from each position. Table 4.3.4 presents a summary of identified sources and eruption correlatives for each glass population level together with interpolated age range based on a limited age-depth model (Fig. 4.3.5). Bivariate plots of diagnostic oxide combinations are shown in Figure 4.3.6 for andesitic and rhyolitic populations in the samples. All elements were considered in correlating deposits and for distinguishing between individual populations in conjunction with age-stratigraphic position. All analysis presented here are normalised to 100 weight (wt) % loss-free basis (Froggatt, 1992; Pearce *et al.*, 2008). Raw, non-normalized analyses are recorded in the Appendices.

The major element composition of glass shards from this site reveal a mix of both rhyolitic (SiO_2 = > 69 wt.%) and intermediate glasses (SiO_2 = 58-70 wt.%) represented by clear and brown shards, respectively (Table 4.3.3; Fig. 4.3.6). The majority of analyses derived from this site are comparable to published analyses for TVZ eruptives (Shane, 2000; Lowe *et al.*, 2008b) and suggest that the cryptotephra populations in this lake site are not subject to any significant chemical alteration.

The analysis of rhyolitic glasses in the core reveals multiple compositional groups. Values for SiO_2 range from 74.08-78.58 wt. % and contain representative populations from Taupo VC and Okataina VC sources (Table 4.3.3; Fig. 4.3.6). Raw analytical totals show a wide range within individual glass shard populations from 93.59->100 wt%, with an average total of 96.88 wt%. For rhyolitic glasses, major element composition was sufficient to identify at least four distinct compositional groups from Taupo and Okataina volcanic centres which include a number of pre-Taupo Tephra deposits preserved in younger stratigraphic levels (Fig. 4.3.6 a, c).

Several glass populations with intermediate chemistry were identified in core LR1. As for Moanatuatua Bog, these are predominantly dacitic glasses (Fig. 4.3.6 a, Table 4.3.3). Individual glass populations comprise typically heterogeneous composition (SiO_2 = 60.52-66.35 wt.%; total alkalis = 5.97- 7.44 wt.%) characterized by high standard deviations for individual oxides compared to rhyolitic glasses. Raw analytical totals for intermediate glasses were typically high, ranging from 97.99-100 wt.%.

Analyses of these intermediate glasses are consistent with Tufa Trig members from Mt Ruapehu volcano (TnG VC) after Donoghue *et al.* (1996; 1997; 2007) (Fig. 4.3.6 d). As determined from Moanatuatua Bog, high-K Egmont sourced tephras were not evident from the selected analyses from this site. All intermediate glasses were evaluated for contamination from microlite phases using the procedure of Platz et al. (2007) (see section 4.2.5; Fig. 4.3.6 b).

Correlatives for dacitic populations were established using age-stratigraphic positions and pre-existing compositional analyses from proximal Tufa Trig members (Donoghue *et al.*, 1995b; 2007). Ages of tephra populations were determined using only a limited age model

(see section 4.2.6) and as a result identifications remain tentative. Interpolated age ranges are based on 2σ age ranges to account for limited numbers of ages (Figs. 4.3.5).

The following descriptions refer to numbered samples shown in Figure 4.3.5 and sample numbers in Tables 4.3.3.

Sample 1 (LR1, 12.5-13 cm): Reworked glass shards from TgVC, Tf members, Taupo VC and Okataina VC with one grain Tuhua Tephra

Sample 1 represents a wide zone of elevated shard concentrations 10-14 cm depth in the core containing predominantly clear type shards. This level in the core also marks the onset of changes to lithology (sediment colour and LOI) and to the pattern of glass shard concentrations in the core (Fig. 4.3.6). Compositionally, this sample contains glasses with rhyolitic and intermediate chemistries that represent an influx of reworked deposits from older stratigraphic levels.

Rhyolitic glasses (10 out of 13 shards analysed) consist of a wide range of compositions that plot into at least four distinct compositional groups (plot of SiO_2 versus total alkalis; Fig. 4.3.6 a) that can be linked to pre- and post-Taupo TVZ tephras (Lowe *et al.*, 2008b). Four of the analyses (40%) fit within the wide compositional range derived for the Taupo Tephra (shown plotted against compositional envelope from Gehrels *et al.*, 2006) but potentially correspond with the older but compositionally similar Opepe Tephra (Taupo VC derived) which is preserved as a thick deposit below the Taupo Tephra in the lake sediments. Four analyses from this level closely correspond with known Okataina VC derived tephras that include Kaharoa and Mamaku tephras (Fig. 4.4.6 a). Of these, two

shard analyses fit into the compositional envelope derived for Kaharoa Tephra from Moanatuatua Bog (Fig. 4.3.6 c). This tephra is identified as a cryptotephra in lower stratigraphic levels in the core (15.5 cm, Sample 2). Kaharoa-derived shards were characterized by higher K_2O (~4.2 wt.%) compared with older Okataina VC derived tephras (Lowe *et al.*, 2008b) and resulted in higher analytical totals (exceeding 99 wt % in most cases). The Mamaku Tephra is an additional pre-Taupo tephra recorded as a visible layer in the site (Lowe, 1988; Table 4.3.1) and was distinguished from Kaharoa shards by much lower K_2O (~3.54 wt.%; Table 4.3.3) and distinctly lower analytical totals obtained (~96 wt.%). These glasses with lower totals effectively contain greater "water" content (Froggatt, 1983).

The remaining analyses of rhyolitic chemistry included one grain labelled "uncorrelated" that fits in a distinct compositional group of uncorrelated analyses from other levels in the core (Fig. 4.3.6 a; Table 3.3.3). These are most likely to represent much older TVZ tephras preserved in lower stratigraphic levels in the lake sediments and possibly reworked from exposures in shallow lake margins or banks around the shoreline. In addition, one shard analysis correlates with the compositionally distinct peralkaline Tuhua Tephra (7005 ± 155 cal yr BP) which is characterized by very high FeO and Na_2O, and low Al_2O_3, compared with other TVZ derived tephras (Manighetti *et al.*, 2003). This tephra has also been observed as a visible unit in the lake sediments at depth (Lowe, 1988a; Green and Lowe, 1994; Table 4.3.1).

Only three analyses were determined from sparse intermediate glasses at this level in the core. These glasses were dacitic in composition and very similar to intermediate glasses from preceding glass population recorded at 15.5 cm (sample 2) that potentially correlate

with Tufa Trig members Tf5, 6 and 8. Because of the high number of analyses linked to older, reworked deposits in this level of the core it is likely these shards may also represent secondary deposition.

Sample 2 (LR1, 16.5-17 cm): Kaharoa Tephra and TnG VC, Tf member 6-8 with reworked shards from Taupo VC and Okataina VC derived tephras

Sample 2 marks a discrete peak in both clear and brown shard concentrations in core LR1 that can be traced through all three sequences (marked by T3; Fig. 4.3.4). This level of the core immediately underlies a lithological change in the sequence marked by an inwashed layer containing plant material (Fig. 4.3.4). Glass analyses revealed a heterogeneous mix of compositional populations that include primary fall and reworked shards from older stratigraphic levels. Partially due to the mix of glasses in this sample only a limited number of analyses were achieved per compositional population and identifications are provisional.

Rhyolitic glasses plot into the same four compositional groups detected in sample 1 (minus Tuhua Tephra). At least six out of the total of nine rhyolitic analyses correspond with OVC derived tephras that include Kaharoa and Mamaku tephras. Only four analyses fit within the compositional range derived for the Kaharoa Tephra from multiple samples from Moanatuatua Bog (Fig 4.3.6 c). However, shards correlating with the Kaharoa Tephra were not detected in the sample immediately below (sample 3). This lack of detection would suggest that this position marks the first occurrence of the tephra and is therefore likely to represent primary fall deposit, albeit mixed with older secondarily deposited tephra.

Table 4.3.3 Electron microprobe analyses of tephra-derived glass shards from 5 sample depths in core LR1, from Lake Rotoroa.

Sampling positions are shown in Figure 4.3.5. Means (in bold) and standard deviations of total number (*n*) analysis (of individual shards) normalized to 100% loss free (wt%). Analysis undertaken at NERC Tephra Analytical Unit, University of Edinburgh, during February and June 2007. Includes individual uncorrelated analyses from each sample position. †Laboratory standard analyzed at regular intervals during analyses of LR1 samples. *Total iron as FeO, **water by difference.

Anal.no.	1a		1b		1c		1d		1e	2a		2b		2c	
Core/depth	**LR1/13 cm**									**LR1/15 cm**					
Source	**TnG VC**		**OVC**		**OVC**		**TVC**		**Mayor Is.**	**TnG VC**		**OVC**		**OVC**	
(Tephra)	**Tufa Trig**		**Kaharoa Tephra**		**Mamaku Tephra**		**Taupo Tephra**		**Tuhua Tephra**	**Tufa Trig**		**Kaharoa Tephra**		**Mamaku Tephra**	
SiO_2	**63.86**	0.76	**78.07**	0.10	**78.16**	0.13	**75.59**	0.19	**74.36** *	**64.02**	0.81	**77.72**	0.26	**78.05**	0.36
$Al2O_3$	**14.57**	0.16	**12.13**	0.09	**11.96**	0.12	**12.90**	0.20	**9.04** *	**14.57**	0.25	**12.19**	0.22	**12.20**	0.18
TiO_2	**1.16**	0.03	**0.07**	0.03	**0.10**	0.02	**0.24**	0.05	**0.28** *	**1.10**	0.08	**0.07**	0.02	**0.10**	0.04
FeO*	**6.41**	0.35	**0.90**	0.14	**1.10**	0.06	**1.81**	0.14	**5.57** *	**6.68**	0.45	**0.87**	0.08	**0.92**	0.06
MnO	**0.14**	0.07	**-0.06**	0.03	**0.04**	0.10	**0.11**	0.07	**0.06** *	**0.09**	0.07	**0.09**	0.04	**0.06**	0.06
MgO	**2.17**	0.10	**0.06**	0.00	**0.12**	0.03	**0.27**	0.01	**0.02** *	**1.95**	0.25	**0.07**	0.00	**0.10**	0.02
CaO	**4.82**	0.45	**0.61**	0.04	**0.79**	0.00	**1.59**	0.04	**0.26** *	**4.80**	0.36	**0.61**	0.03	**0.76**	0.04
Na_2O	**4.02**	0.07	**4.05**	0.21	**4.18**	0.24	**4.60**	0.16	**6.03** *	**4.04**	0.26	**4.20**	0.14	**4.13**	0.11
K2O	**2.63**	0.15	**4.20**	0.13	**3.54**	0.20	**2.87**	0.06	**4.33** *	**2.51**	0.28	**4.17**	0.08	**3.69**	0.05
P_2O_5	**0.23**	0.01	**-0.02**	0.02	**0.01**	0.01	**0.02**	0.02	**0.04** *	**0.23**	0.02	**0.01**	0.01	**0.00**	0.02
*H_2O***	*1.52*	*0.19*	*0.54*	*0.33*	*3.37*	*0.48*	*1.93*	*1.57*	*1.40* *	*1.29*	*0.51*	*1.74*	*0.91*	*4.41*	*0.27*
n	***3***		***2***		***2***		***4***		***1***	***8***		***3***		***3***	

Anal.no	2d		3a		3b		3c		4		5	
Core/depth			**LR1/17 cm**						**LR1/26.5 cm**		**LR1/28 cm**	
Source	**TVC**		**TnG VC**		**OVC**		**TVC**		**TnG VC**		**TVC**	
(Tephra)	**Taupo T.**		**Tufa Trig**		**Mamaku T.**		**Taupo T.**		**Tufa Trig Tf 4**		**Taupo T.**	
SiO_2	**75.19** *		**63.99**	0.89	**78.23**	0.49	**74.08** *		**67.58**	0.77	**74.73**	0.32
Al_2O_3	**13.05** *		**14.06**	0.88	**12.14**	0.01	**13.49** *		**14.58**	0.79	**13.55**	0.22
TiO_2	**0.22** *		**1.17**	0.15	**0.12**	0.01	**0.35** *		**0.94**	0.07	**0.29**	0.03
FeO*	**1.91** *		**7.12**	0.79	**0.76**	0.17	**2.05** *		**4.83**	0.68	**1.87**	0.20
MnO	**0.10** *		**0.08**	0.06	**0.00**	0.09	**0.10** *		**0.06**	0.02	**0.20**	0.03
MgO	**0.28** *		**1.93**	0.21	**0.11**	0.01	**0.28** *		**0.97**	0.28	**0.28**	0.01
CaO	**1.68** *		**4.65**	0.55	**0.87**	0.04	**1.74** *		**4.14**	0.58	**1.59**	0.03
Na_2O	**4.58** *		**3.93**	0.22	**4.08**	0.04	**4.65** *		**3.95**	0.28	**4.59**	0.15
K_2O	**2.93** *		**2.80**	0.37	**3.68**	0.17	**3.24** *		**2.71**	0.27	**2.87**	0.07
P_2O_5	**0.06** *		**0.26**	0.05	**0.02**	0.00	**0.03** *		**0.25**	0.02	**0.03**	0.02
*H_2O***	*1.68* *		*1.30*	*0.39*	*3.28*	*0.32*	*1.75* *		*0.83*	*0.49*	***3.83***	*1.35*
n	***1***		***6***		***2***		***1***		***7***		***3***	

Anal.no.					**Uncorrelated**										
Core/depth	**LR1-13**	**LR1-15**	**LR1-15**	**LR1-17**	**LR1-17**	**LR1-17**	**LR1-17**	**LR1-28.8**	**LR1-28.8**	**R1-28.8**			**Standards**		
Source													**Liparit†**		TB1G†
(Tephra)															
SiO_2	77.35	77.46	77.76	77.76	77.23	77.50	77.77	77.55	77.11	78.13			**74.14**	0.25	**53.92** 0.14
Al_2O_3	12.11	12.35	12.14	12.07	12.30	12.26	12.01	12.87	12.83	12.43			**12.84**	0.10	**16.02** 0.11
TiO_2	0.14	0.12	0.13	0.21	0.15	0.10	0.25	0.15	0.11	0.13			**0.07**	0.03	**0.89** 0.03
FeO*	1.57	1.12	1.16	1.18	1.45	1.54	1.08	0.95	1.20	1.33			**1.58**	0.14	**8.44** 0.28
MnO	0.12	0.14	0.14	0.10	0.01	0.17	0.08	0.02	0.12	0.10			**0.04**	0.05	**0.20** 0.08
MgO	0.12	0.11	0.16	0.16	0.13	0.14	0.12	0.14	0.14	0.11			**0.05**	0.01	**3.62** 0.04
CaO	1.11	1.27	1.14	1.24	1.05	1.11	1.06	0.89	1.09	1.19			**0.74**	0.04	**6.89** 0.11
Na_2O	4.18	3.97	3.46	4.02	4.46	4.19	4.21	4.12	4.15	3.18			**4.17**	0.10	**3.30** 0.07
K_2O	3.33	3.43	3.91	3.22	3.16	2.98	3.28	3.31	3.21	3.38			**5.19**	0.09	**4.47** 0.09
P_2O_5	-0.03	0.04	-0.01	0.04	0.06	0.01	0.13	0.00	0.03	0.02			**-0.01**	0.03	**0.58** 0.04
*H_2O***	*3.73*	*1.35*	*3.74*	*2.76*	*2.84*	*4.30*	*4.15*	*6.41*	*4.72*	*5.91*		*Total*	*98.84*	*0.39*	***98.34*** *0.38*
												n	***25***		***25***

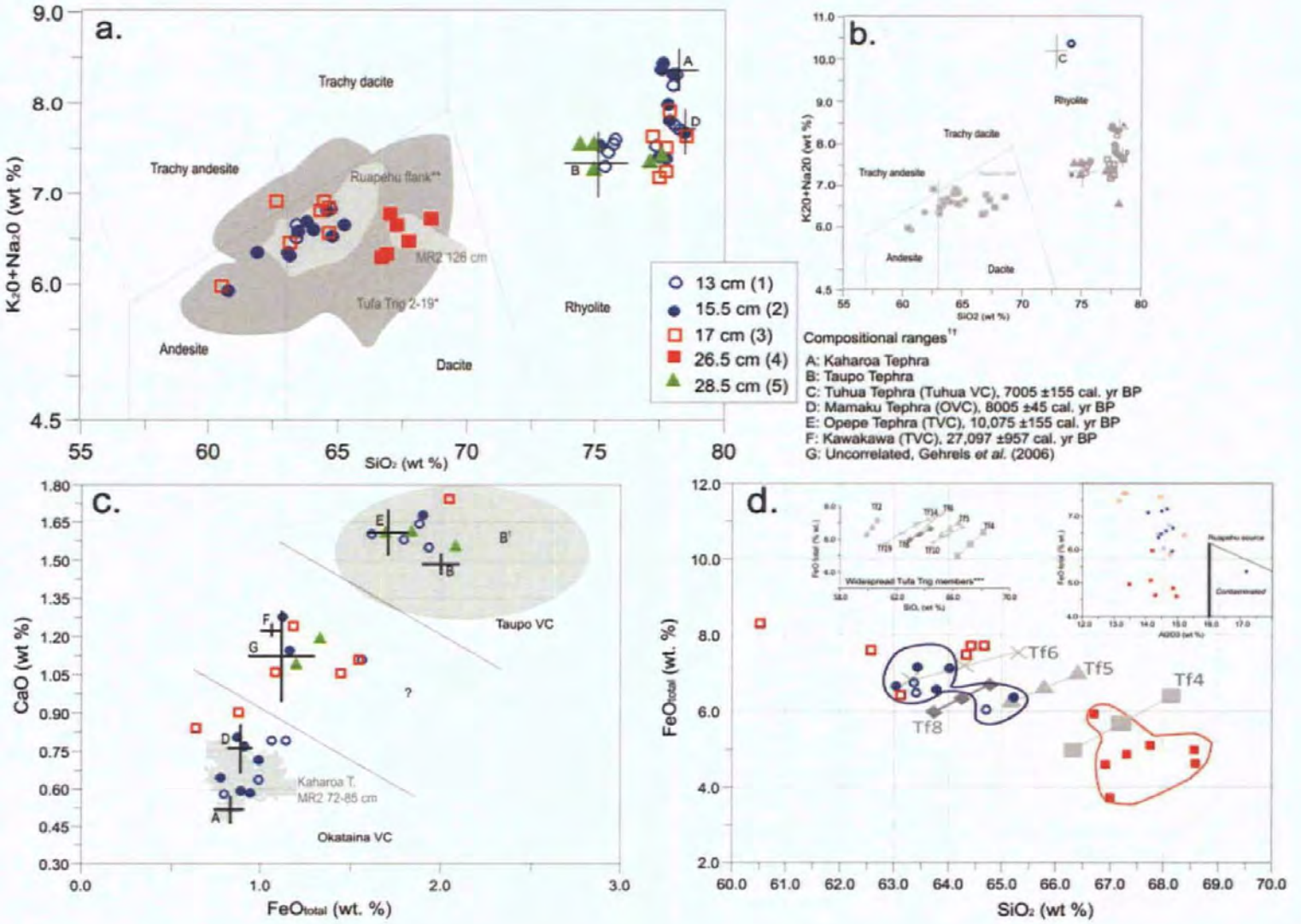
a.
Trachy dacite
Trachy andesite
Ruapehu flank**
MR2 126 cm
Tufa Trig 2-19*
Andesite
Dacite
Rhyolite
A
B
D
13 cm (1)
15.5 cm (2)
17 cm (3)
26.5 cm (4)
28.5 cm (5)
K2O+Na2O (wt %)
SiO2 (wt %)
b.
Rhyolite
Trachy dacite
Trachy andesite
Andesite
Dacite
K20+Na20 (wt %)
SiO2 (wt %)
Compositional ranges††
A: Kaharoa Tephra
B: Taupo Tephra
C: Tuhua Tephra (Tuhua VC), 7005 ±155 cal. yr BP
D: Mamaku Tephra (OVC), 8005 ±45 cal. yr BP
E: Opepe Tephra (TVC), 10,075 ±155 cal. yr BP
F: Kawakawa (TVC), 27,097 ±957 cal. yr BP
G: Uncorrelated, Gehrels et al. (2006)
c.
E
B'
B
Taupo VC
F
G
?
D
Kaharoa T.
MR2 72-85 cm
A
Okataina VC
CaO (wt %)
FeOtotal (wt. %)
d.
Widespread Tufa Trig members***
Ruapehu source
Contaminated
Tf6
Tf5
Tf4
Tf8
FeOtotal (wt. %)
SiO2 (wt %)

Figure 4.3.6 Bivariate plots of normalized analysis from core LR1. All data are normalised to 100% loss free. (a) SiO_2 versus total alkalis (K_2O plus NaO_2) for all glass samples analysed from core LR1 from Lake Rotoroa. Analyses plotted within the compositional scheme for glass chemistry (after Le Bas *et al.*, 1996). Compositional ranges and ages for possible correlative rhyolitic tephras are indicated A-D. (b) Extended plot of (a) to show isolated shard which correlates with geochemically distinct peralkaline Tuhua Tephra. (c) Plot of CaO versus FeO (total) for all rhyolitic glass analysis from OVC and TVC sources. Uncorrelated analyses fit between the two sources. Grey shaded analysis from section MR2 from Moanatuatua Bog identified as Kaharoa Tephra. (d) FeO (total) versus SiO_2 of andesitic/dacitic glass analysis. Analyses of intermediate glasses from Moanatuatua Bog are shown in light grey for comparison. Inset: plot of FeO (total) versus Al_2O_3 used to identify analyses of intermediate glasses affected by microlite contamination following Platz *et al.* (2007).

[1] mean compositional ranges and ages from Lowe *et al.* (2008); [2] compositional envelope of uncorrelated analyses from Gehrels *et al.* (2006); [†] full range of analyses for Taupo Tephra from Gehrels *et al.* (2006))[a] Compositional ranges for Ruapehu Tufa Trig (Tf) members Tf2, 4-6, 9, 10, 14 and 19 from Donoghue *et al.* (2007; data presented are normalized to loss free basis). [b] Tephra sample taken from the flank of Mt Ruapehu in 2005 representing a mix of recent Tf eruptives. [c] Mean and standard deviation of compositions derived from widespread Tufa Trig Formation members from Donoghue et al. (1997; 2007; normalised to loss free basis). Data points represent mean and standard deviation.

Two shards intermixed with the Kaharoa Tephra are characterized by lower K_2O (mean 3.67 wt.%) and correlate more closely with Mamaku Tephra (as for sample 1). Three additional shard analyses also correlate with the Taupo Tephra and an uncorrelated compositional group. Because of the limited number of analyses it is, however, difficult to determine the relative proportions of these groups within the sample.

Only five analyses were obtained of intermediate glass chemistries which form a compositional group distinct from overlying intermediate glass populations (Fig. 4.3.6). The majority of these analyses correlate most closely with Tf members Tf6 and Tf8 which are also found in association with the Kaharoa Tephra in core MR2 from the Moanatuatua peat site. These members are also the most likely candidate source eruptives for the time period represented by the shard concentration in the core.

A small number of minerals (crystals) were also analysed from this level with the hope of identifying biotite which is found associated with the Kaharoa Tephra where it is preserved as a macroscopic layer (Lowe *et al.*, 2008b). The minerals detected, however, included the plagioclase feldspars andesine and labradorite which are associated with many older TVZ tephras in Waikato lakes and are therefore likely to have been reworked with older TVZ tephra derived glasses.

Sample 3 (LR1 17.5 -18 cm): Reworked shards from Taupo VC and Okataina VC derived tephras and TnG VC, Tf member 6

Sample 3 was collected from 1 cm below the preceding glass population (sample 2) and marks the upper limit of elevated concentrations of brown glass between 17 and 22 cm depth in the core. Analysis of the sample from this level also provided an opportunity to assess the vertical spread of Kaharoa shards identified at 15.5 cm in the core.

A total of 13 glass analyses were obtained from this sample, comprising seven analyses of clear rhyolitic glass and six of brown glasses with intermediate composition. The rhyolitic glasses plot into two compositional groups recognized in lower levels of the core which correlate with the Mamaku Tephra and an uncorrelated group most likely representing a mix of older Taupo VC tephras. The shards identified as Mamaku are differentiated from Kaharoa Tephra based on distinctly lower K_2O values (mean 3.16, SD 0.13) and characterised by higher "water" content (mean 3.51 wt.%). One grain tentatively correlates with the Taupo Tephra (Fig. 4.3.6 c).

Analyses of intermediate glasses are recognized as correlatives of the Tufa Trig Formation and appear as a distinct population different from dacite glass analyses lower in the core. Because of the very low number of analyses, however, it is difficult to identify possible correlatives with any certainty. Compositionally, the majority of analyses compare most closely with Tf member Tf6. Tf6 was thought to stratigraphically overlie the Kaharoa Tephra (Donoghue *et al.*, 1995b) which in LR1 occurs above sample 3. However, analyses of a sample of so-called "Kaharoa Tephra" in the Tongariro region collected by Dr Barbara Hobden (formally at University of Waikato) by Prof. David Lowe showed the sample instead to be an Egmont-derived eruptive (Prof. David Lowe, pers. comm. June 2008). Even without the Kaharoa Tephra included in the age model the interpolated age for the peak in shards at this level in the core would be older then the Kaharoa Tephra at ~740-860 cal yr. BP. The occurrence of the Tf6 tephra member at this level in the core could be explained if: (1) the position in the core identified for the primary fall deposits from the Kaharoa Tephra is incorrect; (2) shards from Tf6 have moved vertically in the sediment profile to older stratigraphic levels; or (3) most likely, the stratigraphic relationship between the Kaharoa Tephra and Tf6 has been misidentified in proximal deposits as suggested by the new analysis noted above. It is also possible that the shards are not representative of Tf 6 and instead represent an unknown or uncorrelated Tf member preceding the deposition of the Kaharoa Tephra. This possibility cannot be confirmed with the limited number of analyses obtained.

Sample 4 (LR1 26-26.5 cm): TnG, Tufa Trig member 4

Sample 4 represents a zone of elevated brown shard content which coincides with a decline in the concentration of clear shards above the Taupo Tephra in the core and extends up to ~24 cm. This is a pattern of shards that can be traced through all three cores (labelled T1; Fig. 4.3.5). The shard concentration represents a relatively wide age-stratigraphic position dating to ~1200-1400 cal yr BP (Fig. 4.3.5). The glass population forms a relatively homogenous compositional population that is distinct from all lower positioned analyses of intermediate chemistry and is characterised by higher SiO_2 (67.68, SD 0.77) and lower FeO (4.83, SD 0.68) (Fig.4.3.6 d). These features match the dacitic population identified in Moanatuatua Bog at a similar stratigraphic position and age (MR2 population = 1285-1340 cal. yr BP) and correlate with the compositionally distinct Tufa Trig member Tf4 which stratigraphically lies between the Taupo and Kaharoa tephras. There were no rhyolitic shards analysed from this level.

Sample 5 (LR1 28-28.5 cm): Taupo Tephra with reworked TVC and uncorrelated tephra

Sample 5 is taken from ~2 cm above the visible Taupo Tephra where shard concentrations remain high in the core. This sample was analysed to both confirm the identity of the visible tephra and to assess the contribution of shards from the visible tephra to the attenuating glass concentrations immediately above it. Unfortunately only five shard analyses were obtained from this level which limits the interpretation of the shard sources. The analyses confirmed a rhyolitic chemistry for the glass but these formed two distinct compositional groups. Out of these five analyses, three shards correlate with the Taupo Tephra (Fig. 4.3.6). Two of the analyses represent older tephras and are categorised as uncorrelated.

Table 4.3.4 Summary of glass shard populations analysed and identified in core LR1 including relative ages. Age ranges based on 2 sigma range on age-depth model and taking into consideration the vertical extent of shard concentration and geochemical populations (Fig. 4.3.6 and Table 4.3.3). * Unable to interpolate age.

Sample no. /core	Depth in core (cm) of sample [shard conc.][a]	No. of shards in population analysed	Eruptive source (VC)[b]	Interpolated age in cal. yr BP of shard conc. 2σ range[c]	Identification of tephra (T.) /interpretation	Calendar ages (AD)/ Calibrated ages of correlative tephra in cal. yr BP 2σ range[d]	Primary reference(s): ages[1] major element chemistry[2]
1/LR1	13 [10-14]	(a) 3 (b) 2 (c) 1 (d) 4 (e) 1	Tng OVC OVC TVC Mayor Is.	~490-570	RW Tufa Trig 6-8 RW Kaharoa Tephra RW Mamaku Tephra RW Taupo Tephra RW Tuhua Tephra	* * * * *	[2]Donoghue *et al.*, 1997 [1]Hogg *et al.*, 2003;[2] Newnham *et al.*, 1998 [1,2] Lowe *et al.* 2008
2	15 [15-15.5]	(a) 8 (b) 3 (c) 3 (d) 1	Tng OVC OVC TVC	~700-800	Tufa Trig 6-8 Kaharoa Tephra RW Mamaku Tephra RW Taupo Tephra	post- 636±12 636±12 * *	[1]Wilmshurst *et al.*, 1997; [2]Donoghue *et al.*, 1995 [1]Hogg *et al.*, 2003;[2] Newnham *et al.*, 1998 [1,2] Lowe *et al.*, 2008
3	17 [17-22]	(a) 6 (b) 2 (c) 1	Tng OVC TVC	~740-860	Tufa Trig 67 RW Taupo Tephra RW Mamaku Tephra	post- 636±12 * *	[1]Wilmshurst *et al.*, 1997; [2]Donoghue *et al.*, 1995 [1,2] Lowe *et al.*, 2008
4	26.5 [24-27]	7	Tng	~1200-1400	Tufa Trig 4	?	[1] Lowe *et al.*, 2000;[2]Donoghue *et al.*, 1997
5	28 [27-30]	3	TVC	~1510-1717	RW Taupo Tephra	*	[1,2] Lowe *et al.*, 2008

4.3.7 Summary of findings and resultant issues

1. Lake Rotoroa is a shallow closed basin lake near the urban centre of Hamilton City. Three cores were analysed from the lake, each marked at the base by the ca 1700 BP Taupo Tephra at ca. 30 cm depth. There were several visible tephra layers evident below the Taupo Tephra in the lake sequences.

2. The three sediment sequences comprise organic rich muds. Lithological and stratigraphic observations of the sediment profiles show a change in sedimentary properties approximately half way between Taupo Tephra and the top of the sediment.

3. Dating the sequence using AMS ^{14}C ages proved problematic with samples taken from post-settlement levels in the sequence (marked by Kaharoa Tephra and lithological changes) clearly affected by contamination by older carbon. Such contamination is likely to have resulted from increased inwash of sediments from the catchment. Evidence from nearby sites suggest that deforestation triggers a dramatic change in the hydrological and depositional environment, after which there is a greater propensity for inwash and reworking and, not surprisingly, typically older-than-expected ^{14}C ages (McGlone & Wilmshurst, 1999).

4. Measurements of shard concentrations showed similar issues identified from dating the sequences using AMS ^{14}C ages. The three cores revealed relatively good replicability for the lower sections of the cores where three peaks in shard concentrations were identified. Coincident with the change in lithology approximately halfway up each sequence there is greater variability in shard concentrations with an increase in clear shards and a decline in brown shards and an overall loss of identifiable patterns or

peaks in shards which may be used to identify primary fall deposits. It is very likely that this upper section of the core is affected by increased terriginous inputs caused by human activities in the catchment.

5. At least three primary fall tephras were identified in core LR1 from compositional analyses of shards from selected levels obtained by EMPA (summarised in Table 4.3.4). The Kaharoa Tephra was identified in the core as a cryptotephra but was only represented by a small number of shards amongst a significant background of glasses from older tephras. The position of the Kaharoa Tephra in the core coincides with a change in stratigraphy and inflection in LOI probably reflecting increased terriginous inputs relating to human activities. Dacitic glass was detected in a few positions in the core and could be linked to a small number of post-Taupo eruptions from Tongariro VC known as the Tufa Trig Formation. These include Tf6-8, which were found with the Kaharoa Tephra glasses and Tf4, which is bracketed by the Kaharoa and Taupo tephras and which has been identified in Moanatuatua in similar stratigraphic position marked by the decline in shard concentrations above the Taupo Tephra.

6. EMPA from core LR1 shows that there is considerable contribution from older reworked tephras throughout the sequence. The proportion of older reworked tephra in samples increases markedly in samples representing post-human settlement. These included a number of uncorrelated tephra shards identified in the sequence which are likely to represent a mix of older TVZ tephras reworked within the catchment. The majority of reworked shards from older stratigraphic levels are represented as visible tephras in the lake sediments with a predominance of shards from the youngest of tephra beds which are most likely to be become exposed in nearby sequences.

4.4 Opuatia Bog

Opuatia Bog in the Waikato Region is positioned approximately half way between Moanatuatua Bog and Lake Pupuke. This site was used to provide an additional bog site at an intermediate location for assessing the dispersal range of post-Taupo tephra fall events.

4.4.1 Site description

Opuatia Bog (37°26'00"S, 175°03'40''E) is a young, raised restiad peat bog within a larger wetland area (Opuatia Wetland) situated within the rural landscape of the lower Waikato River basin ~60 km north of Hamilton City and ~70 km south of Auckland City (Fig. 4.4.1). The ~950 ha wetland comprises fen (peat bog), swamp and lakes that form an extensive floodplain for the Opuatia Stream (River) which is a tributary to the Waikato River. Large flood events with an average return period of ~ 15 years from the Waikato River which lies < 0.5 km east of the bog margins are known to periodically flood the wetland and sections of the peat bog (Browne & Campbell, 2005).

The restiad peat bog (fen and young ombrotrophic bog; Fig. 4.4.1; Plate 4.4.1) covers an area ~ 260 ha within the wetland and is one of the youngest of the remaining restiad bogs in the Waikato Region. The peat bog is characterized by its unique plant species composition that forms a distinctive elevated surface (Clarkson *et al.*, 2004). Water table conditions of the bog remain at or just below the surface and recently conducted water table measurements suggest that this has not been affected by any surrounding land

practices of drainage activities (Browne & Campbell, 2005; Fritz *et al.*, 2008). The wetlands are located in low lying areas or the antecedent Opuatia River Valley. They were formed where drainage was impeded by the deposition of thick pumice alluvium from a break-out flood event of the ancestral Waikato River (Manville *et al.*, 1999; 2007; Manville, 2002) approximately 20 years after the Taupo eruption of AD 233 ± 12 (to allow for time for Lake Taupo to refill after the eruption before the break-out flood, Lowe & Green, 1992; Manville, 2001; Manville *et al.*, 2007). This deposit, referred to as the Taupo Pumice Alluvium (TPA), forms the base of the peat sequence of the bog (Clarkson *et al.*, 2004). Radiocarbon dates from wood and peat at the base of the sequence suggest that peat formation began very shortly after the deposition of the TPA (Clarkson *et al.*, 2004). Peat thickness at the site is ~ 3.5 m with an approximate peat accumulation rate of ~1.8 mm yr^{-1}, more than double the rate determined for Moanatuatua Bog (0.8 mm yr^{-1}) (Browne & Campbell, 2005). The peat forms a dome-like raised surface above the influence of drainage from surrounding hill slopes and is rain fed (ombrotrophic).

The present day peat bog fills a relatively narrow, flat valley surrounded by low lying hills used for agriculture and lower lying areas of swamp (Fig. 4.4.1; Plate 4.4.1). The bog forms a long, narrow area ~3 km in length. It is ~1 km at its widest point and is less than 50 m wide at its narrowest point (Plate 4.4.1). The peat bog has a typical hummock-hollow surface and low diversity of plant species. The vegetation is dominated by the jointed rush species *Empodisma minus* which is characteristic of mid-successional phase of restiad bog development and develops thick, dense culms approximately 40-60 cm high (Plate 4.4.2) (Clarkson *et al.*, 2004). Late successional species, such as *Sporadanthus* have yet to fully establish at the site. Swamp ferns (*Gleichenia discarpa)* are abundant in parts of the bog interspersed with the *Empodisma* (Plate 4.4.2). Understory vegetation includes a small

number of bryophyte species. Intermittent species on the bog include the rush *Juncus*, small pine trees *(Pinus radiata)* and flax (*Phormium tenax*) which cluster on drier elevated sections of the bog and can be seen as prominent features when viewed from above (Plate 4.4.3). The introduced grey willow (*Salix cinerea*) (introduced in 1942) is abundant on the margins of the bog and has had to be intensively managed in recent times to reduce its invasive spread on to the bog (Plate 4.4.1) (Browne & Campbell, 2005). Other species on the bog margins include the tea tree (*Manuka*) and flax (*Phormium*) as well as the introduced gorse (*Ulex*). Large parts of the wetland and bog are privately owned but is protected and managed as part of a region-wide initiative to protect native wetland species and maintain biodiversity (Browne & Campbell, 2005).

Opuatia Wetland has been the focus of a recent in-depth investigation and monitoring project funded by Environment Waikato (Waikato Regional Council) which has included evaluating the ecology and hydrology of restiad peat bogs to assess the future management of these types of bogs (Browne & Campbell, 2005). Particular threats identified as affecting Opuatia Bog include sediment and nutrient inputs from adjacent farmland as well as impacts of livestock entering the bog. These factors are thought to have impeded the natural development of parts of the bog (Browne & Campbell, 2005). The spread of non-native plant species has also been identified as problematic. The site was incorporated into one additional study into the peat characteristics and development of lowland restiad peat bogs in the Waikato Region and a small number of radiocarbon dates has been obtained from the base of the sequence (Clarkson *et al.*, 2004). Palaeoenvironmental and tephra records have, however, not previously been investigated at this site.

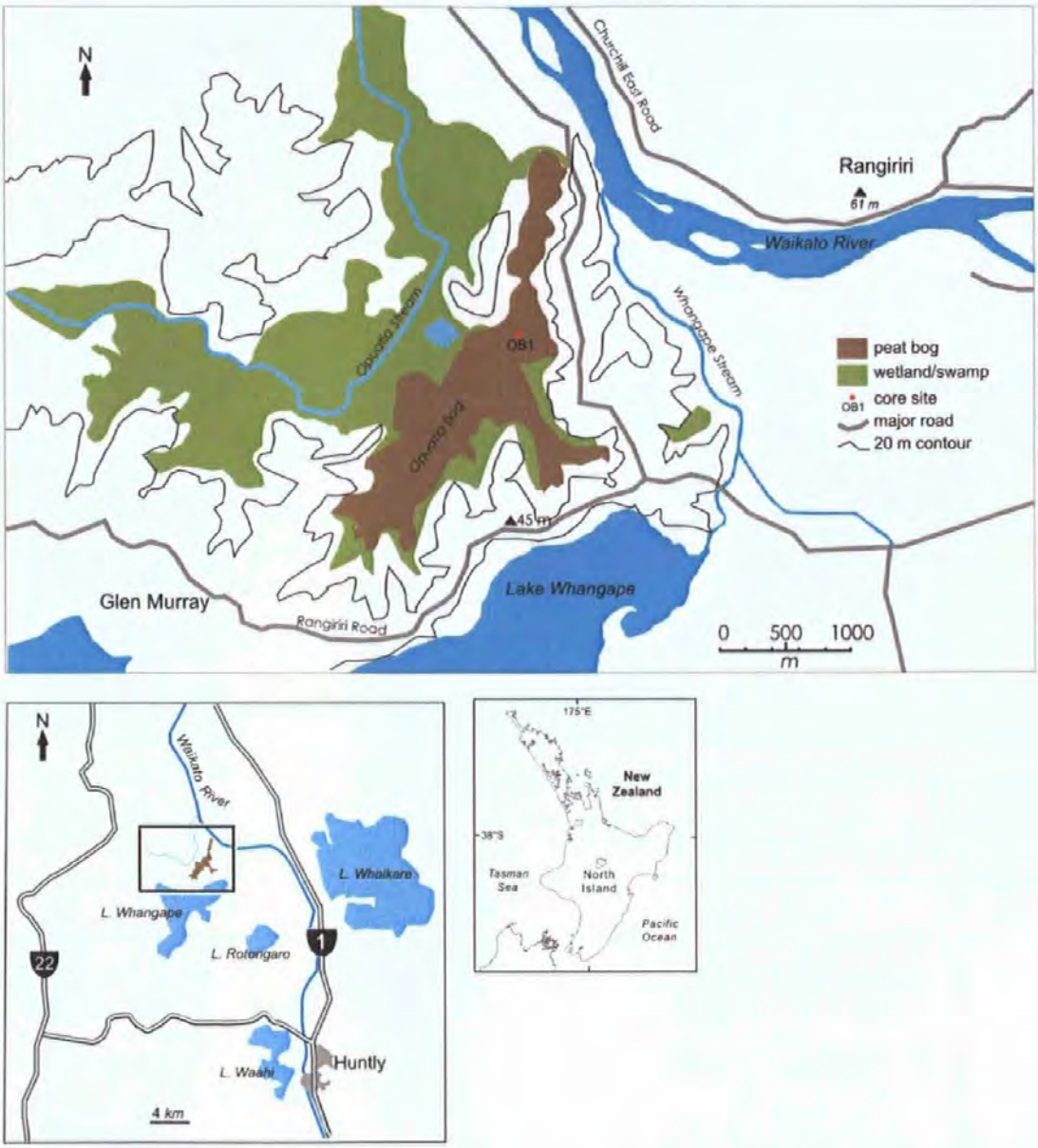

Figure 4.4.1 Location map of Opuatia Bog and core site shown in relation to surrounding wetland, the present course of the Waikato River and Lake Whangape. Small scale maps show the bog site in relation to the nearest major town, Huntly, and other large lakes.

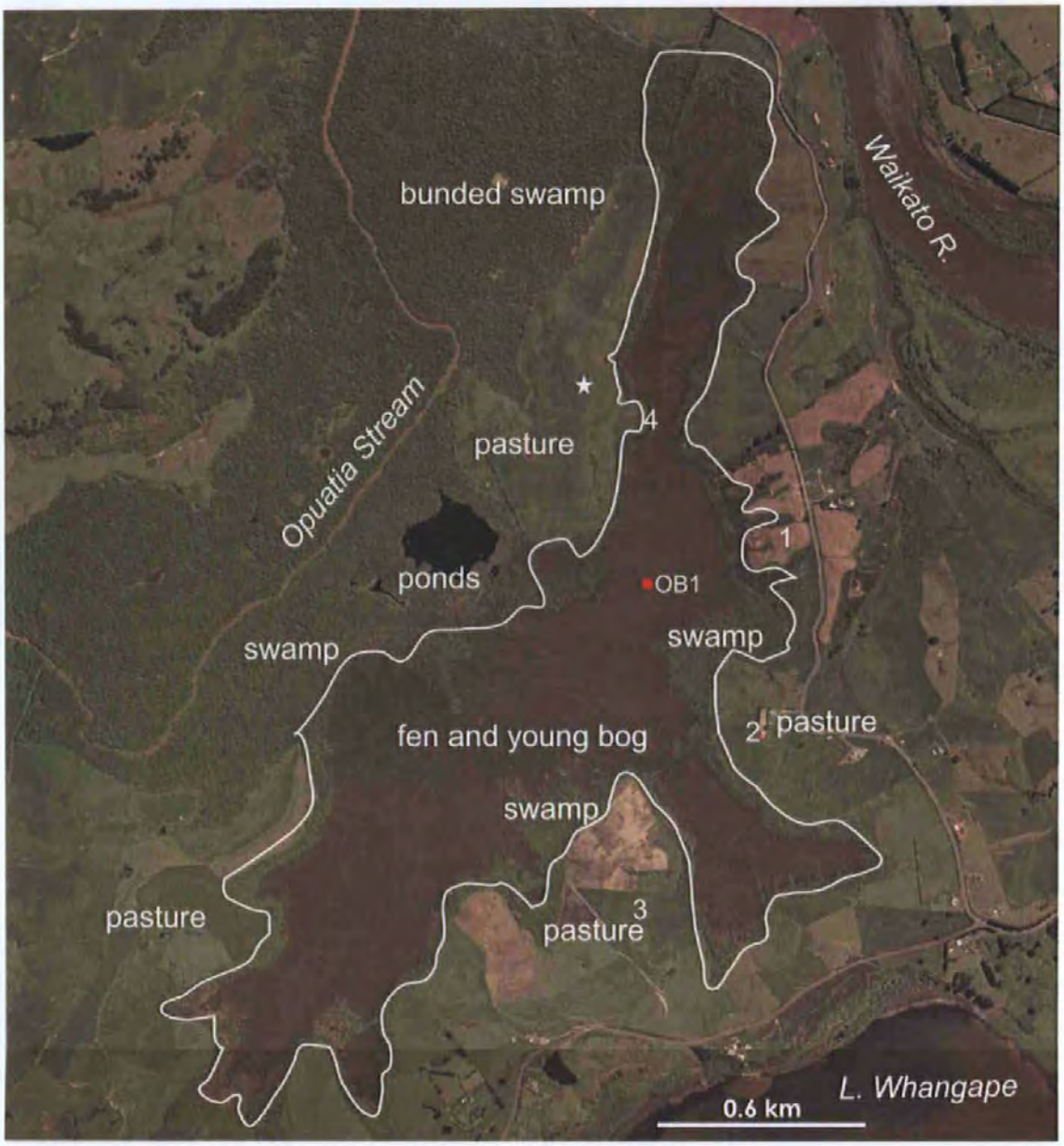

Plate 4.4.1 Annotated satellite image of Opuatia Bog showing surrounding pasture and swamp and the present course of the Waikato River. Image sourced from Orthophoto S13 Huntly (taken 2001/2002), Crown Copyright reserved: http://www.linz.govt.nz/core/topography/aerialandorthophotos/orthophotoindex/aps13/index.html). Bunded swamp refers to restored wetland. Annotations based on image from Browne and Campbell (2005). Numbers 1-4 correspond with numbered features shown on Plates 4.4.3 A and B. White line marks the approximate extent of restiad bog. White star shows the position on the pasture where photographs in Plate 4.4.3 were taken.

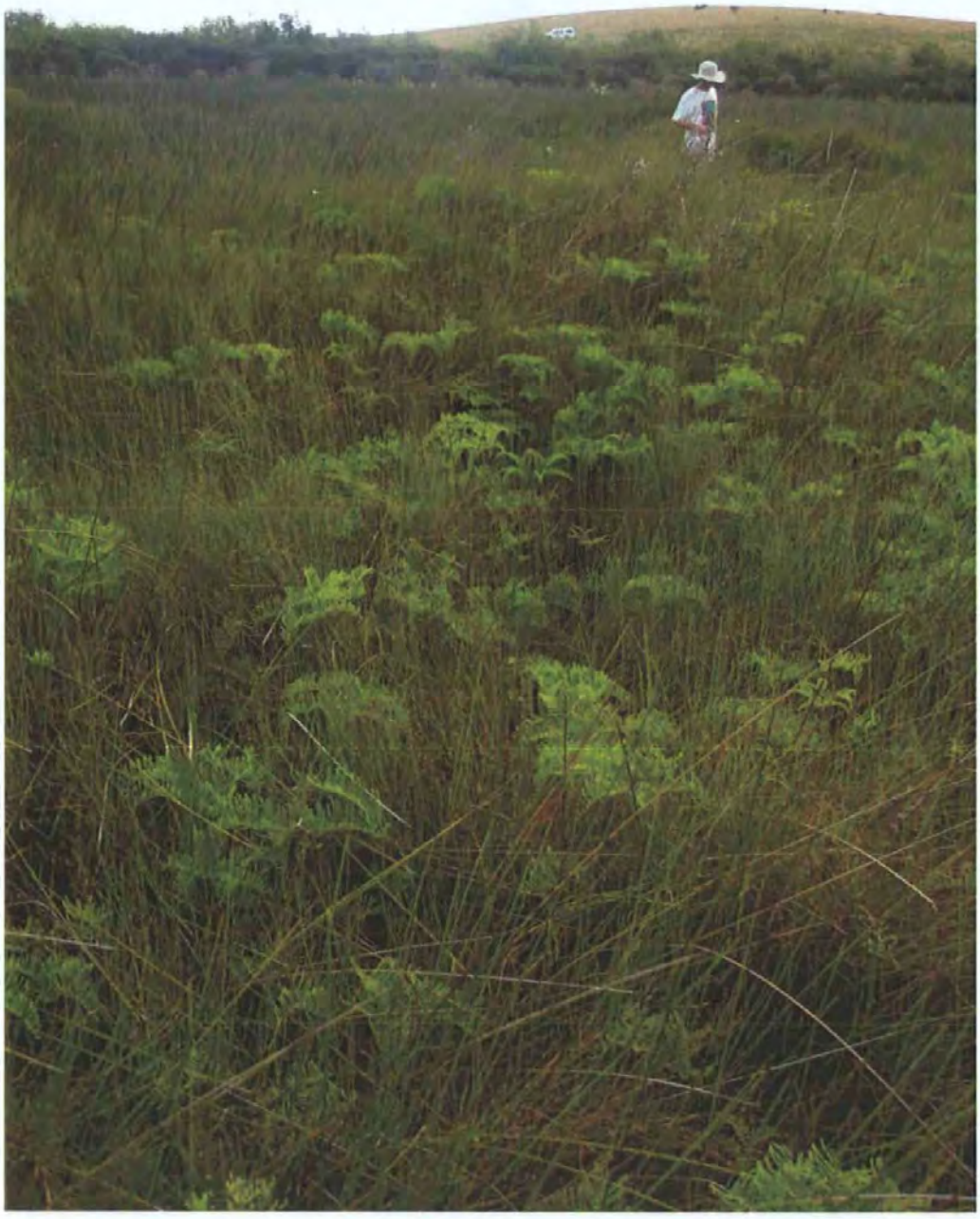

Plate 4.4.2 Surface vegetation of Opuatia Bog. In the foreground the dense stems of *Empodisma* (approx. 50 cm high) are interspersed with fern species *Gleichenia d.* (with Prof. Rewi Newnham in the background). Note the proximity of the hills used for pasture seen in the background of the picture. Also in the background between the hill and the margins of the bog are the dense thickets of grey willow. Images in Plate 4.4.3 are taken from the white vehicle seen on the hill. Photograph taken by author.

Plate 4.4.3. Views over Opuatia Bog. Photographs taken from an adjacent hill. Photographs show the residual hills surrounding the bog, many of which are used for agricultural purposes. The extant of the Grey Willow can also be seen on the margins of the bog. Numbers 1-4 correspond with numbered locations in Plate 4.4.1. White line in A marks the edge of the bog on its eastern margins. Photographs taken by author.

4.4.2 Material collection

One peat sequence (core OB1) was collected from the northern part of Opuatia Bog in February 2005 (Fig. 4.4.1; Plate 4.4.1). Several locations were evaluated using a narrow corer to determine depth of peat and ease of retrieval. The selected location of the cores site (GR: E269346, N641643) was approximately 100 m from the northwest edge of the bog where it was considered the impact of livestock damage and invasive plant species would not have affected the surface peat conditions. In the core location the plant composition appeared natural and undisturbed. The sequence of peat was sampled down to just above the TPA using two different collection methods.

Despite several attempts, complete recovery of the peat sequence proved problematic, possibly due to water pockets in the peat as well as the presence of horizons comprising thick, impenetrable roots. Collection of peat cores from 30-90 cm depth was particularly difficult. As a result a sample was retrieved as one complete ~ 30 x 30 cm section dug out of the surface of the peat bog using spades and knifes to cut though roots down to ~70 cm depth. Collection of this large section ensured that a complete section was retrieved from the top section of the sequence. It was hoped that the large section size would also preserve the integrity of the peat and allow for large samples to be taken for analysis of cryptotephra content. It was anticipated that any glass from historic tephra falls deposited at the site, which is more distal to volcanic sources than the Moanatuatua Bog, site would be preserved in much lower concentrations. The large section also provided archive material for future studies from this site. Sections of the peat below 70 cm depth were retrieved in several sections using a 9-cm wide, 30-cm long Russian-type corer down to TPA at 390 cm

depth. Table 4.4.1 and Figure 4.4.2 provide a summary, description and interpretation of the material collected.

Table 4.4.1 Summary of sections/samples collected from Opuatia Bog with main distinguishable lithological characteristics

Depth of section	Sample collection	Sample Description	Interpretation
0-70	Monolith section dug out from the surface of the peat	Fibrous, poorly humified, water-logged restiad peat containing distinct silty horizons	Acrotelm layer of peat bog. Clayey/silty horizons from flood deposits and increased terrigenous-rich aeolian deposits from deforested hill slopes around the bog
70-110	9 cm wide, 30 cm long Russian-type corer	Poorly retrieved sections containing very fibrous peat	Water pockets in the peat
110-190		Fibrous peat with frequent, thin clayey-silty- peat horizons. Some sections poorly recovered.	Restiad peat with clay layers possibly representing several large flood events from the Waikato River
190-210		Poorly humified peat horizon with distinguishable plant material	?
210-290		Well- moderately-well humified peat with no distinguishable clay-silt horizons	Fully developed restiad peat bog with raised surface - minimal inputs from flooding/in wash events
290-330		Well humified peat with several clayey horizons, possibly displaying some smearing/disturbance during coring	Restiad peat developed but surface still receiving in wash from hill slopes or from flood events
330-390		Clayey peat poorly retrieved that contains abundant wood and woody peat/soil below 360 cm depth	Low lying early peat bog receiving minerogenic rich in wash from surrounding hill slopes. Possibly swampy conditions. Plant composition includes shrubs and pine trees

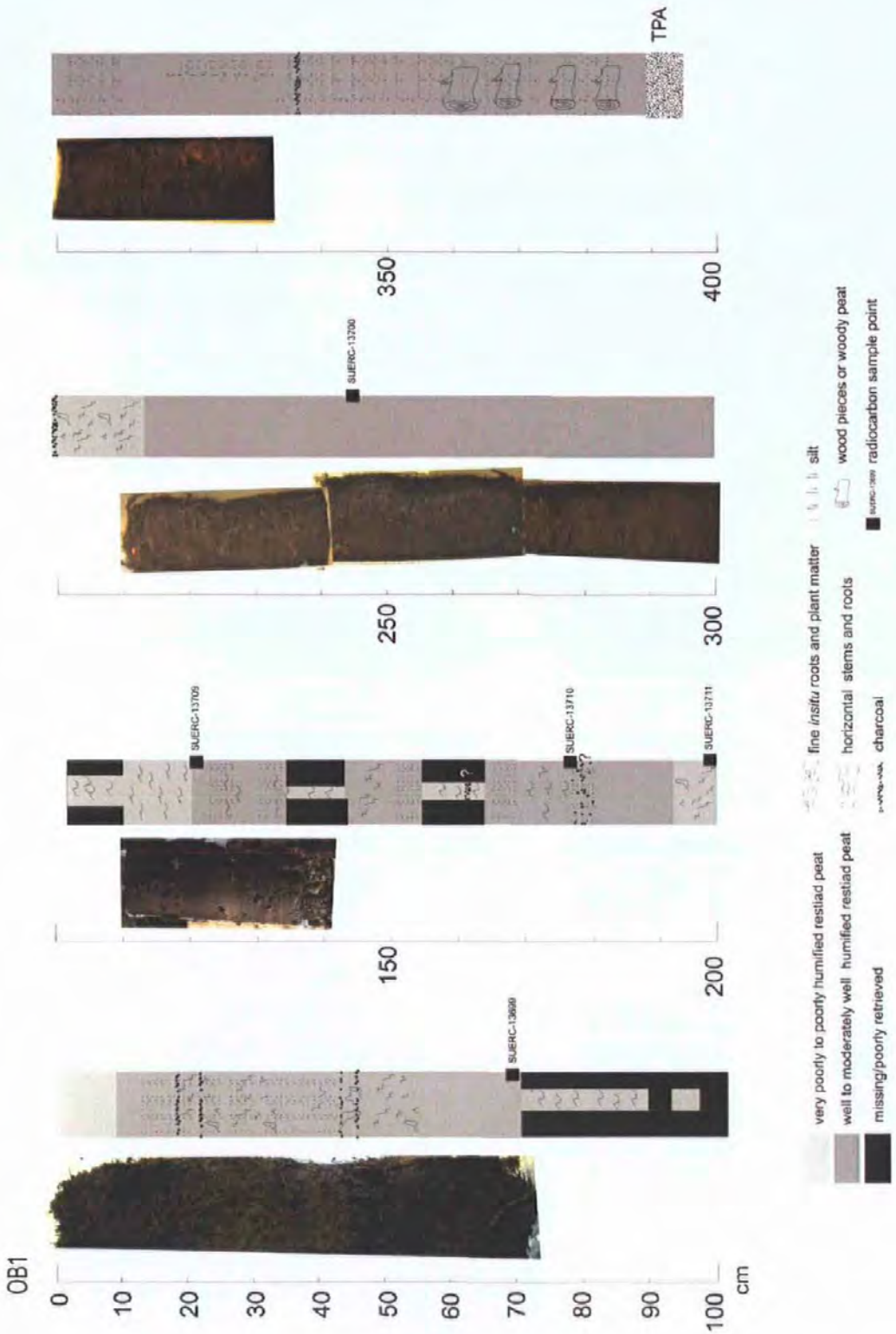

Figure 4.4.2 Section OB1 from Opuatia Bog showing some core sections, observable lithostratigraphic changes and positions of radiocarbon samples. Section 0-70 cm retrieved as a surface monolith, sections 70 - 330 cm collected as several 30 cm long cores. TPA, Taupo Pumice Alluvium.

4.4.3 Lithostratigraphy of sequence OB1

As for Moanatuatua Bog, lithological and sedimentary descriptions of the sequence collected from this site are made using generic descriptions for the restiad peat based on the visual examination of identifiable components (i.e. charcoal, wood, plant fragments) and field techniques (von Post scale) to determine peat texture and decomposition. The lithostratigraphy of the sequence is shown in Figure 4.4.2. The peat samples retrieved from this site show distinct lithological changes up through the sequence that are likely to reflect the growth and development of this young bog as well as the occurrence of flood events and commencement and continuation of human activities in the area around the bog site (Table 4.4.1). Loss on ignition (LOI) measurements from the sequence show a highly fluctuating organic content reflecting these lithostratigraphic changes (shown with glass shard counts in Fig. 4.4.5).

Above the TPA at 390 cm depth in the sequence up to ~ 330 cm the peat comprises of clay-rich woody peat containing some large pieces of wood. These materials are likely to represent the more swampy conditions of a young peat bog which would have been fed by surface runoff rich in terrigenous deposits. Palaeoecological evidence of restiad bog development suggest that an initial phase of development starts with sedges and shrubs (Clarkson *et al.*, 2004) although the large pieces of wood suggest that trees or shrubs were also growing in the waterlogged valley. LOI measurements show that the organic content is only 50-60 % in this lower peat section. Above 315 cm depth there is a general trend of increasing organic content up through the sequence. Above 335 cm and up to ~290 cm the organic content of the peat increases rapidly from ~50% to ~80%. This increase is likely to reflect decreasing terrigenous inputs from hillside drainage and a change to more

hydrologically separate conditions of a raised bog. The position of this change in the peat is marked by a thin charcoal layer that possibly represents a natural fire event near to the site. At 290-335 cm the peat is well developed and clayey peat forms only intermittent horizons. This section of the core, however, appears disturbed which is shown by smearing of a clayey peat horizon through the core which is likely to have occurred during the coring process.

Above 290 cm and up to ~210 cm the peat comprises a well to moderately-well humified restaid peat with no distinguishable clay/silt horizons which would indicate that the restiad bog was now well developed and with a raised surface hydrologically separate and above the influence of sediment rich surface runoff from the hill slopes on the margins of the bog. Organic content in this section of the core fluctuates between 82-93 % which suggests that there are still some inorganic inputs to the peat possibly from aeolian deposition. Microscopic examination shows that these inorganic components include a small amount of silt as well as tephra-derived glass. This section of the peat is also rich in plant phytoliths. At 210 cm and up to ~190 cm in the sequence there is a marked change in lithology to a poorly humified restiad peat consisting of poorly decomposed roots and stems and some layers of horizontally bedded, poorly decomposed plant material. Organic content in this horizon remains above 90%.

Above 190 cm and up to ~ 120 cm depth the peat is moderately well humified with a few poorly humified horizons. The section contains at least five distinct, relatively uniformly spaced, silty to clayey peat horizons marked by rapid inflections in LOI measurements (~10% decrease in LOI). These silty peat horizons potentially represent flood events similar to the 2004 flood event from Waikato River which is known to have flooded the

northern end of the bog close to the core site (Browne & Campbell, 2005). That these horizons were not detected in lower sections of the peat sequence would suggest that such flood events have not occurred throughout the history of the bog and are likely to have started because of changes in the catchment. At 164 cm and 178 cm indistinct charcoal horizons observed through microscopic examination are dispersed over several centimetres in the peat. Organic content in the section of the sequence ranges from 83-96 %, reflecting the clayey horizons interspersed within the organic rich peat (Fig. 4.4.2). At 70-120 cm depth the section was poorly retrieved and comprised very thin, stringy, water logged peat.

Up from ~70 cm depth in the peat there is another distinct change in the lithology of the sediment sequence which is marked by a major inflection in LOI measurements showing a gradual but sustained increase in inorganic contributions to the peat. This trend is a contrast to the distinct narrow, clayey- peat horizons interpreted as flood deposits found lower in the sequence. Organic content remains below 70% from 34 cm to 9 cm depth. Particle size analyses from a few selected levels from this section revealed that the inorganic component of the peat is made up of predominantly silt sized particles. These silts are likely to have derived from windblown soil-derived material from the hill slopes surrounding the bog which would have been exposed and disturbed during deforestation and agricultural practices in recent centuries. Charcoal particles identified throughout this section during the examination of the pollen assemblages are also indicative of sustained land use. Four fine charcoal layers at 18, 22, 44 and 46 cm possibly relate to historical fire events recorded in nearby Whangamarino Wetland (Clarkson, 1997). Above 9 cm there is a gradual increase in organic content up to the surface of the peat bog which is suggestive of a stabilization of the surrounding landscape perhaps as a result of recent changes in land use practices.

4.4.4 Age-depth models

An age model was constructed for the Opuatia Bog sequence using two tephrochronlogical ages from the Taupo and Kaharoa tephras, one AMS ^{14}C age and two pollen markers (Fig. 4.4.3). Tephrochronological ages are derived from the Taupo Tephra (1704-1730 cal yr. BP; Sparks *et al.* 2008) which is represented by the Taupo Pumice Alluvium (TPA) at the base of the sequence. Radiocarbon ages obtained by Clarkson *et al.* (2004) on wood taken immediately above the TPA suggests that it was deposited very shortly after the *ca.*AD 233 Taupo eruption. Manville (2001) suggested that ~20 years elapsed between the eruption and the deposition of the TPA (noted earlier). The Kaharoa Tephra is tentatively identified as a cryptotephra based on derived shard concentrations and a limited number of EMP analyses of glass shards (full details of how these were obtained are provided in later sections). The identification is also supported by interpretations of the stratigraphy which imply the commencement of human induced landscape changes just below the shard concentration, an occurrence observed consistently in sequences containing the Kaharoa Tephra (Newnham *et al.*, 1998).

A total of five AMS ages were originally obtained from selected levels in the sequence corresponding to changing stratigraphy and glass concentrations (Table 4.4.2). Measurements on all samples were performed at the NERC radiocarbon facility, East Kilbride. All samples consisted of a range of handpicked plant macrofossils which included leaves, seeds, twigs and stems (Table 4.4.2). Because there were relatively low quantities of each identifiable plant parts in the samples these were mixed in order to obtain the required sample weight. Unfortunately, four of the five ages were rejected from the age model on the basis that they were determined to be either too young or too old

(rejected ages shown in grey on Fig. 4.4.3). The sample from 244 cm (Table 4.4.2.) was located well below the disturbed section of the peat but returned an age of ~532 cal yr BP, more than 400 years younger than estimated age for this level of the sequence (Fig. 4.4.3). This sample comprised 'woody twigs' as there were few other identifiable plant remains. It is, however, possible that these were misidentified woody roots which could have penetrated down to much older stratigraphic levels in the peat. Samples from 178 cm and 200 cm resulted in very similar age ranges (Table 4.4.2). Only at 200 cm did the derived age (668-766 cal yr. BP) fit with the interpretations of the stratigraphy for a signature of human activities as well as the interpreted position of Kaharoa Tephra (Fig.4.4.3). The sample from 178 cm was taken immediately above a charcoal-rich silty peat horizon most likely representing a flood event. A flood event could have easily remobilized and re-deposited older plant material including leaves, stems and seeds on to the peat surface. The sample from 120 cm also returned an age which represented an age reversal based on accepted ages for the sequence. The position of the sample was also taken immediately above a silty-peat flood horizon which could account for the contamination by older carbon (Fig. 4.4.3). The age determined from sample at 70 cm depth was also considered too old based on the analysis of pollen assemblages (discussed below) and is also likely to have been affected by the contamination by older carbon as a result of disturbance activities on or adjacent to the site.

The analysis of pollen assemblages in the core was undertaken (by Prof. Rewi Newnham, University of Plymouth) with the aim of determining the earliest (lowest) level of introduced pollen in the sequence, which would provide an approximation of the depth equivalent for *ca.* AD 1840 which marks the introduction of exotic species by European settlers. The palynology also provided a test for the ^{14}C chronology in the upper section of

the sequence. The analysis was undermined by the generally low volume and preservation standard of pollen grains, particularly at depths > 40 cm. This meant that it was not practical to count >100 dryland pollen (dlp) grains at sample depths from 0 – 45 cm, normally considered sufficient for a secure interpretation. Below 45 cm to the end of the sampled sequence at 81 cm, pollen was not counted, but slides were scanned rigorously. Figure 4.4.4 shows pollen percentages for the upper 45 cm of the sequence. Table 4.4.3 provides details of slides which were scanned for pollen below 45 cm down to 81 cm depth in the peat.

The pollen content shows no significant changes throughout the upper 45 cm of the sequence with assemblages dominated by wetland (bog) taxa: Cyperaceae, *Empodisma*, *Gleichenia* and *Leptospermum* type, each fluctuating strongly in abundance downcore. In the dryland vegetation, a scattering of pollen from native trees and shrubs is outnumbered throughout by introduced trees, shrubs and herbs (in particular *Pinus* and *Salix*) and by grasses (Poaceae) which are also likely to include introduced species. Charcoal is abundant throughout and is especially prominent from depths 8 – 16 cm. At ~ 45 cm exotic pollen levels constitute c. 50% of the dryland (terrestrial) pollen. These results indicate that vegetation introduced during the European era was already well established in the vicinity of Opouatia Bog at the time of deposition of sediments now at 45 cm depth in the sequence. Indeed, the pollen spectra at 45 cm depth is similar to what would be expected in the pollen rain today at this site. From this evidence the sediments at 45 cm must post-date the early nineteenth century and possibly date to the twentieth century, providing a minimum age of ~100 years BP for this part of the sequence (Fig. 4.4.3).

Below 50 cm to the base of the sampled sequence (at 81 cm) scanning of slides revealed the presence of pine (introduced) pollen down to 79 cm at least, suggesting that this depth is still likely to be less than 200 years old (after AD 1840). This pine pollen forms another tentative minimum age horizon which confirms that the age of the AMS date at 70 cm is too old. However, the poor preservation and low volume of pollen in these lower samples should caution against any confident interpretation.

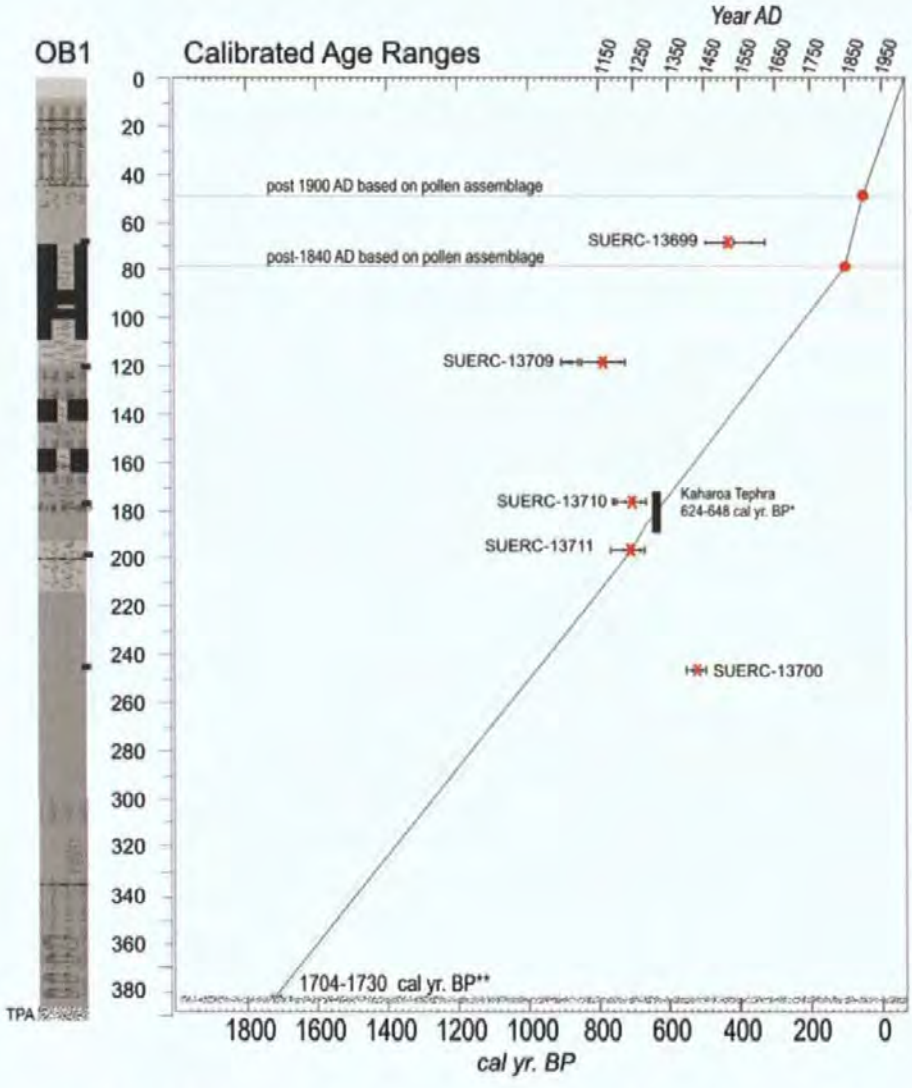

Figure 4.4.3 Age model for core sequence OB1 from Opuatia Bog. Based on a linear interpolation through median age of one AMS ^{14}C date, two tephrochronological dates and two pollen markers. All rejected AMS ^{14}C ages are also shown for illustrative purposes (see text). Refer to sample codes in Table 4.4.2. 2σ error ranges shown by light grey lines between two tephra ages. Tephrochronological dates on the Taupo Tephra (*from Sparks et

al. 2008) and Kaharoa Tephra (wiggle match date from Hogg et al. 2003). TPA, Taupo Pumice Alluvium. Note that the age of the TPA is estimated at ~20 years after Taupo emplacement (Manville, 2001).**

Table 4.4.2 Conventional radiocarbon and calibrated ages on plant macrofossils extracted from section OB1. Sample positions are shown in Figures 4.4.4. *Isotopic fractionation $\delta^{13}C$ is expressed as ‰ wrt PDP(± 0.1 ‰ for NERC-obtained ages). Calibration curve used is shcal 04.14c (Southern Hemisphere calibration curve). *Based on a linear interpolation using tephrochronological age of Taupo Tephra (for TPA) and modern age for the top of the sequence.

Lab code	Sample ID	Stratigraphic position (cm)	Sample material	Conv. RC age years BP ±1sd	$\delta^{13}C_{vpdb}$ ‰ (±0.1)	Estimated age BP*	Calibrated age range (2σ) cal yr BP	Median calibrated age cal. yr BP
SUERC-13699	OB1_70	69-70	stems and seeds	410± 35	-24.5	300	324-500	435
SUERC-13709	OB1_120	120-121	stems, seeds and twigs	924± 37	-25.6	700	724-908	785
SUERC-13710	OB1_178	178-179	stems, seeds and twigs	826± 35	-25.3	800	664-761	705
SUERC-13711	OB1_200	199.5-200	stems and seeds	836± 37	-26.1	900	668-766	710
SUERC-13700	OB1_244	244-245	woody twigs	532± 37	-24.0	1000	495-551	523

Table 4.4.3 Description of Opouatia pollen slides scanned but not counted due to low pollen concentration and poor preservation quality.

Depth (cm)	Pollen count	Introduced pollen?	Comments
40	Too sparse to count	Yes	Charcoal abundant
52	Too sparse to count	Unknown	
56	Too sparse to count	Yes (pine)	
71	Too sparse to count	No	Charcoal abundant
75	Too sparse to count	No	Charcoal present
77	Too sparse to count	Unknown	
79	Too sparse to count	1 pine grain observed	Charcoal abundant
81	Too sparse to count	No	Charcoal abundant

Figure 4.4.4 **Pollen percentage diagram from Opouatia Bog for selected pollen taxa. Vertical scale denotes depth in cm. Below 43 cm, pollen was too sparse to count (see Table 4.4.5).**

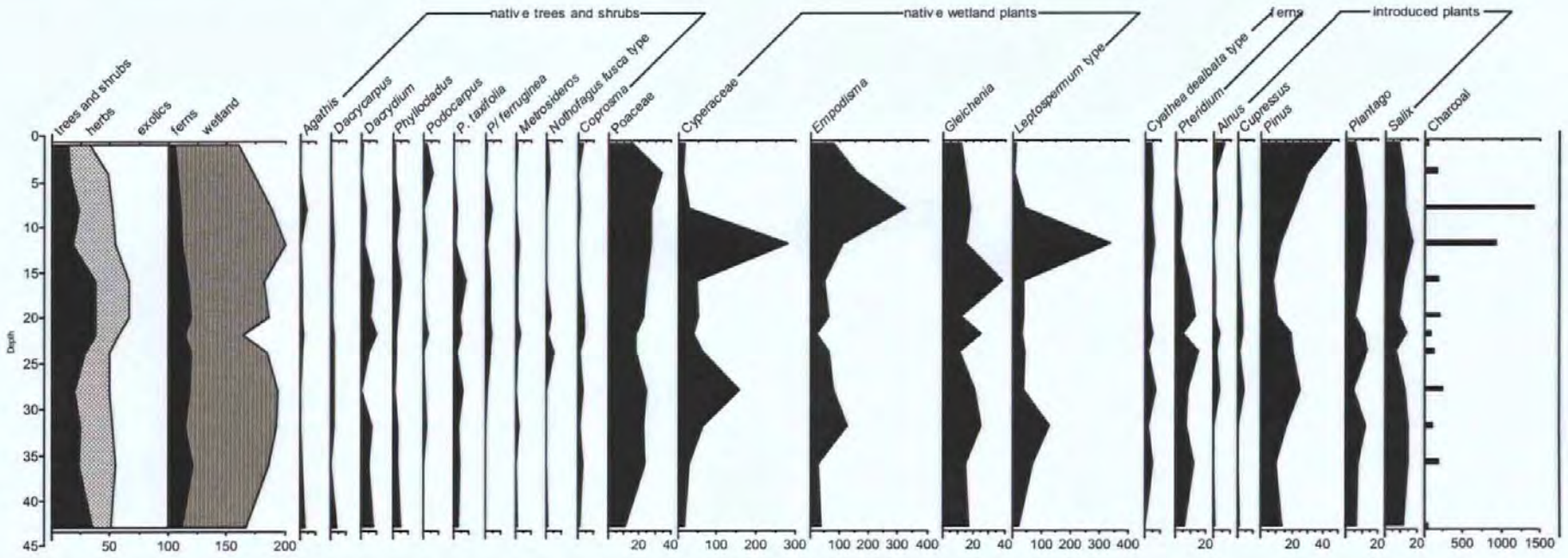

4.4.5 Tephra derived glass-shard content

The glass shard content derived from this site reveals a complex picture of tephra deposition which is likely to reflect natural and human induced changes and developments in and around the site. Processing the samples to extract the glass shard content from the silty clayey horizons proved more problematic and samples required a great deal more processing (mainly sieving) than was the case for the highly organic peat from Moanatuatua Bog. It is possible that this additional processing may have also partly compromised the resulting glass shard concentrations derived from this site. The glass shard content is quantified for both clear and brown shards up through the sequence as shards (glass particles) per mg dry weight (per mg d-wt.) (Fig.4.4.5). Observations of shard character and morphology are described as for previous sites with reference to selected images given in Plate 4.4.2.

The glass shard content from section OB1 is based on 167 samples using a 2-cm-thick contiguous sampling strategy from 340 cm depth up 10 cm depth and 1-cm-thick up from 10 cm up to the surface of the peat bog (Fig.4.4.5.) Below 340 cm the peat was considered too minerogenic and woody to derive a useful record of glass shard content. Clear and brown glass shards were identified throughout the sequence but in relatively low concentrations compared with the other Waikato sites investigated in this study and in varying states of preservation. There are four distinct changes in the pattern and concentrations of glass shards recognized up through the sequence which also coincide with changes in stratigraphy. These changes are shown as four zones (Z1-4) in the sequence in Figure 4.4.5.

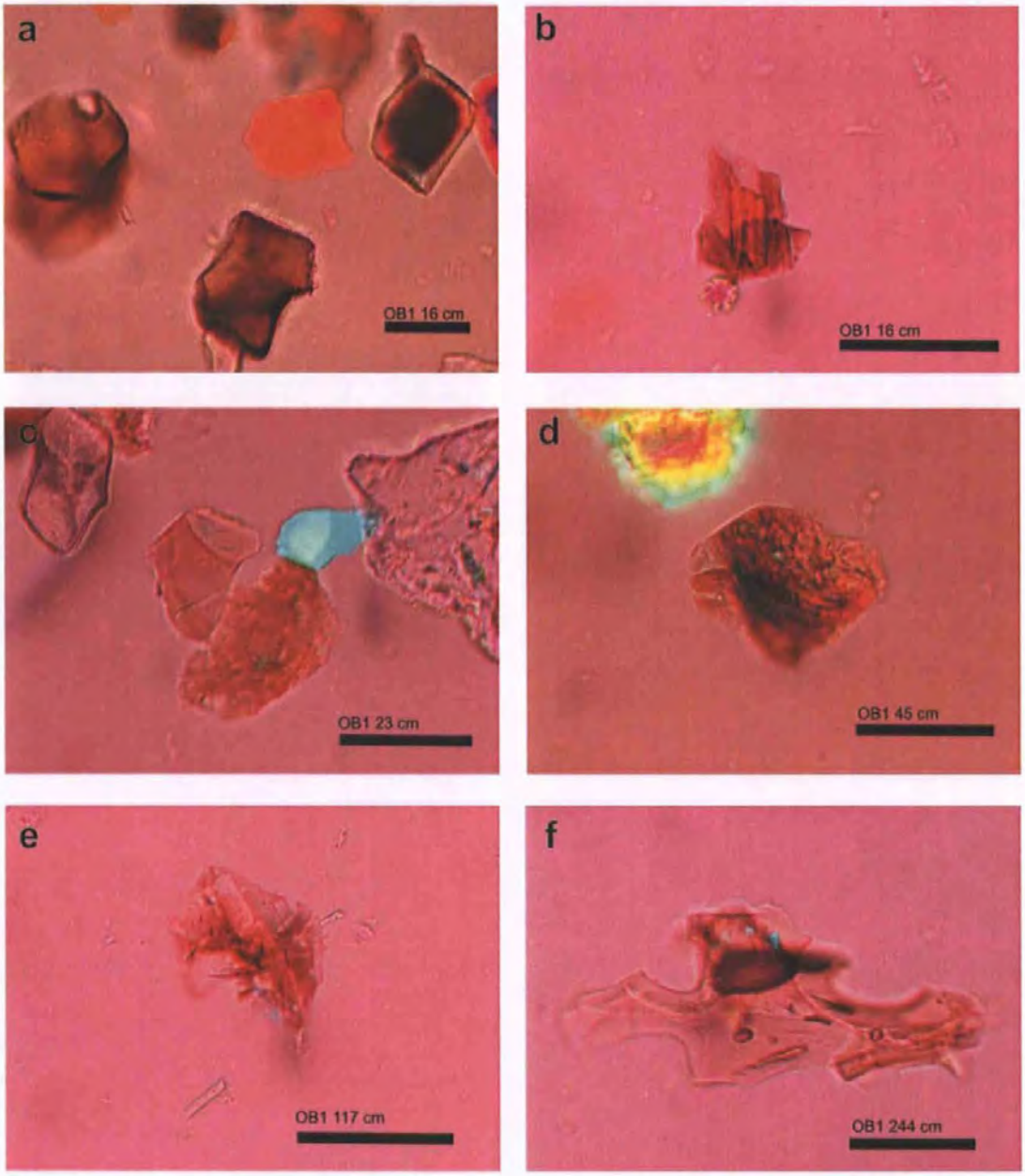

Plate 4.4.4 Photomicrographs of minerals and glass shards from samples taken from OB1 (a-f) (in order of depth in section) as referred to in the text.
All shards are photographed from glass slide setting using manual SLR camera attached to a petrographic microscope and viewed at x400 magnification. Black bar on each image equals 50 µm in length. Section number and depth are labeled on each image.

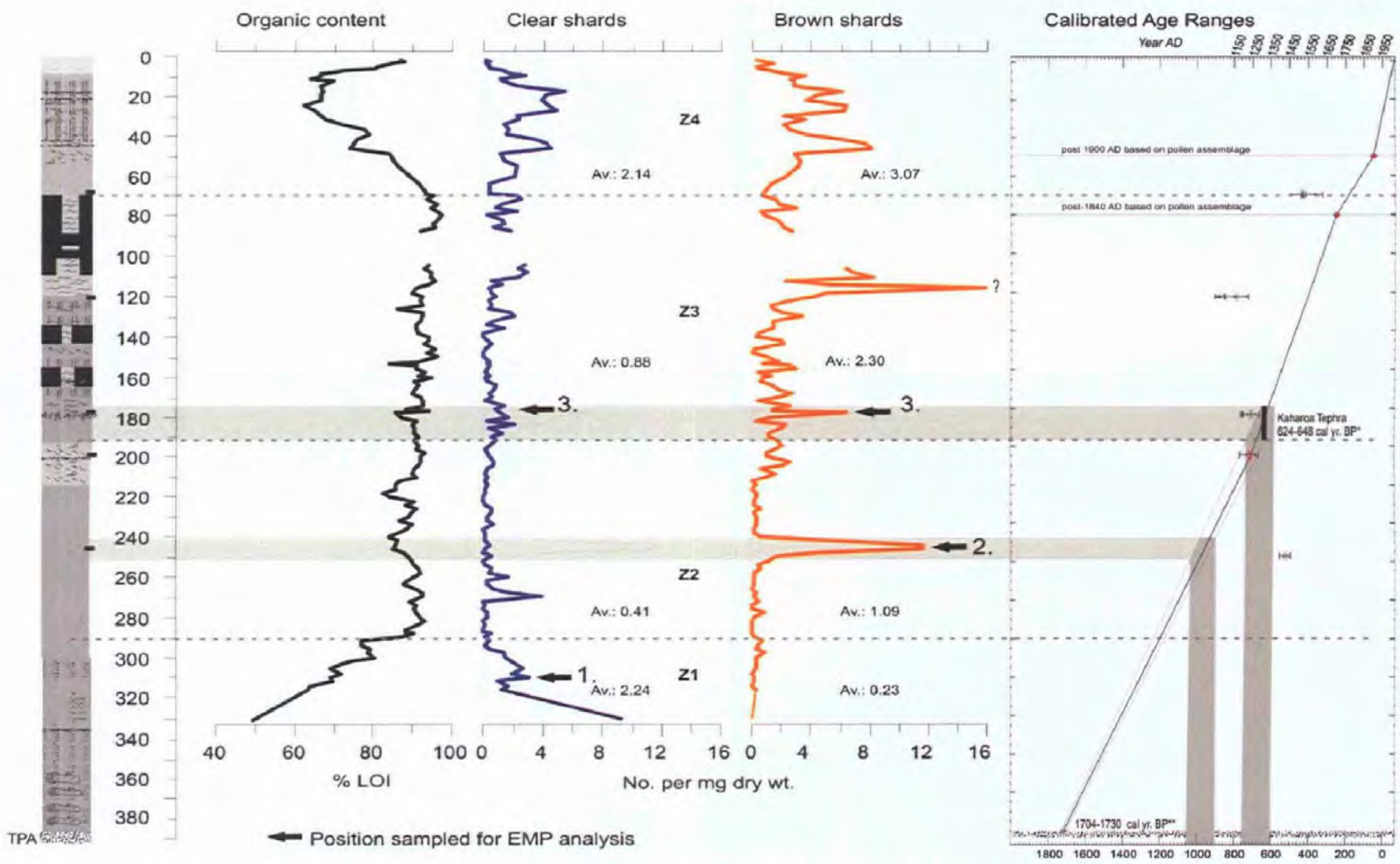

Figure 4.4.5 Results of tephra-derived glass-shard counts derived from core OB1 shown alongside, stratigraphy, organic content and age-depth model. The age-depth model is based on a linear interpolation through median age and 2σ SD points of 2 AMS dates (Table 4.4.2). * Wiggle matched age from Hogg *et al.* (2003); ** from Sparks *et al.* (2008). TPA = Taupo Pumice Alluvium.

From 340 cm depth up to ~290 cm (Z1) there are relatively high concentrations of clear shards which decline in concentration with the decreasing silt content of the peat as reflected by LOI values. Concentrations of brown shards remain very low. Clear shard concentrations comprise some large pumiceous clasts (>100 μm in length) characteristic of many rhyolitic deposits from TVZ eruptions. This level of the sequence is, however, at least 50 cm above the TPA which consists of predominantly in-washed pumice. The clear glass shard content at this position in the sequence is therefore likely to have derived from deposits (predominantly rhyolitic deposits) remobilised from sources adjacent to the site. Shard concentrations comprise some very pristine looking shards as well as some distinctly reworked shards with weathering pits and rounded edges, which are suggestive of differing modes of deposition. The weathered shards are particularly prominent in the silty peat horizons which would suggest that these have been incorporated within in-wash deposits during the early phase of bog development. The more pristine shards may represent windblown deposition from hill slopes on to the peat surface. There are no thick sequences of andesitic tephras (known) in the area around the site that would provide a source of secondary deposits preserved in the bog and this is borne out by the very low concentrations of brown shards in the silty peat in this zone. Despite low overall concentrations, brown shards in this zone lack typical sub-aerial or fluvial weathering features and retain crystal inclusions and thus could represent primary fall deposits.

Above 290 cm and up to ~215 cm (Z2) where the restiad peat is well developed, glass shard concentrations remain at very low background concentrations (<1 shard per mg dry-wt.) reflecting a probable lack of in-washed or aeolian deposits. These concentrations of glass are punctuated by two distinct, discrete peaks in clear and brown glass at 270 cm and 244 cm, respectively. Clear shards in the peak shard concentration at 270 cm depth appear

well preserved but are unlikely to represent a primary fall deposit based on the relative age of the horizon which is too old (at ~1060-1140 cal yr BP; Fig. 4.4.5) for the only known post-Taupo candidate rhyolitic eruption, the Kaharoa Tephra (636 ± 12 cal yr BP; Hogg *et al.* 2003). It is more likely that this peak in shards represents a single erosion event, possibly a wind storm, which resulted in remobilisation of a tephra sequence from a nearby exposure. Brown shards at 244 cm were very distinct in character with clast sizes typically larger than average for brown shards in the sequence at ~50 μm in length. Shards comprised typically dark brown elongate clasts with sparse crystal microlites (Plate 4.4.2 f). The small microlites in the brown shards appear well preserved.

Above 215 cm and up to 70 cm (Z3) where the sequence changes to a possibly more disturbed lithology comprising silty peat horizons, there is a marked change in the concentration of glass shards. Average concentrations of both clear and brown shards increase by more than two-fold compared to the underlying zone of shards (Z2). Brown shards show the most distinct change in concentration and pattern. Clear shard content remains relatively low apart from a few horizons (180-188 cm; 128-130; 102-110 cm) where concentrations exceed 1.7 shards per mg d-wt (twice the calculated average shard concentration for this section of the sequence). These also coincide with increases in brown shards for the same levels in the sequence. Clear shards in these horizons appear well preserved. The peak in clear glass at 188 cm contains shards which are typically larger (70-100 μm in length) than surrounding levels and comprise some distinct shards exhibiting an orange colouration.

The highly fluctuating pattern of brown shard concentrations in this section of the core makes it difficult to identify individual peaks which could be interpreted to represent a primary fall deposit. The fluctuations supports the interpretation of the stratigraphy, that

these silt horizons were deposited under different depositional processes. Only two prominent peaks in shards at 178 cm and 102-110 cm strongly exceed average shard concentration in this part of the sequence. The large peak(s) at 102-110 cm were derived from a very thin fibrous section of peat and calculations of shard concentrations may be artificially high due to low sample weight. Brown shards throughout this zone are typically very small (<40 μm in length) light-brown to yellowish-brown coloured, blocky shaped clasts rich in microlite inclusions. The majority of brown shards do not exhibit any distinct weathering features. In samples taken from the silty peat horizons, shards exhibit some loss of microlites including feldspar crystals and possibly indicating reworking or chemical weathering (Plate 4.4.2 e). There does not appear to be any relationship between shard content and the silty peat horizons as with shard concentrations in Z1 (Fig. 4.4.5). Between 120 and 70 cm the integrity of the peat is uncertain due to poor retrieval but it appears that shard content remains relatively high.

Above 70 cm (Z4), average shard concentrations increase for both clear and brown glass and, as for lowermost section of the sequence (Z1), appear to reflect changing silt content as shown by LOI values. Concentrations derived for clear and brown shards for this section of the sequence also show a very similar pattern in changing shard content up through the section. It is possible that this pattern relates an influx in tephra-rich deposits from surrounding hill slopes which are likely to have been deforested and with soils vulnerable to erosion. This interpretation is supported by the influx of sand-sized minerogenic particles observed in the samples from this part of the sequence (Plate 4.4.2 a) and by pollen analysis indicating European settlement in the region. Whilst clear shards in this section are almost certainly remobilised from nearby deposits and are likely to make up a component of the soils on the adjacent hillslopes, there are likely to be few sources of

brown tephra adjacent to the site. It is therefore likely that the concentrations of brown shards derive from either primary fall deposits onto the bog and on surrounding hill slopes or by reworking from underlying deposits in the peat. It is therefore possible that brown shards represent both primary and secondary deposition on to the bog. On the deforested hill slopes, these thin tephras would form an easily erodible surfical deposit which could explain the continuous concentrations of brown glass in this section of the sequence. Brown shards in this section of the core exhibit a typically blocky or tabular morphology and are very small (<40 μm) indicative of a distal source. Throughout this section, brown shards appear well preserved with very distinct microlite inclusions which show no characteristics suggestive of extensive sub aerial weathering (Plate 4.4.2 b-d).

4.4.6 Geochemical character, correlatives and interpretation

The results of geochemical characterisation of glass shard populations from the Opuatia Bog sequence by electron microprobe analysis are represented by a very limited number of analyses. In total only 24 assays were achieved from three sample levels in the sequence (indicated in Fig. 4.4.5), a smaller number than for the other sites due to problematic nature of the Opuatia sediments. Analyses from this sequence were also hindered by ineffective glass recovery and a high number of analyses were also rejected as analytical outliers or due to microlite contamination. This meant that the number of analyses obtained from each of the three samples and individual geochemical populations was insufficient to identify correlatives with any certainty. A summary of the analyses obtained from each level are shown in Table 4.4.4. Bivariate plots of these data using diagnostic oxide combinations are shown in Figure 4.4.6 (a and b) for glass with rhyolitic and intermediate chemistries. As

with previous sites the values presented are normalised to a 100 wt.% loss free basis (non-normalised analyses are in the appendices).

The major element composition of glass analysed from this site reveal both rhyolitic and intermediate (andesitic-dacitic) chemistries represented by clear and brown shards respectively. These analyses are comparable with values obtained from other sites investigated in this study (Moanatuatua Bog and Lake Rotoroa) which suggests that any physical and chemical weathering of the shards has not compromised the geochemical integrity of the deposits. Rhyolitic glass analyses are representative of at least two geochemical populations within the sequence. Values for SiO_2 range from 74.9 to78.6 wt.% and show corresponding changes in analytical totals (94-99 %) possibly reflecting the source and age (increased hydration with age) of the source tephra.

Intermediate glasses are predominantly dacitic in composition which is characteristic of Tufa Trig Formation tephras which have been identified in the other Waikato sites (Fig. 4.4.6). As with analysis from the other sites, individual glass populations are heterogeneous in composition (Table 4.4.4). There is a wide range for SiO_2 values (62.8-68.7 wt.%) but individual analyses achieve high analytical totals (average 98 wt.%). Analyses of intermediate glasses were evaluated for microlite contamination following methods by Platz *et al.* (2007) and a number of analyses were rejected.

Analyses for the three samples (Fig. 4.4.5) are described and interpreted below in order of occurrence in the sequence.

Table 4.4.4 Electron microprobe analyses of tephra-derived glass shards from three sample depths in core OB1, from Opuatia Bog. Sampling positions are shown in Figure 4.4.5. Mean values (in bold) and standard deviations of total number (*n*) analysis (of individual shards) normalized to 100% loss free (wt%). Analysis undertaken at NERC Tephra Analytical Unit, University of Edinburgh, in February and June 2007. Includes individual uncorrelated analyses from each level. Analyses of laboratory standards commensurate with Lake Rotoroa samples (section 4.3) Full details of laboratory standards are in the appendices. *Total iron as FeO, **water by difference.

Anal.no.	1a		1b		1c		2a		2b		3	
Core/depth	**OB1/180 cm**						**OB1/246 cm**				**OB1/310 cm**	
Source	TnG VC		TnG VC		OVC		TnG VC		TnG VC		TVC	
(Tephra)	Tufa Trig (Tf8)		Tufa Trig (Tf 5)		Kaharoa Tephra		Tufa Trig (Tf4)		Tufa Trig (Tf?)		Taupo Tephra	
SiO_2	**64.15** *		**66.25** *		**77.28**	0.36	**66.94**	1.49	**62.89** *		**75.57**	0.41
Al_2O_3	**14.93** *		**13.78** *		**12.56**	0.25	**14.62**	1.14	**14.85** *		**12.94**	0.23
TiO_2	**1.04** *		**1.12** *		**0.10**	0.01	**0.95**	0.10	**1.06** *		**0.23**	0.03
FeO*	**6.24** *		**6.09** *		**0.93**	0.08	**5.21**	0.73	**6.59** *		**1.88**	0.23
MnO	**0.20** *		**0.07** *		**0.02**	0.03	**0.06**	0.01	**0.17** *		**0.12**	0.06
MgO	**1.74** *		**1.52** *		**0.09**	0.04	**1.15**	0.09	**2.38** *		**0.25**	0.02
CaO	**4.44** *		**4.17** *		**0.73**	0.21	**3.97**	0.94	**5.37** *		**1.60**	0.08
Na_2O	**3.88** *		**3.73** *		**4.17**	0.09	**3.98**	0.29	**3.49** *		**4.48**	0.15
K_2O	**3.13** *		**3.05** *		**4.10**	0.12	**2.86**	0.31	**2.96** *		**2.90**	0.12
P_2O_5	**0.25** *		**0.23** *		**0.02**	0.01	**0.26**	0.04	**0.23** *		**0.05**	0.03
*H_2O***	*1.45* *		*0.89* *		*1.98*	*0.00*	*1.99*	1.00	*1.57* *		*3.20*	*1.71*
n	***1***		***1***		***2***		***4***		***1***		***5***	

Anal.no.	1d	3b	3c	3d	3f
Core/depth	**OB1-180**	**OB1-310**			
	Uncorrelated				
SiO_2	**77.16**	**78.26**	**78.62**	**76.56**	**77.75**
Al_2O_3	**12.33**	**12.10**	**11.94**	**12.62**	**12.21**
TiO_2	**0.17**	**0.11**	**0.14**	**0.14**	**0.10**
FeO*	**1.44**	**1.18**	**0.91**	**1.38**	**0.98**
MnO	**0.09**	**0.02**	**0.00**	**0.18**	**0.02**
MgO	**0.13**	**0.11**	**0.05**	**0.12**	**0.09**
CaO	**1.18**	**1.02**	**0.56**	**1.23**	**0.94**
Na_2O	**4.07**	**3.91**	**3.77**	**4.14**	**3.81**
K_2O	**3.43**	**3.28**	**4.00**	**3.63**	**4.10**
P_2O_5	**0.01**	**0.01**	**0.00**	**0.00**	**0.00**
*H_2O***	*1.63*	*5.76*	*6.02*	*3.46*	*4.91*

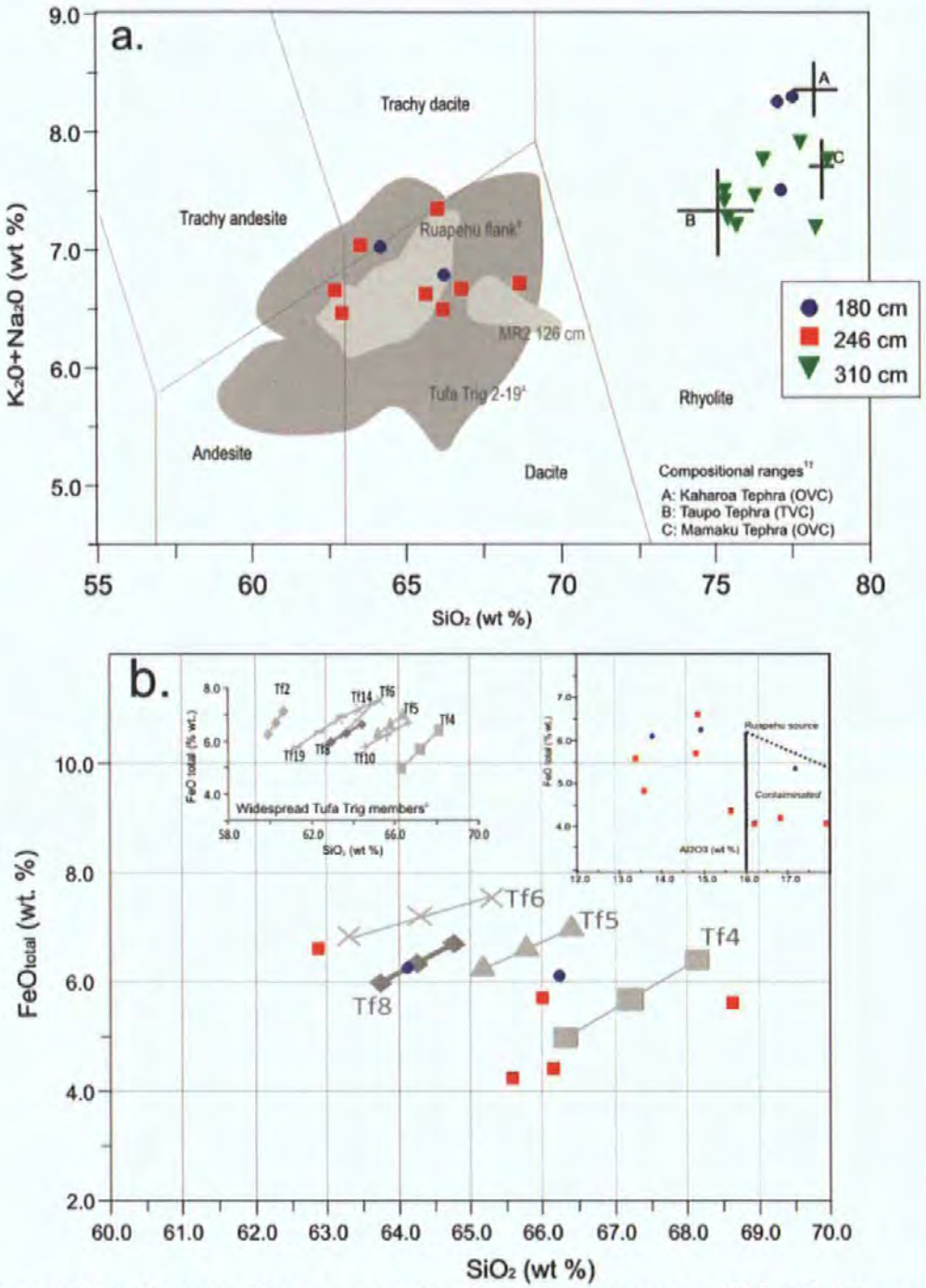

Figure 4.4.6 Bivariate plots of normalized analyses from core OB1. All data are normalised to 100% loss free. (a) Total alkali-silica diagram (TAS; after Le Bas et al. 1986) with compositional ranges and envelopes for potential correlative tephras. (b) Plot of FeO (total) versus SiO_2 for andesitic/dacitic glass analysis. Inset, plot of FeO (total) versus Al_2O_3 used to identify analyses of intermediate glasses affected by microlite contamination following Platz *et al.* (2007).

† mean compositional ranges from Lowe *et al.* (2008). [a] Compositional ranges for Ruapehu Tufa Trig (Tf) members Tf2, 4-6, 9, 10, 14 and 19 from Donoghue *et al.* (2007); data presented are normalized to loss-free basis). [b] Tephra sample taken from the flank of Mt Ruapehu in 2005. [c] Mean and standard deviation of compositions derived from widespread Tufa Trig Formation members from Donoghue et al. (1997; 2007; normalised to loss free basis). Data points represent mean and standard deviation.

Sample 1. OB1- 310 cm: TnG VC Tf4 and one grain uncorrelated Tf tephra

This sample is representative of a zone of declining clear shard content in the lowest section of the sequence ~ 80 cm above the TPA and dates to ~1300-1400 cal yr. BP, ~ 400 years after Taupo Tephra eruption event (Fig. 4.4.5). It was anticipated that analysis of glass from this sample would provide an insight into the sources of the background concentrations of clear shards in the peat.

A total of nine assays were obtained from this sample, all showing a rhyolitic composition (Fig. 4.4.6 a). Five of the eight analyses closely correspond with the Taupo Tephra which although not seen as a fall deposit in the peat sequence is likely to have formed deposits several centimetres thick in the region (e.g. Tonkin, 1967). It is therefore likely that these deposits were incorporated into the soils on surrounding hill slopes which were subject to sustained erosion and deposited by the wind and as inwash on to the early bog site. The other four analyses are uncorrelated to recent tephra units but are likely to represent a mix of much older tephras (e.g. Mamaku Tephra ~8000 cal yr BP; Fig. 4.4.6 a) which are likely to be have been present near the site and also incorporated into the in-wash on to the site (e.g. Lowe, 1988b). These analyses demonstrate the longevity of tephra in the environment from relatively thick rhyolitic sequences and the problems with identifying fine tephra falls in minerogenic rich sequences in volcanic regions.

Sample 2. OB1- 245-247 cm: TnG VC Tf4 and one grain uncorrelated Tf tephra

This sample represents a discrete, prominent peak in brown shards in the undisturbed section of the peat sequence (Fig. 4.4.5). A total of eight assays were obtained from this

glass sample to reveal a predominantly dacite chemistry. These analyses are represented by a typically heterogeneous composition with SiO_2 ranging from 62.9 to 69.7 wt.%. Three of these analyses were, however, rejected due to microlite contamination (Fig. 4.4.6 b inset). When plotted against compositional ranges for candidate Tf member tephras, four of the remaining five glass analyses closely correspond with the Tf4 tephra which has a distinctly higher SiO_2 composition than subsequent Tf members (Donoghue *et al.*, 1997). Glass populations similar in composition to the Tf4 tephra have been detected at similar stratigraphic levels (between the Taupo and Kaharoa tephras and with a significant time separation to subsequent and closely spaced Tf members Tf5-8) in both Moanatuatua Bog and Lake Rotoroa sites. The source of the one analysis that does not correlate with Tf4 remains uncertain but it is possible that this is an analytical outlier or relates to an older reworked Tf member. It could also represent a yet unknown, uncorrelated Tf member. The age range derived for this glass concentration in the sequence is ~910-1040 cal yr BP based on 2σ error age range from the age model (Fig. 4.4.5). This is slightly younger than the same geochemical population identified in Moanatuatua Bog at 1000-1260 cal yr BP. It is likely, however, that that the age model for this site is constrained by the low number and integrity of the ages determined.

Sample 3. OB1- 180-182 cm: two grains of Kaharoa Tephra, two grains of TnG VC (Tf 5-8?), one grain reworked, uncorrelated tephra

Sample 3 marks a peak concentration in clear and brown glass within a wider zone of elevated shard concentrations in the sequence. Problems were encountered in analysing this sample and only five glass analyses were achieved which are insufficient to make any

rigorous interpretations. These analyses included three rhyolitic and two dactic glasses. Of the three rhyolitic glasses, two correlate with the Kaharoa Tephra which has a very distinctive composition characterized by high SiO_2 (77.3 wt.%) and K_2O (~4.1 wt.%) and low CaO (~0.7 wt.%) compared with older OVC derived tephras (Lowe *et al.*, 2008b). As with assays of Kaharoa Tephra-derived shards from the other Waikato sites, these glass analyses also achieved relatively high analytical totals (98 wt.%) compared with older rhyolitic sourced glasses (e.g. Taupo Tephra (core MR2) – av. 96.3 wt.%) which may be indicative of the relatively young age of the tephra. Despite the very low number of analyses these provide some evidence that the Kaharoa was deposited on the site and is preserved in the sequence at or close to the sample position. The age range of the section containing elevated clear shards (175-190 cm depth), based on the age-depth model (Fig. 4.4.5) is ~600-750 cal yr BP which is also in the age range for the deposition of the Kaharoa Tephra (624-648 cal yr BP; Hogg *et al.* 2003).

The additional shard analysis correlates more closely with the Taupo Tephra but could also represent any number of older reworked rhyolitic tephras. These older units are likely to have been disturbed and remobilised as a result of deforestation by early human settlers and, as shown in Moanatuatua Bog and Lake Rotoroa, form the subsequent background glass concentration through the sequence. Analyses from this shard are classified as uncorrelated in Table 4.4.4.

The two dacitic glass analyses fall within the range of Tufa Trig tephras from Mt. Ruapehu and closely correspond with compositional ranges for Tf members Tf5 and Tf8 (Fig. 4.4.6 b). Tephras Tf5 and Tf8 are two widespread Tf members. It is suggested in Wilmshurst (1997) that the Kaharoa Tephra just overlies Tf5. This relationship is not certain because

no data on the positive identification of the Kaharoa Tephra in Hawkes Bay lakes were given by Wilmshurst (1997). The identification of the Kaharoa Tephra in the Tongariro National Park by Donoghue *et al.* (1995b; and Donoghue *et al.*, 1997) may be a miscorrelation because a similar-looking white tephra layer in that area has been identified as deriving from Egmont Volcano (D.J. Lowe pers comm., 2008).

Table 4.4.5 Summary of glass shard populations analysed and identified in core OB1 including relative ages. Age ranges based on 2 sigma range on age depth model and taking into consideration the vertical extent of shard concentration and geochemical populations (Fig. 4.4.4 and Table 4.4.2). * Unable to interpolate age.

Sample no. /core	Depth in core (cm) of sample [a] [shard conc.]	No. of shards in population analysed	Eruptive source (VC)[b]	Interpolated age in cal. yr BP of shard conc. 2σ range[c]	Identification of tephra (T.) /interpretation	Calibrated ages of correlative tephra in cal. yr BP 2σ range[d]	Primary reference(s): ages[1] major element chemistry[2]
1/OB1	310	4	TVC	~740-860	RW Taupo Tephra	*	[1,2]Lowe *et al.*, 2008
2	245-247	(a) 4	Tng	~910-1040	Tufa Trig 4	*	[1,2]Donoghue *et al.*, 1995
3	180-182 [175-185]	(a,b) 2 (c) 2	Tng OVC	~600-750	Tufa Trig 5-8 Kaharoa Tephra	600- 830 636 ± 12	[2]Donoghue *et al.*, 1997 [1]Hogg *et al.*, 2003; [2]Newnham *et al.*, 1998

4.4.7 Summary of findings and resultant issues

1. Opuatia Bog is a young restiad peat bog approximately situated halfway between Moanatuatua Bog and Lake Pupuke and is formed on pumice alluvium (TPA) emplaced several decades after the AD 233 ± 13 Taupo eruption.

2. One peat sequence was collected from the site down to the TPA although some sections of the sequence were poorly retrieved.

3. The lithostratigraphy of the bog reflects the transition of the bog from a low lying valley mire receiving mineral-rich inwash from the surrounding hill slopes to a fully developed ombrogenous restiad bog hydrologically separate from surrounding drainage by ~1200 cal yr. BP. There is a strong change approximately halfway up the sequence marked by an increase in charcoal layers and poorly decomposed plant horizons possibly reflecting initial human activities around the site. Several silty peat horizons which occur above 180 cm depth (after ~600 cal yr BP) are likely to have derived from flood events similar in magnitude to the 2004 Waikato River flood and likely to represent a change in the catchment (possibly also due to human activities). In the upper section of the sequence an increase in silts is likely to have derived from windblown soils remobilized by agricultural activities on adjacent hill slopes. A decrease in silt at the very top of the sequence is likely to reflect changing land use practices to more intensive methods introduced by European settlers.

4. The glass shard content derived for the sequence appears to provide a sensitive indicator of changes in and around the bog which support the interpretation of the

stratigraphy. In the lower section of the sequence representing peat development well before human arrival (>700 cal yr BP), the glass shard content is represented by very low background concentrations but with distinct peaks in glass shards likely to represent primary fall deposits or discrete erosion events. In the upper half of the sequence, concentrations of brown and clear glass shards increase markedly. These are represented by highly fluctuating pattern of shard content - possibly the result of both primary fall deposits as well as sustained remobilization and erosion of tephras by the wind from deforested hill slopes around the bog. This complex pattern of glass shards makes it difficult to identify individual horizons derived from primary fall deposits. In the top ~50 cm of the sequence an additional increase in average glass content coincides with increase in windblown silts and is likely to reflect the intensification of agricultural practices by European settlers resulting in increased remobilization of older deposits from surrounding hill slopes.

5. Table 4.4.5 provides a summary of tephras tentatively identified from the sequence based on a number of criteria including EMPA, age, stratigraphic position and observations of shard preservation. The small number of glass analyses obtained from this site by EMP, provide only a limited insight into the source of glass in the sequence. At the base of the sequence the occurrence of Taupo Tephra (as TPA) and older tephras confirm that older tephras were remobilized and redeposited into the bog and are likely to form the background tephra shard concentrations throughout the sequence. Analysis of the distinct peak in brown shards in the lower section of the sequence confirms this tephra as the compositionally distinct Tufa Trig member Tf4, also identified in other Waikato sites. Analysis of an indistinct horizon of elevated clear shard content in the middle of the sequence confirms the

occurrence of the Kaharoa Tephra preserved as a cryptotephra in the site. This identification is supported by both the sequence stratigraphy and chronology. The zone of clear shards coincides with a peak in brown shards most likely to represent Tufa Trig member tephras Tf5-8 deposited a relatively short time before and after the Kaharoa Tephra.

CHAPTER 5: LAKE PUPUKE, AUCKLAND REGION

5.1 Auckland Region

This chapter presents results from Lake Pupuke of the Auckland Region of the North Island, New Zealand. These results follow the same format used in the previous chapter and include: (1) a description and background to the site; (2) details of the sample collection; (3) core description, including lithostratigraphy and organic content of the sediment sequences; (4) construction of age models; (5) the tephra-derived glass content of each sequence; and (5) geochemical composition and identification of cryptotephras. Finally, a summary of the main findings and issues arising from the site is presented.

The Auckland Region covers an area of 6,059 km^2 between the northern edge of the Waikato Region and the Northland Region to the north and includes the islands of the Hauraki Gulf (Fig. 5.1). In contrast to the Waikato Region, the Auckland Region is much more densely populated. The region as a whole contains ~32.4% of the New Zealand population (1,303,068 people), the majority of whom live within Greater Auckland City (henceforth referred to as Auckland City), by far the most populated urban area in the whole country (Statistics New Zealand, 2008).

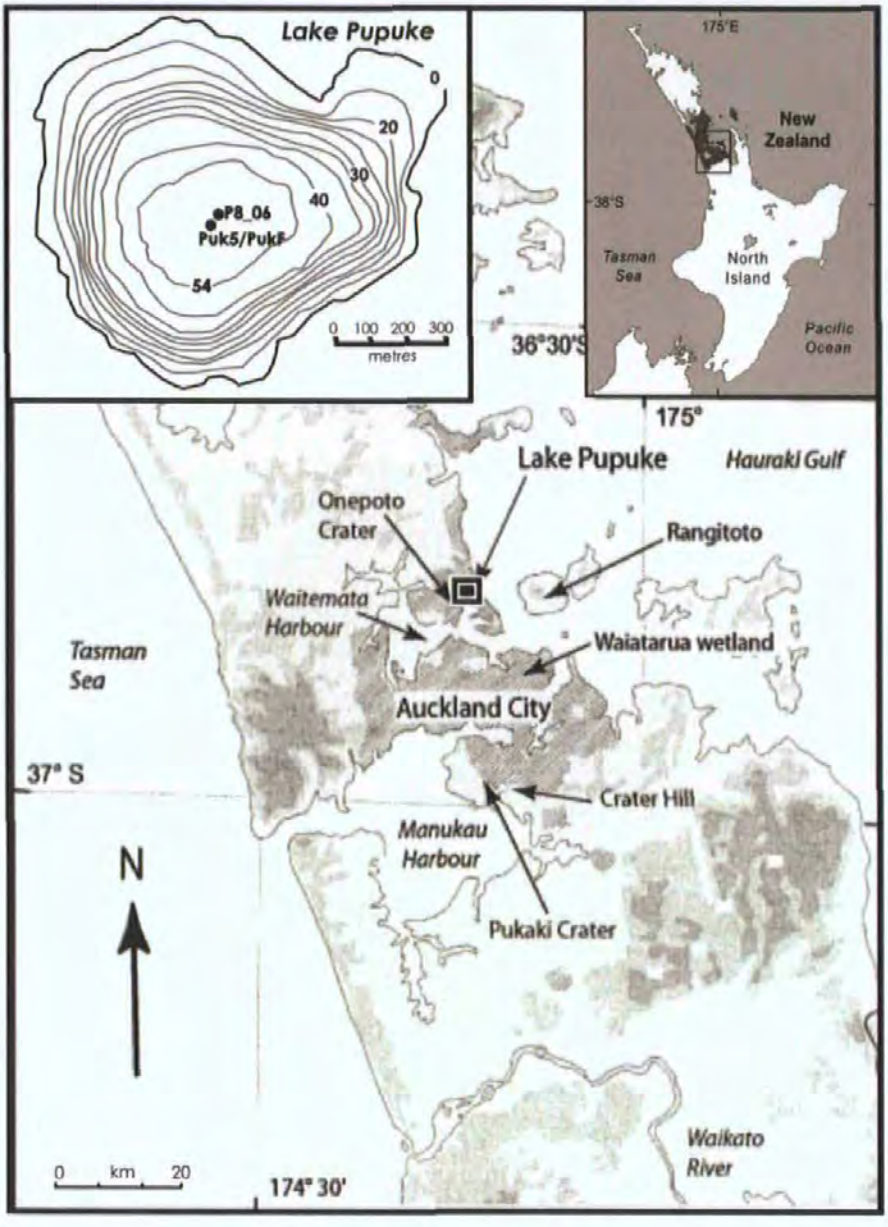

Figure 5.1. Location map of Auckland City and location of Lake Pupuke. Inset left: lake bathymetry (depths in metres) and approximate locations of core sites. Inset right: the Auckland Region shown by dark grey shading. Map modified from Augustinus *et al.* (2006).

The Auckland and Northland regions occupy a fairly narrow northwesterly trending peninsula which has been shaped by the underlying geological structure (Ballance & Williams, 1992). Paleozoic rocks form the main basement rocks of the peninsula and are

overlain by deposits from Tertiary and Quaternary volcanism. Several phases of extension related, intraplate phreomagmatic and magmatic activity have occurred since the early Pleistocene (Cassidy *et al.*, 1999). The youngest of these, the Auckland Volcanic Field (AVF), is confined within the limits of Auckland City covering an area of *c.* 360 km^2 and includes a variety of basaltic structures including lava field, tuff rings, maars, cinder cones, small shield volcanoes and lava lakes (Fig. 5.2) (Ballance & Williams, 1992; Cassidy *et al.*, 1999). Activity in the AVF commenced *ca.* 260,000 years ago (Marra *et al.*, 2006; Smith & Allen, 2007; Augustinus *et al.*, 2008) and has since produced a cluster of ~49 basaltic volcanoes and edifices, most resulting from monogenic activity (i.e., wherein each crater or centre erupts only once). The erupted rocks are predominantly alkali basalts and basanites.

The largest and most recent of AVF activity occurred *ca.* AD 1400 (Nichol, 1992) and resulted in the formation of Rangitoto Island, a shield volcano located near the entrance to Waitemata Harbour (Plate 5.2 a). The eruption of Rangitoto produced 2.3 million cubic metres of lava and 19 million cubic metres of pyroclastic deposits including ash and scoria, found >5 km from the vent, which would have had localised impacts. There is some evidence that ash fall occurred in four separate phases over a relatively short time period (McFadgen, 2007). The actual date or timing of the Rangitoto eruption is, however, a matter of ongoing debate and is complicated by some very recent evidence which suggests that the volcano was the product of possibly several separate eruption events (Nichol, 1992; Cassidy *et al.*, 1999; Needham *et al.*, 2008). There is, however, abundant archaeological evidence that shows the eruption(s) must have been witnessed by early Polynesian (Maori) settlers (Nichol, 1992; Lowe *et al.*, 2000; McFadgen, 2007).

The Auckland Region is characterized by a warm to temperate climate with moderately high annual rainfall. Mean daily temperatures in the region reach 23.7°C in February and 14.5°C in July (NIWA, 2007a). Average annual rainfall in the region is 1240 mm, spread fairly evenly throughout the year. Auckland straddles a distinct boundary between biogeographic zones to the north and south and as a result is particularly important for records of climate change (Newnham *et al.*, 2007a).

5.1.1 Late Quaternary records from Auckland maars

Auckland maars have been an important resource for obtaining high resolution palaeoclimate records which extend for a significant part of the Mid-Late Quaternary (~260 ka) for a number of studies (e.g. Sandiford *et al.*, 2001; Pepper *et al.*, 2004; Horrocks *et al.*, 2005; Augustinus, 2007; Newnham *et al.*, 2007a; Augustinus *et al.*, 2008). Lake Pupuke is, however, the only maar to preserve Holocene lacustrine sediments and as a result provides a key archive for palaeorecords for this time period extending from pre-human settlement to the modern urban environment of today (Newnham & Lowe, 1991). The maars also contain an extensive record of Late Quaternary multi-sourced tephra layers (Newnham *et al.*, 1999a; Sandiford *et al.*, 2001; Shane & Hoverd, 2002; Molloy & Shane, 2007). These tephras provide a detailed chronology and correlative markers to support the palaeoenvironmental records obtained from these sites. More than 70 tephra layers have been preserved as visible layers in the lake sequences since *ca.* 70 ka, derived from distant and local sources (Newnham *et al.*, 1999a; Sandiford *et al.*, 2001; Shane & Hoverd, 2002; Shane, 2005; Molloy & Shane, 2007). The tephra records have also provided very

important insights into the potential frequency of eruptives likely to affect the metropolitan area in the future (Shane, 2005; Molloy & Shane, 2007).

Tephras in the Auckland maar sequences include a large number of rhyolitic layers from Okataina and Taupo volcanic centres as well as a large number of andesitic-dacitic tephras from more voluminous or widely dispersed eruptives from Egmont and Tongariro volcanoes. A total of 43 visible andesitic tephras has been detected in the maar records for the last ~70 ka (Shane, 2005). These records suggest a frequency of fall deposits from andesitic volcanoes of once per ~960 years on average (Molloy & Shane, 2007). The majority derive from Egmont volcano which is located 270 km SW of Auckland. Tephras from TnG VC sources are predominantly in the upper parts of the sequences, within the past *ca.* 15.7 cal. ka (Shane, 2005). Andesitic-dacitic tephras have, however, not been identified in the Lake Pupuke sequence after ~9 cal. ka BP and it is thought that this absence is the result of changing wind patterns after the Last Glacial Maximum (Shane & Hoverd, 2002; Molloy & Shane, 2007). Basaltic tephras from the small scale eruptions in the AVF area also are preserved in the maar sequences, interbedded with well-dated silicic tephras. These sequences have provided an important record for understanding the timing and frequency of AVF eruptions (Shane & Smith, 2000a).

Plate 5.1. Panorama photograph of Lake Pupuke with Rangitoto volcano in the background view. Image taken by author from the western edge of the lake.

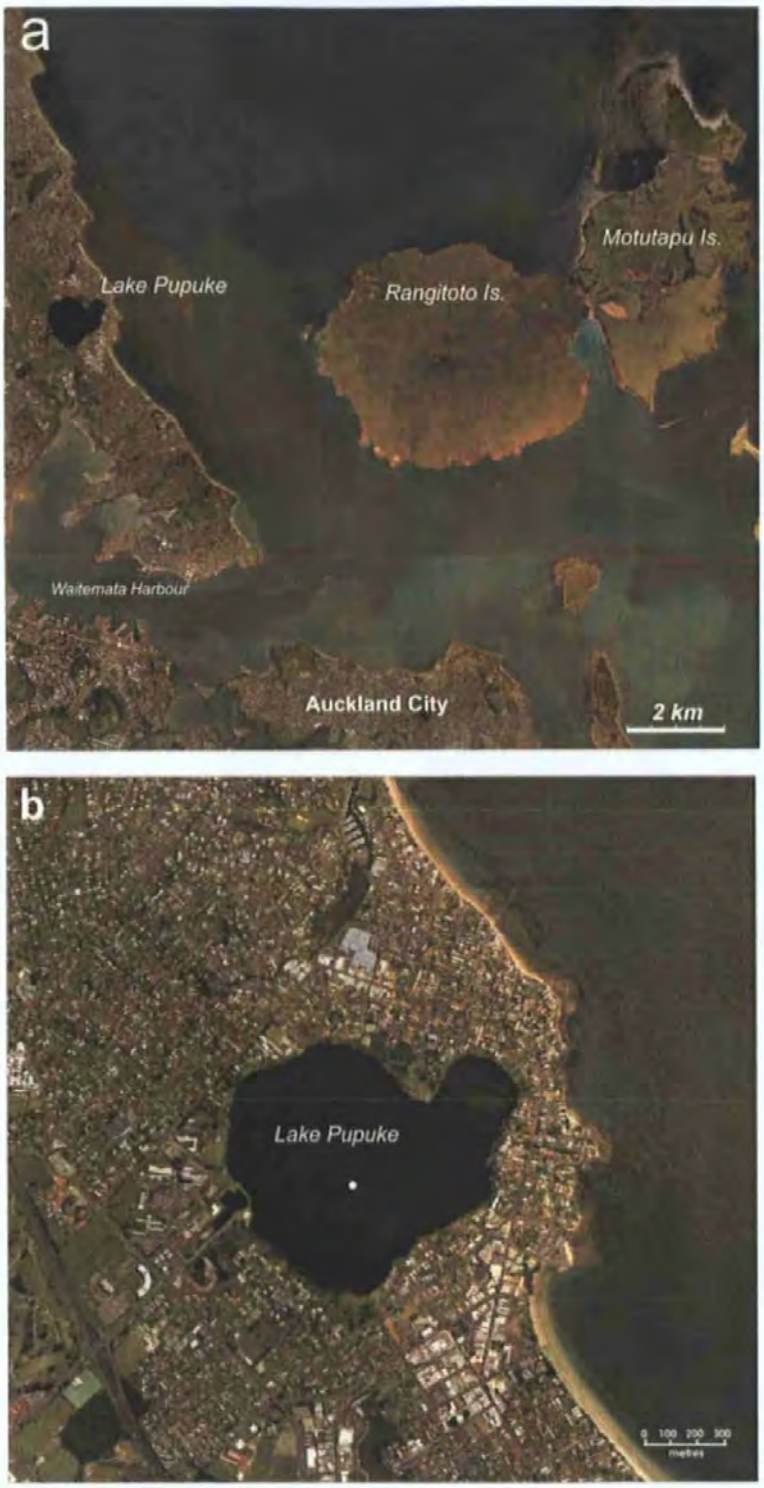

Plate 5.2 Satellite images of Lake Pupuke and surrounds: (a) in relation to Rangitoto volcano and Waitemata Harbour; (b) showing infrastructure around the lake. White dot indicates approximate location of core retrieval (Puk5). Images from Land Information, New Zealand: Orthophoto NZTM BA32 (2003/04).

http://www.linz.govt.nz/core/topography/aerialandorthophotos/nztmorthophotos/ba32/index.html)

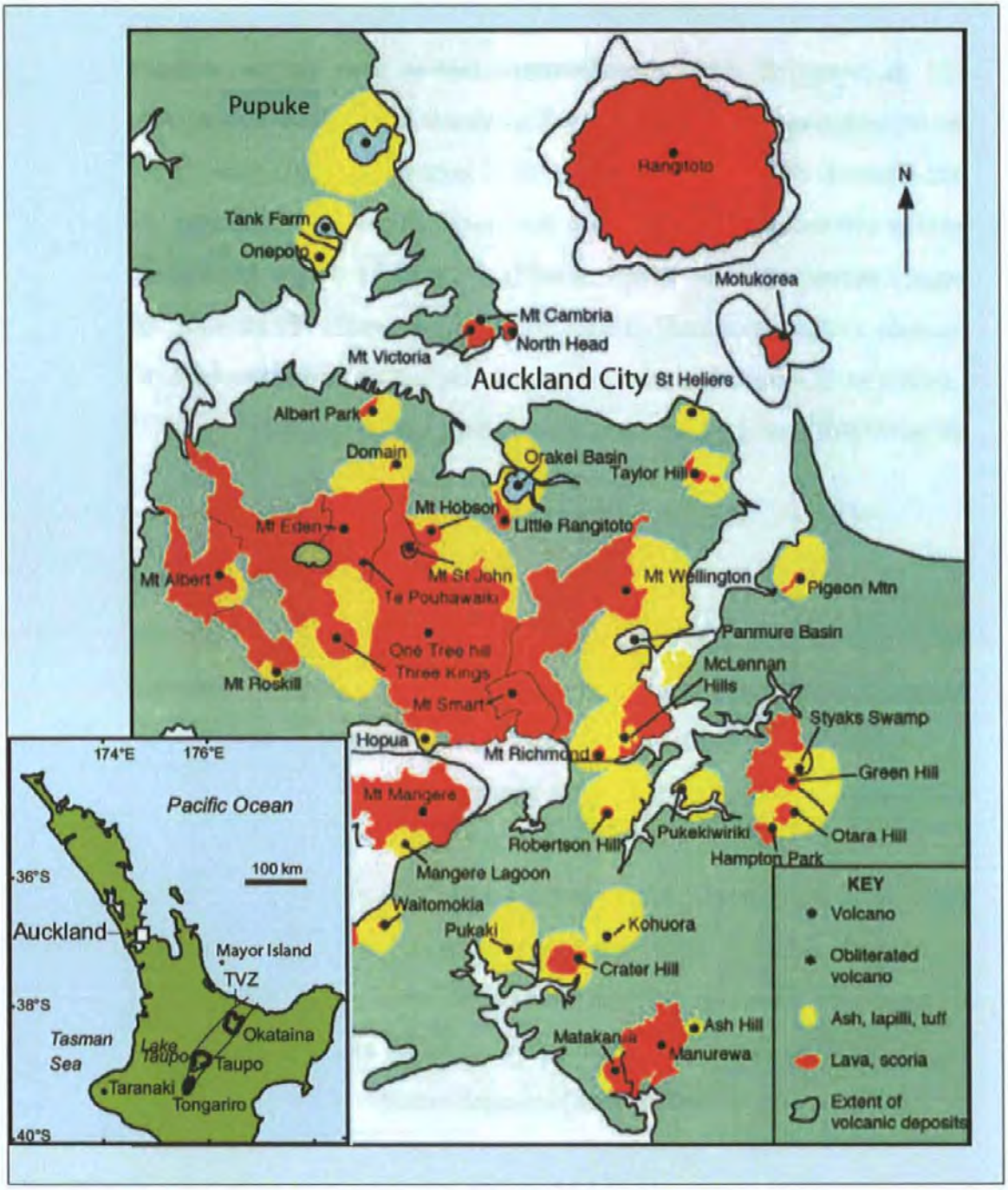

Figure 5.2. Auckland Volcanic Field showing location of named basaltic cones and maar craters in relation to TVZ and Egmont/Taranaki volcano (inset). Figure from: Augustinus (2007).

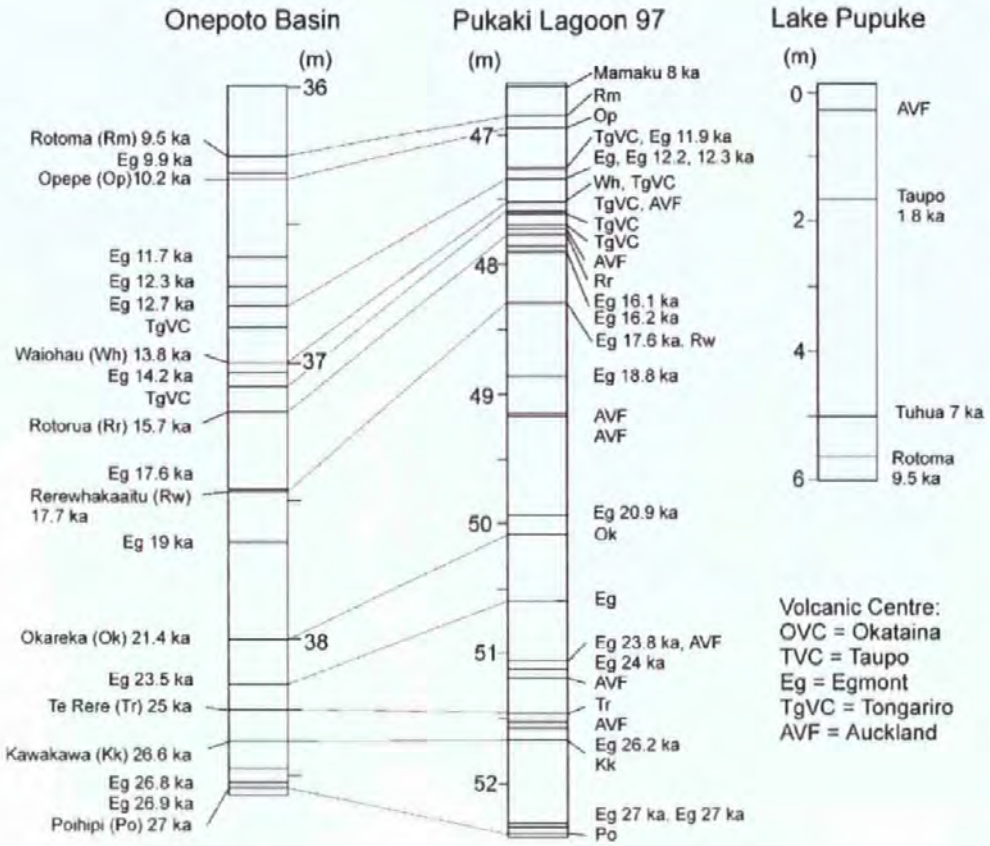

Figure 5.3 Post-26.5 ka tephrostratigraphy of palaeolake sediments from the Auckland area. Figure from Shane (2005).

5.2 Lake Pupuke

Lake Pupuke (36° 46′ 48″ S, 174° 45′ 58″ E) is a large, deep, freshwater maar lake situated in North Shore City, part of the larger Auckland metropolitan area (Fig. 5.1, Plate 5.2 a, b). It is the site most distal from the main CNI volcanoes used in this study and is strategically positioned in New Zealand's most densely populated metropolitan area.

5.2.1 Site description

Lake Pupuke represents one of a number of maar craters of the AVF which formed as a result of ground level explosions from localized intraplate basaltic activity (Fig. 5.2). The formation of the maar craters is the result of phreomagmatic activity – interactions between lava and water which produce large, effectively circular blow-out craters that are surrounded by a tuff ring (Lowe & Green, 1992). Many of the maar craters of the AVF were gradually filled with water and comprised a lake at one time or another in their history. Lake Pupuke, however, is the only remaining freshwater maar in Auckland (Fig. 5.2) (Augustinus, 2007), the other maar lakes having been breached by rising sea level in the early Holocene (~8 cal. ka; Shane, 2005). The Lake Pupuke maar is believed to have formed *ca.* 260,000 years ago (Augustinus *et al.*, 2008).

The lake forms a round, deep basin less than 200 m from the edge of the sea on its eastern margin. Although the lake is only ~5 m above present sea level, it is protected from saltwater influx and erosion by a thick tuff edge (Horrocks *et al.*, 2005). There is no evidence that the lake has ever been breached by the sea (Augustinus *et al.*, 2006). The lake and its catchment are situated entirely in the residential part of the city and private housing extends right up to the lake edge (Plate 5.2 a). The lake occupies ~57% of its catchment area which supplies a small amount of runoff into the lake basin. However, the lake is essentially a hydrologically closed system receiving most of its inputs from rainwater. Minor outputs from the lake occur in the form of coastal springs but evaporation is the dominant means of water loss (Augustinus *et al.*, 2006). In total the lake covers a surface area of 1.1 km^2 and has a bowl-shaped bathymetry which increases in depth toward

the centre (Fig. 5.1). The lake has a volume of 2.9 km^3 and a maximum depth of 57 m (Horrocks *et al.*, 2005).

The environment around the lake has changed dramatically in the last few centuries. Pollen analysis on Auckland sites reveal that during the mid-late Holocene, prior to human arrival, the Auckland Region would have been surrounded by mixed kauri/podocarp angiosperm forest and landscape conditions were considered to have been relatively stable (Newnham & Lowe, 1991; Horrocks *et al.*, 2005). The arrival of Polynesian settlers (Maori) to the area, probably late in the 13th Century or early in the 14th Century, led to rapid deforestation and the start of modifications of many landscape features (Newnham & Lowe, 1991). Abundant archaeological evidence suggests that the region was an important population centre where the Maori population may have peaked at ~20,000. The warm climate and the natural bays meant that, upon the arrival of Europeans to the region in the late 1700s to early 1800s, the area became an important population centre and rapid development followed. Lake Pupuke now has an urban setting surrounded by residential buildings, recreational facilities and parkland. In recent years, along with increased human development around the lake, the lake has provided a number of uses including a repository for raw sewage in the early 1900s and recreational pursuits (Augustinus *et al.*, 2006). The addition of sewage to the lake resulted in problematic algae growth which was treated by the addition of copper sulphate in 1932 and 1939. The addition of these chemicals now provides a clear chemical marker in the lake sediments.

5.2.2 Core collection

Three sequences from Lake Pupuke were used in this study, all collected by Dr Paul Augustinus (University of Auckland) as part of a multi-site, multi-proxy investigation of Auckland maar sequences (NZ-Maar; Augustinus, 2007). Cores Puk5 and PukF were collected in 2002 and P8_06 in 2006 (Fig. 5.4). Core sequences were collected from the deepest part of the lake (Fig. 5.1) using a Mackereth-type corer with 65 mm diameter PVC tubes (Augustinus *et al.*, 2008). Only the upper sections of the sequences, up from the visible component of the Taupo Tephra (1717 ± 13 cal yr BP), were provided for this study.

In core Puk5 the visible Taupo Tephra is identified at 167.3 cm depth but because the top of the sediments was not obtainable, the exact depth from the surface of the modern sediments is uncertain. As a consequence, the top ~84 cm of waterlogged, unconsolidated sediments were collected close to the Puk5 core site using a flat-face freeze corer using CO_2 pellets (dry ice) (Augustinus *et al.*, 2006) (PukF; Fig. 5.4). Samples from Puk5 provided for this study included complete sections of the remaining, dried, core although there were some gaps where large samples had been extracted. PukF was sub-sampled shortly after the section was defrosted at the University of Auckland laboratories.

Core P8_06 was collected in 2006 from a position close to Puk5 to provide for more detailed analysis on the Lake Pupuke maar record (Fig. 5.1). Because of an improved coring technique it was possible to collect a near-complete sequence from surface of the lake bottom (sediment-water interface) down to the visible Taupo Tephra at 210 cm depth. A gap in the core (136-160 cm) may be due to core slippage rather than a missing section of the sequence although this cannot be discounted. Samples provided for this study

included the remains of material used for loss-on-ignition (LOI) measurements taken from 0.5 cm-thick contiguous samples. The samples used for LOI measurements were suitable for glass shard extraction and counting. Samples required for geochemistry were, however, sampled from the original core.

Prior to commencing cryptotephra analysis, it was possible to align the three cores accurately using visible tephra layers and a chemical marker, as shown in Figure 5.4.

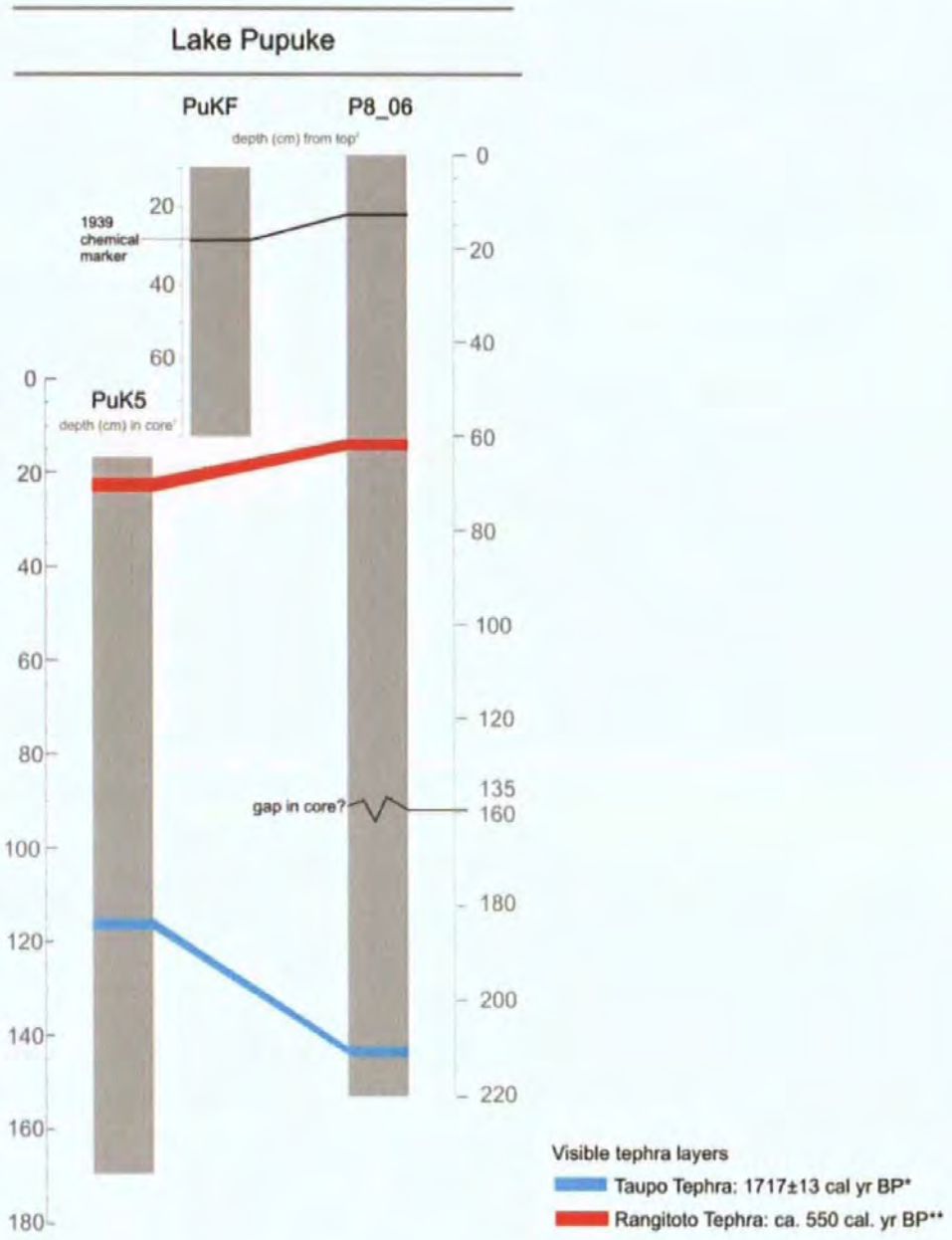

Figure 5.4 Summary of core sections from Lake Pupuke used in this study including visible tephra layers. ‡ from sediment water interface, † from the top of retrieved core. *Ages from Sparks et al., 1995, 2008; ** estimated age from Nichol, (1992). The chemical marker comes from the addition of copper sulphate into the lake in 1939.

5.2.3 Core description: lithostratigraphy, organic content and visible tephrostratigraphy

All sequences from Lake Pupuke used in this study consist of partially laminated sediments of fine organic and diatomaceous rich muds. The laminations in the sequences are millimetre to sub-millimetre-thick alternating dark and light layers consisting of minerogenic and diatom rich deposits, respectively, possibly representing annual or quasi-annual cycles of enhanced summer and reduced winter productivity (Pepper *et al.*, 2004; Augustinus *et al.*, 2008). The lake sediments were also rich in sponge spicules, the mineralised calcareous or siliceous skeletons of sponges.

Both Puk 5 and P8_06 cores contain two visible tephra horizons which include the rhyolitic Taupo Tephra (1717 ± 13 cal yr BP) and the basaltic Rangitoto Tephra (*c.* 550 cal yr BP; Lowe *et al.*, 2000). The Rangitoto Tephra (originally defined by Froggatt and Lowe, 1990) is the product of localised distribution of ash and other pyroclastic material from the largest and most recent AVF eruption which evidentially resulted in the 'main' (alkalic) phase of formation of Rangitoto Island. A likely 'second' or final (tholeitic) phase, identified recently by Needham *et al.* (2008), was less voluminous and produced much thinner ash fallout. A 'precursory' phase (i.e., before the main alkalic phase), also tholeitic, may have occurred as well (Shane and Smith, 2000). Evidence for the occurrence and timing of these three possible phases (precursory, main, second/final) in the formation of Rangitoto Island is presented and discussed below, although it is emphasized that the cryptotepha-derived evidence for the 'precursory' and 'second' phases is provisional because of the possibility of reworking in a lacustrine environment and because of the limited numbers of analyses.

Rangitoto Island is located less than 5 km from Lake Pupuke (Fig. 5.2 a). The precise timing of the main alkalic phase of formation of Rangitoto Island, and the associated visible tephra fall, has been uncertain (Nichol, 1992). The best estimate of age was derived from two radiocarbon ages obtained on short-lived material: 548-434 cal yr BP (AD 1402-1516) (Nichol, 1992; Lowe *et al.*, 2000). A recalibration of these ages using the current Southern Hemisphere calibration series SHCal04 (McCormac *et al.*, 2004) through the calibration programme Calib (Stuiver & Reimer, 2005) (Version 5.0.2html.) refined this age range to 526-451 cal yr BP (2σ range) (AD 1424-1499). This age estimate was supported generally by several additional radiocarbon dates, by hydration age dating and several other lines of evidence including paleomagnetism and thermoluminscence (Lowe *et al.*, 2000).

Detailed lithological, sedimentological and geochemical work has been undertaken on all three core sections used in this study and some of these data have already been published (Horrocks *et al.*, 2005; Augustinus *et al.*, 2006; 2008). The most detailed analyses have so far been undertaken on core P8_06. A selection of the data for this core is shown in Figure 5.5. Measurements of LOI and total organic carbon were carried out on all sections to provide a measure of organic productivity in the lake and provide a useful guide to changing sedimentation in the lake in recent centuries.

In both sequences, particle size analyses show a subtle fining of sediments up the core above the Taupo Tephra from fine to very fine silts. This change to finer sediments has been attributed to increased diatom productivity which has been particularly prevalent in core PukF which represents the last ~200 years of sedimentation (Augustinus *et al.*, 2008). This change in particle size also coincides with a change in sedimentation rates and a

decrease in organic productivity shown by LOI measurements. Using a combination of dating techniques for core Puk5 and PukF, Augustinus *et al.* (2006) recorded a dramatic tenfold increase in sedimentation rates to 4.5 mm/yr for at least the last 190 years in comparison with an average of 0.35 mm/yr between the Taupo and Rangitoto tephras.

Puk5

The two visible tephra layers in Puk5 have been identified in previous investigations and geochemical analyses were undertaken to confirm source and eruption events (Horrocks *et al.*, 2005). The Taupo Tephra is at the base of the sequence used in this study at 168 cm depth and consists of a very thin (~2 mm) coarse ash layer. The Rangitoto Tephra is identified as a single coarse ash layer between 24 and 27 cm depth, 141 cm above the Taupo Tephra. In Horrocks *et al.* (2005) the Rangitoto Tephra in core Puk5 comprised *two* discrete layers separated by laminated lake sediments. However, this separation was difficult to see in the core section when observed at a later date. In the present study, microscopic observations of samples resulted in the discovery of two horizons in the core containing charcoal (not visible from the core stratigraphy) between depths 152 to 155 cm and another relatively fine charcoal horizon at 38 cm. In core Puk5, only low resolution analyses were obtained for LOI measurements. These showed a fluctuation in organic content at around 40% organic matter with a marked excursion to lower organic content from ~15 cm below the Rangitoto Tephra and decrease to less than 30 % organic at the very top of the sequence (Fig. 5.4). Core Puk5 consisted of material that had been air dried over a period of three years after it was initially collected. As a result, some shrinkage of the core material had occurred and hence explains some of the discrepancies between the replicate core P8_06.

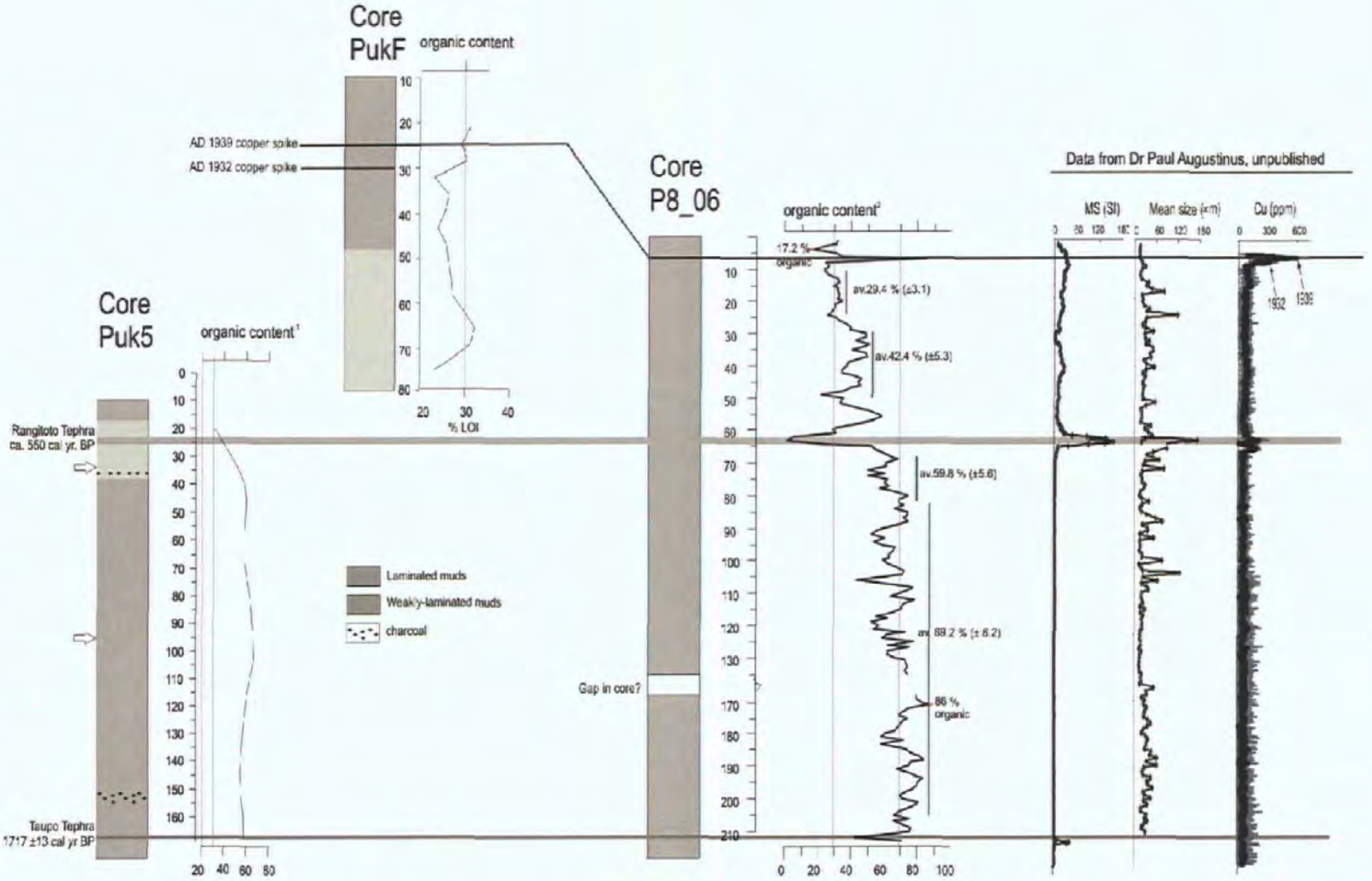

Figure 5.5 Core stratigraphy of sections used in this study showing changes in organic content derived by loss on ignition measurements. The vertical grey line marks 30% organic content. Additional measurements for core P8_06 include magnetic susceptibility (MS), mean grain size and chemical measurements of copper (Cu), data provided by Dr Paul Augustinus (unpublished data).

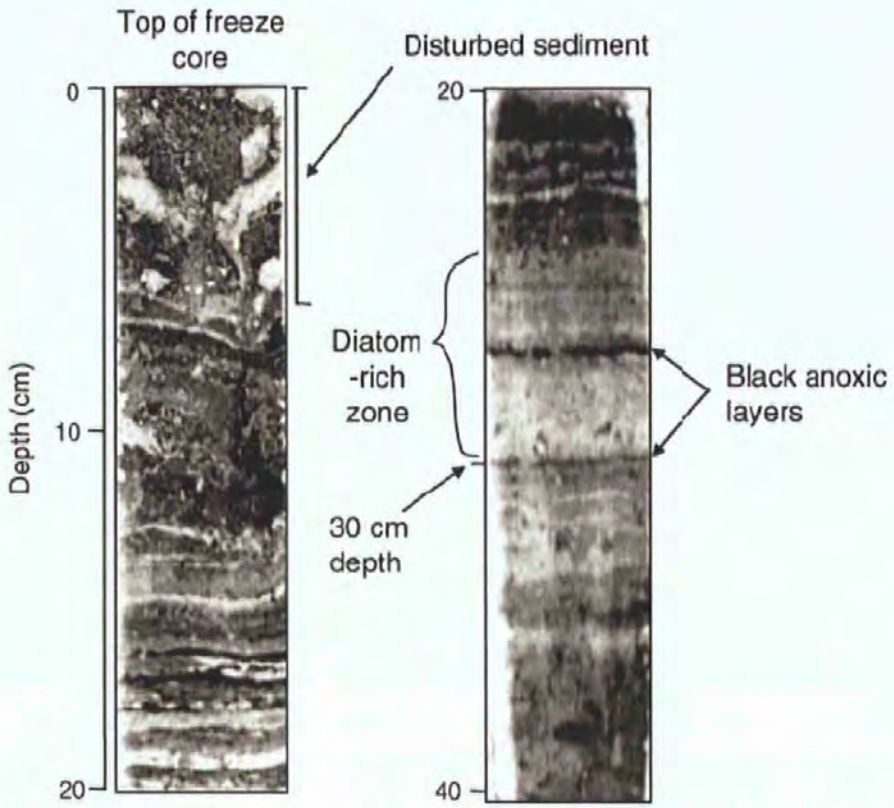

Figure 5.6 Photographs of the top 40 cm of Lake Pupuke sediments obtained as a freeze cores (figure from Augustinus *et al.*, 2006). Note that this photograph is from a replicate sequence and the depths do not match exactly with the core used in this study.

PukF

The freeze core from Lake Pupuke represents the top sediments missing from Puk5 but it was not certain, on collection, whether there was an overlap with section Puk5 (Fig. 5.4). Depths are equal to measurements from the top of the core, not necessarily depths from the actual surface, although this assumption is made with the age model constructed by Augustinus *et al.* (2006). The section consists of finely laminated muds throughout (Fig. 5.6). The laminations are very clear from 44 cm to 10 cm but below 44 cm they are much less clear. The top 10 cm of the sequence was badly disturbed possibly as a result of the

coring method or the sloppy nature of the very surface sediments (Fig. 5.6), or both. The section does not contain the Rangitoto Tephra but does have two visibly dark, 1.5-mm-thick horizons at 30 and 28 cm attributable to copper sulphate applications into the lake in 1939 and in 1932, respectively (Augustinus *et al.*, 2006) (Fig. 5.4). The origin of these layers was confirmed through detailed geochemical analysis. LOI measurements in the core showed an average organic content of 27.5%. This represents a ~10 % decrease in average organic content compared with that recorded in Puk5 (Fig. 5.4). Augustinus *et al.* (2006) attributed this decrease to increased erosion and inwash from around the lake subsequent to Polynesian arrival in the region.

P8_06

Core P8_06 is the most recent sequence collected from Lake Pupuke and represents the longest and most complete of the three cores from the site used in this study (Fig. 5.5). The Taupo Tephra marks the base of the sequence at 210 cm depth and the Rangitoto Tephra forms a single visible ash horizon at 62-63 cm depth (157 cm between the two tephras). Therefore, the length of the core section between the two tephras in P8_06 is 16 cm longer than in Puk5 – if the 30 cm gap in the core represents a missing part of the sequence. If the gap is the result of core slippage, the sediment accumulation would be 24 cm less than Puk5, not accounting for shrinkage in that core. Samples provided from the core were extracted from the fresh, wet core and are unlikely to have been affected by shrinkage as with Puk5.

Measurements of organic content for this core by LOI and provided by Dr Paul Augustinus were obtained from 0.5 cm resolution, contiguous samples and provide a very detailed measure of changing organic productivity and inorganic inputs into the lake since the deposition of the Taupo Tephra (Fig. 5.5). The general trend of organic content shows a steady fluctuation between the Taupo Tephra up to ~80 cm depth with average organic content ~69 % (± 8.2). Above ~80 cm depth there is a slight decline in organic content up to the visible Rangitoto Tephra (av. ~59.8% ± 5.6 organic content) (Fig. 5.5). Above the Rangitoto Tephra up to the top of the core there is a significant decrease in organic content of ~40% compared with average values pre-Rangitoto Tephra shown by two rapid jumps at 53 and 30 cm. At 4 cm depth in the core, 2 cm above the 1930s copper peaks, the lowest values for organic content are recorded. These low values are likely to reflect rapid development around the lake in the 20th Century.

5.2.4 Age-depth models

Age-depth models were developed for all three cores used in this study to facilitate age determinations of identified glass concentrations and for cross-core correlation. The age models for Puk5 and P8_06 were developed using a combination of tephrochronological ages and chemical and pollen markers. The dating of PukF is based on an existing age model using ^{210}Pb measurements, chemical and pollen markers (Augustinus et al., 2006). Radiocarbon dating was not attempted for any of these sequences as a result of previous problems establishing reliable ^{14}C ages for Pupuke and other maar lake sediments (Pepper et al., 2004; Horrocks et al., 2005; Augustinus et al., 2006; 2008). These problems have been attributed to a pervasive old-carbon effect in the lakes that partly arises from a hard-

water effect (e.g., Sandiford et al., 2001) and partly from human-induced inwashing of old carbon from the catchment following Polynesian settlement as has been observed in other lacustrine environments in northern New Zealand (e.g., Newnham et al., 1998; McGlone and Wilmshurst, 1999). Because of the intermittent nature of the laminations in the part of the lake sequence used in this study, layer counting was not deemed feasible as a chronological tool. The Rangitoto Tephra was not added to the age models used here because the age of this tephra is not firmly established and because of the recent evidence that two or three eruptive episodes might have been involved in forming Rangitoto Island. The identification of the Kaharoa Tephra in two of the sequences during the course of this study does, however, provide a more precise and reliable age marker and also presents an opportunity to refine the age of Rangitoto Tephra and the formation of Rangitoto Island volcano.

Age model for Puk5

The age model for Puk5 is constructed from three age markers: the tephrochronological ages of the Taupo Tephra and Kaharoa Tephra and one pollen marker (Fig. 5.7 a). The age model is drawn through the median ages of the tephra layers and shown with 2σ age errors. The age-point for the Taupo Tephra (1717 ±13 cal yr. BP) is at 168 cm depth. As shown below (section 5.2.6), the Kaharoa Tephra (636 ± 12 cal yr BP (AD 1314 ± 12; Hogg *et al.*, 2003), is identified as a cryptotephra in the core and provides an additional, precise marker horizon at the peak glass concentration at 38.5 cm depth in the core. Between the two tephras the sedimentation rate of the core is calculated to be an average of 1.20 mm/yr^{-1}.

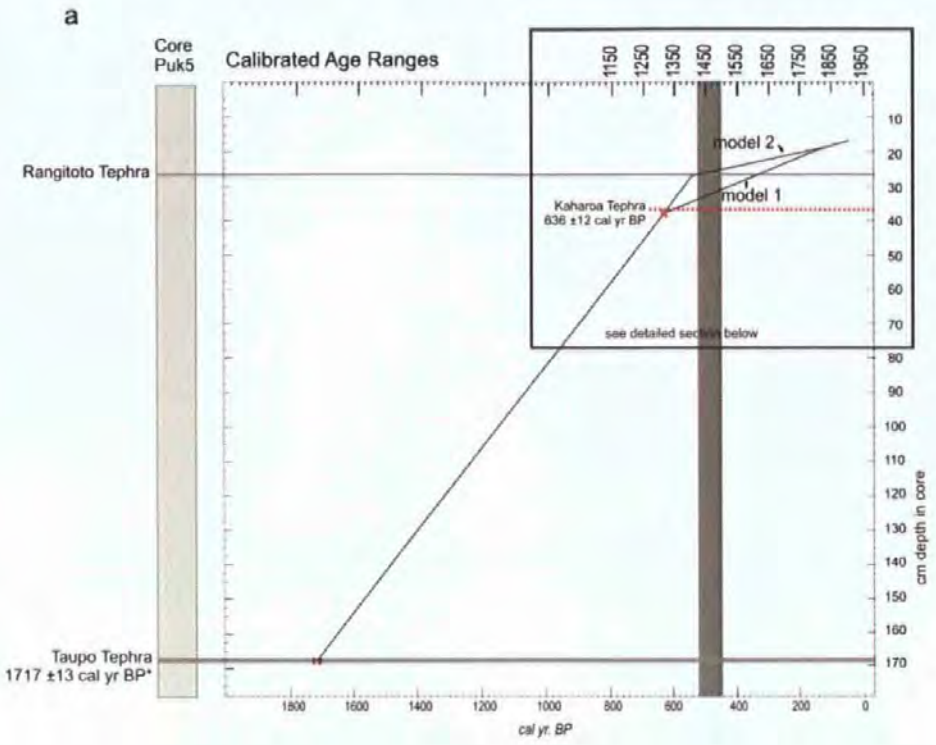

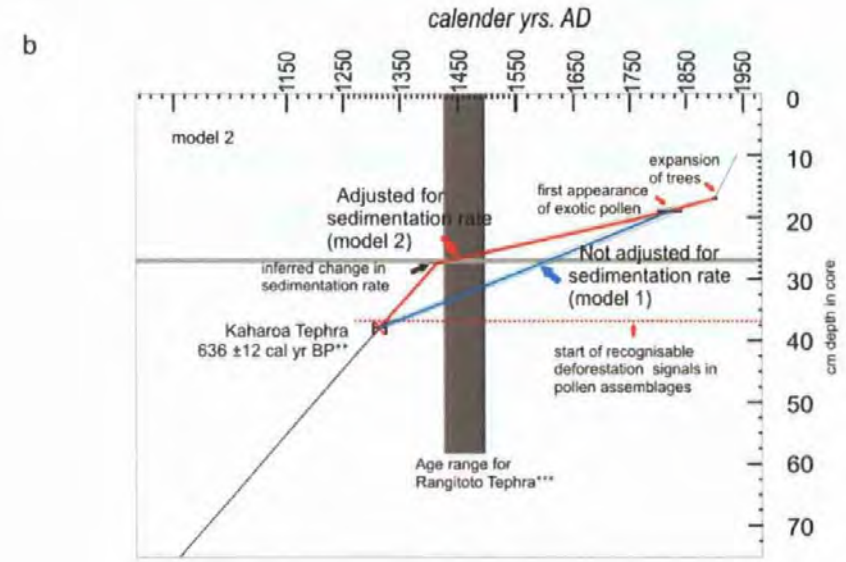

Figure 5.7 (a) Age model for core Puk5 using tephrochronological ages of Taupo Tephra *(Sparks *et al.*, 1995; 2008)and Kaharoa Tephra (Newnham *et al.*, 1998; Hogg *et al.*, 2003) and pollen markers (Fig. 5.8). (b) Detail of two models for the upper section of the core. Model 1 is based on linear interpolation between two age markers. Model 2 is adjusted for a change in sedimentation rate post Rangitoto Tephra, inferred from pollen analyses (Fig. 5.6) and sedimentology and is the preferred model used in this study. ***Age range of Rangitoto Tephra from recalibrated radiocarbon dates from Nichol (1992).

Pollen analysis, undertaken by Professor Rewi Newnham (University of Plymouth), provided two palynostratigraphic age markers to support the age model. The pollen assemblages from 16 to 44 cm depth in the core (Fig.5.8) show two major changes which are attributed firstly to the arrival of Polynesian settlers and, secondly, the arrival of European settlers in the early 1800s.

The first of these changes begins at 37 cm depth (the boundary between zone P1 and P2; Fig. 5.8), and is shown by a decline in trees coupled with a sustained increase in bracken as well as charcoal. These changes are consistent with the current model of early forest clearance in New Zealand by Polynesian settlers (Newnham *et al.*, 1999b). This marked palynological change also occurs only 1 cm above the Kaharoa Tephra (see later sections), consistent with the patterns seen in other pollen records from northern New Zealand, where the tephra is preserved as a visible layer (Newnham *et al.*, 1998; Lowe *et al.*, 2002), and with other evidence for earliest Polynesian settlement and impact (Wilmshurst *et al.*, 2008).

The second major change in pollen assemblages, at 19 cm depth (the boundary between zone P3 and P4; Fig. 5.8), is identified by the appearance of exotic plant species introduced by European settlers upon their arrival in the early 1800s. This boundary is drawn at the first appearance of *Plantago lanceolata* (ribwort plantain), which coincides with a marked sustained increase in Poaceae (grasses) and further elevated level of charcoal. *P. lanceolata* is a weed associated with soil cultivation in Europe. It is highly likely that the plant spread rapidly after its accidental introduction, probably from seed carried in soil by pioneering settlers in the early 1800s. This contention is supported by other features in the pollen diagram, notably increases in other ruderal taxa (*Taraxacum, Rumex* and Poaceae) and

charcoal, marked decline in indigenous tree and shrub taxa, and the subsequent rise in pollen (at *c.*17 cm) of introduced trees (*Pinus cupressus*) which likely occurred in the very early 20th Century. Concurrent with the rise in introduced pollen is the occurrence of spheroidal carbonaceous particles associated with burning of fossil fuels.

Between the Kaharoa Tephra and the introduction of European pollen (assumed *ca.* AD 1800) in the core there are two possible scenarios considered for the age model. The first of these scenarios follows conventional age-model construction, the second takes into account changes in sedimentation rates reflected by LOI measurements. The first model assumes a uniform rate of sediment accumulation between the Kaharoa Tephra and the introduction of European pollen (model 1; Fig. 5.7 a). This shows sedimentation rates decreasing some time after the deposition of the Kaharoa Tephra to 0.4 mm/yr. The inflection in sedimentation rate in this section of the core could, however, occur anywhere between the age points. A problem with this model is that the interpolated age of the Rangitoto Tephra would be as much as 200 years younger that the current best age estimate of ca. AD 1400 (Nichol, 1992). Such a young age is unlikely.

Using this best age estimate as a guide it is more likely that the actual inflection in sedimentation rates occurred after the deposition of the Rangitoto Tephra when LOI measurements reflect a rapid change in organic productivity and sedimentation in the lake. Analysis of the upper part of core PukF by Augustinus *et al.* (2006) also suggests that the change to increased sedimentation rates in the lake did not occur until the arrival of Europeans when organic productivity and terrigenous deposits increased significantly, coincident with marked changes in land use and human activities in the region. Pollen assemblages in the core show that, between the Kaharoa and Rangitoto tephras, changes in

land cover were on a comparatively minor scale and may not have resulted in any significant changes to sediment input into the lake (Fig. 5.7). The deposition of the Rangitoto Tephra into the lake may have also affected sedimentation rates which are largely a function of diatom productivity in this lake. Diatom productivity has been shown to be normally adversely affected by tephra deposition in lake environments (Harper *et al.*, 1986; e.g. Urrutia *et al.*, 2007). The second age model (model 2; Fig. 5.7 b), therefore, assumes the sedimentation rate, as calculated between the Taupo and Kaharoa tephras, remained near-constant up to the Rangitoto Tephra datum. The inflection in sedimentation is taken as immediately below the Rangitoto Tephra where it connects with the upper pollen age marker. This model shows a much better fit with the best age estimates for the Rangitoto Tephra (Fig. 5.7), a finding replicated by the age model for P8_06 (Fig. 5.9). It is this latter model (model 2) which is used therefore for interpolating ages for tephra shard concentrations (cryptotephras) discussed in the following sections.

Above the Rangitoto Tephra, the model assumes constant sedimentation rates until the advent of European pollen (*ca.* AD 1800). Such constancy is unlikely, given the marked changes indicated in pollen and LOI during this interval, but is invoked in the absence of any better age constraints at the present time. In any case, this section of the core is of limited relevance to this specific core study because the post-Rangitoto cryptotephra analyses were based on the other cores.

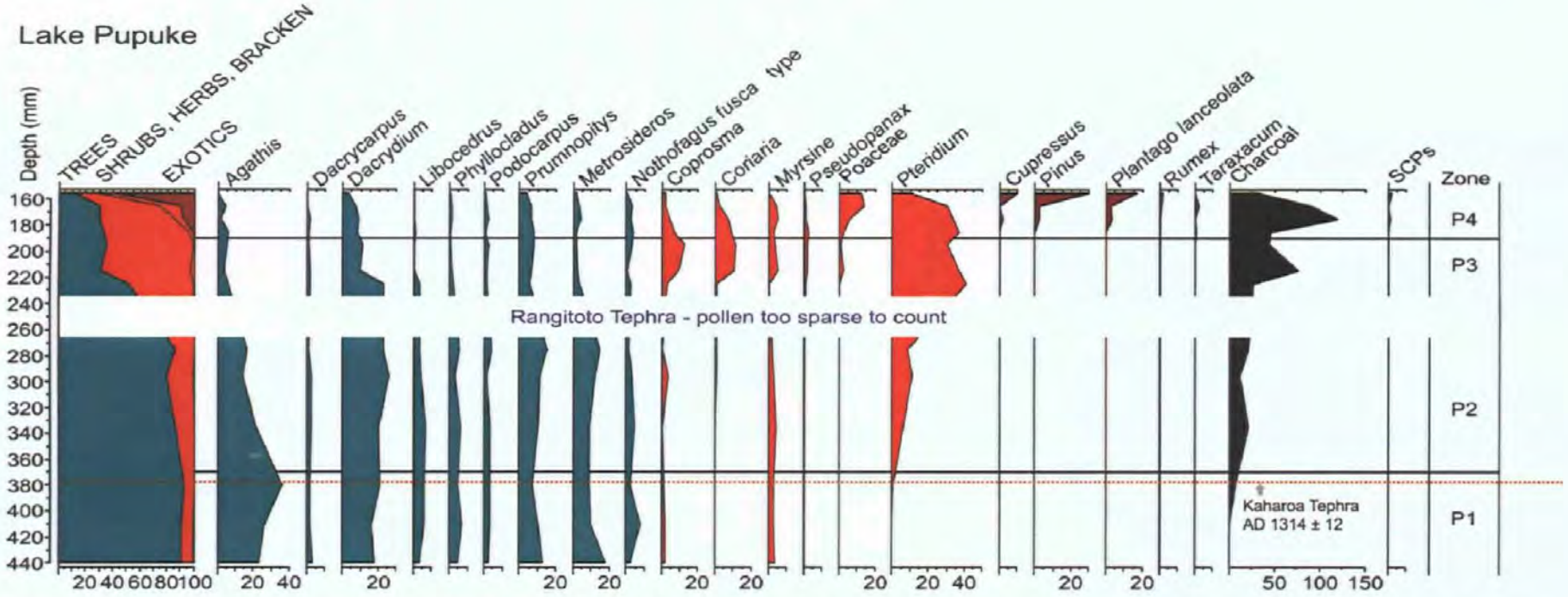

Figure 5.8 Percentage pollen diagram from Lake Pupuke core Puk5 between 44 and 16 cm depth in the core. The position of the Kaharoa Tephra, detected as a cryptotephra, is shown by a dashed red line (from Prof. Rewi Newnham, unpublished data).

Age model for PukF

The age model for PukF sequence is a published model on a replicate freeze core (Augustinus *et al.*, 2006) derived using ^{210}Pb activity and one historical chemical marker to establish sedimentation rates to date the sequence (Fig. 5.9). The age limit of the sediment sequence is also supported by pollen records which record the appearance of exotic plant species (e.g. *Plantago* and *Pinus*) in the lower part of the core, indicative of the arrival of European settlers in the early 1800s. The occurrence of this pollen marker would suggest that there is some overlap between PukF and Puk5 cores.

The historical chemical marker consists of two distinct black anoxic layers at 28 cm and 30 cm in the sediment resulting from the addition of copper sulphate in 1932 and 1939 (Fig. 5.4). The most distinct of these layers is from the 1939 application. These provide two precise age markers for the sequence.

The analysis of ^{210}Pb activity showed a steady decrease in ^{210}Pb down the core which supported the assumption that the laminated sediments were not affected by bioturbation or mixing. The results of ^{210}Pb were used in Augustinus *et al.* (2006) to calculate a model of sedimentation rate which was used to date the sequence. Ages were calculated using the 22.26 year half-life of ^{120}Pb and the assumption that the top of the sequence was representative of the surface sediments from the year the core was collected (December 2002). These ages/datums were used to calculate a mean sedimentation rate of 4.445 ± 0.32 mm/year which was used with the additional age markers to produce an age model (Fig. 5.9). The age model calculates the base of the sequence to start at AD 1822 which means that the sequence represents an essentially complete record since the settlement of Europeans in the region. Although the use of ^{210}Pb back as far as the early 1800s is

questionable, this age model was deemed acceptable for the purposes of this study as it was not required for dating any tephra depositional events.

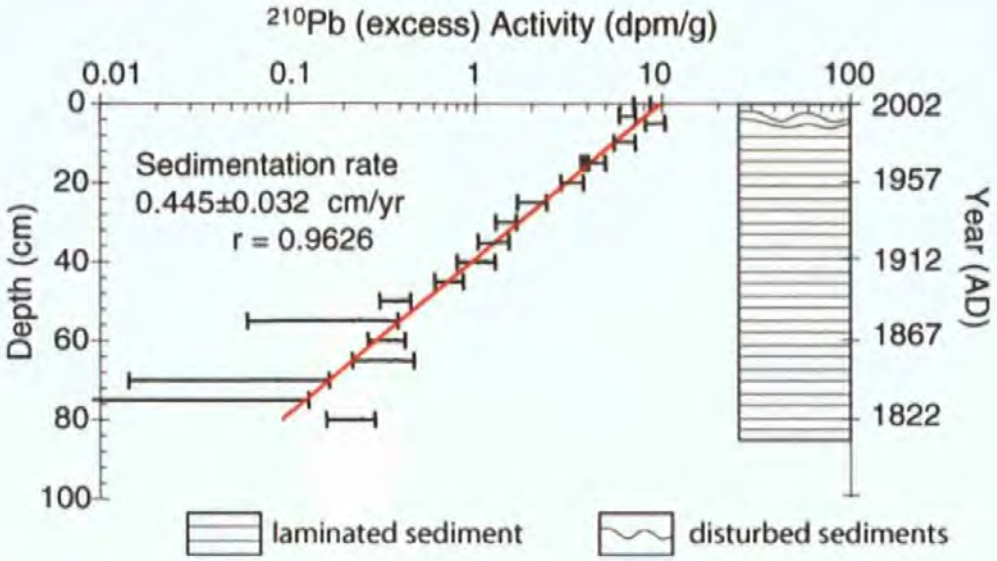

Figure 5.9 Core chronology for Lake Pupuke core PukF using unsupported ^{120}Pb profile to establish sedimentation rates. Figure from Augustinus *et al.* (2006). Below 40 cm the chronology is beyond the limits of 210Pb method and ages are therefore less reliable. The chemical marker in this core (not shown in this published model) is at 30 cm and is believed to correspond with the AD 1934 addition of copper sulphate to the lake.

Age model for P8_06

The age model for sequence P8_06 is also constructed from three age markers: the tephrochrological ages from the Taupo and Kaharoa tephras and the historical 1939 copper marker at the top of the sequence (Fig. 5.10). In the lower part of the core, the model connects between the two tephra ages. This model makes the assumption that the 'gap' in the core is artificial. When plotted to include the gap in the core in the age model there was very little difference in the interpolated ages for glass populations between the Taupo and Kaharoa tephras. The sedimentation rate between the Taupo (T1) and Kaharoa (T2) tephras in the core is calculated to an average of 0.93 mm/yr (distance (cm) interval between T1

and T2 divided by time interval (yrs; from 2σ age range) between T1 and T2). This rate of sedimentation is very slightly slower than that for the replicate core Puk5 (1.20 mm/yr).

As with core Puk5 there are two possible scenarios for the upper part of the core between the Kaharoa Tephra and the chemical marker (model 1 and model 2; Fig. 5.10 b). Model 1 assumes a linear relationship between the Kaharoa Tephra and the upper age marker. In this core the upper age marker is the anoxic black horizon at 7 cm depth in the core. This is believed to represent the 1939 application of copper sulphate which shows up at the uppermost copper spike in the geochemical profile for the sequence (Fig. 5.4). Model 2 adjusts the age model for changing sedimentation rates coincident with the deposition of the Rangitoto Tephra, as for Puk5. Placing the inflection point at this level is also supported by LOI measurements in this core. For this core, both models provide a consistent fit for the best age determinations for the Rangitoto Tephra. The age model does not extend up to the top of the sequence because it is uncertain how much of the upper sediments were lost on retrieval.

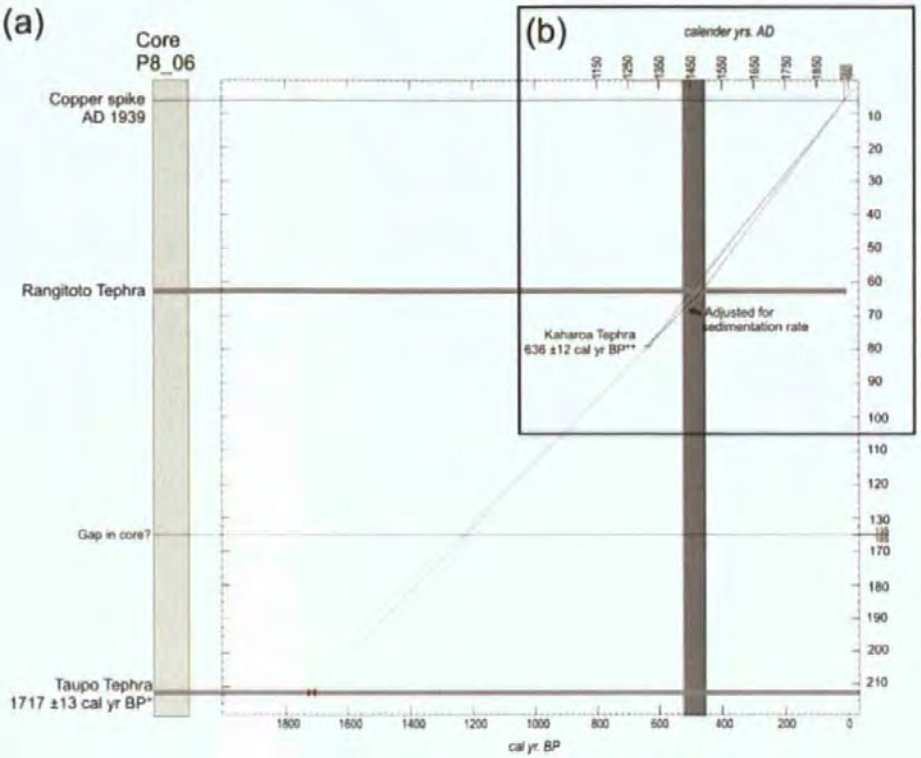

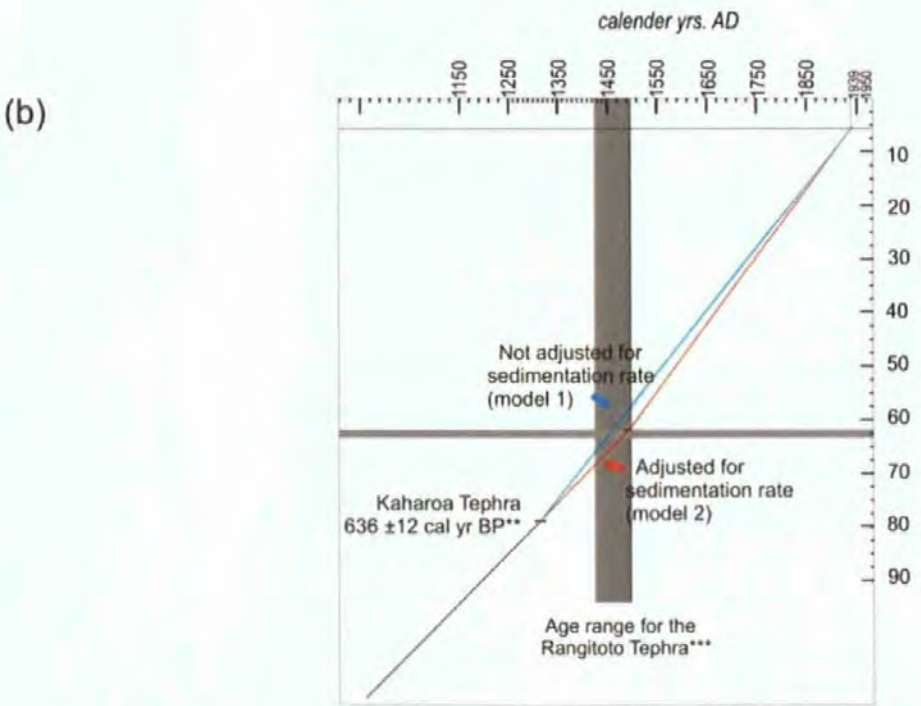

Figure 5.10 (a) Core chronology and age model for Lake Pupuke core P8_06 based on two tephrochronological ages and one historical chemical marker. Tephra ages given in Figure 5.7. (b) Detail of model between the Kaharoa Tephra and AD 1939 chemical marker showing two possible age model scenarios as shown for Puk5 (Fig. 5.7).

5.2.5 *Tephra derived glass-shard content*

As with previous site results the down-core tephra-derived glass shard counts from each section obtained from Lake Pupuke are presented as concentrations of glass shards calculated as particles per mg dry weight (mg d-wt.) (Puk5, Fig. 5.11; PukF, Fig.5.12; P8_06, Fig. 5.13). Three distinct glass shard types were recognized in the sequences from Lake Pupuke, primarily on the basis of colour: clear, brown, and dark brown shards which were tentatively identified prior to geochemical fingerprinting as originating from rhyolitic, andesitic (or dacitic) and basaltic sources, respectively (Shane, 2000). Distinguishing between basaltic and andesitic glass populations was, however, sometimes difficult where the two types were mixed. As a result brown and dark brown shards are combined in the diagrams as 'brown shards' to discount any problems with identification. The following descriptions of shard count results also include reference to shard colour rather than glass chemistry in most cases.

Of the three glass types, the clear (rhyolitic) and brown (andesitic-dacitic) shards identified in the sequences typically exhibited the same characteristics of clear and brown glass observed from the Waikato sites (Chapter 4). Clear shards are typically the larger of the two types of shards (~50-200 μm) and consist of vesicular and bubble wall glass fragments, which were isotropic under crossed polarised light and exhibited a moderate to high degree of stretching. Brown (andesitic-dacitic) shards were highly variable in nature but were typically smaller (~30-60 μm) and orange-brown in colour with a blocky morphology and poorly vesicular with abundant small rod-shaped crystal inclusions. In the visible basaltic tephra layer in the sequences, the basaltic glass was typically dark brown in colour with large, tabular feldspar crystals. Scanning electron microscopy was used to

observe shards in more detail (Plate 5.3) and revealed no distinguishable physical or chemical weathering features on the shards. There was evidence of where diatoms had been attached to the surface of the glass shards but such attachment is unlikely to have affected the structure or the composition of the glass (Plate 5.3 j and k).

Shard contents derived for each sequence are shown for clear and brown shard concentrations alongside measurements of organic content derived from LOI (Figs. 5.9 to 5.11). The glass shard content for each section is described from the base to the top of the sequence for clear and then brown shards, respectively. These descriptions include reference to any observations of shard character and morphology using a combination of generic and technical terms for ash-sized glass shards (Heiken, 1972; Fisher & Schmincke, 1984; Heiken & Wohletz, 1985).

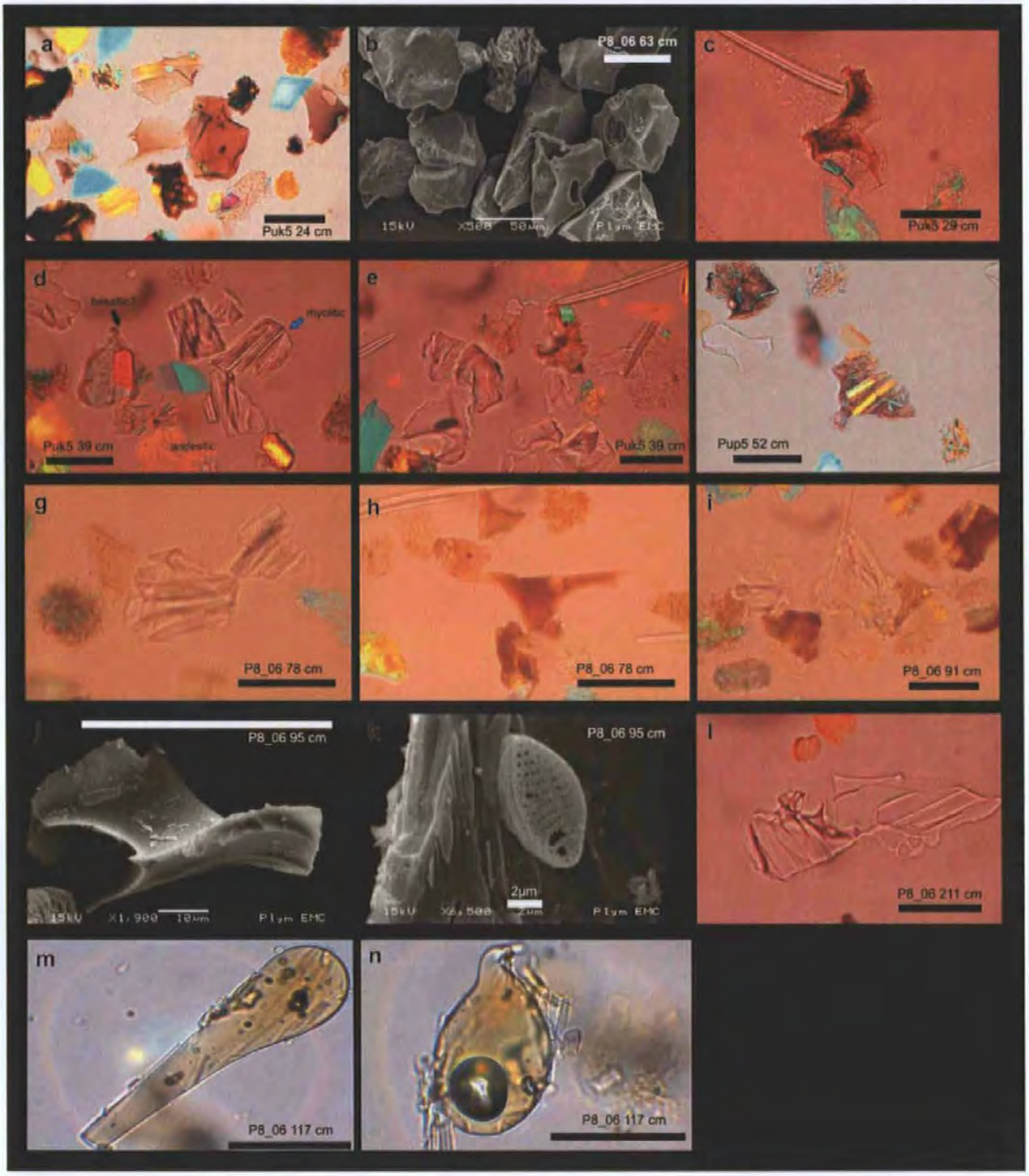

Plate 5.3. Photomicrographs and SEM images of glass shards and other features observed in samples from cores Puk5 and P8_06. Scale bar on images a-l and l-m equals 50 µm in length. Details of individual images referred to in the text.

Glass-shard content Puk5

The results of down-core glass-shard counts for sequence Puk5 are shown in Figure 5.11. The shard content derived from this section is based on analysis of 148 contiguous samples, each 1-cm thick, from the top of the sequence at 16 cm core depth to 169 cm depth just below the Taupo Tephra horizon. Individual glass shards were detected and counted in 96% of samples viewed which comprised a mix of both clear and brown shards in varying proportions. Samples did, however, generally contain a very low concentration of glass shards. More than 60% of samples viewed contained fewer than three clear shards per mg d-wt. More than 80% of samples contained fewer than three brown shards per mg d-wt. And more than 53 % of samples contained no brown shards at all. The highest concentrations of glass were found immediately above and below the visible Taupo and Rangitoto tephras. Additional peak concentrations of glass formed relatively discrete horizons (narrow bands) in the sediments in comparison to the records obtained from the peat sequences from the Waikato Region (Chapter 4).

A number of distinct changes in the concentrations of clear glass shards occur up through the core (Fig. 5.11). Above the Taupo Tephra there is a distinct attenuation of clear shard concentrations, a pattern observed in both peat and lake sites from the Waikato Region. In this section of the core, varying but relatively high concentrations (average 13.4 shard per mg d-wt.; Fig. 5.11) of clear glass were found to extend up to 136 cm depth in the core, 34 cm above the thin (0.5 cm), visible tephra horizon. Shards in this zone typically comprise a mix of pumiceous and striate shards of fine to medium ash size typical of rhyolitic sourced glass shards, comparable to the glass from the visible tephra layer below. Between

136 cm and 71 cm depth in the core (a total of 65 cm, 42 % of the length of the core of interest), clear shards are present in very low numbers with average shard concentrations of 0.9 (± 1.0) per mg dry wt. per sample. This pattern of very low clear shard concentrations in this section of the core is also reflected by similarly low numbers of brown shards. The midpoint in this section of the core also marks higher-than-average organic content. Above 71 cm, clear shard numbers increase in the samples as shown by varying shard concentrations represented by several small peaks where shard concentrations exceed 50 shards per mg-d-wt. This increase coincides with a subtle decline in organic content (Fig. 5.11). Clear glass shards observed in the section 71-50 cm were comparable with shards observed immediately above the Taupo Tephra and included some large, intricate bubble wall and platy shards. There was also a noticeable increase in mineral particles in this section of the core. Between 38 and 39 cm depth in the core there is a large and discrete 'peak' in clear glass content which represents the highest concentration (at 143 shards per mg-d-wt.) of shards from a non-visible tephra horizon in the core. The glass in this section of the core consists of a mix of clear and brown shards. The clear glass shards in this peak concentration were typically small, striate and cuspate shards ~50-70 μm in length which display a moderate to high degree of stretching (Plate 5.3 d and e). Above this glass peak in the core, clear glass concentrations remain relatively low up to the top of the core with a few minor peak concentrations with <13 shards per mg-d-wt.

The content of brown shards determined throughout Puk5 reveals a small number of discrete peaks with typically lower maximum shard concentrations than rhyolitic (clear shard) counterparts. Brown shard concentrations form a number of small peaks within the lowest 30 cm of the core coincident with declining content of clear shards above the Taupo Tephra. There are at least three prominent peaks in brown shard content in this zone at 152,

147 and 140 cm depth in the core. At 140 cm, the largest peak of brown shard concentrations, there are ~19 shards per mg-d-wt. As for clear shards, between 136 and 71 cm depth in the core, brown shard content remains very low with average shard concentrations of only 0.9 (± 0.6) shards per mg-d-wt.

Between 71 cm depth and up to the visible Rangitoto Tephra in the core there are at least three distinct and discrete peaks of elevated brown shard content at 52 cm, between 38 and 39 cm, and at 28 cm. The peak at 52 cm marks a very discrete glass concentration (35 shards per mg-d-wt.) with shard content above and below in the core remaining very low. Glass in this horizon consisted of predominantly blocky-shaped shards, 40-60 μm in length, which are densely packed with microlite crystals (Plate 5.3 f). At 38 cm, brown shard content is marked by the highest concentrations of brown glass for a non-visible horizon in the core with ~89 shards per mg-d-wt. Shard content remains elevated at least 1 cm above and below this peak in brown glass in the core, which also overlaps a peak in clear shards 1 cm below in the core. Brown glass in the sample from this position in the core consisted of pale, orange-brown, blocky and sometimes vesicular shards, 40-60 μm in length and with abundant microlite crystals (Plate 5.3 d). Brown shards at this level in the core were mixed with similar proportions of clear shards (Plate 5.3 e). The peak in brown shards at 29 cm immediately underneath the Rangitoto Tephra is separated by increasing concentrations of basaltic glass by a 1 cm gap where brown shard content is < 1 shard per mg-d-wt. Observations of the shards in this peak concentration revealed mainly dark brown, platy, 'basaltic' shards with large feldspar crystals, similar to shards observed in the visible tephra horizon at 27 cm (Plate 5.3 c). The occurrence of this peak in basaltic shards below the visible layer could be accounted for by a precursory eruption event, an occurrence which has been noted for only one of the previous AVF eruptions (Newnham &

Lowe, 1991), or the peak could be the result of glass sinking through the lower layer into the soft sediment down to an older stratigraphic level. These two hypotheses were proposed by Horrocks *et al.* (2005) to explain the double basaltic horizon observed in the core shortly after retrieval. Basaltic shards from the Rangitoto Tephra are observed in relatively high concentrations for ~ 1 cm above and below the visible layer but remain well contained within the sediment profile. Glass in this zone comprises dark brown to orange brown, blocky and platy shards with low vesicularity and stretching with large rectangular feldspar crystals (Plate 5.3 a, b). Above the Rangitoto Tephra up to the top of the sequence analysed, shard content remains relatively low with one small peak in shard content at 19 cm depth.

Glass-shard content PukF

The results of down-core glass-shard counts for sequence PukF are shown in Figure 5.12. The shard content derived from this section is based on analysis of 64 contiguous samples, each 1-cm thick, from the top of the sequence at 14 cm core depth. The effective retrieval and the counting of glass from samples taken from this section were problematic because of an abundance of fine mineral particles which proved difficult to separate from the glass content. The resulting shard concentrations derived for this section may have been affected as a result.

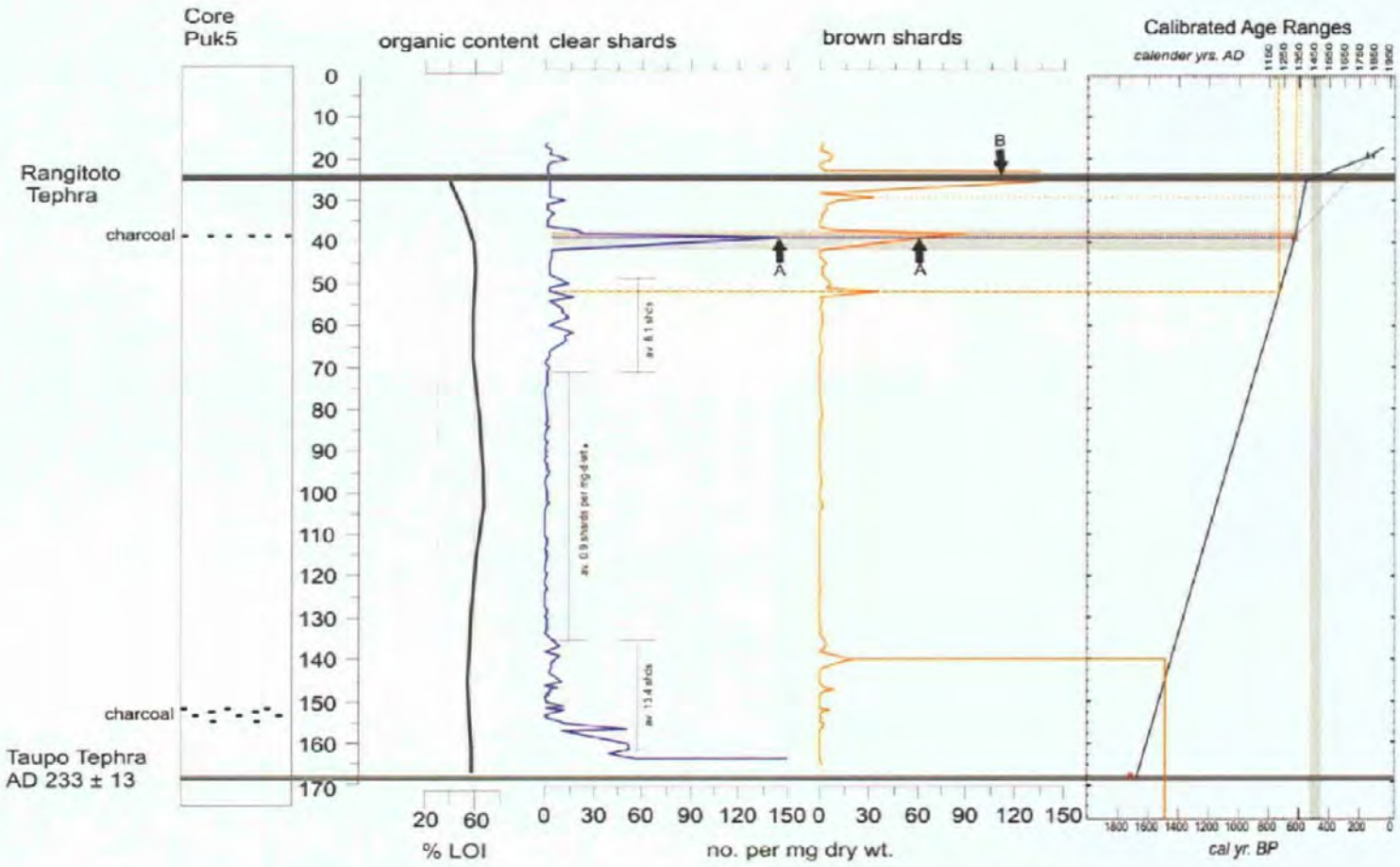

Figure 5.11 Results of glass shard concentrations derived for core Puk5 alongside loss-on-ignition measurements and age model. Shard counts are shown in colour, blue for clear shards and orange for brown shards. Light grey bands mark selected zones of elevated glass concentrations. Arrows indicate position of samples from the core where glass content has been analyzed by EMP.

The results (Fig. 5.12) shows a very variable pattern in shard concentrations, with typically low shard content throughout the section with most samples (80%) containing fewer than 30 shards (clear and brown) per mg dry wt. Both clear and brown shards were, however, detected in every sample viewed, albeit in low concentrations. Clear shard concentrations show the greatest variability with a possible increasing frequency for the top 40 cm of the core. Given the time period that the core represents, it is therefore likely that these fluctuating glass concentrations represent increasing disturbance around the lake resulting in the remobilization of volcanic particles around the lake edge or from the lake catchment. The concentrations of brown shards remain low with no distinguishable peaks except possibly at the lowest part of the core, between 70 and 85 cm depth, where there are three 'peaks' in elevated shard content, and close to the top, at *c.* 12 cm depth.

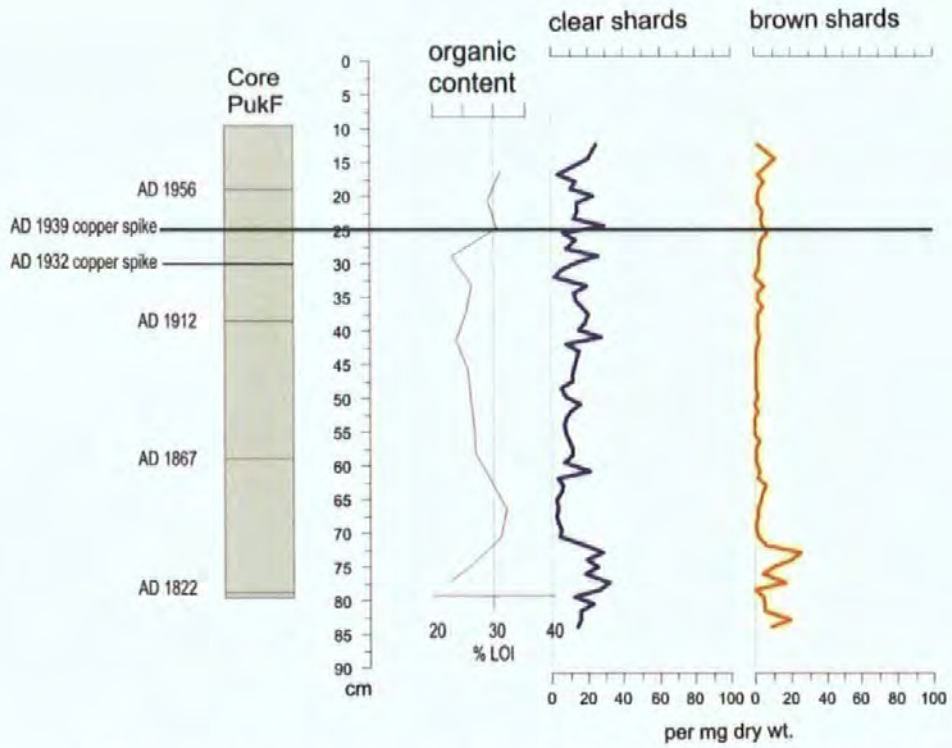

Figure 5.12. Results of glass shard concentrations derived from core PukF shown alongside loss-on-ignition measurements and core chronology. Ages from published age model shown in Figure 5.9.

Glass-shard content P8_06

The results of down-core glass-shard counts for sequence P8_06 are shown in Figure 5.13. The shard content derived from this section is based on analysis of 180 contiguous samples, each 1-cm thick, from below the top of the core down to the Taupo Tephra at 213 cm depth (a total of 199 cm of sediment minus the core gap). Individual glass shards were detected and counted in every sample, which included a mix of clear, brown and dark brown shards in varying proportions. In contrast to core Puk5, there were slightly higher average shard concentrations derived from P8_06 core with only 49% of samples containing <3 clear shards per mg d-wt. (60% in Puk5) and 66% of samples containing <3 brown shards per mg d-wt. (80% in Puk5). This discrepancy could relate to differences in sample sizes (age intervals represented by each sample) because of variations in sedimentation rates in the different core locations. It is also possible the core 'gap' in P8_06 may have included a number of samples where shard concentrations were low (as shown between 70 and 130 cm in Puk5). Only 11% of samples contained no brown shards at all, in contrast to 53 % of samples in Puk5. Glass 'peaks' in the core also showed more variable shard content than in Puk5 with a number of peaks which were not replicated in similar stratigraphic levels in Puk5 (Fig. 5.11).

Clear glass shards show a very variable pattern of shard content up through the core which is replicated by changes in organic content only where shard concentrations are relatively high (Fig. 5.13). Concentrations of clear shards in the core show a generally fluctuating pattern with increasing concentrations of glass within the middle third of the core (between 180 and 80 cm depth) bracketed by relatively low shard concentrations in the upper and lower sections of the core. Unlike Puk5, the concentrations of clear shards above the visible Taupo Tephra in P8_06 decline rapidly, reaching low levels ~ 3 cm above the

visible layer at 211 cm depth. Above this horizon, between 206 and 180 cm depth, clear shards remain in very low concentrations with an average of only 1.57 (± 1.0) shards per mg d-wt. per sample. A comparable zone in Puk5, however, extends for 65 cm of the core in contrast to 26 cm of P8_06 (Fig. 5.11). In both cores this zone coincides with the highest measurements of organic content. There are three possible explanations for the discrepancy between the cores where shard concentrations remain low: (1) the part of the lake where core P8_06 was taken receives greater or different sediment inputs from Puk5; (2) the equivalent part of the core in Puk 5 is represented by the 'missing' section of the core (core gap, 136-160 cm), or (3) part of the core has been replicated as a result of coring errors.

Between 180 and 80 cm in the core there is a distinct increase in the number of clear shards which are represented by variable but almost continuous concentrations in this section of the core. More than 60% of samples viewed in this section contained >10 clear shards per mg d-wt. Between 89 and 100 cm there is another distinct jump in concentrations of clear shards which peaks at 95 cm. Observations of glass in this section of the core during microscopy revealed rhyolitic, basaltic and andesitic/dacitic glasses mixed with abundant mineral particles (Plate 5.3 i). Closer examination of a sample from 95 cm in the core using scanning electron microscopy revealed that these shards preserved a number of small pitting and abrasion features indicative of weathering (Plate 5.3 j). Interestingly, the shards also appear to have been host to a large number of diatom species (Plate 5.3 k). In contrast to the pattern of shards between 180 and 80 cm, there is a distinct and discrete peak in clear shards between 78 and 79 cm depth which coincides with a similarly distinct peak in brown shards. Glass at 78 cm consists of a mix of striate and bubble-wall clear shards, 40-60 μm in length, which displays a moderate degree of stretching and vesicularity (Plate 5.3 g). These are mixed with similar proportions of brown shards which include some pale

brown shards with microlite crystals (Plate 5.3 h) and dark brown, platy shards which look similar to the basaltic shards observed in the Rangitoto Tephra horizon.

The content of brown shards determined throughout P8_06 reveals a small number of discrete peaks with typically lower maximum shard concentrations than for the rhyolitic (clear shard) spectrum. Above the Taupo Tephra at 211 cm up to 109 cm (102 cm of the total core), 89% of samples counted contained fewer than two brown shards per mg d-wt. In this section of the core there is only one small glass peak (with nine shards per mg d-wt.) at 185 cm. Between 108 and 105 cm depth there is a large peak concentration in brown shards. The glass observed in the sample from this level consisted of dark brown basaltic shards and minerogenic particles. This peak in brown shards is also marked by a distinct excursion in organic content (Fig. 5.12). There are four smaller, discrete peaks in brown glass at 92, 88, 80 and 72 cm depth. These comprised predominantly a distinct mix of brown shards. The dominant shards type were pale brown, blocky to platy shards with abundant, fine, microlite crystals characteristic of andesitic/dacitic shards found in other sites. These were mixed with a lesser content of darker, platy shards with large tabular feldspar crystals (Plate 5.3 i).

In core P8_06, as in Puk5, there appears to be a spread of basaltic glass above and below the visible layer of Rangitoto Tephra. Elevated concentrations of brown glass with basaltic appearance (Plate 5.3 a, b) start at 68 cm depth in the core, 5 cm below the visible tephra layer, and extend up to 53 cm, 9 cm above the visible tephra. As for Puk5, it is possible to surmise that a small percentage of glass, from a relatively thick tephra layer, could sink through soft surface sediments and thus account for glass found below the tephra layer, whilst reworking of mobile basaltic tephra in the catchment may explain the occurrence of

an attenuated glass concentration above the visible layer. Alternatively, these peaks could represent fallout from extended activity of Rangitoto Island volcano as discussed below. Above the zone of glass around the Rangitoto Tephra, there are two further small peaks in brown glass concentrations at 35 and 27 cm. Above 23 cm, brown glass content remains very low (<5 shards per mg d-wt.) up to the top of the core.

In addition to brown glass detected in this sequence, but not in Puk5, were Pele's Tears, tear-shaped droplets of basaltic glass, 60-150 μm in length, which are the product of explosive products of basaltic eruptions (Plate 5.3 m, n) (Heiken & Wohletz, 1985). Because of the persistent nature of these features through the sequence it is possible that they derive from exposures at the margins of the lake or make up part of the tuff ring on the lake edge.

5.2.6 Geochemical character, correlatives and interpretation

A total of 187 individual analyses of major element composition of cryptotephra populations based on 12 samples were determined by electron microprobe analysis (EMP) (Fig. 5.14). Selection of samples for EMP analysis was based primarily on peak glass concentrations identified in the cores with a small number of samples targeted to establish the origin of background glass concentrations. Glass samples were also taken from visible tephras to confirm the original identifications in the cores. From the Lake Pupuke sequences, ten samples in total were analysed from section P8_06 (shown by numbered levels in Figure 5.13, which correspond with sample numbers detailed below) and two samples from Puk5 (Fig. 5.11). For this site sequence P8_06 is used a 'master section' for the analysis of glass-shard major element geochemistry.

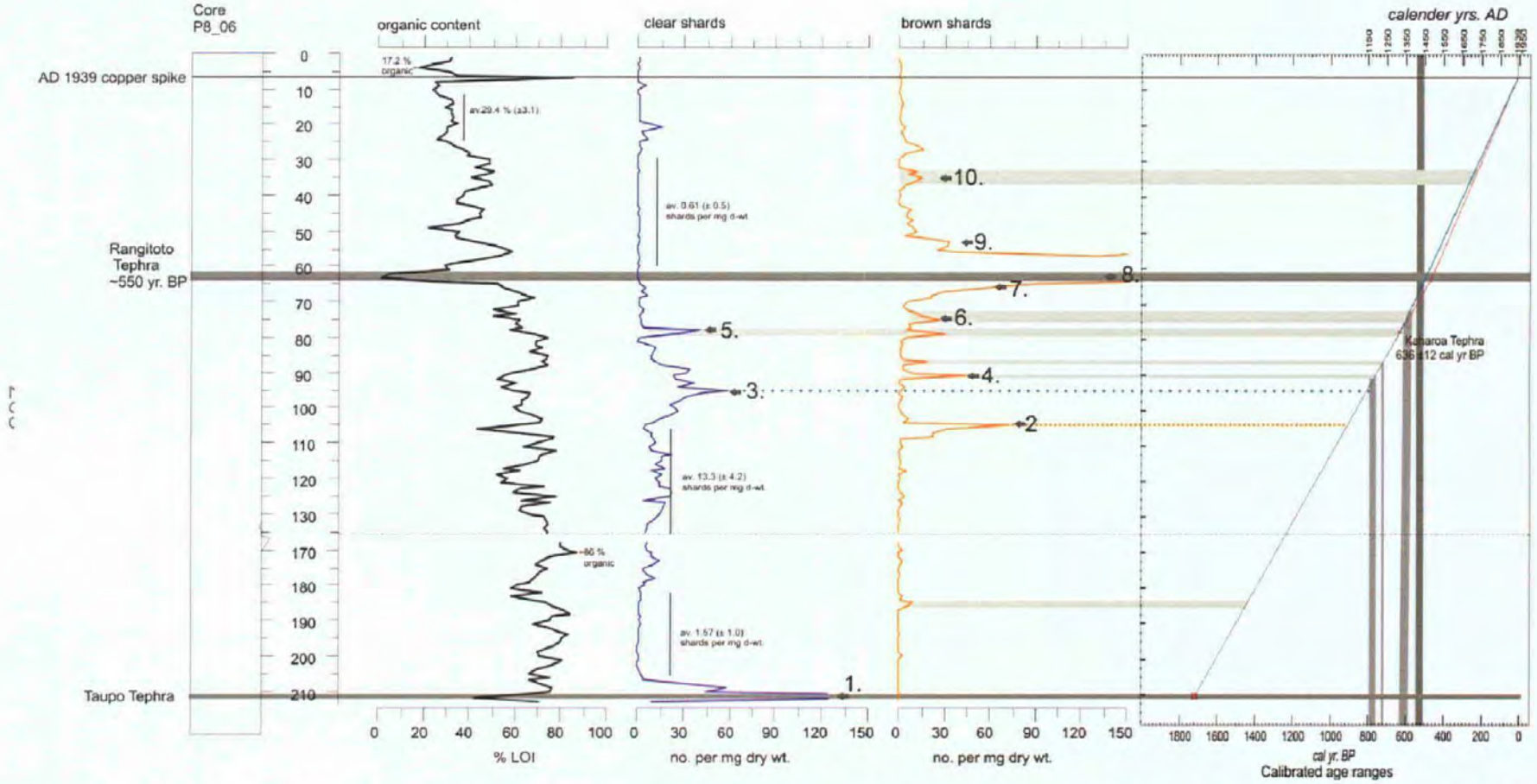

Figure 5.13. Results of glass shard concentrations derived from core P8_06 shown alongside loss-on-ignition measurements and core chronology. Numbered arrows point to sampling positions in the core where glass content has been analysed by electron microprobe analysis.

Table 5.1 provides a summary of analysis for glass populations from each level sampled. Table 5.2 provides a summary of the identified sources and eruption correlatives for each level together with interpolated age range and reference sources for tephra ages and geochemistry. The bivariate plots of selected oxides from these analyses are shown in Figures 5.14 to 5.17 and represent the most diagnostic oxide combinations to differentiate between individual geochemical populations for the three major glass chemistries (Shane, 2000). As with analyses from previous sites, other elements were also considered in correlating deposits and for distinguishing between individual populations. All analyses presented here have been normalized to 100 weight (wt.) % loss-free basis to account for hydration (Froggatt, 1992; Shane, 2000; Pearce *et al.*, 2008) The following descriptions of these analyses also refer to normalized values. Raw, non-normalized analyses can be found in the Appendices.

The major element composition of glass samples from this site fall into three main glass chemistries as illustrated on a total alkalis silica diagram (TAS; Le Bas *et al.*, 1986): rhyolite (SiO_2 => 69 wt.%), andesite to dacite (SiO_2 = 58-69 wt.%) and basanite to trachy-basalt (alkaline series; Irvine & Baragar, 1971) (SiO_2 = 43.3–51.9 wt.%) (Table 5.1; Fig. 5.14). The majority of analyses for these andesite/dacite and rhyolite tephra-derived glasses are comparable to previously obtained compositional ranges for TVZ eruptives and it was therefore possible to derive correlative sources and/or eruption events for the majority of samples analysed (Shane, 2000; Lowe *et al.*, 2008b). There were some discrepancies between analyses obtained for basaltic glass from the sequences and previous analyses from glasses from Auckland Volcanic Field (AVF) (Shane & Smith, 2000a). This discrepancy may be the result of differences in analytical conditions or natural variability (including possible inadvertent assay of microlites) but because of the

paucity of published analyses from these sequences it is difficult to confirm either of these options.

Rhyolite glasses analysed from the site are represented by a wide range of SiO_2 compositions (SiO_2 72-78 wt.%) that are indicative of tephras from the two main rhyolitic centres active over the Holocene, the Taupo and Okataina volcanic centres (Fig. 5.14). The examination of the major element composition of rhyolite glass was sufficient to differentiate between primary and secondary (reworked) deposits of rhyolite glass. Primary fall deposits have been linked with published values for known rhyolitic tephras (Shane & Smith, 2000a; Lowe *et al.*, 2008b). Secondary, reworked glass from older deposits is easily distinguished on bivariate plots because of marked differences from known compositional ranges for candidate tephras for the cores (Fig. 5.15). The secondary deposits possibly represent several different older tephras and are indicated as 'uncorrelated'. Glass analyses of primary fall deposits confirm the identification of the visible Taupo Tephra in this site and the presence of the Kaharoa Tephra in the cores represented by the additional zone of shards. Unlike the peat sites from the Waikato Region, the small quantities of glass shards of rhyolite chemistry which form the background concentrations of clear glass appear to derive from tephras which are much older than the Taupo Tephra and likely reflect the available sources in the catchment of the lake.

Glasses with intermediate chemistries, as with previous sites in this study, consist predominantly of dacitic and andesitic glasses (SiO_2 = 61-69 wt.%) and a few individual analyses fitting into trachy-dacite and trachy-andesite chemistries (Fig. 5.16). Individual populations typically comprise a heterogeneous set of glass analyses (SiO_2 = 61.0-69.0 wt.%; $Na_2O + K_2O$ (total alkalis) = 5.48-7.72 wt.%) characterized by high standard

deviations for individual oxides (e.g. SD: 1.00-2.22 for SiO_2; Table 5.1) compared with rhyolitic counterparts. Consistent with findings from the Waikato sites, the analytical totals of glasses of intermediate chemistry, remained consistently high, ranging from 98.1-100 wt.%.

As for the Waikato sites, the majority of dacitic glasses identified in the Lake Pupuke cores were characteristic of tephras of the Tufa Trig Formation (Tf) from Ruapehu volcanic centre (SiO_2= av. 63.0 wt.%; total alkalis = av. 6.5 wt.%) (Donoghue & Neall, 1996) (Fig. 5.16). Only a few shards analysed from the site have compositions similar to known Egmont-sourced tephras. Egmont VC derived tephras typically have much higher K_2O contents than other andesitic-dacitic tephra sources. All intermediate glasses were evaluated for "contamination" from microlite phases using the procedure of Platz *et al.* (2007), which estimates plagioclase feldspar microlite proportions in contaminated glass (Fig. 5.16).

As for intermediate glass identified in the Waikato sites, the identification of correlative eruptions is constrained by a limited number of published compositional data and/or age determinations for recent andesitic tephras (Shane & Smith, 2000a; Donoghue *et al.*, 2007). Individual populations identified in the Lake Pupuke cores are thus tentative associations based on compositional disparity or distinctness, where possible, together with stratigraphic position and relative age where the age range for a deposit is well constrained. Where possible, these attributes are linked with available compositional data for Tf members sampled from proximal sources (Donoghue *et al.*, 1995b; 1997; 2007). Consideration of potential Tf candidate correlatives is also given to the thickness of the deposit in proximal sequences which are thought to have resulted in more widespread

dispersal (Donoghue *et al.*, 1995b). Compositional ranges from these tephra units are plotted for the mean and standard deviations in Figure 5.16 (b, inset). However, direct correlation between these published datasets and analyses obtained from the sites presented here remain tentative. Differences in analytical conditions may also limit confidence in correlations, and as possible discrepancies between the composition of proximal and distal deposits are another potential source of uncertainty.

Glass with basaltic chemistry represented the third type of glass type encountered in the sequences and comprises about 33% of the total glass analyzed (Fig. 5.17). Analyses classify in the TAS diagram mostly as basanites and trachybasalts but include a minor population that classify as basaltic, basaltic-andesite and basaltic trachy-andesite (Fig. 5.17). Totals for glass analyses were typically high, ranging from 97 to 99.8 wt.%. The glass shards are characterized by a wide range in SiO_2 contents of between 43 and 51 wt. %, which is comparable to limited numbers of reported values by Shane and Smith (2000) from analyses of AVF glasses, primarily from proximal deposits, and whole rock analyses (24-50 wt.%). The compositions of the glasses are also characterized by high component of other oxides with ranges comparable to those of previous analyses of AVF tephras (ranges from Shane and Smith, 2000, in brackets): Al_2O_3 = 11.6-15.8 wt.% (12-17 wt.%); FeO = 8.9-12.6 wt.% (8-14 wt.%), and CaO = 8.7-12.6 wt.% (10-12 wt.%). Individual glass analyses do not, however, fit directly within compositional envelopes of previous analyses obtained from proximal deposits. The difference between distal and proximal AVF tephras was noted by Shane and Smith (2000). They suggested that proximal deposits were likely to be an amalgamation of some or all eruptive phases (i.e., composite units) whilst distal deposits must represent only a single phase of the eruption. The majority of glass analyses from this study are relatively homogenous and as a result it was difficult to differentiate

between primary fall and glass derived from older reworked deposits. Almost none of the analyses fit within the compositional envelope for analysed, pre-Rangitoto AVF tephras but this does not exclude the possibility of reworked older AVF glass occurring in the cores (Fig. 5.17).

The following sections provide details of analyses from samples selected from cores P8_06 (samples 1- 10) and Puk5 (samples A and B). Depths refer to positions in the core shown by numbered arrows in Figures 5.13 and 5.11. The numbered samples are listed in order of occurrence and therefore relative age in the individual sequences. Interpolated age ranges for all tephra units described below are based on 2σ-age ranges derived from the age-depth model for individual cores unless otherwise stated (Figs. 5.9 and 5.10).

Table 5.1 Electron microprobe analyses of tephra-derived glass shards from ten sample depths in core P8_06 and two samples from core Puk5, Lake Pupuke. Sampling positions for P8_06 are shown in Figure 5.11and for Puk5 in Fig. 5.9. Means (In bold) and standard deviations of total number (*n*) analysis (of individual shards) normalized to a 100% loss-free basis (wt%). Analysis undertaken at NERC Tephra Analytical Unit, University of Edinburgh, February and June 2007. †Mean values for analysis in this study of independently characterized laboratory standards. TB1G and Lipari analysed at 3-4 hours intervals during analyses of glass samples from this site. Full details of standards including inter-laboratory statistics are provided in the appendices. *Total iron as FeO; ** Water by difference.

Anal.no.	1a	1b	2	3	4	5a	5b	6a
Core/depth	P8-06/212 cm		P8-06/105 cm	P8-06/95 cm	P8-06/91 cm	P8-06/78 cm		P8-06/75 cm
Source (Tephra)	Taupo VC Taupo T.	Okataina VC?	AVF	OVC	TnG VC Tf5	OVC Kaharoa T.	TnG VC Tf6	OVC
SiO_2	**75.30** 0.22	**78.24** 0.15	**45.56** 0.51	**78.25** 0.47	**65.83** 1.72	**77.81** 0.21	**64.27** 1.03	**75.38** 0.84
Al_2O_3	**13.23** 0.13	**12.08** 0.21	**14.62** 1.09	**12.21** 0.25	**14.12** 1.68	**12.15** 0.16	**14.27** 0.83	**11.59** 0.23
TiO_2	**0.26** 0.02	**0.14** 0.01	**3.19** 0.13	**0.16** 0.03	**1.07** 0.13	**0.08** 0.03	**1.12** 0.16	**0.11** 0.03
FeO*	**1.98** 0.10	**1.24** 0.23	**11.58** 0.74	**0.99** 0.13	**5.81** 1.44	**0.88** 0.14	**6.63** 0.96	**0.90** 0.19
MnO	**0.08** 0.05	**0.09** 0.05	**0.19** 0.05	**0.07** 0.05	**0.08** 0.07	**0.05** 0.06	**0.07** 0.06	**0.07** 0.05
MgO	**0.26** 0.01	**0.13** 0.03	**5.50** 1.13	**0.15** 0.01	**1.96** 1.64	**0.07** 0.01	**1.95** 0.50	**0.10** 0.03
CaO	**1.54** 0.05	**1.03** 0.15	**12.71** 1.53	**0.90** 0.05	**4.25** 0.82	**0.59** 0.05	**4.87** 0.54	**0.73** 0.16
Na_2O	**4.49** 0.15	**3.87** 0.18	**4.49** 0.64	**4.01** 0.19	**3.64** 0.36	**4.25** 0.11	**3.84** 0.21	**3.92** 0.39
K_2O	**2.81** 0.03	**3.16** 0.07	**1.49** 0.26	**3.27** 0.12	**3.01** 0.47	**4.10** 0.10	**2.73** 0.34	**3.55** 0.37
P_2O_5	**0.04** 0.02	**0.01** 0.01	**0.67** 0.12	**-0.01** 0.03	**0.23** 0.05	**0.00** 0.02	**0.26** 0.05	**0.00** 0.03
H_2O**	*1.92 1.29*	4.24 0.93	*2.25 1.04*	*4.49 0.85*	*1.16 1.01*	*1.28 0.92*	*1.21 0.52*	*3.67 1.47*
n	*7*	*3*	*10*	*9*	*16*	*11*	*11*	*7*

Anal.no.	6b	6c	6d	7	8	9a	9b	10
Core/depth	P8-06/75 cm			P8-06/56 cm	P8-06/63 cm	P8-06/54 cm	P8-06/63 cm	
Source (Tephra)	TnG VC	AVF	AVF	AVF Rangitoto T.	AVF Rangitoto T.	AVF Rangitoto T.	AVF	TnG VC Tf14
SiO_2	**63.56** 2.22	**44.13** 0.55	**50.62** 0.45	**45.01** 0.57	**45.20** 0.62	**45.02** 0.74	**50.92** 0.58	**65.12** 0.83
Al_2O_3	**14.56** 0.79	**14.46** 1.06	**13.10** 0.07	**15.11** 0.19	**15.08** 0.26	**15.13** 0.50	**13.24** 0.18	**14.34** 0.26
TiO_2	**1.19** 0.04	**3.24** 0.18	**3.06** 0.08	**3.23** 0.13	***3.19*** *0.11*	**3.27** 0.15	**3.26** 0.31	**1.13** 0.04
FeO*	**6.32** 1.77	**11.63** 1.07	**12.84** 0.56	**12.15** 0.39	***12.04*** *0.43*	**12.12** 0.58	**13.69** 0.68	**6.29** 0.41
MnO	**0.10** 0.10	**0.17** 0.07	**0.22** 0.04	**0.18** 0.08	***0.19*** *0.07*	**0.19** 0.06	**0.26** 0.06	**0.06** 0.05
MgO	**1.83** 1.15	**5.37** 1.20	**4.63** 0.07	**5.01** 0.20	**5.02** 0.33	**5.01** 0.46	**4.28** 0.56	**1.62** 0.20
CaO	**4.63** 0.77	**12.55** 2.00	**9.06** 0.28	**12.06** 0.29	**12.17** 0.41	**12.26** 0.97	**8.89** 0.96	**4.37** 0.16
Na_2O	**4.14** 0.35	**4.59** 0.87	**3.55** 0.62	**4.89** 0.24	**4.78** 0.35	**4.74** 0.62	**3.75** 0.40	**3.94** 0.14
K_2O	**2.58** 0.37	**1.55** 0.32	**1.11** 0.05	**1.61** 0.12	**1.59** 0.17	**1.52** 0.17	**1.20** 0.24	**2.90** 0.08
P_2O_5	**0.26** 0.04	**0.75** 0.16	**0.46** 0.05	**0.75** 0.07	**0.75** 0.12	**0.73** 0.13	**0.51** 0.06	**0.23** 0.03
H_2O**	*0.82 0.73*	*1.56 0.55*	*1.37 0.54*	*1.85 0.56*	1.94 0.64	1.20 1.37	*0.65 0.48*	*1.11 0.59*
n	*4*	*14*	*5*	*16*	*16*	*4*	*7*	*7*

Table 5.1 Continued.

Anal.no.	A				B			
Core/depth	Puk5/ 38 cm				Puk5/ 24 cm			
Source	TnG VC		Okataina		AVF			
(Tephra)	Tf6		Kaharoa T.		Rangitoto T.			
SiO_2	64.32	1.30	77.68	0.08	45.87	0.38	51.33	0.69
Al_2O_3	14.52	0.64	12.19	0.12	14.86	0.22	13.35	0.27
TiO_2	1.14	0.09	0.09	0.00	3.09	0.13	3.16	0.30
FeO*	6.09	1.15	0.95	0.08	11.91	0.13	13.16	0.61
MnO	0.08	0.04	0.12	0.02	0.15	0.02	0.22	0.04
MgO	1.98	0.55	0.08	0.01	5.17	0.15	4.28	0.67
CaO	4.88	0.64	0.61	0.02	12.27	0.20	8.86	1.10
Na_2O	4.03	0.30	4.21	0.11	4.55	0.22	3.98	0.33
K_2O	2.70	0.35	4.07	0.00	1.47	0.06	1.14	0.39
P_2O_5	0.26	0.03	0.00	0.01	0.68	0.07	0.51	0.07
*H_2O***	*1.36*	*0.51*	*1.85*	*0.16*	*2.26*	*0.78*	*1.32*	*1.10*
n	*9*		*2*		*4*		*7*	

Anal.no.	Standards†											
Sample	TB1G		Lipari		Wollstonite		Spinel		Jadite		Orthoclase	
SiO_2	53.83	0.37	74.11	0.44	51.46	0.39	0.10	0.02	60.60	0.33	64.57	0.65
Al_2O_3	16.06	0.24	12.80	0.23	0.01	0.03	71.53	0.94	25.60	0.47	17.56	0.31
TiO_2	0.88	0.04	0.07	0.02	0.00	0.01	0.01	0.01	0.01	0.01	0.02	0.01
FeO*	8.49	0.29	1.56	0.15	0.34	0.09	0.01	0.02	0.05	0.05	0.46	0.12
MnO	0.20	0.07	0.05	0.05	0.07	0.06	0.04	0.04	0.02	0.03	0.01	0.03
MgO	3.60	0.05	0.04	0.01	0.20	0.05	28.32	0.29	0.01	0.01	0.00	0.00
CaO	6.89	0.10	0.74	0.04	47.84	0.29	0.01	0.01	0.03	0.02	0.01	0.02
Na_2O	3.30	0.07	4.14	0.09	0.01	0.01	0.00	0.01	15.22	0.23	1.08	0.05
K_2O	4.47	0.08	5.18	0.08	0.00	0.01	0.00	0.00	0.00	0.00	15.30	0.10
P_2O_5	0.59	0.04	0.00	0.02	0.42	0.03	0.00	0.00	0.00	0.00	0.00	0.00
Total	*98.31*	*0.46*	*98.71*	*0.49*	*100.36*	*0.56*	*100.03*	*0.96*	*101.55*	*0.59*	*99.01*	*0.52*
n	*84*		*63*		*12*		*13*		*9*		*10*	

Sample 1. P8_06 – 212 cm: Taupo VC, Taupo Tephra (1717 ± 13cal.yr BP) (number of analyses (n) =7) and analyses of uncorrelated shards (n = 3)

The sample was taken from the top of the visible component of a thin, visible tephra identified as the Taupo Tephra in the core by field characteristics and stratigraphic positions (Fig. 5.13). The Taupo Tephra has been identified by microprobe analysis at comparable stratigraphic level in previous cores (Puk5) extracted from the site (Horrocks *et al.*, 2005). Analyses of shards from this sample confirm the occurrence of the Taupo Tephra which comprises a relatively homogenous set of rhyolitic glass analysis (SiO_2 =

75.3 ± 0.22; K_2O = 2.18 ± 0.03 wt. %; CaO = 1.54 ± 0.05 (Table 5.1; Fig. 5.15). Seven of the ten analyses reveal compositional ranges consistent with published analyses for the AD 233 ± 13 Taupo Tephra event (Unit Y) (SiO_2 = 75.04 wt% ± 0.19; K_2O = 2.85 ± 0.07 wt%; CaO = 1.47 ± 0.05 (Lowe *et al.*, 2008b)). Three analyses from the sample do not correlate with the Taupo Tephra and exhibit much higher SiO_2 values (~ 78 wt%) and higher K_2O (~3.16 wt%) characteristic of glass from pre-Taupo Tephra events from Okataina VC and Taupo VC (Fig. 5.15). The occurrences of outliers and uncorrelated analyses associated with the Taupo Tephra have been noted in analyses from Waikato sites (this study), and from previous studies (Gehrels *et al.*, 2006), and are most likely attributed to the incorporation of older deposits into the eruption column or possibly magma mingling (Lowe *et al.*, 2000; Siebert & Simkin, 2002). These non-Taupo Tephra analyses correlate quite well with Okataina VC-derived Mamaku Tephra (~8000 cal. yrs. BP) that, although not identified in the Lake Pupuke sequences, has been found in Waiatarua wetland (Newnham & Lowe, 1991; Newnham *et al.*, 1999a) and in Pukaki Lagoon, which is located just south of Auckland City (Shane, 2005).

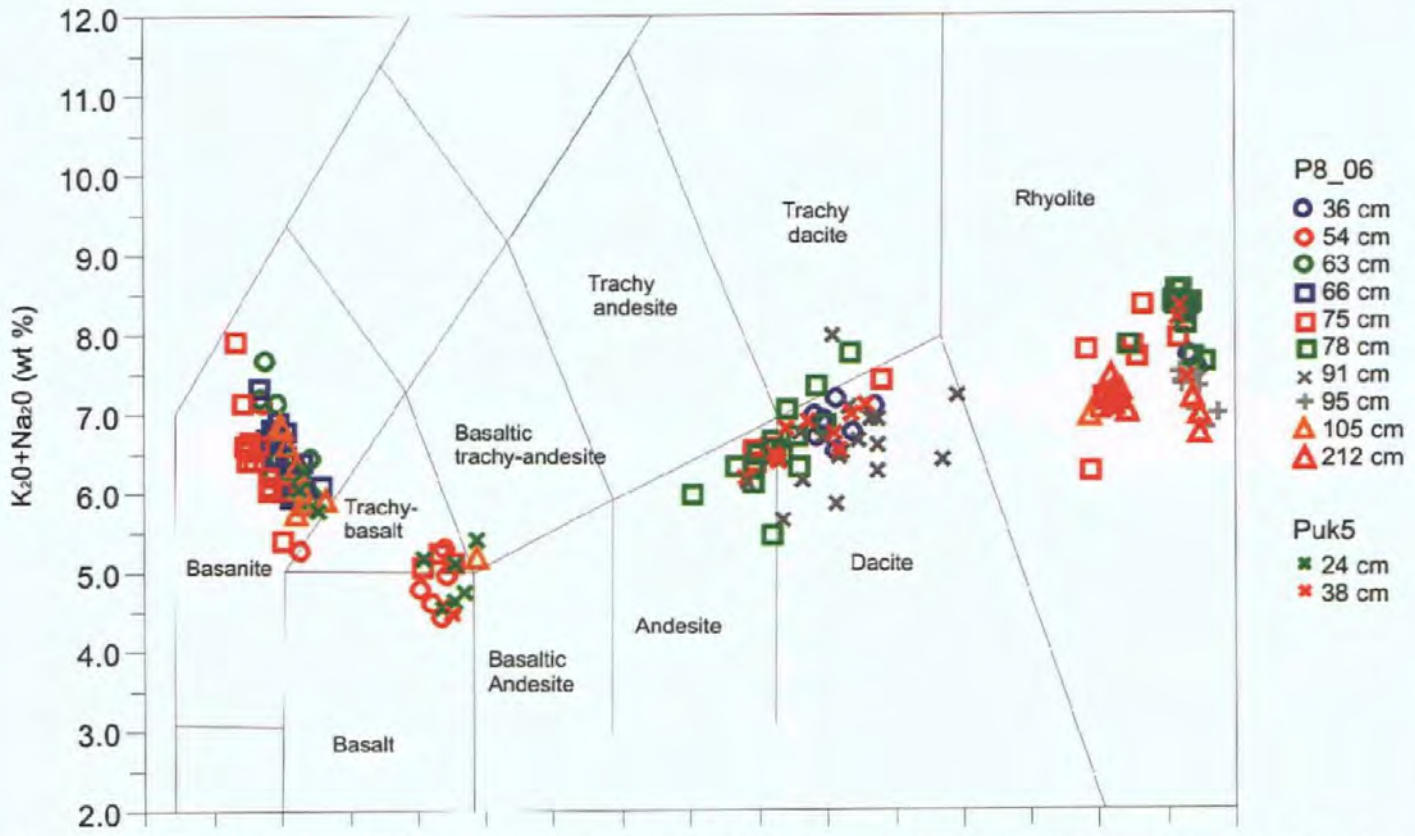

Figure 5.14 Bivariate plot of SiO_2 versus total alkalis of individual glass shard analyses from Lake Pupuke cores using TAS scheme of Le Bas *et al.* (1986).

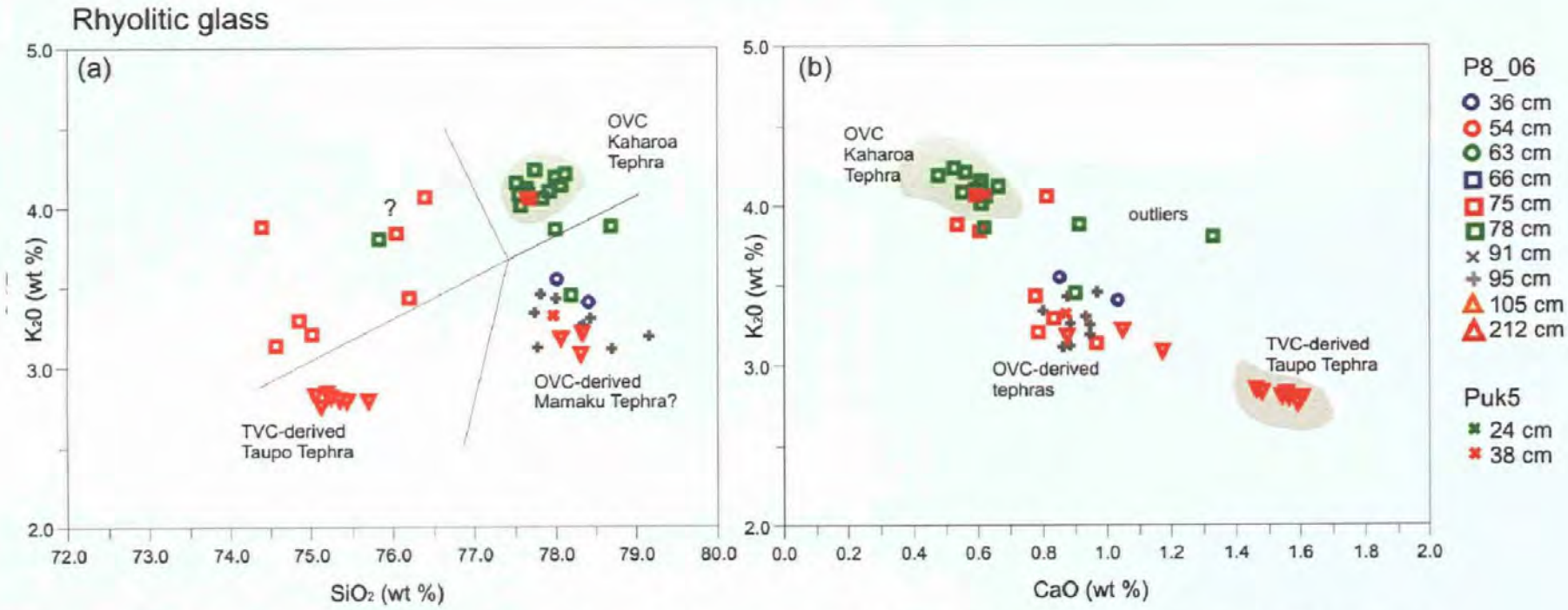

Figure 5.15 Bivariate plots of individual glass analyses of rhyolitic chemistry from Lake Pupuke core sequences P8_06 and Puk5. Outliers identified from a range of compositional plots.

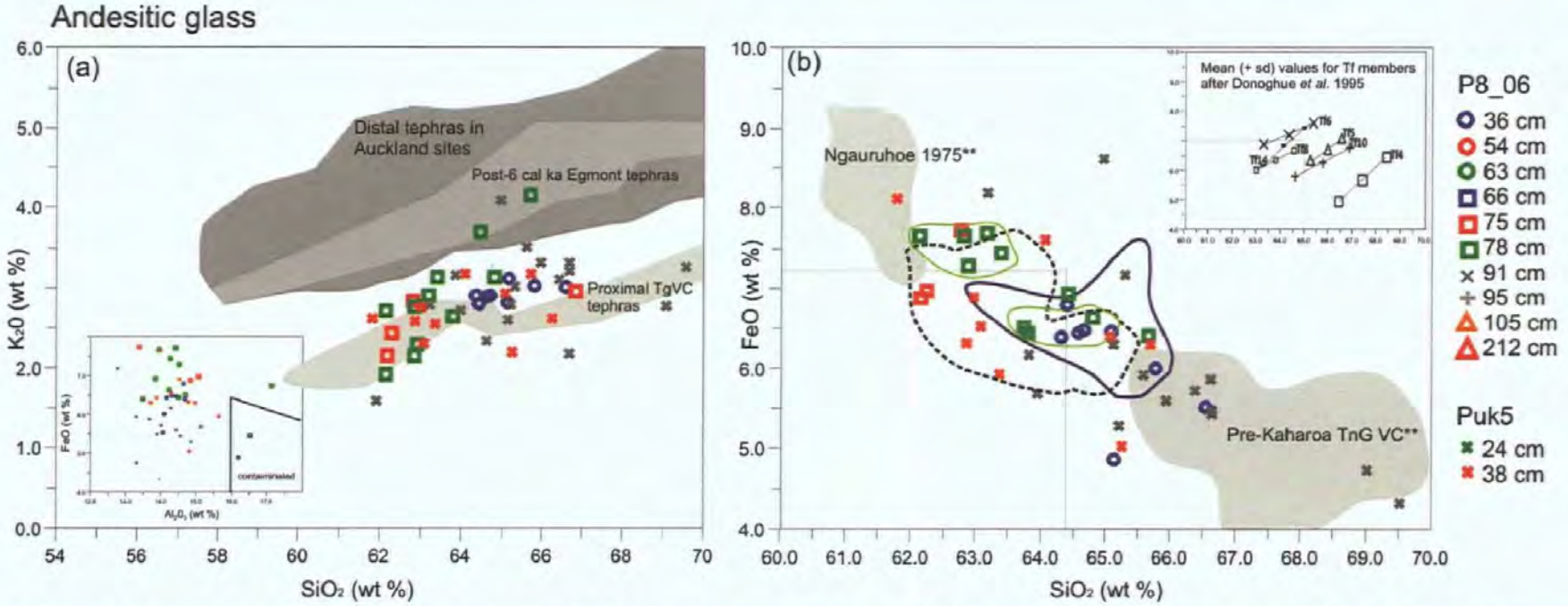

Figure 5.16 Bivariate plots of individual glass analyses of intermediate chemistry from Lake Pupuke sequences P8_06 and Puk5. (a) Grey compositional envelopes for Egmont and Tongariro VC (TnG) volcanic centres from Shane (2005); (b) Compositional envelopes with grey fill and dashed lines are traced from glass analyses from Waikato sites (Chapter 4). Compositional envelopes from glass populations identified in Waikato sites: dashed line represents dacite populations associated with the Kaharoa Tephra, blue solid line shows dacite glass population identified as Tf14. Inset: bivariate plot used to identify analyses contaminated by inclusion using known limit of plagioclase phase for Mt Ruapehu tephra following method of Platz *et al.* (2007).

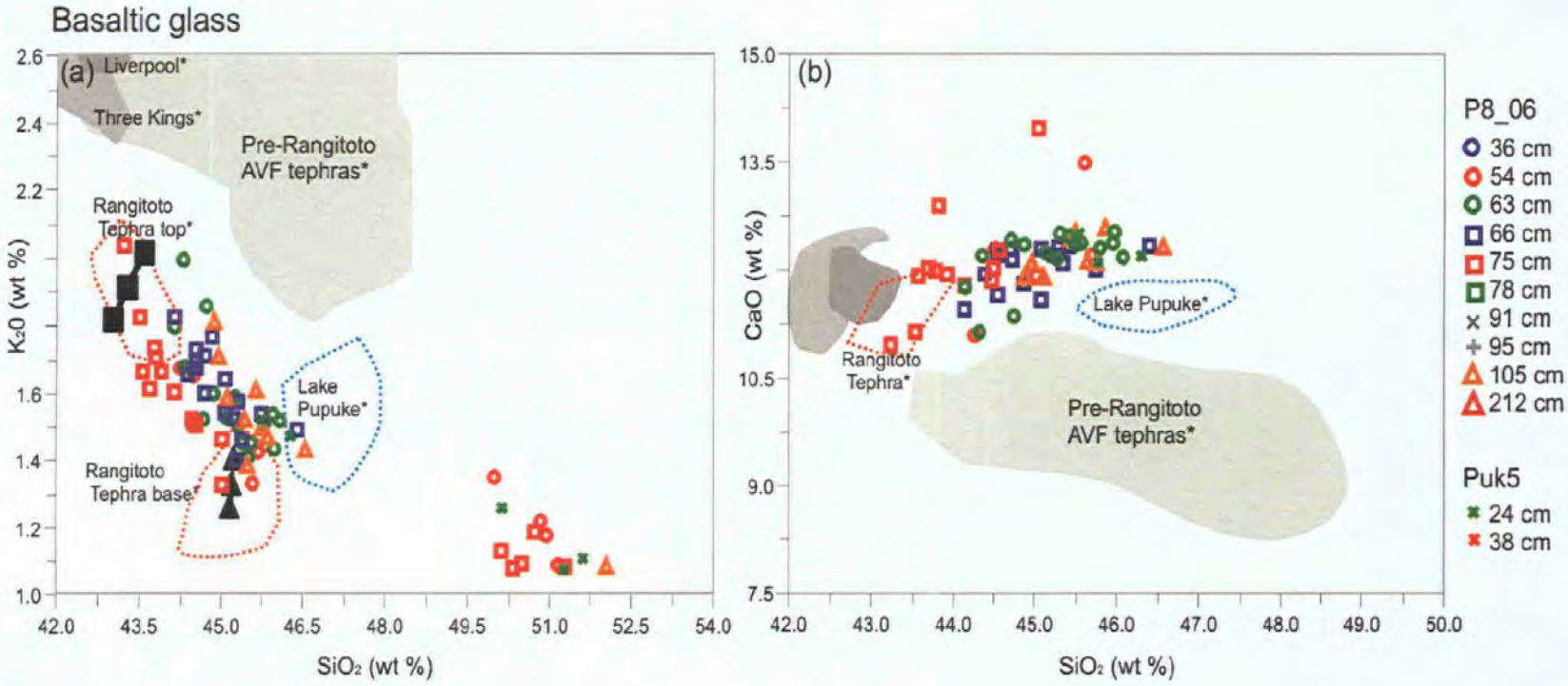

Figure 5.17 Bivariate plots of individual glass analyses of alkaline chemistry from Lake Pupuke sequences P8_06 and Puk5. Grey envelopes show compositional ranges for pre-Rangitoto AVF tephras, using normalised data from Shane and Smith (2000a). Dashed red line = full compositional range for the top and base of Rangitoto Tephra identified in proximal deposits. Black symbols **represent mean and standard deviations of these data. Blue dashed line represents compositional envelope for tephra from Lake Pupuke tuff ring. * data from Shane and Smith (2000).**

Sample 2. P8_06 – 105 cm: AVF-derived basaltic glass (n = 10)

Sample 2 marks a very prominent peak in brown glass concentrations spread between depths 108 to 105 cm depth in the core (Fig. 5.13). Despite the high concentrations of glass encountered in the core during shard counts, the recovery of glass for microprobe analysis was relatively poor and only ten analyses from the sample were completed. This glass peak is not replicated in core Puk5 and it was anticipated that glass from this level in the core was derived probably from reworked basaltic glass deposits.

The sample comprised a relatively homogenous set of glass analyses (SiO_2 = 45.56 wt% ± 0.51; FeO = 11.58 wt% ± 0.74; MgO = 5.50 wt% ± 1.13) with nine analyses which classify as basanites on the TAS diagram (Fig. 5.14). The majority of analyses overlap with other glass assays from younger levels in the core including from samples taken from the visible Rangitoto Tephra (63 cm in P8_06) (Fig. 5.17 a, b), but do not fit within the envelopes for most of pre-Rangitoto AVF tephras (identified by Shane and Smith, 2000). In Figure 5.17 (a and b), analyses from this sample plot between the compositional ranges determined by Shane and Smith (2000) for glass from Rangitoto Tephra and from the tuff ring of Lake Pupuke. On an individual basis, the majority of the glass analyses from this position in the core are closer to the compositional range for glass from the Pupuke maar tuff ring (SiO_2 = 46.4 wt% (± 0.44); CaO = 11.5 wt% (± 0.45); Shane and Smith, 2000) (Fig. 5.17 b). There is only a slim possibility that this glass concentration could represent a previously unknown, local minor eruption from the AVF. The interpolated age range of the glass concentration is ~910-940 cal yr BP (Fig. 5.10) and there is currently no evidence for any

eruption activity from the AVF between 9 cal. ka (Mt Wellington or Maungarei) and the eruption of the Rangitoto Tephra (~0.55 cal. ka). Therefore, on the basis of present knowledge, it is more likely that this glass concentration derives from the tuff ring of the Pupuke maar possibly as a result of a localised erosion event.

Sample 3. P8_06 – 95 cm: Reworked Okataina VC-derived glass (n = 9)

This sample marks a peak concentration of clear glass within a wide zone of elevated glass content between 100 and 89 cm depth in the core (Fig. 5.13). This sample was selected to establish the source of the clear shards in this section of the core. The glass analysis represents a fairly homogenous compositional population with rhyolite chemistry (Figs. 5.12, 5.13). The high values for SiO_2 = 78.3 wt% (± 0.47) obtained for this sample are characteristic of Okataina VC derived glass (77-78 wt%) as well as some pre-20 cal ka Taupo VC tephras (Lowe *et al.*, 2008b). Values for K_2O (3.27 wt% ± 0.12), and other oxides, are not consistent with Kaharoa Tephra which is detected in higher stratigraphic level in the core sequence (78 cm, sample 5) (Fig. 5.15). Because there are no known candidate rhyolitic eruptives between the Taupo and Kaharoa tephras, it is most likely that the glass concentration represented by this sample derives from reworked deposits in or close to the site. Okataina-derived tephras are the most frequently-deposited rhyolitic tephras identified in Auckland maar sequences – six out of eight of the most recent rhyolitic tephras detected in the region (for the last 27 cal. ka) are Okataina VC-derived (Fig. 5.3). Glass shards from Okataina VC tephras are therefore the most likely source of secondary or reworked glass deposits in such sites.

Sample 4. P8_06 – 91 cm: Ruapehu VC-derived Tufa Trig member (Tf5) (n = 15)

Sample 4 from P8_06 represents a well defined peak in brown glass at 91 cm in the core (Fig. 5.13). A total of 15 analyses were conducted from this sample, and 13 shards classify as dacitic which is characteristic of Ruapehu-derived glass identified in the Waikato sites (Fig. 5.16). However, the glass population is compositionally heterogeneous with a wide spread of values for SiO_2 ranging from 63 to 69 wt% (Table 5.1). Only one of the analyses from this sample fits within the envelope for post-6 cal. ka Egmont-derived tephras detected in Auckland sites which are notably enriched in K_2O (3-5 wt%) compared with Tongariro-derived glass (Shane, 2005) (Fig. 5. 16 a).

In attempting to identify possible correlatives for this glass population, individual clusters of analyses were examined. Ten out of the 15 analyses from the sample fit within, or very close to, the compositional envelope of pre-Kaharoa dacite glass identified in the Moanatuatua Reserve sequence (Chapter 4.2) which were found to be distinct from post-Kaharoa dacitic glass at the site (Fig. 5.16 b). Intermediate glass detected below the Kaharoa Tephra in Moanatuatua Reserve exhibited higher SiO_2 (65-70 wt%) and lower values of FeO (4-7 wt.%) compared with post-Kaharoa glass (Fig. 5.16 b). The five additional analyses overlap with a number of additional dacitic glass populations in the core and do not exhibit any distinct clustering and overlap with a number of other dacite glass analyses from the core. The glasses comparable to pre-Kaharoa glass in Waikato sites plot between mean compositional ranges for Tufa Trig members Tf4 and Tf5 identified by Donoghue *et al.* (1995b). Although poorly dated and with limited stratigraphic control, these tephra members are thought to have been deposited before the Kaharoa Tephra (Eden & Froggatt, 1996; Wilmshurst, 1997). Only Tf4 has been identified in Waikato sites

(described in Chapter 4) which provides some additional age controls for this unit based on radiocarbon chronologies obtained for the Waikato sequences. The glass population in core P8_06 has an interpolated age range of 765-795 cal yr BP between the Taupo and Kaharoa tephras (Fig. 5 13). This age range falls between the two possible ages for Tf4 and Tf5 tephra members. Tf4 was identified in multiple cores from the Waikato sites and has an age range of 1060-1300 cal yr BP. Tf5 has an age range of 540-660 cal yr BP based on radiocarbon ages of peat above and below the tephra in a site proximal to Ruapehu volcano (Donoghue *et al.*, 1995b; Eden & Froggatt, 1996; Wilmshurst, 1997). It is possible therefore that either the age model for P8_06 core, or the ages derived for the Tf5 tephra, or both, are inaccurate. A peak in brown shards in core Puk5, which is at a comparable stratigraphic level to the glass peak in P8_06 in relation to the Kaharoa Tephra (Figs. 5.9 and 5. 11), has an age range estimate of 595-660 cal yr BP. This is very similar to the age range established for Tf5. Unfortunately, there are no probe data available from this unit in core Puk5 but it is likely that the prominent glass peak in the cores represents the same tephra (given the similar stratigraphic juxtaposition). Alternatively, the glass concentration from 91 cm depth in core P8_06 could represent a previously unidentified pre-Kaharoa eruption event from Mt Ruapehu.

Sample 5. P8_06 –78 cm: Okataina VC, Kaharoa Tephra (n = 11) with Ruapehu VC-derived Tufa Trig member (Tf6) (n = 11)

This sample marks a position in the core comprising discrete peak concentrations of both clear and brown glass between 77 and 79 cm depth (Fig. 5. 13). The EMP analyses from this sample reveal two main glass chemistries: rhyolite and andesite-dacite (Fig. 5.14). The

rhyolite glass comprises a homogenous glass composition with three to four possible analytical outliers (Fig. 5.15). Bivariate plots of various oxide combinations show that the majority of analyses from this sample form a tight cluster which is distinct from analyses of other rhyolitic glass from the core. The high values obtained for SiO_2 (77.8 wt% ± 0.2) and K_2O (4.1 wt% ± 0.1) and very low values for CaO (0.5 wt% ± 0.05) are characteristic of the compositionally distinct Okataina VC-derived Kaharoa Tephra (636 ± 12 cal. yr BP).

The occurrence of this tephra in the Lake Pupuke site was considered very likely. Isopach maps of the limits of the visible (*ca.* 3 cm thick) Kaharoa Tephra show a north-west trajectory extending up to the Bay of Islands in Northland, more than 100 km northwest of the Lake Pupuke (Fig. 3.2; Lowe *et al.*, 1998). The geochemical confirmation of the occurrence of Kaharoa Tephra in Lake Pupuke represents the first identification of this tephra in Auckland and provides a precise age marker for the sequence. This novel identification also marks the first known occurrence of the Kaharoa and Rangitoto tephras preserved together in the same sequence. For the first time it has thus been demonstrated that Rangitoto Tephra stratigraphically overlies Kaharoa Tephra, a relationship previously the subject of conjecture (e.g., Lowe *et al.*, 2000; McFadgen, 2007).

The intermediate glass population in the sample comprises a predominantly dacite chemistry with a few analyses of andesite and trachy-dacite composition (Fig. 5.14). The majority of these analyses fit closely with the known compositional range of Ruapehu VC derived Tufa Trig tephras and overlaps with a number of intermediate glass populations from other levels in the core (Fig. 5.16). The glass population is compositionally distinct from the underlying dacite population at 91 cm. Two of the analyses from this sample fit

within the compositional range of glass from post-6 cal. ka Egmont VC-derived tephras identified in Auckland sites (Fig. 5.16 a). These possible Egmont glasses are in very low numbers so may represent reworked glass or analytical outliers rather than primary fall deposits. The majority of dacite and andesite glasses comprise a relatively heterogeneous composition that is characteristic of dacitic glasses identified in the Waikato sites used in this study. Bivariate plots of oxides SiO_2 and FeO show a possible bi-modal population for dacite glass from this sample (Fig. 5.16): pop. 1: SiO_2 = 62.2- 63.5 wt%, FeO = 7.3-7.7 wt%; pop. 2 (minus Egmont glasses): SiO_2 = 63.8- 64.8 wt%, FeO = 6.4-6.6 wt%. Bi-modal geochemical populations have been identified from Mt Ruapehu-derived glass in the Waikato Region sites.

Potential correlatives include a number of post-Kaharoa Tephra Tf members. The glass analyses plot either side of the compositional range derived for Tufa Trig member Tf6 but also overlap with the compositional range of a number of other dacite populations associated stratigraphically with Kaharoa Tephra glass identified in the Waikato Region sites (dashed line; Fig. 5.16 b). The majority of dacite analyses from this sample appear to be slightly more enriched in FeO (6.9 wt% ± 0.7) than for comparable units in the Waikato sites (mean FeO = 6.5 wt% ± 0.6), which possibly reflects different preservation conditions of the sites. The most likely candidate Tf member based on the known distribution of the proximal deposits (Donoghue *et al.*, 1995b) is Tf6. Tf6 forms one of the thickest and most widespread of the proximal units. A maximum age for Tf6 of 535-660 cal yr BP has been derived from a radiocarbon age (Wk1488) on peat taken between Tf5 and Tf6 units (Donoghue *et al.*, 1995b). This age range overlaps with the age of the Kaharoa Tephra (636 ± 12 cal. yr BP) which is preserved in the same (or very slightly overlapping) stratigraphic position in the core.

Sample 6. P8_06 – 75 cm: Auckland Volcanic Field-derived tephra (reworked pre-Rangitoto tephra?) (n= 19) with reworked glass from Okataina VC (n=7) and Ruapehu VC-derived Tufa Trig members (n = 4)

Sample 6 is from a discrete peak in brown shard concentrations 10 cm below the visible Rangitoto Tephra (Fig. 5.13). EMP analyses reveal glass contributions from the three main glass chemistries identified in the core (rhyolitic, andesite-dacite, and basanite) (Fig. 5. 14). A large proportion of the eight rhyolite glass shards from the sample exhibit a wide spread of analyses that cannot be correlated to any individual rhyolitic tephra and most likely represent a mix of old, possibly Okataina VC-derived, tephras reworked from in or near the catchment. Only one glass analysis in the sample correlates with the Kaharoa Tephra, which is preserved only 3 cm deeper in the sequence.

The four glass analyses in the sample with intermediate composition overlap with a number of dacite-andesite glass populations identified in lower levels in the core. Because of the low numbers of analyses, establishing a correlative, whether from primary or secondary deposition, is problematic. The large proportion of reworked rhyolitic glass in this sample would, however, support the idea that this glass population is also possibly the result of secondary deposition.

The glass population in the sample with an alkaline chemistry mostly plot as basanite with a few analyses forming a separate sub-population with basalt to trachy-basalt chemistry (Fig. 5.14). The basanite population (n = 14: SiO_2 = 44.1 wt% ± 0.6; FeO= 11.6 wt% ± 1.1; MgO = 5.4 wt.% ± 1.2) forms a subtly different population from alkaline glass found in higher and lower levels in the core (Fig. 5.17). None of the analyses overlaps with compositional ranges of pre-Rangitoto tephras but several analyses overlap with the

established compositional ranges of glass from the Rangitoto Tephra (Shane & Smith, 2000a). Basanite glass from this level actually shows better correlation with established compositional range for the Rangitoto Tephra than with the glass taken from the visible layer at 63 cm depth in the core. These glass analyses show close correspondence to ranges for the two Rangitoto components – base and top – which most likely represent a change in eruptive style during the eruption sequence(s) (Fig. 5.17 a) (Shane and Smith, 2000). The trachy-basalt sub-population (n = 5: SiO_2 = 50.6 wt% ± 0.5; FeO = 12.8 wt% ± 0.6; MgO = 4.6 wt.% ± 0.1) overlaps with a number of sparse analyses from other levels in the core (Fig. 5.17 a). Because of the low numbers of shards it remains possible that these represent reworked glass from older AVF derived deposits or accidental ejecta. Shane and Smith (2000) noted that a large number of the AVF tephras examined contained outliers which were attributed to accidental ejecta from earlier eruptions. Glasses with a trachy-basalt composition are also thought to have resulted from phreatomagmatic activity, which precedes the eruption of magmatic units in a number of older AVF tephras (Shane and Smith, 2000).

The actual source of the basanite glass population at this level in the core is uncertain. The glass peak is separated by a gap of 60-90 years of shard content before the visible Rangitoto tephra based on the age model for the core (Fig. 5.13). There are several possible explanations for this gap, as follows.

(1) The glass population represents an eruption event prior to the main Rangitoto eruption event as represented by the visible tephra layer, and well before the postulated 'precursory' phase. Before the findings of Needham *et al.* (2008), Rangitoto Island was thought to have formed as a result of several eruptive phases that occurred in quick succession over a

relatively short time period, i.e. within less than 10 years (Nichol, 1992; Cassidy *et al.*, 1999; McFadgen, 2007), as would be expected for a typical intraplate basaltic episode. Evidence for a longer or multiphase eruption was disputed by Nichol (1992) using a wide range of counter-evidence. Critically, most of the ages on wood and charcoal used to suggest several distinct (separate) eruption phases were shown by Nichol (1992) to be flawed (e.g., Lowe *et al.*, 2000; McFadgen, 2007). However, as noted earlier, the recent study by Needham et al. (2008) has reignited this debate. Analysis of tephras contained in a core taken from the nearby Motutapu Island suggested that Rangitoto Island was formed in two separate and compositionally distinct phases (referred to above as 'main' and 'second' or 'final' phase) separated by some decades (on the basis of ~20–30 cm of sediment occurring between the two basaltic tephras) (Needham *et al.*, 2008). These two phases were differentiated by geochemistry with an early alkalic phase and a later tholeitic phase. Sample 6 from core P8_06 is essentially tholeitic, not alkalic, hence does not match the main (alkalic) phase recognised by Needham et al. (2008).

The timing of the main Rangitoto eruption is still, however, a matter of debate (see below).

(2) It is possible that a small amount of glass from the Rangitoto Tephra had sunk through the soft upper sediments down to a lower stratigraphic level, a process that has been observed for tephra layers in other lake environments (Anderson *et al.*, 1984; Beierle & Bond, 2002). Sinking of the tephra was the mechanism suggested by Horrocks *et al.* (2005) for the observed double layer originally observed in Puk5 core. The basaltic glass is denser than rhyolitic or andesitic glass and thus would be more likely to sink. (3) The lack of laminations in this section of the core possibly indicates a period of disturbance or mixing in the lake sediments. (4) The glass could represent a reworked deposit from older AVF

tephra for which there are no compositional data. (5) The section of core has been affected by smearing or replication during coring.

Sample 7. P8_06 – 66 cm: Auckland VF-derived tephra (Rangitoto Tephra 'precursory' phase?) (n = 16)

Sample 7 was taken 3 cm below the visible Rangitoto Tephra where brown glass concentrations were found to be high (Fig. 5.13). The EMP analyses reveal a homogenous glass population with basanite glass chemistry (SiO_2 = 45.0 wt% ± 0.6; FeO= 12.2 wt% ± 0.4; MgO = 5.0 wt.% ± 0.2) which correlates very closely with analyses from the visible component of the Rangitoto Tephra (SiO_2 = 45.2 wt% ± 0.6; FeO= 12.0 wt% ± 0.4; MgO = 5.0 wt.% ± 0.3) (Fig. 5.17). The range of analyses from this sample falls between the two units of Rangitoto Tephra (top and base) established by Shane and Smith (2000), which possibly suggests that the sample may contains components from both eruptive phases. It is also possible that the compositional ranges established by Shane and Smith (2000) do capture the range of compositions from the Rangitoto Tephra. The occurrence of Rangitoto Tephra-derived glass below the visible tephra layer can be explained if: (1) the deposit reflects the time-transgressive, possibly decade-long nature of the eruption (Nichol, 1992), (2) the deposit represents a separate 'precursory' eruptive phase (perhaps a decade or so before the main phase), or (3) because of density differences, a small component of glass from the tephra layer sank through the underlying soft sediments.

Sample 8. P8_06 – 63 cm: Auckland VF-derived Rangitoto Tephra: main (alkalic) eruptive phase of Rangitoto Island (ca. AD 1469 ± 22) (n = 16)

Sample 8 was taken from the visible component of the Rangitoto Tephra between 62 and 63 cm to confirm the identification of this tephra in the core and to facilitate the correlation of any additional basaltic glass detected in the sequence. As with the sample from 66 cm (sample 7), this sample consists of a homogenous set of glass analyses with basanite (alkalic) chemistry. The analyses also plot between the established compositional ranges for the top and base components of the Rangitoto Tephra recognized in proximal deposits (Shane and Smith, 2000) which suggests this sample represents either a mix of the two components (top and base) or, as suggested by Shane and Smith (2000), a single phase represented by a distinct composition not recognized from more heterogeneous proximal deposits. Furthermore, the alkalic composition of this sample is consistent with the early ('main') Rangitoto-eruption phase recognized by Needham *et al.* (2008). The interpolated age for the visible tephra unit in the core is determined by extrapolating the sedimentation between the Taupo Tephra and Kaharoa Tephra up to the base of the Rangitoto Tephra (model 2; Fig. 5.10). This model provided the means to calculate the age interval between the Kaharoa Tephra, and the base of the Rangitoto Tephra. Using the 2σ-age ranges of the Taupo and Kaharoa tephras the age for the base of the Rangitoto Tephra is estimated to be 481 ± 22 cal. yr BP (AD 1469 ± 22). This age range overlaps the best estimate age range for the Rangitoto Tephra established from a range of different dating methods of 526-451 cal. yr BP (2σ range) (AD 1424-1499) (recalibrated from Nichol, 1992) (see also Lowe *et al.*, 2000; McFadgen, 2007).

Sample 9. P8_06 – 54 cm: Second or final Rangitoto eruptive episode (ca. AD 1545), or reworked glass (?) from AVF-derived tephras (n = 11)

Sample 9 represents the upper limit of elevated concentrations of brown glass found up to 9 cm above the visible Rangitoto Tephra in the core. The resulting glass analyses comprise a mix of alkaline glasses with basanite and trachy-basalt to basalt chemistries, comparable with analyses from other levels in the core. However, only a minor component of the glass sample (4 out of 11 shards analysed) correlated with the Rangitoto Tephra glass from 63 cm. The majority of the glasses in the sample (7 out of 11) were basaltic or trachy-basalt (tholeitic) in chemistry. In older deposits from AVF these latter compositions have been attributed to early phreatomagmatic activity during the initial phases of an AVF eruption (Shane and Smith, 2000). The position of this sample 9 cm above the visible tephra unit would represent *ca.* 76 calendar years since the deposition of the Rangitoto Tephra (based on the newly interpolated age of the latter tephra in this core). This interval is well beyond the most likely time period (≤ 10 years) over which the Rangitoto eruption was believed to have taken place as suggested by Nichol (1992), but would fit with the time frame for the later 'tholeitic' phase recognised tentatively by Needham *et al.* (2008). A similar, later peak in basaltic shards is also recognised in core Puk5 at 18 cm but there are no geochemical data to confirm whether these shards could represent a similar composition. Provisionally, the sample may thus record the second (tholeitic) phase of eruption of Rangitoto Island at *ca.* AD 1545 ± 22 (AD 1469 ± 22 plus ~76 years).

If correct, this finding generally supports the palaeomagnetic data of lava flow activity on the island used by Robertson (1986) to suggest that Rangitoto Island developed over three phases; between AD 850 and AD 1500, with a maximum of activity between *ca.* AD 1200

and AD 1500. Although the earlier ages (*ca.* AD 850 and *ca.* AD 1200) are not upheld as the presence of the *ca.* AD 1314 Kaharoa Tephra precludes them.

Alternatively, this glass concentration could just represent the reworked deposits of older AVF tephras as well as the remains of Rangitoto Tephra glass from in and around the lake catchment.

Sample 10. P8_06 – 36 cm: Ruapehu VC-derived Tufa Trig member (Tf14) (n = 7) plus reworked glass from Okataina VC (n=10)

Sample 10 marks a peak concentration of brown glass between 33 and 36 cm in the core. The sample comprises a relatively homogenous composition of dacite glasses. All analyses were checked for contamination by microlites phase following the method by Platz *et al.* (2007) and one glass analysis was rejected (Fig. 5. 16). The analyses show a tight clustering on the bivariate plot of SiO_2 and K_2O which overlaps with a number of other Tufa Trig compositional groups identified in the core. Potential correlatives could include a number of post-Kaharoa Tufa Trig members. The most likely correlative Tf member based on evidence from proximal deposits would be Tf14, one of the thickest tephras in proximal sequences and with one of the most widespread dispersals in the proximal and medial zone around the volcano (Donoghue *et al.*, 1995b; 1997). In the bivariate plot in Figure 5.16 b, this glass population overlaps with the known compositional range for this tephra from proximal deposits and with the compositional range of Tf14 tentatively identified in Moanatuatua Reserve (envelope with solid blue line). This tephra is not dated directly but it does represent one of the most recent of the Tufa Trig members identified in

proximal sequences. In the Moanatuatua sequence the age of the unit is constrained by radiocarbon chronology to between 160 and 300 cal yr BP. In the Lake Pupuke sequence, which has a limited chronology, the interpolated age of the deposit is 220-275 cal yr BP (from models 1 and 2; Fig. 5.13). The overlap of ages supports the premise that the prominent glass peak in the two sites may represent the same eruption event. Alternatively, sample 10 in P8_06 could represent an older Tf member not represented or recognised as a prominent glass concentration in Waikato sites.

The composition of two analyses of two clear glass shards compare with a number of uncorrelated glass analyses in the core and most likely derive from Okataina-derived glass deposits (not including the Kaharoa Tephra) that may have been reworked from exposures in or near the site (Fig. 5. 15). There were a number of additional glass peaks in the core (e.g. at 30 cm) which were not analysed because of time constraints and poor glass recovery.

Descriptions of the following two samples are from a limited set of analyses obtained from core Puk5 (Fig. 5.11) to support correlative tie points with core P8_06.

Sample A. Puk5 - 38 cm: Ruapehu VC-derived Tufa Trig member (n = 9) and Okataina VC-derived Kaharoa Tephra (n = 3)

Sample A marks two overlapping, prominent peaks in brown and clear glass concentrations between 38 and 39 cm depth in the core, 13 cm below the visible Rangitoto

Tephra. The glass concentrations at this position in the core were considered the most likely correlatives to the double peak identified in P8_06 at 78 cm depth comprising the Kaharoa Tephra and Tf member Tf6. Unfortunately, glass recovery from this sample was poor due to insufficient material available. It was only possible to obtain analyses from three clear glass shards from the sample and it was likely that the extracted sample 'missed' the peak concentration in clear glass which was identified immediately below the peak in brown glass from the glass counts (Fig. 5.11). A larger sample size may have resulted in more representative glass composition.

The results of the EMP analysis revealed predominantly dacite glass with a composition characteristic of Ruapehu derived Tufa Trig members identified in core P8_06 (Fig. 5.16). The dacite analyses overlap with a number of analyses from post-Kaharoa Tf members from P8_06 and from Waikato sites. The analyses show good correspondence with the composition of Tufa Trig member Tf6 which also exhibits a relatively wide spread of compositions and includes a number of analyses with high FeO values – a distinguishing characteristic of Tf6 from other Tf members in proximal deposits (Donoghue & Neall, 1996; Donoghue *et al.*, 2007) (Fig. 5.16 b).

For the three analyses obtained of the clear glass in the sample, only two show a clear correlation with the compositionally distinct Kaharoa Tephra (Fig. 5.15). The identification of this unit, although tentative, is supported by similarities in the pattern of glass concentrations in core P8_06 (double peak in clear and brown shards), and by its stratigraphic position relative to other features in the core.

Sample B. Puk5- 24 cm: Auckland VF, Rangitoto Tephra (n=10)

Sample B was taken from the top of the visible Rangitoto Tephra in the core to confirm the initial identification in the core and to support analyses of the visible basaltic tephra from replicate core P8_06. Unlike the sample from P8_06, this sample also contains a significant proportion of shards with a trachy-basalt and basaltic chemistry which are only recognised in the cryptic component above the Rangitoto Tephra. Although it is recognised that there is substantial variability/heterogeneity in many of the basalts (noted earlier), it is possible that this sample could represent a mix of the two phases recognised by Needham *et al.* (2008). In this core Horrocks *et al.* (2005) did recognise two thin basaltic layers but they were separated by only 1 cm of sediment. Given the sedimentation rates of the core, the single centimetre is unlikely to represent the longer interval recognised by Needham *et al.* (2008) between the two phases, unless core loss or mixing had occurred. Because of a paucity of data in this core it is not possible to make any definitive links neither with the record of Needham et al. (2008), nor with the samples from core P8_06.

The calculated age of the Rangitoto Tephra from this core, based on a model of constant sedimentation (model 2; Fig. 5.7), is 544 ± 20 cal. yr BP (AD 1406 ± 20) based on an age-depth model adjusted for changing sedimentation rates after the deposition of the Rangitoto Tephra (Fig. 5.7). This age range overlaps with the best estimate age of the Rangitoto Tephra at 526-451 cal. yr BP (2σ range) (AD 1424-1499) (recalibrated from Nichol, 1992), but is somewhat younger than the age estimated using core P8_06 (AD 1469 ± 22).

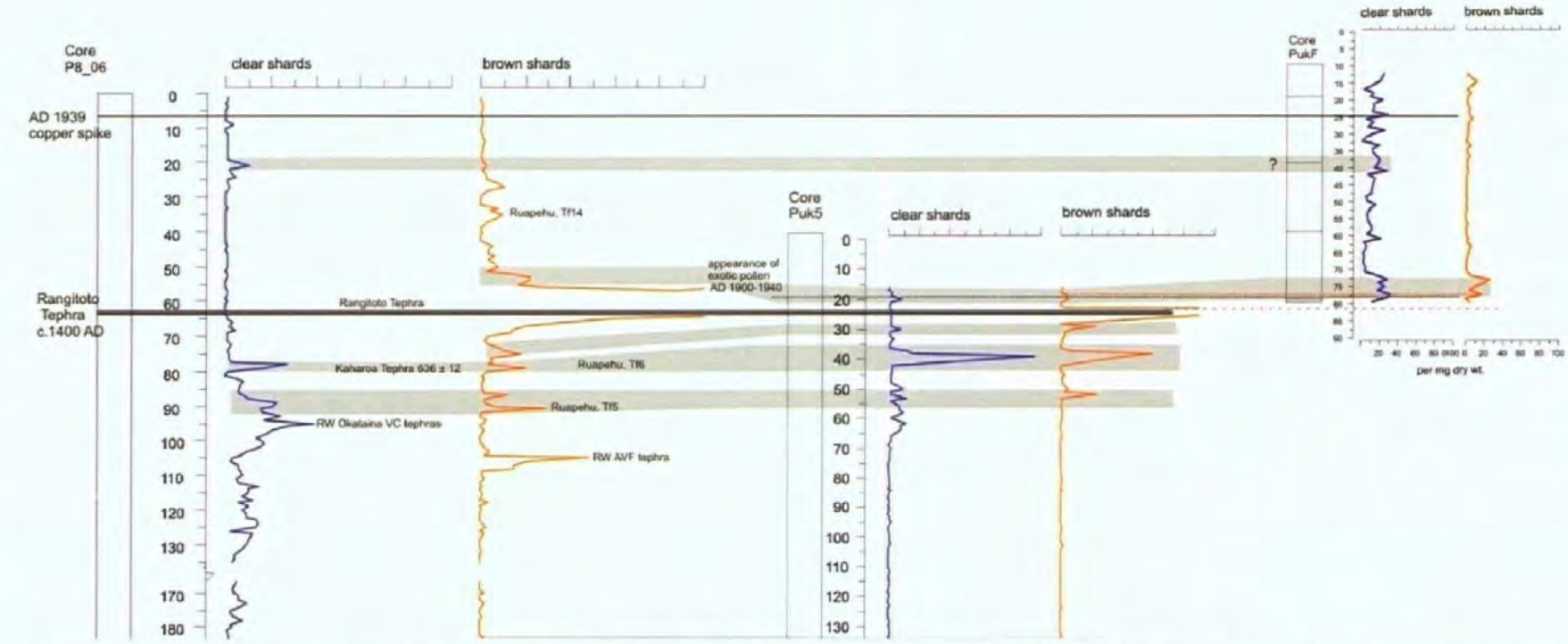

Figure 5.18 Combined results of glass shard counts from all three cores (l-r: P8_06; Puk5; PukF) shown with tie-points between peak concentrations based on stratigraphic position, age. Indicated correlatives are supported by major element composition of glass shards from one or more cores determined by electron microprobe analysis. RW, reworked.

Table 5.2 Summary of cryptic and visible tephras identified in cores P8_06 and Puk5 including their relative ages. Age ranges based on 2-sigma range of age depth model and taking into consideration the vertical extent of cryptotephra zone considered to represent a primary fall event or depositional event identified from shard counts (Figs. 5.11 and 5.13) ,and from analysis of geochemical populations (Table 5.1). * Unable to interpolate age; **age ranges interpolated between ages with Kaharoa Tephra removed from age model. RW = reworked (secondary deposition). § Original dates recalibrated in Calib Southern Hemisphere calibration curve: SHCal04

Sample no. /core	Depth in core (cm) [of sample shard conc.][a]	No. of shards in population analysed	Eruptive source (VC)[b]	Interpolated age of glass conc. in cal. yr BP 2σ range[c]	Identification of tephra (T) /interpretation	Calibrated ages of tephras in cal. yr BP 2σ range[d]	Primary reference(s): ages[1] major element chemistry[2]
1/P8_06	212 [212-213]	12	TVC	*	Taupo Tephra	1717 ± 13	[1,2] Lowe *et al.* (2008)
2	105 [105-108]	10	AVF	910-940	RW AVF tephra poss. Lake Pupuke tuff ring	*	[2] Shane and Smith (2000)
3	95 [89-100]	9	OVC?	740-890	Mixed RW tephras	*	[2] Lowe *et al.* (2008)
4	91	15	Tng	765-795	Ruapehu, Tf 5	540-660	[1] Lowe *et al.* (2000) [2] Donoghue *et al.* (1995)
5	78 [77-79]	(a) 11	OVC	ca. 775**	Kaharoa Tephra	624-646	[1] Hogg *et al.*, 2003; [2] Lowe *et al.* (1998); Newnham *et al.* (1998)
		(b) 11	Tng	590-630	Ruapehu, Tf 6	535-600	[1] Lowe *et al.* (2000) [2] Donoghue *et al.* (1997)
6	75	(a) 19 (b) 7 (c) 4	AVF OVC Tng	610-650	RW Rangitoto Tephra RW OVC tephra RW (?) Tong tephra	ca. 550	[1] Nichol (1992) [2] Shane and Smith (2000) [1] Lowe *et al.* (2008) [2] Donoghue *et al.* (1995)

Sample no. /core	Depth in core (cm) [of sample shard conc.][a]	No. of shards in population analysed	Eruptive source (VC)[b]	Interpolated age of glass conc. in cal. yr BP 2σ range[c]	Identification of tephra (T.) /interpretation	Calibrated ages of tephras in cal. yr BP 2σ range[d]	Primary reference(s): ages[1] major element chemistry[2]
7	66	16	AVF	445-530	Rangitoto Tephra	526-451[1]	[1]Nichol (1992) [2]Shane and Smith (2000)
8	63 [62-63]	16	AVF	466-497	Rangitoto Tephra	526-451[1]	as for sample 7
9	54	11	AVF	395-430	RW Rangitoto Tephra	526-451[1]	as for sample 7
10	36	7	Tng	220-275	Ruapehu, Tf 14	?	as for sample 7
A/Puk5	38	(a) 9	Tng	580-660	Ruapehu, Tf 6	624-648	[1]Newnham *et al.* (1998); [2]Hogg *et al.* (2003)
		(b) 3	OVC	ca. 770**	Kaharoa Tephra	535-600	[1]Lowe *et al.* (2000) [2]Donoghue *et al.* (1997)
B/Puk5	24	10	AVF	530-558	Rangitoto Tephra	526-451[1]	[1]Nichol (1992) [2]Shane and Smith (2000)

5.2.7 Summary of findings and resultant issues

1) Cryptotephra analyses were conducted on three lake sediment sediments core from Lake Pupuke that collectively span the interval from the deposition of the Taupo Tephra at AD 233 ± 13 up to the near present. Unlike sequences from the Waikato sites, the Lake Pupuke cores contain an additional visible tephra layer – the Rangitoto Tephra, the locally derived basaltic (mainly alkalic) tephra deposited between *ca.* AD 1400 and *ca.* AD 1500 (see 3a below) during the main phase of the eruption of Rangitoto Island.

2) The results of shard counts for the three cores reveal almost continuous background concentrations of clear and brown tephra-derived glass punctuated by several discrete 'peaks' in glass concentrations attributed to primary or secondary tephra depositional events. The discrete peaks in glass showed little evidence of sustained reworking or downward movement in the sediments. Background glass was identified as deriving from much older tephras which occur in the lake catchment. There were some variations in glass content between the different cores, despite their proximity to one another, and this variation has been attributed to localised differences in sedimentation in the lake.

3) The results of single-shard analysis by electron microprobe revealed glass in the cores was derived from rhyolitic, andesitic-dacitic and basaltic sources. Analyses on selected levels from the core suggest that peak shard concentrations can represent both primary fall deposits and secondary (reworked deposits). Distinguishing between these two origins is not straightforward but has been based on replication between the core sequences, homogeneity of glass chemistry and the use of stratigraphic and age

relationships to correlate with eruptive events recognised at more proximal localities. Primary fall tephras are identified as cryptotephras in the lake sequences from major element glass compositions and supported by age models constructed for each core.

Primary fall tephras identified include the rhyolitic Kaharoa Tephra, at least three andesitic tephras from Mt Ruapehu's Tufa Trig Formation: Tf5, Tf4 and Tf14, and the widespread, visible, basaltic Rangitoto Tephra noted above. It is now possible that another basaltic tephra was erupted about 76 years after Rangitoto Tephra during a final (tholeitic) eruption phase of Rangitoto Island. It is also possible that a precursory tephra (also tholeitic) fell one or two decades before the main (alkalic) eruption phase. It is emphasised that the evidence for both the 'precursory' and 'final' events is uncertain. Figure 5.18 provides a composite of results from all three cores and shows possible tie lines based on the results of glass concentrations and compositional analyses of glass samples from one or more of the cores. Table 5.2 provides a summary of the main tephras identified by glass-shard major element composition in the core, indicating source and interpolated age of each deposit.

a) The identification of the Kaharoa Tephra in the core represents the first reported occurrence of this critical marker of initial human (Polynesian) settlement in an Auckland site. This is the first record that shows the Kaharoa Tephra in the same stratigraphic sequence as another archaeologically significant marker, the Rangitoto Tephra. As a consequence, the current age estimate of the Rangitoto Tephra is revised to between 564-459 cal. yr BP (AD 1386-1491) based on the 2σ-age models from two cores from Lake Pupuke: age from core P8_06, 481 ± 22 cal yr BP (AD 1469 ± 22); age from core Puk5, 544 ± 20 cal. yr BP (AD 1406 ± 20). This

age range confirms the updated age estimates of 526-451 cal. yr BP (AD 1424-1499) (recalibrated from Nichol, 1992) and estimates using other data including obsidian hydration dating, thermoluminescence and paleomagnetism (Lowe *et al.*, 2000).

b) The three shard concentrations of intermediate chemistry identified in the cores are linked to Mt Ruapehu Tufa Trig members Tf4, Tf5 and Tf14 based on compositional analyses and interpolated ages. The compositions and interpolated ages of the Tf members can also be linked with shard concentrations identified in the Waikato sites. This record represents the first occurrence of andesitic tephras, deposited within the last 9 cal ka, within any Auckland sequence (and the first from Tongariro Volcanic Center to be recorded in the Holocene). It is possible that a number of additional andesitic tephras are also preserved in the core but have not been analyzed for geochemistry. No glass was detected (other than a few single-shard occurrences) which could be correlated to any recent Mt Egmont derived eruptives, the source of most andesitic tephra found in the maar sequences before 9 cal ka. Shane (2005; 2007a) has suggested that changing wind conditions, in particular reduced westerlies, after the Last Glacial Maximum, may explain the lack of andesitic tephras found in Auckland Holocene records (see also Magill, 2007). The results from Lake Pupuke show a prevalence of TnG VC-derived tephras from a more southerly sector and consistent with this hypothesis. This finding could result in these Tongariro VC volcanoes being more significant for future ash-fall hazard models.

c) The frequency of eruptions from andesitic volcanoes identified in the cores so far exceeds previous estimates of andesitic falls in the Auckland Region of one per 960 years. The new record from Lake Pupuke reveals that since 1700 cal yrs BP, or since the eruption of the Taupo Tephra, the frequency of andesitic tephras is one per 567 years. The analysis of further glass concentrations in the cores, which have not been analysed for geochemistry, could further increase this frequency.

d) Much of the glass of alkaline (basaltic) chemistry identified in the cores does not correlate directly with previously established compositions of the Rangitoto Tephra or older Auckland Volcanic Field-derived tephras. This finding supports the assertion by Shane and Smith (2000) that there are likely to be compositional differences between proximal and distal AVF tephras. Basaltic glass identified immediately below the visible Rangitoto Tephra may represent reworked deposits of the tephra although the possibility that there was a minor precursory tholeitic phase cannot be ruled out (i.e. a precursory phase prior to the main alkalic Rangitoto Island-forming event that generated Rangitoto Tephra). Basaltic glass identified 9 cm above, and separated from the visible Rangitoto Tephra in core P8_06 by about 76 years, may represent a later tholeitic phase (as proposed by Needham *et al.*, 2008), or reworked glass. Glass of basaltic composition identified at other levels of the cores are thought to represent older, reworked AVF tephras including glass from the tuff ring of Lake Pupuke itself.

CHAPTER 6: DISCUSSION

6.1 Introduction

The main aim of this research is to establish a post-Taupo Tephra record of tephra fall preserved as cryptotephra from sediment sequences collected from peat and lake sites in northern New Zealand. The results described in Chapters 4 and 5 revealed a complex record of tephra deposition at each site, a consequence of both primary fall events from rhyolitic and andesitic sources and redeposition from older tephra units. These records provide considerable insight into both the frequency and distribution of tephra-fall events in the region as well as site specific and regional environmental changes since the Taupo Tephra eruption of AD 233 ± 13.

Determining the mode of deposition and, in particular, differentiation between primary fall and redeposited tephra was a major challenge and, during the course of this study, a protocol was developed to assist with this task. This chapter begins with a description and discussion of this protocol which serves two purposes: (1) an explanation of how decisions were made in this study on the likely mode of deposition of cryptotephra, and (2) a working model that may usefully inform future investigations. This discussion includes appraisal of the principal investigative methods used in this study (section 6.2). The

remainder of this chapter provides a summary of the main tephra correlatives identified in this study which form the basis for an enhanced (more comprehensive) tephrostratigraphic framework for the Waikato-Auckland region (section 6.3), a review of site and environmental factors determining the preservation and identification of cryptotephra identified in this study (section 6.4) and finally, the implications of these cryptotephra records as discussed with respect to regional volcanic hazards assessment (section 6.5).

6.2 Distinguishing primary tephra fall from redeposited tephra

The tephra-derived glass shard concentrations reveal a detailed, and in some cases, complex pattern of tephra deposition and redeposition at each site. In all sequences, clear and brown coloured glass shards, corresponding to rhyolitic and andesitic (and/or basaltic in Lake Pupuke) volcanic sources, respectively, were found in near continuous, albeit mostly very low, concentrations. This background continuum of shards is marked by distinct and sometimes discrete elevated 'peaks' or zones of shards, the result of depositional events of primary fall and secondary reworking of tephra. Identifying and differentiating between the different sources of tephra from the complex pattern of shards was one of the main challenges of this study.

The complexity of the tephra content observed in the different sites used in this study was not unexpected. In addition to primary fall, sedimentary and taphonomic processes operating at each site were important factors in determining the pattern of distribution of shards obtained. All the peat and lake sites used in this study are medially positioned, ~100–300 km away from a range of volcanic sources which have experienced prolific and

sometimes simultaneous explosive volcanic activity in the recent past (Shane, 2000). Sources for secondary reworking were also abundant in and around each site in the form of pre-existing tephra deposits.

Candidate tephras for the sites included the Taupo and Kaharoa tephras, both the product of large scale eruptions from rhyolitic calderas, and preserved across much of the North Island and beyond (e.g. Lowe *et al.*, 2008b). In addition to these two primary fall rhyolitic tephras identified in the sites, deposits from rhyolitic volcanoes were found to provide a major source of reworked tephras at all the sites. The region's andesitic volcanoes, on the other hand, have been very frequently active in recent times producing much smaller volumes of tephra which were thought to be confined to mainly proximal sites with only a few of the largest eruptions (or smaller-volume events with wider dispersal by exceptionally strong winds) depositing ash in medially positioned sites (Alloway *et al.*, 1995; Eden & Froggatt, 1996; Hobden *et al.*, 2002). In this study at least nine andesitic tephras were detected in the post-Taupo sediments with possibly many more preserved as smaller concentrations of shards. The basaltic eruptions of the Auckland Volcanic Field (AVF) have occurred relatively infrequently resulting in only localized distribution of tephra (Shane & Smith, 2000a). The AVF eruptions were found to provide a source of primary fall and reworked tephra in the Auckland site. In addition to the potential sources of tephra, the condition and history of the sedimentary environments was considered an important factor for the preservation and identification of cryptotephras in the different sediment profiles. Section 6.4 in this chapter evaluates the different sedimentary archives with respect to the preservation of cryptotephras.

6.2.1 *Developing a protocol for identifying primary fall tephras*

Identifying primary tephra fall events from the complex cryptotephra records, one of the primary objectives of this study, was not straightforward. Unlike the isolated shard concentrations typically obtained from cryptotephra sites located very distally from volcanic sources (e.g. Hang *et al.*, 2006), the shard content from the sites used in this study represent multiple and sometimes simultaneous depositional events (from primary and secondary sources) resulting in multiple and in some cases overlapping peaks in shard concentrations. In the peat sites, there was the added complication that shard concentrations were typically disseminated over several centimetres in the peat.

During the course of this study, a working procedure was developed to distinguish primary fall-tephra layers from these non-primary sources. It should be noted that the procedure, described below and in Fig 6.1, was not always followed rigidly particularly during the early, developmental stages of the study. It is presented here both to indicate in broad fashion how key decisions were made and as a protocol to guide future investigations of similar phenomena based on the cumulative experiences and findings of this study. Even so, this protocol should be applied with caution and discretion and no doubt could be improved with further application. For example, relatively little detailed compositional data are available on andesitic glass shards (e.g. Shane, 2005; Shane *et al.*, 2008a) and the level of heterogeneity for individual eruptive events needs further testing to confirm the principle of homogeneity used in the model. Further, although the lack of replication between cores or sites suggests strongly that an heterogeneous glass concentration is probably reworked (Fig. 6.1, panel at bottom right), a primary-fall origin cannot definitively be ruled out in each case because insufficient cores may have been examined,

or sediments preserved in a core might have been compromised in some way leading to missing units.

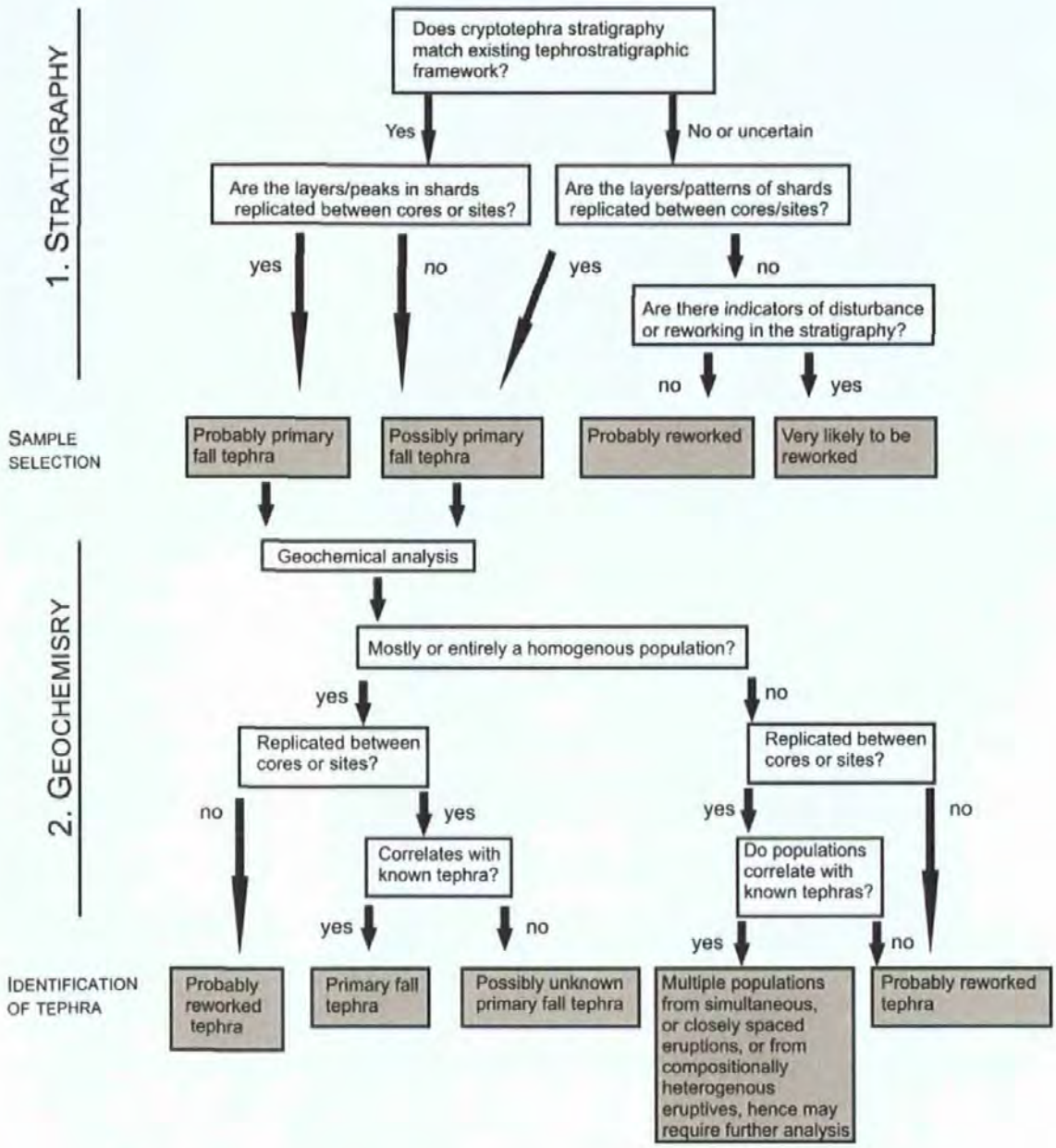

Figure 6.1. Proposed model for identifying primary-fall tephras from cryptotephra content.

The procedure consists of a sequence of enquiries in two phases. The first stage uses stratigraphic information to differentiate between shard concentrations most likely to be derived from primary fall deposits and reworked deposits in order to target samples for the second stage, geochemical analysis. This two-stage procedure recognises that all cryptotephra work will include stratigraphic analyses but not all will have the resources to undertake geochemistry. Those that do will require a judicious sampling strategy, informed by the results of the first, stratigraphic, stage. It therefore allows both for informed decisions to be made based on stratigraphy alone as well as for confirmation and substantiation to be achieved from geochemical analysis undertaken at varying degrees of resolution.

(1) Stratigraphy stage

In the first stage of this approach, the shard counts were compared with the existing tephrostratigraphic framework for the region. In this study, the reconciliation of these records was relatively straightforward because the tephrostratigraphic records for the region's rhyolitic and andesitic volcanoes are generally well known. The distributions of the individual tephras beyond the visible limits were unknown. Information from the tephrostratigraphic records which were also useful to this study included known dispersal range and thickness of proximal deposits which helped to narrow down the most likely candidate eruptions. It is noted, however, that the frequently-erupting andesitic volcanoes have complex proximal records in detail and many 'units' are composites of multiple events erupted over considerable time periods (e.g. Donoghue *et al.*, 1995b).

Matching the patterns of clear (rhyolitic) shards to the known tephrostratigraphic record was the most straightforward for the different tephra types identified. In the time period investigated in this study, there was only one rhyolitic candidate eruptive since the Taupo Tephra eruption – the Kaharoa Tephra which has a well defined dispersal range as a visible unit and which was a very likely candidate for detection in all the sites (Newnham *et al.*, 1998). Because the Kaharoa Tephra is also well dated it was possible to estimate the approximate location in the cores where the cryptotephra would be preserved using the age model for the core as a location 'device'. Additional peaks in clear shards were therefore likely to be derived from reworked sources.

Matching the peaks or concentrations of brown (andesitic) shards with the known eruptions from andesitic eruptions was less straightforward, because (a) there were many more candidate eruptions, (b) the distribution of the tephras was typically not so well defined, and (c) the ages of the individual eruptions were poorly constrained. It was, however, anticipated that the brown shard concentrations were less likely to derive from secondary reworking as there were no known exposures of andesitic tephras in or around the sites. The fall deposits were also likely to have been quite thin at the sites and were therefore less likely to be disseminated in the sediments than is the case with the thicker tephras (e.g. Taupo and Kaharoa tephras). Although not yet explored fully, it is possible that some apparently disseminated andesitic shard concentrations actually represent volcanic 'events' that comprise several phases that occur over an extended length of time (Magill *et al.*, 2006a; Jenkins *et al.*, 2007). In the upper section of the Moanatuatua Bog core (MR2) it was eventually possible (following geochemical analysis) to link shard concentrations to well documented historical eruptions (i.e. since around the mid-1800s in New Zealand) using the age model for the core. Because some of the shard concentrations for these

eruptions were relatively small it is possible that additional, unknown pre-historic eruptives represented by similarly small concentrations of shards had not been recognized from the cryptotephra content in the lower sections of the cores. Because glass concentrations from historic eruptives (e.g. from 1974-1975 Ngauruhoe eruption) were manifested as simple isolated concentrations in the cores (with no or very few shards immediately above or below in the peat), it is also possible that similar-sized concentration peaks also represent primary fall events rather than secondary or reworked shards from a pre-existing layer or zone. The absence of any such antecedent zone/concentration to provide a source for reworking implies that the isolated peak must have arrived through aerial deposition and hence represents a primary depositional event.

After consideration of the existing tephrostratigraphic framework, the second stage was to assess the degree of replicability in tephra shard concentrations between cores. In this study primary fall tephras were almost always well replicated in the cores from the individual sites, whereas reworked shards typically formed spatially variable patterns. The cores from Lake Pupuke (P8_06 and Puk5; Fig. 5.18) provide a particularly good example of this. All primary fall tephras were replicated between the two main cores whereas concentrations found to derive from reworked sources were only evident in one core (P8_06), probably as a result of localised reworking. By comparing cryptotephra records between the different sites it was also possible to identify comparable patterns which are more likely to derive from primary fall tephras. This was particularly useful for evaluation of the Opuatia Bog core where there was no replicate core. For example, a peak in brown shards coinciding with the decline in clear shards above the Taupo Tephra was identified in cores from Moanatuatua Bog (Figs. 4.2.7-8) and Lake Rotoroa (Fig. 4.3.4). It was therefore likely that a similar pattern of shards in the other two sites would represent the same

tephra. It is still possible, however, that primary fall tephras may be better preserved in some sites or parts of the site than others; for example, where the occurrence of reworked shards obscures primary fall deposits.

Where replication does not or cannot provide sufficient information to distinguish between primary and secondary deposited tephras, other stratigraphic evidence may also be informative, in particular where there is evidence for reworking or disturbance in the sediment sequences. Where this is the case it may not be beneficial to take samples for geochemistry. In Opuatia Bog, for example, the presence of silt or clay layers in the upper section of the sequence provided an indication that the bog had been inundated during recent flooding events (section 5.3). It is likely that such events would have had a significant disturbance effect on the site including redeposition of tephra by water movement. Indeed, the occurrence of high concentrations of clear shards in this section of the core, which were stratigraphically well above the cryptic Kaharoa Tephra, provided clear evidence for the presence of reworked tephras. In this case it was considered that the concentrations of brown shards at the same levels were also likely to be reworked. In a Lake Rotoroa core (LR1) the age reversals obtained from two radiocarbon dates were suggestive of reworking of older carbon in the catchment (section 4.3.4). This interpretation was supported by the results of geochemistry which revealed a significant contribution of reworked (much) older tephras. Other stratigraphic evidence for reworking identified in this study included evidence for fires from charcoal layers, irregularities in the pollen records, and changes in the sediment composition including increases in mineral particles. In many cases, stratigraphic evidence for disturbance and reworking coincided with clear signals of human activities in the region indicated by pollen analysis, age

models or loss-on-ignition measurements (as described, for example, in Newnham *et al.*, 1998).

The use of these three stratigraphic criteria – comparison with existing tephrostratigraphic framework, replicability, and independent disturbance indicators – allows a preliminary assessment of primary tephra-fall events to be made. For some studies this will be the end result. For studies that are supported by geochemical analysis of glass shards, the results of this stratigraphic stage can be used to select candidates for these analyses, to confirm or refute the preliminary assessment of fall provenance, underpin tephra identification and correlation, as well to identify mixed or heterogeneous populations, as outlined below.

(2) Geochemistry stage

In the description below, it is assumed that the selected candidates for geochemistry are considered likely to be primary-fall tephra, based on the stratigraphy phase. The first step in interpreting any geochemical analysis of tephra shards is to determine whether the sample consists of an entirely (or mostly) homogenous population. This step is indicative rather than diagnostic. A homogenous geochemical population implies primary fall provenance but that may not always be the case, as noted above. In some cases in this study there was evidence for reworking of a single prominent tephra, e.g. the Taupo Tephra. Conversely, a heterogeneous population may point to reworking, but this also is not necessarily always the case. As alternative scenarios, the mixed population may match a known tephra correlative with a heterogeneous composition arising through magmatic processes (e.g., Shane *et al.*, 2008b) or may reflect two or more overlapping fall events.

At this point, it is necessary to consider the varying degrees of complexity that may be seen in mixed populations. A large number of samples analyzed in this study showed mixed geochemical populations. In most samples there was a small background concentration of reworked tephras (e.g. 1-3 shards for every 10 shards analyzed), mainly from rhyolitic sources, with the majority of shards having homogeneous geochemistry. In this study a population was considered mixed when it consisted of a greater degree of heterogeneity (e.g. < 60% of shards share the same geochemistry). It was sometimes possible to conclude, on the basis of other key criteria of the protocol, that mixed populations actually consisted of one or more primary fall tephras and/or one or more geochemical populations from reworked tephras. In one sample from Lake Rotoroa it was possible to identify five separate geochemical populations (section 4.2). In this case, the multiple populations represented several depositional events including closely spaced or effectively simultaneous eruptions (Kaharoa Tephra and Tufa Trig tephra) in addition to significant and multiple contributions from reworked deposits. In the case of multiple populations it is beneficial to undertake a much larger number of analyses to account for the different populations (as recommended by Shane *et al.*, 2008b). It may also be necessary to obtain further (more closely spaced) samples to determine the stratigraphic position of individual primary fall tephras.

The second step considers the degree to which the patterns of geochemistry are replicated between sequences. If this is clearly not the case, (it is considered judicious to apply the precautionary principle and conclude that) the tephra is probably reworked, regardless of whether geochemistry populations were homogenous or not. On the other hand, if comparable geochemical data are attained in similar stratigraphic pattern in different sequences, even when mixed populations are involved (see above), it is less likely that the

shard concentration or peak is derived from the more localized distribution of reworked tephras. The determination of primary fallout in such cases is further strengthened if, in the final (third) step, a satisfactory tephra correlative match can be achieved from the geochemistry. However, if the geochemistry is replicated but the tephra cannot be correlated with a known event then it is still likely to be primary fall, but derived from an unknown eruption or volcanic source in which case further investigation may be warranted especially where the number of cores or samples examined has been limited.

6.3 An enhanced post-Taupo (crypto) tephrostratigraphic framework for the Waikato-Auckland region, New Zealand

By following the protocol summarized in the previous section it was possible to identify a number of key primary tephra fall events which can be linked to known eruptive events in the region. These correlatives include the rhyolitic Kaharoa Tephra and nine tephras from andesitic volcanic sources (Fig. 6.2). Figure 6.2 provides a composite of the results of cryptotephra analysis from representative cores from each site and shows where these can be correlated between the different sites. All cryptotephras identified in this study provide a significant extension or addition to the known dispersal range of the tephras based on the visible range of the deposits (Fig. 6.3). The following section provides a summary of each of the tephra correlatives from rhyolitic and andesitic sources identified in this study with reference to the compositional characteristics, age, stratigraphic position and dispersal range of the deposit. Where appropriate, variability in the tephra records between the different sites is also discussed.

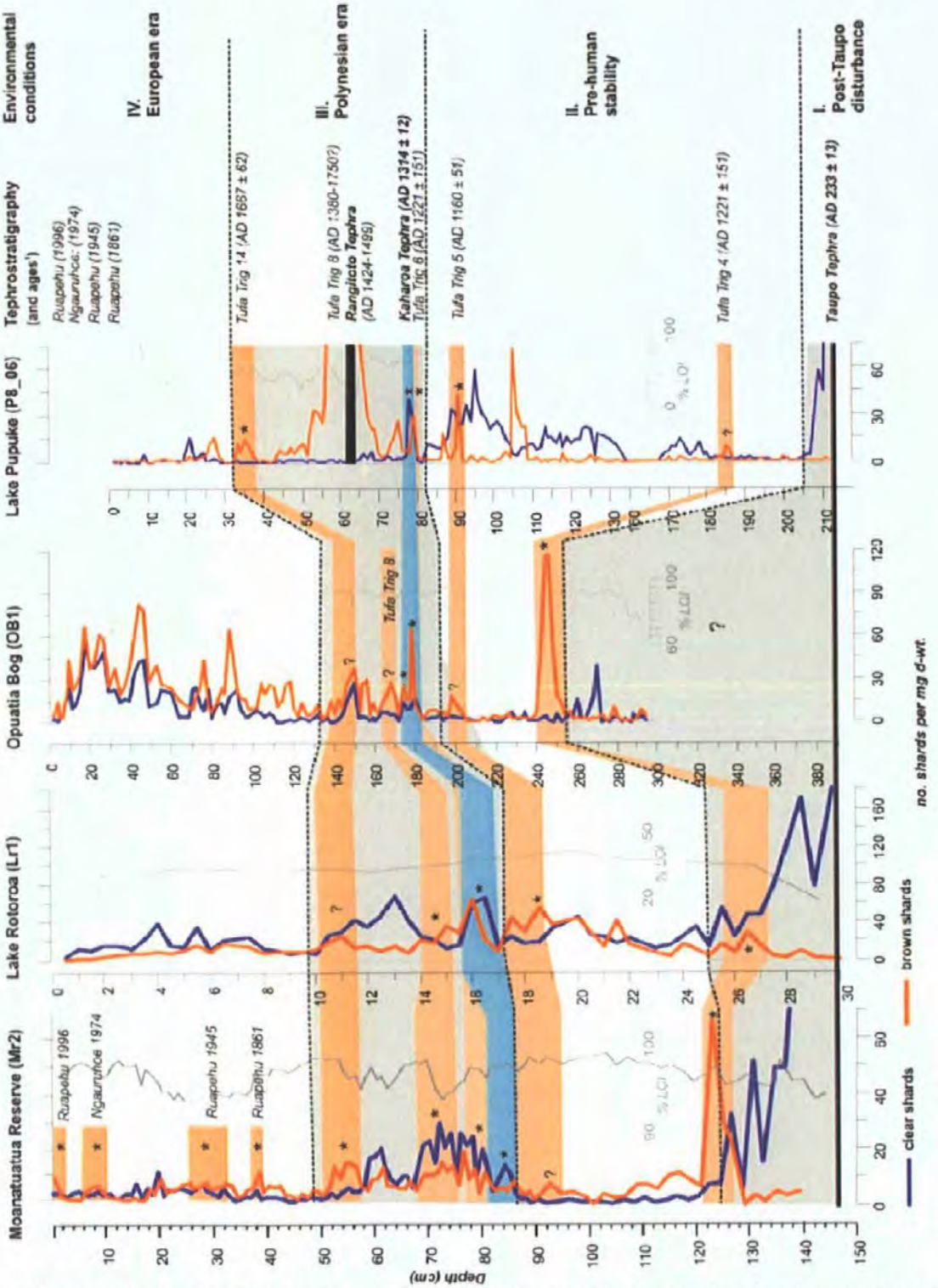

Figure 6.2 Composite results of counts of clear and brown shards shown as number of shards per mg dry weight (no. shards per mg d-wt.), from representative cores from each site, shown against loss on ignition (LOI), in light grey. Orange tie points connect individual identified tephras: * = correlation supported by geochemistry. ? = a tentative correlation based on stratigraphic position and shard distribution ? pattern (no geochemistry available). Dates for Taupo and Kaharoa tephras are 2sd range; other dates are also 2sd ranges.

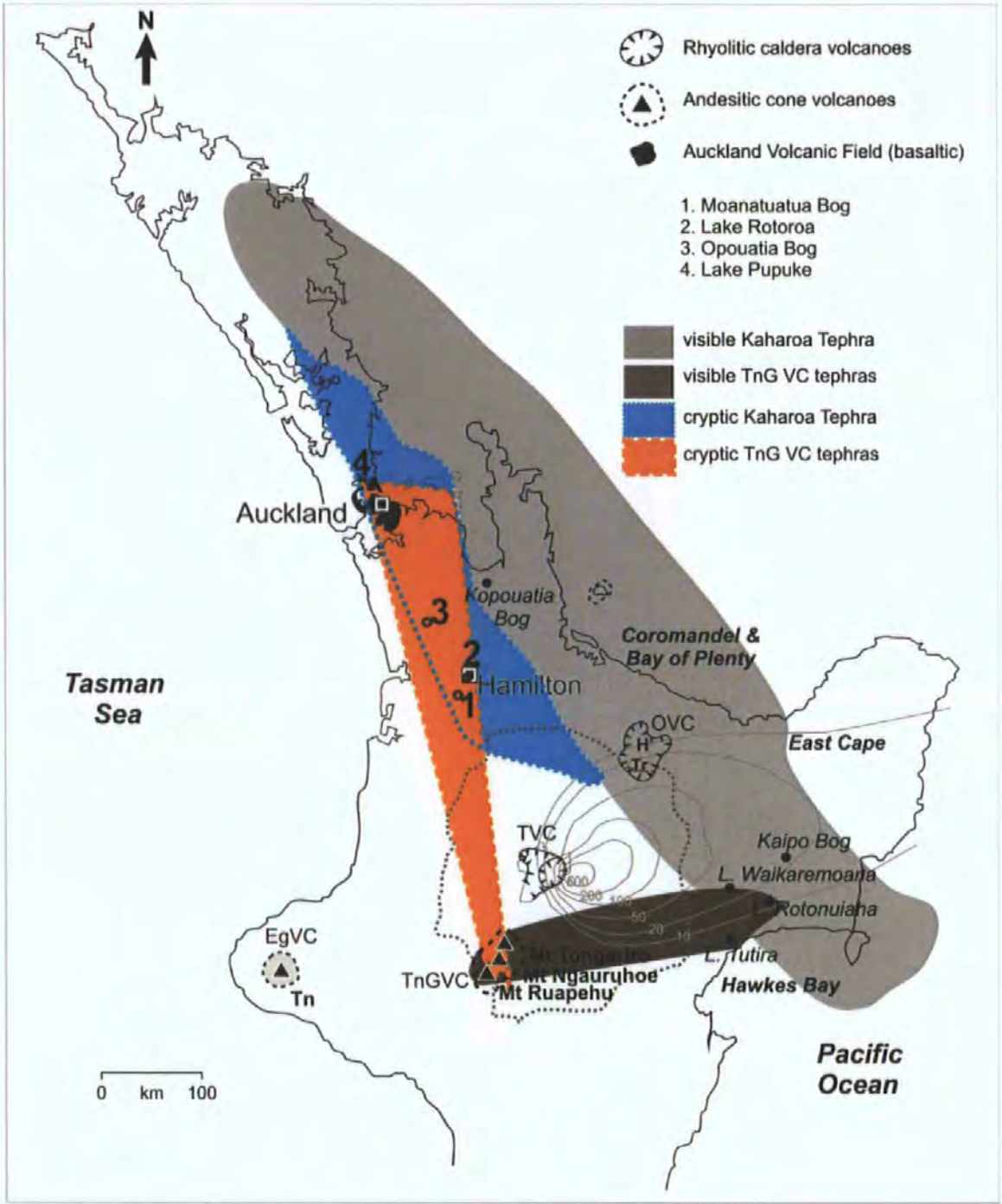

Figure 6.3 Known dispersal range of the visible Kaharoa Tephra (after Lowe *et al.*, 1998) and post-Taupo Tongariro Volcanic Centre (TnGVC)-derived eruptives (after Donoghue *et al.*, 1995b; Eden and Froggatt, 1996) with extension or dispersal axis of cryptotephras identified in the sites used in this study (shown by numbers 1-4). Distribution of Taupo ignimbrite radially around Lake Taupo (dashed grey line) and tephra fallout isopachs (in cm) derived from the Taupo eruption (from Wilson & Walker, 1985; from Wilson & Leonard, 2008). The occurrence of Taupo Tephra (<10 cm thick) in the Waikato and Auckland regions has been documented by Tonkin (1967), Pullar and Birrell (1973), Pullar *et al.* (1977), Lowe *et al.* (1988b), Horrocks *et al.* (2005), Gehrels *et al.* (2006) and others. EgVC, Egmont VC (Mt Taranaki, Tn); TVC, Taupo VC; OVC, Okataina VC.

6.3.1 *Rhyolitic tephrostratigraphy (visible and cryptic tephras)*

Glass shard concentrations derived from rhyolitic sources provided a significant contribution to the tephra content of most sites, derived from both primary fall events and reworked tephra components. Apart from the visible Taupo Tephra, the Kaharoa Tephra from the Okataina VC was the only candidate eruptive from a rhyolitic volcanic source in the region that was likely to be found as a cryptotephra in the post-Taupo Tephra sediments. The 1886 Mt Tarawera eruption, also from the rhyolitic Okataina VC, was basaltic, however, and, although very explosive for a basaltic event, produced fallout essentially confined to the Bay of Plenty -eastern Coromandel- East Cape regions and northwards because of strong southerly winds (Lowe *et al.*, 2002; Sable *et al.*, 2006). Both Taupo and Kaharoa tephras were identifiable from glass shard geochemistry and were found to contribute to the background concentrations of clear shards in many of the cores. Pre-Taupo rhyolitic shards were also identified in some sites. Identifying and differentiating between the different sources of rhyolitic glass was relatively straightforward in this study using geochemical analyses of the shard concentrations.

Taupo Tephra AD 233 ± 13 (1717 ± 13 cal. yr BP)

The Taupo Tephra forms a distinct visible horizon at three sites investigated in this study and was identified in the core by physical characteristics and stratigraphic position. All sites fall within the known range of visible Taupo Tephra. The Waikato sites match approximately the thicknesses recorded for Taupo Tephra by Tonkin (1967) and Pullar and Birrell (1973) although there is considerable variation (~1-10 cm) because of possible

reworking or compaction; at Moanatuatua Bog and Lake Rotoroa the tephra is less than 1 cm thick. At Opuatia Bog, pumiceous alluvium formed the base of the sequence, derived from the break-out flood resulting from, and occurring shortly after, the AD 233 ± 13 Taupo eruption (Manville *et al.*, 1999; 2007). Geochemical analysis was used to confirm the field identification of the visible tephra in selected sites and it was easily distinguishable from pre-Taupo VC derived tephras and from other rhyolitic sources by its unique geochemical composition. In comparison to Okataina VC-derived tephras, the shard composition of Taupo VC tephras has characteristically lower SiO_2 (74.8-76.7 wt %) and K_2O (2.44-3.62 wt %). The geochemical composition of the Taupo Tephra shards analysed from the sites used in this study corresponds with the climactic (ultra)plinian phase of the Taupo Tephra event (Unit Y after Wilson, 1993) (SiO_2 = 75.04 ± 0.19 wt%; K_2O = 2.85 ± 0.07 wt%) which is consistent with the findings from the tephra identified in other North Island sites (Gehrels *et al.*, 2006; Lowe *et al.*, 2008b). Unit Y5 is compositionally identical to Unit Y7, the 'Taupo ignimbrite' phase (Stokes *et al.*, 1992). The only slight discrepancy with published analyses is that there are slightly higher mean SiO_2 values in the analyses from this study. However, these higher values appear to be characteristic of most of the subsequent correlatives and probably relate to small differences in analytical conditions (e.g. Lowe *et al.*, 1999).

Glass shards correlating with the Taupo Tephra were also found to be a significant contributor to the cryptotephra content of the sites. These included clear glass shards found in high concentrations immediately above the visible tephra as well as background concentrations of clear shards mixed with andesitic populations. In Lake Rotoroa these included mostly pre-Taupo tephras. In some cases Taupo Tephra-derived shards were found persisting right to the very top of a sequence. There were no significant variations in

composition observed between the visible and cryptic components of the tephra which indicates that reworking of the shards has not had a perceptible impact on the shard geochemistry (Fig. 6.4).

In all sites, analysis of the visible and cryptic component of the Taupo Tephra revealed a minor population of glass shards (e.g. 2 out of 16 [13%] shards analyzed in sample MR2 145 cm) with similar composition to a number of post-22 ka Okataina VC derived tephra. As well, a few additional analyses suggest possible derivation from older Taupo VC-derived tephras (Fig. 6.4). The inclusion of an older unit with Okataina VC-like glass within the distal deposits associated with the Taupo Tephra layer has been noted in previous studies (Stokes & Lowe, 1988; Lowe, 1988b; Clarkson *et al.*, 1995; Gehrels *et al.*, 2006). It has been attributed to contamination (during analysis, coring or mixing during eruption) or to a separate (compositionally different) phase of the Taupo eruption or a hitherto unknown Okataina eruption that occurred simultaneously with the Taupo Tephra eruption. There is otherwise no known evidence for an Okataina eruption around this time and there is little current evidence to suggest additional phases of the Taupo eruption. It is thus more likely that the shards represent some form of contamination. Because the contamination is consistent in all cores (Fig.6.4) it is probable that it actually relates to the eruption. The Taupo Tephra eruption was an extremely powerful event and it erupted through many metres of volcanic deposits built up in the caldera which could thus have become incorporated within the Taupo Tephra plume. It is also possible that contamination in the cryptic component of the tephra could be attributed to post-eruption environmental instability (see section 6.3.2).

Glass analysis from the Taupo Tephra also exhibits very subtle variations between some of the different sites (Fig. 6.4). These variations could arise for a number of reasons: (1) unidentified changes in analytical conditions between samples; (2) compositional variations between the different phases of the eruption; (3) physical or chemical weathering effects in the different sedimentary environments. Alternatively, the 'variations' are not significant and simply lie within the error ranges for the analyses.

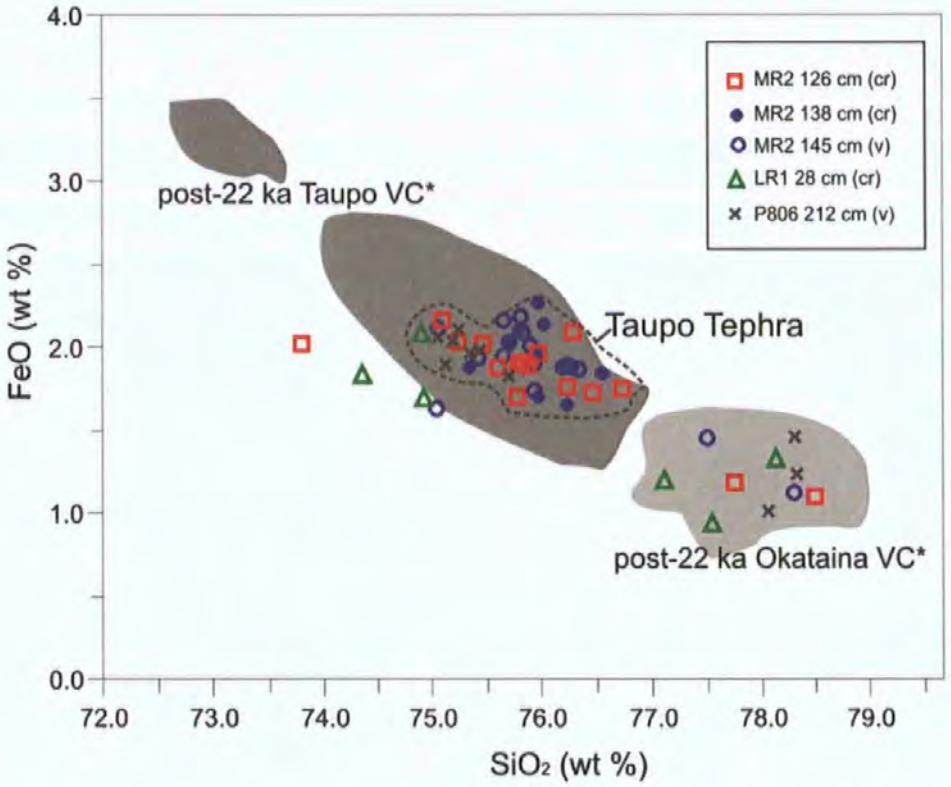

Figure 6.4. Compositional analysis of glass shard samples from the visible (v) and cryptic (cr) components of the Taupo Tephra in cores MR2, LR1 and P806. * Grey fields represent compositional ranges of post-22 ka Taupo and Okataina VC-derived tephras from Shane (2000).

Kaharoa Tephra AD 1314 ± 12 (636 ± 12cal.yr BP)

The Kaharoa Tephra was identified as a cryptotephra from distinct elevated concentrations of clear shards in all sites, located approximately halfway between the Taupo Tephra and the top of the cores. Compositional analysis, stratigraphic position and relative age all provided definitive evidence to support the identification of this tephra in all sites. The identification of Kaharoa Tephra in the sites provides an extension of the dispersal range of the tephra based on visible (3 mm isopach) deposits alone (Fig. 6.3; Newnham *et al.*, 1998). In Moanatuatua Bog the cryptotephra identification represents a *ca.* 40 km extension to the known visible limit. These findings support the hypothesis proposed by Newnham *et al.* (1998) that the tephra would be detectable beyond the visible limit in the Waikato and Auckland regions. Given the high concentrations of shards representing the cryptotephra in the sites used in this study, and the ease with which it was detected, it is very likely that that the Kaharoa Tephra is detectable as cryptotephra over much of the northern and middle part of the North Island and probably beyond. Because the Kaharoa Tephra represents a critical stratigraphic marker for late Holocene palaeoenvironmental and archaeological studies (Lowe *et al.*, 1998; Hogg *et al.*, 2003), these findings open up the potential for its use at a greater number of sites in the North Island.

Geochemical analysis of the rhyolitic glass concentrations representing this tephra were typically homogenous geochemically and were characterized by high analytical totals compared with older rhyolitic tephras, consistent with assays from previous work (e.g. Shane and Ingraham, 2002). Most Holocene tephra beds contain up to 4 wt% water, the degree of hydration depending on geographic location and age (e.g. Froggatt, 1983; 1992; Shane, 2000; Shane & Ingraham, 2002). The deficiency in analytical total from 100% in

electron microprobe analyses of volcanic glass shards is due mostly to secondary water not analysed (Shane, 2000). The shard concentrations correlate well with published values for the Kaharoa Tephra which is a compositionally distinct tephra from the Okataina VC, readily distinguishable from the Taupo Tephra and preceding Okataina VC derived tephras (Fig. 6.5 a; Table 6.1).

Table 6.1 shows a summary of analyses from the different sites used in this study compared with the published values of the tephra (Newnham *et al.*, 1998; Lowe *et al.*, 2008b). Analyses from the different sources all show quite consistent values for this tephra supported by low standard deviations for most oxides. Analyses from this study also show good correspondence with published values for most oxides. As with the Taupo Tephra, SiO_2 values from this study are typically very slightly higher and Al_2O_3 slightly lower than for the most recent published values (Lowe et al., 2008), probably reflecting small differences in analytical conditions (Table 6.1). The most recent published values for the Kaharoa Tephra include Type 1 (T1) and Type 2 (T2) compositions which represent subtle variations in the composition of the tephra recognized by Smith *et al.* (2005) (Lowe *et al.*, 2008b). T1 and T2 magma types correspond with tephra units from early and later phases of the eruption (respectively) which represent the tapping of separate batches of magma (Smith *et al.*, 2005; Shane *et al.*, 2008b). The units are recognized in proximal deposits: A-I (early phases), units J to L (intermediate phase), and units M+ (later phases) (Fig. 6.4 b; Shane *et al.*, 2008b). The early and later phases are represented by the southeast and northwest plumes from the volcano, respectively (Fig. 6.3) (Nairn *et al.*, 2001; 2004).

Figure 6.5 b, a bivariate plot of analyses from this study overlain by the compositional ranges for the different units, shows that the majority of analyses fall within the range for

unit M+ (later phases, generally blown north or northwestwards; Nairn et al., 2001). Table 6.1 highlights the diagnostic oxides for the tephra (SiO_2, CaO, K_2O and FeO) and shows that the analysis from this study also corresponds better with the later phases (T2 from Lowe *et al.*, 2008b). T2 tephra exhibits slightly higher SiO_2, CaO, and FeO and lower K_2O than the T1 population, although it is emphasized that these are very small differences and with errors they are indistinguishable (Table 6.1).

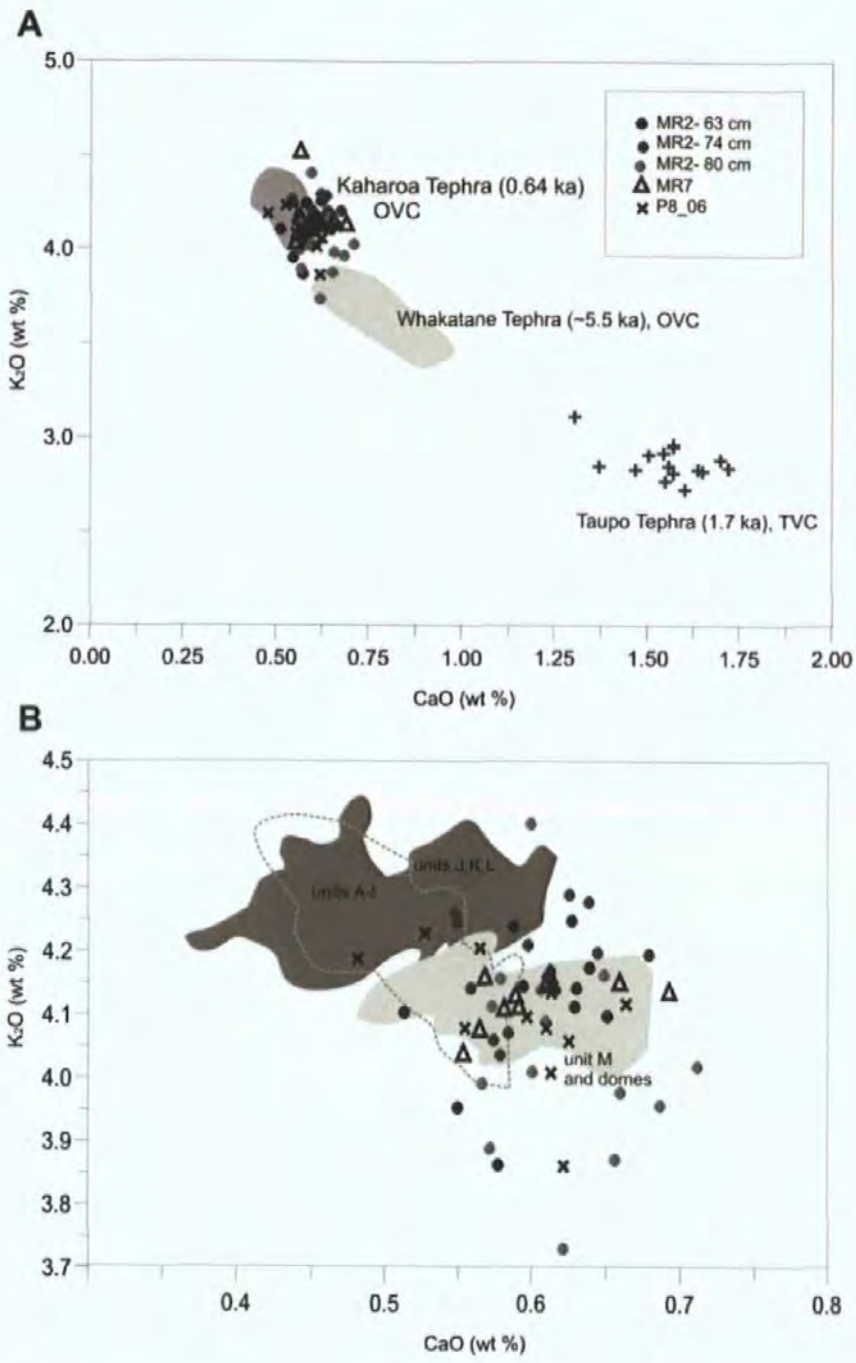

Figure 6.5. Bivariate plots of CaO versus K_2O for glass analysis of the Kaharoa Tephra from three sites: A, shown in relation to analysis from the Taupo Tephra; B, analysis shown in relation to ranges of the three compositional units identified from Shane *et al.* (2008b).

Table 6.1 Summary of major element composition of the Kaharoa Tephra identified in sites from this study compared with summary analyses from Lowe *et al.* (2008) and mean values from six sites in the Waikato and Bay of plenty from Newnham *et al.* (1995), * mean values of analyses from six sites from Bay of Plenty and Waikato regions. Mean values in bold. Normalised to 100% loss free (wt.%). In published analysis P_2O_5 is replaced by Cl. Grey boxes highlight diagnostic elements.

	SiO_2		Al_2O_3		TiO_2		FeO		MnO		MgO		CaO		Na_2O		K_2O		P_2O_5		H_2O		*n*
MR2 (85 cm)	**77.74**	0.29	**12.27**	0.15	**0.06**	0.02	**0.86**	0.09	**0.06**	0.06	**0.07**	0.01	**0.62**	0.05	**4.13**	0.13	**4.18**	0.11	**0.00**	0.03	**1.16**	1.64	**10**
MR2 (80 cm)	**78.20**	0.45	**12.14**	0.14	**0.08**	0.03	**0.85**	0.11	**0.11**	0.04	**0.07**	0.01	**0.62**	0.05	**3.89**	0.29	**4.04**	0.16	**0.00**	0.03	0.86	1.14	***14***
MR2 (76 cm)	**77.79**	0.28	**12.24**	0.20	**0.09**	0.10	**0.81**	0.10	**0.06**	0.05	**0.07**	0.01	**0.59**	0.04	**4.18**	0.12	**4.17**	0.10	**0.00**	0.01	1.23	1.28	***12***
MR2 (74 cm)	**77.68**	0.17	**12.19**	0.14	**0.08**	0.02	**0.86**	0.10	**0.04**	0.07	**0.07**	0.01	**0.60**	0.04	**4.28**	0.14	**4.18**	0.08	**-0.02**	0.02	1.41	0.98	***13***
MR2 (72 cm)	**77.63**	0.57	**12.14**	0.07	**0.09**	0.02	**0.88**	0.12	**0.05**	0.06	**0.07**	0.01	**0.60**	0.02	**4.09**	0.11	**4.05**	0.07	**-0.02**	0.02	**0.77**	0.48	***9***
MR2 (63 cm)	**77.97**	0.21	**12.19**	0.14	**0.08**	0.04	**0.75**	0.12	**0.06**	0.03	**0.07**	0.01	**0.60**	0.04	**4.16**	0.11	**4.11**	0.11	**0.00**	0.02	0.50	0.62	***11***
MR2 (61 cm)	**77.97**	0.25	**12.06**	0.06	**0.08**	0.05	**0.86**	0.08	**0.04**	0.02	**0.07**	0.01	**0.62**	0.03	**4.24**	0.10	**4.06**	0.10	**-0.01**	0.01	1.55	0.80	***5***
MR7 (90 cm)	**77.92**	0.87	**11.97**	0.31	**0.11**	0.07	**0.92**	0.35	**0.07**	0.07	**0.09**	0.07	**0.69**	0.30	**4.16**	0.20	**4.05**	0.40	**0.02**	0.02	**1.00**	1.36	***12***
LR1 (15 cm)	**77.72**	0.26	**12.19**	0.22	**0.07**	0.02	**0.87**	0.08	**0.09**	0.04	**0.07**	0.00	**0.61**	0.03	**4.20**	0.14	**4.17**	0.08	**0.01**	0.01	1.74	0.91	***3***
P8_06 (78 cm)	**77.81**	0.21	**12.16**	0.16	**0.08**	0.03	**0.88**	0.14	**0.05**	0.06	**0.07**	0.01	**0.59**	0.05	**4.25**	0.11	**4.10**	0.10	**0.00**	0.02	1.28	0.92	***11***
Total analysis	**77.84**	0.17	**12.16**	0.09	**0.08**	0.01	**0.85**	0.05	**0.06**	0.02	**0.07**	0.01	**0.61**	0.03	**4.16**	0.11	**4.11**	0.06	**0.00**	0.01	**1.15**	0.38	**100**
Lowe *et al.* (2008)																							
T1 (early phase)	**77.61**	0.19	**12.39**	0.11	**0.12**	0.06	**0.79**	0.07	**0.08**	0.05	**0.05**	0.04	**0.51**	0.05	**4.04**	0.12	**4.26**	0.08	-	-	**4.93**	**2.00**	***84***
T2 (late phase)	**77.75**	0.18	**12.32**	0.07	**0.13**	0.05	**0.82**	0.07	**0.07**	0.05	**0.05**	0.04	**0.58**	0.05	**4.01**	0.13	**4.13**	0.15	-	-	**1.83**	**0.50**	***30***
Newnham *et al.* (1998)																							
Kopouatai Bog	**78.22**	0.31	**12.49**	0.15	**0.13**	0.04	**0.76**	0.26	**0.09**	0.13	-	-	**0.55**	0.06	**3.42**	0.19	**4.22**	0.43	-	-	**0.93**	**0.68**	***10***
L. Waiaremoaona	**77.44**	0.28	**12.83**	0.14	**0.12**	0.03	**0.88**	0.10	**0.08**	0.03	-	-	**0.52**	0.07	**3.89**	0.13	**4.09**	0.25	-	-	**6.31**	**1.39**	***11***
Mean values*	**78.00**	0.10	**12.55**	0.06	**0.11**	0.01	**0.81**	0.04	**0.10**	0.01	-	-	**0.55**	0.03	**3.67**	0.06	**4.05**	0.06	-	-	**2.32**	**0.41**	***82***

6.3.2 *Andesitic-dacitic tephras*

Tephras from andesitic volcanoes formed the greater part of primary fall tephras identified in the post-Taupo sequences in this study. Using glass shard geochemistry, stratigraphic information from proximal deposits and in some cases, the established age of the tephra, it was possible to link shard concentrations to known eruption events from the region's andesitic volcanoes. In total it was possible to identify at least nine individual post-Taupo tephras with andesite-dacite chemistry from Mt Ruapehu (Tufa Trig eruptives) and Mt Ngauruhoe of the Tongariro VC (Table 6.2). It is possible that more andesitic tephras are preserved but have not been identified in the sites.

Somewhat surprisingly, none of the individual shard analyses from the sites investigated in this study could be linked to tephras from Mt Egmont (Taranaki; Fig. 6.3) volcano (pre- and post- Taupo Tephra) or any other known pre-Taupo Tephra andesitic tephras. Eruptions from Mt Egmont have been less frequent than from Tongariro (TnG) VC volcanoes but typically significantly larger in size (volume). In the early part of this study, Egmont-derived tephras were considered highly likely candidates to be identified in the sites. This assumption was based largely on past records which showed a prevalence of Mt Egmont-derived tephras in pre- and early Holocene sequences in the Waikato Region and as far as Auckland (e.g., Shane, 2005). In comparison, only very few Tongariro-derived tephras were found in these sites (Lowe, 1988b; Cronin *et al.*, 1996b; Shane *et al.*, 2002; Shane, 2005; Lowe *et al.*, 2008b). The findings from this study suggest there may have been a marked change in the distribution of Egmont tephras in the late Holocene. As suggested in Chapter 5, changes in wind patterns at the end of the last glaciation may help account for the apparent lack of these tephras in Late Holocene sediments in Auckland and

Waikato regions. Egmont-derived Burrell tephras have been identified, although not definitively, in Hawke's Bay sites and may represent the northerly limit of the ash from these post-Taupo eruptions from this volcano (Eden & Froggatt, 1996). The paucity of these tephras in the sites from this study also implies that perhaps, in terms of contemporary volcanic hazard assessment to Auckland and Waikato regions, Egmont eruptions are less significant (in terms of frequency) than previously thought compared with eruptions from Tongariro VC eruptions, (Shane, 2005).

Given the small eruptive volumes of Holocene Tongariro VC tephras, their limited dispersal as a visible tephra unit and 'high weatherability' of the andesitic glasses, previous studies suggest that andesitic tephras would be of much less value than rhyolitic tephras for stratigraphic studies (Donoghue & Neall, 1996; Shane, 2000) (Fig. 6.3). In contrast, this study has shown that andesitic cryptotephras can potentially provide identifiable and distinguishable stratigraphic marker tephras and may have greater resolution than rhyolitic tephras for time periods poorly represented by all other tephras. Especially where identified in combination with the Kaharoa Tephra, as was the case in this study, it is possible that these andesitic tephras could provide very useful stratigraphic markers for a critical time period in New Zealand's history which marks the first arrival of humans on the islands (Lowe *et al.*, 2000). These findings should encourage further work on these tephras including developing a more comprehensive database of the composition of the individual tephras, more comprehensive assessments of their homogeneity or heterogeneity, and the use of trace- and rare-earth elements to help differentiate between different tephra members more effectively. Further work would also be necessary to refine the dates of individual pre-historic tephras if they are to provide definitive age markers for post-Taupo sediments.

The identification of so many andesitic tephras in the medial to distal sites in this study was somewhat surprising given that brown (andesitic) shards were not recorded at all in a previous cryptotephra investigation of a ~5000 year pre-Taupo Tephra sequence from another Waikato peat bog (Gehrels *et al.*, 2006), although some Ruapehu derived tephras have been identified as visible tephras in early Holocene sequences as far as Auckland (Shane & Hoverd, 2002; Shane, 2005). An explanation of this unexpected finding remains unclear but seems likely to involve changes in the dynamics of the Ruapehu Volcano and changes in wind patterns. Mt Ruapehu eruptives were less frequent prior to the Taupo eruption but consisted of many larger magnitude events (Donoghue *et al.*, 1995a; 1995b). This possibility, in combination with changing wind or atmospheric circulation patterns may have resulted in stronger dispersal of Ruapehu-derived tephras across the Waikato and Auckland regions.

Tufa Trig Formation tephras

The andesite-dacite tephras from Mt. Ruapehu volcano formed the dominant source of andesitic volcano derived cryptotephras (eight out of nine) identified in the four sites (Table 6.2). All shard concentrations were found to correlate with Tufa Trig Formation tephras, a group of at least 19 tephra units erupted from Mt Ruapehu since the Taupo Tephra which are compositionally distinct both from older (pre-Taupo Tephra) Mt Ruapehu tephras and from tephras from other Tongariro VC volcanoes (Ngauruhoe and Tongariro) (Donoghue *et al.*, 1995b). The 19 Tufa Trig Formation tephras are recognized as distinct and mappable units in proximal sequences and include the most recent 1995-96 eruptives from the volcano (Tf19) (Donoghue *et al.*, 1995b). The Tufa Trig tephras

identified in the study include some of the larger (more explosive and voluminous) eruptions from the volcano (with a volcanic explosivity index, VEI, of 3 or more) with an eruption frequency of 50-100 years. The Tf members identified in Moanatuatua Reserve include a number of historical eruptions, some of which were likely to have been smaller than some of the pre-historic eruptions identified (i.e. VEI 2).

Previous studies suggested that Tufa Trig tephras, as visible units, have a confined dispersal pattern principally to the east of the volcano and mostly within 20 km of the vent (Donoghue et al., 1997). Few studies have identified the Tufa Trig tephras much beyond the proximal zone of the volcano. The most distal sites where some of these tephras have been identified (Tf5, 6 and 8) (lakes Tutira and Rotonuiaha) are located in Hawkes Bay *ca.* 100 km east of the Tongariro volcanoes (Eden & Froggatt, 1996; Wilmshurst *et al.*, 1997) (Fig. 6.3). The Lake Tutira record consists of cryptic (described as microscopic or very thin) and visible andesitic tephras, mostly derived from Tufa Trig members shown by continuous shard counts. It is possible to identify a number of similarities with the post-Taupo tephra record from Moanatuatua Bog (Fig. 6.5). For example, additional glass concentrations in the Lake Tutira record, attributed to reworking and storm pulses, may in fact represent (primary) cryptotephras when compared with the Moanatuatua record (e.g. Tufa Trig 4, see Fig. 6.6). One difference between the records is the occurrence of an andesitic glass peak in the Tutira record attributed to one of the Burrell Formation tephras (age ca. 295 cal yr BP; Eden and Froggatt, 1996) from Egmont VC. It is possible that this represents the (recognizable) limit of dispersal of the post-Taupo Egmont tephras, none of which have been identified in this study. It is also possible that the tephra may have been misidentified or represents a reworked unit although this is less likely if identified in two cores (Eden & Froggatt, 1996).

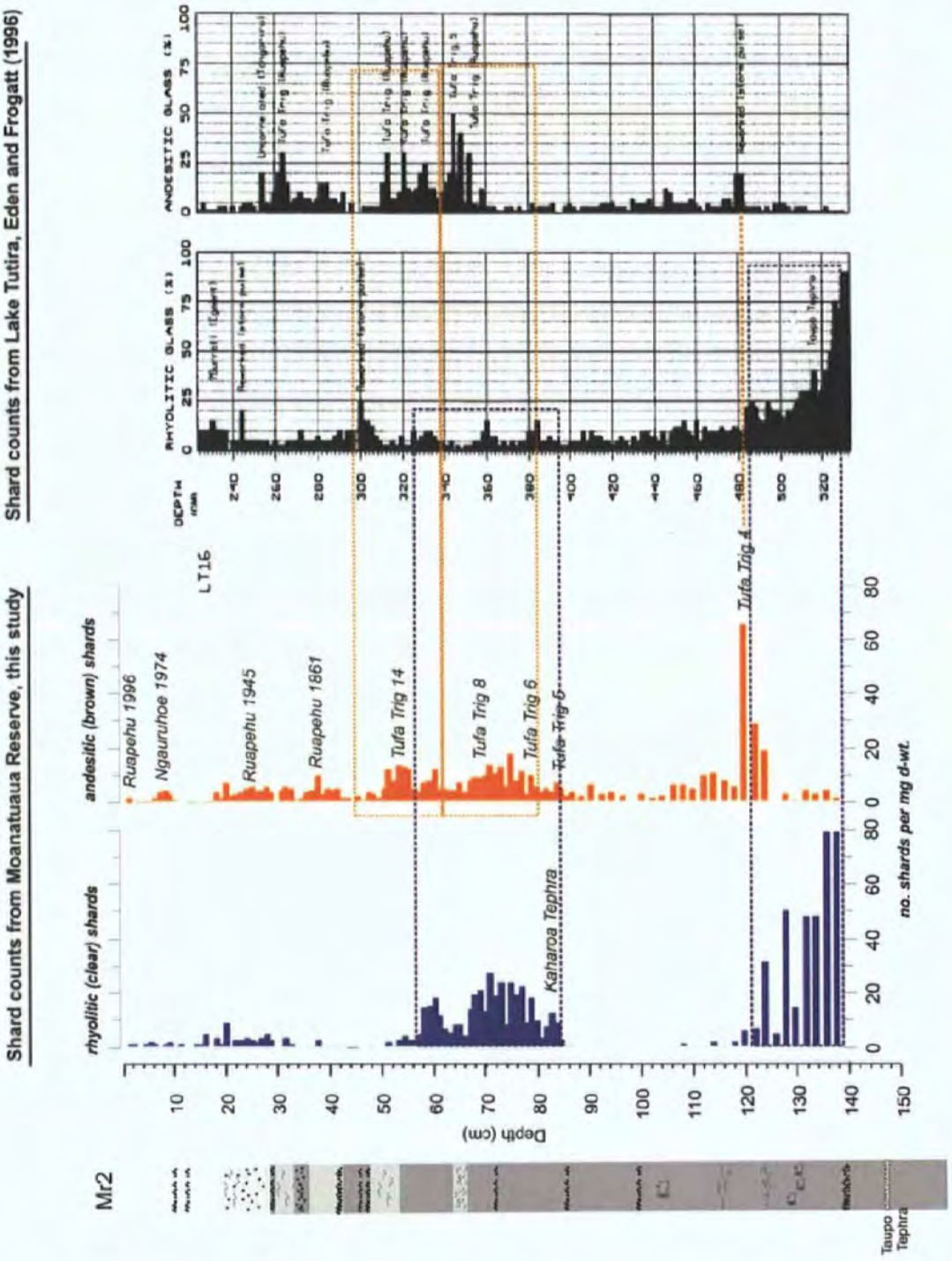

Figure 6.6 Glass shard counts from Moanatuatua Reserve compared with shard counts from Lake Tutira by Eden and Froggatt (1996) (core LT16) showing possible linkages between the different records.

The identification of Tufa Trig tephras as cryptotephra in this study shows that the dispersal ranges of these tephras have been significantly underestimated. The Hawke's Bay sites support a strong eastwards dispersal index of the ash from these eruptions as identified by proximal to medial exposure of the tephras (Donoghue *et al.*, 1995b) (Fig. 6.3). The cryptotephras from this study express northwestwards dispersal (Fig. 6.3). Only much older Ruapehu derived tephras (> ca. 10 000 years BP) have previously been identified in sequences as far north as Auckland (Shane, 2005). As a result of examining the cryptotephra records, it is shown that the Tufa Trig tephras have a much more widespread dispersal than previously demonstrated. Variable dispersal patterns can also be attributed to the contrasting influence of stratospheric and tropospheric winds on the eruption column (Bursik, 1998). Satellite images of the eruption of Mt Ruapehu in 1995-1995, for example, showed that the direction of the eruption column of the different phases of the eruption varied significantly with the wind conditions and the height of the eruption column (Johnston *et al.*, 2000) resulting in multidirectional deposition of ash (Fig. 6.7).

Unlike the caldera volcanoes, the eruptions from the andesitic volcanoes are considerably more moderate in size. The ash plumes from these eruptions are more likely to have been influenced by the turbid westerly winds of the troposphere which extend up to about 17-20 km (varies seasonally) above the Earth's surface at these latitudes (Buck, 1985). This explains why there is a strong eastwards dispersal index for the majority of tephras (including the Tufa trig members, Fig. 6.3) from New Zealand (e.g. Buck, 1985; Nelson *et al.*, 1986; Carter *et al.*, 1995; Donoghue *et al.*, 1995b). However, observations of the 1995 and 1996 events from Mt Ruapehu also showed that the ash plumes of some of the most energetic eruption phases of the eruption extending up into the stratospheric winds, which exert a stronger southwesterly force. This may explain why the finest ash from the most

powerful Tufa Trig eruptions was dispersed in a northeastwards direction from the volcanic source. Further work (including more coring sites) would of course be needed to qualify this more rigorously. It should also be pointed out that further investigations of cryptotephra over a wider region of the North Island may show an even greater variability in dispersal patterns than identified in this study and from visible deposits.

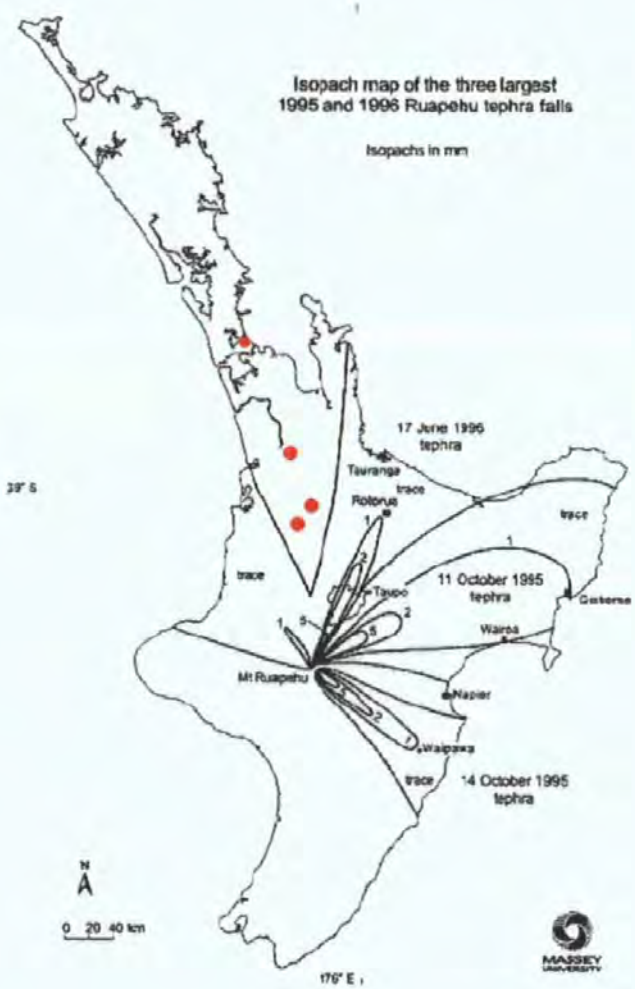

Figure 6.7. Isopach map of ash deposits from three of the main ash-fall events from the 1995 and 1996 Mt Ruapehu eruption. Image from Cronin *et al.* (1998). Dots show the positions of the four sites used in this study.

Differentiating between Tufa Trig tephra members

Tufa Trig tephras were identified using a combination of glass shard characteristics, shard counts and single shard analysis. The stratigraphic context of the shard concentrations was also used to correlate the different units between the sites (Table 6.2). Tufa Trig tephras typically comprised orange-brown blocky shards with abundant mineral inclusions. The distinct geochemical composition of the shards made it possible to identify the source volcano and differentiate the tephras from older andesitic units. Unfortunately, correlating the deposits definitively with individual Tf members was constrained by the fact that there are few published compositional analyses for the different Tufa Trig tephras. The majority of data used were derived from a detailed investigations of proximal deposits by Donoghue et al. (1995b; also see: Donoghue & Neall, 1996; Donoghue *et al.*, 2007). Identification and correlation of the tephras were further limited by the fact that there were very few published ages attached to these tephras.

The compositional analyses of the individual Tufa Trig members from this study and from published analyses presented heterogeneous compositions for the different units (Fig. 6.8a). In most cases there were only very subtle variations between the units identified in the proximal sequences and in some cases it was not possible to distinguish between the different units (Fig. 6.8a) (Donoghue & Neall, 1996). In this study it was possible to recognize a number of compositionally distinct populations by comparing the different glass concentrations. In some cases it was also possible to link these with the published geochemical analysis when supported by other stratigraphic information relating to the thickness of the tephra in proximal sequences. All the prehistoric Tf member tephras identified in this study were linked to the most distinct units in the proximal sequences

(Donoghue *et al.* 1995b). The thickness of the deposit was attributed to the magnitude or productivity of the individual eruption events from the volcano which would normally support a more widespread dispersal. Tufa Trig tephras Tf1, 2, 4, 5, 6, 8 and 14 formed the thickest deposits in the proximal sequences and thus were assumed to be the most likely units to be identified as more widespread tephras. Donoghue *et al.* (1995b) suggested that some of the very thin units identified in the proximal sequences (Tf7, 9, and 15-18) may represent very small eruption events which were thus less likely to have been transported very far from the volcano ring plain. It is possible, however, that the proximal deposits do not adequately reflect the potential for widespread dispersal.

Figure 6.8b shows the mean ranges of the Tufa Trig tephras identified in this site alongside the analyses of Tufa Trig members identified in proximal deposits (Donoghue & Neall, 1996). This diagram shows very good correspondence between the two sources, thus supporting the initial identification of these units (Fig. 6.8b). In comparison, analyses from this study do show slightly greater heterogeneity for all Tufa Trig members, possibly the result of contamination by older Tufa Trig members, because of inherent variability (magma mingling and mixing), or because of the possible impact of microlites during glass analyses (discussed earlier). In general, most Tufa Trig member tephras identified in this study exhibit higher mean SiO_2 values than published analysis which could relate to analytical conditions (Fig. 6.8b; Table 6.3). There is also an apparent trend toward decreasing SiO_2 content for Tufa Trig members through time, at least between Tf4 and Tf8 (Fig. 6.8b). The identification and differentiation between the different member tephras are discussed under the headings for the different units below.

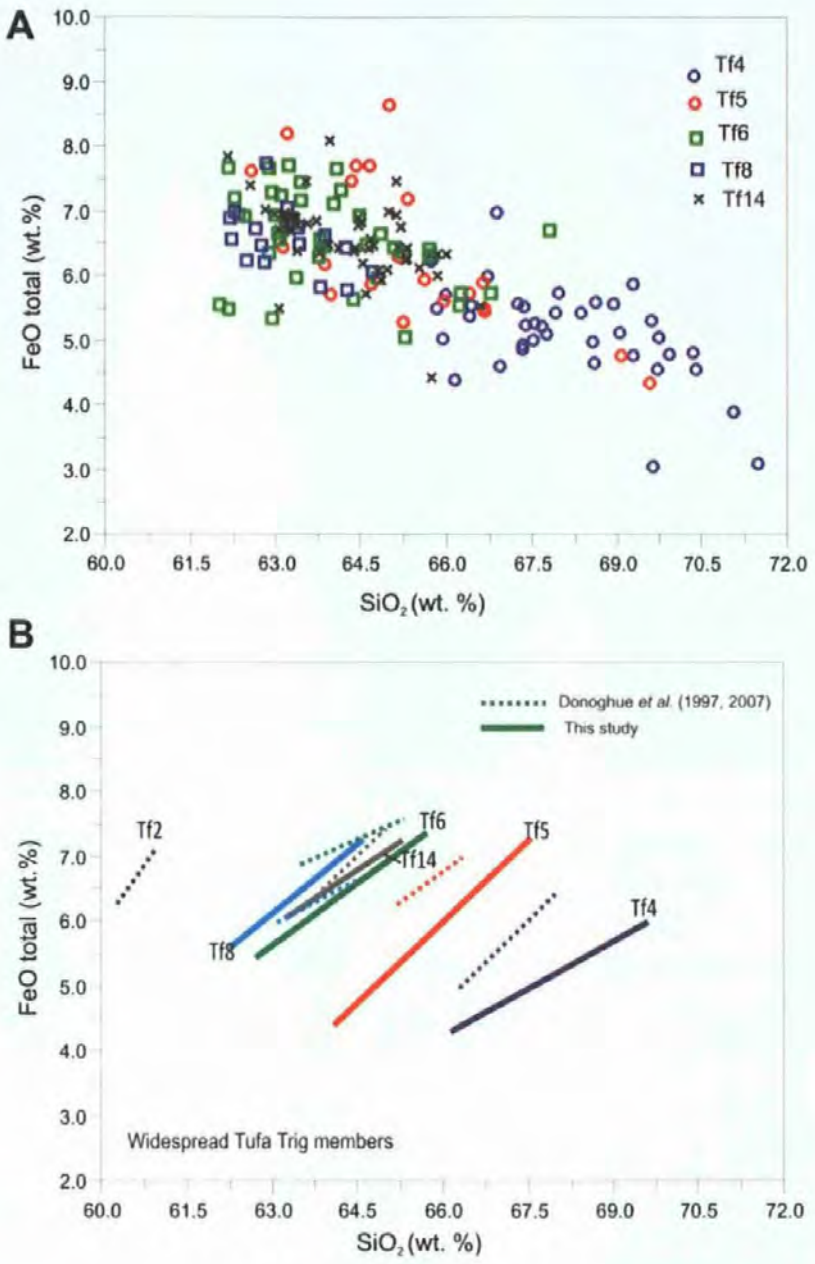

Figure 6.8 Compositional analyses of prehistoric Tufa Trig (Tf) member tephras. A. comparison between the four sites separated into different Tf members. B. Mean and standard deviations of compositional analysis of Tufa Trig tephras from Donoghue *et al.* (1997; 2007) identified in proximal sequences (dashed line) and analyses from this study (shown by solid line).

Table 6.2. Summary of andesitic tephras identified in the four sites including stratigraphic position and interpolated ages. Sites: MR, Moanatuatua Reserve; LR, Lake Rotoroa; OB, Opuatia Bog; LP, Lake Pupuke. Ages: *limitations to age model or glass concentration poorly defined; **significant limitations to age model or glass concentrations poorly defined.

Andesitic tephras identified	Site (core)	Stratigraphic context	Geochemistry And=andesite Dac=dacite	Interpolated age of deposit - cal yr BP (calender date AD) from age models	Pooled age- cal yr BP cal date AD, 2 sd.range (minus **ages)	Published ages - cal yr BP (AD)	References: 1. ages, 2. major element geochemistry
Tufa Trig Tf4	MR (MR2), MB, OB,	Coincides with deline in rhyolitic glass concentrations above Taupo Tephra.	And-dac	1000-1260 (AD 950-690) 1285-1340 (AD 665-610)* 910-1040 (AD 1040-910)**	1221 ±151 (AD 729 ± 151)	1210 ± 150 (AD 740 ± 150)	1. Lowe *et al.* (2000). 2. Donoghue *et al.* (1997)
Tf5	LR, LP (P8_06)	Precedes Kaharoa Tephra (KT)	And-dac	740-860 (AD 1210-1090)* 765-795 (AD 1185-1155)	790 ±51 (AD 1160 ± 51)	Minimum age 571-898 (AD 1378-1052)	1. Wilmhurst *et al.* (2000), 1,2. Donoghue *et al.* (1995)
Tf6	MR (MR2) LR OB LP (P8_06) LP (Puk5)	Mixed with KT glass/coincides with KT or possibly slightly after	And-dac	620-890 (1330-1060)** 700-800 (1250-1150)** 600-750 (1350-1200)* 590-630 (1360-1320) 580-660 (1370-1290)*	635 ±63 (AD 1315 ± 63)	Maximum age 535-660 (AD 1415- 1290)	1,2. Donoghue *et al.* (1997)
Tf8	MR (MR2) MR (MR7) LR	Mixed with reworked KT shards Occurrence post- KT	And-dac	200-440 (1750-1510) 290-330 (1660-1620)* 490-570 (1460-1380)**	315 ± 99 (AD 1635 ± 99)		2. Donoghue *et al.* (1997)
Tf14	MR (MR2) LP (P8_06)	Mixed with Kaharoa Tephra shards	And-dac	160-300 (1790-1650) 220-275 (1730-1675)	238 ±62 (AD 1667 ± 62)		2. Donoghue *et al.* (1997)
Ruapehu 1861 (Tf?)	MR (MR2)		And-dac			AD 1861, February	
Ruapehu 1945 (Tf?)	MR (MR2)		And-dac			AD 1945	1. Gregg (1960); 2. Donoghue *et al.* (1996)
Ngauruhoe 1974	MR (MR2)		And	Age constrained by two historical charcoal layers		AD 1974, 19th February	1.Nelson, (1975); Nairn and Self (1978); 2. Nelson (1975), Donoghue (1995)
Ruapehu 1996 (Tf19)	MR (MR2)	Just below surface	And-dac			AD1996, June 17-18th	2. Donoghue *et al.* (1997)

Table 6.3 Summary compositional analyses of Tufa Trig member tephras (normalised to 100% loss free and averaged) Analysis in bold combined from the sites used in this study, where identified, compared with correlative Tufa Trig tephra members (in normal font) identified in proximal deposits from Donoghue *et al.* (1997 and/or 2007). † Total Fe expressed as FeO. * Cl analysed instead.

Tephra	SiO_2	Al_2O_3	TiO2	FeO†	MnO	MgO	CaO	Na2O	K2O	P_2O_5	H_2O	*n*
Tf4	**67.88 (1.73)**	**13.90 (1.08)**	**1.01 (0.16)**	**5.11 (0.85)**	**0.08 (0.05)**	**1.09 (0.31)**	**3.72 (0.83)**	**3.81 (0.30)**	**3.00 (0.60)**	**0.24 (0.05)**	**1.37 (0.74)**	***42***
Donoghue et al. (2007)	67.24 (0.90)	14.38 (0.53)	1.16 (0.08)	4.77 (0.60)	0.19 (0.11)	1.44 (0.60)	3.70 (0.47)	2.77 (0.44)	3.29 (0.51)	*	0.67 (0.47)	*10*
Tf5	**65.83 (1.72)**	**14.12 (1.68)**	**1.07 (0.13)**	**5.81 (1.44)**	**0.08 (0.07)**	**1.96 (1.64)**	**4.25 (0.82)**	**3.64 (0.36)**	**3.01 (0.47)**	**0.23 (0.05)**	**1.16 (1.01)**	***16***
Donoghue et al. (2007)	65.78 (0.60)	14.36 (0.45)	1.27 (0.14)	5.57 (0.31)	0.17 (0.08)	1.52 (0.31)	4.19 (0.42)	3.08 (0.36)	2.80 (0.35)	*	0.29 (0.53)	*16*
Donoghue et al. (1997)	64.49 (1.02)	15.20 (0.73)	1.03 (0.13)	5.85 (0.40)	0.14 (0.03)	1.82 (0.44)	4.98 (0.50)	3.79 (0.41)	2.66 (0.38)	*	1.00 (0.91)	*12*
Tf6	**64.81 (1.52)**	**14.84 (0.83)**	**1.08 (0.14)**	**5.95 (0.99)**	**0.09 (0.05)**	**1.66 (0.55)**	**4.82 (0.67)**	**4.63 (0.33)**	**1.87 (0.48)**	**0.24 (0.04)**	**1.81 (0.65)**	***43***
Donoghue et al. (2007)	64.30 (0.97)	14.66 (0.50)	1.22 (0.07)	6.01 (0.29)	0.21 (0.13)	1.77 (0.29)	4.36 (0.36)	3.13 (0.49)	2.98 (0.48)	*	0.76 (0.58)	*16*
Tf8	**63.43 (1.17)**	**14.47 (0.57)**	**1.14 (0.09)**	**6.37 (0.83)**	**0.11 (0.08)**	**2.05 (0.57)**	**4.82 (0.45)**	**3.93 (0.29)**	**2.70 (0.32)**	**0.24 (0.03)**	**1.21 (0.62)**	***17***
Donoghue et al. (1997)	63.74 (0.74)	14.87 (0.37)	1.08 (0.07)	6.33 (0.33)	0.19 (-)	2.30 (0.34)	5.08 (0.42)	3.85 (0.24)	2.66 (0.38)	*	0.74 (0.47)	*12*
Tf14	**64.28 (1.05)**	**14.39 (0.59)**	**1.12 (0.10)**	**6.59 (0.59)**	**0.09 (0.06)**	**1.91 (0.35)**	**4.72 (0.44)**	**3.91 (0.24)**	**2.77 (0.30)**	**0.23 (0.04)**	**0.94 (0.72)**	***52***
Donoghue et al. (2007)	64.06 (0.79)	15.18 (0.41)	1.03 (0.22)	5.67 (0.52)	0.17 (0.05)	2.02 (0.32)	4.08 (0.48)	3.94 (0.39)	2.60 (0.78)	*	1.14 (1.00)	*11*
Donoghue et al. (1997)	63.63 (0.29)	14.87 (0.19)	1.08 (0.08)	6.59 (0.19)	0.28 (-)	2.21 (0.11)	5.04 (0.19)	3.81 (0.18)	2.70 (0.22)	*	1.11 (0.61)	*14*
Tf19	**65.34 (1.03)**	**14.12 (0.59)**	**1.12 (0.08)**	**6.25 (0.42)**	**0.10 (0.07)**	**1.68 (0.44)**	**4.33 (0.44)**	**4.08 (0.49)**	**2.75 (0.64)**	**0.23 (0.03)**	**1.49 (0.55)**	***13***
Donoghue et al. (2007)	62.37 (1.11)	15.73 (1.07)	1.01 (0.12)	5.31 (0.50)	0.23 (0.10)	2.42 (0.69)	5.69 (0.79)	3.73 (0.23)	2.34 (0.29)	*	2.35 (1.16)	*17*
Donoghue et al. (1997)	61.98 (1.12)	16.04 (1.05)	0.99 (0.09)	6.19 (0.52)	0.25 (0.10)	2.43 (0.31)	5.99 (0.63)	3.77 (0.21)	2.22 (0.19)	*	2.54 (0.54)	*8*

Ages of Tufa Trig Members

Observational records of eruptions from Ruapehu volcano since 1861 have enabled accurate age determinations of prominent shard concentrations from historic eruptions identified in this study. However, there are few independent ages for the pre-historic Tufa Trig tephras available from previous work. In proximal sequences the different units are identified on the basis of stratigraphic position and visible characteristics of the deposits (Donoghue et al., 1995b). Radiocarbon dates are associated only with Tufa Trig member Tf5 which in turn provide limiting ages for the bracketing tephras Tf4 and Tf6. The relationship of Tufa Trig tephras with well dated post-Taupo eruptions has not been established from previous studies. Eden and Froggatt (1996) found a tephra layer between the Tf5 and Tf6 tephras in Lake Tutira which they identified as the Kaharoa Tephra based on the stratigraphic relationship identified in proximal sequences by Donoghue *et al.* (1995b). However, neither study had geochemical analysis to confirm the identification of the Kaharoa Tephra. What was thought to be the equivalent interbedded tephra, namely Kaharoa, in proximal sequences (e.g. see Price *et al.*, 2000) was later identified as an uncorrelated Egmont VC-derived eruptive based on major element analysis undertaken at a later date (Prof. David Lowe, pers. comm.) (from sample TG561 obtained in 2000 by Dr Barbara Hobden from the Mt Ngauruhoe area: see Price *et al.*, 2000). In this study, the identification of the Kaharoa Tephra interbedded with Tufa Trig tephras for the first time provides more definitive evidence for the stratigraphic relationship between these tephras.

In this study it was possible to establish ages of the different pre-historic Tufa Trig members using age models for the different sites to interpolate shard concentrations. Table

6.2 shows the range of ages from the different cores, including mean (pooled) ages that use the most reliable ages from the different cores – i.e. where glass concentrations are relatively well defined or where the age model of the core is considered fairly robust, or both. Some cores show a very broad age range for certain Tufa Trig members because of the wide spread of the glass concentration in the sediments. Figure 6.9 provides a graphical summary of the age ranges from the different sites for the different Tufa Trig members and includes published ages (red line) and pooled ages (blue lines; also see Table 6.1). The age of the Kaharoa Tephra is also shown in relation to the different Tufa Trig member tephras identified in the sites.

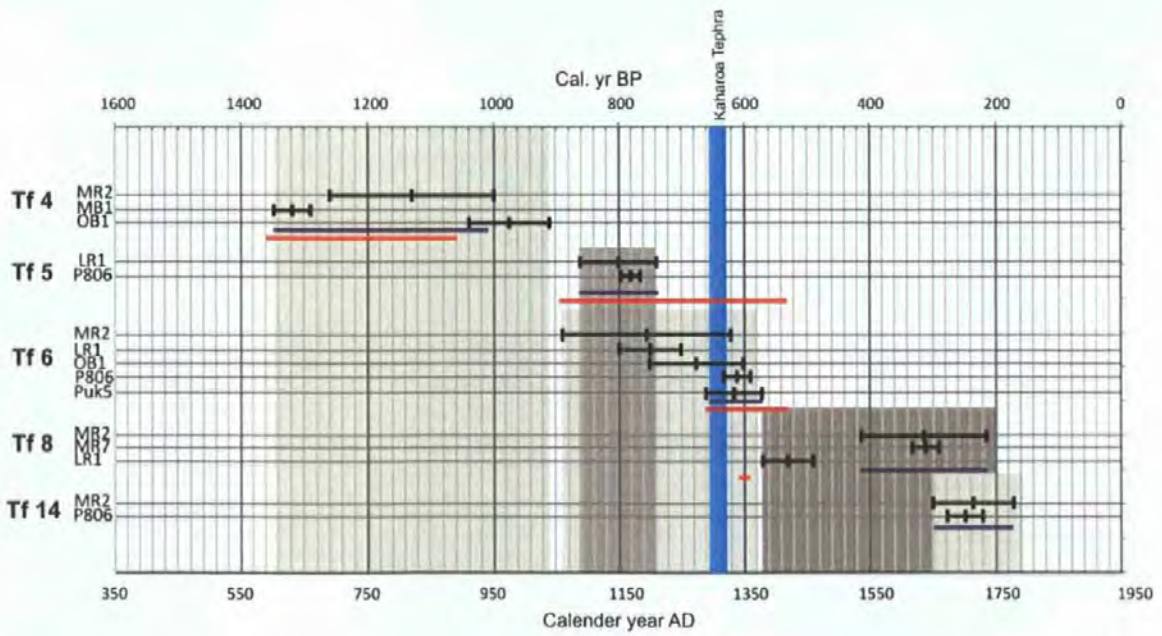

Figure 6.9 Age ranges (2sd) of Tufa Trig member tephras (Tf) identified in the four sites used in this study. Red lines show published age ranges (for references see Table 6.1). Dark blue line indicates mean ages (see Table 6.2). Age of Tf6 is also adjusted to take account of stratigraphic relationship with the Kaharoa Tephra (light blue vertical line).

Tufa Trig Tf4, AD 729 ± 151 (1221 ± 151 cal. yr BP)

Tufa Trig member Tf4 was identified as a distinct peak in brown glass concentrations coinciding with the decline in clear shards above the Taupo Tephra in all sites from the Waikato Region. A possible peak in brown shards in the Lake Pupuke cores is tentatively linked to this tephra based on interpolated age and stratigraphic position but no geochemical analyses were undertaken to support this possible correlation (Fig. 6.2). In proximal deposits the Tf4 tephra is identified as a relatively thin but distinct deposit that stratigraphically overlies the Taupo Tephra (Donoghue *et al.*, 1995b). The Tf4 tephra presents a compositionally distinct population from previous (e.g. Tf2; Fig. 6.8) and all subsequent Tufa Trig members shown from this study and published analysis (Fig. 6.10a; Table 6.3). A comparison with published compositional analysis shows that there is a particularly good correspondence with values for SiO_2 and FeO which are quite distinct from those of other Tufa Trig members (Fig. 6.8; Table 6.3).

The only published age for this tephra is AD 740 ± 150 (1210 ± 150 cal. yr BP), derived from Siebert and Simkin (2002), although the original source is uncertain. It is possible that the age cited represents an interpolation between the Taupo Tephra and the radiocarbon date obtained for the Tf5 tephra in proximal deposits (see Tf5 below; Table 6.2). Nevertheless, the pooled age of this tephra from this study at AD 729 ± 151 (1221 ± 151 cal. yr BP) is compatible with the published age (Table 6.1) despite the variable quality of age models for the different sequences.

Tufa Trig Tf5 AD 1160 ± 51 (790 ± 51 cal. yr BP)

The Tf5 tephra was only identified as a distinct peak in brown shards in the Lake Pupuke cores, stratigraphically underlying the Kaharoa Tephra (Fig. 6.1). A few brown shard analyses were obtained from levels below the Kaharoa Tephra in the Waikato sites but there were insufficient numbers to provide a definitive identification of the tephra in these locations. The Tf5 Member tephra is thought to be the most widely dispersed of the Tufa Trig tephras and has been identified as a visible tephra in a number of Hawke's Bay sites located ~100 km east of the volcano (Eden & Froggatt, 1996; Donoghue & Neall, 1996; Wilmshurst, 1997; Lowe *et al.*, 2002). In some of these sites the Tf5 tephra (in conjunction with pollen analysis) has been used to constrain the onset of human impact in the region in the absence of the Kaharoa Tephra (Wilmshurst, 1997). In proximal deposits the Tf5 tephra forms one of the thickest of the Tufa Trig deposits (Donoghue *et al.*, 1995b).

Compositional analyses of the shard concentrations reveal a heterogeneous population characterized by high standard deviations for individual elements/oxides (Table 6.3). Despite the heterogeneity, the population is compositionally distinct from that of the preceding tephra Tf4 (Fig. 6.10a) and shows subtle variations from subsequent Tufa Trig members (Fig. 6.11a). In Figure 6.8b, mean values of the diagnostic elements SiO_2 and FeO for Tf5 fit between values for Tf4 and Tf6 which follows the pattern of decreasing SiO_2 with decreasing age of Tufa Trig members Tf4-8 shown by published analyses. Other elements show fairly good correspondence with published analyses (Table 6.3). A couple of outlier analyses that correlate with the earlier Tf4 tephra indicate that contamination from older Tf members is a potential problem with subsequent analyses where the compositional differences are less distinct. The composition of glass concentrations

initially identified as Tf5 from Lake Rotoroa shows a quite distinct population from the Tf5 identified in Lake Pupuke. This difference suggests that this tephra may have been misidentified in Lake Rotoroa and could represent (a) a younger Tufa Trig tephra, (b) a reworked unit, or (c) less likely, an unidentified Tufa Trig member which preceded the Kaharoa Tephra. There are, however, several problems associated with the Lake Rotoroa cryptotephra record (see section 4.3) and it is difficult to identify this tephra with any certainty. As a result the Tf 5 analyses from this site were omitted from Table 6.3.

The Tf5 tephra is the only Tufa Trig member that has been targeted for dating in a previous study (Donoghue *et al.*, 1995b). The published ages for this tephra derive from two radiocarbon ages from peat samples taken immediately below (830 ± 60 ^{14}C yrs BP; Wk1489) and above (650 ± 50 ^{14}C yrs BP; Wk1488) the Tf5 tephra (Donoghue *et al.*, 1995b) (Table 6.2). When these dates are calibrated with the current calibration programme (Calib 5.0.2; Stuiver & Reimer, 2005) using the Southern Hemisphere calibration curve (SHCal04), the 2σ age ranges are as follows: 571-898 cal. yr BP below, and 535-660 cal yr BP above. These calibrated dates present a wide potential age range for the deposition of the tephra between 535 and 898 cal. yr BP (AD 1052– AD 1415) (Fig. 6.9). The best age estimates from the cores from this study derive from Lake Pupuke where Tf5 tephra forms a distinct and discrete horizon. The interpolated age (2sd range) for the tephra from this core is 790 ± 51 cal. yr BP (AD 1160 ± 51) which does fit within the known age range for this tephra and possibly provides a more precise age for the tephra (Figure 6.9; Table 6.2). The identification of this tephra at the site also provides more definitive evidence for its stratigraphic relationship with the Kaharoa Tephra. Providing the

age and identification of Tf5 tephra in Lake Pupuke are reliable, the Tf5 tephra would have been deposited *ca.* 103 to 205 years before the Kaharoa tephra.

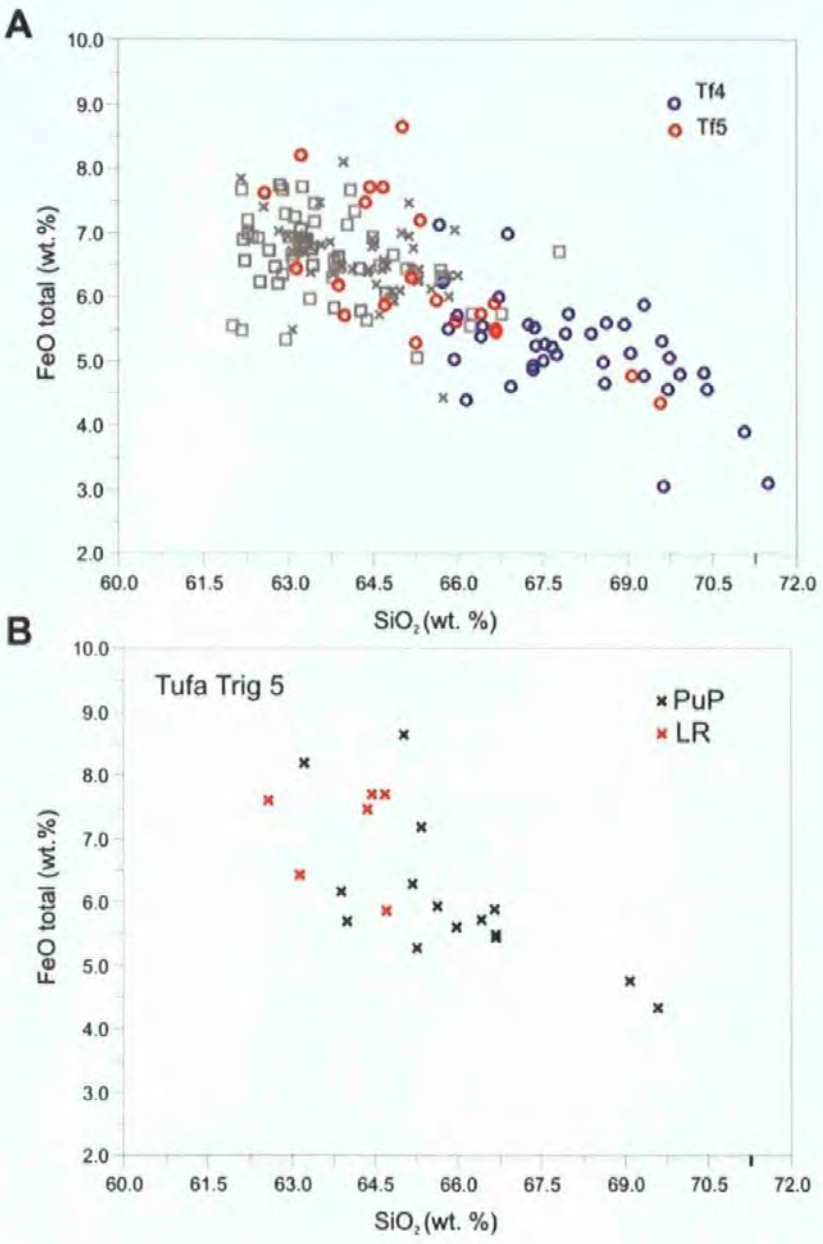

Figure 6.10 compositional analysis of Tufa Trig members. A, Tf4 and Tf5, shown in relation to the post-Kaharoa Tephra Tufa Trig members (in grey). B, Tf5 analysis from the two different cores where it has been identified. Pup, Lake Pupuke cores; LR, Lake Rotoroa.

Tufa Trig Tf6 ca. AD 1314 ± 12 (636 ± 12cal.yr BP)

The Tf6 tephra was identified by a quite distinct peak in brown shards in all sites mixed or slightly overlapping with the cryptic Kaharoa Tephra shard concentration (Fig. 6.1). It is difficult to discern from shard concentrations whether the tephra were deposited simultaneously or a very short time period apart. The Tf6 tephra is identified as a relatively thick and distinct deposit in proximal sequences (Donoghue *et al.*, 1995b). The tephra has been identified in a number of medially positioned sites in sequence together with Tf5 tephra (e.g. Eden & Froggatt, 1996).

The geochemical composition of the Tf6 samples shows one of the most heterogeneous populations of the Tufa Trig member tephras characterized by high standard deviations for individual oxides (Fig. 6.11a; Table 6.3). Plotted using diagnostic oxides SiO_2 and FeO, the Tf6 tephra forms a distinct compositional population from earlier member Tf5 and later member Tf8 (Fig. 6.11a). Separation of the analyses from the different sites reveals that the tephra is inherently heterogeneous and does not show any distinct variability between the different sites (Fig. 6.11b). Compositional analyses show good correspondence with published analyses for the Tf6 tephra particularly with diagnostic oxides SiO_2 and FeO (Table 6.3; Fig. 6.8b).

The maximum age of the Tf6 tephra in published records is 535-660 cal yr BP (AD 1290 to AD 1415) provided from the radiocarbon age obtained from peat taken above the Tf5 tephra in a proximal sequence (see Tf5 above) (Donoghue *et al.*, 1995b). In this study it was difficult to define the exact position of the tephra in all the sites. In Moanatuatua Reserve, for example, the tephra formed a similar spread in shards as the Kaharoa Tephra hence the wide age range estimate at this site. However, in the rest of the sites this tephra is

found more tightly coincident with the well dated Kaharoa Tephra which means that it is possible to constrain the age of the tephra to *ca.* 636 ± 12 cal. yr BP (AD 1314 ± 12) (Hogg *et al.*, 2003).

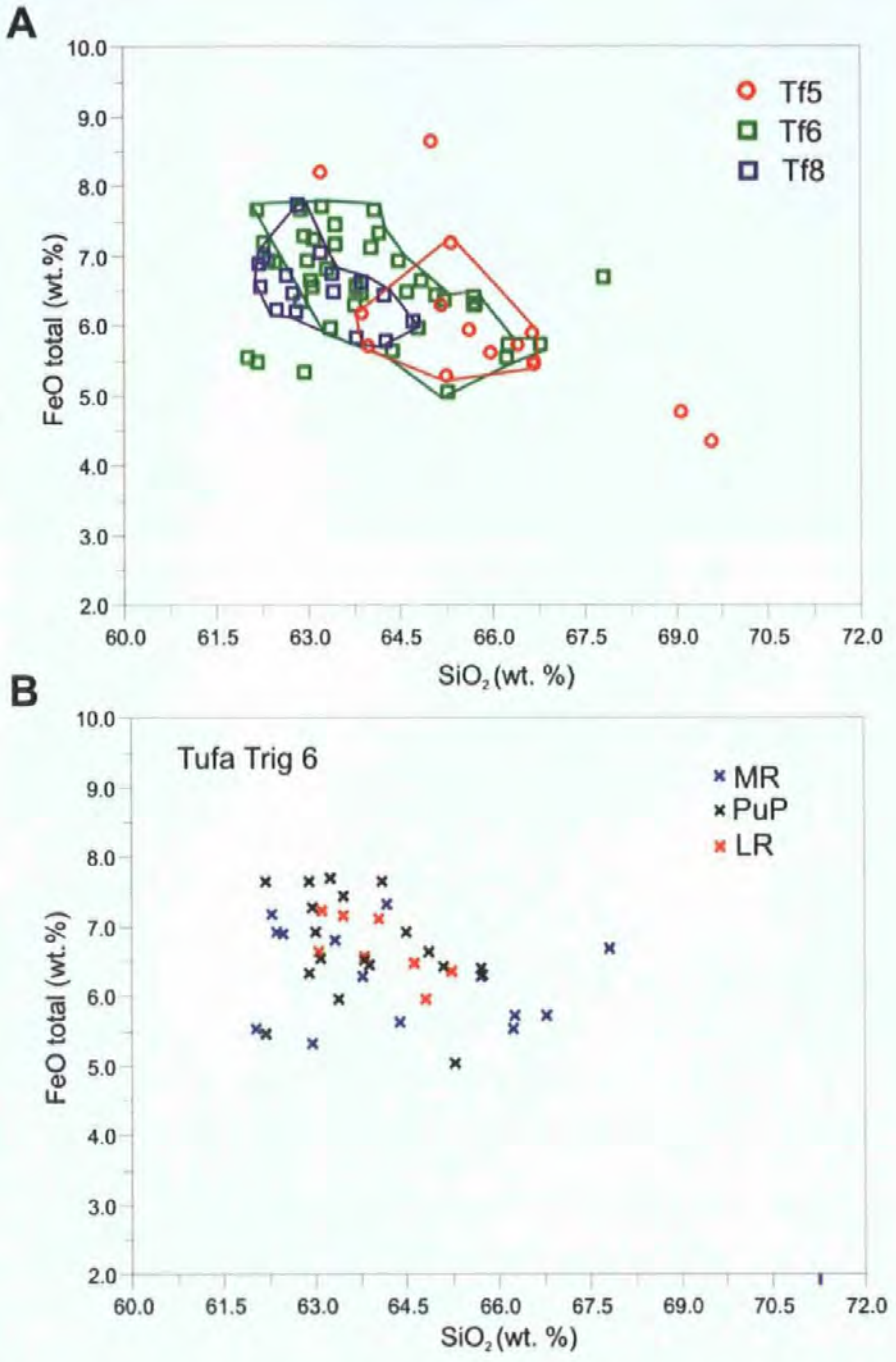

Figure 6.11 compositional analyses of Tufa Trig members. A, Tf5, Tf6 and Tf8. B, Tf6 analysis from three cores. MR, Moanatuatua Reserve; Pup, Lake Pupuke cores; LR, Lake Rotoroa.

Tufa Trig Tf8 ca. AD 1635 ± 99 (315 ± 99cal.yr BP)

The Tf8 tephra was identified in Moanatuatua Reserve and Lake Rotoroa from elevated brown shard concentrations overlying the Kaharoa Tephra in the sediment sequences (Fig. 6.1). A peak in brown shards in Opuatia Bog could be attributed to the Tf8 tephra but there are only few analyses from this site. Tf8 tephra was not identified in Lake Pupuke but it is possible that the tephra could be masked by shards from the local Rangitoto Tephra. The Tf8 tephra is found as one of the thickest deposits of Tufa Trig tephras in proximal sequences and as a result is likely to have been widely dispersed (Donoghue *et al.*, 1995b).

The compositions of the Tf8 tephra from the two sites reveal a relatively homogenous and distinct population compared with preceding Tufa Trig tephras (Fig. 6.11a) and subsequent Tf14 tephra (Fig. 6.12). The analyses for this tephra show very good correspondence with published values for the Tf8 tephra, particularly with the most diagnostic oxides for the Tufa Trig tephras, SiO_2 and FeO (Table 6.3; Fig. 6.8b). The approximate age given to the Tf8 tephra in Donoghue et al. (1995b) was *ca.* 600 cal years BP (*ca.* AD 1350) based on its stratigraphic position relative to the radiocarbon ages for Tf5 and Tf6 tephras (Table 6.2). However, the pooled interpolated ages of Tf8 tephra from the sites used in this study places the age of deposition at 315 ± 99 cal yr BP (AD 1635 ± 99) which is much younger than the previous estimated age (Fig. 6.9). However, there are problems with this interpolated age mainly because the shard concentrations representing this tephra are poorly defined in the sites (see section 6.4). In both sites the Tf8 tephra is preserved within a relatively disturbed zone of the cores which coincides with the early Polynesian era and so the exact (true) isochron of the tephra may be incorrectly identified (Fig. 6.1). The well constrained ages of the bracketing tephras Tf6 (AD 1314 ± 12) and Tf14 (AD 1667 ± 62; see below)

do, however, provide a limiting age range for the deposition of this tephra. In this time interval, the Tf8 eruption could have occurred shortly before, during or shortly after the deposition of the Rangitoto Tephra (dated in this study to AD 1424-1499) which could explain why the tephra was not identified in the Lake Pupuke cores. In Lake Pupuke basaltic shards are persistent in the cores for several centimetres above the visible basaltic tephra which could potentially have obscured any low concentration andesitic tephras deposited at the site.

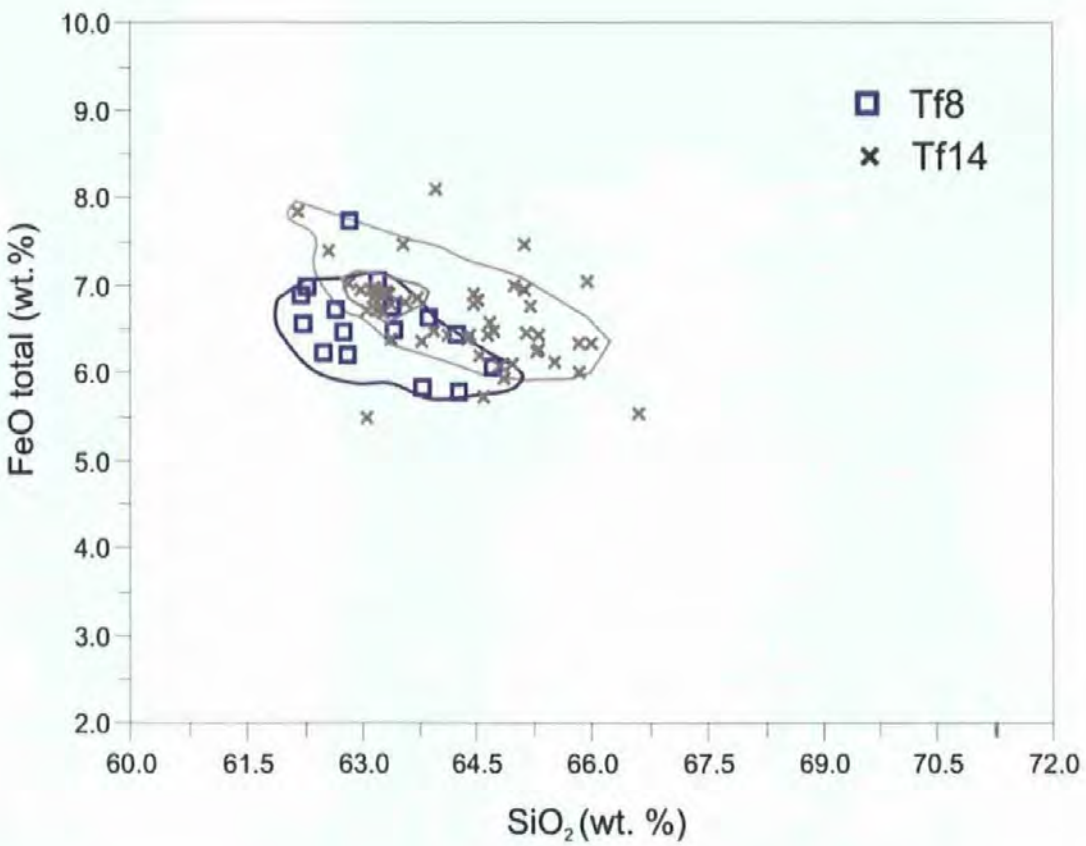

Figure 6.12 Combined compositional analyses of Tufa Trig members Tf8 and Tf14 from the different sites (refer to sections on each tephra).

Tufa Trig Tf14 ca. AD 1667 ± 62 (238 ± 62cal.yr BP)

The Tf14 tephra was identified as a discrete and distinct peak in brown shards in Moanatuatua Reserve and Lake Pupuke (Fig. 6.1). It is likely that it is also preserved in the intervening sites (Lake Rotoroa and Opuatia Bog) but only limited numbers of samples were analyzed from these sites. In Lake Pupuke, Tf14 was identified above the Rangitoto Tephra and before pollen evidence for the arrival of European settlers. Together with Tf8, Tf14 represents the thickest of the Tufa Trig tephras in proximal deposits as identified by Donoghue et al. (1995b) and hence was identified as one of the most likely candidates for widespread dispersal. As a result, the Tf14 tephra member was seen as being the most likely candidate tephra for the cryptotephra identified in the Waikato and Auckland sites.

The Tf14 cryptotephra forms a relatively heterogeneous composition which appears distinguishable from that of the preceding Tf8 composition. The composition also appears to comprise a bimodal population (Fig. 6.12) that is also characteristic of subsequent historical eruptives (Fig. 6.13). Plotted together, the two populations (P1 and P2) appear as one tight cluster (P1: SiO_2 = 63.69 ± 0.27 wt%; FeO = 6.69 ± 0.24 wt%) and one more widely spread population (P2: SiO_2 = 64.69 ± 1.14 wt%; FeO = 6.52 ± 0.75 et%) (Fig. 6.13), possibly representing magma mingling observed in other recent Tongariro VC derived tephras (Griffin, 2007) and in some earlier eruptives (Shane *et al.*, 2008a). Mean values for Tf14 tephra and subsequent Tufa Trig tephras also show a change in the trend evident for Tf4-8, namely decreasing SiO_2 through time, which corresponds with the trend for analyses by Donoghue *et al.* (1995b) (Fig. 6.8b). Analyses of Tf14 and all subsequent Tufa Trig tephras identified in this study appear indistinguishable from one another when plotted in various element combinations (Fig. 6.13). However, the rest of the analyses for

Tf14 do show fairly good correspondence with the two sets of published values for the tephra (Table 6.3; Fig. 6.8b) (Donoghue *et al.*, 1995b; 2007). The variations in the two sets of published data from Donoghue *et al.* (1995; 2007; Table 6.3) are not explained but potentially reflect changes in analytical precision or analytical conditions, or both. It is also possible that the two sets of analyses relate to different populations identified in the cryptic tephras, e.g. as for P1 and P2 detailed above.

There are no published ages for the Tf14 tephra member but it was undoubtedly a fairly voluminous eruption in comparison with other post-Taupo andesitic eruptions and is likely to have occurred prior to European settlement. Where identified in this study, the Tf14 cryptotephra is also separated by several centimetres of sediment from the previous Tufa Trig tephra Tf8 (Fig. 6.1) which could represent a significant time period between these two eruptions. The interpolated ages of the Tf14 tephra from the two sites are in good agreement and provide a pooled age of 238 ± 62 cal. yr BP (AD 1667 ± 62) (Table 6.2; Fig. 6.9). This age determination does overlap significantly with the interpolated age for the Tf8 tephra which was not expected based on the stratigraphic separation of the two tephras. The problems with interpolating an age for the Tf8 tephra, detailed above, are consequently not resolved.

Historical eruptions, identification and significance

Four cryptotephras from Moanatuatua Bog were linked to recorded historical eruptions from volcanoes of Tongariro VC. The preservation quality of cryptotephras in the other three sites used in this study were thought to be compromised as a result of disturbance and

reworking, most likely caused by an intensification of human activities in the last two to three centuries. This disturbance does not, however, preclude the possibility that tephras from these same historical eruptions were deposited at these other three sites. At Moanatuatua Bog, all four historical tephras were identified from elevated concentrations of brown shards. In all cases these tephras appear as relatively low concentrations of shards compared with the peaks of shards from the pre-historic eruptions. It is possible that the higher minerogenic component of samples in this section of the core may have had a dilution effect on the concentration, resulting in an apparently lower total concentration of shards. Further work would be needed to test and adjust (if necessary) for this effect.

The identified tephras include three from Mt Ruapehu eruptives and one from Mt Ngauruhoe. The Ruapehu tephras belong to Tufa Trig members although it is not possible to ascertain from the literature the exact correlative Tufa Trig member name for each of these eruptions because they are characterized by stratigraphic position and not numerical age (Donoghue *et al.*, 1995b). Only the most recent eruption from 1995-1996 is assigned Tf19 in the literature and is the latest in the sequence of Tufa Trig members (Donoghue *et al.*, 2007). The most recent Tf members in proximal deposits, Tf15 to Tf18, were described as very thin, discontinuous deposits close to the soil surface in proximal sequences and each member is likely to be a composite of several ash phases (Dr Sue Donoghue pers. comm., 23 Dec 2008). The description of these historic tephras does, of course, have implications for the potential dispersal range of the other thin Tufa Trig members which were considered to have resulted in only very localized dispersal. There are at least ten other Tufa Trig members identified as thin units in the proximal deposits (Donoghue *et al.*, 1995b). It is therefore possible that one or more of these additional units has the potential to be present in one of the sites.

The identification of the tephra from the 1975 Ngauruhoe eruption was a significant find in this study because it was the only tephra from that source. The 1975 eruption was possibly the largest (in terms of volume and dispersal) of the eruptions from this volcano for several thousand years (Donoghue *et al.*, 1995b; Hobden *et al.*, 2002), which may help explain why additional Ngauruhoe tephras have not been identified in this study. The 1975 event was the only historical eruption that was accompanied by an observation of ash fall on Moanatuatua Bog at the time (Prof. David Lowe pers. comm.). Interestingly, although the original ash fall on the site was visible on the surface of the bog, the consequent shard concentration was manifested as a cryptotephra in the peat rather than as a visible layer. It is likely that the brown colour of the shards means that the tephra is easily obscured in the organic rich or dark coloured sediments or peat. This potential obscuration has implications for interpretation of additional shard concentrations in the sequences which are represented by equal or larger concentrations of glass shards.

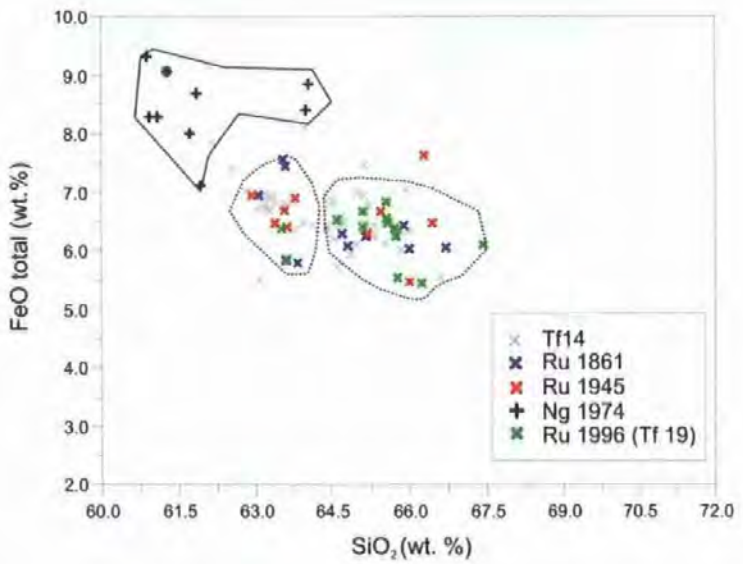

Figure 6.13 Compositional analyses of glass concentrations from historical eruptions shown in relation to Tf14 shard analyses. Ru, Ruapehu Volcano; Ng, Ngauruhoe Volcano

Analyses from all historical tephras exhibit heterogeneous populations (Fig. 6.13). All the Ruapehu-derived tephras showed similar compositions to the Tf14 tephra and are inseparable based on compositional analyses alone. As with Tf14 tephra, it is possible to recognize bi- or multi-modal populations in all the historical Ruapehu tephras. More analyses of these units would be needed to demonstrate the entire range and if there were any differences relating to spatial distribution. There were very limited compositional analyses for the historical Ruapehu tephras, apart from the most recent 1995-1996 eruption (e.g. Nakagawa *et al.*, 2002; Donoghue *et al.*, 2007). The geochemistry from the 1996 eruption and the analyses found in this study did not match well and it was concluded that perhaps the cryptotephra identified on Moanatuatua Bog represented a separate phase or phases of that eruption. There were compositional differences between published analysis from the 1995 and 1996 eruption phases and differences in published analysis of the 1996 eruption depending on the location of the deposits, a reflection of changing magma during the course of the eruption (Donoghue *et al.*, 2007; Platz *et al.*, 2007). As a result, the identification of the historical tephras was thus mainly achieved by comparing the interpolated age of the tephra to the historical records of eruptions. In all cases these were linked to the more voluminous or widely dispersed eruptions from the volcano supported by observational accounts and records. For example, observations of the 1945 Ruapehu eruption recorded widespread dispersal over much of the North Island (McSaveney *et al.*, 2007).

The compositional analysis of the Ngauruhoe tephra is distinct from all Ruapehu-derived tephras identified in this study and it is the only intermediate tephra with a purely andesite chemistry (Fig. 6.13). Because previous compositional analyses of this tephra were limited to mainly X-ray fluorescence, it was not possible to correlate directly the tephra with

proximal deposits using geochemistry although it was possible to use these to identify certain characteristics of the tephra – e.g. high FeO and low SiO2 compared with assays of Tufa Trig members. In addition to the unique composition, the age model of the core, the occurrence of historical charcoal layers, the recorded history of the tephra fall as well as the depth of the tephra in the core, all helped to definitively identify this tephra at the site.

6.3.3 Basaltic tephrostratigraphy

In addition to the rhyolitic and andesitic-dacitic tephras at Lake Pupuke, basaltic tephra-derived glass shards were also identified. The basaltic Rangitoto Tephra, locally an archaeologically significant marker, represents by far the largest (58% of total volume of the field) and most recent eruption of the Auckland Volcanic Field. The eruption resulted in a distinct visible tephra being deposited at the site, recognized in previous studies (Horrocks *et al.*, 2005; Augustinus *et al.*, 2006; Augustinus *et al.*, 2008). Basaltic shards were also present as cryptotephra associated with the Rangitoto Tephra. Concentrations of basaltic glass from reworked older basaltic units were also identified in the site, some most likely derived from the margins of the maar crater.

In this study, the analysis and identification of cryptotephras provided an opportunity to determine the date or timing of the Rangitoto eruption which has been a matter of ongoing debate. Most recently, age modelling has been complicated by evidence from a core taken on adjacent Motutapu Island which suggests that the volcano was the product of two eruption events separated by some time (Nichol, 1992; Cassidy *et al.*, 1999; Horrocks *et al.*, 2005; Needham *et al.*, 2008). On Motutapu Island, Needham *et al.* (2008) reported a

~10-100 cm thick deposit of alkalic basaltic scoria and ash, overlain by 30-50 cm of non-volcanogenic sediment (possibly representing several decades?), and in turn overlain by a much thinner (<5 cm) tholeitic basaltic tephra. Previously, Horrocks *et al.* (2005) had found two thin (1 and 2 mm thick) coarse basaltic ash layers only about 1 cm apart in a core from Lake Pupuke. These were interpreted as separate (but presumably closely spaced) eruptive episodes tapping a changed magma composition during the evolution of Rangitoto volcano because the upper layer was higher in SiO_2. An alternative suggestion, less favoured because of the fresh character of the ash grains, was that the upper layer was reworked detritus from the Pupuke crater rim (Horrocks *et al.*, 2005). In this study, the identification of different compositional groups of basaltic glass in the cryptotephra component adjacent to Rangitoto (9 cm above) is tentatively linked to a possible separate phase or eruption as identified by Needham et al. (2008) and Horrocks et al. (2005) but would require much more detailed work to verify this.

Turning to the timing of the main Rangitoto eruption, assuming this to be expressed as the visible layer in the Lake Pupuke cores, the occurrence of the Kaharoa Tephra and the Rangitoto Tephra in the same stratigraphic sequence represents the first record of these two archaeologically important tephras together. This unequivocal juxtaposition facilitates an independent check on previous estimates for the age of the Rangitoto Tephra, based on the established precise age of the Kaharoa Tephra. The age of the (main) Rangitoto eruption estimated in this way is 564-459 cal. yr BP (AD 1386-1491) based on the 2σ-age models from two cores from Lake Pupuke. This age range aligns well with previous age estimates of 526-451-cal. yr BP (AD 1424-1499) (recalibrated from Nichol, 1992) and estimates using other data including obsidian hydration dating, thermoluminescence and paleomagnetism (Lowe *et al.*, 2000).

6.3.4 Summary

The detection and analysis of cryptotephra in the post-Taupo sediments provides an enhanced tephrostratigraphic record for the sites investigated and offers considerable insights into the eruption history and dispersion of tephra in the region. In addition to the visible Taupo Tephra at the sites, the Kaharoa Tephra and nine andesitic tephras from Mts Ruapehu (8 tephras) and Ngauruhoe (1 tephra) from the Tongariro VC are preserved as cryptotephra, many of which have been recognised in more than one site. The identification of the Kaharoa Tephra in the sediments at all sites provides an extension to this valuable stratigraphic marker to new sites. Because this critical marker tephra is also recorded for the first time in direct stratigraphic association both with Tufa Trig tephras and with the Rangitoto Tephra, it provides an opportunity to establish definitively the stratigraphic relationship between these tephras as well as to date these stratigraphically important but until now poorly dated tephras. The identification of at least eight cryptotephras from the Mt Ruapehu volcano, in addition to the unexpected absence of Egmont tephras, has significant implications for future hazard assessment for the Waikato and Auckland regions. The examination of the visible and cryptotephra components of the Rangitoto Tephra in the Lake Pupuke site also provided additional evidence for ongoing investigations of this archaeologically important tephra and, critically for volcanology, the possible two-stage development of Rangitoto Island. The variability in the cryptotephra records for the different sites was attributed primarily to the varying quality of the sediments in each site which were the result of site specific factors and wider scale environmental conditions. The following section deals with these particular issues.

6.4 Site and environmental factors in the preservation and detection of cryptotephra

As described above, at least ten post-Taupo tephra fall events have been identified from the different sites used in this study, but only four cryptotephras (i.e. the Kaharoa Tephra and three Tufa Trig members) have been identified in all four sites (Fig. 6.2). Although volcanological and meteorological conditions are critically important factors in the spatial and temporal patterns of tephra fall, it is recognised in this study, and in a number of previous tephra studies (e.g. Boygle, 1999; Wastegård *et al.*, 2000a; Enache & Cumming, 2006; de Fontaine *et al.*, 2007; S.M. Davies *et al.*, 2007), that discontinuities in tephra records are also strongly linked to the variable nature of site and environmental conditions at the time of deposition. In this study it has been found that these conditions strongly control the preservation potential of primary fall tephras. It is therefore possible that additional cryptotephras in the sites were simply not recognised, because the shards were poorly preserved or concealed by reworked shards. In the following section, site-specific and environmental factors are discussed in the context of preservation and identification of cryptotephra.

6.4.1 Site Factors

Preservation of primary fall cryptotephra is variable in the four sites and this presented obstacles for tephra identification and for defining accurately the stratigraphic levels in the sediment sequence that mark the primary ash-fall event. Several sedimentary and taphonomic processes were recognized as key determinants for the preservation quality of

cryptotephras (Table 6.4). Sedimentary processes and the geomorphological setting of the peat and lake sites controlled how discretely the tephra layers were preserved and the contributions of reworked shards and minerogenic (non-volcanic ash) particles to the sites. Taphonomic processes, such as bioturbation, can cause post-depositional remobilisation of shards.

It is possible that in some very acidic peats low-silica glass shards (e.g. andesitic tephras) may have been lost due to dissolution (e.g. Hodder *et al.*, 1991). It is important to acknowledge that it is also possible that some shard loss occurred as a result of sample processing. Samples with a large component of minerogenic material required intensive chemical treatment and repeated sieving. Listed below are the main factors identified as beneficial or detrimental for the preservation of cryptotephra in peat and lake sites in this study.

Table 6.4 Summary of site-specific factors affecting cryptotephra preservation

	Sites	Depositional environment	Air fall tephras	Slope wash	Flood in wash	Catchment reworking by wind	Bioturbation	Sediment focusing
Peat sites	**Moanatuatua Bog**	*Raised restiad bog in open plain*	√	—	—	√	?	—
	Opuatia Bog	*Valley restiad bog*	√	—	√	√	?	—
Lake sites	**Lake Rotoroa**	*Enclosed, shallow lake (< 6 m deep)*	√	√	—	√	—	√
	Lake Pupuke	*Deep maar lake (>50 m deep)*	√	√	—	√	—	√

Peat sites

Peat bogs are considered to be effective sediment archives for the preservation and detection of fine tephra falls (e.g. van den Bogaard *et al.*, 2002; Kilian *et al.*, 2003; Payne & Blackford, 2004; Gehrels *et al.*, 2006; Hang *et al.*, 2006; Gehrels *et al.*, 2008) except in special circumstances (e.g. Hodder *et al.*, 1991). The vegetation and moisture of peat-accumulating environments are effective traps for fall-out tephras and, unlike in lakes, glass shards are, in theory, affected by minimal post-depositional remobilisation. The raised surface of ombrogenous bogs, such as those in this study, are isolated from overland flow and inwash and this limits the inputs of non-aeolian minerogenic sediments. The compositional contrast between the peat and the shards allow for easy extraction and identification of cryptic tephra.

The analysis of glass shard content from Moanatuatua Bog resulted in the greatest number of cryptotephras identified of all the sites examined. While the site was the closest of the four to active volcanic sources, a combination of favorable site conditions also meant that it was possible to detect and identify cryptotephras in the sediment sequences with relative ease. The raised surface of the bog and location of the site in an open plain, away from hill slopes, resulted in minimal contributions of reworked shards and minerogenic inputs to the highly organic peat. As a result, cryptotephra content of the different cores from the site showed good replication and an even distribution of ash fall over the site. As suggested in section 6.1, replication in cryptotephra records is an effective way of distinguishing between primary fall and secondary deposited tephras from the shard counts.

It was observed, however, that in Moanatuatua Bog cryptotephra layers were not always preserved as discrete horizons in the peat but were also found as attenuated zones of

shards. In some cases the shards of cryptotephra with a consistent geochemical signature appeared to be spread over several centimetres in the peat. Single or multiple peaks in shard concentrations were found with tails above and below the levels of maximum concentrations (see Fig. 6.2). This attenuated pattern of shards in crypto- and visible-tephra horizons has been observed in cores from other sites and has been attributed to a combination of sedimentary and taphonomic processes (e.g. Hogg, 1979; Zoltai, 1989; Ranner *et al.*, 2005; Gehrels *et al.*, 2006; Hang *et al.*, 2006; Payne *et al.*, 2008; Matthews, 2008).

Shard attenuation poses two main problems for cryptotephra studies. Firstly, it may be difficult to identify the primary fall layer or isochron of the cryptotephra, which can limit the potential of the tephra to provide an accurate and precise age marker. Secondly, because of the relatively slow accumulation rates of peat it may not be possible to distinguish between closely spaced tephra depositional events. In Moanatuatua Bog, the Tufa Trig tephras 5-8 and the Kaharoa Tephra (see Fig. 6.2) formed a complex pattern of overlapping shard concentrations and it was difficult to distinguish between the individual tephras based on the shard counts alone.

Conventionally, cryptotephra investigators in peat sites have placed the original stratigraphic position of the tephra at the maximum concentration of shards in the peat (e.g. Zoltai, 1989; Payne & Blackford, 2004; Ranner *et al.*, 2005; Hang *et al.*, 2006). In doing so these authors assumed that lower concentrations upwards and downwards in the peat resulted from secondary deposition and bioturbation (e.g. Payne & Blackford, 2005). Evidence from this study and from unpublished experimental work sheds new light on these interpretations.

In Moanatuatua Bog, glass shards of the Kaharoa Tephra were found throughout a ~20 cm core section. The primary ash-fall horizon was identified by predicting the stratigraphic position of the well-dated tephra using an independent age model (see section 4.2.6). The age model placed the primary fall layer at the first distinguishable occurrence of the tephra, and not at the highest peak in shards. Assuming the age model is correct, this positioning indicates that downward movement of the glass from Kaharoa Tephra in the peat was not significant, a finding that is supported by recent experimental work (Payne & Gehrels in prep.). A possible explanation is that the primary ash-fall deposits on the bog would have been relatively thin. Subsequent transport (by wind) of tephra to the bog from exposures adjacent to the site would have been persistent for a considerable time so that secondary deposits of the tephra appear in significant concentrations higher in the peat column. Only when the 'source' of the secondary tephra starts to become exhausted do shard concentrations decline – hence the attenuated pattern up through the peat.

Secondary remobilisation and re-deposition of glass shards from exposures or surfaces immediately adjacent to the site may not explain the attenuation of cryptotephra shards in all cases. A number of alternative mechanisms were identified in a previous cryptotephra study of restiad peat bogs (Gehrels *et al.*, 2006). These included the redistribution of tephra on the surface of the bog itself (from hummock to hollow) as a result of localised ponding of rainwater or vertical reworking as a result of bioturbation from plant roots and insect activity. Worms and beetles are abundant in the peats of restiad bogs (Dr Beverley Clarkson, pers. comm. 2007). However, bioturbation would work shards downward into the profile and in the case of the Kaharoa Tephra this mechanism can therefore be discounted.

The identification of primary fall cryptotephras in Opuatia Bog, also a raised restiad peatland but much smaller in area than Moanatuatua, was problematic for other reasons than those identified in Moanatuatua Bog. The complex pattern of cryptotephra contained significant contributions from reworked tephras which are likely to have masked many additional primary fall tephras. It is very likely that the source of this reworked material came from the valley slopes adjacent to the bog (see section 4.4.1) and was transported to the surface of the bog by overland flow or aeolian processes. The impact of periodic flood events from the nearby Waikato River proved to be a significant obstacle for cryptotephra analyses at Opuatia Bog. The floods are recorded by numerous silt-rich layers in the peat sequence, and by historical observations. In these sections of the core, the peat samples required additional physical and chemical treatment to extract the shards, which was not only very time consuming but also may have resulted in some shard loss. Problems in establishing a reliable radiocarbon chronology in parts of the Opuatia Bog sequence may also be the result of the delivery of allochthonous organic material to the site during flood events. These results highlight the importance of geomorphological setting in the selection of suitable sites for cryptotephra investigations.

Lake sites

Lakes are recognized as efficient archives of low concentration tephras (e.g. Ranner *et al.*, 2005; de Fontaine *et al.*, 2007) and, as with peat bogs, represent an almost continuous accumulation of sediments. The maar lakes in Auckland contain long sedimentary sequences that span several glacial-interglacial cycles (Pepper *et al.*, 2004; Shane, 2005; Molloy & Shane, 2007). It is acknowledged, however, that lakes potentially present more

problems for cryptic and visible tephra preservation than peat bogs (S.M. Davies *et al.*, 2007). Slumping, turbidity (wind- generated mixing) and bioturbation are processes which can affect the preservation of cryptic or visible tephra within a lake (Thompson *et al.*, 1986; Boygle, 1999; Wastegård *et al.*, 2000a; Beierle & Bond, 2002; Enache & Cumming, 2006; de Fontaine *et al.*, 2007; S.M. Davies *et al.*, 2007). The reworking and re-deposition of shards from the surrounding catchment can result in significant complications for the interpretation and application of tephra records in lakes (Wastegård *et al.*, 2000a; S.M. Davies *et al.*, 2007). On the other hand, concentrations of tephra can also be enhanced due to the characteristic bathymetry of maar lakes (e.g. Fig. 5.1) and the transport of the shards along the steeply sloping lake bed to the deepest part of the basin ('sediment focusing'). The cryptotephra content of the two contrasting lake sites used in this study highlighted the key roles of sedimentation processes, accumulation rates, lake morphology and catchment conditions for effective preservation and identification of cryptotephra concentrations in lake sediments.

In Lake Rotoroa, a small, shallow basin lake, it was possible to identify four cryptotephra. The enclosed nature of the lake meant that there were very low inputs of minerogenic material into the lake resulting in very slow accumulation rates of organic rich sediments. As a result, cryptotephra were identified as fairly distinct peaks. Extraction of the tephra content from the highly organic sediments was also achieved with relative ease reducing the possibility of shard loss. The four tephras identified in the site, however, represent only half the number identified in Moanatuatua Bog which is located less than 20 km away.

Problems with identifying additional cryptotephra in Lake Rotoroa can be attributed to three main site-specific factors. First, accumulation of the lake sediments was very slow

(~0.17 mm yr^{-1}) and as a result, even with sampling at very high resolution (0.5 cm) it may have not been possible to distinguish between some closely spaced depositional events (e.g. Tufa Trig members 6 to 8). Second, significant contributions of reworked tephra shards were found which are likely to have masked or obscured the occurrence of additional primary fall tephras. As at Opuatia Bog, reworked tephra also proved problematic for the geochemical analyses of the tephras. Shards were likely derived from exposures towards the edge of the lake where older tephra deposits are sometimes exhumed by wave and wind action (Plate 6.1). Although the catchment of Lake Rotoroa is relatively small (138 ha), it is possible that reworked tephra is washed into the lake by overland flow from surrounding hill slopes (slope wash). Third, sediment focusing played a possible role in reworking tephra shards from shallow to deeper parts of the lake (see Blais & Kalff, 1995). Although the lake is shallow (2-6 metres), there were still quite significant variations in the tephra content between the different cores analyzed from the lake. The lack of strong replicability in the cores meant it was difficult, in some cases, to differentiate between primary tephra fall and reworked deposits.

In Lake Pupuke, four post-Taupo cryptotephra were identified from peaks in shards that were easily distinguishable from a low background concentration of reworked glass shards. This lake is a closed basin, like Lake Rotoroa, with a small, steep-sided catchment. The steep bathymetry results in sediment focusing into the deepest parts of the lake where high sedimentation rates make it possible to resolve closely spaced tephra depositional events. This large and deep lake presents several other advantages for tephra preservation (also see de Fontaine *et al.*, 2007). The bottom sediments are unlikely to have been affected by wind driven currents that might lead to sediment mixing. At depth, reduced oxygen in bottom waters produces minimal activity of bioturbating benthic organisms. Large, deepwater

lakes form a stratified water column with favorable conditions for diatom production and the formation of laminated sediments (Sancetta, 1996). Although there are laminations in some sediments from Lake Pupuke, it has not been established if they are annual (see chapter 5). Annually deposited laminae are particularly beneficial for dating tephra layers (Turney & Lowe, 2001). The laminations also provide evidence of the stratigraphic integrity of the sediments and tephras. The chemical extraction of tephra shards from calcareous rich sediments is normally relatively straightforward (Rose *et al.*, 1996). Good replicability was achieved between the two cores from Lake Pupuke for primary fall tephras. However, in one core there were pulses of reworked shards not evident in the other core, possibly indicating localized reworking or slumping of the sediments along the steeply sloping lake bed.

Plate 6.1. Pale yellowish ~8.0 cal ka Mamaku Ash, exposed and hence potentially actively reworked at the peaty edge of Lake Maratoto, North Island. Dinghy paddle for scale. The lake is near both Lake Rotoroa and the Moanatuatua Reserve sites (see Green and Lowe, 1985). Photograph by Prof. David Lowe.

Summary

Peat bogs and lakes offer variable attributes for the preservation and identification of primary fall cryptotephra. Peat bogs are effective traps of fine tephra and the identification of the cryptotephra is straightforward due to the distinct compositional contrasts and relatively fast rates of peat accumulation. The attenuated pattern of cryptotephra in peat can be problematic for establishing the precise stratigraphic position of the primary fall layer and for resolving between closely spaced ash-fall events. Evidence from this study suggests that the first discernable occurrence of the tephra, rather than the level with maximum concentration, is most likely representative of the primary fall layer and thus the mappable and datable isochron. Reworking of allochthonous shards into a bog can result in a vertical spread of shards above the primary fall layer. In selecting peat bogs for cryptotephra studies it is important to consider the geomorphological setting of the site and the possibility of inputs of windblown or fluvial sediments, or both.

Preservation of cryptotephra in lakes can vary significantly depending on the bathymetric and catchment conditions. The two lakes used in this study are closed basins with small catchment areas. They contain homogenous sediments with inputs of reworked shards and minerogenic material which can hinder the identification of cryptotephra. Deep lakes contain better cryptotephra archives than shallow lakes due to the focusing of tephra and reduced potential for disturbance and bioturbation. Finely laminated sediments in deep lakes preserve discrete peaks in shards that are easy to identify and they resolve closely spaced depositional events. Nonetheless, steep catchments deliver allochthonous shards and minerogenic sediments to both shallow and deep lakes, which dilute the primary cryptotephra.

This study has also indicated that anthropogenic activity in the catchment can result in further complications of tephra taphonomic processes, as discussed in the subsequent section.

6.4.2 Environmental factors

This investigation has recognized four distinct temporal patterns in the sedimentary and cryptotephra records, consistent between all sites, suggesting that they could be linked to environmental changes operating at the regional scale (Fig. 6.2). Similar phases of environmental change, resulting from significant natural and anthropogenic events, have been reported previously from this region and elsewhere in New Zealand (e.g. Wilmshurst *et al.*, 1997; Wilmshurst, 1997; McGlone & Wilmshurst, 1999; Newnham *et al.*, 1999b; Lowe *et al.*, 2000; Gomez *et al.*, 2007). Gomez *et al.* (2007), for example, separated the sedimentation record of the last 2 (cal) ka into four main phases: (I) Pre-Polynesian, (II) Maori, (III) European, and (IV) deforestation. The cryptotephra records of this study correspond well to this subdivision but also indicate a period of environmental disturbance following the Taupo eruption as an additional and significant phase (Fig. 6.2). As well, the deforestation record of Gomez *et al.* (2007) is combined with the European arrival (phase IV) in this study. This subdivision of the last ca 2 (cal) ka based on cryptotephra records is explained in the following sections with reference to key correlative tephras and additional chronological information.

Post-Taupo eruption disturbance (phase I)

Earlier work on cryptotephra from the study area (Ballinger, 2003; Gehrels *et al.*, 2006) reported cryptotephra persisting in stratigraphic sequence above the visible Taupo Tephra layer in very high concentrations. A variable but typically progressively attenuating pattern suggests that the Taupo Tephra depositional event was followed by a sustained period of reworking. A similar pattern was observed in all the sequences reported here, consistently following the emplacement of Taupo Tephra and also on occasions postdating other tephra layers. This investigation therefore included opportunity to provide further insight into this phenomenon, referred to as cryptotephra attenuation (Gehrels *et al.*, 2006).

The vertical spread in shards shown by the cryptic Kaharoa Tephra at Moanatuatua Bog and by the visible Rangitoto Tephra at Lake Pupuke accompanied the sustained disturbance activities (deforestation by burning) of early Polynesian settlers (McGlone & Wilmshurst, 1999; Augustinus *et al.*, 2006) as discussed later in this section (see phase III below). In contrast, anthropogenic disturbance cannot be invoked as a factor contributing to the post-Taupo Tephra attenuation because the land was not inhabited until much later. EMPA results showed that the attenuated cryptotephra derives not just from the visible Taupo layers, which at the sites investigated here are not prominent (typically <1 cm thick), but from older tephra sources as well. Also, age models suggest that the time interval between the visible tephra layer and the end of the cryptotephra attenuation may be in the order of *ca.* 300-500 years. Similar studies of the vertical range of tephras (and cryptotephra) have shown that under certain environmental conditions, taphonomic and sedimentary processes can result in the remobilization and re-deposition of components of tephra deposits (mainly glass) for very long periods (Thompson *et al.*, 1986; S.M. Davies

et al., 2007; Matthews, 2008). In addition to this study and earlier work by the author (Gehrels *et al.*, 2006), the post-Taupo attenuation of shards is recognised in a number of spatially disparate sites (Eden & Froggatt, 1996; Wilmshurst *et al.*, 1999; Gomez *et al.*, 2007). Collectively this evidence indicates that a lengthy period of environmental instability with widespread impacts followed the *ca.* AD 233 Taupo eruption.

The most likely cause of this environmental instability is the impact of the eruption itself. A number of sedimentary and palaeoecological records show significant environmental degradation after the eruption, possibly exacerbated by increasing climate variability and fire incidence (Wilmshurst & McGlone, 1996; Horrocks & Ogden, 1998; Wilmshurst *et al.*, 1999; Gomez *et al.*, 2007). The impacts seem similar in pattern although much smaller in scale to those that followed the *ca.* 27.1 cal. ka Oruanui (Kawakawa) eruption, also from the Taupo VC, which occurred at a time of very marked climatic instability early in MOIS 2 and prior to the LGM. This eruption led to widespread and long-lived environmental impact resulting in aeolian and fluvial remobilisation of the tephra for several thousands of years after the eruption (Manville & Wilson, 2004).

Although the Taupo Tephra is relatively thin (<1 cm) in the sites investigated in this study, the eruption was still exceptional in many aspects. The Taupo Tephra event was the most powerful and energetic eruption to have occurred in the world during the last 7000 years. The eruption (in late summer-early autumn AD 233 ± 13, noted earlier) was complex, generating five phases of plinian and phreatomagmatic fall activity and the climax was the extremely violent emplacement of Taupo Ignimbrite, erupted cataclysmically over about 400 seconds by an extremely energetic, hot, ground-hugging pyroclastic flow (density current) moving at 200-300 m/s over a near circular area (~80 km radius) of ~20;000 km^2

around the vents (Wilson, 1985, 1993; Wilson and Walker, 1985; Smith and Houghton, 1995). Its temperature was about 400-500° C at ~50 km from the vents (McClelland *et al.*, 2004). It is likely that the ignimbrite emplacement phase generated a volcano-meteorological tsunami (Lowe and de Lange, 2000). A total eruptive bulk volume for the Taupo event is about 100 km^3 (~30 km^3 as dense-rock equivalent). The thickest fall deposits are found directly to the east of the volcano in the direction of the prevailing winds during the eruption. Areas of the Waikato and Auckland regions received less than ~10 cm (original thickness) of pyroclastic fall (including co-ignimbrite ash) deposits (Wilson & Walker, 1985; Wilson & Leonard, 2008) (see Fig. 6.3). Studies of the impact of the eruption are, as a result, primarily confined to sites very proximal or to the east of the volcano. For example, pollen analyses and palaeoecological studies of post-Taupo sequences are mainly confined to the ignimbrite zone around the volcano or within the ≤~10 cm tephra fallout isopachs (Wilmshurst & McGlone, 1996; Wilmshurst *et al.*, 1997; Horrocks & Ogden, 1998; Wilmshurst *et al.*, 1999) (Fig. 6.3). In these proximal to medial areas there is consistent evidence of a significant reduction in tall forest taxa and a disruption to vegetation succession as a result of the eruption (Horrocks & Ogden, 1998). Within ~80 km radius of Lake Taupo the forests were all flattened by the shock wave generated by the emplacement of the ignimbrite and burnt (the ignimbrite contains numerous charred logs and charcoal). Beyond this zone, tree felling (toppling), burial and defoliation were primary causes for the disruption. Some of these impacts may have been fairly localised (e.g. 80 km zone, Clarkson *et al.*, 1992; Wilmshurst & McGlone, 1996). Within this zone full recovery of forests is thought to take 100-200 years (Wilmshurst & McGlone, 1996) with 'full forest' recovery taking up to ~400 years (Prof. Bruce Clarkson pers. comm.).

In more distal areas, the impact on vegetation is not well established but is likely to have been significant as even small quantities of ash can have detrimental effects on sensitive vegetation (Clarkson, 1990; Kent *et al.*, 2001; Hall, 2003; Hotes *et al.*, 2004). The widely reported increases in fire incidence were partly the result of increases in volumes of dead, or standing trees stripped of leaves, that provided drying fuel, and partly because of a drying climate (Horrocks & Ogden, 1998; Ogden *et al.*, 1998; Gomez *et al.*, 2007). In this investigation, abundant charcoal layers were observed in association with the attenuated post-Taupo cryptotephra at a number of sites. The reduced and more open vegetation cover, due to this combination of volcanic and fire impacts, would have resulted in increased exposure and erosion of the unconsolidated volcanic debris in the area. The breakout flood event and fluvial reworking associated with the thicker Taupo deposits would have also remobilised and transported large quantities of tephra down river systems across much of the North Island for several decades or longer after the eruption (Manville *et al.*, 1999; 2002; 2005; Segschneider *et al.*, 2002). This reworking would have brought additional sources of tephra closer to the study sites. Although Wilson and Walker (1985) suggested that the proximal fall deposits from this eruption appeared to have been little affected by [aeolian] reworking, subsequent work at distal locations including this investigation suggests that remobilisation and transportation of tephra by water and wind occurred on a wider scale and that the prolonged impact of the eruption may have been more widely registered that previously thought.

In summary, it is suggested that a combination of the initial catastrophic environmental impacts of the eruption at proximal and medial sites was followed by frequent and large scale fires in the region as a result of more fire-prone dead and dry standing timber being available, and drier climate conditions, could have resulted in tephra being blown into

depositional sites for possibly hundreds of years following the eruption. The consequence of the high concentrations of shards above the Taupo Tephra is that it was not possible to identify any andesitic cryptotephras within the same stratigraphic interval. If small concentrations of andesitic tephras were preserved, they are likely to be masked by clear shards. In at least two sites used in this study a correlated andesitic cryptotephra (Tufa Trig 4) was identified immediately above the decline in cryptotephra shards to background concentrations, and provides a tie point for this section of the core between the different sites (Fig. 6.2).

Comparative environmental stability (pre-human settlement) (phase II)

Above this interval of the Taupo Tephra attenuation up to where the Kaharoa Tephra is preserved as a cryptotephra there is a fairly distinct pattern in cryptotephra concentrations and core stratigraphy that is suggestive of comparative environmental stability in all the sites (Fig. 6.2). At most sites used in this study, this interval in the cores is characterized by the lowest background concentrations of clear shards and higher than average measurements for organic content (see Fig. 6.2). The only exception to this is at Lake Pupuke where high concentrations of presumably reworked shards recorded in one core only (P8_06) are attributed to a localized erosion event. This exception apart, the comparative environmental stability and reduction in reworked shards meant that it was easier to identify andesitic shard concentrations which were more likely to have derived from primary fall deposits, and two Tufa Trig tephras (Tf4 and Tf5) were consistently found.

These findings are consistent with pollen and other palaeoenvironmental records from the region that indicate that this time interval was a period of relative environmental stability, characterized by dense forest cover (Newnham *et al.*, 1998; 1999b) and a low incidence of natural fires (Horrocks *et al.*, 2005). A more complete vegetation cover and lower fire hazard would have made volcanic deposits less prone to remobilization and reworking. Interestingly, studies from some east coast sites (Lake Tutira and Waipaoa sedimentary system in Hawkes Bay; Fig. 6.3) (Wilmshurst *et al.*, 1997; Gomez *et al.*, 2007) show that although sedimentary conditions (organic content, sedimentation rates etc.) did not appear to return to pre-Taupo Tephra conditions, a new equilibrium of stability appeared to have been reached for this time period. These records also indicate some intermittent disturbances (e.g. fires and landslides) in this time interval, but these are inferred to possibly represent smaller, localised scale events, for example, as a result of tectonic displacements (earthquakes) which are common in that region (Manville & Wilson, 2003).

Arrival of Polynesian settlers and the start of sustained environmental change (phase III)

At all sites the interval bracketed by the Kaharoa and Tufa Trig Tf14 tephras shows a marked change in the pattern of both clear and brown glass shards that corresponds to the period of Polynesian arrival and subsequent moderate environmental impacts (Fig. 6.13). Within this interval, shard concentrations remain elevated and in some cases form very complex patterns. Nevertheless, up to four primary fall tephras were identified in the different sites, including the rhyolitic Kaharoa Tephra and at least three Tufa Trig tephras (Tf6, Tf8, Tf14). In Lake Pupuke this interval also includes the visible Rangitoto Tephra. Geochemical analyses show that there is a degree of reworking of most of these tephras

which has resulted in persistence of the tephras up through the sediment profiles. This is exemplified at Moanatuatua Reserve, where the attenuation of Kaharoa Tephra up through the peat includes multiple peaks that are interpreted as frequent depositional events reflecting disturbance of the tephra near the site.

The evidence pointing to an anthropogenic cause of these disturbances is strong. Kaharoa Tephra, which typically marks the beginning of the disturbance phase, provides a definitive marker for evidence of early human impact associated with the arrival of Polynesian settlers in New Zealand sedimentary sequences (Newnham *et al.*, 1998; Lowe *et al.*, 1998; Wilmshurst *et al.*, 1999; McGlone & Wilmshurst, 1999; 2002; Lowe & Newnham, 2004). In this study, the occurrence of the cryptic Kaharoa Tephra also corresponds with a significant increase in charcoal layers and minerogenic input at both peat and lake sites that can be attributed to human activities in and around the sites. Early Polynesian settlers cleared forest mainly with the use of fire and records of increased charcoal are evident across large areas of New Zealand (e.g. Ogden *et al.*, 1998). Charcoal records from this investigation and in previous studies show a peak frequency in burning events between 700 and 500 (cal) years BP (Ogden *et al.*, 1998). Pollen analysis at Lake Pupuke shows forest clearance commenced soon after deposition of the Kaharoa Tephra but became more pronounced following the Rangitoto Tephra and so may reflect an initially comparatively moderate phase in land clearance followed by later stronger activity in the Auckland Region. In Opuatia Bog this interval also marks the onset of flooding events on the bog from Waikato River which could also be related to human activities.

The period immediately before and after the Kaharoa Tephra also marks a period of increased activity from Ruapehu volcano. The Tufa Trig tephras identified at the sites

include three of the most distinct Ruapehu eruptive units (Donoghue *et al.*, 1995b), each marked by a distinct increase in brown shards (Tf 5, 6, and 8; Fig. 6.2).

Arrival of European settlers and accelerated environmental change (phase IV)

The Tufa Trig tephra Tf14 marks another distinct change in shard concentrations in the different sites that coincides approximately with the arrival of European settlers (late 1700s to early 1800s) and the dramatic changes in the natural environment that followed. Marked changes in the surrounding environment have resulted in very different patterns of shard distribution for each site. In Opuatia Bog, an increase in flood events, in addition to agricultural activities in the hills surrounding the site, resulted in a dramatic increase in reworked shards (Fig. 6.1). In lakes Rotoroa and Pupuke there is an apparent decline in shard concentrations which is the result of increased minerogenic input (shown by increased LOI) and increased sedimentation rates in the lakes. At sites where this minerogenic flux is particularly pronounced, tephra-derived glass concentrations have been diluted and it was not possible to identify any primary fall tephras that could be attributed to historical eruption events. In Moanatuatua Bog, the level of the core marked by an increase in charcoal and a decrease in organic content corresponds with the commencement of large scale drainage of the bog and associated agricultural activity. Fires became more frequent due to sparks from machinery (Clarkson, 1997). Such activity would have resulted in increased disturbance of older tephras. It is not surprising that this interval of the peat included an increase in reworked rhyolitic tephras. Where the very top parts of the sequences are preserved (i.e. Moanatuatua Reserve and Opuatia Bog) it is, however, possible to see a return to more stable conditions in the sites with decline in

reworked tephras and increase in organic content which may be linked to a stabilization of environmental conditions in recent decades as disturbances from agricultural activities were reduced and more land set aside for conservation. For the most part, however, this phase is marked by severe instability and is generally the most problematic in terms of detecting primary fall cryptotephra.

Summary

It is possible to subdivide the *ca.* 1800 year time interval of this investigation into four environmental phases based on the cryptotephra records and other sedimentological indicators. During the first of these intervals (phase I) the disturbance impacts of the Taupo Tephra eruption are indicated by persistence of clear shards above the visible layer possibly resulting from widespread damage of vegetation, increased occurrence of fire and changes in sedimentary processes. Variable climate conditions are likely to have enhanced and extended this period of disturbance meaning that reworking of tephra extended for probably several hundred years following the eruption. The extended reworking of rhyolitic glass meant that it was not possible to identify andesitic tephras in this interval.

The following interval (phase II), bracketed by Tufa Trig members Tf4 and Tf5, reflects the comparative environmental stability after the impact of the Taupo eruption had ceased and before human impacts commenced. This period is characterized by a decrease in reworked shards, linked presumably to increased vegetation cover, which enabled the identification of andesitic primary fall tephras.

The next section, phase III, is bracketed by the Tf5 and Tf14 tephras and represents the commencement of human activities, and perhaps increased activity of Ruapehu volcano. Despite some evidence for disturbance in and around the sites, the effects were comparatively moderate and it was still possible to identify individual cryptotephras.

Following this phase, from Tf14 up to the surface of the cores, phase IV represents a period of more intense environmental changes resulting from the arrival and subsequent activities of European settlers. The result is intense erosion and reworking of tephra deposits and dramatic changes in sedimentation in some sites, making it difficult to identify cryptotephra. Near the top of the sequence (in Moanatuatua Bog) it is possible to identify stabilization following earlier settlement which enabled the identification of deposits from two very recent historical eruptions in 1945 and 1975.

Linking environmental change to cryptotephrostratigraphy represents an important advance in this study in two contrasting ways. These records show on the one hand that the cryptotephra content of a site can be a sensitive indicator of wider scale environmental conditions driven by natural and anthropogenically forced changes in the landscape. On the other hand, it is important to recognize that the relationship of the cryptotephrostratigraphy to the record of ash-fall-producing eruptions is dependent to some extent upon environmental conditions at the depositional site and in particular the degree to which disturbance at the site and in the wider catchment results in remobilized and redeposited tephra. A significant development from this study therefore is recognition that environmental stability acts as a filter which may at times help to reveal and at other times mask the record of volcanic ash fall at that site.

6.5 Implications for volcanic hazard assessment

6.5.1 Introduction

Ash fallout from rhyolitic, andesitic and basaltic eruptions poses one of the most significant threats to New Zealanders living in the region investigated here, with potentially widespread and wide ranging impacts (Scott et al., 1995; Poirot et al., 2004; Bebbington et al., 2008). With an expanding population, an increasingly sophisticated infrastructure and highly developed economy, the population is growing more vulnerable to these impacts (Johnston et al., 2000). Recognition that even very thin deposits of ash can have a significant impact on human and farm animal health and on community infrastructure, both in towns and rural sectors, means that a rigorous assessment of the full range of threats are all the more pertinent (Smith, 2000; Zimanowski *et al.*, 2003; Forbes *et al.*, 2003; US Geological Survey, 2004; Horwell & Baxter, 2006; Newnham *et al.*, 2008). This threat was brought into sharp focus by the 1995-1996 eruption events from Mt. Ruapehu (TnG VC) (Weinstein & Patel, 1997; Cronin *et al.*, 1998; Johnston *et al.*, 2000; Becker *et al.*, 2001; Cronin *et al.*, 2003). Such recent ash-fall events provide a valuable benchmark for understanding the wider threats of this type of eruption, but the very short history of documented events (~170 years) in the region provides only a limited record from which to assess the likely future hazard (Rhoades et al., 2002). Models and estimates of the frequency, thickness and location of future ash fall from the region's volcanoes are therefore determined primarily from the stratigraphic record of tephras (Table 6.5) (Hurst & Smith, 2004; Poirot *et al.*, 2004; Magill & Blong, 2005a; Magill *et al.*, 2006a; 2006b; Bebbington *et al.*, 2008). In this context, the enhanced record of ash-fall events for the

Waikato and Auckland regions developed in this investigation through cryptotephrostratigraphic techniques has critical implications for the assessment of ash-fall hazards in this region.

Table 6.5. Summary of active volcanoes in the North Island and their estimated frequency of occurrence for range of eruption sizes. Source: After Ministry of Agriculture and Forestry (MAF, 2002). Data based on historical, dendrochronological, and tephrostratigraphic records (see Lowe *et al.*, 2002).

Volcano		Last known eruption	Future eruption size (km^3)	Estimated frequency of occurrence
Auckland		~600 cal yr B.P.	small - medium (0.1-2.0)	1000-2000 years
Mayor Island		Probably within last c. 3000 yrs	small - medium (0.1-1)	?1000 years
			large (>1.0)	?10 000 years
White Island		1998 AD	small (<0.01)	1-5 years
			medium (0.01-0.1)	?100 years
			large (> 0.1)	?10 000 years
Tongariro Volcanic Centre	Ruapehu	1996 AD	small (0.01-0.1)	20 years
			medium (0.1-1.0)	100-500 years
			large (>1)	10 000 years
	Ngauruhoe	1975 AD	small (< 0.01)	10-20 years
			medium (0.01-0.1)	100-200 years
	Tongariro	1896 AD	small (<0.01)	100 years
			medium (0.01-0.1)	1000 years
			large (0.1-1)	10 000 years
Egmont		c. 1755 AD	small (<0.01)	300-500 years
			medium (0.01-0.1)	1300-1600 years
			large (<.1)	10 000 years
Taupo		233 ± 13 AD	small (0.1-0.9)	1300-1600 years
			medium (1-10)	2500-5000 years
			large (10-100)	5000-10 000 years
Okataina		1886 AD	medium (1-10)	1500-2000 years
			large (10 20)	2000 5000 years

In this study cryptotephrostratigraphic techniques were used to identify fine ash-fall events in sites in or near to the major population centres of Auckland and Hamilton. The population of greater metropolitan area of Auckland is ca. 1.4 million, approximately one third of the New Zealand population (Statistics New Zealand, 2008). Auckland is also the

country's economic and industrial hub and contains buildings and infrastructure which are extremely vulnerable to the impacts of future ash fall including oil refineries, major power lines and the county's largest international airport. Public health is always at risk to some degree (Johnston *et al.*, 2000; Newnham *et al.*, 2008). Tephra fall from central North Island volcanoes is thought to represent a significant threat to the region in the near future (Newnham *et al.*, 1999a; Edbrooke *et al.*, 2003; Magill & Blong, 2005b; Magill *et al.*, 2006a). Hamilton City and surrounding towns represent the fourth largest urban area in New Zealand with a current population of ca. 200, 000 (based on 2006 census, Statistics New Zealand, 2008). The wider Waikato Region also represents some of the North Island's most productive farmland and cropping land that is recognised as very vulnerable to ash-fall from volcanoes (Gregory & Neall, 1996; MAF, 2002; e.g. Cronin *et al.*, 2003). Also at risk in the Waikato region are hydroelectric and thermal power stations and associated transmission structures, transport and water supply networks, and plantation forests.

It is widely recognised that wind direction and intensity have a major influence over the dispersal of ash and are an important component in modelling future ash fall probabilities (Magill *et al.*, 2006a; Shane, 2007b). The record of ash fall may thus be distorted by prevailing wind patterns which no longer apply to the present (Shane, 2007b). For example, changing wind patterns have been invoked to explain the change in the number of distal andesitic tephras identified in Auckland sites since the end of the last ice age (see Fig. 6.13) (Shane & Hoverd, 2002; Shane, 2007b), although Magill (2007) noted that other processes are important as well with regard to the deposition and preservation of tephras. It has therefore been argued that only recent (Holocene) tephra records can provide realistic scenarios for ash fall distribution and impact to a particular region (Shane, 2007b). This

study focussed on the time period since the AD 233 ± 13 Taupo Tephra eruption to include the most recent ash-fall events which are unlikely to have been deposited under significantly different wind conditions than currently prevail. Investigating this recent time period also provided an opportunity to verify accounts of historically documented ash fall events. Lowe *et* al. (2002) focussed on this time period in evaluating potential impacts of volcanism on early Maori society.

6.5.2 An enhanced records of recent ash fall

As detailed in the previous sections of this chapter, the use of cryptotephrostratigraphic techniques meant it was possible to identify at least ten post-Taupo Tephra (1717 ± 13 cal. yr BP) ash-fall events in the sediments of the four sites within the Waikato and Auckland regions. None of these ash-fall deposits had previously been recognised in any lake sediments or peats in these regions. Nine of the ash-fall events were from the andesitic volcanoes of the Tongariro VC; four of the ash-fall events were identified at the Auckland site. This considerable extension to the known range of ash fallout from these eruption events implies the threat to the Waikato and Auckland regions from future eruptions of these volcanoes is greater than previously thought. Further, the identification of the rhyolitic Kaharoa Tephra as a cryptotephra in the sites also demonstrates that Kaharoa ash was deposited over a much wider area than previously known and hence the potential impact of ash fall from similar rhyolitic eruptions is now evidently much greater and more extensive than considered in any previous hazard modelling (e.g. Bonadonna *et al.*, 2005).

Figure 6.14 shows a comparison of the frequency of ash fall events (calculated to eruptions per 1000 years) obtained from the cryptotephra record from this study (representing the last ~1700 years) and the number of identified visible tephra from published records[3] (representing the last *ca.* 11.5 cal ka, and pre-Holocene, *ca.* 11.5-20 ka[4]) from the vents of the Tongariro Volcanic Centre. No Egmont tephras were identified in this study and cannot be compared. For the ash-fall events from the Tongariro VC at least, Fig. 6.14 illustrates that the detailed cryptotephra records represent an order of magnitude increase in the frequency of events compared with those represented by visible Holocene deposits. The ash-fall events identified in this study can be used to inform assessments of ash-fall hazards in two main ways: (1) by providing an extension to the known range and possible impact of eruption events from the different volcanic sources, and (2) by supporting recalculation of the likely reoccurrence of similar size eruptions from the different volcanic sources affecting the regions in the future. The enhanced records of the main andesitic volcanoes are discussed below.

[3] These records are patchy and very likely incomplete thus far but are the focus of ongoing work (e.g. Molloy & Shane, 2007).

[4] Note that pre-Holocene records of andesitic tephras extend much further back in time. This time period was selected to demonstrate differences between records over a similar time period.

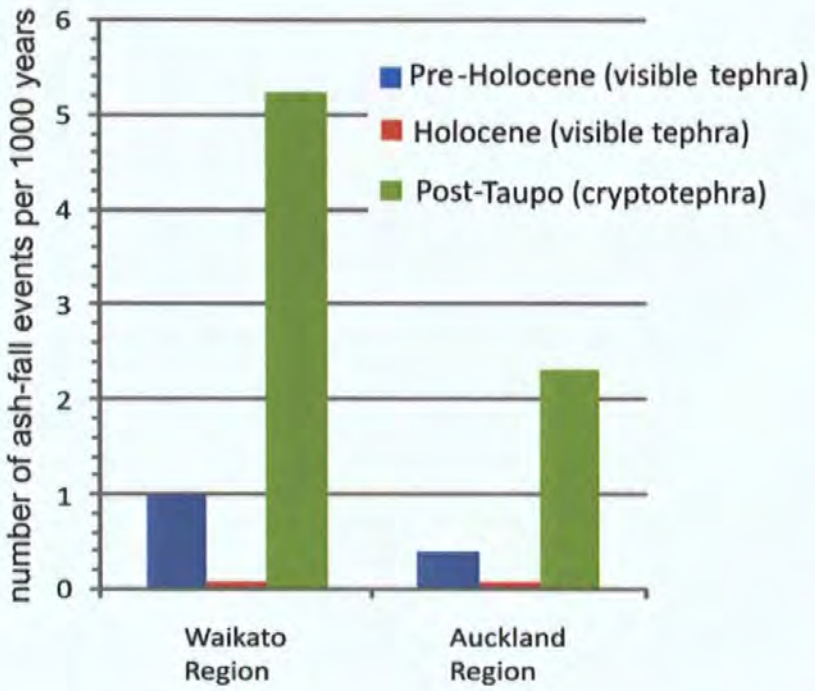

Figure 6.14 Frequency of ash fall events (per 1000 years) from Tongariro Volcanic Centre (TnG VC) identified in sites in the Waikato and Auckland regions. Pre-Holocene, c. 11.5-20 cal. ka; Holocene is post-*ca.* 11.5 cal. ka period. Post-Taupo Tephra record (after 1717 ± 13 cal. yr BP) from this study. For TnG VC tephras, vent sources are combined or undifferentiated. Data sources for number of visible tephras (pre-Holocene and Holocene records) from Lowe *et al.* (1988a; 1988b); Sandiford *et al.* (2001); Shane and Hoverd (2002); Shane (2005); Molloy and Shane (2007).

6.5.3 Threat from Tongariro Volcanic Centre (TnG VC) volcanoes

All nine of the andesitic ash-fall events identified in the Waikato and Auckland sites in this study were derived from Tongariro Volcanic Centre (TnG VC) volcanoes. The three main active vents of the TnG VC, Mt Ruapehu, Mt Tongariro and Mt Ngauruhoe, have been very frequently active in the recent past and are the source of almost all of the most significant andesitic eruptions for mainland New Zealand in historic times (IGNS, 2004). (Offshore White Island or Whakaari has also been very active but eruptions have been of minor significance to North Island coastal communities: Lowe *et al.*, (2002)). During

these historic events, and in particular during the most recent eruptions from Mt Ruapehu (1995-6) and Ngauruhoe (1974-5), ash dispersal was widespread and impacts were significant despite deposition of only very thin ash. The stratigraphic records of post-Taupo ash-fall events from these volcanoes are primarily confined to sites proximal to the volcano (Donoghue *et al.*, 1995b; Donoghue & Neall, 1996; Cronin & Neall, 1997; Hobden *et al.*, 2002).

Only one TnG VC-derived tephra (undifferentiated by vent) has previously been identified as a visible layer in Holocene-aged sequences in distal sites of the Waikato Region (Lowe, 1988a) and as far as Auckland (Sandiford *et al.*, 2001; Shane & Hoverd, 2002; Shane, 2005; Molloy & Shane, 2007) (Fig. 6.14). TnG VC tephras are more prominent in pre-Holocene sequences with ~10 tephras in the Waikato and Auckland regions (Lowe, 1988a; Sandiford *et al.*, 2001). This prominence is probably as a result of stronger wind conditions during the earlier, cold climate phase (Shane, 2005). It is also possible that these represent a different, more powerful, phase of activity from the volcanoes (Neall *et al.*, 1995; Donoghue *et al.*, 1995b).

In this study the identification of ash fall events from TnG VC volcanoes in post-Taupo sediments represents a frequency of ~5.2 events per 1000 years in Waikato Region and ~2.3 eruptions per 1000 years in Auckland compared to 0.1 events per 1000 years from the visible Holocene records (Fig. 6.14).

Ruapehu

Eight out of the nine post-Taupo andesitic tephras identified in this study were linked to the Tufa Trig Formation which represents the most recent phase of eruption activity of the Mt Ruapehu volcano. All tephras were linked to the thickest of ash-fall events from the volcano identified in proximal sequences (Donoghue *et al.*, 1995b) and the largest events of the historic eruptions (1861, 1945 and 1995-1996). The identification of Ruapehu-derived tephras at the sites in Waikato and Auckland regions demonstrates much greater dispersal range of ash fall from this volcano than previously recognised from the tephrostratigraphic record (Fig. 6.3). The tephrostratigraphic records of these recent ash-fall events from the volcano indicate a fairly limited dispersal with most tephras preserved at proximal sites around the volcano (Donoghue *et al.*, 1995b). Several of the thickest (or more voluminous) pre-historic Tufa Trig tephras have been identified as visible and cryptotephra at sites *ca.* 100 km to the east of the volcano in the direction of the prevailing winds (Eden & Froggatt, 1996). The records from this study show dispersal of at least four Ruapehu tephras at least as far as Auckland *ca.* 300 km to the north of the volcano (Fig. 6.3). Because the one visible tephra identified in Holocene sequences is not linked to a particular vent from the TnG VC, these records cannot be compared directly to pre-Taupo Tephra andesitic records. Nevertheless, it has been estimated that pre-Taupo phases of activity from Mt Ruapehu are likely to have consisted of greater magnitude events than the Tufa Trig eruptions (Donoghue *et al.*, 1995b).

Based on the eight ash-fall events identified in the Waikato and Auckland sites, the frequency of ash fall from Ruapehu Volcano represents an average of one per ca. 215 years since the Taupo Tephra. Interestingly, the cryptotephra record shows an increase in ash

fall events in these regions in the latter part of the record consistent with interpretations of proximal deposits (Donoghue *et al.*, 1995b). Seven eruptions are identified in the last *ca.* 900 years (which represents one eruption per 128 years) and three historical ash-fall events large enough to leave a trace in the Waikato Region are identified in the last ca. 170 years (one eruption per ~57 years).

Tongariro

No Mt Tongariro-derived tephras were identified in the post-Taupo sequences in the Waikato and Auckland regions. This volcano has been active for about 260,000 years (Hitchcock & Cole, 2007) and is likely to be the source of at least one substantial ash-fall-generating event (Mangamate Formation) identified in pre-Holocene distal sequences (Lowe, 1988b; Sandiford *et al.*, 2001; Hitchcock & Cole, 2007). The volcano itself is composed of at least 12 separate cones with Mt Ngauruhoe the vent for the most recently active phases of the volcano.

Ngauruhoe

The only additional andesitic cryptotephra identified from the sites in this study is linked to the ash fall of the 1974-1975 eruption from Mt Ngauruhoe. This is the youngest vent in the Tongariro VC and has only been active during the last ~2,500 years. Mt Ngauruhoe was, until 1975, one of the world's most active volcanoes and more than 45 eruptive events or phases occurred during the 20th Century alone (Hobden *et al.*, 2002). The 1975 phase of the eruption was the largest and most recent activity from this volcano in historic times. Although it left a trace in the Waikato Region at the time of the eruption in the form of a

dusting of ash fallout on cars and other surfaces (Nelson, 1975), no ash had been recorded in sedimentary archives (Lowe, 1988b). The cryptotephra was identified only at Moanatuatua Bog, the nearest of the four study sites to the volcanic centre. It is possible that comparatively poor preservation of historically aged sediments prevented detection of this event at the other three sites.

Most activity from this volcano has been small in magnitude (as measured by volume and dispersal for example). The cryptotephra records from this study suggest that previous ash-fall events were not sufficiently large to deposit ash as far as Waikato sites, or possibly that unfavourable winds were prevalent, or both. Earlier, pre-Taupo phases of activity (2500 ± 200 cal. yr BP; Hobden *et al.*, 2002) from the volcano are thought to have been more significant in size than the majority of historically observed tephra-generating events and have been identified in sites several kilometres from the volcano (e.g., the Mangatawai Tephra) (Donoghue *et al.*, 1995b; Hobden *et al.*, 2002). This tephra is very likely preserved at much greater distances as a cryptotephra. A return period of ~1250 years for events of the scale of the 1975 and the Mangatawai Tephra events implies that ash fall from Ngauruhoe does not pose a considerable threat to the Waikato Region in the near future, although the propinquity of the most recent event should caution against complacency.

6.5.4 Threat from Egmont (Taranaki) Volcano

No Egmont Volcano-derived tephras were identified as cryptotephra in any of the sites investigated in this study. Egmont volcano has been frequently active in the recent past, although not in historic times, and has resulted in a number of much larger eruptions compared with those of TnG volcanoes (e.g. Lowe *et al.*, 2002). Visible Egmont-derived

tephras have been identified in a number of distal sites at much greater frequency than TnG VC tephras. As many as 43 (visible) Egmont tephras have been identified in sequences in Auckland spanning the last 70 ka (Sandiford *et al.*, 2001; Shane & Hoverd, 2002; Shane, 2005; 2007b), although almost all of these are restricted to pre-Holocene sequences (Shane, 2005). Only one ash-fall event of Holocene age has been identified in any Auckland site (Sandiford *et al.*, 2001). At least four mid-Holocene Egmont tephras have, however, been found in Waikato peat bogs and lakes (Lowe, 1988b). At least two post-Taupo Tephra aged Egmont-derived tephras have also been tentatively identified in a Hawkes Bay sequence on the east coast of the North Island (Eden & Froggatt, 1996). Based on these records and models of prevailing wind directions, it was previously thought that Taranaki posed the most significant risk to Auckland and Waikato regions from central North Island eruptive centres (Magill & Blong, 2005a; Magill *et al.*, 2006a; 2006b). The findings from this study suggest that this view may need to be revised.

There are a number of possible explanations for the lack of Egmont tephras identified in the sequences from this study. Firstly, it is possible that atmospheric circulation/wind patterns, perhaps in combination with the style of eruptions, have changed since the Late Glacial to favour dispersal from volcanoes in the central North Island, but not from Egmont Volcano. It is also possible that the time period investigated in this study is too short to capture the complete ash-fall record from this volcano. Based on the limited records of these tephras in Holocene sequences, ash-fall events represent an average frequency of one per 2.5 ka. It is also possible that some cryptotephra were inaccurately attributed to TnG VC events using glass chemistry, although this is unlikely. The correlation of the cryptotephra to TnG VC tephras showed a close match to the composition of proximal deposits and can be linked to known events based on stratigraphic

position and relative age. Egmont derived tephras are also typically characterised by much higher K_2O and SiO_2 compositions compared with those of TnG VC tephras (Shane, 2005) (see section 4.2.6 in this thesis). However, the geochemistry of recent Egmont-derived tephras in distal settings is not known with certainty.

6.5.5 Threats from other North Island volcanoes

Okataina Volcanic Centre

The rhyolitic Kaharoa Tephra (Mt Tarawera, Okataina Volcanic Centre, OVC) was the only additional cryptotephra identified in this study in the Auckland and Waikato sites. It derived from the most recent rhyolitic eruption (AD 1314 ± 12) of the region's rhyolitic volcanoes. The most recent activity of the OVC occurred on 10 June, 1886 (the Tarawera eruption) but that event was basaltic. Nevertheless, it is one of only a handful of plinian basaltic eruptions known and the phreatomagmatic phase resulted in locally catastrophic impacts (Lowe, 1990; Nairn *et al.*, 2005). After Taupo VC, the OVC is the second most productive and frequently active large caldera volcano in the world (Wilson, 1993) with an estimated frequency of eruptions of between 1.5 and 5 ka (Table 6.5) (Smith *et al.*, 2006). The identification of the Kaharoa Tephra in all the sites in this study represents an extension to the known range of the ash fall as defined by the visibly preserved tephra and demonstrates that such an eruption today would pose a considerable threat, not previously considered in probabilistic modelling, to these regions. For example, Bonadonna *et al.* (2005) concluded from such modelling that ..."the areas NW, west, and south of Tarawera are likely to receive little tephra fall from a Kaharoa-type eruption. Therefore key cities

such as Hamilton, Auckland, and Wellington are relatively safe from hazardous tephra fall from Tarawera." (p.18). Even though the exact meaning of "little tephra fall" is not given, the probability models imply that nil or negligible fallout is likely to occur on Auckland and Hamilton, which contradicts the new cryptotephra-based findings here. Therefore, the conclusion of Bonadonna *et al.* (2005) that Hamilton and Auckland "are relatively safe from hazardous tephra fall from Tarawera" must now be considered unsound.

Auckland Volcanic Field

The Auckland Volcanic Field has been active for *ca.* 260 ka and has produced at least 49 basaltic volcanoes (Ballance & Williams, 1992). The ash fall from the most recent, and by far the largest (by volume) eruption from Rangitoto Volcano (ca. 550 cal yr BP, refer to section 4.2.1), was preserved as a visible tephra layer. The analysis of basaltic shards from the cryptic tephra-shard component adjacent to the visible tephra did reveal the possibility of additional eruptive phases or eruption events from Rangitoto Volcano (see section 4.2.1 and 6.5.3). If supported, the identification of a second eruptive phase for Rangitoto Island has the potential to develop further recent ideas about multiple events of the Auckland Volcanic Field volcanoes (Needham *et al.*, 2008) rather than the previously held model of monogenetic eruptions (Cassidy *et al.*, 1999). This has the potential to significantly alter perceptions and planning for volcanic hazards in Auckland. The threat from future activity from the AVF is so far unknown because eruption activity in the past has been sporadic and infrequent through time and the probable location of a new vent is uncertain. What is known, however, is that if an eruption of a similar magnitude to Rangitoto were to occur in

the future within the boundaries of Auckland City this would have catastrophic impacts (Edbrooke *et al.*, 2003; Chick *et al.*, 2004; Smith & Allen, 2007; Newnham *et al.*, 2008).

6.5.6 *How can cryptotephra records be used to inform the assessment of ash-fall hazards?*

This study has demonstrated that ash-fall events in the recent past are capable of much greater dispersal range than previously considered. However, one question which may arise from modellers of ash-fall hazards, and planners who attempt to mitigate for such hazards (e.g. Environment Waikato, 1999a) is how cryptotephra records can translate to original ash-fall thickness or some other quantitative parameter such as total mass or mass per unit area from which isomass maps can be drawn (e.g. Connor *et al.*, 2001; Scollo *et al.*, 2006). The thickness of tephra layers is an important guide to potential hazards posed by individual eruptions. There is, for example, a considerable difference between the impacts expected from a very thin (<1 mm) deposit of ash on infrastructure compared with ash layers 1–2 mm or 5–10 mm or more thick (MAF, 2002). Tephra thickness is also an essential component of ash-fall-based numerical models (together with distribution, density, atmospheric considerations, and physics, etc) which provide a measure in which to estimate the original volume or mass of ash (Hurst & Smith, 2004; Poirot *et al.*, 2004; Magill *et al.*, 2006a; Magill *et al.*, 2006b). Although beyond the scope of this thesis, this topic is recognised as an important direction for future work.

6.5.7 Summary

Ten post-Taupo Tephra ash-fall events were identified as cryptotephra in sites from the Waikato and Auckland regions which represents a substantial enhancement to the record of recent ash-fall events in these regions. The nine andesitic tephras from the TnG VC volcanoes, mostly from the Ruapehu Volcano, represent a considerable extension to the known range of many of the pre-historic ash-fall events. In addition, they provide the first geological evidence that match observations of these ash-fall events in historic times. The findings from this study suggest that ash fall from Mt Ruapehu is a much greater threat to regions such as Waikato and Auckland than previously thought. The most recent records suggest future ash fall events could re-occur as frequently as every ~57 years. On the basis of the findings from this study and from the Holocene record of visible tephras, ash fall from Egmont Volcano does not pose as great a threat in terms of return period to the Waikato and Auckland regions in the future. The identification of Kaharoa Tephra also demonstrates a wider dispersal range than previously documented and thus fallout from similar rhyolitic events in the future poses a substantial threat to Auckland and Hamilton regions. The cryptotephra investigations of Rangitoto Tephra and associated basaltic deposits also support the idea that eruptions from Auckland Volcanic Field may be more complex and not monogentic and therefore more of a hazard than previously thought.

CHAPTER 7: CONCLUSIONS, RECOMMENDATIONS AND FUTURE WORK

7.1 Conclusions

The main aim of this study was to develop an enhanced stratigraphic record of ash fall events since deposition of the AD 233 ± 13 Taupo Tephra at selected sites in the Waikato and Auckland regions of the North Island, New Zealand. Cryptotephrostratigraphic techniques were used to detect, quantify and characterise primary tephra-fall events preserved as cryptotephra in sediment cores from two peat bogs (Moanatuatua Bog and Opuatia Bog) and two lakes (Lake Rotoroa and Lake Pupuke). Stratigraphic position, major element geochemistry of glass, and age were used to link identified cryptotephras to volcanic source and where possible to correlate individual eruptive events. This investigation resulted in the following advances and findings.

1. The cryptotephra content derived from the four sites revealed a complex record of tephra deposition, a consequence of both primary fall events from rhyolitic and andesitic volcanic sources and redeposition from older (pre-Taupo) tephra units. A two-stage protocol using stratigraphic and geochemical analysis was developed to differentiate between shard concentrations derived from these two main sources.

This protocol allows for informed decisions to be made based on stratigraphy alone in addition to providing more rigorous assessment though geochemical analysis.

2. Ten individual post-Taupo tephra-fall events were identified as cryptotephra from the four sites, none of which had previously been recognised in the Waikato and Auckland regions. This recognition represents a substantial enhancement to the pre-existing record of ash-fall events. The cryptotephra identified here include the Kaharoa Tephra (AD 1314 ± 12) and nine andesitic tephras from the volcanoes of Mts Ruapehu (8 tephras) and Ngauruhoe (1 tephra) of the Tongariro Volcanic Centre. The TnG VC-derived tephras included five pre-historic Ruapehu-derived tephras of the Tufa Trig Formation (Tf): Tf4, Tf5, Tf6, Tf8 and Tf14. Four cryptotephras were linked to historic ash-fall events including the 1861, 1945 and 1996 events from Mt Ruapehu and the 1975 ash-fall event from Mt Ngauruhoe.

The identification of the Kaharoa Tephra at all sites provides an extension of this valuable stratigraphic marker to new areas of the North Island. This tephra was recorded for the first time in direct stratigraphic association both with prehistoric Tufa Trig tephras and with the Rangitoto Tephra. Such interbedding provided an opportunity to establish definitively the stratigraphic relationship between these tephras as well as providing calendar ages for them (previously these stratigraphically important tephras were poorly or not dated). The new ages established for the Tufa Trig (Tf) tephras are as follows: Tf4, AD 678-780; Tf5, AD 1109-1211; Tf6, AD 1302-1326; Tf8, AD 1635-1734; Tf14, AD 1605-1729.

For the Rangitoto Tephra the age derived from Auckland lake sediment cores is AD 1386-1491 (564-459 cal. yr BP). The examination of the visible and cryptotephra components of the Rangitoto Tephra (derived from the main eruption event) in Lake Pupuke also revealed additional compositional groups which point to the possibility of a two-stage development of Rangitoto Island, an hypothesis which is under examination by other researchers.

3. The geomorphological setting, site and environmental conditions proved to be important factors affecting the preservation and identification of cryptotephra. The protocol for distinguishing primary fall from reworked cryptotephra (see point 1 above) was further developed to take account of these environmental and local site factors. At all sites, reworking of tephra-derived glass shards by lacustrine, aeolian, and fluvial (at Opuatia) or other processes is likely to have obscured some primary fall cryptotephras. This complication is aggravated where sediment accumulation rates are slow, thereby further reducing capacity to distinguish between closely spaced depositional events. At peat sites, the vertical attenuation of cryptotephra proved problematic for establishing the precise stratigraphic position or isochron of the primary fall layer and for resolving between closely spaced ash-fall events. Detailed analysis of the Kaharoa Tephra at one site showed that the first discernable occurrence of the tephra, rather than the level with maximum concentration, is most likely representative of the time of the primary fall layer. At all sites, anthropogenic disturbance resulted in further complications due to greater reworking of catchment material, including glass shards.

4. Cryptotephra from the different sites provided a sensitive indicator of regional environmental changes. It was possible to subdivide the *ca.* 1800-year time interval of this investigation into four environmental phases, based on the cryptotephra records and sedimentological indicators. Because these environmental phases are distinguished largely by the relative degree of reworking of tephra, some broad generalisations can be drawn in terms of the comparative efficacy of cryptotephra techniques for detecting primary fallout layers within each phase. Phase I (*ca.* AD 233–500) represents an extended period of environmental disturbance following, and probably resulting from, the Taupo eruption. This was indicated by the persistence of clear shards above the visible tephra layer probably resulting from widespread damage of vegetation, increased occurrence of fire and changes in sedimentary processes. As a consequence of this extended period of increased reworking, detection of cryptotephra was highly problematic within this interval. Phase II (*ca.* AD 500–1300) reflects a period of comparative environmental stability after the impacts of the Taupo eruption had ceased or diminished and before human impacts commenced. This period is characterized by a decrease in reworked shards, linked presumably to greater catchment stability in general and increased vegetation cover. As a consequence, a comparatively rich suite of andesitic primary fall cryptotephras was detected during this phase. Phase III (*ca.* AD 1300–1800) represents the commencement of human activities in the region. Despite some evidence for disturbance in and around the sites, the effects were at first comparatively moderate and it was still possible to identify individual fallout cryptotephras. Phase IV (after *ca.* AD 1800) represents a period of more intense environmental changes resulting from the arrival and subsequent activities of

European settlers. The attendant severe erosion and reworking of tephra deposits and dramatic changes in sedimentation during this latest phase proved problematic for identifying cryptotephra at all four sites. It follows from these observations that environmental, and catchment stability, in particular, is an important factor in the potential for cryptotephra analyses to determine primary tephra-fall events.

5. The identification of ten post-Taupo Tephra cryptotephra ash-fall events, previously undetected in the Waikato and Auckland regions, has important consequences for the assessment and mitigation of future ash-fall hazard scenarios in these regions. Relative to current knowledge, the record of nine andesitic ash-fall events represents a near five-fold increase in frequency of such events. These records show that ash fall from Mt Ruapehu is a much greater threat to regions such as Waikato and Auckland than previously thought and could re-occur as frequently as every ~57 years. On the basis of the findings from this study, ash fall from the Egmont Volcano does not pose as great a threat in terms of return period to the Waikato and Auckland regions in the future. The identification of Kaharoa Tephra also demonstrates a wider dispersal range than previously documented and thus fallout from similar rhyolitic events in the future poses a substantial threat to Auckland and Hamilton regions, contrary to current modelling-based predictions. The cryptotephra investigations of Rangitoto Tephra and associated basaltic deposits also support the emerging view that ash-fall events from Auckland Volcanic Field may be more complex and more frequent than previously thought.

7.2 Recommendations

Although some limitations have been highlighted, it is clear that considerable future advances in the field of tephrostratigraphy will be made through the careful and judicious application of the techniques and methodology developed and applied in this investigation. In particular, this study has demonstrated that cryptotephrostratigraphic techniques can be applied at medial to distal sites in the North Island of New Zealand to: (1) increase the number of potential isochronous markers in the tephrostratigraphic records from ash-fall events; (2) extend the geographic coverage and hence application of key chronostratigraphic marker tephras (e.g. Kaharoa Tephra); and (3) enhance the historical and geological record of ash-fall events as a guide to future hazard assessment for the main population centres. It is recommended that further investigations that develop these three important research fronts continue apace in this region and other regions of similar setting.

In addition the following specific recommendations are made for future cryptotephra investigations of medial to distal sites in New Zealand or similar volcanic regions.

1. When propensity for reworking is strong, it is advisable to adopt a high resolution sampling strategy both for quantifying cryptotephra content and for geochemical glass analysis, using replicate sequences to help differentiate between primary fall and reworked tephra.
2. Care must be taken with the selection of sites for this type of study to ensure effective preservation and identification of cryptotephra. It is important to consider geomorphological setting of the site in terms of possible inputs of reworked tephra

shards from windblown and or fluvial sediments. Rates of sediment accumulation are an important factor in determining whether closely spaced ash-fall events can be differentiated. It is also important to consider the possible impacts of anthropogenic activity and other exogenous sources of disturbance in or around the site which can result in further complications of tephra taphonomic processes.

7.3 Future work

On completing this study it is recognised that much potential exists for further development in the investigation and application of cryptotephra in this region building on and testing the conclusions described here. Three key areas are identified as important for future work.

1. Further enhancement of the tephra record in these regions by incorporating cryptotephra analysis as a routine adjunct to standard tephrostratigraphic work.

In particular, more records should be developed at sites positioned more distally to volcanic source and representing different time periods. Investigating a longer time period, for example through the Holocene, would increase the possibility of obtaining a more comprehensive record of ash fall (and thus eruption history) from the andesitic volcanoes in the region, including those from Egmont Volcano which have not been recognised in the sites or time period investigated in this study and are poorly represented as visible tephra in Holocene-aged sequences.

Allied to this effort, it is necessary to develop a more comprehensive database of the geochemical fingerprint of andesitic ash-fall events in proximal, medial and distal sites. Such a database would promote the use of these tephras for regional scale correlation, which in turn would help to improve the dating of key events and thus their role as isochrons in high resolution studies. The application of laser ablation ICP-MS for determining the trace and rare-earth elemental composition of individual tephras may prove beneficial for differentiating effectively between compositionally similar andesitic tephra members.

Further application of these methods would provide opportunity to investigate more thoroughly the use of cryptotephras as a sensitive environmental indicator, thus testing the four-phased environmental history of last ~1800 years identified in this study and perhaps contributing to the investigation of environmental change during other intervals and in other regions

2. Methodological developments

If the 'protocol' developed in this study for differentiating between primary fall and reworked cryptotephra is robust, then it should be applicable at other sites in these regions as well as in investigations of other regions where tephra is abundant in the environment and has a propensity to be reworked. It is hoped that future investigations will attempt to apply this protocol and report on its potential as a routine methodological tool in cryptotephra analysis.

3. Informing the modelling and management of ash-fall hazards in the Auckland and Waikato regions.

The enhanced tephrostratigraphic record developed here carries some fundamental ramifications for hazards assessment in these regions. An important development is the realisation that large centres of population such as Auckland may be at far greater risk than previously thought from future andesitic eruptions of Ruapehu in particular. Cryptotephra work is critical to this work on two counts: first it concerns the higher frequency events, previously considered to be of insignificant magnitude, but now recognised as posing a potential threat to human health (as well as societal infrastructure); second, it concerns the detailed, microscopic examination of volcanic particles at the scale most relevant to the human respiration system. For example, although not within the scope of this study, particle size analysis of the finer fraction of cryptotephra in distal sites would enable estimation of the volume of respirable-sized material which in turn could contribute to a probabilistic risk assessment of the ash-fall hazard (e.g. Horwell & Baxter, 2006).

Similarly, as discussed earlier, with further work it should be possible to develop a method for estimating the original mass or thickness of ash on a given site from cryptotephra concentrations in the sediment. It has long been recognised that the thickness of tephra layers is an important guide to potential hazards posed by individual eruptions but growing population concentrations at locations within reach of fine ash-fall events make it increasingly important to incorporate cryptotephra and sub-millimetre scale events in to ash dispersal and depositional models and in to hazards assessment generally.

A final example of the potential role of cryptotephra in hazards assessment arises from the developing notion that volcanoes in the Auckland Volcanic Field may have experienced multiple eruptions, including possibly small scale precursors to the main event(s). If true, there are considerable implications for volcanic planning in Auckland, which hitherto has assumed the AVF volcanic centres are essentially monogenetic. This study points the way to using cryptotephra to investigate these possibilities further.

References

Aaby B, Berglund BE. 1986. Characterization of peat and lake deposits. In: Bergland BE, ed. *Handbook of Holocene Palaeoecology and Palaeohydrology*. John Wiley & Sons Ltd., 231-246.

Alloway B, Neall VE, Vucetich CG. 1995. Late Quaternary (post 28,000 year BP) tephrostratigraphy of northeast and central Taranaki, New Zealand. *Journal of the Royal Society of New Zealand* **25:** 385-458.

Alloway BV, Larsen G, Lowe DJ, Shane PAR, Westgate JA. 2007. Tephrochronology. In: Elias SA, in chief, eds. *Encyclopaedia of Quaternary Science*. London: Elsevier, 2869-2898.

Anderson RY, Nuhfer EB, Dean WE. 1984. Sinking of volcanic ash in uncompacted sediment in Williams Lake, Washington. *Science* **225:** 505-508.

Augustinus P. 2007. NZ-Maars: Extracting high resolution palaeoclimate records from maar lakes, Auckland, New Zealand. *Pages News* **15:** 18-20.

Augustinus P, Bleakley N, Deng YB, Shane P, Cochran U. 2008. Rapid change in early Holocene environments inferred from Lake Pupuke, Auckland City, New Zealand. *Journal of Quaternary Science* **23:** 435-447.

Augustinus P, Reid M, Andersson S, Deng Y, Horrocks M. 2006. Biological and geochemical record of anthropogenic impacts in recent sediments from Lake Pupuke, Auckland City, New Zealand. *Journal of Paleolimnology* **35:** 789-805.

Ballance PF, Williams PW. 1992. The Geomorphology of Auckland and Northland. In: Soons JM, Selby MJ, eds. *Landforms of New Zealand*. Auckland, New Zealand: Longman Paul, 210-232.

Ballinger MJ. 2003. *Developing methods for identifying cryptic tephra in peat cores from the Waikato region, North Island, New Zealand.* MRes, The University of Plymouth, UK.

Barber KE. 1993. Peatlands as scientific archives of past biodiversity. *Biodiversity and Conservation* **2:** 474-489.

Bebbington M, Cronin SJ, Chapman I, Turner MB. 2008. Quantifying volcanic ash fall hazard to electricity infrastructure. *Journal of Volcanology and Geothermal Research* **177:** 1055-1062.

Becker J, Smith R, Johnston DM. 2001. Effects of the 1995-1996 Ruapehu eruptions on communities in central North Island, and people's perceptions of volcanic hazards after the event. *The Australasian Journal of Disaster and Trauma Studies* **2001-1**.

Beierle B, Bond J. 2002. Density-induced settling of tephra through organic lake sediments. *Journal of Paleolimnology* **28:** 433-440.

Bell BD. 1986. The Conservation status of New Zealand wildlife. Occasional Publication 12. Wellington, New Zealand, New Zealand Wildlife Service, Department of Internal Affairs.

Bennett K, Boreham S, Sharp MJ, Switzur VR. 1992. Holocene history of environment, vegetation and human settlement on Catta Ness, Lunnasting, Shetland. *Journal of Ecology* **80:** 173-241.

Blackford JJ, Chambers FM. 1993. Determining the degree of peat decomposition for peat-based palaeoclimate studies. *International Journal of Peat* **5:** 7-24.

Blais JM, Kalff J. 1995. The Influence of Lake Morphometry on Sediment Focusing. *Limnology and Oceanography* **40:** 582-588.

Blockley SPE, Lane CS, Lotter AF, Pollard AM. 2007. Evidence for the presence of the Vedde Ash in Central Europe. *Quaternary Science Reviews* **26:** 3030-3036.

Blockley SPE, Pyne-O'Donnell SDF, Lowe JJ, Matthews IP, Stone A, Pollard AM, Turney CSM, Molyneux EG. 2005. A new and less destructive laboratory procedure for the physical separation of distal glass tephra shards from sediments. *Quaternary Science Reviews* **24:** 1952-1960.

Bonadonna C, Connor CB, Houghton BF, Connor L, Byrne M, Laing A, Hincks TK. 2005. Probabilistic modeling of tephra dispersal: Hazard assessment of a multiphase rhyolitic eruption at Tarawera, New Zealand. *Journal of Geophysical Research-Solid Earth* **110**.

Boygle J. 1999. Variability of tephra in lake and catchment sediments, Svinavatn, Iceland. *Global and Planetary Change* **21:** 129-149.

Briggs RM, Houghton BF, Mcwilliams MO, Wilson CJN. 2005. 40Ar/39Ar age of silicic volcanic rocks in the Tauranga-Kaimai area, New Zealand: dating the transition between volcanism in the Coromandel Arc and the Taupo Volcanic Zone. *New Zealand Journal of Geology and Geophysics* **48:** 459-469.

Browne K, Campbell DI. 2005. Ecohydrological characteristics of Opuatia Wetland and recommendations for future management. Brown, E. 2005/17, 1-50. 2005. Hamilton, New Zealand, Envronment Waikato, Waikato Regional Council. Environment Waikato Technical Report.

Buck MD. 1985. An assessment of volcanic risk on and from Mayor Island, New Zealand. *New Zealand Journal of Geology and Geophysics* **28:** 283-298.

Buckland PC, Foster P, Perry DW, Savory D. 1981. Tephrochronology and Palaeoecology: The value of Isochrones. In: Self S, Sparks RSJ, eds. *Tephra Studies - Proceedings of the NATO Advanced Study Institute "Tephra Studies as a tool in Quaternary Research", held in Laugarvatn and Reykjavick, Iceland, June 18-29, 1980.* Dordrecht: D.Reidal Publishing Company, 381-389.

Bursik M. 1998. Tephra Dispersal. In: Gilbert JS, Sparks RSJ, eds. *The physics of Explosive Volcanic Eruptions*. London: Geological Society Special Publications 145, 115-144.

Campbell DI, Laybourne CE, Blair IJ. 2002. Measuring peat moisture content using the dual-probe heat pulse technique. *Australian Journal of Soil Research* **40:** 177-190.

Campbell EO. 1975. Peat deposits of northern New Zealand as based on identification of plant fragments in the peat. *Proceedings of the New Zealand Ecological Society* **22:** 57-60.

Carter L, Nelson CS, Neil HL, Froggatt PC. 1995. Correlation, Dispersal, and Presentation of the Kawakawa Tephra and Other Late Quaternary Tephra Layers in the Southwest Pacific-Ocean. *New Zealand Journal of Geology and Geophysics* **38:** 29-46.

Carter L, Shane P, Alloway B, Hall IR, Harris SE, Westgate JA. 2003. Demise of one volcanic zone and birth of another - A 12 my marine record of major rhyolitic eruptions from New Zealand. *Geology* **31:** 493-496.

Cassidy J, Locke CA, Miller CA, Rout DJ. 1999. The Auckland Volcanic Field, New Zealand: geophysical evidence for its eruption history. In: Firth CR, McGuire WJ, eds. *Volcanoes in the Quaternary*. Geological Society, London, Special Publication 161, 1-10.

Chambers FM, Daniell JRG, Hunt JB, Molloy K, O'Connell M. 2004. Tephrostratigraphy of An Loch Mor, Inis Oirr, western Ireland: implications for Holocene tephrochronology in the northeastern Atlantic region. *Holocene* **14:** 703-720.

Charman DJ, West S, Kelly A, Grattan J. 1995. Environmental-Change and Tephra Deposition - the Strath-Of-Kildonan, Northern Scotland. *Journal of Archaeological Science* **22:** 799-809.

Chick L, Williams A, Linzey A, Williams K. 2004. Cities on Volcanoes - Preparing for an eruption from Auckland Volcanic Field. *TEPHRA.Living with Volcanoes* **21:** 32-37.

Clarkson B. 2004. Vegetation and peat characteristics in the development of lowland restiad peat bogs, North Island, New Zealand. *Wetlands* **24:** 133-151.

Clarkson BD. 1990. A Review of Vegetation Development Following Recent (Less-Than 450 Years) Volcanic Disturbance in North Island, New-Zealand. *New Zealand Journal of Ecology* **14:** 59-71.

Clarkson BR. 1997. Vegetation recovery following fire in two Waikato peatlands at Whangamarino and Moanatuatua, New Zealand. *New Zealand Journal of Botany* **35:** 167-179.

Clarkson BR. 2002. Swamps, fens and bogs. In: Clarkson, B. D., Merrett, M., and Downs, T. Botany of the Waikato. Waikato Botanical Society.
Ref Type: Serial (Book,Monograph): 49-58.

Clarkson BR, Clarkson BD, Patel RN. 1992. The pre-Taupo eruption (c. AD 130) forest of the Bennydale-Pureora district, central North Island, New Zealand. *Journal of the Royal Society of New Zealand* **22:** 61-76.

Clarkson BR, McGlone MS, Lowe DJ, Clarkson BD. 1995. Macrofossils and Pollen Representing Forests of the Pre-Taupo Volcanic-Eruption (C.1850 Yr Bp) Era at Pureora and Benneydale, Central North-Island, New-Zealand. *Journal of the Royal Society of New Zealand* **25:** 263-281.

Clarkson BR, Schipper LA, Lehmann A. 2004. Vegetation and peat characteristics in the development of lowland restiad peat bogs, North Island, New Zealand. *Wetlands* **24:** 133-151.

Clayton JS, de Winton MD. 1994. *Lake Rotoroa: Change in an urban lake.* NIWA Ecosystems Publication No.9.

Cole JW. 1990. Structural Control and Origin of Volcanism in the Taupo Volcanic Zone, New-Zealand. *Bulletin of Volcanology* **52:** 445-459.

Connor CB, Winfrey B, Franklin NM, LaFemina PC. 2001. 2001. Estimation of volcanic hazards from tephra fallout. . *Natural Hazards Review* **2:** 33-42.

Cronin SJ, Hedley MJ, Neall VE, Smith RG. 1998. Agronomic impact of tephra fallout from the 1995 and 1996 Ruapehu Volcano eruptions, New Zealand. *Environmental Geology* **34:** 21-30.

Cronin SJ, Neall VE. 1997. A late Quaternary stratigraphic framework for the northeastern Ruapehu and eastern Tongariro ring plains, New Zealand. *New Zealand Journal of Geology and Geophysics* **40:** 185-197.

Cronin SJ, Neall VE, Lecointre JA, Hedley MJ, Loganathan P. 2003. Environmental hazards of fluoride in volcanic ash: a case study from Ruapehu volcano, New Zealand. *Journal of Volcanology and Geothermal Research* **121:** 271-291.

Cronin SJ, Neall VE, Palmer AS, Stewart RB. 1997. Methods of identifying late Quaternary rhyolitic tephras on the ring plains of Ruapehu and Tongariro volcanoes, New Zealand. *New Zealand Journal of Geology and Geophysics* **40:** 175-184.

Cronin SJ, Neall VE, Stewart RB, Palmer AS. 1996a. A multiple-parameter approach to andesitic tephra correlation, Ruapehu volcano, New Zealand. *Journal of Volcanology and Geothermal Research* **72:** 199-215.

Cronin SJ, Wallace RC, Neall VE. 1996b. Sourcing and identifying andesitic tephras using major oxide titanomagnetite and hornblende chemistry, Egmont volcano and Tongariro Volcanic Centre, New Zealand. *Bulletin of Volcanology* **58:** 33-40.

Davies SE, Turney CSM, Hall VA, Kershaw P, Harberle SG, Denham TP. 2007. The characterisation of local and distal tephras in the northern sector of Greater Australia including some preliminary high-precision correlations between significant archaeological sites in Papau New Guinea (PNG). *Quaternary International.*

Davies SM, Branch NP, Lowe J, Turney CSM. 2002. Towards a European tephrochronological framework for termination 1 and the early Holocene. *Philosophical Transactions of the Royal Society of London Series A-Mathematical Physical and Engineering Sciences* **360:** 767-802.

Davies SM, Elmquist M, Bergman J, Wohlfarth B, Hammarlund D. 2007. Cryptotephra sedimentation processes within two lacustrine sequences from west central Sweden. *The Holocene* **17:** 319-330.

Davies SM, Hoek WZ, Bohncke SJP, Lowe JJ, O'Donnell SP, Turney CSM. 2005. Detection of Lateglacial distal tephra layers in the Netherlands. *Boreas* **34:** 123-135.

Davies SM, Lowe JJ. 2004. Detection of Volcanic Ash Layers in Northern Ireland: New Additions to the European Tephrochronology Framework. *Swansea Geographer.*

Davies SM, Wastegård S, Rasmussen TL, Svensson A, Johnsen SJ, Steffensen JP, Andersen KK. 2008. Identification of the Fugloyarbanki tephra in the NGRIP ice core: a key tie-point for marine and ice-core sequences during the last glacial period. *Journal of Quaternary Science* **23:** 409-414.

Davies SM, Wastegård S, Wohlfarth B. 2003. Extending the limits of the Borrobol Tephra to Scandinavia and detection of new early Holocene tephras. *Quaternary Research* **59:** 345-352.

de Fontaine CS, Kaufman DS, Scott Anderson R, Werner A, Waythomas CF, Brown TA. 2007. Late Quaternary distal tephra-fall deposits in lacustrine sediments, Kenai Peninsula, Alaska. *Quaternary Research* **68:** 64-78.

de Lange PJ, Heenan PB, Clarkson BD, Clarkson BR. 1999. Taxonomy, ecology, and conservation of Sporadanthus (Restionaceae) in New Zealand. *New Zealand Journal of Botany* **37:** 413-431.

de Lange PJ, Lowe DJ. 1990. History of Vertical Displacement of Kerepehi Fault at Kopouatai Bog, Hauraki Lowlands, New-Zealand, Since C 10700 Years Ago. *New Zealand Journal of Geology and Geophysics* **33:** 277-283.

De Vleeschouwer F, van Vliët-Lanoé B, Fagel N. 2008. Long term mobilisation of chemical elements in tephra-rich peat (NE Iceland). *Applied Geochemistry* **23:** 3819-3839.

Denton JS, Pearce NJG. 2008. Comment on "A synchronized dating of three Greenland ice cores throughout the Holocene" by B. M. Vinther et al.: No Minoan tephra in the 1642 B.C. layer of the GRIP ice core. *Journal of Geophysical Research-Atmospheres* **113.**

Donoghue S, Neall VE, Palmer AS, Steward RB. 1997. The volcanic history of Ruapehu during the past 2 millennia based on the record of Tufa Trig tephras. *Bulletin of Volcanology* **59:** 136-146.

Donoghue SL, Gamble JA, Palmer AS, Stewart RB. 1995a. Magma mingling in an andesite pyroclastic flow of the Pourahu Member, Ruapehu volcano, New Zealand. *Journal of Volcanology and Geothermal Research* **68:** 177-191.

Donoghue SL, Neall VE. 1996. Tephrostratigraphic studies at Tongariro volcanic centre New Zealand: An overview. *Quaternary International* **34-6:** 13-20.

Donoghue SL, Neall VE, Palmer AS. 1995b. Stratigraphy and chronology of Late Quaternary andesitic tephra deposits, Tongariro Volcanic Center, New Zealand. *Journal of the Royal Society of New Zealand* **25:** 115-206.

Donoghue SL, Vallance J, Smith IEM, Stewart RB. 2007. Using geochemistry as a tool for correlating proximal andesitic tephra: case studies from Mt Rainier (USA) and Mt Ruapehu (New Zealand). *Journal of Quaternary Science* **22:** 395-410.

Dugmore AJ, Larsen G, Newton AJ. 1995. Seven tephra isochrones in Scotland. *The Holocene* **5:** 257-266.

Dugmore AJ, Newton AJ. 1992. Thin Tephra Layers in Peat Revealed by X-Radiography. *Journal of Archaeological Science* **19:** 163-170.

Dugmore AJ, Newton AJ, Sugden DE, Larsen G. 1992. Geochemical stability of fine-grained silicic Holocene tephra in Iceland and Scotland. *Journal of Quaternary Science* **7:** 173-183.

Edbrooke SW, Mazengarb C, Stephenson W. 2003. Geology and geological hazards of the Auckland urban area, New Zealand. *Quaternary International* **103:** 3-21.

Eden DN, Froggatt PC. 1996. A 6500-year-old history of tephra deposition recorded in the sediments of Lake Tutira, eastern North Island, New Zealand. *Quaternary International* **34-6:** 55-64.

Einarsson T. 1986. Tephrochronology. In: Berglund BE, ed. *Handbook of Holocene Palaeoecology and Palaeohydrology*. John Wiley & Sons Ltd., 329-342.

Enache MD, Cumming BF. 2006. The morphological and optical properties of volcanic glass: A tool to assess density-induced vertical migration of tephra in sediment cores. *Journal of Paleolimnology* **35:** 661-667.

Environment Waikato, 1999a. Volcanic contingency plan of the Waikato Region. Environment Waikato Policy Series 1999/04, -52pp. 1999a.

Environment Waikato. 1999b. Wetlands in the Waikato Region. *http://www.ew.govt.nz/enviroinfo/water/wetlands/whatwetlands/wetlandsmap.htm.*

Feakins SJ, Brown FH, deMenocal PB. 2007. Plio-pleistocene microtephra in DSDP site 231, Gulf of Aden. *Journal of African Earth Sciences* **48:** 341-352.

Fisher RV. 1961. Proposed classification of volcaniclastic sediments and rocks. *Geological Society of America Bulletin* **72:** 1409-1414.

Fisher RV, Schmincke HU. 1984. *Pyroclastic rocks*. Berlin: Springer-Verlag.

Fitzsimons SJ. 2001. Denudation, weathering, and slope development. In: Melbourne: Oxford University Press, 240-253.

Forbes L, Jarvis D, Potts J, Baxter PJ. 2003. Volcanic ash and respiratory symptoms in children on the island of Montserrat, British West Indies. *Occupational and Environmental Medicine* **60:** 207-211.

Fritz C, Campbell DI, Schipper LA. 2008. Oscillating peat surface levels in a restiad wetland, New Zealand - magnitude and spatiotemporal variability. *Hydrological Processes* .

Froggatt PC. 1983. Toward a comprehensive upper Quaternary tephra and ignimbrite stratigraphy in New Zealand using electron microprobe analysis of glass shards. *Quaternary Research* **19:** 188-200.

Froggatt PC. 1992. Standardisation of the chemical analysis of tephra deposits. Report of the ICCT working group. *Quaternary International* **13/14:** 93-96.

Froggatt PC, Lowe DJ. 1990. A Review of Late Quaternary Silicic and Some Other Tephra Formations from New-Zealand - Their Stratigraphy, Nomenclature, Distribution, Volume, and Age. *New Zealand Journal of Geology and Geophysics* **33:** 89-109.

Froggatt PC, Rogers GM. 1990. Tephrostratigraphy of high-altitude peat bogs along the Axial Ranges, North Island, New-Zealand. *New Zealand Journal of Geology and Geophysics* **33:** 111-124.

Gamble JA, Wood CP, Price RC, Smith IEM, Stewart RB, Waight T. 1999. A fifty year perspective of magmatic evolution on Ruapehu Volcano, New Zealand: verification of open system behaviour in an arc volcano. *Earth and Planetary Science Letters* **170:** 301-314.

Gardner JV, Nelson CS, Baker PA. 1985. Distribution and character of pale green laminae in sediment from Lors Howe Rise: a probable late Neogene and Quaternary tephrostratigraphic record. *Initial Reports of the Deep Sea Drilling Project* **XC:** 1145-1159.

Gehrels MJ, Lowe DJ, Hazell ZJ, Newnham RM. 2006. A continuous 5300-yr Holocene cryptotephrostratigraphic record from northern New Zealand and implications for tephrochronology and volcanic hazard assessment. *Holocene* **16:** 173-187.

Gehrels MJ, Newnham RM, Lowe DJ, Wynne S, Hazell ZJ, Caseldine C. 2008. Towards rapid assay of cryptotephra in peat cores: review and evaluation of various methods. *Quaternary International* **178:** 68-84.

Giles TM, Newnham R, Lowe DJ, Munro AJ. 1999. Impact of tephra fall and envronmental change: a 1000 year record from Matakana Island, Bay of Plenty, North Island, New Zealand. In: Firth CR, McGuire WJ, eds. *Volcanoes in the Quaternary.* Geological Society, London, Special Publication 161, 11-26.

Gomez B, Carter L, Trustrum NA. 2007. A 2400 yr record of natural events and anthropogenic impacts in intercorrelated terrestrial and marine sediment cores: Waipaoa sedimentary system, New Zealand. *Geological Society of America Bulletin* **119:** 1415-1432.

Grange LI. 1931. Volcanic ash showers: a geological recconnaissance of volcanic showers of the central part of the North Island. *New Zealand Journal of Science and Technology* **12:** 228-240.

Grattan J, Gilbertson D, Charman D. 1999. Modelling the impact of Icelandic volcanic eruptions upon the prehistoric societies and environment of northern and western Britain. In: Firth CR, McGuire WJ, eds. *Volcanoes of the Quaternary.* Geological Society Special Publication No.161, 109-124.

Green JD, Lowe DJ. 1985. Stratigraphy and development of c.17000 year old Lake Maratoto, North Island, New Zealand, with some inferences about postglacial climatic-change. *New Zealand Journal of Geology and Geophysics* **28:** 675-699.

Green JD, Lowe DJ. 1994. Origin and development. In:*Lake Rotoroa: Changes in an urban lake.* NIWA Ecosystems Publication No.9, 13-23.

Gregg DR. 1960. Volcanoes of Tongariro National Park - A New Zealand Geological Survey Handbook. In: New Zealand Department of Scientific and Industrial Research, - 82.

Gregory NG, Neall VE. 1996. Volcanic hazards for livestock. *Outlook on Agriculture* **25:** 123-129.

Griffin AM. 2007. *Products and Processes of Cone-Building Eruptions from North Crater, Tongaririro.* Master of Science, The University of Waikato.

Hall VA. 2003. Assessing the impact of Icelandic volcanism on vegetation systems in the north of Ireland in the fifth and sixth millennia BC. *Holocene* **13:** 131-138.

Hall VA, Pilcher JR. 2002. Late-Quaternary Icelandic tephras in Ireland and Great Britain: detection, characterization and usefulness. *The Holocene* **12:** 223-230.

Hall VA, Pilcher JR, McCormac FG. 1993. Tephra-Dated Lowland Landscape History of the North of Ireland, Ad 750-1150. *New Phytologist* **125:** 193-202.

Hang T, Wastegård S, Veski S, Heinsalu A. 2006. First discovery of cryptotephra in Holocene peat deposits in Estonia, eastern Baltic. *Boreas* **35:** 644-649.

Harper MA, Howorth R, McLeod M. 1986. Late Holocene diatoms in Lake Poukawa: effects of airfall tephra and changes in depth. *New Zealand Journal of Marine and Freshwater Research* **20:** 107-118.

Hazell ZJ. 2004. *Holocene palaeoclimate reconstruction from New Zealand peatlands.* PhD, The University of Plymouth.

Heiken G, Wohletz K. 1985. *Volcanic Ash.* Berkely: University of California Press.

Heiken G. 1972. Morphology and petrography of volcanic ashes. *GSA Bulletin* **83:** 1961-1987.

Hitchcock DW, Cole JW. 2007. Potential impacts of a widespread subplinian andesitic eruption from Tongariro volcano, based on a study of the Poutu Lapilli. *New Zealand Journal of Geology and Geophysics* **50:** 53-66.

Hobden BJ, Houghton BF, Lanphere MA, Nairn IA. 1996. Growth of the Tongariro volcanic complex: New evidence from K- Ar age determinations. *New Zealand Journal of Geology and Geophysics* **39:** 151-154.

Hobden BJ, Houghton BF, Nairn IA. 2002. Growth of a young, frequently active composite cone: Ngauruhoe volcano, New Zealand. *Bulletin of Volcanology* **64:** 392-409.

Hodder APW, Delange PJ, Lowe DJ. 1991. Dissolution and depletion of ferromagnesian minerals from Holocene tephra layers in an acid bog, New-Zealand, and implications for tephra correlation. *Journal of Quaternary Science* **6:** 195-208.

Hogg AG. 1979. *Identification and correlation of thinly bedded Late Quaternary tephras of Coromandel Peninsula, New Zealand.* Unpublished PhD thesis, University of Waikato, New Zealand.

Hogg AG, Higham TFG, Lowe DJ, Palmer JG, Reimer PJ, Newnham RM. 2003. A wiggle-match date for Polynesian settlement of New Zealand. *Antiquity* **77:** 116-125.

Hogg AG, Lowe DJ, Hendy CH. 1987. University of Waikato Radiocarbon dates I. *Radiocarbon* **29:** 263-301.

Hogg AG, McCraw JD. 1983. Late Quaternary Tephras of Coromandel Peninsula, North-Island, New-Zealand - A Mixed Peralkaline and Calcalkaline Tephra Sequence. *New Zealand Journal of Geology and Geophysics* **26:** 163-187.

Horrocks M, Augustinus P, Shane P, Deng Y, Andersson S. 2005. Holocene vegetation, environment, and tephra recorded from Lake Pupuke, Auckland, New Zealand. *New Zealand Journal of Geology and Geophysics* **48:** 85-94.

Horrocks M, Ogden J. 1998. The effects of the Taupo Tephra eruption of c. 1718 BP on the vegetation of Mt Hauhungatahi, central North Island, New Zealand. *Journal of Biogeography* **25:** 649-660.

Horwell CJ, Baxter PJ. 2006. The respiratory health hazards of volcanic ash: a review for volcanic risk mitigation. *Bulletin of Volcanology* **69:** 1-24.

Hotes S, Poschlod P, Takahashi H, Grootjans AP, Adema E. 2004. Effects of tephra deposition on mire vegetation: a field experiment in Hokkaido, Japan. *Journal of Ecology* **92:** 624-634.

Houghton BF, Wilson CJN, Mcwilliams MO, Lanphere MA, Weaver SD, Briggs RM, Pringle MS. 1995. Chronology and Dynamics of A Large Silicic Magmatic System - Central Taupo Volcanic Zone, New-Zealand. *Geology* **23:** 13-16.

Hunt JB, Hill PG. 1993. Tephra geochemistry: a discussion of some persistant analytical problems. *The Holocene* **3:** 271-278.

Hunt JB, Hill PG. 1996. An inter-laboratory comparison of the electron probe microanalysis of glass geochemistry. *Quaternary International* **34-36:** 229-241.

Hunt JB, Hill PG. 2001. Tephrological implications of beam size - Sample-size effects in electron microprobe analysis of glass shards. *Journal of Quaternary Science* **16:** 105-117.

Hurst T, Smith W. 2004. A Monte Carlo methodology for modelling ashfall hazards. *Journal of Volcanology and Geothermal Research* **138:** 393-403.

IGNS. 2004. Volcanoes in New Zealand. http://www.gns.cri.nz/what/earthact/volcanoes/ . Institute of Geological and Nuclear Sciences Ltd.

Irvine TN, Baragar WRA. 1971. A guide to the chemical classification of the common volcanic rocks. *Canadian Journal of Earth Sciences* **8:** 523-548.

Jenkins SF, Magill CR, McAneney KJ. 2007. Multi-stage volcanic events: A statistical investigation. *Journal of Volcanology and Geothermal Research* **161:** 275-288.

Johnston DM, Houghton BF, Neall VE, Ronan KR, Paton D. 2000. Impacts of the 1945 and 1995-1996 Ruapehu eruptions, New Zealand: An example of increasing societal vulnerability. *Geological Society of America Bulletin* **112:** 720-726.

Kamp PJJ. 1992. Tectonic Architecture. In: Soons JM, Selby MJ, eds. *Landforms of New Zealand*. Auckland, New Zealand: Longman Paul, 1-30.

Kent M, Owen NW, Dale P, Newnham RM, Giles TM. 2001. Studies of vegetation burial: a focus for biogeography and biogeomorphology? *Progress in Physical Geography* **25:** 455-482.

Kilian R, Hohner M, Biester H, Wallrabe-Adams HJ, Stern CR. 2003. Holocene peat and lake sediment tephra record from the southernmost Chilean Andes (53-55 degrees S) 47. *Revista Geologica de Chile* **30:** 23-37.

Kittleman LR. 1979. Geologic methods in studies of Quaternary tephra. In: Sheets PD, Grayson DK, eds. *Volcanic Activity and Human Ecology*. New York: Academic Press, 49-82.

Kristjansdottir GB, Stoner JS, Jennings AE, Andrews JT, Gronvold K. 2007. Geochemistry of Holocene cryptotephras from the north Iceland shelf (MD99-2269): intercalibration with radiocarbon and palaeomagnetic chronostratigraphies. *Holocene* **17:** 155-176.

Lakeman TR, Clague JJ, Menounos B, Osborn GD, Jensen BJL, Froese DG. 2008. Holocene tephras in lake cores from northern British Columbia, Canada. *Canadian Journal of Earth Sciences* **45:** 935-947.

Le Bas MJ, Le Maitre RW, Streckeisen A, Zanettin B. 1986. A chemical classification of volcanic rocks based on the total alkali silica diagram. *Journal of Petrology* **27:** 745-750.

Leathwick J, Wilson G, Rutlege D, Wardle F, Morgan F, Johnston K, McLeod M, Kirkpatrick R. 2003. *Land Environments of New Zealand.* Auckland, New Zealand: David Bateman Ltd.

Lim CW, Ikehara K, Toyoda K. 2008. Cryptotephra detection using high-resolution trace-element analysis of Holocene marine sediments, southwest Japan. *Geochimica et Cosmochimica Acta* **72:** 5022-5036.

Lowe DJ. 1981. Late Quaternary tephras in the Hamilton Basin, North Island, New Zealand. In: Howorth R, Froggatt P, Vucetich CG, Collen JD, eds. *Proceedings of Tephra Workshop.* Victoria: University of Wellington, 68-75.

Lowe DJ. 1986. Revision of the age and stratigraphic relationships of Hinemaiaia Tephra and Whakatane Ash, North Island, New-Zealand, using distal occurrences in organic deposits. *New Zealand Journal of Geology and Geophysics* **29:** 61-73.

Lowe DJ. 1988a. Late Quaternary Volcanism in New Zealand: towards an integrated record using distal airfall tephras in lakes and bogs. *Journal of Quaternary Science* **3:** 111-120.

Lowe DJ. 1988b. Stratigraphy, age, composition, and correlation of Late Quaternary tephras interbedded with organic sediments in Waikato lakes, North Island, New Zealand. *New Zealand Journal of Geology and Geophysics* **31:** 125-165.

Lowe DJ. 1990. Tephra Studies in New-Zealand - An Historical Review. *Journal of the Royal Society of New Zealand* **20:** 119-150.

Lowe DJ. 2008. Globalisation of tephrochronology: new views from Australasia. *Progress in Physical Geography* **32:** 311-335.

Lowe DJ, Green JD. 1992. Lakes. In: Soons JM, Selby MJ, eds. *Landforms of New Zealand, 2nd Edition.* Auckland: Longman Paul, 107-143.

Lowe DJ, Hogg AG, Green JD, Boubee JAT. 1980. Stratigraphy and Chronology of Late Quaternary Tephras in Lake Maratoto, Hamilton, New-Zealand. *New Zealand Journal of Geology and Geophysics* **23:** 481-485.

Lowe DJ, Hogg AG, Hendy CH. 1981. Detection of thin tephra deposits in peat and organic lake sediments byrapid x-radiography and x-ray fluorescence techniques. Proceedings of tephra workshop, July 30th-July 1st 1980, Victoria University of Wellington. Howorth, R., Froggatt, P. C., Vucetich, C. G., and Collen, J. D.

Lowe DJ, Hunt JB. 2001. A summary of terminology used in tephra-related studies. *Les Dossiers de l'Archeo-Logis* **1:** 17-22.

Lowe DJ, McFadgen BG, Higham TFG, Hogg AG, Froggatt PC, Nairn IA. 1998. Radiocarbon age of the Kaharoa Tephra, a key marker for late- Holocene stratigraphy and archaeology in New Zealand. *Holocene* **8:** 487-495.

Lowe DJ, Newnham RH, Ward CM. 1999. Stratigraphy and chronology of a 15 ka sequence of multi- sourced silicic tephras in a montane peat bog, eastern North Island, New Zealand. *New Zealand Journal of Geology and Geophysics* **42:** 565-579.

Lowe DJ, Newnham RM. 1999. Advances in Quaternary tephrostratigraphy and tephrochronology in New Zealand. *Quaternary Australasia* **17:** 12-19.

Lowe DJ, Newnham RM. 2004. Role of tephra in dating Polynesian settlement and impact, New Zealand. *Pages News* **12:** 5-7.

Lowe DJ, Newnham RM, McCraw JD. 2002. Volcanism and early Maori Society in New Zealand. In: Torrence R, Grattan J, eds. *Natural Disasters and Cultural Change*. London: Routledge, 126-161.

Lowe DJ, Newnham RM, McFadgen BG, Higham TFG. 2000. Tephras and New Zealand archaeology. *Journal of Archaeological Science* **27:** 859-870.

Lowe DJ, Smith RT, Jones HS. 2008a. Introduction to Quaternary volcanism, tephras and tephra-derived soils in New Zealand. *In*: Lowe, D.J. (editor) Nov. 2008. In: Lowe DJ, ed. *Guidebook for Pre-conference North Island Field Trip A1 'Ashes and Issues', Australian and New Zealand 4th Joint Soils Conference)November 2008)*. Massey University, Palmerston North: New Zealand Society of Soil Science, 10-26.

Lowe DJ, Shane PAR, Alloway BV, Newnham RM. 2008b. Fingerprints and age models for widespread New Zealand tephra marker beds erupted since 30,000 years ago: a framework for NZ-INTIMATE. *Quaternary Science Reviews* **27:** 95-126.

Mackie EAV, Davies SM, Turney CSM, Dobbyn K, Lowe JJ, Hill PG. 2002. The use of magnetic separation techniques to detect basaltic microtephra in last glacial-interglacial transition (LGIT; 15- 10 ka cal. BP) sediment sequences in Scotland. *Scottish Journal of Geology* **38:** 21-30.

MAF. 2002 Volcanic Hazards in New Zealand. Ministry of Agricuture and Forestry website.

Magill C, Blong R. 2005a. Volcanic risk ranking for Auckland, New Zealand. I: Methodology and hazard investigation. *Bulletin of Volcanology* **67:** 331-339.

Magill C, Blong R. 2005b. Volcanic risk ranking for Auckland, New Zealand. II: Hazard consequences and risk calculation. *Bulletin of Volcanology* **67:** 340-349.

Magill CR, Hurst AW, Hunter LJ, Blong RJ. 2006a. Probabilistic tephra fall simulation for the Auckland Region, New Zealand. *Journal of Volcanology and Geothermal Research* **153:** 370-386.

Magill C. 2007. Reply to comments on "Probabilistic tephra fall simulation for the Auckland region, New Zealand by P. Shane". *Journal of Volcanology and Geothermal Research* **159:** 423-424.

Magill C, Blong R, McAneney J. 2006b. VolcaNZ--A volcanic loss model for Auckland, New Zealand. *Journal of Volcanology and Geothermal Research* **149:** 329-345.

Maher LJ. 1981. Statistics for microfossil concentration measurements employing samples spiked with marker grains. *Review of Palaeobotany and Palynology* **32:** 153-191.

Manighetti B, Palmer A, Eden D, Elliot M. 2003. An occurrence of Tuhua Tephra in deep-sea sediments from offshore eastern North Island, New Zealand. *New Zealand Journal of Geology and Geophysics* **46:** 581-590.

Manville V. 2001. Environmental impacts of large-scale explosive rhyolitic eruptions in the central North Island. In: Smith RT, ed. *"Fieldtrip Guides" Geological Society of New Zealand annual conference, University of Waikato.* Hamilton: Geological Society of New Zealand Miscellaneous Publication 110B, 64-68.

Manville V. 2002. Sedimentary and geomorphic responses to ignimbrite emplacement: Readjustment of the Waikato River after the AD 181 Taupo Eruption, New Zealand. *Journal of Geology* **110:** 519-541.

Manville V, Hodgson KA, Nairn IA. 2007. A review of break-out floods from volcanogenic lakes in New Zealand. *New Zealand Journal of Geology and Geophysics* **50:** 131-150.

Manville V, Newton EH, White JDL. 2005. Fluvial responses to volcanism: resedimentation of the 1800a Taupo ignimbrite eruption in the Rangitaiki River catchment, North Island, New Zealand. *Geomorphology* **65:** 49-70.

Manville V, Segschneider B, White JDL. 2002. Hydrodynamic behaviour of Taupo 1800a pumice: implications for the sedimentology of remobilized pyroclasts. *Sedimentology* **49:** 955-976.

Manville V, White JDL, Houghton BF, Wilson CJN. 1999. Paleohydrology and sedimentology of a post-1.8 ka breakout flood from intracaldera Lake Taupo, North Island, New Zealand. *Geological Society of America Bulletin* **111:** 1435-1447.

Manville V, Wilson CJN. 2003. Interactions between volcanism, rifting and subsidence: implications of intracaldera palaeoshorelines at Taupo volcano, New Zealand. *Journal of the Geological Society* **160:** 3-6.

Manville V, Wilson CJN. 2004. The 26.5 ka Oruanui eruption, New Zealand: a review of the roles of volcanism and climate in the post-eruptive sedimentary response. *New Zealand Journal of Geology and Geophysics* **47:** 525-547.

Marra MJ, Alloway BV, Newnham RM. 2006. Paleoenvironmental reconstruction of a well-preserved Stage 7 forest sequence catastrophically buried by basaltic eruptive deposits, northern New Zealand. *Quaternary Science Reviews* **25:** 2143-2161.

Matthews I. 2008. Holocene tephrochronology and wetland archaeology in the British Isles: new developments. IAVCEI 2008 General Assembly, Reykjavik, Iceland. 17-22 August, 2008. 2008.

Mc Lay CDA, Allbrook RF, Thompson K. 1992. Effect of development and cultivation on physical properties of peat soils in New Zealand. *Geoderma* **54:** 23-37.

McCormac FG, Hogg AG, Blackwell PG, Buck CE, Higham TFG, Reimer PJ. 2004. SHCal04 Southern Hemisphere calibration, 0-11.0 cal kyr BP. *Radiocarbon* **46:** 1087-1092.

McCraw JG. 2002. Physical environment. In: Clarkson BD, Merrett M, Downs T, eds. *Botony of Waikato*. Hamilton: Waikato Botanical Society, 13-22.

McFadgen BG. 2007. *Hostile Shores: Catastrophic Events in Prehistoric New Zealand and their Impact on Maori Coastal Communities*. Auckland: Auckland University Press.

McGlone MS, Wilmshurst JM. 1999. Dating initial Maori environmental impact in New Zealand. *Quaternary International* **59:** 5-16.

McSaveney E, Stewart C, Leonard G. 2007 'Historic volcanic activity'. Te Ara - the online Encyclopedia of New Zealand. Accessed: 16-3-2008.

Meney KA, Pate JS. 1999. Morphological and anatomical descriptions of Restionaceae. In: Meney KA, Pate JS, eds. *Australian Rushes: Biology, Identification and Conservation of Restionacaeae and Allied Families*. Nedlands, Western Australia: Western Australia Press, 160-464.

Mobis A, Cronin S, Lube G, Turner M, Nemeth K. 2008. The birth and growth of a stratovolcano recorded in medial tephras- Mount Ngauruhoe, Tongariro Volcanic Centre, New Zealand. IAVCEI 2008 General Assembly, Rekjavik, Iceland, 17-22 August 2008.

Molloy C, Shane PAR. 2007. New multi-source tephra record in Auckland maars: Implications for volcanic frequencies and hazards. XVII INQUA Congress, Cairns, Australia, 28 July – 3 August 2007.

Molloy L, Christie Q. 1998. *The Living Mantle: Soils in the New Zealand Landscape*. Canterbury: New Zealand Society of Soil Science, Lincoln University.

Mullan B, Tait A, Thompson C. 2007. 'Climate', Te Ara - the Encyclopedia of New Zealand, updated 21-Sep-2007. URL: http://www.TeAra.govt.nz/EarthSeaAndSky/ClimateAndAtmosphere/Climate/en .

Nairn IA, Hedenquist JW, Villamor P, Berryman KR, Shane PA. 2005. The ~AD1315 Tarawera and Waiotapu eruptions, New Zealand: contemporaneous rhyolite and hydrothermal eruptions driven by an arrested basalt dike system? *Bulletin of Volcanology* **67:** 186-193.

Nairn IA, Self S. 1978. Explosive eruptions and pyroclastic avalanches from Ngauruhoe in February 1975. *Journal of Volcanology and Geothermal Research* **3:** 39-60.

Nairn IA, Self S, Cole JW, Leonard GS, Scutter C. 2001. Distribution, stratigraphy, and history of proximal deposits from the c. AD 1305 Kaharoa eruptive episode at Tarawera Volcano, New Zealand. *New Zealand Journal of Geology and Geophysics* **44:** 467-484.

Nairn IA, Shane PR, Cole JW, Leonard GJ, Self S, Pearson N. 2004. Rhyolite magma processes of the similar to AD 1315 Kaharoa eruption episode, Tarawera volcano, New Zealand. *Journal of Volcanology and Geothermal Research* **131:** 265-294.

Nakagawa M, Wada K, Wood CP. 2002. Mixed magmas, mush chambers, and eruption triggers: evidence from zoned clinopyroxene phenocrysts in andesitic scoria from the

1995 eruptions of Ruapehu volcano, New Zealand. *Journal of Petrology* **43:** 2279-2303.

Neall V, Cronin SJ, Donoghue SL, Hodgson KA, Lecointre J, Purves AM. 1995. The Potential Threat at Ruapeahu. *TEPHRA* **12:** 23-29.

Neall VE. 2001. Volcanic landforms. In: Melbourne: Oxford University Press, 39-60.

Neall VE, Alloway BV. 1996. Volcanic hazard map of western Taranaki. Massey University Department of Soil Science Occasional Report 12.

Needham AJ, Lindsay JM, Smith IEM. 2008. The eruptive history of Rangitoto Island, Auckland Volcanic Field, New Zealand. Geological Society of New Zealand Miscellaneous Publication 124A , 156. 2008. Wellington. Geosciences '08 Te Papa, Wellington, November 23-26, 2008.

Nelson CS. 1975. Ngauruhoe ashfall in Waikato. *Geological Society of New Zealand Newsletter* **39:** 41-42.

Nelson CS, Froggatt PC, Gosson GJ. 1986. Nature, Chemistry, And Origin of Late Cenozoic Megascopic Tephras in Leg 90 Cores from the Southwest Pacific. *Initial Reports of the Deep Sea Drilling Project* **90:** 1161-1171.

Newnham RM, Lowe DJ, Giles T, Alloway BV. 2007. Vegetation and climate of Auckland, New Zealand, since ca.32 000 cal. yr ago: support for an extended LGM. *Journal of Quaternary Science* **22:** 517-534.

Newnham RM, Delange PJ, Lowe DJ. 1995. Holocene vegetation, climate and history of a raised bog complex, northern New-Zealand based on palynology, plant macrofossils and tephrochronology. *Holocene* **5:** 267-282.

Newnham RM, Eden DN, Lowe DJ, Hendy CH. 2003. Rerewhakaaitu Tephra, a land-sea marker for the Last Termination in New Zealand, with implications for global climate change. *Quaternary Science Reviews* **22:** 289-308.

Newnham RM, Gehrels MJ, Dirks K. 2008. Have we underestimated the distal volcanic hazard? Lessons from multidisciplinary investigations at Auckland, New Zealand. The 33rd International Geological Congress, Oslo. August 6-14th 2008. 2008.

Newnham RM, Lowe DJ. 1991. Holocene vegetation and volcanic activity, Auckland Isthmus, New Zealand. *Journal of Quaternary Science* **6:** 177-193.

Newnham RM, Lowe DJ, Alloway BV. 1999a. Volcanic hazards in Auckland, New Zealand: a preliminary assessment of the threat posed by central North Island silicic volcanism based on the Quaternary tephrostratigraphic record. In: Firth CR, McGuire WJ, eds. *Volcanoes of the Quaternary. The Geological Society of London Special Publications* **161**: 27-45.

Newnham RM, Lowe DJ, Green JD. 1989. Palynology, vegetation and climate of the Waikato Lowlands, North Island, New-Zealand, since c18,000 years ago. *Journal of the Royal Society of New Zealand* **19:** 127-150.

Newnham RM, Lowe DJ, McGlone MS, Wilmshurst JM, Higham TFG. 1998. The Kaharoa Tephra as a critical datum for earliest human impact in northern New Zealand. *Journal of Archaeological Science* **25:** 533-544.

Newnham RM, Lowe DJ, Williams PW. 1999b. Quaternary environmental change in New Zealand: a review. *Progress in Physical Geography* **23:** 567-610.

Newnham RM, Vandergoes MJ, Garnett MH, Lowe DJ, Prior C, Almond PC. 2007b. Test of AMS C-14 dating of pollen concentrates using tephrochronology. *Journal of Quaternary Science* **22:** 37-51.

Nichol R. 1992. The eruption history of Rangitoto - reappraisal of a small New Zealand myth. *Journal of the Royal Society of New Zealand* **22:** 159-180.

NIWA. 2007a. Climate Summaries: averages for 1971-2000. http://www.niwascience.co.nz/edu/resources/climate/summary.

NIWA. 2007b Climate variability and change. http://www.niwa.cri.nz/ncc/clivar/scenarios . NIWA National Climate Centre.

Norton DA, de Lange PJ. 2003. Fire and vegetation in a temperate peat bog: Implications for the management of threatened species. *Conservation Biology* **17:** 138-148.

Ogden J, Basher L, McGlone MS. 1998. Fire, Forest Regeneration and Links with Early Human Habitation: Evidence from New Zealand. *Annals of Botany* **81:** 687-696.

Palmer DJ, Höck BK, Lowe DJ, Dunningham AG, Payn TW. 2009. Developing national-scale terrain attributes for New Zealand (TANZ). *Scion Research Bulletin* **232:** 81.

Payne R, Blackford J. 2005. Simulating the impacts of distal volcanic products upon peatlands in northern Britain: an experimental study on the Moss of Achnacree, Scotland. *Journal of Archaeological Science* **32:** 989-1001.

Payne R, Gehrels MJ. 2009. The formation of tephra layers in peatlands. *in prep.*

Payne RJ, Blackford JJ. 2004. Distal micro-tephra deposits in southeast Alaskan peatlands. *Yukon Exploration and Geology* 191-197.

Payne R, Blackford J, van der Plicht J. 2008. Using cryptotephras to extend regional tephrochronologies: An example from southeast Alaska and implications for hazard assessment. *Quaternary Research* **69:** 42-55.

Pearce NJG, Bendall C, Westgate JA. 2008. Comment on "Some numerical considerations in the geochemical analysis of distal microtephra" by A.M. Pollard, S.P.E., Blockley and C.S. Lane. *Applied Geochemistry* **23:** 1353-1364.

Pearce NJG, Westgate JA, Perkins WT, Eastwood WJ, Shane P. 1999. The application of laser ablation ICP-MS to the analysis of volcanic glass shards from tephra deposits: bulk glass and single shard analysis. *Global and Planetary Change* **21:** 151-171.

Pearce NJG, Westgate JA, Perkins WT, Preece SJ. 2004. The application of ICP-MS methods to tephrochronological problems. *Applied Geochemistry* **19:** 289-322.

Pepper AC, Shulmeister J, Nobes DC, Augustinus PA. 2004. Possible ENSO signals prior to the Last Glacial Maximum, during the last deglaciation and the early Holocene, from New Zealand. *Geophysical Research Letters* **31:** art-L15206.

Pilcher JR, Hall VA. 1992. Towards a tephrochronology for the Holocene of the north of Ireland. *The Holocene* **2:** 255-259.

Platz T, Cronin SJ, Smith IEM, Turner MP, Steward RP. 2007. Improving the reliability of microprobe-based analyses of andesitic glasses for tephra correlation. *The Holocene* **17:** 573-583.

Poirot T, Cole J, Elms DG. 2004. Ash fall prediction in New Zealand. *Bulletin of the New Zealand Society for Earthquake Engineering* **37:** 181-194.

Pollard AM, Blockley SPE, Lane CS. 2006. Some numerical considerations in the geochemical analysis of distal microtephra. *Applied Geochemistry* **21:** 1692-1714.

Price RC, Gamble JA, Waight TE, Stewart RB, McIntosh W, Smith I. 2000. Geology of the Whakapapa skifield and Turoa-Upper Mangaturuturu areas. In: Price RC, Gamble JA, Hobden BJ, eds. *"State of the Arc 2000: Guidebook for field excursions on Ruapehu and Tongariro volcanoes"*. 7-24.

Price RC, Gamble JA, Smith IEM, Stewart RB, Eggins S, Wright IC. 2005. An integrated model for the temporal evolution of andesites and rhyolites and crustal development in New Zealand's North Island. *Journal of Volcanology and Geothermal Research* **140:** 1-24.

Pullar WA, Birrell KS. 1973. Age and distribution of late Quaternary pyroclastic and associated cover deposits of the Rotorua and Taupo area, North Island, New Zealand. *New Zealand Soil Survey Report 1.*

Pullar WA, Kohn BP, Cox JE. 1977. Air-fall Kaharoa Ash and Taupo Pumice, and sea-rafted Loisels Pumice, Taupo Pumice, and Leigh Pumice in northern and eastern parts of the North Island, New Zealand. *New Zealand Journal of Geology and Geophysics* **20:** 697-717.

Pyne-O'Donnell SDF, Blockley SPE, Turney CSM, Lowe JJ. 2008. Distal volcanic ash layers in the Lateglacial Interstadial (GI-1): problems of stratigraphic discrimination. *Quaternary Science Reviews* **27:** 72-84.

Ranner PH, Allen JRM, Huntley B. 2005. A new early Holocene cryptotephra from northwest Scotland. *Journal of Quaternary Science* **20:** 201-208.

Rhoades DA, Dowrick DJ, Wilson CJN. 2002. Volcanic hazard in New Zealand: Scaling and attenuation relations for tephra fall deposits from Taupo Volcano 10. *Natural Hazards* **26:** 147-174.

Robertson DJ. 1986. A palaeomagnetic study of Rangitoto Island, Auckland, New Zealand. *New Zealand Journal of Geology and Geophysics* **29:** 405-411.

Rose NL, Golding PNE, Battarbee RW. 1996. Selective concentration and enumeration of tephra shards from lake sediment cores. *The Holocene* **6:** 243-246.

Sable JE, Houghton BF, Wilson CJN, Carey RJ. 2006. Complex proximal sedimentation from Plinian plumes: the example of Tarawera 1886. *Bulletin of Volcanology* **69:** 89-103.

Sancetta C. 1996. Laminated diatomaceous sediments: controls on formation and strategies for analysis. *Geological Society, London, Special Publications* **116:** 17-21.

Sandiford A, Alloway B, Shane P. 2001. A 28 000-6600 cal yr record of local and distal volcanism preserved in a paleolake, Auckland, New Zealand 13. *New Zealand Journal of Geology and Geophysics* **44:** 323-336.

Sarna-Wojcicki A. 2000. Tephrochronology. In: Stratton Noller J, Sowers JM, Lettis WR, eds. *Quaternary Geochronology, Methods and Applications.* Washington, DC: American Geophysical Union, 357-377.

Schipper LA, McLeod M. 2002. Subsidence rates and carbon loss in peat soils following conversion to pasture in the Waikato Region, New Zealand. *Soil Use and Management* **18:** 91-93.

Scollo S, Del Carlo P, Coltelli M. 2006. Tephra fallout of 2001 Etna flank eruption: Analysis of the deposit and plume dispersion. *Journal of Volcanology and Geothermal Research* **160:** 147-164.

SCOTAV list server 2007. A query about hydrogen peroxide. http://www.jiscmail.ac.uk/cgi-bin/webadmin?A0=TEPHRA. 2007.

Scott BJ, Houghton BF, Wilson CJN. 1995. Surveillance of New Zealand's Volcanoes. Volcanic Hazards in New Zealand. A special feature in association with Ruapehu '95 Volcanic Hazard Awareness Week, 16-23 October 1995. TEPHRA 14 [2], 14-22.

Segschneider B, Landis CA, Manville V, White JDL, Wilson CJN. 2002. Environmental response to a large, explosive rhyolite eruption: sedimentology of post-1.8 ka pumice-rich Taupo volcaniclastics in the Hawke's Bay region, New Zealand. *Sedimentary Geology* **150:** 275-299.

Selby MJ, Lowe DJ. 1992. The Middle Waikato Basin and Hills. In: Soons JM, Selby MJ, eds. *Landforms of New Zealand.* Auckland: Routledge, 232-255.

Shane P. 2000. Tephrochronology: a New Zealand case study. *Earth-Science Reviews* **49:** 223-259.

Shane P. 2005. Towards a comprehensive distal andesitic tephrostratigraphic framework for New Zealand based on eruptions from Egmont volcano. *Journal of Quaternary Science* **20:** 45-57.

Shane P. 2007. Comment on: "Probabilistic tephra fall simulation for the Auckland region, New Zealand by Magill et al. (2006)". *Journal of Volcanology and Geothermal Research* **159:** 421-422.

Shane P, Doyle LR, Nairn IA. 2008a. Heterogeneous andesite-dacite ejecta in 26-16.6 ka pyroclastic deposits of Tongariro Volcano, New Zealand: the product of multiple magma-mixing events. *Bulletin of Volcanology* **70:** 517-536.

Shane P, Hoverd J. 2002. Distal record of multi-sourced tephra in Onepoto Basin, Auckland, New Zealand: implications for volcanic chronology, frequency and hazards. *Bulletin of Volcanology* **64:** 441-454.

Shane P, Lian OB, Augustinus P, Chisari R, Heijnis H. 2002. Tephrostratigraphy and geochronology of a ca. 120 ka terrestrial record at Lake Poukawa, North Island, New Zealand. *Global and Planetary Change* **33:** 221-242.

Shane P, Martin SB, Smith VC, Beggs KF, Darragh MB, Cole JW, Nairn IA. 2007. Multiple rhyolite magmas and basalt injection in the 17.7 ka Rerewhakaaitu eruption episode from Tarawera volcanic complex, New Zealand. *Journal of Volcanology and Geothermal Research* **164:** 1-26.

Shane P, Smith I. 2000a. Geochemical fingerprinting of basaltic tephra deposits in the Auckland Volcanic Field. *New Zealand Journal of Geology and Geophysics* **43:** 569-577.

Shane PAR, Ingraham N. 2002. dD values of hydrated volcanic glass: a potential record of ancient meteoric water and climate in New Zealand. *New Zealand Journal of Geology and Geophysics* **45:** 453-459.

Shane P, Nairn IA, Martin SB, Smith VC. 2008b. Compositional heterogeneity in tephra deposits resulting from the eruption of multiple magma bodies: Implications for tephrochronology. *Quaternary International* **178:** 44-53.

Sharp TG, Stevenson RJ, Dingwell DB. 1996. Microlites and "nanolites" in rhyolitic glass: microstructural and chemicla charachterisation. *Bulletin of Volcanology* **57:** 631-640.

Shearer JC. 1997. Natural and anthropogenic influences on peat development in Waikato/Hauraki Plains restiad bogs. *Journal of the Royal Society of New Zealand* **27:** 295-313.

Siebert L, Simkin T. 2002- Volcanoes of the World: an Illustrated Catalogue of Holocene Volcanoes and their Eruptions. Global Volcanism Program, Digital Information Series, GVP-3 Global Volcanism Program, Digital Information Series, GVP-3. 2002. Smithsonian Institution. Accessed: 9-3-2008.

Smith DGW, Westgate JA. 1969. Electron probe technique for characterising pyroclastic deposits, *Earth and Planetary Science Letters. Earth and Planetary Science Letters* **5:** 313-319.

Smith IEM, Allen SR. 2007. New Zealand Volcanoes: Auckland. http://www.gns.cri.nz/what/earthact/volcanoes/ .

Smith K. 2000. *Environmental Hazards: Assessing Risk and Reducing Disaster.* London: Routledge.

Smith RT, Lowe DJ, Wright IC. 2007. Volcanoes. http://www.TeAra.govt.nz/EarthSeaAndSky/NaturalHazardsAndDisasters/Volcanoes/en New Zealand Ministry for Culture and Heritage, Wellington.

Smith VC, Shane P, Nairn IA. 2005. Trends in rhyolite geochemistry, mineralogy, and magma storage during the last 50 kyr at Okataina and Taupo volcanic centres, Taupo Volcanic Zone, New Zealand. *Journal of Volcanology and Geothermal Research* **148:** 372-406.

Smith VC, Shane PA, Nairn IA, Williams CM. 2006. Geochemistry and magmatic properties of eruption episodes from Haroharo Linear Vent Zone, Okataina Volcanic Centre, Taupo Volcanic Zone, New Zealand during the last 10 kyr. *Bulletin of Volcanology* **69:** 57-88.

Soons JM, Selby MJe. 1992. *Landforms of New Zealand.* Auckland: Longman Paul.

Sparks RJ, Graham IJ, Morgenstern U. 2008. Cosmic chronometers. In: Graham IJce, ed. *A Continent On The Move: New Zealand Geoscience Into The 21st Century.* Lower Hutt, New Zealand: Geological Society of New Zealand, Miscellaneous Publication 124, 64-67.

Sparks RJ, Melhuish WH, Mckee JWA, Ogden J, Palmer JG, Molloy BPJ. 1995. C-14 calibration in the southern hemisphere and the date of the last Taupo eruption: evidence from tree-ring sequences. *Radiocarbon* **37:** 155-163.

Statistics New Zealand. 2008. 2006 census of population and dwellings. http://www.stats.govt.nz/census/census-outputs/default.htm. Last updated 4/4/08.

Stockmarr J. 1971. Tablets with spores used in absolute pollen analysis. *Pollen et Spores* **13:** 615-621.

Stokes S, Lowe DJ. 1988. Discriminant Function-Analysis of Late Quaternary Tephras from 5 Volcanos in New-Zealand Using Glass Shard Major Element Chemistry. *Quaternary Research* **30:** 270-283.

Stuiver M, Reimer PJ. 2007. Calib Radiocarbon Calibration programme. [Calib Version 5.0.2html.]. 2005.

Tanner CC, Clayton JS. 1990. Persistence of arsenic 24 years after sodium arsenite herbicide application to Lake Rotoroa, Hamilton, New Zealand. *New Zealand Journal of Marine and Freshwater Research* **24:** 173-179.

Tanner CC, Clayton JS, Coffey BT. 1990. Submerged-vegetation changes in Lake Rotoroa (Hamilton, New Zealand) related to herbicide treatment and invasion by *Egeria densa*. *New Zealand Journal of Marine and Freshwater Research* **24:** 45-57.

Taylor R, Smith I, and others. 1997. The Place and the People. In:*The State of New Zealand's Environment 1997 (online publication).* Wellington: The Ministry for the Environment and GP Publications, 3-27.

Telford RJ, Heegaard E, Birks HJB. 2004. All age-depth models are wrong: but how badly? *Quaternary Science Reviews* **23:** 1-5.

TEPHRATRACE. 2002. International Virtual Workshop: Towards a European Framework for Correlating Records of Abrupt Environmental Change. http://mediator.ads.qab.ac.uk/ms/virtual . Queen's University, Belfast. Last updated: 15-4-2002.

Thompson MA, Campbell DI, Spronken-Smith RA. 1999. Evaporation from natural and modified raised peat bogs in New Zealand. *Agricultural and Forest Meteorology* **95:** 85-98.

Thompson R, Bradshaw RHW, Whitley JE. 1986. The distribution of ash in Icelandic lake sediments and relative importance of mixing and erosion processes. *Journal of Quaternary Science* **1:** 3-11.

Thorarinsson S. 1981. The Application of Tephrochronology in Iceland. In: Self S, Sparks RSJ, eds. *Tephra Studies - Proceedings of the nATO Advanced Study Institute "Tephra Studies as a tool in Quaternary Research", held in Laugarvatn and Reykjavick, Iceland, June 18-29, 1980.* Dordrecht: D.Reidal Publishing Company, 109-134.

Tonkin PJ. 1967. A note on the occurrence of Taupo Pumice in the Hamilton Basin. *Earth Science Journal* **1:** 31-32.

Troels-Smith J. 1955. Karakterisering af lose jordater. Characterisation of unconsolidated sediments. *Danmarks Geolosika Undersogelse* **4:** 39-73.

Turner MB, Cronin SJ, Smith IE, Stewart RB, Neall VE. 2008. Eruption episodes and magma recharge events in andesitic systems: Mt Taranaki, New Zealand. *Journal of Volcanology and Geothermal Research* **177:** 1063-1076.

Turney CSM. 1998. Extraction of rhyolitic component of Vedde microtephra from minerogenic lake sediments. *Journal of Paleolimnology* **19:** 199-206.

Turney CSM, Lowe JJ. 2001. Tephrochronology. In: Last WM, Smol JP, eds. *Tracking Environmental Change Using Lake Sediments: Volume 1: Basin Analysis, Coring and Chronological Techniques.* Dordrecht, The Netherlands: Kluwer Academic Publishers, 451-471.

Turney CSM, Lowe JJ, Davies SM, Hall V, Lowe DJ, Wastegård S, Hoek WZ, Alloway B. 2004. Tephrochronology of Last Termination Sequences in Europe: a protocol for improved analytical precision and robust correlation procedures (a joint SCOTAV-INTIMATE proposal). *Journal of Quaternary Science* **19:** 111-120.

Turney CSM, Lowe JJ, Harkness DD. 1997. The use of microtephra horizons to correlate Late-Glacial lake sediment successions in Scotland. *Journal of Quaternary Science* **12:** 525-531.

Urrutia R, Araneda A, Cruces F, Torres L, Chirinos L, Treutler HC, Fagel N, Bertrand S, Alvial I, Barra R, Chapron E. 2007. Changes in diatom, pollen, and chironomid assemblages in response to a recent volcanic event in Lake Galletue (Chilean Andes). *Limnologica* **37:** 49-62.

US Geological Survey. 2004. Volcanic ash: effects & mitigation strategies. http:volcanoes.usgs.gov/ash/ashfall.html .

van den Bogaard C, Dorfler W, Glos R, Nadeau MJ, Grootes PM, Erlenkeuser H. 2002. Two tephra layers bracketing late Holocene paleoecological changes in northern Germany. *Quaternary Research* **57:** 314-324.

Vucetich CG, Puller WA. 1964. Stratigraphy of Holocene Ash in the Rotorua and Gisborne Districts. Part 2. *New Zealand Journal of Geology and Geophysics.*

Walker MJC. 2005. *Quaternary Dating Methods.* Chichester: Wiley.

Wastegård S. 2002. Early to middle Holocene silicic tephra horizons from the Katla volcanic system, Iceland: new results from the Faroe Islands. *Journal of Quaternary Science* **17:** 723-730.

Wastegård S, Turney CSM, Lowe JJ, Roberts SJ. 2000a. New discoveries of the Vedde Ash in southern Sweden and Scotland. *Boreas* **29:** 72-78.

Wastegård S, Wohlfarth B, Subetto DA, Sapelko TV. 2000b. Extending the known distribution of the Younger Dryas Vedde Ash into northwestern Russia. *Journal of Quaternary Science* **15:** 581-586.

Weinstein P, Patel A. 1997. The Mount Ruapehu eruption, 1996: a review of potential health effects
25. *Australian and New Zealand Journal of Public Health* **21:** 773-778.

Westgate JA, Perkins WT, Fuge R, Pearce NJG, Wintle AG. 1994. Trace-element analysis of volcanic glass shards by laser ablation inductively coupled plasma mass spectrometry: application to tephrochronological studies. *Applied Geochemistry* **9:** 323-335.

Wilmshurst JM. 1997. The impact of human settlement on vegetation and soil stability in Hawke's Bay, New Zealand. *New Zealand Journal of Botany* **35:** 97-111.

Wilmshurst JM, Anderson AJ, Higham TFG, Worthy TH. 2008. Dating the late prehistoric dispersal of Polynesians to New Zealand using the commensal Pacific rat. *Proceedings of the National Academy of Sciences USA* **105:** 7676-7680.

Wilmshurst JM, Eden DN, Froggatt PC. 1999. Late Holocene forest disturbance in Gisborne, New Zealand: a comparison of terrestrial and marine pollen records. *New Zealand Journal of Botany* **37:** 523-540.

Wilmshurst JM, Higham TFG. 2004. Using rat-gnawed seeds to independently date the arrival of Pacific rats and humans in New Zealand. *The Holocene* **14:** 801-806.

Wilmshurst JM, McGlone MS, Leathwick J, Newnham RM. 2007. A pre-deforestation pollen-climate calibration model for New Zealand and quantitative temperature reconstructions for the past 18000 years BP. *Journal of Quaternary Science* **22:** 535-547.

Wilmshurst JM, McGlone MS, Partridge TR. 1997. A late Holocene history of natural disturbance in lowland podocarp/hardwood forest, Hawke's Bay, New Zealand. *New Zealand Journal of Botany* **35:** 79-96.

Wilmshurst JM, McGlone MS. 1996. Forest disturbance in the central North Island, New Zealand, following the 1850 BP Taupo eruption. *The Holocene* **6:** 399-411.

Wilson CJN. 1993. Stratigraphy, Chronology, Styles and Dynamics of Late Quaternary Eruptions from Taupo Volcano, New-Zealand. *Philosophical Transactions of the Royal Society of London Series A-Mathematical Physical and Engineering Sciences* **343:** 205-306.

Wilson CJN, Houghton BF, Mcwilliams MO, Lanphere MA, Weaver SD, Briggs RM. 1995. Volcanic and Structural Evolution of Taupo Volcanic Zone, New- Zealand - A Review. *Journal of Volcanology and Geothermal Research* **68:** 1-28.

Wilson CJN, Leonard G. 2008. Slumbering giants . In: Graham IJce, ed. *A Continent on the Move: New Zealand Geoscience Into the 21st Century*. Geological Society of New Zealand Miscellaneous Publication 124, 166-169.

Wilson CJN, Scott BJ, Houghton BF. 2004. Volcanoes of New Zealand. *TEPHRA.Living with Volcanoes* **21:** 2-11.

Wilson CJN, Walker GPL. 1985. The Taupo Eruption, New-Zealand .1. General-Aspects. *Philosophical Transactions of the Royal Society of London Series A-Mathematical Physical and Engineering Sciences* **314:** 199-228.

Zimanowski B, Wohletz K, Dellino P, Buttner R. 2003. The Volcanic Ash Problem. *Journal of Volcanology and Geothermal Research* **122:** 1-5.

Zoltai SC. 1989. Late Quaternary Volcanic Ash in the Peatlands of Central Alberta. *Canadian Journal of Earth Sciences* **26:** 207-214.